PROCEEDINGS OF SPIE

SPIE—The International Society for Optical Engineering

Laser Optics 2000

Ultrafast Optics and Superstrong Laser Fields

Alexander A. Andreev
Vladimir E. Yashin
Editors

26–30 June 2000
St. Petersburg, Russia

Organized by
Institute for Laser Physics (Russia)
All-Russia Scientific Center, S.I. Vavilov State Optical Institute
General Physics Institute, Russian Academy of Sciences
P.N. Lebedev Physical Institute, Russian Academy of Sciences
A.F. Ioffe Physico-Technical Institute, Russian Academy of Sciences
Russian National Center of Laser Physics, St. Petersburg State University
St. Petersburg Institute of Fine Mechanics and Optics (Russia)
Scientific Council on Coherent and Nonlinear Optics, Russian Academy of Sciences
SPIE—The International Society for Optical Engineering
SPIE Russia Chapter
OSA—Optical Society of America
ROS—Rozhdestvensky Optical Society (Russia)
Government of St. Petersburg (Russia)
ISTC—International Scientific and Technological Center

SPIE P PROCEEDINGS SERIES

Volume 4352

REPORT DOCUMENTATION PAGE

Form Approved OMB No. 0704-0188

1. AGENCY USE ONLY (Leave blank)	2. REPORT DATE	3. REPORT TYPE AND DATES COVERED
	14 September 2001	Conference Proceedings

4. TITLE AND SUBTITLE

Laser Optics 2000: Ultrafast Optics and Superstrong Laser Fields (Volume 4352)

5. FUNDING NUMBERS

F61775-00-WF

6. AUTHOR(S)

Conference Committee

7. PERFORMING ORGANIZATION NAME(S) AND ADDRESS(ES)

Institute for Laser Physics
12 Birzhevaya line
St. Petersburg 199034
Russia

8. Performing Organization Report Number

N/A

9. SPONSORING/MONITORING AGENCY NAME(S) AND ADDRESS(ES

EOARD
PSC 802 Box 14
FPO 09499-0200

10. SPONSORING/MONITORING AGENCY REPORT NUMBER

CSP 00-5049

11. SUPPLEMENTARY NOTES

Conference Proceedings in five volumes. Proceedings of SPIE – The International Society for Optical Engineering, 26-30 June 2000, St. Petersburg, Russia. Volumes 4350 (Solid State Lasers), 4351 (High-Power Gas Lasers), 4352 (Ultrafast Optics and Superstrong Laser Fields), 4353 (Control of Laser Beam Characteristics and Nonlinear Methods for Wavefront Control), and 4354 (Semiconductor Lasers and Optical Communication), ISSN 0277-786X

12a. DISTRIBUTION/AVAILABILITY STATEMENT

Approved for public release; distribution is unlimited.

12b. DISTRIBUTION CODE

A

ABSTRACT (Maximum 200 words)

The Final Proceedings for the Tenth Conference on Laser Optics, 26-30 June 2000. This is an interdisciplinary conference. Topics include generation of ultrashort light pulses, application of nonlinear correction techniques in adaptive optics and lasers, advanced methods of beam control and pointing; diode-pumped solid state lasers; high average power gas and solid-state lasers; and lasers in medicine and medical applications.

14. SUBJECT TERMS

EOARD, Adaptive optics, Gas lasers, Solid state lasers, Aberration correction

15. NUMBER OF PAGES

Five bound volumes

16. PRICE CODE

17. SECURITY CLASSIFICATION OF REPORT	18. SECURITY CLASSIFICATION OF THIS PAGE	19. SECURITY CLASSIFICATION OF ABSTRACT	20. LIMITATION OF ABSTRACT
UNCLASSIFIED	UNCLASSIFIED	UNCLASSIFIED	UL

PROCEEDINGS OF SPIE

SPIE—The International Society for Optical Engineering

Laser Optics 2000

Ultrafast Optics and Superstrong Laser Fields

Alexander A. Andreev
Vladimir E. Yashin
Editors

26–30 June 2000
St. Petersburg, Russia

Organized by
Institute for Laser Physics (Russia) • All-Russia Scientific Center, S.I. Vavilov State Optical Institute • General Physics Institute, RAS • P.N. Lebedev Physical Institute, RAS • A.F. Ioffe Physico-Technical Institute, RAS • Russian National Center of Laser Physics, St. Petersburg State University • St. Petersburg Institute of Fine Mechanics and Optics (Russia) • Scientific Council on Coherent and Nonlinear Optics, RAS • SPIE—The International Society for Optical Engineering • SPIE Russia Chapter • OSA—Optical Society of America • ROS—Rozhdestvensky Optical Society (Russia) • Government of St. Petersburg (Russia) • ISTC—International Scientific and Technological Center

Supported by
Ministry of Science and Technical Policy of the Russian Federation • Ministry for Economics of the Russian Federation • Ministry of Education of the Russian Federation • Federal Agency for Conventional Weapons (Russia) • Russian National Foundation for Basic Research • SPIE—The International Society for Optical Engineering • Lawrence Livermore National Laboratory (USA) • European Office of Aerospace Research and Development (USA) • OSA—Optical Society of America • ISTC—International Scientific and Technological Center • Amada Corporation (Japan) • Jenoptic GmbH (Germany) • Corning Inc. (USA) • IRE-Polus Group (Germany)

Volume 4352

Published by
SPIE—The International Society for Optical Engineering

Please use the following format to cite material from this book:

Author(s), "Title of paper," in *Laser Optics 2000: Ultrafast Optics and Superstrong Laser Fields*, Alexander A. Andreev, Vladimir E. Yashin, Editors, Proceedings of SPIE Vol. 4352, page numbers (2001).

ISSN 0277-786X
ISBN 0-8194-4042-6

Published by
SPIE—The International Society for Optical Engineering
P.O. Box 10, Bellingham, Washington 98227-0010 USA
Telephone 1 360/676-3290 (Pacific Time) • Fax 1 360/647-1445
http://www.spie.org/

Printed in the United States of America.

Contents

Laser Optics 2000 Program Committee

Chair

Artur A. Mak, Institute for Laser Physics (Russia)

Vice-Chairs

Alexander A. Andreev, Institute for Laser Physics (Russia)
Vladimir Yu. Venediktov, Institute for Laser Physics (Russia)

Scientific Secretary

A. F. Vassil'yev, Institute for Laser Physics (Russia)

Members

Zhores I. Alferov, A.F. Ioffe Physico-Technical Institute (Russia)
Pavel A. Apanasevich, B.I. Stepanov Institute of Physics (Belarus)
Sergey N. Bagaev, Institute for Laser Physics (Russia)
Nikolai G. Basov, P.N. Lebedev Physical Institute (Russia)
Yuri D. Berezin, Institute for Laser Physics (Russia)
Viktor I. Bespalov, Institute of Applied Physics (Russia)
Ernest V. Boiko, Military Medical Academy (Russia)
F. V. Bunkin, General Physics Institute (Russia)
Oleg B. Danilov, Institute for Laser Physics (Russia)
Eugeni M. Dianov, General Physics Institute (Russia)
Sergei A. Dimakov, Institute for Laser Physics (Russia)
Alexander V. Dotsenko, Corning Scientific Center (Russia)
Valentin Gapontsev, IPG Laser GmbH (Germany)
Yu. D. Golyaev, Research and Development Institute Polyus (Russia)
Vyacheslav M. Gordienko, M.V. Lomonosov Moscow State University (Russia)
Serguei A. Gurevich, A.F. Ioffe Physico-Technical Institute (Russia)
Valerii P. Kandidov, M.V. Lomonosov Moscow State University (Russia)
Yakov I. Khanin, Institute of Applied Physics (Russia)
I. V. Kovsh, Laser Association (Russia)
O. N. Krohin, P.N. Lebedev Physical Institute (Russia)
Vladimir V. Lyubimov, Institute for Laser Physics (Russia)
Alexander A. Manenkov, General Physics Institute (Russia)
Yuri T. Mazurenko, S.I. Vavilov State Optical Institute (USA)
Anatoly P. Napartovich, Troitsk Institute for Innovation and Fusion Research (Russia)
Anatoly N. Oraevsky, P.N. Lebedev Physics Institute (Russia)
Vladislav Ya. Panchenko, Scientific Research Center for Technological Lasers (Russia)
Pavel P. Pashinin, General Physics Institute (Russia)
G. T. Petrovskiy, S.I. Vavilov State Optical Institute (Russia)
N. N. Rozanov, Institute for Laser Physics (Russia)
Alexander S. Rubanov, B.I. Stepanov Institute of Physics (Belarus)
Marat S. Soskin, Institute of Physics (Ukraine)

Victor A. Serebryakov, Institute for Laser Physics (Russia)
Ivan A. Shcherbakov, General Physics Institute (Russia)
Vladimir E. Sherstobitov, Institute for Laser Physics (Russia)
Leonid N. Soms, Institute for Laser Physics (Russia)
V. B. Smirnov, St. Petersburg State University (Russia)
Anatoli P. Sukhorukov, M.V. Lomonosov Moscow State University (Russia)
Vladimir I. Ustyugov, Institute for Laser Physics (Russia)
V. V. Valuev, GPO Almaz (Russia)
V. N. Vasilev, St. Petersburg State Institute of Fine Mechanics and Optics (Russia)
Evgeny A. Viktorov, Institute for Laser Physics (Russia)
Vadim P. Veiko, St. Petersburg State Institute of Fine Mechanics and Optics (Russia)
Vladimir E. Yashin, Institute for Laser Physics (Russia)
Georgii M. Zverev, Research and Development Institute Polyus (Russia)

High-precision long-distance remote sensing using chirped-pulse interferometry.

A.B.Vankov and V.E.Yashin
Institute for Laser Physics, Birzhevaya line, 12, 199034 St.Petersburg, Russia
e-mail: yashin@ilph.spb.su

ABSTRACT

The use of a new method of interferometry of chirped pulse for precise remote measurement of lengths and velosities is proposed, evaluated and tested in experiments. The potentialities of the method in comparison with conventional methods are considered, and its possible applications are discussed.

Keywords: chirped pulses, remote sensing, interferometry, range finders, lidars.

1. INTRODUCTION

Pulsed lidars and laser range finders with pulse duration from micro- to nanoseconds are currently extensively used for measuring distances and velocities[1-4]. Such durations impose substantial restrictions on resolution of such systems. A change to pica- and femtosecond duration ranges is restrained by manifistation of different nonlinear effects accompanying the propagation of pulses with high peak power in the air. These effects can be suppressed using the method proposed in[5]. It uses pulse lengthening in time by diffraction gratings[6] and subsequent compression of the pulse reflected from a target. The measurement of its time delay relative to a reference pulse makes it possible to measure distances with submillimeter accuracy. However, the employment of this method in practice requires expensive high-sensitive instruments with high time resolution, such as a streak camera, or a high radiation power in the case of employment of an autocorrelator.
On the other hand, it is known that distances can be precisely measured by interferometric methods. However, interferometry of narrow-band radiation, which provides a high accuracy, gives no way of measuring distances in a wide range. Similar problems associated with a limited coherence length of broadband radiation[7]. These problems can be partially solved using methods of two-wave interferometry in combination with heterodyne measurements[8]. However, these methods call for extremely stable laser sources. Moreover, such advantages of the pulse method as high sensitivity and, consequently, large measurable distances are lost in this case.
In the papers[9,10] it is shown that the combination of pulsed and interferometric methods supplemented with the use of special wide-band chirped pulses makes it possible to combine the advantages of these two methods of distance measurement. The method, which was referred to as the interferometry of chirped pulses, can be used to measure not only distances, but velocities of objects as well, which makes it possible to design laser radars and lidars.

2. PRINCIPLE OF THE METHOD

The principle of the method consists in recording and analysing an interference pattern formed by two pulses, a reference pulse and a pulse reflected from an object, with frequency modulation that is linear in time. One can easily obtain such pulses by means of lengthening an initial short pulse with the use of diffraction gratings[6]. Such pulses are extensively used in the chirped pulse amplification technique (CPA)[11]. It is important that such nonlinear processes as small-scale self-focusing accompanying the pulse propagation are efficiently suppressed for relatively long pulses (0.5-3 ns) formed in this way. The interference pattern formed by two light waves with quadratically varying phases in the Michelson interferometer is not steady state, because the pulse frequency varies in time. However, the temporal Fourier transformation is stationary

Laser Optics 2000: Ultrafast Optics and Superstrong Laser Fields, Alexander A. Andreev, Vladimir E. Yashin, Editors, Proceedings of SPIE Vol. 4352 (2001) © 2001 SPIE · 0277-786X/01/$15.00

and carries information on pulse phase at a given moment of time, which makes possible precise measuring of distances. Let us analyze the general case of interference of two linearly chirped pulses.
The electric fields of two light waves with Gaussian intensity profiles and quadratically varying phases are described by the expressions

$$E^{(1)}{}_0(t) = A_1\exp(-\beta_1 t^2)\exp(i(\alpha_1 t^2+\varphi_1)) \qquad (1)$$
$$E^{(2)}{}_0(t) = A_2\exp(-\beta_2 (t-\tau)^2)\exp(i(\alpha_2 (t-\tau)^2+\varphi_2))$$

where $A_{1,2}$ are the amplitudes of light waves, $-\beta_{12}$ are the half-widths of the Gaussian envelopes, τ is the mutual time delay, $\alpha_{1,2}$ are the rates of frequency variation, and $\varphi_{1,2}$ are initial phases.
The Fourier transform of the resulting wave is described by the expression

$$I(\omega)= |E_\omega|^2 = A_1^2K_1^2\pi\exp(-K_1^4\beta_1\omega^2)+A_2^2K_2^2\pi\exp(-K_2^4\beta_2\omega^2)+2A_1A_2K_1K_2\pi\exp(-K_1^4\beta_1\omega^2/2)\exp(-K_2^4\beta_2\omega^2/2)\cos(\omega\tau+\omega^2(K_1^4-K_2^4)/4)++\mathrm{arctg}(\alpha_2/\beta_2)-\mathrm{arctg}(\alpha_1/\beta_1)+\varphi_1-\varphi_2) \qquad (2)$$

where $K_{1,2}=(\alpha_{1,2}^2+\beta_{1,2}^2)^{-1/4}$
Let us consider some particular cases of this expression important for practical cases.
The pulses have the same amplitudes, A1=A2, and chirp rates, $\alpha 1=\alpha 2$, but are separated it time by the interval τ. This gives

$$I(\omega) = A_1^2K_1^2 4\pi\exp(-K_1^4\beta_1\omega^2)\cos(\omega\tau+\varphi_1-\varphi_2) \qquad (3)$$

The pulses are characterized by the time delay τ and have the same chirp rates $\alpha_1=\alpha_2$ but different amplitudes $A_1\neq A_2$. In this case

$$I(\omega) =K_1^2\pi\exp(-K_1^4\beta_1\omega^2)(A_1^2+A_2^2+2A_1A_2\cos(\omega\tau+\varphi_1-\varphi_2)) \qquad (4)$$

The pulses are characterized by the time delay τ and have the same amplitudes $A_1=A_2$ but different chirp rates $\alpha_1\neq\alpha_2$. This gives

$$I(\omega)=A_1^2\pi(K_1^2\exp(-K_1^4\beta_1\omega^2)+K_2^2\exp(-K_2^4\beta_1\omega^2)+2K_1K_2\exp(-K_1^4\beta_1\omega^2/2)\exp(-K_2^4\beta_1\omega^2/2)\cos(\omega\tau+\omega^2(K_1^4-K_2^4)/4+\mathrm{arctg}(\alpha_2/\beta_1)-\mathrm{arctg}(\alpha_1/\beta_1)+\varphi_1-\varphi_2) \qquad (5)$$

Expressions (3) and (4) shows that the spectral expansion contains information on the time delay of two interfering pulses. The period of spectral modulation $\Delta\omega$ is inversely proportial to the mutual time delay of the pulses:

$$\tau=2\pi/\Delta\omega$$

Therefore, one can measure with high accuracy the period of spectral modulation and calculate the distance to an object.
The contrast of the corresponding oscillations can be determined from expression (4)

$$I(\omega)^{max} / I(\omega)^{min}=(A_1+A_2)^2/(A_1-A_2)^2 \qquad (6)$$

One can see from expression (6) that the maximum contrast (the maximum measurement accuracy) can be obtained by way of equalizing amplitudes of the reference and object beams, although this is not the necessary condition of measurements.

3. EXPERIMENT

The optical schematic of the device based on this method is shown in Fig.1. The chirped pulse with duration of about 500 picosecond (ps) and energy of 0.5 μJ after the master oscillator (MO) on Nd:glass with mode locking and stretcher is sent into a Q-switched regenerative amplifier (RA) with negative feedback. A part of the pulse train from this amplifier is directed at the target then comes back and interferes with pulses present in the amplifier. The spectral information on this interference is analysed at the output of RA by a diffraction grating and CCD camera.

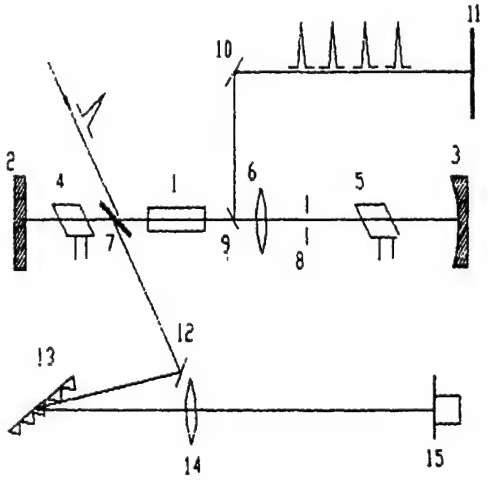

Fig.1. Schematic of the regenerative amplifier for remote sensing.
1-Nd:glass rod, 2,3-mirrors, 4,5-Pockels cells, 6-lens, 7-polariser, 8-aperture 9,10,12-mirrors, 11-object, 13 diffraction grating, 14-lens, 15-CCD camera

As a result of interference of overlapped chirped pulses displaced in time by interval τ a temporal amplitude modulation arises which easily can be observed in the radiation spectrum, as it is shown in Fig.2. It is easy to show, that the period $\Delta\omega$ of these spectral modulations is dentically connected with the time delay: $\tau=2\pi/\Delta\omega$

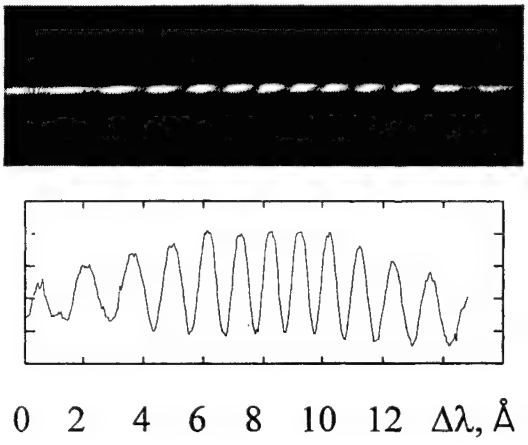

Fig.2. Spectrum of interfering chirped pulses at the output of the regenerative amplifier

Thus, it is possible to precisely measure the temporal shift, and consequently distance to an object $l=c\tau$, by measuring the period of spectral modulations. The model tests carried out with the initial picosecond pulse and 450 ps pulse length after stretching have shown an opportunity of measurement of distances with accuracy of 0.1 mm (see Fig. 3).

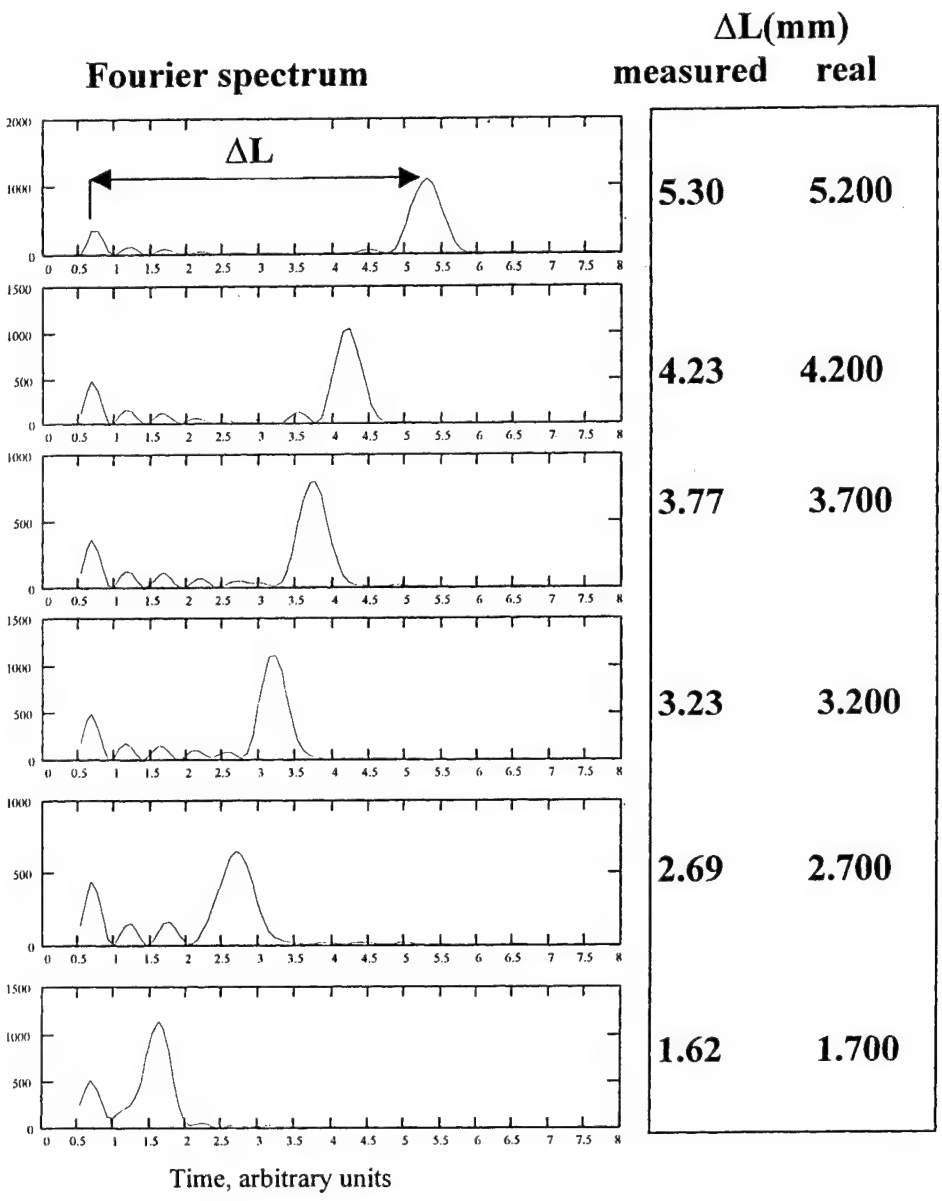

Fig.3. Fourier transforms of experimental spectra for different distances to the object and real and measurend changing of length at the object

4. POTENTIALITIES OF THE METHOD

Using results of calculations and experiments we shall discuss potentials of the considered method of distance and velosity measurement.

Limiting precision of measurement

The limiting precision and resolution of the given method are determined by the reciprocal width of the harmonic function envelope. Note that envelope width represents the spectral width $\Delta\omega$ of a laser pulse. Thus, the theoretical limit of an absolute error of distance determination is given by the quantity $\sigma=c/\Delta\omega$, where c is light velosity and $\Delta\omega$ the spectral width of the used pulse. This conclusion is confirmed by the results of experiment. So, for example, for the Nd:YLF laser medium the accuracy of measurements is about 1 mm, for Nd:glass 0.2 mm, and for Ti:Al_2O_3 30 μm. The same accuracy is obtained in the case of employment a pulse compressor followed by an autocorrelator or a streak camera [5] under the condition that the initial pulse is bandwidth limited. In the represented technique only a diffraction grating, lens and CCD-camera are used. In this case, sensitivity to weak reflected pulses is increased by several orders of magnitude in comparison with sensitivity of the correlation method, the range of measurable distances being several times wider.

Sensitivity to Weak Reflected Pulses.

Rejection of the use of instruments with high time resolution sharply increases the sensitivity of the method to weak reflected signals. Indeed, only noise and sensitivity of a CCD camera limit the signal-to-noise ratio of the system. Noises of amplifier, the frequency filters, and the analog-to-digital converters, which are used in direct distance measurements, to say nothing about distance measurements with an autocorrelator or a streak camera, are eliminated [3]. Thus, the interferometry of chirped pulses makes it possible to reach the theoretical limit of the signal-to-noise ratio, which is determined by shot noise of a cooled CCD.

In view of the fact that the cavity of the regenerative amplifier perceives only single-mode radiation, the speckle composition of the beam reflected from the target surface is of no importance, and only the energy of a separate speckle is significant. This makes it possible to measure distances to rough surfaces and aerosol.

Range of Measurable Distances

The measurement technique presented in paper[5] has a strong disadvantage. It requires a reference pulse coinciding in time with the object pulse, so that the both pulses are within the capture range of a streak camera or a correlator. One is forced to place a semitransparent mirror close to the surface under study and measure in actuality the difference of distances between them or make a series of measurements with a streak camera in order to obtain the required accuracy of absolute measurements of distance.

In the configuration presented in Fig. 1, chirped pulses with a virtually constant temporal structure are found in the regenerative amplifier during several tens of microseconds. In our measurements, a pulse train from the regenerative amplifier was directed onto the target surface. These pulses returned back from the target and interfered with pulses in the regenerative amplifier. The latter pulses were used as reference pulses. We measured distance directly by the delay of the first pulse of the train. This value was accurate within the pulse period in the train, which was equal to 13 ns. The exact value of distance within this range was determined from the interference spectrum.

In view of the fact that the capture range depends only on the spectral instrument resolution, one can cover the double pass along a RA cavity with several channels and obtain the instrument measuring distances of at least several hundreds meters with an accuracy of the order of 100 μm. The lack of uniqueness caused by the signal symmetry in respect to the zero position is eliminated in a similar way.

Velocity Measurement

The given approach allows measuring not only a distance, but also a velocity of targets by Doppler shift of pulse frequency. A train of chirped pulses whose frequency linearly varies in time is directed onto a moving object being studied. The pulses reflected from the object enter the input of a regenerative amplifier (RA) and are amplified (or attenuated) in it to the desired level. This is accompanied by their overlap in time. The overlap causes multibeam interference, which is recorded at the output by a spectrometer. The motion of the object produces the phase shift of separate pulses in the train, which causes easily recorded changes in the spectrum.

The frequency shift of the pulse results in displacement of spectral modulations, which will be the more, the more is velocity of the object. The displacement by a half of an interference pattern strip which can be easily registered at moderate spectral resolution, occurs at speed $v=\lambda/4T$, where λ is the wavelength and T is the train period.

The experiments which have been carried out on the Nd:glass CPA laser system[10] have shown an opportunity of measurement of velocity in the range of 5-50 m/s with accuracy of measurement of 5% for the given configuration of the

laser (cavities of master oscillator and regenerative amplifier have the length about 2m). Thus the total energy of the order of 10 nJ at the input of the regenerative amplifier is sufficient to perform measurements, which is comparable in sensitivity with those by the heterodyne method[1-4].
The bottom border of measurable velocities can be lowered approximately to 1 m/s by using statistical processing of the output spectra. The top limit of velocities can be extended by the order by decreasing the time of round trip along the RA cavity. In particular, a cavity 20-cm long makes it possible to measure velocities up to 500 m/s.

5. CONCLUSIONS

Thus the considered methods of remote measurement of distances and velocities of objects have the following advantages before other approaches.

1. The accuracy of distance measurement is defined by spectrum width of pulse and can amount to several tenth microns for distances of several kilometres.
2. Use for measurements in the atmosphere of rather long pulses (ns- and subns) suppresses such nonlinear effects, as small-scale self-focusing filamentation which can interfere with the measurements for more short pulses.
3. Implementation of measurements does not need a complex and expensive equipment with high temporal resolution (streak camera or broadband photodetectors and oscilloscopes).
4. The simultaneous measurements of distances and velocities of objects with high accuracy are possible with the rather simple equipment

These features favourably distinguish this method from the known and give the basis to hope for its practical applications in laser rangefinders and lidars. The development of the specialised complex with the use of simple and cheap laser sources is necessary for this purpose. As such sources the diode pumped solid-state lasers and also picosecond diode lasers are most attractive.

REFERENCES

1. R.T Menzies., and R.M Hardesty., Proc. IEEE, , **77**, 449-462 (1989).
2. T.J. Kane, W.J. Kozlovsky, R.L. Byer and C. Byvik, Optics Lett., **12**, 239-241 (1987).
3. M.J. Kavaya, S.M. Henderson, J.R. Magee, C.P. Hale, and R.M. Huffaker, Optics Lett., **14**, 776-778 (1989).
4. K.P. Chan and D.K. Kilinger, Optical. Engineering, , **30**, 49-54 (1991).
5. A. Braun, C.Y.Chien, S. Coe, and. G. Mourou, Opt Commun, **105**, 63-65 (1994).
6. E.B. Treacy, IEEE J. Quant. Electron.,**QE-5**, 454-460 (1969).
7. D.A. Pol" Introduction in optics ", 1947, OGIZ, p.150.
8. R. Danliker, R.Thalman, and D.Prongue, Opt. Lett., **13**, 339-341 (1988).
9. A.B.Van'kov, A.A. Kozlov , S.A.Chizhov, and V.E. Yashin, Optics and spectroscopy, **84**, 94-99 (1998).
10. A.B. Van'kov, A.A. Kozlov, S.A. Chizhov, and V.E Yashin. Optics and spectroscopy, , **84**, 672-676 (1998).
11. P. Maine, D. Strickland, P. Bado., M Pessot., and G. Mourou, IEEE J. Quant. Electron., , **24**, 398-405 (1988).

Femtosecond two-photon excitation spectra of condensed matter

Thomas Roth and Robert Laenen

Physik-Department E11, Technische Universität München, James-Franck-Str., D-85748 Garching, Germany

ABSTRACT

Tunable femtosecond laser pulses in a large spectral range of 0.41 to 5.5 μm are used for non-collinear two-photon absorption in condensed matter. The spectral properties of two examples are discussed in detail: diamond of type IIa and neat water at room temperature. The generation of free carriers and results on the subsequent relaxation dynamics are presented.

Keywords: two-photon absorption, IR-spectroscopy, diamond, water

1. INTRODUCTION

The two-photon absorption (TPA) is a well-known phenomenon which already has been predicted for the first time in 1931 by Goeppert-Meyer[1] and was experimentally verified by Kaiser and Garret[2] in 1961. This absorption-mechanism appears mainly in two different situations:

1. In the degenerate case simultanous absorption of two photons of an intense light field oscillating at frequency ω is observed. The absorption shows a resonance at 2ω. The degenerate two-photon absorption coefficient $\beta(\omega_{Pu}, \omega_{Pu}) \equiv \beta$ is defined by the relation:

$$dI_{Pu}/dz = -\beta(\omega_{Pu}, \omega_{Pu})\, I_{Pu}^2 - \sigma\, n\, I_{Pu}, \tag{1}$$

   where $I_{Pu}(z)$ denotes the intensity of the light pulse depending on the sample depth z. Linear losses $-\alpha I_{Pu}$ are neglected. The second term takes into account the absorption of the pump pulse by the generated carriers with density n. σ is the appropriate absorption cross section.

2. By using two independent light pulses at frequencies ω_{Pu} and ω_{Pr} the simultanous absorption of one photon of each pulse is caused by a resonance at $\omega_{Pu}+\omega_{Pr}$. This is the same experimental situation pertaining at the same time to the classical setup of pump-probe-experiments. As a rule of thump the TPA will become a dominant influence in pump-probe-measurements if the total available energy of pump- and probe-field is deep in the absorption-regions of the sample. As most samples show strong electronic absorption in the ultraviolet part of the electromagnetic spectrum TPA is expected with the application of two light pulses with

Further author information: (Send correspondence to R. Laenen)

E-mail: rlaenen@ph.tum.de

Laser Optics 2000: Ultrafast Optics and Superstrong Laser Fields, Alexander A. Andreev, Vladimir E. Yashin, Editors, Proceedings of SPIE Vol. 4352 (2001) © 2001 SPIE · 0277-786X/01/$15.00

frequencies in the blue to ultraviolet part of the spectrum.
For pump-probe TPA one has to extend Eq. (1)[3]:

$$dI_{pr}/dz = -\beta(\omega_{pu},\omega_{pr})\, I_{pu}\, I_{pr} - \sigma\, n\, I_{Pr} \quad (2)$$

$$dI_{pu}/dz = -\beta(\omega_{pu},\omega_{pr})\, I_{pu}\, I_{pr} - \sigma\, n\, I_{Pu} - \beta(\omega_{pu},\omega_{pu})\, I_{pu}^2 \quad (3)$$

The nondegenerate two-color TPA coefficient $\beta(\omega_{pu},\omega_{pr})$ is in general different from $\beta(\omega_{pu},\omega_{pu})$. The second term in Eq. (2) takes into account the absorption of the probe-pulse by carriers generated by the intense pump-pulse. Note that the first term on the right side of Eq. (2) increases linearily with the pump-pulse intensity ($\sim I_{pu}$), whereas the second term has a quadratic dependence since $n \sim I_{pu}^2$. Experimental results have shown that the term $-\beta(\omega_{pr},\omega_{pr})\, I_{pr}^2$ describing TPA of the probe-pulse alone is negligible for the applied probe intensities in our experiments and can therefore be omitted in Eq. (2).

In the following we will discuss at first our experimental setup into detail. Special consideration will be focused on the methods of parametric frequency-conversion enabling time-resolved spectroscopy in a wide spectral range from 410 to 5500 nm with high temporal resolution down to < 100 fs. It will be stressed that especially this considerable scope of available information leads to novel results concerning ultrafast processes in condensed matter. As an example for solid samples we show data on time-resolved spectroscopy on a diamond sample of type II a. Similar measurements were in addition performed on a sample in the liquid state, this time we invesigated neat water.

2. EXPERIMENTAL SETUP

Wavelength	820 nm
Repetitionrate	1kHz
Pulselength	80 - 120 fs
Pulseenergy	600 μJ

Figure 1. Specifications of the laser output.

The experimental data shown in the next two sections were obtained with a home built Ti:Sa laser utilizing regenerative amplification of one pulse out of the pulse train of the respective oscillator at a repetition rate of 1 kHz. The specifications of the laser-system are listed in Fig. 1. The laser pulse at the fundamental wavelength is split into three parts for further conversion to different frequencies.
250 μJ of the amplified laser pulse is used for the generation of a 270 nm UV pulse by frequency-tripling of the fundamental. A scheme of the respective setup is depicted in Fig. 2. The combination of the halfwave-plate $\lambda/2$ and thin-film-polarizer TFP allows for a variable splitting of the energy of the input pulse into the two beam lines. The perpendicular polarized part is frequency-doubled in a 1 mm-long BBO-crystal. The frequency doubled pulse at 410 nm is subsequently overlapped in space and time (VD) with the parallel polarized remainder at 820 nm in a second BBO-crystal of 0.3 mm length. Utilizing Type I-phasematching the fundamental and the frequency-doubled pulses generate the desired radiation at 270 nm. The overall conversion efficiency amounts to 3.5% equal to 9 μJ of available UV energy.
The remainder of the available laser energy is converted to wavelengths ranging from 410 to 5500 nm

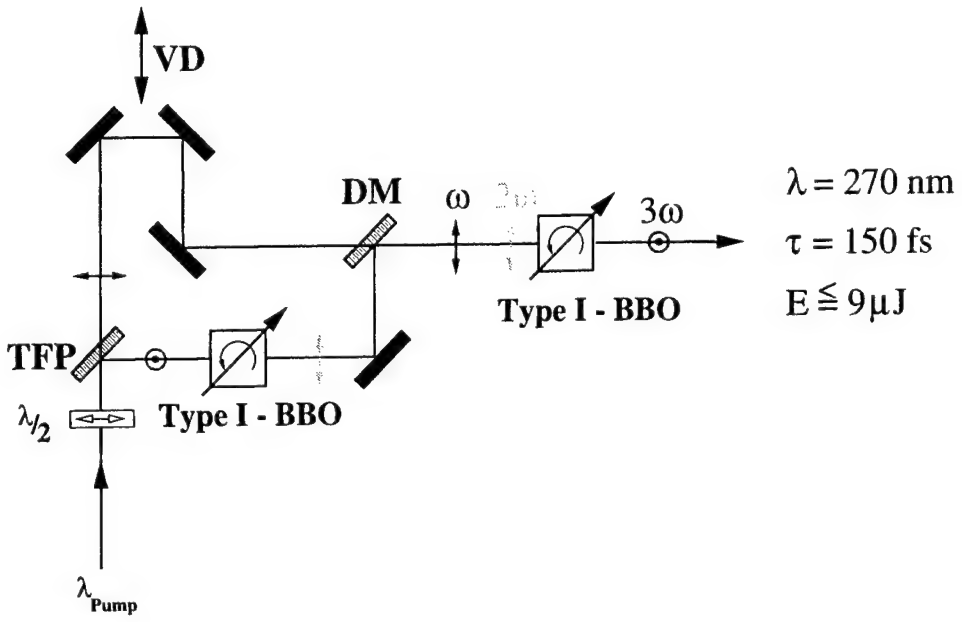

Figure 2. Scheme of the setup used for generation of the third harmonic of the laser at 270 nm; TFP: thin film polarizer; DM: dichroic mirror; VD: variable delay.

by two different techniques. A smaller part is used for generation of a white light continuum offering suitable probing pulses in the range of 410 to 930 nm. The wavelength selection is realized by inserting different interference filters into the beam line with a spectral transmission width of ca. 10 nm.

The larger part of the laser-energy of $\simeq 350\ \mu$J is converted to the IR by parametric amplification and subsequent frequency down conversion in a special setup. A small part of the laser pulse is

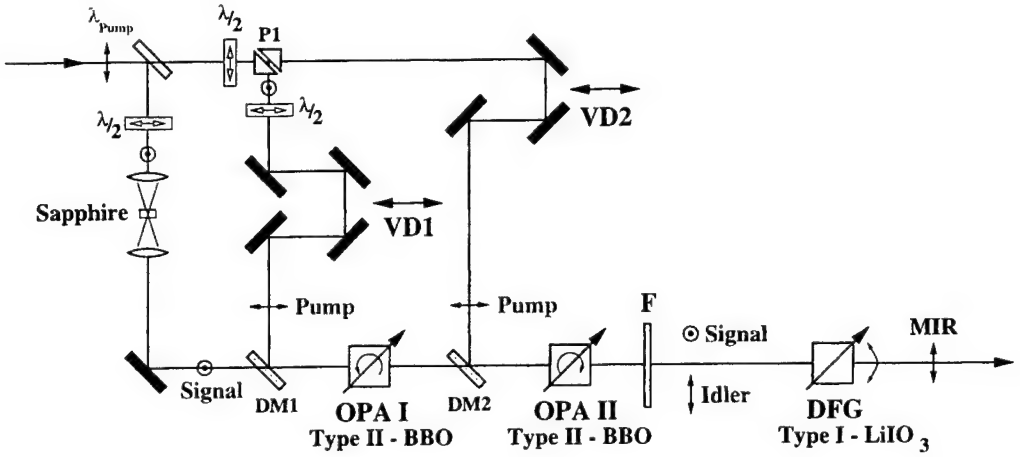

Figure 3. Schematic setup of the two-stage parametric amplifier and frequency down conversion used for the generation of intense NIR to MIR radiation; DM1, DM2: dichroic mirrors; VD1,2 : variable delays; F: filter.

focused into a specimen of sapphire for the generation of a white light continuum providing near-infrared wavelength components, too, as an initial seed for a subsequent parametric amplification step. By the help of the dichroic mirror DM1 the continuum and part of the laser fundamental are focused collinearly into the first nonlinear crystal. The variable delay VD1 enables the synchronization of the seed-pulse with the laser pulse allowing for optimization of the conversion. Due to the exceptional low groupvelocity dispersion of BBO in the NIR-region a 4 mm long crystal could be employed without detrimental pulse-lengthening of the resulting signal and idler pulses due to the different respective wavelengths. In this way the optimum temporal resolution of the experiment is preserved at a high energy conversion level. This first amplification stage is followed by a second identical setup which allows for further amplification of the signal and idler fields. The optimum synchronization of the two parametric components and the laser pulse is adjusted by a second variable delay VD2. Wavelength selection is realized by employing Type II-phasematching in the two BBO crystals resulting in the parametric amplification of a comparably small frequency range of the continuum obeying the phasematching condition.[4] Additionally this scheme allows for easy separation of signal and idler components with a suitable polarizer. This setup enables the generation of tunable signal pulses from 1.22 μm to 1.65 μm with pulse energies up to 6 μJ and from 1.65 μm to 2.5 μm with pulse energies up to 5 μJ for the idler, respectively. The tuning range is limited by the onset of absorption in the BBO crystal for wavelengths exceeding $\simeq$ 2.5 μm. Extension of the available probing range is achieved by difference-frequency generation between the signal and idler pulse in a $LiIO_3$-crystal of length of 2.5 mm. The experimentally generated MIR pulses enables probing from 2.5 to 5.5 μm with typical energies of < 0.5 μJ.
Fig. 4 shows schematically the setup for the generation of three light pulses at different colors and the noncollinear pump-probe experiment. Having passed the variable translation stage VD1 the UV pulse is focused into the sample. Two silicon detectors record the transmission of the pump pulse through the sample. The time-resolved transmission change $\Delta OD(t) = -\log\left(\frac{T_{Pump}(t)}{T_0}\right)$ of the sample is determined by subsequent blocking of every second pump pulse with a chopper. Depending on the desired probing wavelength either the continuum is utilized for probing of the induced change in sample transmission in the visible or the IR-pulse is focused into the excited region of the sample while polarization resolved recording of the transmission is accomplished. Silicon detectors are used for the visible spectral range and liquid nitrogen cooled HgCdTe-photoresistors for the IR. To avoid for accumulative thermal effects in the water sample a jet is utilized which ensures exchanges of the excited volume from one laser shot to another. In addition coherent artefacts of the measured signal transients are avoided arising from pump-probe coupling in the sample windows which would deteriorate the data. A jet thickness of 75 μm is used to minimize the complicating influence of the different groupvelocities of the UV-pump and MIR-probe pulses.

3. TWO-PHOTON ABSORPTION IN DIAMOND

In the following we present the experimental results obtained for a diamond sample. Fig. 5 shows some measured signal transients taken at four different probing wavelengths in the range of 410 nm to 3.28 μm. A 100 μm-thick diamond-specimen of type II a (nitrogen-free) was used in the experiments. The intensity of the UV-pulse was kept constant within an accuracy of $\pm$20% within all

experiments. For this reason the strength of the induced absorption at all different probing wavelengths is directly comparable. As can be seen from Fig. 5 the signal transients exhibit two major contributions. The signal around delay time zero (optimum overlap between pump and probe) is dominated by a crosscorrelation peak between pump and probe which is gradually disappearing in amplitude for longer wavelengths. For delay times > 0.5 ps a longlived contribution shows up in the measurements with an amplitude which is increasing with longer wavelengths. The lines in Fig. 5 are calculated with the help of equations 2 discussed in the introduction with typical numbers of σ and n as discussed in the following.

Diamond is belonging to the group of indirect semiconductors with an indirect bandgap of $E_{ind} = 5.48$ eV.[5] Concerning the energy width of the direct bandgap different values can be found in the literature. Numbers are reported in between $E_{dir} = 6.5$ eV[6] and $E_{dir} = 7.3$ eV.[7] TPA-measurements offer a further possibility in determination of the energy of the direct band gap as will be outlined in the following.

In Fig. 6 the maximum transient absorption ΔOD_{max} of the crosscorrelation-peak as derived from measurements shown for example in Fig. 5 is shown versus the sum of the photon energy of pump and probe pulse. The probe light undergoes an induced absorption at delay time zero as it is able to generate electron-hole pairs together with the UV-pump in the diamond. Therefore the two-color TPA is a very sensitive method for investigations of different excitations in semiconductors. As the generation of charges below the direct bandgap proceeds phonon-assisted this contribution to the induced absorption is obviously hindered and depends strongly on the temperature. Above the direct bandgap this constriction is elucidated and as shown in Fig. 6 for the smallest probing

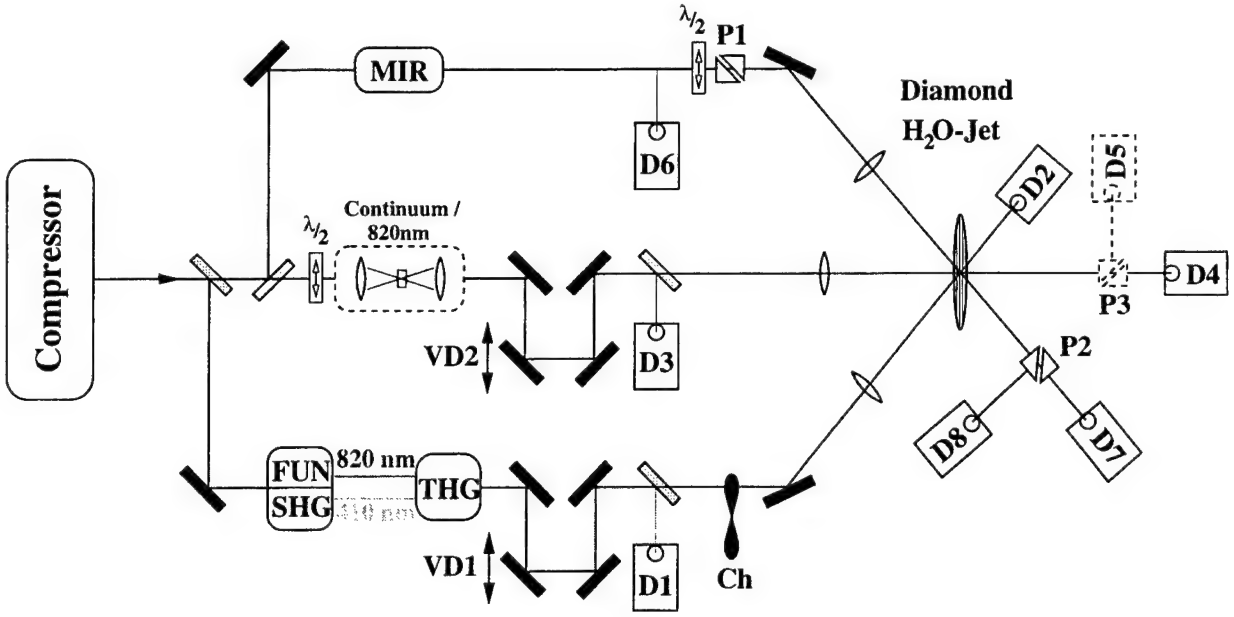

Figure 4. Schematic of the complete setup for the frequency conversion and the noncollinear pump-probe experiment; D1-8: detectors; Ch: Chopper; Compressor: pulse-compression unit after the regenerative amplification.

wavelength of 410 nm the crosscorrelation-peak is increasing significantly. With decreasing overall photon energy of the two-photon excitation the induced absorption above the indirect bandgap is decreasing slowly as the density of states of the thermally excited acoustical phonons is decreasing. Following Fermi's 'Golden Rule' the absorption crossection shows the same behaviour. Below the indirect bandgap an additional induced absorption is developing which can presumably be attributed to the generation of excitons. As is suggested by the measurement at $\lambda_{Pr} = 580$ nm corresponding to a total photon energy of $\simeq 6.6$ eV the direct bandgap seems to be located higher than this value. As can be seen from the shortest probing wavelength of 410 nm the direct bandgap has to be lower then 7.5 eV.

The longlived contribution to the induced absorption in diamond shows a variation with frequency, too. In Fig. 7 the absorption-coefficient derived from fitting of the latter data is plotted logarithmically versus wavelength. It is evident that the absorption for the longer wavelengths $\lambda > 1\mu$m observes a powerlaw $\sim \lambda^{2.7}$. This finding can be interpreted as the well-known free-carrier absorp-

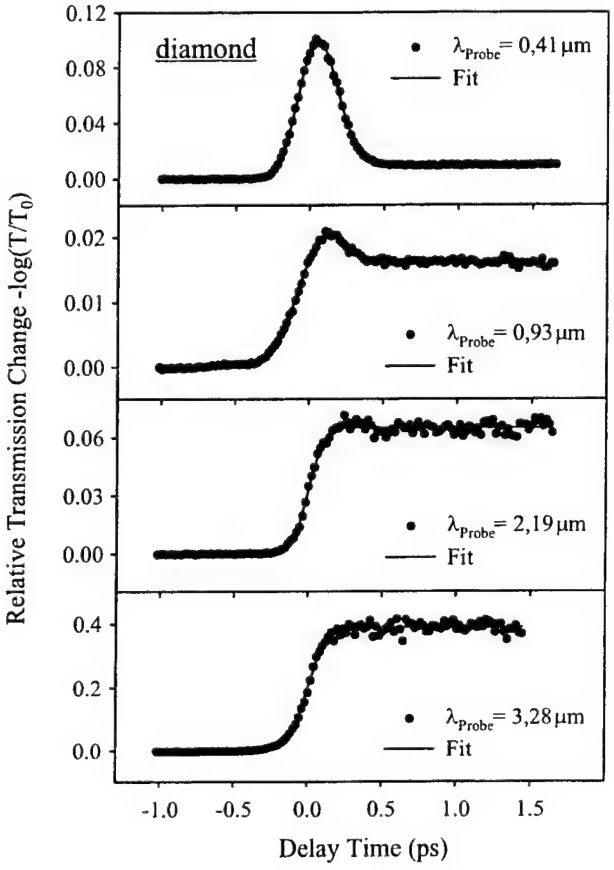

Figure 5. Induced absorption of a 100 μm-thick diamond-sample (type II a); measured data, calculated line.

tion in semiconductors. In the following a quantitative analysis with the 'Drude'-model allows to extract the generated electron-density in the sample:
The frequency-dependence of the dielectric function is described in the 'Drude'-model as

$$\epsilon(\omega) = n^2(\omega) = \epsilon_\infty - \frac{n_c e^2}{m^* \epsilon_0 (\omega^2 + i\omega/\tau)} \tag{4}$$

with ϵ_∞ as nonresonant dielectric constant, n_c as density of carriers, m^* as effective mass of the carriers and τ as collision-time depending on the mobility of the carriers. For sufficiently high frequencies ($\frac{1}{\omega\tau} << 1$) the dielectric function can be expanded and split into real and imaginery parts:

$$\begin{aligned} \epsilon(\omega) &\simeq \epsilon_\infty - \frac{n_c e^2}{m^* \epsilon_0 \omega^2} \cdot \left(1 - \frac{i}{\omega\tau}\right) \\ &\simeq \underbrace{\epsilon_\infty \left(1 - \frac{\omega_p^2}{\omega^2}\right)}_{\epsilon_r(\omega)} + i \underbrace{\frac{\epsilon_\infty}{\omega\tau} \frac{\omega_p^2}{\omega^2}}_{\epsilon_i(\omega)} \quad , \qquad \text{with} \quad \omega_p^2 = \frac{n_c e^2}{m^* n_r^2 \epsilon_0} \end{aligned} \tag{5}$$

as the plasma-frequency.
With the assumption that the index of refraction n_r is independent of the frequency the following

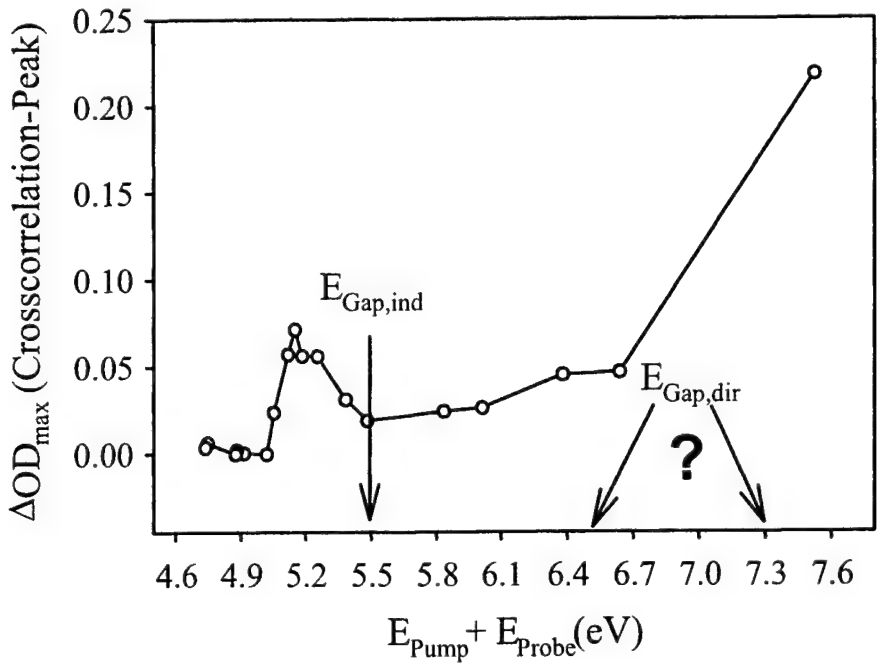

Figure 6. Maximum transient absorption ΔOD_{max} of the crosscorrelation-peak versus the sum of the pump and probe photon energy, the energy of the direct and indirect bandgaps are indicated in the figure as reported from the literature (see text).

expression is derived:

$$\alpha(\omega) \simeq 2\frac{\omega}{c} n_i(\omega) \simeq \frac{\omega \epsilon_i(\omega)}{c n_r} \simeq \frac{n_r}{c\tau}\frac{\omega_p^2}{\omega^2} \tag{6}$$

Taking the electron-mobility in diamond with $\mu_e = 2000\ \frac{cm^2}{Vs}$[9] and an averaged effective mass of $m^* = \sqrt[3]{m_l m_t^2} = 0,57 m_e$ (m_l: longitudinal electron-mass , m_t: transversal electron-mass) into account the collision-time τ evolves as:

$$\tau = \frac{m^* \sigma}{n_e e^2} = \frac{m^* e n_e \mu_e}{n_e e^2} = \frac{m^* \mu_e}{e} = 0,65\,\text{ps} \tag{7}$$

The electron-density n_e in the plasma-frequency ω_p alone is left as an adjustable parameter and is for this reason fitted to the data according to Eq. (6). Fig. 7 contains the solid line as a fit with an electron-density of $1.1 \cdot 10^{19} cm^{-3}$. Additionally the exponent of the wavelength powerlaw acts as the second adjustable parameter of the fit to the data shown in the figure. It is well-known that the scattering upon the deformation potential by phonons and the scattering upon lattice-imperfections through doped nitrogen is responsible for deviations from Eq. (6). Depending on the semiconductor this modifies the exponent of the frequency dependency of α between 2 to 3.[8] In diamond the free-carrier-absorption decreases apparently with $\simeq \lambda^{2.7}$, as deduced from fitting of the data.

For photon-energies exceeding $\simeq$ 1 eV the absorption-coefficient α decreases with a smaller exponent in the powerlaw. If the energy of the direct bandgap with 6.5 eV applies the electrons can be elevated with E_{Pr} = 1 eV to the conduction-band using a suitable phonon for conservation of

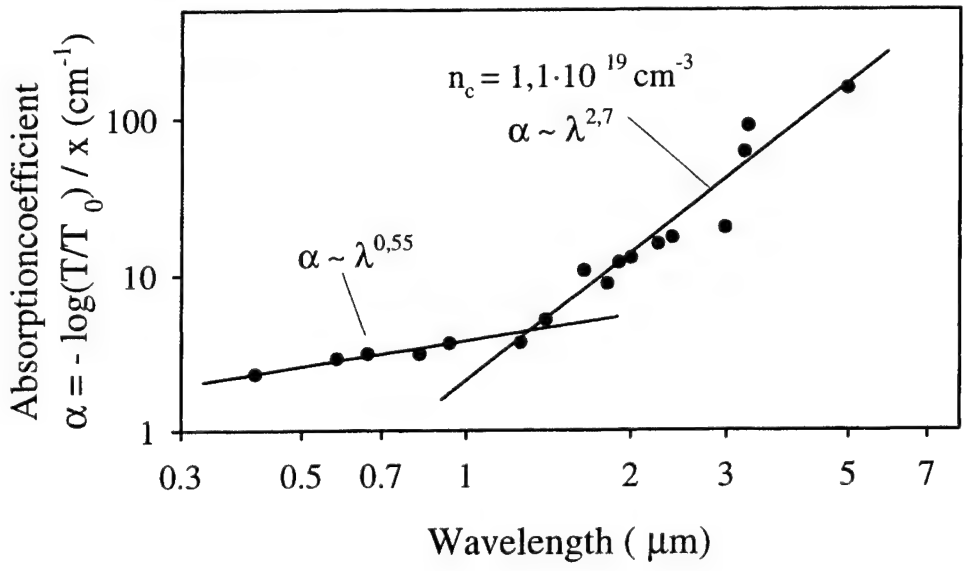

Figure 7. Absorption-coefficient $\alpha(\lambda)$ deduced from the longlived contribution to the induced absorption in the diamond-sample.

momentum. As the curvature of the conduction-band is disappearing in this region of k-space, the density of states is increasing together with the transition-probability. This in turn causes a slower decline of the absorption-coefficient with smaller wavelength. Fig. 7 allows the conclusion that the direct bandgap is more in the vicinity of 6.5 than 7.3 eV.

4. TWO-PHOTON ABSORPTION OF NEAT WATER

The TPA is one of the most important tools for generating charges in liquids serving there as a local probe for the structural and dynamical properties of the surrounding molecules. In this way it is possible to get new insights in the dynamics of H-bonded networks and the physics of these complex systems in general. Most prominent representative of these systems due to its omnipresence in nature, biology and chemistry is water. As the ionization of bulk-water is believed to start at ca. 6.4 eV[10,11] it is possible to generate electrons with up to 2.6 eV kinetic energy with our laser-system. The equilibration of this species has been subject to intense scrutiny for many

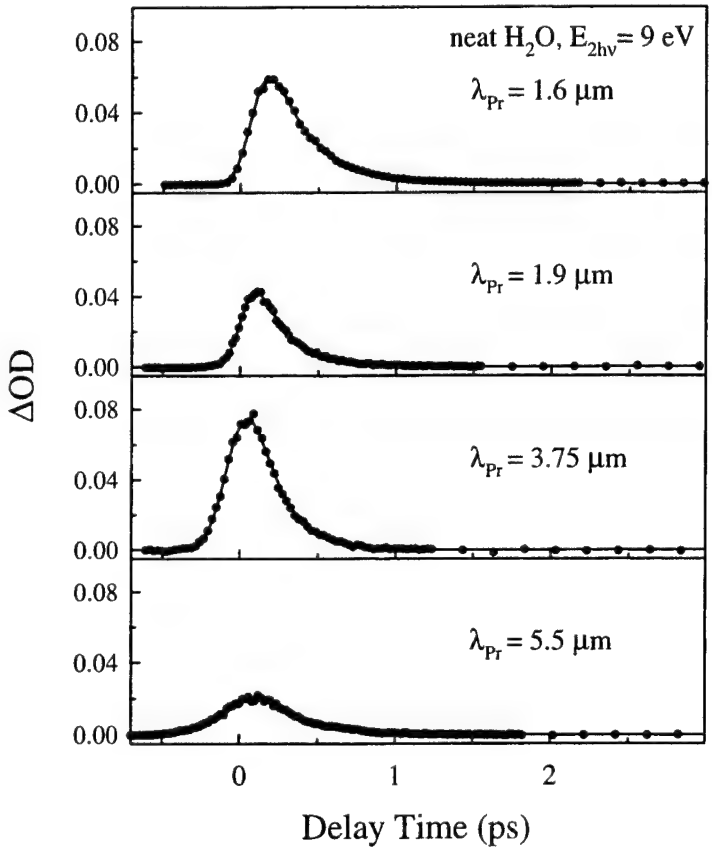

Figure 8. Four selected signal transients show the temporal evolution of the induced sample absorption after two-photon excitation of water in between 1.6 and 5.5 μm.

years. It has been recognized early in the time-resolved investigations that the generated carriers show partly relaxation to the so-called solvated electron. This species is believed to be a bound electron in a potential which results from an interaction between the electron and the surrounding water molecules oriented with the hydrogens to the electron. The first results from investigations of the process of equilibration of the generated electrons in water have been conducted with probing in the visible.[12,13] With the availability of the IR probing pulses of our laser system we are able to determine for the first time the induced sample absorption after two-photon excitation of water up to wavelengths of 5.5 μm. From the respective experiments we determined novel precursors of the solvated electron. Fig. 8 presents some selected signal transients with probing in the near and mid infrared. The delay time zero has been determined from additional measurements on a diamond specimen which have been conducted for every probing wavelength as outlined in section 3. A first glance at the presented data shows that the induced absorption has already disappeared around 1 ps after delay time zero between pump and probe pulse in the investigated IR-region. A closer look reveals that the response in the mid-infrared, e.g. at 3.75 or 5.5 μm, seems to be instantanous within the time-resolution of our experiment. On the contrary the near-infrared measurements show a delayed onset of the induced absorption and a slower decay. As already outlined in section 3 again the pump intensity was kept constant within $\pm 20\%$ during all measurements shown here. A major maximum of ΔOD centered at the frequency position of the OH-stretching mode (not shown) is derived from the data as well as a second smaller maximum in the near infrared at 1.6 μm. In the course of this study at least 23 mearurements at different wavelength positions in the IR have been made in neat water. A self-consistent fit of all signal transients measured in between 410 nm and 5.5 μm to a multi energy level system suggested[14] the existence of two new precursors to the up to now known intermediate called wet electron[13] which finally relaxes to the solvated electron. A comparison with the results from gasphase experiments strongly supports the following interpretation:

The first species which is seen after two-photon excitation of water results from an ultrafast proton-transfer along an H-bridge-bond leaving behind a OH:e^- complex with an enhanced dipole moment and a remarkably strong absorption with maximum of up to 120000 $M^{-1}cm^{-1}$. The next species builts up with a time constant of $\tau_{CT} = 110 \pm 40$ fs and this can be understood as an envelope of the absorption-bands of electrons within traps consisting of an increasing number of water molecules. As the surrounding water molecules do not have enough time to react completely to the presence of the newly generated charge the system can be compared to some extent to a very small water-cluster with an electron. With increasing delay time more and more water molecules reorient within the vicinity of the electron resulting in a continous blue-shift of the absorption of the corresponding trapped electron. With a second time constant of $\tau_{trap} = 200 \pm 50$ fs the already well-known wet electron builds up, the final precursor of the solvated electron.

5. CONCLUSION

In this work we have shown that TPA is a very suitable method for the generation of charges in condensed matter. It offers the possibility to monitor the subsequent dynamics of equilibration of these generated charges with femtosecond time resolution. To get the most complete picture of the

involved species after photoexcitation the broadest possible probing range has to be accomplished. In the case of diamond we found strong hints that the energy of the direct band gap is close to 6.5 eV from the frequency dependent maximum induced absorption. In the case of a neat water sample new insights are obtained on the equilibration mechanism of the generated electrons and the response of the surrounding molecules. This work gives evidence for the existence of two novel precursors to the solvated electron absorbing in the IR-region. These are interpreted as the first steps of electron-separation and the subsequent structural relaxation of the surrounding water molecules which takes place with time constants of 110 fs and 200 fs, respectively.

REFERENCES

1. M. Goeppert-Meyer, Ann. Phys. (Leipzig) **9**, pp 273 (1931)
2. W. Kaiser and G. B. C. Garrett, Phys. Rev. Lett. **7**, pp 229 (1961)
3. C. Rauscher and R. Laenen, J. Appl. Phys. **81**, pp 2818 (1997)
4. F. Seifert, V. Petrov, and F. Noack, Opt. Lett. **19**, pp837 (1994)
5. C. Clark, P. Dean, and P. Harns, Proc. Roy. Soc. London **A 277**, pp 312 (1964)
6. H. Armon and J. P. F. Sellschop, Phys. Rev. **B 26**, pp 3289 (1982)
7. R. A. Roberts and W. C. Walker, Phys. Rev. **161**, pp 730 (1967)
8. P. Yu and M. Cardona, *Fundamentals of Semiconductors*, Springer (1989)
9. F. Nava, C. Canali, C. Jacoboni, and L. Reggiani, Solid State Commun. **33**, pp 475 (1980)
10. J. McGowen, H. Ajo, J. Zhang, and J. Schwartz, Chem. Phys. Lett. **231**, pp504 (1994)
11. D. Nikogosyan, A. Oraevsky, and V. Rupasov, Chem. Phys. **77**, pp 131 (1983)
12. A. Migus, Y. Gauduel, J. L. Martin, and A. Antonetti, Phys. Rev. Lett. **15**, pp 1559 (1987)
13. H. Lu, F. H. Long, and K. B. Eisenthal, J. Opt. Soc. Am. **B7**, pp 1511 (1990)
14. R. Laenen, T. Roth, and A. Laubereau, Phys. Rev. Lett. **85**, tentatively scheduled for 3rd of July 2000

Ultrafast relaxation of induced anisotropy in condensed media studied by forced light scattering using broadband laser radiation with variable spectral width

A.I. Vodchits[1] and A. Lau[2]

[1]B.I. Stepanov Institute of Physics, National Academy of Sciences of Belarus, Fr. Scaryna Ave. 68, Minsk 220072, Belarus, E-mail: vodchits@dragon.bas-net.by

[2]Gesellschaft zur Förderung angewandter Optik, Optoelektronik, Quantenelektronik und Spektroskopie e. V., Rudower Chaussee 29 / IGZ, D12489 Berlin, Germany

ABSTRACT

The ultrafast relaxation of induced anisotropy in condensed media (organic liquids and their mixtures) is studied by forced light scattering using broadband dye laser radiation with variable spectral width. The influence of the finite spectral width of an exciting laser pulse on the observed relaxation dynamics of the investigated samples (so-called spectral-filter effect) is demonstrated for the first time in transient spectroscopy with incoherent light.

1. INTRODUCTION

The investigations of ultrafast relaxation processes in condensed matter give insight into the nature of the different intra- and intermolecular interactions. As a rule, these processes are studied using femtosecond laser pulses[1,2]. Alternative approach is already well-known transient correlation spectroscopy with incoherent light[3-8].

It is known that in the frequency domain a femtosecond optical pulse acts as a frequency filter of the intrinsic nonlinear response of the investigated sample, if its spectral width is narrower than that of the response[9]. Therefore, in general case the relaxation dynamics of the sample will be determined not only by its response but also by the spectral content of the optical pulse. This so-called spectral-filter effect must be taken into account when interpreting relaxation measurements.

In this paper we demonstrate for the first time to our knowledge the spectral-filter effect in transient spectroscopy with incoherent light for the case of forced light scattering (FLS). Up to now incoherent laser pulses were applied in the scheme of FLS to measure the dephasing times of electronic transitions and molecular vibrations in organic liquids and dye solutions[7,8]. Here we apply such pulses for measuring the ultrafast relaxation of induced anisotropy in the transparent organic liquids under the low-frequency resonance conditions.

2. EXPERIMENT

The optical scheme of the experiment is shown in Fig. 1 (a view from the top). A home-made broadband dye laser BDL and narrowband dye laser NDL with an amplifier A were used in the experiment. The both dye lasers with circulating methanol solution of DCM dye were transversely pumped by the second harmonic radiation of a nanosecond Nd:YAG-laser

Laser Optics 2000: Ultrafast Optics and Superstrong Laser Fields, Alexander A. Andreev, Vladimir E. Yashin, Editors, Proceedings of SPIE Vol. 4352 (2001) © 2001 SPIE · 0277-786X/01/$15.00

(Continuum, Surelight) using mirrors M1-M5 and cylindrical lenses L1-L3. The central wavelengths of the broadband and narrowband lasers were equal to about 638 nm and 636.3 nm, respectively. The telescopes T1 and T2 were used for the optimization of the divergence of the output laser beams and the two Glan polarizers G1, G2 were applied to make an appropriate polarization configuration of the beams. The both broadband and narrowband beams had the same vertical linear polarization. The two broadband beams splitted from the one in a Michelson interferometer (prisms P4-P8 and mirrors M6, M7) and one narrowband laser beam (after prisms P1-P3 and mirror M8) propagated in a parallel direction with the same distance of about 3.5-4 mm between all beams (two broadband beams propagate one under the other in this figure). The beams were focused into a sample in a folded box arrangement using a lens L4 of 10 cm focal length. The energies of all beams after lens were about the same and equal approximately to 20-30 μJ per a pulse. The broadband beams induce a refractive index grating inside the investigated sample IS and a part of the probe narrowband beam (FLS-signal beam) is diffracted in the direction of phase-matching for FLS[7,8]. The three-dimensional picture of phase-matching for FLS is shown in Fig. 2. The FLS-signal (see Fig. 1) passed through an aperture D, telescope T3 and after the mirrors M11, M12, lens L6 and neutral-filter box F2 it was introduced into a monochromator M for the spectral selection. The signal was detected by a photomultiplier PM as a function of the time delay between the two broadband beams by changing one arm of the Michelson interferometer (prism P5 with changeable position). One of the broadband beams after the sample was introduced into an optical multichannel analyzer OMA using mirrors M9, M10, lens L5, neutral-filter box F1 and diffusive plate DP for measuring its spectrum. Controlling the experiment and gathering the data were realized by a computer PC.

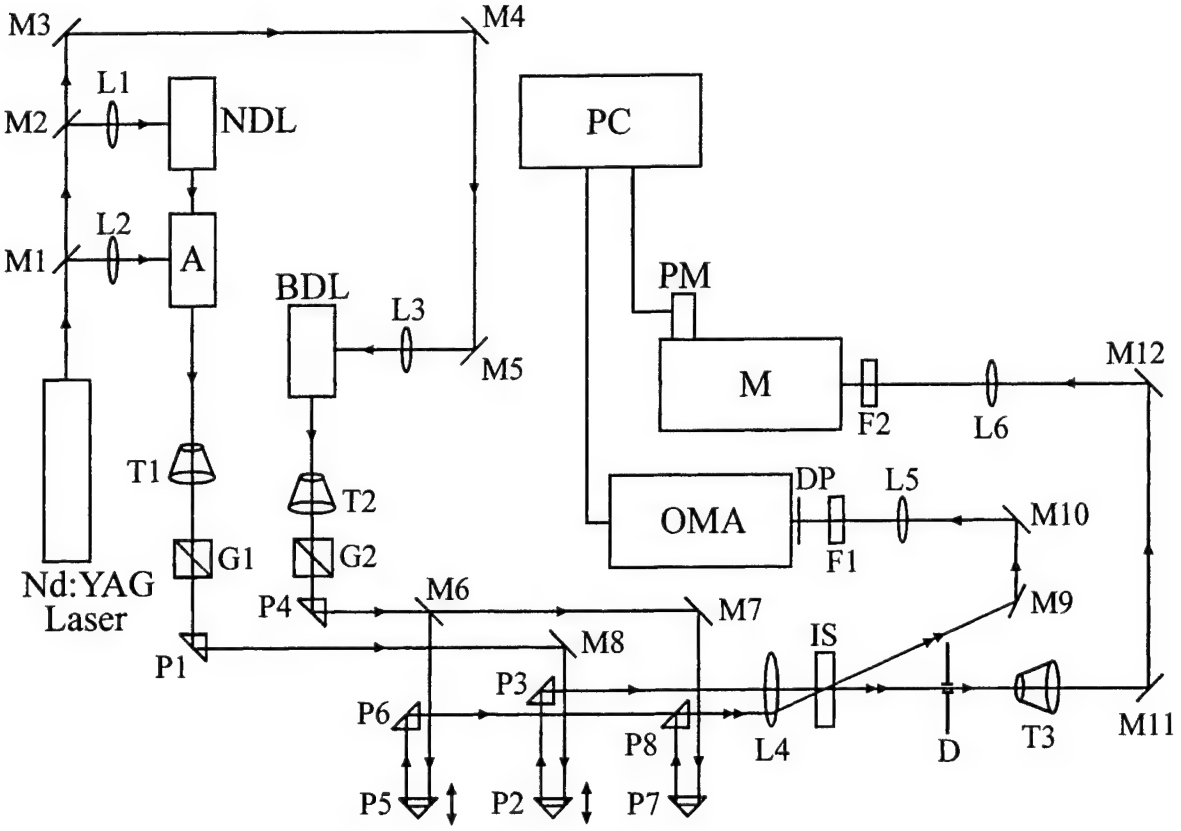

Fig. 1. The experimental setup (see the details in the text above).

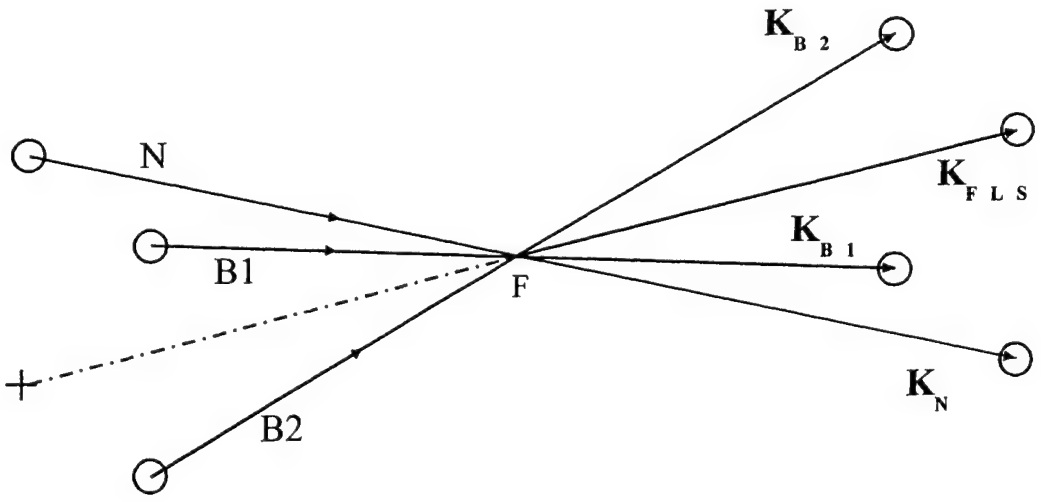

Fig. 2. The three-dimensional picture of phase-matching for FLS, $\mathbf{k}_{FLS} = \mathbf{k}_N + (\mathbf{k}_{B2} - \mathbf{k}_{B1})$. The circles from the left depict the beam spots on lens L4 (the cross is its optical center). The circles from the right side depict the beam spots on an arbitrary screen after the sample: N- narrowband laser beam; B1, B2 –broadband beams; F- focal point of lens L4 (inside the sample); $\mathbf{k}_{B1}$, $\mathbf{k}_{B2}$, $\mathbf{k}_N$ and $\mathbf{k}_{FLS}$ – wave vectors of broadband beams, narrowband beam and FLS-beam, respectively

The time resolution of the measurement of grating relaxation is determined by the auto-correlation time of the broadband laser radiation. Assuming a Gaussian statistics for the noisy radiation of the broadband dye laser, a simple relation between the spectral bandwidth of the radiation and the width of its intensity autocorrelation function is given by the Wiener-Khintichine's theorem[10,11]. The validity of this was proved by simultaneous measuring the spectrum of the broadband laser radiation and its intensity second–order autocorrelation function (ACF) by means of non-collinear second harmonic generation (NSHG) in a BBO-crystal of 200 μm thickness. The correlation time was altered from about 60 fs and up to 230 fs by changing the spectral width of the broadband laser radiation (without changing its central wavelength) with the help of interferometric filters.

3. THEORY

The principle idea of transient incoherent light spectroscopy is based on using noisy properties of the broadband laser radiation[3-8]. The broadband laser light, otherwise known as incoherent light, can be described as a sequence of random ultrashort spikes. The process of the interaction of such a light with matter consists of an ensemble of transient processes caused by various combinations of these spikes. To study the relaxation processes in such a way, it is necessary to know the statistical properties of noisy light and one must record the statistically averaged signal of the interaction versus the time delay between the two correlated flows of such a radiation. In this case one can reach the time resolution which is determined by the correlation time of broadband radiation and not its pulse width. The correlation time (or the averaged time duration of random ultrashort spikes) is inversely proportional to the spectral bandwidth of the radiation. It enables one to apply non-transform-limited pulses from comparatively simple and cheap broadband nanosecond lasers for reaching pico- and femtosecond resolution while studying ultrafast relaxation processes in the substance.

In our case of FLS the broadband laser beam is splitted into the two beams of about equal intensity and these beams are focused into the sample under a certain angle. In such a way, a refractive index grating will occur in the sample which is probed by the narrowband laser beam for the different time delays between the two broadband beams.

The physical mechanisms which are responsible for the grating formation can be different. When there is an

absorption of the radiation by the sample, a population grating will be induced which causes the changes of the refractive index due to heating the sample after the transformation of the absorbed energy to the thermal energy of the molecular motion[7,8]. In our case there is no any absorption of the radiation by the sample and physical mechanisms of grating formation are different. To our opinion, these mechanisms are due to the anisotropy of the sample induced by the broadband laser radiation. These are the low-frequency motions of the molecules or the mechanisms of Kerr nonlinearity (in particular, libration, translation and orientation of the molecules in light field and also electronic mechanism of Kerr nonlinearity). These motions can contribute to the signal observably because of accumulative nature of the signal formation (each random spike excites the sample and the excitation is sustained during the broadband nanosecond laser pulse) and because of low-frequency resonances between the different spectral components of the two broadband laser beams.

Let us consider the two identical time-delayed noisy flows of the broadband laser radiation with electric fields given by[7,8]

$$E_{b1}(\mathbf{r}, t) \approx E_0(t)R(t_r + \tau)\exp(-i\omega_b\tau) \text{ and } E_{b2} \approx E_0(t)R(t_r), \tag{1}$$

where $E_0(t)$ is the amplitude of the envelope of the broadband laser pulse, t_r is the reduced time

$$t_r = t - (\mathbf{k_{b1}} + \mathbf{k_{b2}})\mathbf{r}/2\omega_b, \tag{2}$$

τ is the time delay between the two broadband laser beams and $R(t)$ is a complex random function describing the statistical properties of the broadband laser radiation. The function $E_0(t)$ is a slowly varying function of time in comparison with the correlation time of the radiation. We assume that the statistical properties of the broadband radiation are described by a stationary random Gaussian process given by the following relations

$$\begin{aligned} &\langle R^*(t)R(t+\tau)\rangle = G(\tau), \\ &\langle R(t)R(t+\tau)\rangle = \langle R^*(t)R^*(t+\tau)\rangle = 0, \\ &\langle R(t)\rangle = \langle R^*(t)\rangle = 0. \end{aligned} \tag{3}$$

Here the symbol <...> denotes the statistical average and $G(\tau)$ is the autocorrelation function of the incoherent light. Assuming a Gaussian spectral density of the light, $G(\tau)$ is given as

$$G(\tau) = (\tau_c\sqrt{2\pi})^{-1}\exp[-\tau^2/(2\tau_c^2)], \tag{4}$$

where τ_c is the autocorrelation time of noisy radiation.

The delay-time dependence of the detected intensity of FLS-signal J_s is given as

$$J_s(\tau) = AJ_n n_\Delta^2(\tau) \propto \left|\int_{-\infty}^{+\infty} D(s-\tau)\exp(-g(|s|))ds\right|^2, \tag{5}$$

where A is a constant, J_n is the intensity of the probing narrowband laser radiation, n_Δ is the nonlinear change of the refractive index and $g(s)$ is a response function of the sample.

Assuming a Gaussian response function of the sample we obtain

$$J_s(\tau) \propto \left| \int_{-\infty}^{+\infty} \exp\left[-(s-\tau)^2 / 2\tau_c^2\right] \exp\left(-s^2 / 2T_r^2\right) ds \right|^2 , \qquad (6)$$

where T_r is the relaxation time of the sample response which is looked for.

From the experiment the FLS-signal versus the time delay between the two broadband beams is measured. If we denote the full width at half maximum (FWHM) of this dependence as T_m, then T_r can be determined from the relation

$$T_r = \sqrt{2T_m^2 - \tau_c^2} \ . \qquad (7)$$

The correlation time τ_c was measured directly by measuring intensity ACF in the scheme of NSHG. Also, it was calculated from the measured spectrum of the broadband radiation using Wiener-Khintichine's theorem.

4. RESULTS AND DISCUSSION

The measured FLS-curves are well fitted by Gaussian curves. For example, Fig. 3 shows the typical FLS-signal versus the time delay in neat nitrobenzene.

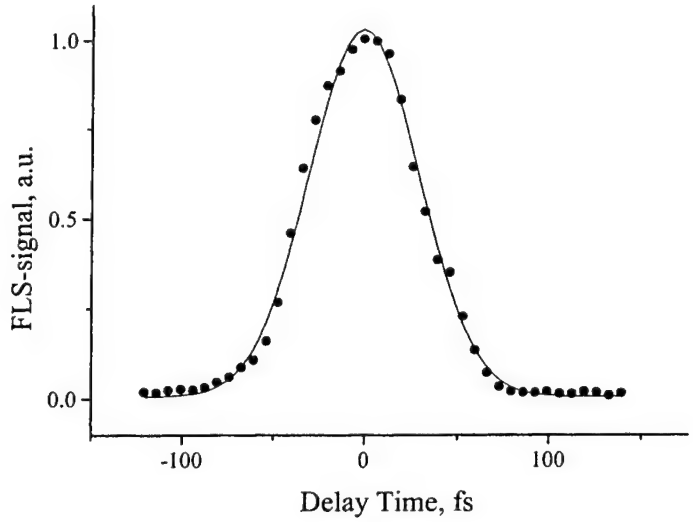

Fig. 3. FLS-signal (points) versus the time delay between the two broadband laser beams in neat nitrobenzene. The correlation time of the broadband radiation is about 60 fs. The solid line is a fitting Gaussian curve.

We have studied the ultrafast dephasing processes of Kerr type in neat nitrobenzene, the mixtures of nitrobenzene with carbon tetrachloride and in neat carbon bisulphide. The determined values of the relaxation times are given in Fig. 4 for neat nitrobenzene and the mixtures of nitrobenzene with carbon tetrachloride and in Fig. 5 for carbon bisulphide together with the corresponding correlation times of the exciting broadband laser radiation as a function of the half width at the half maximum (HWHM) of the broadband laser spectrum. It must be noted that these relaxation times are some effective relaxation times which take account of the contributions of the different physical mechanisms to the signal.

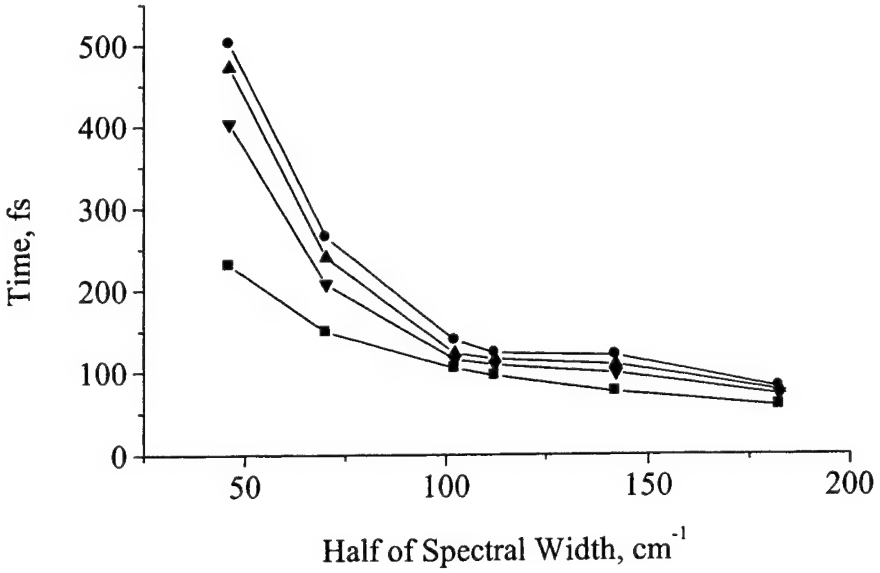

Fig. 4. The ultrafast relaxation times for neat nitrobenzene (circles), the mixtures of nitrobenzene with carbon tetrachloride (up triangles – 70 % of nitrobenzene; down triangles – 50 % of nitrobenzene) and the values of the auto-correlation time (squares) of broadband laser radiation versus its spectral width.

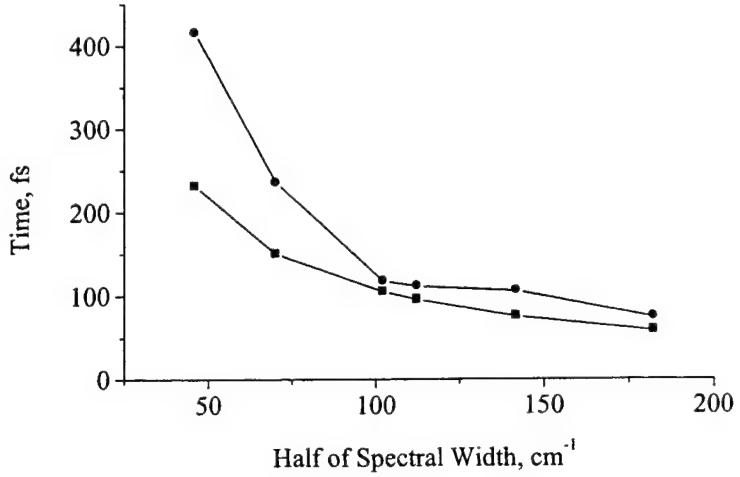

Fig. 5. The ultrafast relaxation times for neat carbon bisulphide (circles) and the values of the auto-correlation time (squares) of broadband laser radiation versus its spectral width.

From this figure it is seen that the relaxation time of the observed responses strongly depends on the spectral width (or the correlation time) of the exciting broadband laser radiation.

Theoretically, in (7) T_m depends on τ_c. This leads to the different relaxation times of the molecules as long as T_m is not much larger than τ_c. Physically, it means that different parts of the low-frequency mode spectrum of the sample are excited because the spectral bandwidth of the broadband laser is smaller than that of the mode spectrum. This effect was demonstrated earlier in the experimental studies of ultrafast relaxations using femtosecond laser pulses and was called as "filter effect"[9].

We modelled this effect for the two most interesting cases: a) the spectrum of the low-frequency modes of the sample is homogeneously broadened and b) this spectrum is inhomogeneously broadened. The corresponding spectra together with the different spectrums of the broadband exciting radiation are schematically shown in Fig. 6.

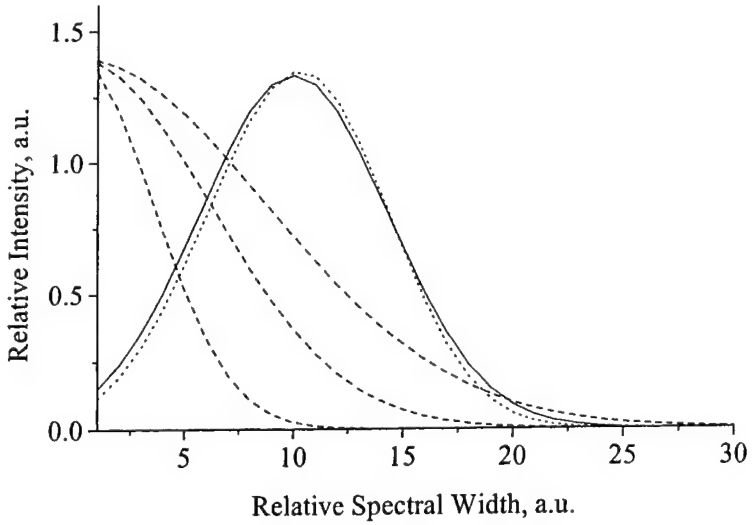

Fig. 6. The homogeneously (solid line) and inhomogeneously (dotted line) broadened spectrums of the low-frequency molecular motions in condensed media and the halves of the spectrums of exciting broadband laser radiation for the different spectral widths (broken lines).

The observed molecular response is determined by the excitation of the molecular motions which are related to the different overlapping between the broadband laser spectrum and mode spectrum. To simulate this we used an integral of convolution of the corresponding spectra for the different spectral widths of the exciting broadband laser. As a result, we calculated the relaxation time of the low-frequency modes versus the spectral width of broadband laser. The typical result is shown in Fig. 7.

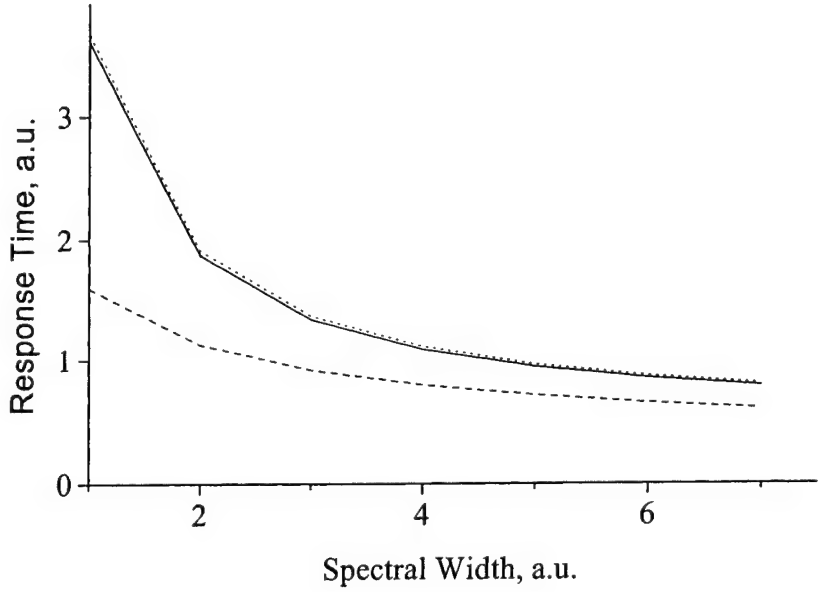

Fig. 7. The relative relaxation time of the sample response (solid line - the case of inhomogeneous broadening; dotted line – the case of homogeneous broadening) and the correlation time (broken line) of the broadband laser radiation versus its relative spectral width.

It is seen that there is a difference between the values of the correlation time and the relaxation times of the response which becomes smaller for the broader spectral widths of the laser radiation. This difference is due to the excitation of the different parts of the mode spectrum. It is also seen that the relaxation times of the response for the cases of homogeneous and inhomogeneous broadening are approximately the same. But this is true only if the sub-bands of the mode spectrum are modelled by smooth curves like Lorentzian or Gaussian ones. If sub-bands are modelled by rectangular-shaped curves (for the simplicity) there will be substantial difference for the homogeneous and inhomogeneous cases. This conclusion is in agreement with the theoretical calculations of Mukamel[12]. To distinguish between both cases Mukamel introduced an additional independent variable – a second time delay. This second variable can not be realized in the experiments concerning the study of the third-order nonlinearity but only in the higher-order nonlinearity experiments.

However, our theoretical model reflects the behaviour of the experimental curves rather well, showing its applicability. On the other hand, our results show that the spectral bandwidth of the broadband laser can not be used as a second independent variable to reasonably distinguish between the homogeneous and inhomogeneous broadening of the low-frequency mode spectrum in our kind of the experiment.

4. CONCLUSIONS

In conclusion, we measured the relaxation times of the induced anisotropy in some Kerr organic liquids and their mixtures in femtosecond time region by FLS using broadband laser light with variable spectral width. Our results demonstrate for the first time to our knowledge the so-called spectral-filter effect in transient spectroscopy with incoherent light. I.e. the broadband non-transform-limited optical pulse with variable spectral width acts as a frequency filter of the intrinsic nonlinear response of the investigated sample which is excited by it. This spectral-filter effect must be taken into account for the interpretation of the relaxation measurements. Therefore, one can conclude that the transient spectroscopy with incoherent light is characterized by the same main features and limitations as the transient spectroscopy based on ultrashort laser pulses.

5. ACKNOWLEDGEMENTS

The support of the International Bureau of the BMBF of Germany (grant WEI-006-98) is gratefully acknowledged.

6. REFERENCES

1. In: "*Ultrashort Laser Pulses and Applications*"/ Ed. W. Kaiser, Berlin, 1988.
2. D. McMorrow, W.T. Lotshaw and G.A. Kenney-Wallace, "Femtosecond optical Kerr studies on the origin of the nonlinear responses in simple liquids", IEEE J. Quant. Electron., **24**, pp. 443-454, 1988.
3. M.A. Vasil'eva, V.I. Malyshev, A.V. Masalov and P.S. Antsiferov, "The investigation of ultrafast relaxation of media by the method of spatial and temporal modulation of exciting light", Bull. Acad. Sci. USSR. Phys. Ser. , **46**, pp. 167-171, 1982.
4. N. Morita and T. Yajima, "Ultrahigh-time-resolution coherent transient spectroscopy with incoherent light", Phys. Rev. A, **30**, pp. 2525-2536.
5. P.A. Apanasevich, V.P. Kozich and A.I. Vodchits, "Time-delayed three-wave mixing of nanosecond incoherent laser beams for measuring short relaxation times", J. Mod. Opt., **35**, pp.1933-1938, 1988.

6. T. Kobayashi, A. Terasaki, T. Hattori and K. Kurokawa, "The application of incoherent light for the study of femtosecond-picosecond relaxation in condensed phase", Appl. Phys. B, **47**, pp. 107-125, 1988.

7. A. Kummrow, S. Woggon and A. Lau, "Forced light scattering by broad-bandwidth incoherent pump lasers", Phys. Rev. A, **50**, pp.4264-4275, 1994.

8. A. Kummrow and A. Lau, "Dynamics in condensed molecular systems studied by incoherent light", Appl. Phys. B, **63**, pp. 209-223, 1996.

9. D. McMorrow and W.T. Lotshaw, "The frequency response of condensed-phase media to femtosecond optical pulses: spectral-filter effects", Chem. Phys. Lett., **174**, pp.85-94, 1990.

10. S.A. Akhmanov, Yu.E. D'yakov and A.S. Chirkin, "*Introduction to the statistical radiophysics and optics*", Nauka, Moscow, 1981.

11. J.W. Goodman, "*Statistical optics*", Wiley, New York, 1985.

12. S. Mukamel, "*Principles of nonlinear optical spectroscopy*", Oxford University Press, New York, 1995.

Ultrabroadening of light beam spatial spectrum when self-focusing.

S.A.Izyurov, S.A.Kozlov, C.R.Simovskiy

Institute of Fine Mechanics and Optics (Technical University)
197101, 14 Sablinskaya st., St. Petersburg, Russia

ABSTRACT

New nonlinear equations for the dynamics of spatial spectrum of a self-focusing monochromatic wave in a medium with cubic nonlinearity is derived in the nonparaxial approximation. The formation of optical beams with cross section on the order of a wavelength is considered. Backward self-reflection is found to be the fundamental cause for the limitation of optical self-focusing.

Keywords: monochromatic light self-focusing, nonparaxial beam

Self-focusing in media with positive refractive nonlinearity of refractive index is a classical phenomenon of nonlinear optics. Since the early 1960s, hundreds of publications were devoted to this phenomenon. An excellent and detailed review of these works is given, e.g, in monograph [1]. In most of them, the theory of monochromatic radiation self-focusing in isotropic media was based on an analysis of the solution of cubic Shrodinger equation, to which the Maxwell equations are reduced in the approximation of paraxial optical beams. However, the theoretical description in this approximation leads to the catastrophic character of self-focusing with field collapsing into a point. The behavior of light field in the vicinity of singularity, where the paraxial approximation does not apply, was analyzed in many works and also reviewed in [1]. Rigorous solutions of the Maxwell equations for isotropic media with cubic nonlinearities were obtained only for the stationary (i.e., in terminology of [1], independent of the coordinate along the light propagation axis) nonparaxial optical beams (see also [2] and the review given therein). The nonstationary (in the above-mentioned sense) field evolution in the course of a deep self-focusing was studied on a basis of various modifications of Shrodinger equations. A critical review of the approximation used in these treatments is given, e.g., in [3]. Note, for our part, that, in the majority of works, rigorous description was not suggested even for the linear diffraction of narrow optical beams. Although the linear nonparaxial diffraction was correctly treated in [4] (this is likely the most popular work on the nonparaxial self-focusing), the vector character of the three-dimensional nonlinear field evolution was not taken into account in [4], rendering the treatment incorrect on this point [1, 2].

In this work (letter [5] is a brief variant of it), a new nonlinear equation is derived for the nonparaxial self-focusing of monochromatic radiation in an isotropic medium with cubic nonlinearity. It describes the evolution of the spatial spectrum of optical beam rather than the evolution of its field. When linearized, this equation exactly describes the diffraction of a unidirectional wave, including the situation where its spatial spectrum involves components with spatial frequencies exceeding the wave number. This components are corresponding to the evanescent waves instead of traveling waves. The method of deriving of spectral equation is based on the requirement that its solution of unidirectional wave type be a partial solution of the nonreduced nonlinear wave equation. The reduced wave equation, an analogue of the spectral equation derived in this work, is nontrivial. This is probably the reason why it was not obtained for a rather long time. Numerical analysis of the new solutions is used to discuss the ultrabroadening of the spatial spectrum of radiation and the formation of a self-focusing beam with cross section on the order of a wavelength. It is shown that the backward self-reflection of radiation may be the natural reason for preventing the self-focusing collapse.

In describing the propagation of a monochromatic radiation in an isotropic dielectric medium with cubic nonlinearity, the Maxwell equations can be reduced to the form [1]

$$\nabla \times (\nabla \times \bar{E}) - k_0^2 \bar{D} = 0, \qquad (1)$$

where $\bar{E}$ is the complex amplitude of electric field $\bar{E}' = \frac{1}{2}\bar{E}e^{-i\omega t} + \text{c.c.}$ of the optical wave; $\bar{D} = \varepsilon \bar{E} + 12\pi\chi^{1111}(\bar{E}\bar{E}^*)\bar{E} + 12\pi\chi^{1221}\bar{E} \times (\bar{E}^* \times \bar{E})$ is the complex amplitude of electric induction

Laser Optics 2000: Ultrafast Optics and Superstrong Laser Fields, Alexander A. Andreev, Vladimir E. Yashin, Editors, Proceedings of SPIE Vol. 4352 (2001) © 2001 SPIE · 0277-786X/01/$15.00

$D' = \frac{1}{2} D e^{-i\omega t}$ +c.c.; ω is the light frequency; $k_0 = \frac{\omega}{c}$ is the wave number in vacuum; ε is the dielectric constant of medium; χ^{1111}, χ^{1221} are the tensor components of its nonlinear susceptibility, and c is the light speed in vacuum. In deriving Eq. (1) , the generation of new optical harmonics was not taken into account.

To demonstrate the spectral method of self-focusing analysis, we restrict ourselves to the two-dimensional linearly polarized TE beams . In this case, Eq. (1) takes the form [1]

$$\Delta E + k^2 E + \chi |E|^2 E = 0, \tag{2}$$

where E is the complex amplitude of a field polarized along the y-axis, $\Delta = \frac{\partial^2}{\partial z^2} + \frac{\partial^2}{\partial x^2}$ is the two-dimensional Laplasian, $k = \sqrt{\varepsilon} k_0$, $\chi = 12\pi \frac{\omega^2}{c^2} \chi^{1111}$.

Choosing the z-axis as the propagation direction (in the numerical calculations, the two-dimensional field $E(x,z)$ is assumed to be symmetric about this axis), let us recast Eq. (2) for the spatial spectrum $G(k_x, z) = \int_{-\infty}^{\infty} E(x,z) \exp(-ik_x x) dx$ as:

$$\frac{\partial^2 G}{\partial z^2} + (k^2 - k_x^2) G + \frac{\chi}{4\pi^2} \iint G^*(\alpha - k_x) G(\alpha - \beta) G(\beta) d\alpha d\beta = 0. \tag{3}$$

The linearized Eq. (3) has the solution

$$G = C_1(k_x) e^{i\sqrt{k^2 - k_x^2} z} + C_2(k_x) e^{-i\sqrt{k^2 - k_x^2} z}, \tag{4}$$

where the first and the second terms correspond to the radiation propagation in the positive and negative direction of the z-axis, respectively. The linear diffraction of a unidirectional wave (i. e., $C_2 = 0$) is described by the equation

$$\frac{\partial G}{\partial z} - i\sqrt{k^2 - k_x^2} G = 0. \tag{5}$$

Evidently, the solution of reduced Eq. (5) is simultaneously a partial solution of linearized Eq. (3). Physically, the reduction of linearized Eq. (3), i.e., transition to Eq. (5) containing lower-order z-derivative, is carried out with the aim of analyzing the diffraction of a unidirectional wave.

Let us generalize Eq. (5) to the nonlinear medium. The reduced nonlinear equation is sought in the form

$$\frac{\partial G}{\partial z} - i\sqrt{k^2 - k_x^2} G + \chi N(G) = 0, \tag{6}$$

where $N(G)$ is an unknown nonlinear operator. It will be found from the requirement that the solution of Eq. (6) be simultaneously a solution of nonreduced spectral Eq. (3). Differentiating Eq. (6) with respect to z and expressing $\frac{\partial G}{\partial z}$ through G from the same equation, one gets

$$\frac{\partial}{\partial z}\left(\frac{\partial G}{\partial z}-i\sqrt{k^2-k_x^2}G+\chi N(G)\right)=$$
$$=\frac{\partial^2 G}{\partial z^2}+(k^2-k_x^2)G+\chi(i\sqrt{k^2-k_x^2}N(G)+\frac{\partial}{\partial z}N(G))=0. \quad (7)$$

Comparing (7) and (3), one obtains the following relationship for the $N(G)$ operator

$$i\sqrt{k^2-k_x^2}N(G)+\frac{\partial}{\partial z}N(G)=\frac{1}{4\pi^2}\int_{-\infty-\infty}^{\infty}\int^{\infty}G^*(\alpha-k_x)G(\alpha-\beta)G(\beta)d\alpha d\beta. \quad (8)$$

Let us seek $N(G)$ in the form

$$N(G)=\int_{-\infty-\infty}^{\infty}\int^{\infty}\varphi(k_x,\alpha,\beta)G^*(\alpha-k_x)G(\alpha-\beta)G(\beta)d\alpha d\beta, \quad (9)$$

where $\varphi(k_x,\alpha,\beta)$ is an unknown function

Then, using the fact that the relationships

$$\frac{\partial G(\alpha-\beta,z)}{\partial z}\approx i\sqrt{k^2-(\alpha-\beta)^2}G(\alpha-\beta,z),$$
$$\frac{\partial G(\beta,z)}{\partial z}\approx i\sqrt{k^2-\beta^2}G(\beta,z), \quad (10)$$
$$\frac{\partial G^*(\alpha-k_x,z)}{\partial z}\approx -i\left(\sqrt{k^2-(\alpha-k_x)^2}\right)^*G^*(\alpha-k_x,z),$$

hold to higher-order small terms, it is straightforward to obtain from Eqs. (8) and (9)

$$\varphi(k_x,\alpha,\beta)=-\frac{i}{4\pi}\frac{1}{\sqrt{k^2-k_x^2}-\left(\sqrt{k^2-(k_x-\alpha)^2}\right)^*+\sqrt{k^2-(\alpha-\beta)^2}+\sqrt{k^2-\beta^2}}. \quad (11)$$

Therefore, the reduced equation for the dynamics of spatial spectrum of a unidirectional optical wave in a nonlinear medium takes the form

$$\frac{\partial G}{\partial z}-i\sqrt{k^2-k_x^2}G=$$
$$=i\frac{\chi}{4\pi^2}\int_{-\infty-\infty}^{\infty}\int^{\infty}\frac{G^*(\alpha-k_x)G(\alpha-\beta)G(\beta)d\alpha d\beta}{\sqrt{k^2-k_x^2}-\left(\sqrt{k^2-(k_x-\alpha)^2}\right)^*+\sqrt{k^2-(\alpha-\beta)^2}+\sqrt{k^2-\beta^2}} \quad (12)$$

Applying manipulations (7)-(11) to this equation, one arrives at nonreduced Eq. (3) accurate to the terms fifth order in G (because of the approximation (10). However, this accuracy is quite sufficient because Eqs (2) and (3) are derived with the same accuracy [1].

Eq. (12) can also be used to obtain a nonlinear reduced equation for the field

$E(x,z) = \frac{1}{2\pi}\int_{-\infty}^{\infty} G(k_x,z)\exp(ik_x z)dk_x$. However, it is more complicated than Eq. (12) and, even being linearized, remains an integro-differential equation [6].

One of our numerical results is presented in Fig. 1, where the dynamics of spatial spectrum is illustrated for a beam having Gaussian shape $E(x,0) = E_0 \exp(-\left(\frac{x}{6\lambda}\right)^2)$ at the input of the medium.

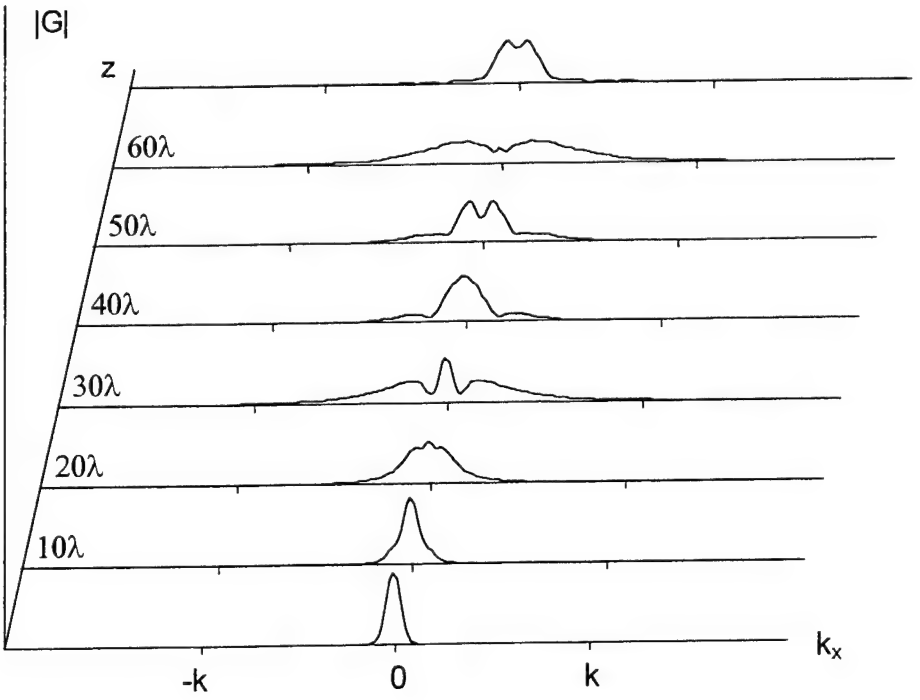

Fig.1. Dynamics of spatial spectrum for the radiation in a nonlinear medium

The nonlinear component of refractive index in the input of medium was $\frac{\chi|E_0|^2}{2k^2} = 0.02$. One can see in Fig. 1 that the spectrum changes in quasi-periodic manner. At a distance of approximately 30 wavelengths, its width becomes maximum and comparable with the wave number. Such a ultrabroadened spatial spectrum (this term is employed by analogy with the term "spectrum ultrabroadening" for a pulse with spectral width comparable to the mean frequency [7]) contains spatial harmonics with frequencies exceeding the wave number. The second term in Eq. (12) becomes real for these harmonics.. Hence, they correspond to the field exponentially decreasing along z and analogous to the field appearing upon the total internal reflection. One can see that if the second term in Eq. (12) is real then the corresponding components in the spectrum of the direct wave decrease, so that the back wave should appear in a transparent medium. Inasmuch as the energy loss due to the exponentially decaying field components of the radiation in the positive direction of the z-azis was small (less than 10%) in out numerical experiment, the influence of back wave on the self-focusing of direct wave was ignored in this work.

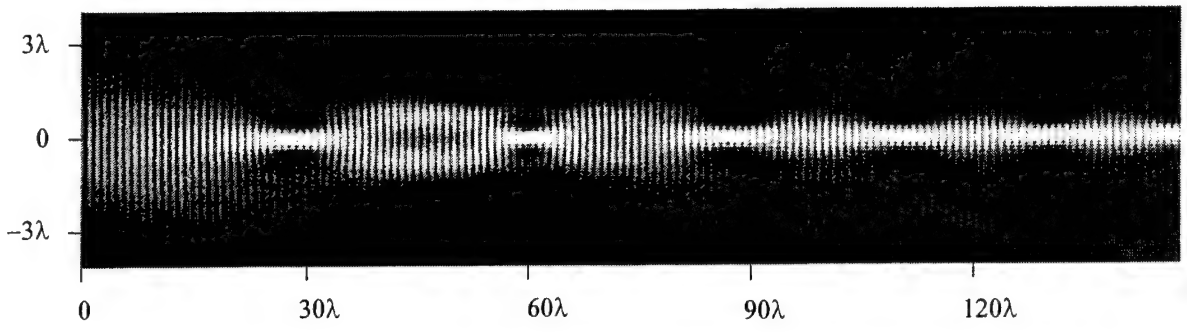

Fig.2. Snapshot of self-focusing optical beam

Figure 2 is a snapshot of the self-focusing beam field obtained by inverse transformation of the calculated spectrum dynamics. To make the image more pictorial, the transverse and longitudinal scales are different in Fig. 2. The quasi-periodicity of the spatial spectrum corresponds to the quasi-periodicity of the beam cross section. In the focuses, the spatial spectrum acquires high-frequency components that are responsible for the radiation self-reflection. The field dynamics in Fig. 2 is shown for larger distances than in Fig. 1. It demonstrates not only the oscillatory character of changing the cross-sectional field structure but also the gradual damping of these oscillations and the formation of a quasi-stationary beam with cross section close to wavelength.

The dynamics of the spatial spectrum of radiation can be also analyzed in paraxial approximation. This approach is described by approximate equation

$$\frac{\partial G}{\partial z} - ik(1 - \frac{k_x^2}{2k^2})G = i\frac{\chi}{8\pi^2}\int_{-\infty}^{\infty}\int_{-\infty}^{\infty} G^*(\alpha - k_x)G(\alpha - \beta)G(\beta)\,d\alpha\,d\beta\,, \qquad (13)$$

and also demonstrate the multifocus structure. The analysis shows not only quantitative difference in focuses locations, but also a qualitative difference. The ultrabroadening of the spatial spectrum beyond the limits of $-k \le k_x \le k$ leads to the decrease of the energy of radiation, propagating in positive direction (see Fig.3). This phenomenon can not be deduced in the paraxial approximation.

In summary, a new (spectral) method is suggested in this work for an analysis of the nonparaxial self-focusing. This method is more convenient than the field method. It is tested by the two-dimensional self-focusing, which is not catastrophic in the paraxial approximation. Nevertheless, it is clear from above that the radiation self-reflection would be the fundamental cause for field limitation in focuses in the case of the collapsing three-dimensional paraxial self-focusing as well.

This work was partly supported by INTAS (project 97-31777)

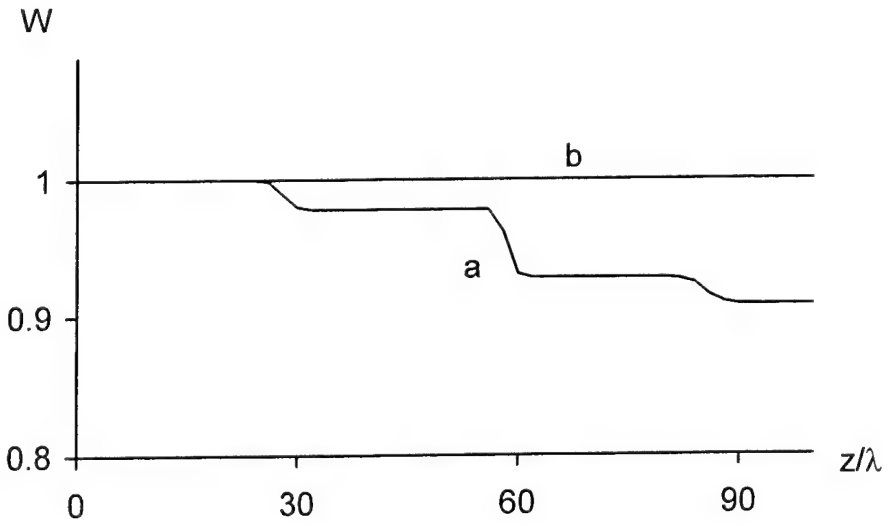

Fig.3. The evolution of the energy W of self-focusing beam: a – calculated from Eq. (12), b – calculated in paraxial approximation from Eq. (13)

REFERENCES

1. S.V.Vlasov, and V.I.Talanov, "Self-Focusing of waves" (Inst. Prikl. Fiz. Ros. Akad. Nauk, Nizhni Nocgorod, 1999).
2. V.E.Semenov, N.N.Rozanov, and N.V.Vysotina. "Supernarrow beams of radiation in Kerr media" – Jh. Exp. Teor Fiz. 116, pp.458-468, 1999.
3. S. Chi , and Q. Guo "Vector theory of self-focusing of an optical beam in Kerr media" – Opt. Lett., v.20, N15, pp. 1598-1600, 1995.
4. M.D.Feit, and J.A.Fleck "Beam nonparaxiality, filament formation, and beam breakup in self-focusing of optical beams" – J. Opt. Soc. Am. B, v.5, N3, pp. 633-640, 1988.
5. S.A.Iz"yurov, and S.A.Kozlov "Dynamics of spatial spectrum of self-focusing optical wave in a nonlinear medium" – JETP Letters, v.71, N11, pp. 453-456, 2000
6. L. Fishman L., and J.J.McCoy, "Derivation and application of extended parabolic wave theories" – J. Math. Phys., v.25, N2, pp. 285-308, 1984.
7. V.G.Bespalov, S.A. Kozlov, A.N.Sutyagin, and Yu. A. Shpolyanskii, "Ultrabroadening of spectrum of intensive femtosecond laser pulses and its time compression to one light field oscillation" – Opt. Zh., v.65, N10, pp.85-88., 1998.

Ultrashort optical pulse propagation in Kerr medium with quasi-resonant impurities

A.M.Basharov[1], and A.I.Maimistov[2]

Moscow Engineering Physics Institute, Moscow, 115409 Russia

Abstract

A nonlinear evolution equation describing an ultrashort optical pulse propagation under quasi-resonant condition is derived by the unitary transformation method. This method allowed us to obtain the terms which are not taken into account within the framework of the adiabatic following approximation. The analysis of the nonlinear evolution equation and example of its application are given.

PACS number: 42.65.Dr, 42.65.Tg

Keywords: resonance, impurities, fiber, adiabatic following, nonlinear Schrödinger equation

1. Introduction

The fiber containing impurity atoms is of interest in the field of nonlinear optics [1-18]. The fiber doped by Er^{3+} ions serves as an active medium of fiber amplifiers if the population of resonant levels is inverted by an additional pumping [1,2]. The fiber directed coupler with resonant impurities in channels can be used as all-optical switcher [3,4]. The self-induced transparency can be observed in doped fibers [5-10] under some conditions. Experimental observation of the self-induced transparency in optical fiber containing Er^{3+} ions [12] has given rise to further investigations of the coherent ultrashort optical pulses propagation in the medium of this kind. The ultrashort pulses amplification was considered in [12-18]. New regimes of the optical pulses propagation were studied in [19-21]. Further generalization of the models of resonant and non-resonant subsystems were proposed in [22-24]. For example, the nonlinear absorption, which appears under the two-photon resonance, was studied in [11].

When the self-induced transparency condition does not hold, impurities can result in additional losses. As it is indicated in [12], the energy of optical soliton propagating in the nonlinear fiber without absorbing impurities is approximately hundreds times less than it is required to invert the population of the resonant levels. Thereby the influence of the impurities on the optical solitons in the fiber results only in absorption (if only special measures are not undertaken as in [12]). The frequency detuning $\Delta\omega$ from resonance can reduce losses. In this case the role of impurity atoms leads to modification of refraction in fiber in the main. In addition frequency detuning does not need to be too high, otherwise it is not necessary to consider the resonance condition. This situation meets the condition of *quasi-resonance*. The quasi-resonance is characterized by inequalities $\Delta\omega << \omega$, $\Delta\omega << |\omega_{ab}|$ and $\Delta\omega >> \Omega_R$ where ω is a carrier wave frequency, $|\omega_{ab}|$ is a typical frequency of nonresonant atomic transition and $\hbar\Omega_R$ is a typical interaction energy between an impurity atom and an electromagnetic wave.

The ultrashort optical pulses propagation theory under quasi-resonant conditions was developed rather long ago [25-27] on the base of *adiabatic following approximation* (AFA). It is expected that the

[1] electronic address bash@pico.mephi.ru

[2] electronic address maimistov@pico.mephi.ru

Laser Optics 2000: Ultrafast Optics and Superstrong Laser Fields, Alexander A. Andreev, Vladimir E. Yashin, Editors, Proceedings of SPIE Vol. 4352 (2001) © 2001 SPIE · 0277-786X/01/$15.00

variation of the optical pulse envelope emerges slowly in comparison with the time $\Delta\omega^{-1}$. This allows to substitute initial system of equation with one nonlinear wave equation for slowly varying complex envelope of the pulse. However, the initial system of the Maxwell-Bloch equations had already been obtained under *slow varying envelope and phase approximation* (SVEPA). There are some effects such as the Stark shifts of the energy levels, which are not taken into account by this method. The resonant (or quasi-resonant) condition selects a pair of levels from the total spectrum of the impurity atoms and thereby introduces a two-level atom as a model of resonant medium. Developing the method of AFA in terms of density matrix equation of the two level atoms without any SVEPA is more correct approach.

In this article the adiabatic following method is introduced from the two-level atoms model without using the Bloch equations in the rotating waves approximation. It allows to present the expression for the polarization of resonant subsystem more exactly. Non-resonant contributions can be introduced by the phenomenological nonlinear susceptibility. Thus the results from the papers [25-27] can be corrected. The unitary transformation method is quite efficient tool in nonlinear optics [28-30]. This method allows us to get more exact solution of the Bloch equations describing the evolution of the state of the two-level atom as it was done in [25]. The expression for polarization is obtained as a series in powers of the ratio of the instant Rabi frequency to the frequency detuning. The presented expressions are distinguished from the known ones [25-27]. Here we take into account the dispersion of the nonlinear response of the system As an example of using general equations we consider initial stage of optical shock wave formation in the fibers containing quasi-resonant impurities.

The paper has the following structure. Section 1 is devoted to the formulation of the problem. In section 2 the method of unitary transformation has been developed to correct consideration of the quasi-resonant case. The resonant polarization of medium under quasi-resonance condition is given in section 3. In section 4 the nonlinear equation governing the dynamics of ultrashort pulse envelope is discussed. Some examples of the effect of the impurities are presented in section 5.

2. Formulating the problem

Let the electric field strength of electromagnetic radiation be presented in the form

$$\vec{E} = \vec{\mathcal{E}} e^{-i\Phi} + \vec{\mathcal{E}}^{*} e^{i\Phi}, \ \Phi = kz - \omega t - \varphi_0 \tag{1}$$

where $\omega = k v_{ph}$ is a carrier frequency of wave (v_{ph} is a phase velocity). The wave propagates along the z axis in the medium which contains the resonant atoms as impurities. We consider the resonant impurities as two-level atoms.

The main equations for description of wave propagation in this medium are the Maxwell wave equations

$$\frac{\partial^2}{\partial z^2}\vec{E} - \frac{1}{c^2}\frac{\partial^2}{\partial t^2}\vec{E} = \frac{4\pi}{c^2}\frac{\partial^2 \vec{P}}{\partial t^2} \tag{2}$$

and equations defining the polarization of medium. As the polarization of medium is a dipole moment of unit volume we present it as a sum of two terms: $\vec{P} = \vec{P}_m + \vec{P}_{im}$ where $\vec{P}_m$ describes a medium without the impurity atoms and $\vec{P}_{im}$ presents the result of the interaction of electromagnetic wave with impurities. Value $\vec{P}_m$ is connected with the strength of the electric field by means of optical susceptibilities.

Here we take into account the third order susceptibility which describes the high frequency Kerr effect. Value $\vec{P}_{im}$ is defined by the impurity atoms and can be determined by the density matrix ρ_{im}:

$$\vec{P}_{im} = Sp(\rho_{im}\vec{d}_{im}) \ . \tag{3}$$

Here $\vec{d}_{im}$ is an operator of a dipole moment of a two-level atom. We normalize the density matrix ρ_{im} to make $Sp(\rho_{im})$ be a density of atoms in the unit volume.

The density matrix of the impurity atoms is governed by the following equation

$$i\hbar\left(\frac{\partial}{\partial t}+\hat{\Gamma}\right)\rho_{im} = \left(H_0 - \vec{E}\vec{d}_{im}\right)\rho_{im} - \rho_{im}\left(H_0 - \vec{E}\vec{d}_{im}\right), \tag{4}$$

where $\hat{\Gamma}$ is the relaxation operator, and the Hamiltonian H_0 has the eigenvectors $|a\rangle$ and $|b\rangle$:

$$H_0|a\rangle = E_a|a\rangle, \ H_0|b\rangle = E_b|b\rangle, \ E_b - E_a = \hbar\omega_{ba}.$$

We will neglect the polarization effects assuming that all the vectors are defined by their values ($\vec{\mathcal{E}} = \mathcal{E}\vec{e}_x, \vec{P}_{im} = P_{im}\vec{e}_x, \vec{d}_{im} = d\vec{e}_x$) and they are parallel to the x axis. For slowly varying envelope of the electric field $\mathcal{E} = \mathcal{E}(z,t)$ (1) we have the reduced wave equation

$$\left[-2ik\left(\frac{\partial}{\partial z}+\frac{1}{v_g}\frac{\partial}{\partial t}\right)+\frac{1-kv'_g}{v_g^2}\frac{\partial^2}{\partial t^2}\right]\mathcal{E}(z,t) = \\ = \frac{12\pi k^2}{\varepsilon(\omega)}\chi^{(3)}(-\omega;\omega,-\omega,\omega)\left|\mathcal{E}(z,t)\right|^2\mathcal{E}(z,t) + 4\pi\frac{k^2}{\varepsilon(\omega)}\mathcal{P}_{im}, \tag{5}$$

where v_g is the group velocity, $v'_g = dv_g/d\omega$, $\varepsilon(\omega)$ is a dielectric permeability and $\chi^{(3)}(-\omega;\omega,-\omega,\omega)$ is third order susceptibility of medium without impurities. The slowly varying envelope of the polarization is defined as

$$P_{im} = \mathcal{P}_{im}e^{-i\Phi} + \mathcal{P}^*_{im}e^{i\Phi} \ . \tag{6}$$

The effects of optical harmonic generations are neglected in our treatment.

Equations (3)-(5) describe an electromagnetic solitary wave propagation in the nonlinear medium containing impurity atoms.

2. Method of unitary transformation for adiabatic following

Let us now consider the case where frequency detuning from the resonance $\Delta = \omega - \omega_{ba}$ greatly exceeds the Rabi frequency $\Lambda = 2\mathcal{E}d_{ba}/\hbar$ and the width of spectral line $1/\gamma$ but it is less than the frequency of the carrier wave:

$$|\Delta| >> |\Lambda|, \ |\Delta| >> 1/\gamma, \ |\Delta| << \omega \ . \tag{7}$$

Condition (7) relates to adiabatic following approximation. The polarization of the resonant atoms follows the variation of the envelope of optical pulse. Usually this polarization is presented by expanding

the solution of equation for density matrix into power series. However, here we will use a more elegant method of the unitary transformation demonstrating its efficiency in different problems of nonlinear optics.

Instead of solving the equation (4) we transform the density matrix and Hamiltonian of the impurities in the field (1) so that the Hamiltonian becomes diagonal. Herewith, the relaxation operator can be omitted according to the condition (7). Thus, we get

$$\tilde{\rho} = e^{-iS}\rho_{im}e^{iS}\,,\quad i\hbar\frac{\partial}{\partial t}\tilde{\rho} = \left[\tilde{H},\tilde{\rho}\right],\quad \tilde{H} = e^{-iS}H_0e^{iS} - e^{-iS}Ede^{iS} - i\hbar e^{-iS}\frac{\partial}{\partial t}e^{iS} \tag{8}$$

We note that the operator e^{-iS} should be unitary, and S be a Hermitian one. This transformation, however, can not be obtained exactly. So we expand the operator S and the efficient Hamiltonian in power series of degrees of the electrical field strength:

$$S = S^{(1)} + S^{(2)} + \ldots, \qquad \tilde{H} = \tilde{H}^{(0)} + \tilde{H}^{(1)} + \tilde{H}^{(2)} + \ldots.$$

As a result we have

$$\tilde{H} = H_0 - i\left[S,H_0\right] - \frac{1}{2}\left[S,\left[S,H_0\right]\right] - \ldots - Ed + i\left[S,Ed\right] + \frac{1}{2}\left[S,\left[S,Ed\right]\right] + \ldots - i\hbar e^{-iS}\frac{\partial}{\partial t}e^{iS},$$

then

$$\tilde{H}^{(0)} = H_0\,, \tag{9a}$$

$$\tilde{H}^{(1)} = -Ed - i\left[S^{(1)},H_0\right] + \hbar\frac{\partial}{\partial t}S^{(1)} \tag{9b}$$

$$\tilde{H}^{(2)} = \frac{i}{2}\left[S^{(1)},Ed\right] - \frac{i}{2}\left[S^{(1)},\tilde{H}^{(1)}\right] - i\left[S^{(2)},H_0\right] + \hbar\frac{\partial}{\partial t}S^{(2)}\,, \tag{9c}$$

$$\tilde{H}^{(3)} = \frac{i}{2}\left[S^{(2)},Ed\right] - \frac{i}{2}\left[S^{(1)},\tilde{H}^{(2)}\right] - \frac{i}{2}\left[S^{(2)},\tilde{H}^{(1)}\right] + \frac{1}{12}\left[S^{(1)},\left[S^{(1)},Ed\right]\right] + \frac{1}{12}\left[S^{(1)},\left[S^{(1)},\tilde{H}^{(1)}\right]\right] -$$
$$- i\left[S^{(3)},H_0\right] + \hbar\frac{\partial}{\partial t}S^{(3)}\,, \tag{1.9d}$$

Let us assume that the following conditions are held:

$$\tilde{H}^{(1)} = 0\,,\ \tilde{H}^{(2)}_{\alpha\alpha'} = E^{(2)}_{\alpha}\delta_{\alpha\alpha'}\,,\ \tilde{H}^{(3)}_{\alpha\alpha'} = E^{(3)}_{\alpha}\delta_{\alpha\alpha'}\,, \tag{10}$$

where $E^{(2)}_{\alpha}$ and $E^{(3)}_{\alpha}$ do not contain oscillating exponents $e^{im\Phi}$, $m = \pm1, \pm2, \ldots$ Then the transformed density matrix will be diagonal $\tilde{\rho}_{\alpha\alpha'} = \tilde{\rho}^{(0)}_{\alpha}\delta_{\alpha\alpha'}$. The indeces α and α' mark the energy levels of the two-level system.

Polarization (3) of the two-level atoms with the frequency detuning from resonance Δ is defined by the formula

$$P_{im}(\Delta) = Sp(\tilde{\rho}e^{-iS}de^{iS}) = Sp\left\{\tilde{\rho}\left(d - i\left[S,d\right] - \frac{1}{2}\left[S,\left[S,d\right]\right] + \frac{i}{6}\left[S,\left[S,\left[S,d\right]\right]\right] + \ldots\right)\right\}. \tag{11}$$

In order to find this value in the third order of the field strength it is necessary to obtain the expressions for $S^{(1)}, S^{(2)}$ and $S^{(3)}$. From the equation (9b), taking into account (10), one has

$$\frac{\partial}{\partial t} S^{(1)}_{\alpha\alpha'} + i\omega_{\alpha\alpha'} S^{(1)}_{\alpha\alpha'} = d_{\alpha\alpha'} \hbar^{-1} (\mathcal{E} e^{-i\Phi} + \mathcal{E}^* e^{i\Phi}).$$

This equation with regard to adiabatic turning on electromagnetic field strength leads to

$$S^{(1)}_{\alpha\alpha'} = d_{\alpha\alpha'} \hbar^{-1} \int_{-\infty}^{t} e^{i\omega_{\alpha\alpha'}(t'-t)} \left\{ \mathcal{E}(t') e^{-i\Phi'} + \mathcal{E}^*(t') e^{i\Phi'} \right\} dt', \qquad \Phi' = \omega t' - kz .$$

Integration by parts results in series

$$\begin{aligned} S^{(1)}_{\alpha\alpha'} = {} & \frac{d_{\alpha\alpha'}}{\hbar} \left\{ \frac{\mathcal{E} e^{-i\Phi}}{i(\omega_{\alpha\alpha'} - \omega)} + \frac{\mathcal{E}^* e^{i\Phi}}{i(\omega_{\alpha\alpha'} + \omega)} \right\} + \frac{d_{\alpha\alpha'}}{\hbar} \left\{ \frac{e^{-i\Phi}}{(\omega_{\alpha\alpha'} - \omega)^2} \frac{\partial \mathcal{E}}{\partial t} + \frac{e^{i\Phi}}{(\omega_{\alpha\alpha'} + \omega)^2} \frac{\partial \mathcal{E}^*}{\partial t} \right\} - \\ & - \frac{d_{\alpha\alpha'}}{\hbar} \left\{ \frac{e^{-i\Phi}}{i(\omega_{\alpha\alpha'} - \omega)^3} \frac{\partial^2 \mathcal{E}}{\partial t^2} + \frac{e^{i\Phi}}{i(\omega_{\alpha\alpha'} + \omega)^3} \frac{\partial^2 \mathcal{E}^*}{\partial t^2} \right\} - \\ & - \frac{d_{\alpha\alpha'}}{\hbar} \left\{ \frac{e^{-i\Phi}}{(\omega_{\alpha\alpha'} - \omega)^4} \frac{\partial^3 \mathcal{E}}{\partial t^3} + \frac{e^{i\Phi}}{(\omega_{\alpha\alpha'} + \omega)^4} \frac{\partial^3 \mathcal{E}^*}{\partial t^3} \right\} + \ldots \end{aligned} \tag{12}$$

In addition to conditions (7), let us require the variations of the electric field envelope to emerge in time interval τ_p fast enough:

$$\frac{\Delta}{\omega} (\Delta\tau_p) << 1 . \tag{13}$$

Then the expression (12) can be reduced to

$$S^{(1)}_{ba} = \frac{d_{ba}}{\hbar} \left\{ \frac{i}{\Delta} \mathcal{E} + \frac{1}{\Delta^2} \frac{\partial \mathcal{E}}{\partial t} - i \frac{1}{\Delta^3} \frac{\partial^2 \mathcal{E}}{\partial t^2} - \frac{1}{\Delta^4} \frac{\partial^3 \mathcal{E}}{\partial t^3} \right\} e^{-i\Phi} = S^{(1)*}_{ab} , \quad S^{(1)}_{bb} = S^{(1)}_{aa} = 0 .$$

From equation (9c) it follows

$$E^{(2)}_a = \frac{|d_{ba}|^2}{\hbar} \left\{ \frac{|\mathcal{E}|^2}{\Delta} + \frac{i}{2\Delta^2} \left(\mathcal{E} \frac{\partial \mathcal{E}^*}{\partial t} - \mathcal{E}^* \frac{\partial \mathcal{E}}{\partial t} \right) - \frac{1}{2\Delta^3} \left(\mathcal{E}^* \frac{\partial^2 \mathcal{E}}{\partial t^2} + \mathcal{E} \frac{\partial^2 \mathcal{E}^*}{\partial t^2} \right) \right\} = -E^{(2)}_b ,$$

$$S^{(2)}_{\alpha\alpha'} = 0 .$$

Finally, the expression (9d) leads to the following equation

$$\frac{\partial}{\partial t} S^{(3)}_{ba} + i\omega_{ba} S^{(3)}_{ba} = \frac{i}{\hbar} S^{(1)}_{ba} E^{(2)}_a - \frac{1}{6\hbar} \left(|S^{(1)}_{ba}|^2 E d_{ba} - S^{(1)2}_{ba} E d_{ab} \right). \tag{14}$$

Taking into account (13) and retaining only the terms proportional to $e^{\pm i\Phi}$ we get

$$S_{ba}^{(3)} = -i\frac{4}{3}\frac{|d_{ba}|^2 d_{ba}}{\hbar^3}\left\{\frac{1}{\Delta^3}\mathcal{E}|\mathcal{E}|^2 + i\frac{1}{2\Delta^4}\left(\mathcal{E}^2\frac{\partial\mathcal{E}^*}{\partial t} - 3|\mathcal{E}|^2\frac{\partial\mathcal{E}}{\partial t}\right)\right\}e^{-i\Phi}. \qquad (15)$$

The results obtained are sufficient to evaluate the polarization (11) of the two-level impurities with an accuracy of the third order in the field inclusive. However, we shall further suppose that $\tilde{\rho}_a^{(0)} = N_{im}$. Thus, we have

$$P_{im}(\Delta) = N_{im}\left(-i(S_{ab}^{(1)}d_{ba} - d_{ab}S_{ba}^{(1)})(1-\frac{2}{3}|S_{ba}^{(1)}|^2) - i(S_{ab}^{(3)}d_{ba} - d_{ab}S_{ba}^{(3)})\right),$$

and as a result

$$\mathcal{P}_{im}(\Delta) = iN_{im}d_{ab}\left(S_{ba}^{(1)}(1-\frac{2}{3}|S_{ba}^{(1)}|^2) + S_{ba}^{(3)}\right)e^{i\Phi}.$$

From theses results we can get the following expression for polarization

$$\mathcal{P}_{im}(\Delta) = N_{im}\frac{|d_{ab}|^2}{\hbar}\left\{-\frac{1}{\Delta}\mathcal{E} + \frac{i}{\Delta^2}\frac{\partial\mathcal{E}}{\partial t} + \frac{1}{\Delta^3}\frac{\partial^2\mathcal{E}}{\partial t^2} - \frac{i}{\Delta^4}\frac{\partial^3\mathcal{E}}{\partial t^3} + \right.$$
$$\left. + \frac{|d_{ba}|^2}{\hbar^2\Delta^3}\left(2\mathcal{E}|\mathcal{E}|^2 - \frac{6i}{\Delta}|\mathcal{E}|^2\frac{\partial\mathcal{E}}{\partial t} + \frac{4i}{3\Delta}\frac{\partial(\mathcal{E}|\mathcal{E}|^2)}{\partial t}\right)\right\} \qquad (16)$$

3. Contribution of the quasi-resonant atoms to polarization

Equation (16) allows to find a polarization of the two-level system in the case of both homogeneous and inhomogeneous broadening of spectral line of the impurity atoms:

$$\mathcal{P}_{im} = <\mathcal{P}_{im}(\Delta)> \equiv \int_{-\infty}^{\infty}\mathcal{P}_{im}(\Delta)g(\Delta)d\Delta \ .$$

Here, function $g(\Delta)$ takes account for frequency dispersion of the impurities around the central frequency. Herewith we consider that the value of dipole moment of the quasi-resonant transition does not depend on the detuning Δ. This expression and the equation (5) for polarization lead to a new wave equation, which determines the ultrashort electromagnetic pulses propagation in Kerr medium containing two-level impurities in the framework of the modified adiabatic following approximation.

Expression for the polarization $\mathcal{P}_{im}$ is correct for any kind of spectral line broadening. Here we shall consider only the Lorentz broadening which is typical for the case of impurities in solids. Let us suppose that the form factor $g(\Delta)$ is given by the distribution

$$g(\Delta) = \frac{\gamma/\pi}{\gamma^2 + (\Delta - \Delta_0)^2}, \qquad (17)$$

where Δ_0 is frequency detuning from center of inhomogeneous line, and γ is defined by the reversible relaxation time T_2^*, i.e., $\gamma = 1/T_2^*$. In this case

$$<1/\Delta^n>=(T_2^*)^n\frac{1}{\pi}\int_{-\infty}^{\infty}\frac{dx}{(1+x^2)(x+v)^n}\equiv(T_2^*)^n I_n(v),$$

where the normalized frequency detuning $v=\Delta_0 T_2^*$ was used. To evaluate integrals $I_n(v)$ one can exploit recursion relation

$$I_{n+1}(v)=-\frac{1}{n}\frac{dI_n(v)}{dv}\ ,\ \text{and}\ I_1(v)=\frac{v}{(1+v^2)}.$$

Thus, we get

$$I_2(v)=\frac{v^2-1}{(1+v^2)^2},\quad I_3(v)=\frac{v(2v^2-3)}{(1+v^2)^3},\quad I_4(v)=\frac{2v^4-7v^2+1}{(1+v^2)^4}.$$

Now, the polarization of the two-level system of the impurity atoms can be written as

$$\begin{aligned}\mathcal{P}_{im}&=N_{im}\frac{|d_{ab}|^2}{\hbar}\left(-J_1\mathcal{E}+iJ_2\frac{\partial\mathcal{E}}{\partial t}+J_3\frac{\partial^2\mathcal{E}}{\partial t^2}-iJ_4\frac{\partial^3\mathcal{E}}{\partial t^3}\right)+\\&+N_{im}\frac{2|d_{ba}|^4}{\hbar^3}\left(J_3\mathcal{E}|\mathcal{E}|^2-3iJ_4|\mathcal{E}|^2\frac{\partial\mathcal{E}}{\partial t}+\frac{2i}{3}J_4\frac{\partial(\mathcal{E}|\mathcal{E}|^2)}{\partial t}\right).\end{aligned}\qquad(18)$$

where $J_n=(T_2^*)^n I_n(T_2^*\Delta_0)$. This expression takes into account the dispersions of the group velocities up to the third order (terms with second and third order derivatives with respect to time) and dispersion of the nonlinear response of quasi-resonant atoms (the two last terms in (18)). These terms distinguish our results from the ones earlier discovered in the framework of the adiabatic following approximation [25-27].

4. Nonlinear equation for optical pulse envelope

Let us now rewrite the equation (5) in the following form

$$i\left(\frac{\partial}{\partial z}+\frac{1}{v_g}\frac{\partial}{\partial t}\right)\mathcal{E}-\frac{1}{2}D\frac{\partial^2\mathcal{E}}{\partial t^2}+\frac{6\pi\omega\chi^{(3)}}{cn(\omega)}|\mathcal{E}(z,t)|^2\mathcal{E}(z,t)=-\frac{2\pi\omega}{cn(\omega)}\mathcal{P}_{im},\qquad(19)$$

where $n(\omega)$ is a refractive index of the optical fiber core at the carrier wave frequency and $D=(1-kv_g')k^{-1}v_g^{-2}=(1/2)(d^2k^2/d\omega^2)$ is a dispersion parameter characterizing a group-velocity dispersion of the second order in fiber without impurities.

There are two characteristic lengths - the length L_a of resonant absorption for pulse with duration t_p and length L_D of dispersion: $L_a=cn(\omega)\hbar(2\pi\omega N_{im}|d_{ba}|^2 t_p)^{-1}$ and $L_D=t_p^2/2|D|$. Here the pulse duration t_p was chosen as typical time of the problem under consideration. Let us introduce new dimensionless variables: $\tau=(t-z/v_g)t_p^{-1}$, $\zeta=z/L_a$, $q=A_0^{-1}\mathcal{E}$. Then the equation (19) taking account of (18) can be rewritten as

$$i\frac{\partial q}{\partial \zeta}-\frac{\sigma}{2}\varepsilon_D\frac{\partial^2 q}{\partial \tau^2}+\mu|q|^2 q=J_1 q-iJ_2\frac{\partial q}{\partial \tau}-J_3\frac{\partial^2 q}{\partial \tau^2}+iJ_4\frac{\partial^3 q}{\partial \tau^3}-$$
$$-\frac{\varepsilon_R^2}{2}J_3|q|^2 q+i\frac{\varepsilon_R^2}{2}J_4\left(3|q|^2\frac{\partial q}{\partial \tau}-\frac{2}{3}\frac{\partial(|q|^2 q)}{\partial \tau}\right), \tag{20}$$

where $\sigma=\operatorname{sgn} D$, $\mu=6\pi\omega\chi^{(3)}A_0^2 L_a/cn(\omega)$, $\varepsilon_D=L_a/L_D$, $\varepsilon_R=(2|d_{ba}|A_0^2/\hbar)t_p=\Omega_R t_p$. If we use the nonlinear refractive index n_2 related to nonlinear cubic susceptibility $\chi^{(3)}$ as $n_2=3\pi\chi^{(3)}/n(\omega)$, then the parameter μ can be rewritten as $\mu=2(\omega/c)n_2 A_0^2 L_a$. The high-frequency Kerr effect results in the phase shift of wave $\Delta\varphi=(\omega/c)n_2 A_0^2 L$, where L is the distance of propagation. Thus, the parameter μ can be interpreted as a phase shift of the wave propagating in the distance of the two absorption lengths.

In this consideration we have assumed that $\Delta_0 t_p>>1$. Let us now regard that an inhomogeneous broadening line is sufficiently narrow, i.e., $\Delta_0 T_2^*>>1$. In this case coefficients in equation (20) can be estimated as $J_1\approx(\Delta_0 t_p)^{-1}$, $J_2\approx(\Delta_0 t_p)^{-2}$, $J_3\approx 2(\Delta_0 t_p)^{-3}$, and $J_4\approx 2(\Delta_0 t_p)^{-4}$.

If we exploit the new variables $\eta=\tau-(\Delta_0 t_p)^{-2}\zeta$ and $\tilde{q}(\zeta,\eta)=q\exp[i\zeta/\Delta_0 t_p]$, then the equation (20) can be written in the following form

$$i\frac{\partial \tilde{q}}{\partial \zeta}+\tilde{\varepsilon}_D\frac{\partial^2 \tilde{q}}{\partial \eta^2}+\tilde{\mu}|\tilde{q}|^2\tilde{q}=iJ_4\frac{\partial^3 \tilde{q}}{\partial \eta^3}+i\frac{\varepsilon_R^2}{2}J_4\left(3|\tilde{q}|^2\frac{\partial \tilde{q}}{\partial \eta}-\frac{2}{3}\frac{\partial(|\tilde{q}|^2\tilde{q})}{\partial \eta}\right), \tag{21}$$

where $\tilde{\varepsilon}_D=-\sigma\varepsilon_D/2+(\Delta_0 t_p)^{-3}$ and $\tilde{\mu}=\mu+(1/2)\varepsilon_R^2(\Delta_0 t_p)^{-3}$. Thus, we get generalized nonlinear Schrödinger equation (GNLS). The effects of the third order group-velocity dispersion and dispersion of nonlinear response have appeared here as a result of the influences of the impurity atoms.

5. Some examples of the influence of the quasi-resonant impurities

Going back to the original independent variable t and z one can find the correction to the group velocity due to the impurities. The re-normalized group velocity is defined by the expression

$$\frac{1}{V_g}=\frac{1}{v_g}+\frac{t_p}{L_a(\Delta_0 t_p)^2}=\frac{1}{v_g}+\frac{2\pi\omega N_{im}|d_{ba}|^2}{cn(\omega)\hbar(\Delta_0)^2}. \tag{22}$$

It should be noted that $\varepsilon_R^2 J_3\approx(\Omega_R/\Delta_0)^2(\Delta_0 t_p)^{-1}$ and $\varepsilon_R^2 J_4\approx(\Omega_R/\Delta_0)^2(\Delta_0 t_p)^{-2}$, whereas $J_4\approx 2(\Delta_0 t_p)^{-4}$. In the range of the picosecond optical pulses a dispersion length is of the order of hundred meters. It is much longer than a resonant absorption length. By taking $L_a<<L_D$ and omitting terms which are proportional to $(\Delta_0 t_p)^{-3}$ and $(\Delta_0 t_p)^{-4}$ we can reduce the equation (21) to the following one

$$i\frac{\partial \tilde{q}}{\partial \zeta}+\tilde{\mu}|\tilde{q}|^2\tilde{q}=i\beta\left(3|\tilde{q}|^2\frac{\partial \tilde{q}}{\partial \eta}-\frac{2}{3}\frac{\partial(|\tilde{q}|^2\tilde{q})}{\partial \eta}\right), \tag{23}$$

where $\beta = \varepsilon_R^2 J_4 / 2 \approx (\Omega_R / \Delta_0)^2 (\Delta_0 t_p)^{-2} / 2$. It is suitable to use real-valued variable by assuming $\tilde{q} = a \exp(i\phi)$. In these terms equation (23) can be represented as a system of real equations

$$\frac{\partial a}{\partial \zeta} - \beta a^2 \frac{\partial a}{\partial \eta} = 0, \quad \frac{\partial \phi}{\partial \zeta} - \frac{7}{3} \beta a^2 \frac{\partial \phi}{\partial \eta} = \tilde{\mu} a^2 .$$

The first equation of these systems presents an equation of a simple wave with velocity depending on their own amplitude. The solution of that can be written in an implicit form

$$a(\eta, \zeta) = f(\eta + \beta a^2(\eta, \zeta)\zeta) ,$$

where function $f(\eta) = a(\eta, \zeta = 0)$ is determined by the initial profile of incident optical pulse. If $\beta > 0$ ($\beta < 0$), then the maximum of pulse is moved with the velocity that is faster (slower) than the group velocity. There the self-steepening of the incident wave front (tail of pulse) occurs and the shock wave will eventually be formed. It should be pointed out that cast-off terms in the equation (21) in the shock wave limit case become important. Their influence prevents a breakup of a wave front (tail of pulse). Conversely, the oscillation of the pulse envelope appears and pulse decay develops in the susequent stage.

6. Conclusion

In the presented paper we have shown that the method of the unitary transformation allows to obtain a nonlinear evolution equation describing an ultrashort optical pulse propagation under quasi-resonant condition. Herewith we get the terms which had no been obtained previously in the framework of the adiabatic following approximation. As an example of the physical situations, where this method proves to be useful, we have considered the ultrashort optical pulse propagation in the nonlinear (Kerr type) fiber containing impurities. When the corrections of the order of $(\Delta_0 t_p)^{-2}$ and above were omitted, the nonlinear Schrödinger equation occurs. However, the coefficients in this equation were re-normalized due to the influence of the impurities. Taking into account the terms up to the forth order in $(\Delta_0 t_p)^{-1}$, one gets a generalization NLS equation. This equation allows for the effects of the group-velocity dispersion of the third order and dispersion of nonlinear response. If the dispersion length is much longer than an absorption length, one can obtain an equation describing the self-steepening of the wave front and the optical shock wave formation.

Acknowledgement

This work has been supported by INTAS under grant No 96-0339

References

1. B.J. Ainslie, *J.Lightwave Technol.* **9** (1991) 220.
2. N.J. Miniscalco, *J.Lightwave Technol.* **9** (1991) 234.
3. A. Guzman, M. Romagnoli, and S. Wabnitz, *Appl.Phys.Letts.* **56** (1990) 614.
4. A. Guzman, F.S. Locati, and S. Wabnitz , *Phys. Rev.* A, **46** (1992) 1594.
5. A.I. Maimistov, and E.A. Manykin, *Zh.Eksp.Teor.Fiz.* **85** (1983) 1177 [*Sov. Phys. JETP* **58** (1983) 685].

6. A.M. Basharov, and A.I. Maimistov, *Opt.Spektrosk.* **66** (1989) 167.
7. R.A. Vlasov, and E.B. Doctorov, *Dokl. AN BSSR*, **26** (1982) 322 .
8. R.A. Vlasov, and E.B. Doctorov, *Dokl. AN BSSR*, **32** (1988) 790.
9. S. Karplyuk, *Opt.Spektrosk.* **67** (1989) 626.
10. F.Kh. Abdullaev, and S.A. Tadjimuratov, *Dokl. AN USSR.* **316** (1991) 337.
11. Y. Silberberg, *Opt.Letts.* **15** (1990) 1005.
12. M. Nakazawa, Y. Kimura, K. Kurokawa, and K. Suzuki, *Phys.Rev. A.* **45** (1992) R23.
13. M. Nakazawa, K. Suzuki, Y. Kimura, and H. Kubota, *Phys.Rev. A.* **45** (1992) R2682.
14. M. Nakazawa, K. Suzuki, H. Kubota, and Y. Kimura, *Opt.Lett.* **18** (1993) 6123.
15. A.B. Grudinin, E.M. Dianov, D.V. Korobkin, A.M. Prokhorov, V.A. Semenov, I.Yu. Khrushchev, *Kvantovaya Elektron.* (*Moscow*) **17** (1990) 1070 [*Sov. J.Quantum Electron.* **20** (1990) 984].
16. I.V. Mel'nikov, R.F. Nobiev, and A.V. Nazarkin, *Opt.Letts.* **15** (1990) 1348.
17. A.I. Maimistov, *Kvantovaya Elektron.* (*Moscow*) **19** (1992) 295 [*Sov. J.Quantum Electron.* **22** (1992) 271].
18. V.V. Kozlov, *Zh.Eksp.Teor.Fiz.* **107** (1995) 360.
19. V.V. Kozlov, and E.E. Fradkin, *Zh.Eksp.Teor.Fiz.* **106** (1994) 1572.
20. V.V. Kozlov, and E.E. Fradkin, *Opt. Letts.* **21** (1995) 2165.
21. V.V. Kozlov, and E.E. Fradkin, *Zh.Eksp.Teor.Fiz.* **109** (1996) 89.
22. K. Porsezian, and K. Nakkeeran, *Phys.Rev. Letts.* **74** (1995) 2941.
23. S. Kakei, and J. Satsuma, *J.Phys.Soc.Japan.* **63** (1994) 885.
24. K. Porsezian, and K. Nakkeeran, *J. Mod.Opt.* **42** (1995) 1953.
25. D. Grischkowsky, *Phys.Rev. A* 7 (1973) 2096.
26. M.D. Crisp, *Phys.Rev. A*, **8** (1973) 2128.
27. R.H. Lehmberg, and J, Reintjes, *Phys.Rev.* A **12** (1975) 2574.
28. M.Takatsuji, *Physica* **51** (1971), 265; *Phys.Rev. A* **11** (1975), 619.
29. A.M. Basharov A.M., *Photonics. Method of unitary transformation in the nonlinear optics* (MEPhI, Moscow, 1990).
30. A.I.Maimistov, and A.M.Basharov, Non-linear optical waves, Kluwer Academic, Dordrecht, (1999).

Investigation of Kerr lens mode locking in lasers with composite active media

V.I.Trunov, A.V.Kirpichnikov, E.V.Pestryakov, V.V.Petrov, A.K.Komarov[a], K.P.Komarov[a]

Institute of Laser Physics of Siberian Branch of RAS, Novosibirsk, 630090, Russia

[a]Institute of Automation and Electrometry of Siberian Branch of RAS; Novosibirsk, 630090, Russia

ABSTRACT

One of the possible methods of realization of active medium with anomalously wide bandwidth has been described. Composite active medium, consisting of several laser active centers with overlapping gainbands in common resonator has been created. In this case gain contour has complex shape with local extremums. Method of numerical simulation of the formation dynamics of ultrashort pulse at passive mode locking in laser with arbitrary spectral gain contour has been performed. The main parameters for the generation of ultrashort pulse in a laser with a composite active medium are obtained and investigated. The conditions of realization of stationary regime in the form of ultrashort pulse generation with duration determined by combined gain bandwidth are calculated.

Keywords: composite active media, self-mode locking, nonlinear absorber, Kerr nonlinearity

1. INTRODUCTION

At the present time, the minimum duration of ultrashort optical pulses generated directly in tunable lasers (e.g., the Kerr-lens mode-locked $Al_2O_3:Ti^{3+}$ laser) is less than 6 femtoseconds[1, 2]. It is close to the inverse spectral bandwidth of the active medium of this laser. Further decrease of pulses duration is possible either by using methods of nonlinear optics[3], rotational molecular modulation[4] or active media with anomalously broad band gain contours. Early in our work[5], we proposed to use a laser with a composite active medium for the generation of extremely short optical pulses. The medium consists of several laser active media with overlapping gainbands placed in a common cavity. It may also consist of a number of color centers, ions in common host or a set of semiconductor lasers. This opens up new possibilities for the creation of an ultrawide gainband and allows one to advance into the subfemtosecond time scale at optimum conditions. In all these cases, the spectral gain contour has a complex shape with a local extremums. It was shown[6] that in the case of symmetrical form of the unsaturated gain contour with a local minimum, a stationary regime in the form of ultrashort pulse generation with the duration determined by the combined gain bandwidth, can be realized under certain conditions.

In this paper, the dynamics of development of ultrashort pulses in a laser with a composite active medium with an arbitrary spectral gain contour is investigated under passive mode locking using noninertial saturated losses by methods of numerical simulation. Earlier all theoretical studies of the dynamics of formation of optical pulses were limited only by the parabolic profile of the spectral gain contour[7].

2. GENERAL FORMULATION

In the model of an active uniformly filled medium, we analyze the equations describing the evolution of intracavity radiation in the system of coordinates of a moving pulse. In this case, at unidirectional generation in a ring laser with noninertial nonlinear saturating losses, the equations can be written in nondimensional variables[8]:

For further author information:
E-mail: trunov@laser.nsc.ru
Fax: 7 (3832) 332067

Laser Optics 2000: Ultrafast Optics and Superstrong Laser Fields, Alexander A. Andreev, Vladimir E. Yashin, Editors, Proceedings of SPIE Vol. 4352 (2001) © 2001 SPIE · 0277-786X/01/$15.00

$$\frac{\partial}{\partial t}E(z,t)=\frac{1}{2}\left(\hat{G}_1+\hat{G}_2-\sigma_0-\frac{\sigma}{1+\xi\left|\mathrm{E}(z,t)\right|^2}\right)E(z,t) \tag{1}$$

Here E(z,t) is a slow field amplitude, the operators $\hat{G}_1$ and $\hat{G}_2$ determine the action of the first and the second active media on the light pulse, respectively, σ_0 denotes the cavity losses; the last term in the right side describes nonlinear losses. It is assumed that as an ultrashort pulse passes through the *i*-th active medium, the gain of the spectral component of the field E(k,t) is described by the following equation:

$$\frac{\partial}{\partial t}E(k,t)=\frac{1}{2}\left(\frac{D_i N_i}{1+\chi_i\int\left|E(k,t)\right|^2 L(k-k_i,\Gamma_i)dk}L(k-k_i,\Gamma_i)\right)E(k,t). \tag{2}$$

Here $L(k-k_i,\Gamma_i)$ is the Lorentz function determined by the formula:

$$L(k-k_i,\Gamma_i)=\frac{1}{1+\left(\frac{k-k_i}{\Gamma_i}\right)^2}. \tag{3}$$

Here k is the wave vector of the appropriate spectral component; k_i is the wave vector corresponding to the spectral gainband center of the *i*-th active medium, Γ_i is the half width on half maximum gainband of this active medium, χ_i, D_i, and N_i are its saturation parameter, the Einstein gain coefficient, and the inversion in the absence of field, respectively. Relation (2) is determined the corresponding operators $\hat{G}_i$ in (1). The nonlinear diffraction losses in the chosen model of passive mode locking are determined by the following two parameters: the single pass diffraction losses σ and the parameter ξ. Calculation of these parameters through the parameters of the laser system may be done as follows[9]:

$$\xi=n_2\frac{l\omega}{\mathscr{L}\sigma}\left(\frac{\sigma\omega r^2}{c^2}\right) \tag{4}$$

Here l and $\mathscr{L}$ are the lengths of the active medium and of the cavity, respectively; ω is the light frequency, n_2 is the nonlinear refraction index; r is the light beam radius. The factor in round brackets is assumed to be smaller than unity or of the order of unity[9]. In the chosen model, nonlinear diffraction losses decrease with increase of the intensity and approach zero at high intensities. The evolution of a pulse as it passes through an element with nonlinear losses and reflects on the mirrors in accordance with (1) is determined by the following equation:

$$\frac{\partial}{\partial t}E(z,t)=\frac{1}{2}\left(-\sigma_0-\frac{\sigma}{1+\xi\left|E(z,t)\right|^2}\right)E(z,t) \tag{5}$$

The modification of the pulse as it passes through the active medium is described by the equation (2). In this case, the spectral components of the field in this equation are calculated by the Fourier transform of the time profile of the pulse. Then the inverse Fourier transform was carried out and the changes in the pulse parameters due to linear losses in the cavity and nonlinear diffraction losses are analyzed by means of the equation (5). This cycle was repeated several times during the numerical simulation. Thus, the evolution of an ultrashort pulse versus the gain media parameters and other characteristics of laser elements were investigated. The algorithm under consideration can be extended to any number of active media in the cavity and for any spectral gain profiles of active media.

3. NUMERICAL SIMULATION: RESULTS AND DISCUSSION

The dynamics of formation and the parameters of ultrashort pulses after the transient process using different gain saturation parameters, nonlinear losses, widths of spectral gain contours, distances between maxima in the spectral gain contour, and depths of minima appearing in the total unsaturated spectral gain contour of a composite active medium are investigated.

The results of the calculations are shown that ultrashort pulses with carrying frequencies are formed in a laser with two active media with separated spectral gain contours, under weak nonlinear losses (much smaller than the depth of the minimum in the total spectral gain contour). The carrying frequencies correspond to two gain maxima. Each active medium forms its own structure of ultrashort pulses with its own carrying frequency. Then two parallel processes take place. The separation of the most intensive pulse and the suppression of weaker pulses occur within each structure. Since nonlinear losses are the same for pulses belonging to both structures, the more intensive pulse of one structure, by saturating losses, leads to the generation, in its spatial volume, of an ultrashort pulse with the carrying frequency corresponding to the other structure of pulses. As a result of the transient process, a pair of pulses remains in the cavity. One of them is gained due to the first active medium and has the corresponding carrying frequency. The other pulse is gained due to the second active medium and has the carrying frequency corresponding to the gain maximum of the second active medium. These pulses are in the same volume. As a result of interference, the envelope of the total intensity turns out to be frequency-modulated. Its frequency corresponds to the differences between the gain maxima of these active media, and the intracavity radiation has the form of a train of ultrashort pulses. When nonlinear losses are comparable to the depth of the minimum in the total spectral gain contour, a single spike remains from the train of ultrashort pulses, and two intracavity active media work as a united gain medium.

Analysis of the results of numerical calculations shows that the dynamics of development is determined by the two main parameters C and Q. The parameter C is determined by the following expression:

$$C = \frac{\xi}{\sqrt{2}\pi\chi_i\Gamma_i L} \tag{6}$$

i. e., this is the ratio between the saturation intensity of nonlinear losses and the saturation intensity of gain. Q is the ratio between the diffraction losses of a single pass and the total linear intracavity losses of a single pass. For solid state active media with broad gainbands, the parameter C lies in a range from 10^{-3} (for Mg_2SiO_4:Cr) to 1 (for $LiF:F_2^+$) if their own Kerr nonlinearities are used. In this case the spatial size of the generation area is simultaneously the saturation area size of nonlinear losses and the value of C is determined by the ratio between the parameters of the active medium and its Kerr nonlinearity. The use of an additional nonlinear absorber in the cavity greatly increases the possibilities of varying the parameter C. The magnitudes of Q for most frequently used solid state lasers are in a range from 10^{-2} to $5\ 10^{-1}$.

For active media with equal saturation parameters and the equal pumping, Q determines an admissible depth of the minimum in the initial unsaturated gain contour at which one pulse for the period of the cavity with the duration determined by the width of the total unsaturated gain contour can be generated. As Q increases (the other parameters being equal), the admissible depth of the minimum in the initial unsaturated gain contour for this generation mode also increases. Fig.1 shows Q as a function of frequency difference between the spectral gain maxima $\Delta\omega$ (in unites of FWHM gain band) for two active media with equal pumping and laser parameters (like $Al_2O_3:Ti^{3+}$) under fourfold threshold pump. In Fig.1 value Q define the possibility of single pulse generation with the ratio peak pulse intensity to background more than one order of magnitude. In this case there exists an optimal value of the parameter C, at which a pulse of minimum duration is generated. For small values of C, quick saturation of nonlinear absorption takes place. This nonlinear shaping mechanism stops, and a long pulse is generated. For large values of C, the gain of the active medium is quickly saturated with low intracavity intensity, and nonlinear absorption turns out to be weak. In this case a train of pulses in the axial period is generated even at values of the parameters Q that are close to unity or higher than unity. Active media with the parameter C in a range from $5\ 10^{-2}$ to $2\ 10^{-1}$ is near optimal for the generation of extremely short pulses in a laser with a composite active medium. In this case in accordance with calculations, an increase of the parameter Q from 0.5 to 0.9 leads to narrowing of the pulse by a factor of two, and its spectral width approaches a half width of the unsaturated gain band. Fig.2 shows time (a) and spectral (b) profiles of pulses generated in a laser with a composite active medium for variable values of the parameter Q and twofold threshold pump with the initial depth of the minimum in the unsaturated gain contour of 30%. For comparison, the time profiles of the generated pulses in the case of zero spectral difference, the other parameters being the same, are shown in Fig.2(a) by a dotted line.

When the composite medium consists of active media with differing parameters C, a single pulse in the axial period can be generated under smaller parameters Q, in contrast to the above case. The formation dynamics becomes much more sensitive to the ratio between the pumping levels for each of the active media. For equal initial pumping levels, quick saturation of one active medium occurs, and the duration of the generated pulse is determined by the gain bandwidth of the active medium with higher saturation intensity. At an appropriate choice of the pumping levels, generation starts with the initial asymmetric unsaturated total gain contour. In the stationary mode, however, an optical pulse with the duration

determined by the combined spectral gain width is generated. The formation dynamics of development in a laser with a such type of composite active medium is presented in Fig.3. Here the difference between the maxima of active media is the same as in Fig.2, but the parameter C differs by an order of magnitude (C_1=0.1 for LiSAF:Cr, C_2=1 for LiF:F_2^+). Given generation mode is realized under double exceeding of pump threshold level for the first active medium and tenfold for the second.

Let us consider the case of three or more active media in a common cavity. Depending on the separation between the gain contour maxima, both a single optical pulse in the axial period with the duration determined by the total width of the unsaturated gain contour and a pulse train with an ultrahigh repetition rate can be generated. When a pulse train is generated in such a laser, there is a time gap between pulses comparable to their duration (in contrast to two equal active media, when there is no such time gap). Fig.4 shows time (a) and spectral (b) profiles of radiation generated in a laser with three like LiSAF:Cr active media versus the separation between the spectral maxima. Passing it through a saturated absorber can increase the contrast in the train of generated pulses.

4. CONCLUSION

A method of numerical simulation of formation of optical pulses in lasers with composite active medium and complex spectral gain contour was developed. We presented the results of our simulations for two and three active media with Lorentz form of spectral gainband in common cavity. This consideration may be extended for composite medium with an arbitrary number of active media and arbitrary shape of spectral gain contour. Analysis of numerical simulation was shown, that the development of generation is defined by two main parameters: first -ratio of initial nonlinear losses to all linear one pass intracavity losses, and second- ratio of nonlinear losses saturation intensity to gain saturation intensity of each laser medium, including in composite medium. The main parameters for the generation of extremely short optical pulses whose duration is determined by the width of a combined spectral gain contour in a laser with a composite active medium were obtained for active media with equal and unequal saturation parameters. Numerical data have been shown that the experimental realization of discussed above ultrashort optical pulses generation may be done with broadband solid state tunable lasers widely used at present time.

5. ACKNOWLEDGEMENTS

This work was performed in part under the support of the Russian National Foundation for Basic Research grant No.99-02-17117 and by the Russian Governmental Program " Fundamental Metrology".

6. REFERENCES

1. D.H.Sutter, G.Steinmeyer, L.Gallamann, N.Matuschek, F.Morier-Genoud, U.Keller,. V Scheuer, G.Angelov, and T. Tschudi, "Semiconductor saturable-absorber assisted Kerr-Lens mode-locked Ti:Sapphire laser producing pulse in the two-cycle regime" Optics.Lett., **24**, pp. 631-633, 1999.
2. U.Morgner, F.X.Kartner, S.H.Cho, Y.Chen, H.A.Haus, J.G.Fujimoto, E.P.Ippen, V. Scheuer, G.Angelov, and T. Tschudi, "Sub-two-cycle pulses from a Kerr-lens mode-locked Ti:Sapphire laser" Optics.Lett., **24**, pp.411-413, 1999.
3. Z.Chang, A.Rundquist, H.Wang, M.M.Murnane and H.C.Kapteyn, "Generation of Coherent Soft X Rays at 2.7 nm High Harmonics", Phys. Rev. Lett., **79**, pp. 2967-2970,1997.
4. A.V.Sokolov, D.D.Yavuz, S.E.Harris, "Subfemtosecond pulse generation by rotational molecular modulation" Optics.Lett., **24**, pp. 557-559, 1999.
5. V.I.Trunov, A.V.Kirpichnikov, E.V.Pestryakov, V.V.Petrov, K.P.Komarov, "Generation of femtosecond pulses in lasers with composite active media", Russisches- Deutsch Lasersymposium, RGLS-97, Novosibirsk, Russia, Technical Digest, p. P9, 1997.
6. E.V.Pestryakov, V.V.Petrov, A.V.Kirpichnikov,V.I.Trunov, K.P.Komarov, A.I.Alimpiev, "Ultrabroadband active media for generation of ultrashort optical pulses", Laser Physics, **8**, pp. 612-619, 1998.
7. H.A.Hauss, J.G.Fujimoto, E.P.Ippen, "Structures for additive pulse mode locking", J. Opt. Soc. Am. **2B**,pp. 2068-2076, 1991.
8. K.P.Komarov, "On Transient Evolution and Steady-State Conditions of the Passively Mode-Locked Laser Action" Sov.J. Quantum Electron. **13**, pp. 166-169, 1986.
9. K.P. Komarov, A.S. Kuch'yanov, "Formation of ultrashort pulses in lasers with nonlinear diffraction loss", SPIE's Proceedings, **2513**, pp. 512-519, 1995.

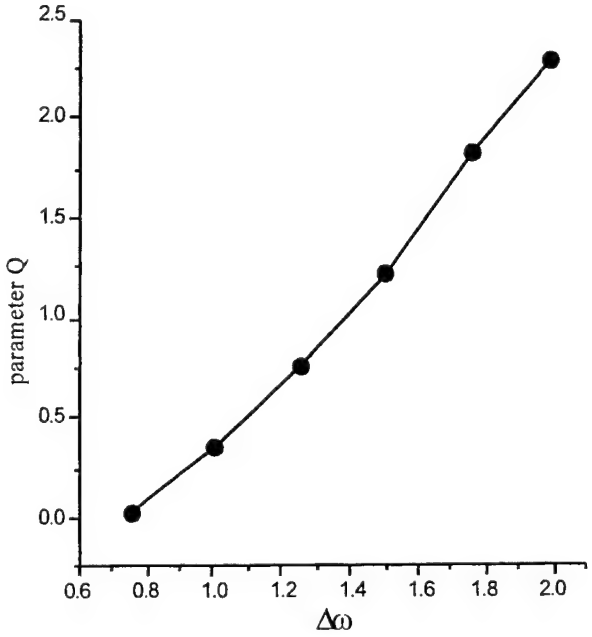

Fig.1

Parameter Q as a function of frequency difference Δω between the spectral gain maximums for two like $Al_2O_3:Ti^{3+}$ active media .

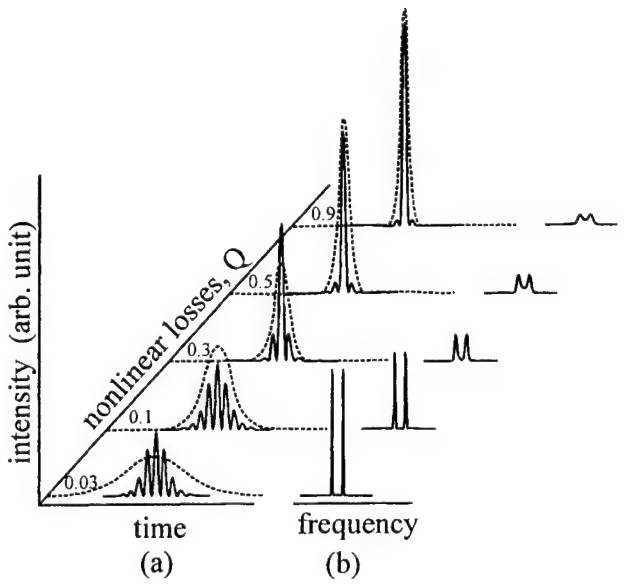

Fig.2

Steady-state temporal (a) and spectral (b) profiles of pulses in the laser with two active medium for set values of Q for Δω=1 (solid curves) and Δω=0 (dashed curves).

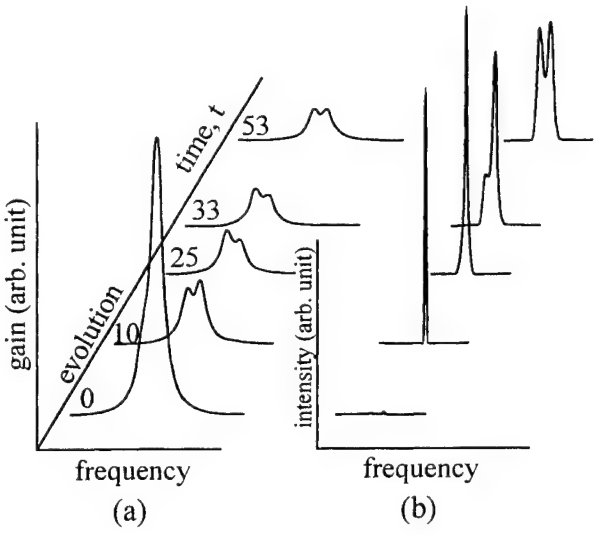

Fig. 3

Evolution of the ultrashort pulses in the laser with the composite active media with similar in Fig.2, but parameters C differ by the order of magnitude.

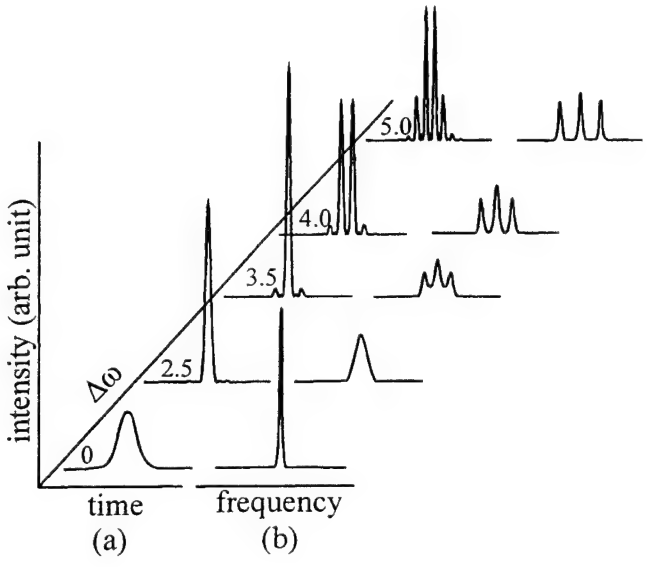

Fig.4

Temporal (a) and spectral (b) profiles of stationary pulses in the laser with three active media in dependence on Δω for Q=0.3.

Synthesis of dispersion-controlled mirror based on the semiconductor materials for near IR femtosecond lasers

N.D.Goldina, E.V.Pestryakov, V.I.Trunov,

Institute of Laser Physics SB RAS, Novosibirsk, Russia

ABSTRACT

It has been proposed the design of mirrors for near IR femtosecond lasers with given phase characteristics based on the III-V compound semiconductors using MBE-technologies with reproducible phase parameters due to precise control of the layer parameters. The designed structure of two-part multilayer mirror includes the bottom part with a great number of AlGaAs-pairs and the top several antireflection layers. The specified negative near-constant group delay dispersion can be realized at certain band of spectrum.

Keywords: semiconductor mirror, group-delay dispersion, thin-film design, femtosecond laser

1. INTRODUCTION

The group delay dispersion of cavity elements is one of the important factor that determinate the possibility of femtosecond pulse generation and their duration in broadband solid-state lasers[1]. For stable work of such laser system the full group delay dispersion of laser cavity must be remained small negative after compensation of their positive part from active medium and other intracavity optical elements.

The dispersive properties of laser cavity reflectors are discussed for various femtosecond systems in a wide spectral range[2,3]. One of the methods of a solution of this problem is the use so-called chirped mirrors[3], permitting smoothly regulate full group delay dispersion of laser cavity over a wide range. The practical realization of such type of mirrors is complicated and connected with the high technological requirements demanded during their making, in particular, for the reproducibility of layers parameters. The reproducibility is determined in main by accuracy of monitoring of layers thickness and refraction index of used materials. It is worthwhile to investigate the new materials and new technology for femtosecond laser mirrors and to consider the possibilities of its design with of required phase characteristics.

In the present work we demonstrate the synthesis of the multilayer structure based on the III-V compound semiconductors using molecular beam epitaxy (MBE) technology. In MBE-technology the monitoring of a layers thickness is possible to within a monolayer (less 3A for GaAs using of a method of a electron diffraction) and even with the greater accuracy after some its updating. The factor of nonreproducibility connected with a spread of refraction index magnitude is absent under the using of the given technology. The grown III-V compound semiconductors structures using MBE-technology in the range near and longer of wavelength 1 μm, have a low absorption level . They can be used for generation of femtosecond pulses in laser crystals and glasses [4,5], and particular in crystals activated by trivalent ytterbium ions. The lasers based on such type of active mediums are widely investigated now [6].

One such variant of mirror design is the change of thickness ratio inside couple of layers in the direction from substrate to incident medium (as shown in[5]) . In that case is synthesized the graded – index layer system. The depth of

Further author information –
E-mail: ngold @laser.nsc.ru, trunov @laser.nsc.ru

Laser Optics 2000: Ultrafast Optics and Superstrong Laser Fields, Alexander A. Andreev, Vladimir E. Yashin, Editors, Proceedings of SPIE Vol. 4352 (2001) © 2001 SPIE · 0277-786X/01/$15.00

penetration optical field in structure is increased with wavelength with the result that is extended time delay for longer part of spectrum.

2. MIRROR DESIGN

Our design of the simplest type mirror may be divided into two stacks. The lower building block adjacent to GaAs substrate consists of the alternate discrete layers of materials with a refractive high-index (H) and a low-index (L). The dispersion of materials no account has been taken. The thickness of layers varies on the specific law in a direction that is normal to the coating with the goal of creating the graded system. As a consequence of interference of multiple reflections at layer boundaries is attained the linear change of the group delay of all system in the high-reflection spectral region. The important part of the synthesis is the matching-problem of the mirror surface and the surrounding medium (air). For the purpose of elimination of large undesirable reflection from the boundary air – semiconductor is added a top two-material multilayer consisting several layers of antireflection (AR) coating. The synthesis of AR-coating includes the analytical starting design based on the equivalent-index method and followed by a numerical refinement procedure. The matching layers give the symmetrical change with wavelength of complex amplitude reflectance of produced reflecting interference system, which is the nonminimal – phase system.

In this report we present two different examples of coating design. The bottom main structure is made from two-material layers GaAs/AlAs by MBE-technology. For the design is chosen the spectral region around 1 μm. The high reflection R>99% with these materials is attained in standard quarterwave stack with bandwidth about 60 nm when the number of layer pairs is more than 15. The layer couple GaAs/AlAs has a small ratio $\Delta n/n_{ave}$ =0.5/3.25, where Δn - the difference between refractive indices of H- and L-layer, n_{ave} - average index. One way to synthesize dielectric mirror with prescribed dispersion properties involves the increasing of the number of layer pairs. The greater is the number of layers, the longer is the penetration depth of electric field in the layer structure. Consequently, a higher value of negative group delay dispersion can be obtained. The optimal practical solution is dictated by experimental possibilities. In the GaAs/AlAs case can be imposed the constraints on the total thickness of mirror or limited maximal thickness by one layer any of two materials.

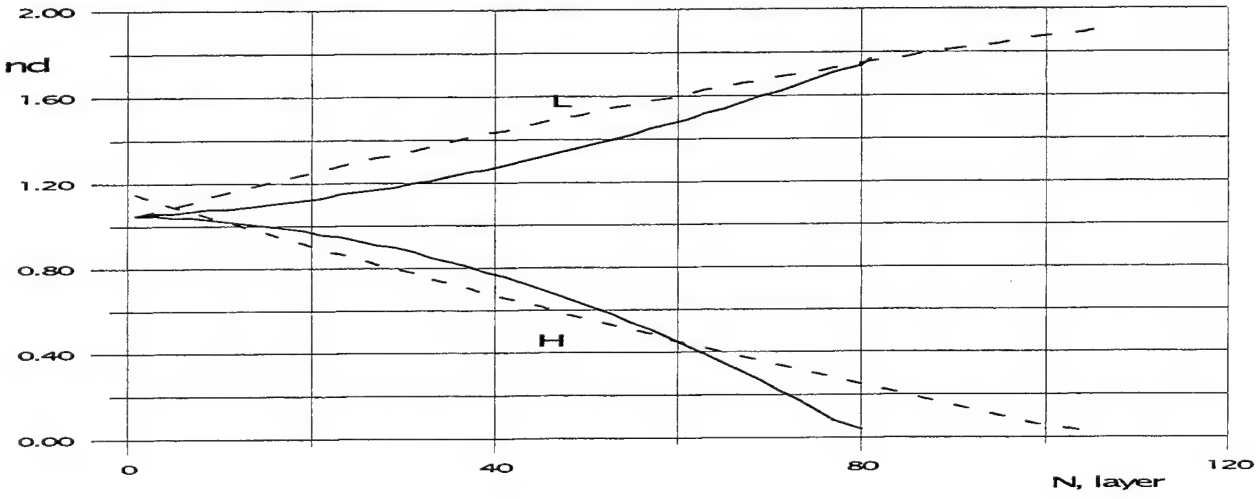

Fig.1. Optical thickness (λ /4 units) of the layers for bottom structures of two mirrors (——- 81 layers, - - - - 105 layers).

Figure 1 shows the calculated dependence of layer thickness (in units of quarter-wave) for bottom structure of 81 (solid line) and 105 (dashed line) layers. The top AR-coating in both cases consists three layers TiO_2 /SiO_2.

Unfortunately, these coatings must be obtained by other deposition technology. Today CaF_2 can be possible constituent material of AR-coating in semiconductor technology. The overall physical thickness **d** of bottom binary structure equal 6.7 μm for first mirror and 8.8 μm - for second; in either case the thickness of H-layers are about 2 μm. The thickness of L-layers grows to the direction of incoming medium for both examples. Although can be treated the version with increasing of H-layer thickness. As seen from figure 1 the different dependencies of thickness change on the number of layer are applied in two cases.

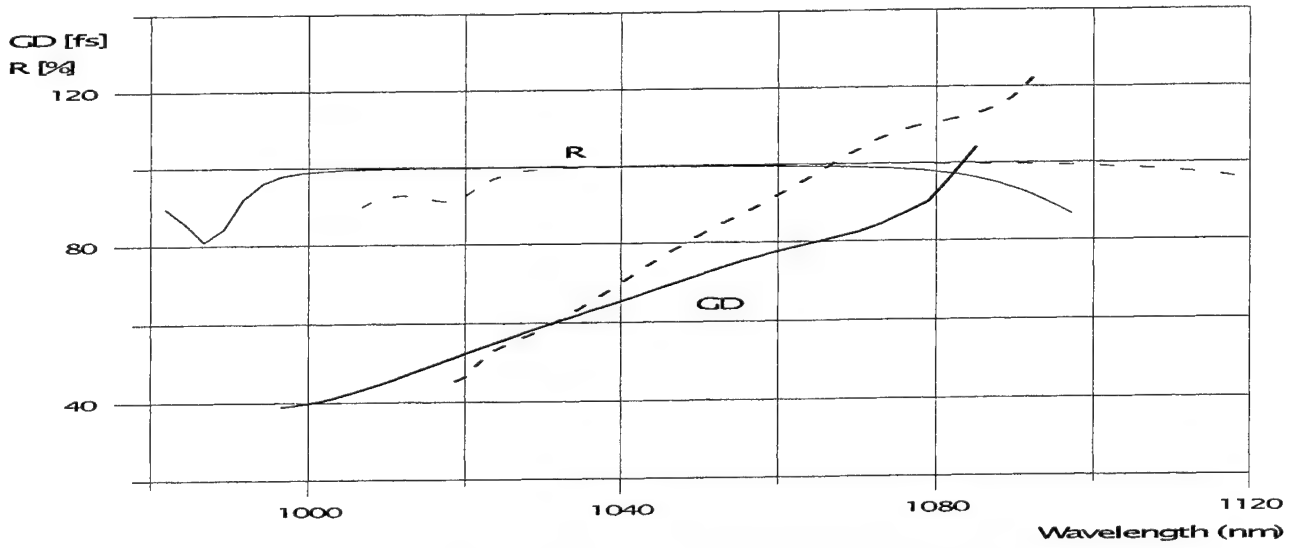

Fig.2. Computed group delay (GD) and reflectance (R) vs. wavelength function for two mirrors (—— - 84 layers, - - - - 108 layers).

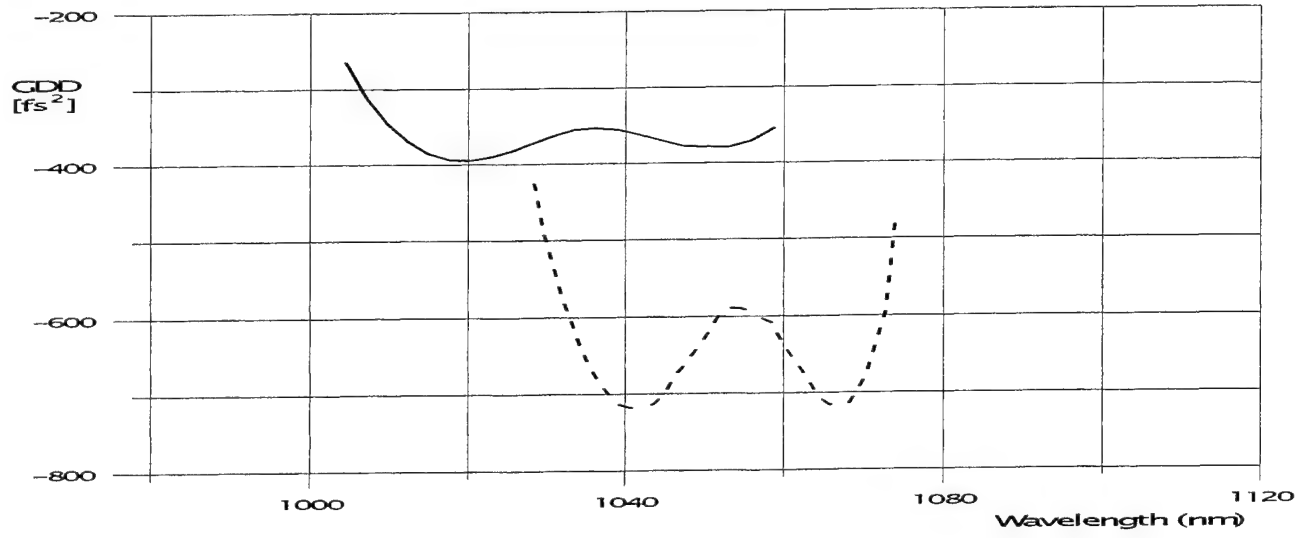

Fig.3. Calculated group delay dispersion of two mirrors with wavelength (—— - 84 layers, - - - - 108 layers).

The group delay linearly grows with wavelength in high-reflection spectral region over about 40 nm bandwidth (figure 2) for both of these mirrors. The spectral reflection coefficients R of both mirrors are shown on figure 2. The maximum of reflectance is equal 99.8% for 84 layer- and 99.9% for 108-layer mirror; the reflection coefficients are fall

slightly at the edges of the stop-band. Figure 3 represents corresponding group delay dispersion over those intervals.

As one would expect a higher number of layer pairs gives the possibility to increase the level of negative GDD for fully dispersion compensation in a femtosecond laser cavity as a result a single bounce on such a semiconductor mirror. In modern practice the upper limit of the layer number is set by the absorption losses in thin-film used materials and another limitations (stress in coating, for example).

3. CONCLUSION

While GaAs/AlAs mirror has not large operating spectral region and consists of the great number of layers, it nevertheless provides large negative group delay dispersion, necessary for sufficient compensation dispersion after one reflection. In addition the advantages of GaAs/AlAs structure is the fact that the deposition procedure can be as integral part of semiconductor technology.

MBE-technology allows to realize the designed structures with the highest reproducibility. The use of other technologies (metalorganic chemical vapor deposition, etc.) does not allow to control the thickness of layers using fast electron diffraction. Furthermore in these technologies the semiconductor structure grows in quasiequilibrium system subject to influence of thermal fluctuations. In MBE-technology a main factor of the nonreproducibility during the structure growth is the modification of the electronic beam parameters forming the Ga and As atoms beams. They can be controlled and be corrected with a higher accuracy than for other technologies.

4. ACKNOWLEDGEMENTS

The authors express their gratitude to Drs A.I. Toropov and V.A. Haisler for helpful discussion about possibilities of MBE technology. This work was supported by the Russian Fundamental Research Foundation (grant N99-02-17117 and grant N99-02-39135)

5. REFERENCES

1. C.Spielman, P.F.Curley, T.Brabec, F.Krausz, "Ultrabroadband femtosecond lasers", *IEEE J.Quantum Electron.*,**QE-30**, pp.1100-1114, 1994.
2. J.Kuhl and J.Heppner, "Compression of fs-optical pulses with dielectric multilayer interferometers", *IEEE J.Quantum Electron.*,**QE-22**, pp.182-185, 1986.
3. R.Szipocs and A.Kohazi-Kis, "Theory and design of chirped dielectric laser mirrors", *Appl.Phys.*, B**65**, pp.115-135, 1997.
4. S.R.A.Dodds and M.Ogura, "Dispersive mirror in AlGaAs designed by inverse spectral theory", *Appl.Opt.*, **36,** pp.7741-7751, 1997.
5. R.Paschotta, G.J.Spuhler, D.H.Sutter, N.Matuschek, U.Keller, M.Moser, R.Hovel, V.Scheuer, G.Angelow and T.Tschudi, "Double-chirped semiconductor mirror for dispersion compensation in femtosecond lasers", *Appl.Phys.Lett.* ,**75**, pp.2166-2168, 1999.
6. C.Honninger, F.Morier-Genoud, M.Moser etc., "Efficient and tunable diode-pumped femtosecond Yb:glass lasers", *Opt.Lett.*, **23**, pp.126-128, 1998.

Stimulated Raman scattering in compressed gases by short laser pulses

A. I. Vodchits[a], W. Werncke[b], S. Hogiu[b] and V. A. Orlovich[a]

[a]B.I. Stepanov Institute of Physics, National Academy of Sciences of Belarus,
Fr. Scaryna Ave. 68, Minsk 220072, Belarus

[b]Max-Born-Institut, Max-Born-Strasse 2A, D-12489 Berlin, Germany

ABSTRACT

Stimulated Raman scatterimg (SRS) excited by picosecond pulses (3.5-4 ps) of a synchronously pumped dye laser has been studied in compressed methane, hydrogen and their mixture. Physical energetic SRS-efficiencies (corrected for the linear losses of the optical elements) up to about 55-60 % and 35-37 % for the generation of the first vibrational Stokes radiation were reached in methane at a pressure of 60 bar and at excitation wavelengths near 600 nm and 740 nm, respectively. SRS-efficiencies versus pump pulse energy, pressure of gas and temporal duration of laser pulses were studied at 600 nm in methane. A very rich spectrum of Raman lines (including some vibrational, vibrational-rotational and combination Raman lines) was observed in the mixture of methane (35 bar) and hydrogen (25 bar). The energy efficiency of SRS-conversion to the 1-st rotational Stokes Raman line of hydrogen reached about 20 % in the mixture. In contrast, the 1-st vibrational Stokes components of hydrogen and methane were substantially suppressed in this mixture. Our measurements demonstrate that methane is one of the most suitable Raman media for obtaining effective SRS-generation especially at pico- and femtosecond excitation because of its suitable parameters controlling the SRS-process and that the mixtures of compressed gases are rather promising Raman media for extending the tuning range of pico- and femtosecond laser systems and for optimizing the efficiencies of SRS-conversion to the different Raman components.

Keywords: stimulated Raman scattering, compressed gas, methane, hydrogen, gas mixture, picosecond laser pulse, efficiency, Raman line, combination line

1. INTRODUCTION

Nowadays one of the most important tasks of ultrafast laser techniques and technologies is the extension of the tuning range of pico- and femtosecond laser radiation from the infrared (IR) to the ultraviolet (UV) spectral region. In particular, it is necessary for improving the possibilities of application of Ti:Sapphire laser systems for pump-probe spectroscopy, e.g. for the development of time-resolved Raman spectrometers.

In this connection stimulated Raman scattering (SRS) in compressed gases is a rather convenient and simple method to extend (due to the frequency conversion of laser radiation) the tuning range of ultrashort laser systems to the other spectral regions. The advantages of SRS in comparison with other techniques (for example, optical parametric generation) are low cost of the appropriate equipment, little problems with damage and a comparatively simple experimental setup. Gases such as hydrogen and methane are well known to be suitable gases for Raman shifting. They have well-characterized SRS spectra, large vibrational and rotational Stokes frequency shifts, relatively high values of Raman gain, and low group velocities dispersion between the pumping and Stokes waves. These gases can be mixed in arbitrary ratios and stored at high pressures without condensation. They are transparent to radiation throughout most of the UV, visible and IR spectral regions.

However, SRS in most compressed gases excited by the short laser pulses with the time duration less than several picoseconds is a highly transient non-linear optical process which is not as well studied as in the steady-state regime of

Laser Optics 2000: Ultrafast Optics and Superstrong Laser Fields, Alexander A. Andreev, Vladimir E. Yashin, Editors, Proceedings of SPIE Vol. 4352 (2001) © 2001 SPIE · 0277-786X/01/$15.00

SRS excited typically by nanosecond laser pulses. Therefore, in the last years several studies devoted to pico- and femtosecond SRS have been published[1-5].

Nevertheless, there are still a number of open questions concerning the transient SRS excited by the laser pulses shorter than 10 ps. These are the conditions for the maximum efficiencies of SRS-conversion of pumping radiation at different wavelengths to the different SRS-components, for the suppression of white light continuum generation and for the generation of the frequency-shifted pulses with desirable temporal and spectral properties.

Furthermore, it seems to be very promising to obtain sub-femtosecond optical pulses by mode locking of high-order stimulated Raman lines which are generated by four-wave Raman mixing. Realizing this idea demands for detailed studies of the transient SRS and related parametric processes in compressed gases[6]. In this connection it should be noted that little attention (if any) was paid to the studies of highly transient SRS excited by laser pulses shorter than 10 ps in the mixtures of different gases. Meanwhile, studies carried out under the conditions of steady-state SRS in gas mixtures demonstrated considerable possibilities concerning an effective generation of a larger number of Raman lines or a more effective generation of known Raman lines in the comparison with the neat gases[7-11].

In this report we present the results of experimental studies of some peculiarities of transient SRS excited by picosecond laser pulses in compressed methane and hydrogen. In addition, some preliminary results on the study of SRS in a mixture of methane and hydrogen are presented.

2. EXPERIMENT

The experimental setup is shown in Fig. 1. SRS was excited by short pulses generated by a laser system used for our time-resolved Raman spectrometer[12]. It is based on a dye laser synchronously pumped by the second harmonic (SH) radiation of a mode locked Nd:YAG-laser (Quantronix 4216, 76 MHz, pulse-width of 100 ps). Dye laser pulses of 3.5-4 ps pulse duration exceeding the transform-limited spectral bandwidth about two times were amplified by a three-stage dye amplifier. It was pumped by the SH-radiation of a regenerative amplifier (Continuum RGA-50, repetition rate of 50 Hz). After amplification, pulse energies up to 250 μJ were obtained at about 600 nm and up to 150 μJ near 730-740 nm depending on the actual dye used (rhodamin 6G or pyridin 2 in ethylene glycol, respectively). The temporal width of the pulse could be tuned from 3.5 and up to about 25 ps by changing the length of dye laser resonator. The pulse-width (FWHM) was measured by non-collinear SH-generation in BBO-crystals (thickness 500 μm) using a home-made auto-correlator (not shown in the figure). Frequency doubling of the fundamental radiation could be performed in an additional BBO-crystal of 2 mm thickness with an efficiency up to 25 %.

The gas was filled into a special high pressure Raman cell of about 25 cm working length equipped with quartz windows. Maximum gas pressure did not exceed the value of 60 bar. Lenses with different focal lengths (15-50 cm) were used for focusing the pumping laser beam into the cell. For measuring the SRS-conversion efficiency the light beam was dispersed after the cell by a prism. The different spectral components were spatially discriminated by an aperture and measured by a power meter (ZWG, PEM521). The measured energies were corrected for the losses in the optical elements including the cell windows, the lens after the cell and the dispersive prism. These losses were determined experimentally. Therefore, the SRS-conversion efficiencies presented are the "physical" SRS-conversion efficiencies calculated for the center of the Raman cell, unless otherwise stated. In addition, the spectrum of SRS could be measured using a spectrograph (SOPRA SpectraPro-275) and a liquid-nitrogen-cooled CCD camera (Spectroscopy and Imaging, LN/CCD 1100PB/UVAR CCD, back illuminated). For this purpose a right-angle prism was inserted into the beam of scattered light and the beam was directed to the spectrograph. An appropriate polarization of the pumping laser beam was obtained by using polarizers (Glan prisms) and phase rotators (λ/4-plates) which are not shown in Fig. 1.

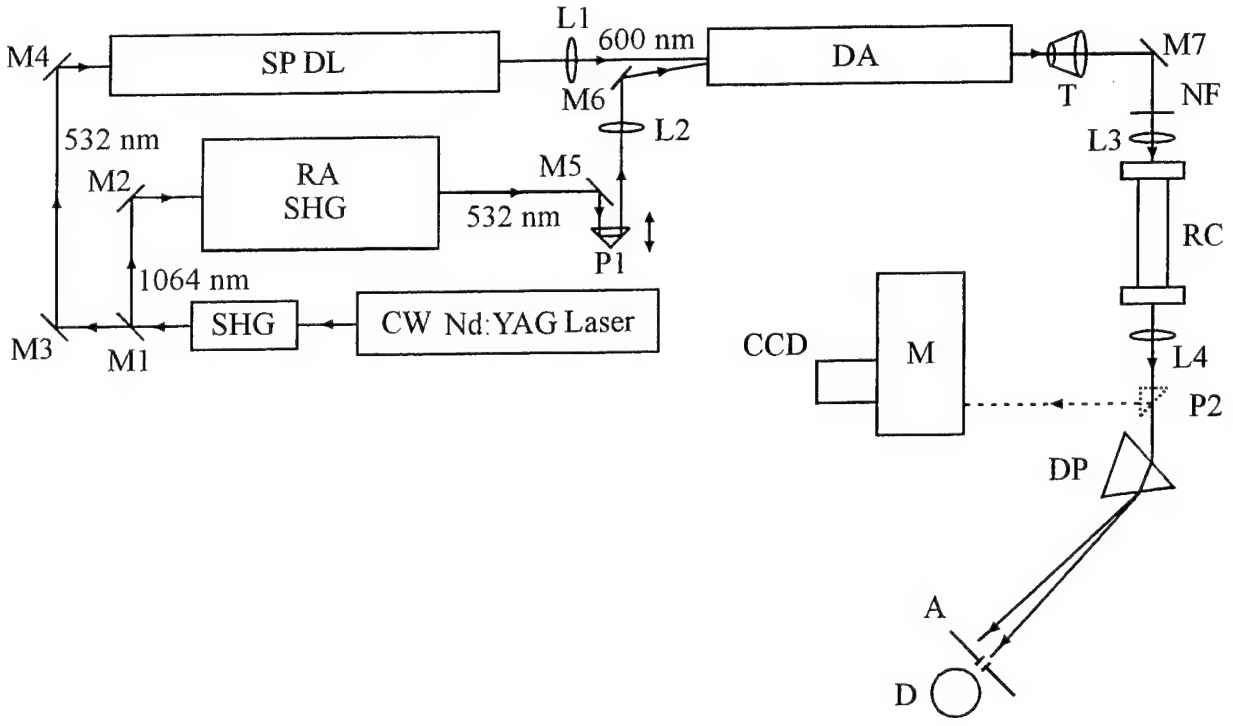

Fig. 1. The experimental setup:
SHG – second harmonic generator; RA – regenerative amplifier; SP DL - synchronously pumped dye laser; DA – dye amplifier; M1-M7 – mirrors; L1-L4 –lenses; P1, P2 – prisms; T – telescope; NF – neutral filters; RC – Raman cell; M – spectrograph; CCD – CCD-camera; DP – dispersive prism; A – aperture; D – energy meter

3. RESULTS AND DISCUSSION

Fig. 2 shows the dependence of the first Stokes pulse energy on the pump pulse energy for SRS in methane compressed to 60 bar excited by 3.5 ps laser pulsed radiation at about 600 nm. For measuring this dependence the linear polarized laser radiation was focused into the Raman cell by a positive spherical lens of about 25 cm focal length. In this case, on a white screen after the dispersive prism we were able to observe the axial components of the 1-st Stokes and 2-nd Stokes radiation and parametric ring components of the 1-st anti-Stokes and 2-nd anti-Stokes radiation visually. The energies of the 2-nd Stokes, 1-st and 2-nd anti-Stokes pulses were below the threshold of measurement (10 μJ). Below the value of about 60 μJ for the pump pulse energy, the energy of the 1-st Stokes pulse dropped rapidly exhibiting large fluctuations. Near the pump energy of about 15-20 μJ we reached the threshold of SRS-generation for the 1-st Stokes radiation. This value of SRS-threshold was estimated by visual control and by observing the presence of the Stokes radiation with the CCD-camera.

From Fig. 2, it is seen that above a pump pulse energy of 60 μJ the energetic efficiency of SRS-conversion to the 1-st Stokes radiation remains approximately constant at a very high value of about 55 %. It corresponds to the technical SRS-efficiency (determined as a ratio of the Stokes pulse energy after the dispersive prism to the pump pulse energy before the input window of the cell) of about 30 %. The main condition for obtaining such an effective generation was the good quality of laser beam, i.e. an energy distribution in the cross-section close to Gaussian. In the case of some distortion of the beam quality the SRS-efficiency dropped substantially to a value 30-40 %. Some small saturation of the 1-st Stokes pulse energy at the highest pump energies is due to the increase of the 2-nd Stokes pulse energy. It should be noted that our results concerning SRS-efficiency were not very sensitive to the polarization properties of the pumping radiation.

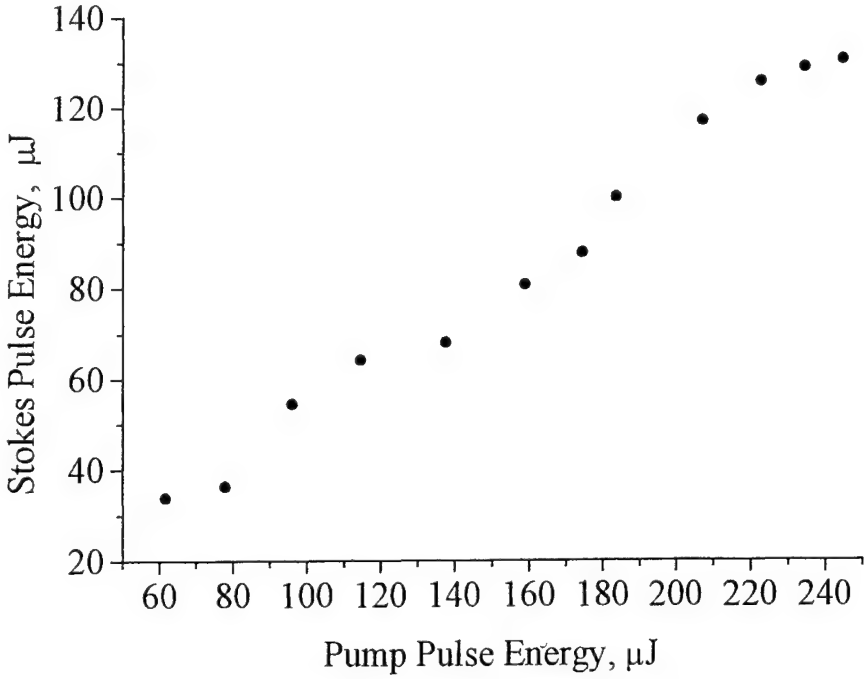

Fig. 2. The 1-st Stokes pulse energy versus the pump pulse energy for SRS in methane compressed to 60 bar and excited by a 3.5 ps laser pulse at 600 nm.

When we changed the focal length of the focusing lens from 15 to 50 cm the character of SRS generation was not changed dramatically. Decreasing the focal length facilitated the SRS-generation of anti-Stokes components. Increasing it above 25 cm results in a reduced SRS-efficiency for the generation of the 1-st Stokes radiation and high-order components were partly suppressed.

Decreasing the pressure of methane resulted in a considerable reduction of the 1-st Stokes SRS-conversion efficiency (35 % at 35 bar). In this case the threshold of SRS-generation was increased to 30-40 μJ of pump pulse energy. As a preliminary test of non-stationarity we measured the efficiency of SRS-conversion to the 1-st Stokes radiation versus the temporal duration of pumping laser pulse between 3.5 ps and 25 ps. For all pulse widths we reached a limit of the efficiency of SRS-conversion ranging from 55 and up to 60 % indicating that the efficiency depends on the pump pulse energy under our experimental conditions.

At an excitation wavelength of the pumping laser radiation of about 740 nm the maximum efficiency for the 1-st Stokes SRS-generation in compressed methane (60 bar) of about 35-37 % was obtained (which corresponds to the technical SRS-efficiency of about 20 %). This value slightly exceeds the efficiency reported in[5] for the case of the SRS-excitation with 140 fs pulses from Ti:Sapphire-laser tuned at 750 nm.

Under our experimental conditions of using short laser pulses we didn't observe any backward SRS which limits the conversion efficiency in the case of long pulses. In addition, we didn't observe the generation of white light continuum; its appearance is a serious problem for the spectroscopic applications of SRS excited by the shorter laser pulses[1,2].

Some peculiarities of SRS in compressed methane which we observed are close to the results presented elsewhere[1,3,5]. Anyway, to our knowledge such high efficiencies for the SRS-generation of the 1-st Stokes radiation in compressed methane was not reached earlier under excitation with laser pulses shorter than 10 ps.

Using hydrogen instead of methane we couldn't reach the threshold of SRS at 740 nm excitation even at the maximum pressure of 60 bar and an energy of the 3.5 ps laser pulse of about 150 μJ. Also at 370 nm excitation with the

energy of 35-40 μJ no detectable SRS-conversion was obtained.

Our results demonstrate that, in accordance with[5], methane is one of the most suitable Raman media for obtaining highly effective SRS at pico- and femtosecond excitation because of its rather advantageous combination of the main parameters which are responsible for the SRS-process. In particular, these are the steady-state Raman gain coefficient g and the dephasing time T_2. For the simplicity we don't take into account the manifold of additional factors influencing SRS too, such as the intensity of the laser radiation, the interaction length, the spatial distribution of the laser beam, the group-velocity mismatch, and competitive processes. In the high-gain-limit of transient SRS, the gain increment G is proportional to[1,3,13]

$$G \propto \sqrt{\frac{g}{T_2}} \ . \qquad (1)$$

Although the gain coefficient for SRS-generation to the 1-st vibrational Stokes component in methane is a several times smaller than that in hydrogen[1] the dephasing time in methane is more than 10 times shorter than that in hydrogen[1,3]. Therefore, the SRS-gain increment may be considerably higher in methane in comparison to hydrogen, which is known to be rather suitable for SRS-generation.

Searching for possibilities to extend the number of Raman lines generated by SRS, we have carried out some preliminary studies of SRS in a mixture of methane and hydrogen. The partial pressure of methane was equal to 35 bar and that of hydrogen 25 bar. The elliptically polarized pumping laser radiation at about 600 nm was focused inside the Raman cell with a lens of 25 cm focal length. The energy of the pump laser pulse (3.5-4 ps) was equal to about 200 μJ. In this case we observed a very rich spectrum of SRS after the dispersive prism. Visually we observed 13 SRS-components in the Stokes and anti-Stokes region on the white screen behind the prism. The strongest Raman line was the line S_{01} (Raman shift of about 587 cm^{-1}) of rotational SRS (RSRS) in hydrogen. The efficiency of SRS-conversion to this line was equal to about 20 %. The vibrational SRS (VSRS) to the 1-st Stokes components of hydrogen and methane (S_{10} lines with the Raman shifts of 4155 and 2917 cm^{-1}, respectively) was considerably suppressed in comparison with the case of neat gases. The energies of these components as well as of other observable Raman lines were below the our detection limit of 10 μJ. At present the reasons for this observation are not very clear. However, at least partly this may be associated with the comparatively low pressures of gases and suppression of VRSR-gain at sharp focusing of the laser beam[14-16].

Using the CCD-camera we detected the spectrum of SRS in the mixture. More than 30 lines in Stokes and anti-Stokes regions were observed from the mixture by CCD. One could observe some rotational, vibrational and vibrational-rotational lines of hydrogen, vibrational lines of methane. Besides the known lines for neat hydrogen and methane, we observed some combination lines from both gases. The frequencies of the latter lines can be expressed as

$$\omega_L + n\Omega_{H_2} + m\Omega_{CH_4} \ , \qquad (2)$$

where ω_L is the frequency of the exciting laser line, Ω_{H_2} and Ω_{CH_4} are the Raman shifts of hydrogen and methane and $n, m = 0, \pm 1, \pm 2, \ldots$. In particular, we observed Raman lines originating from the rotational shift S_{01} of hydrogen and vibrational shift S_{10} of methane (overall Raman shift is equal to 587 cm^{-1} + 2917 cm^{-1} = 3504 cm^{-1}) and from vibrational shifts S_{10} of hydrogen and methane (overall Raman shift is equal to 4155 cm^{-1} + 2917 cm^{-1} = 7072 cm^{-1}), respectively. It is known that rotational scattering in methane is forbidden by the symmetry of the molecule[1].

Despite the rather weak intensities of the lines observed in our experiment, we believe that there is a possibility to obtain even higher efficiencies of SRS-conversion with respect to certain Raman components in the mixtures of gases than in the case of neat gases, e.g. by changing the partial pressures of the gas components, the geometry of focusing and the parameters of the pumping laser beam. A number of studies carried out under the conditions of steady-state SRS support this idea[14-20]. Such a work is in progress now.

4. CONCLUSIONS

In conclusion, SRS in compressed methane, hydrogen and their mixture under the excitation with 3.5-4 ps laser pulses has been experimentally investigated. The efficiencies of SRS-conversion up to about 55-60 % and 35-37 % for the generation of the 1-st vibrational Stokes component radiation have been obtained in methane compressed to 60 bar at an excitation wavelengths near 600 nm and 740 nm, respectively. SRS-efficiencies versus pump energy, gas pressure and temporal duration of the laser pulse were studied at 600 nm excitation more in detail. Our results demonstrate unique properties of methane as a Raman medium for obtaining very effective SRS especially at picosecond and probably also at femtosecond excitation, because its material parameters are suitable for SRS under non-stationary conditions.

To our knowledge for the first time we observed a very rich spectrum of Raman lines (including some vibrational, vibrational-rotational and combination Raman lines) in the mixture of methane (35 bar) and hydrogen (25 bar) at highly transient SRS excited by 3.5 ps laser pulses at 600 nm. Under these conditions the efficiency of SRS-conversion to the strongest 1-st Stokes rotational Raman line S_{01} of hydrogen reached about 20 % in the mixture. It is noted that the mixtures of compressed gases are rather promising Raman media for extending the tuning range of pico- and femtosecond laser systems, optimizing the efficiencies of SRS-conversion to the different Raman components and probably for obtaining sub-femtosecond pulses by mode locking of stimulated Raman lines which are generated by four-wave Raman mixing.

5. ACKNOWLEDGEMENTS

Support of the International Bureau of the BMBF of Germany (grant WEI-006-98) is gratefully acknowledged.

6. REFERENCES

1. V. Krylov, O. Ollikainen, U.P. Wild, A. Rebane, V.G. Bespalov, and D.I. Staselko, "Femtosecond stimulated Raman scattering in pressurized gases in the ultraviolet and visible spectral ranges", J. Opt. Soc. Am. B, **15**, pp. 2910-2916, 1998.
2. I. Fisher, and T. Schultz, "Generation of tunable visible and near-IR light from 2.5 ps, high-power Ti:sapphire pulses by Raman shifting in hydrogen", Appl. Phys. B, **64**, pp. 15-20, 1997.
3. Y. Uesugi, Y. Mizutani, S.G. Kruglik, A.G. Shvedko, V.A. Orlovich, and T. Kitagawa, "Characterization of stimulated Raman scattering of hydrogen and methane gases as a light source of picosecond time-resolved Raman spectroscopy", to be published in J. Raman Spectr.
4. L. Zhu, J. Kim, and R.A. Mathies, "Picosecond time-resolved Raman system for studying photochemical reaction dynamics: application to the primary events in vision", J. Raman Spectrosc., **30**, pp. 777-783, 1999.
5. I.G. Koprinkov, A. Suda, P. Wang, and K. Midorikawa, "High-energy conversion efficiency of transient stimulated Raman scattering in methane pumped by the fundamental of a femtosecond Ti:sapphire laser", Opt. Lett., **24**, pp. 1308-1310, 1999.
6. H. Kawano, Y. Hirakawa, and T. Imasaka, "Generation of high-order rotational lines in hydrogen by four-wave Raman mixing in the femtosecond regime", **34**, pp. 260-268, 1998.
7. J.A. Duardo, L.J. Nugent, and F.M. Johnson, "Combination lines in stimulated Raman emission from gas mixtures", J. Chem. Phys., **46**, pp. 3585-3591, 1967.
8. T.R. Loree, R.C. Sze, D.L. Barker, and P.B.Scott, "New lines in the UV: SRS of excimer laser wavelengths", IEEE J. Quantum Electron., **QE-15**, pp. 337-342, 1979.
9. G.B. Jarvis, S. Mathew, and J.E. Kenny, "Evaluation of Nd:YAG-pumped Raman shifter as a broad-spectrum light source", **33**, pp. 4938-4946, 1994.
10. S.V. Melchenko, and V.F. Tarasenko, "SRS-transformation of high-power UV-lasers radiation in gases and vapors", The Proceedings of the High Education Schools (Russia), Series "Physics", N3, pp. 90-116, 1998 (in Russian).
11. J. Wang, Y. Siegel, C. Lii, E. Mazur, and J. Reintjes, "Subpicosecond stimulated Raman scattering in high pressure hydrogen", J. Opt. Soc. Am. B, **11**, pp. 1031-1037, 1994.

12. S. Hogiu, W. Werncke, M. Pfeiffer, A. Lau, and T. Steinke, "Picosecond time-resolved CARS spectroscopy of a mixed excited singlet state of diphenylhexatriene", Chem. Phys. Lett., **287**, pp. 8-16, 1998.
13. R.L. Carman, F. Shimizu, C.S. Wang, and N. Bloembergen, "Theory of Stokes pulse shapes in transient stimulated Raman scattering", Phys. Rev. A, **2**, pp.60-72, 1970.
14. F. Hanson, and P. Poirier, "Stimulated rotational Raman conversion in H_2, D_2, and HD", IEEE J. Quant. Electr., **29**, pp. 2342-2345, 1993.
15. M.R. Perrone, V. Piccino, G.De Nunzio, and V. Nassisi, "Dependence of rotational and vibrational Raman scattering on focusing geometry", IEEE J. Quant. Electr., **33**, pp. 938-944, 1997.
16. M.R. Perrone, G.De Nunzio, and C. Panzera, "Competition between vibrational and rotational Raman scattering in H_2", Opt. Commun., **145**, pp.128-134, 1998.
17. S.V. Melchenko, A.N. Panchenko, and V.F. Tarasenko, "SRS-transformation of electro-discharge XeCl-laser radiation", Sov. Quant. Electron., **13**, pp.1496-1500, 1986.
18. S.V. Melchenko, A.N. Panchenko, and V.F. Tarasenko, "The investigation of SRS-transformation of ultraviolet radiation in compressed gases", Sov. Opt. and Spectrosc., **61**, pp.303-307, 1986.
19. A. Luches, V. Nassisi, and M.R. Perrone, "Stimulated Raman scattering in H_2-Ar mixtures", Opt. Lett., **12**, pp.33-35, 1987.
20. A.D. Papayannis, G.N. Tsikrikas, and A.A. Serafetinides, "Generation of UV and VIS laser light by stimulated Raman scattering in H_2, D_2, and H_2/He using a pulsed Nd:YAG laser at 355 nm", Appl. Phys. B, **67**, pp. 563-568, 1998.

Active mode-locking: is everything clear?

A.Apolonski[1,2], V.Yakovlev[1,2]

1. Institute of Automation and Electrometry RAS, 630090 Novosibirsk, Russia.
2. Institut für Photonik, Technische Universität Wien, Gusshausstrasse 27/387, A-1040 Wien, Austria.

Active mode-locking itself provides pulses not shorter than picoseconds. Nevertheless, this regime is useful for many laser systems including powerful ones where strict synchronization with external periodic signal is needed. Another growing field where active mode-locking is widely used is fiber laser systems. 30 years passed since D.Kuizenga and A.Siegman (K-S) [1] developed their (presently well-known) theoretical model for active mode-locking. Hence many other models have been published, all of them (including K-S) are not completely adequate for the real laser systems. That conclusion was pointed out by one of the authors for the gas, dye and solid-state lasers and presented in many publications and conference papers [2]. In this paper we present results of successful numerical modelling for the mode-locked Ar-ion laser, which are in qualitative agreement with the experiment. Disagreement of the known models (or not revealed stuff from them) with the experiment can be formulated in such common items:

a) an optimum pulse position inside the temporal mode-locker window: dependence on the gain, mode-locker parameters;

b) phase characteristics (pulse position inside the mode-locker window);

c) pulse amplitude and duration versus the mode-locker parameters.

1 Numerical simulations

We use a model based on the Maxwell-Bloch equations [3]

$$\frac{\partial \Omega(\tau,\xi)}{\partial \xi} = g\int_{-\infty}^{\infty} \rho(\Delta) P(\tau,\xi,\Delta) d\Delta, \tag{1a}$$

$$\frac{\partial P(\tau,\xi,\Delta)}{\partial \tau} = (-\gamma_2 + i\Delta)P + \Omega D, \tag{1b}$$

$$\frac{\partial D(\tau,\xi,\Delta)}{\partial \tau} = -\gamma_1(D - D_0) - \Re(\Omega^* P), \tag{1c}$$

Laser Optics 2000: Ultrafast Optics and Superstrong Laser Fields, Alexander A. Andreev, Vladimir E. Yashin, Editors, Proceedings of SPIE Vol. 4352 (2001) © 2001 SPIE · 0277-786X/01/$15.00

where

- $\Re$ denotes the real part;
- τ, ξ are the co-moving coordinates: $\tau = t - x/c$, $\xi = x/c$;
- Δ is the inhomogeneous detuning;
- $\rho(\Delta)$ specifies the inhomogeneous line broadening;
- Ω is the complex Rabi frequency;
- D is the normalized inversion;
- g is a constant that represents gain;
- γ_1, γ_2 are the longitudinal and transverse relaxation rates;
- D_0 it the equilibrium inversion without an applied field.

Experimental parameters [2] were used for calculations. These parameters were chosen different from those in [3]. Namely, $T_1 = 5$ ns ([4], 3 times larger than those in [3]) and the output-coupler loss 15% (4 times more than those in [3]). Calculations and comparison with the experiment have been done for the 514.5 nm line.

2 Results

A 3D picture of the pulse evolution is shown in Fig.1. Pulse shape is shown in Fig.2 at different frequency detunings. The optimal position of the pulse at the zeroth value of detuning is remarkably not at the center of the mode-locker window, in agreement with the experiment [2]. At large negative detunings the satellite has chaotic nature and we used averaging over 4000 pulses to get these smooth realizations which are close to the experimental observations with a stroboscopic oscilloscope. In Fig.3 it can be seen that the pulse changes its symmetry in dependence on its position inside the mode locker window. The most symmetric pulse shape occurs near the center of the mode-locker window, and the symmetry (ratio of the leading part of the pulse to the tailing one relative to the pulse maximum) changes as the pulse position crosses the zeroth point. The pulse asymmetry occurs due to the additional losses of the leading/tailing parts of the pulse in the mode-locker. When the pulse is symmetric, its shape in most cases is close to the Gaussian one.

The dependence of the pulse parameters on the mode-locker modulation depth has been shown in Fig.4. To get an agreement with the experimental curves (namely, strong dependence of the pulse duration on the modulation depth, Fig.4b, and the decrease of the pulse amplitude as the modulation depth increases, Fig.4c) we have introduced additional losses in the

mode-locker which are dependent on the modulation depth owing to the a) additional acoustic modes of higher orders and b) increase of the running acoustic wave as the electrical RF power is increased.

The pulse position is different at different gain values, Fig.5., demonstrating the pulse velocity variations. It is clearly seen that the satellite position does not depend on the main pulse position revealing its nature: the satellite begins at the minimum mode-locker losses owing to the inversion recovery.

The model above does *not* allow stable pulses to exist at positive detuning. But in out experiments it was demonstrated that the laser can produce stable pulses even at positive detunings. In our calculations we used oversimplified model for the noise and found the effect of extension of the detuning range, where the pulse is stable, to positive values, Fig.6. (see for comparison [2a]). Before in [5] it was shown that the noise leads to a possibility for the laser to operate in a quasi-steady-state mode-locked regime at zeroth detuning, when the pulse train is episodically disrupted by so-called phase waves. It is worth noting that in our experiments we did not obtain the enhanced noise at positive detuning as in [6]. That was perhaps, because of higher value of the output coupler loss we used. As of now, we have no physical explanation for this effect.

Coherence effects can be seen in Figs.1,2 (afterpulse(-s) ringing at the distance of some hundreds of ps from the main pulse). Experimental realizations for that have been done in [7]. Ripples at the top of the spectrum can be seen in the spectral domain, when the pulse duration is shorter than the value of T_2 (dephasing time). At fixed $T_2 = 0.5$ ns, decrease of T_1 (population inversion decay time) from 5 ns to 0.05 ns leads to many-pulse regime (inside the mode-locker window) and irregular spectrum. At fixed T_1 and variation of T_2 from 1.5 ns to 0.1 ns the coherent satellites become less prominent, the satellite distance from the main pulse decreases, the spectrum is smooth. The spectrum may contain a central dip (in averaged over the 5000 round trips realization) at higher pulse energy inside the cavity, but we do not connect it with the coherence effects.

3 Conclusion

In conclusion, we have shown:

1. The pulse and satellite positions in the temporal mode-locker window. The pulse and satellite evolution is rather complex as detuning occurs.

2. So-called phase characteristics occur for both positive and negative frequency detunings.

3. Dependence of the pulse duration as well as the pulse amplitude, pulse position on the modulation depth.

Acknowledgment. This research is supported in part by the INTAS foundation under grant 97-1058. We thank J.M. Dudley for discussions and giving us a relevant reference [5].

Correspondence should be addressed to V.S. Yakovlev, viakovle@pop.tuwien.ac.at.

References

[1] D.Kuizenga, A.Siegman. **QE-6**, 694 (1970).

[2] See, for example: A.Apolonski et al. **Opt. Communs.**, 98, 291 (1993); **Proc. SPIE**, 2041, 385 (1993); **Kvantovaja Elektronika (Russian)**, 24, 998 (1997).

[3] J.M.Dudley, C.M.Loh, J.D.Harvey. **Quantum Semiclass. Opt.** 8, 1029 (1996).

[4] A.Apolonsky, S.A.Babin, T.T.Timofeev. **Opt. Spectrosc. (USSR)** 59, 714 (1985).

[5] P.D.Drummond, J.D.Harvey, J.M.Dudley, D.B.Hirst, S.J.Carter. **Phys.Rev.Lett.**, 78, 836 (1997).

[6] H.D.Harvey, N.Christensen , J.M.Dudley and D.B.Hirst. **Opt. Communs.**, 97, 219 (1993).

[7] A.Apolonsky. **Opt. Spectrosc.(USSR)**, 61, 564 (1986); J.M.Dudley, J.D.Harvey, R.Leonhardt. **J.Opt.Soc.Am.B**, 10, 840 (1993).

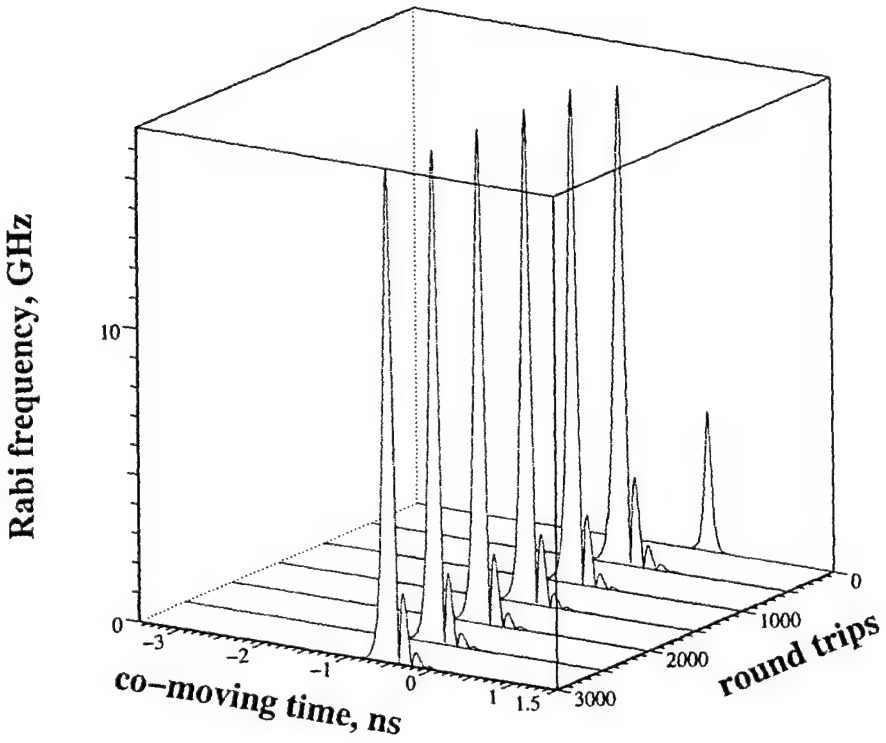

Fig. 1. The pulse shape evolution vs. number of round trips

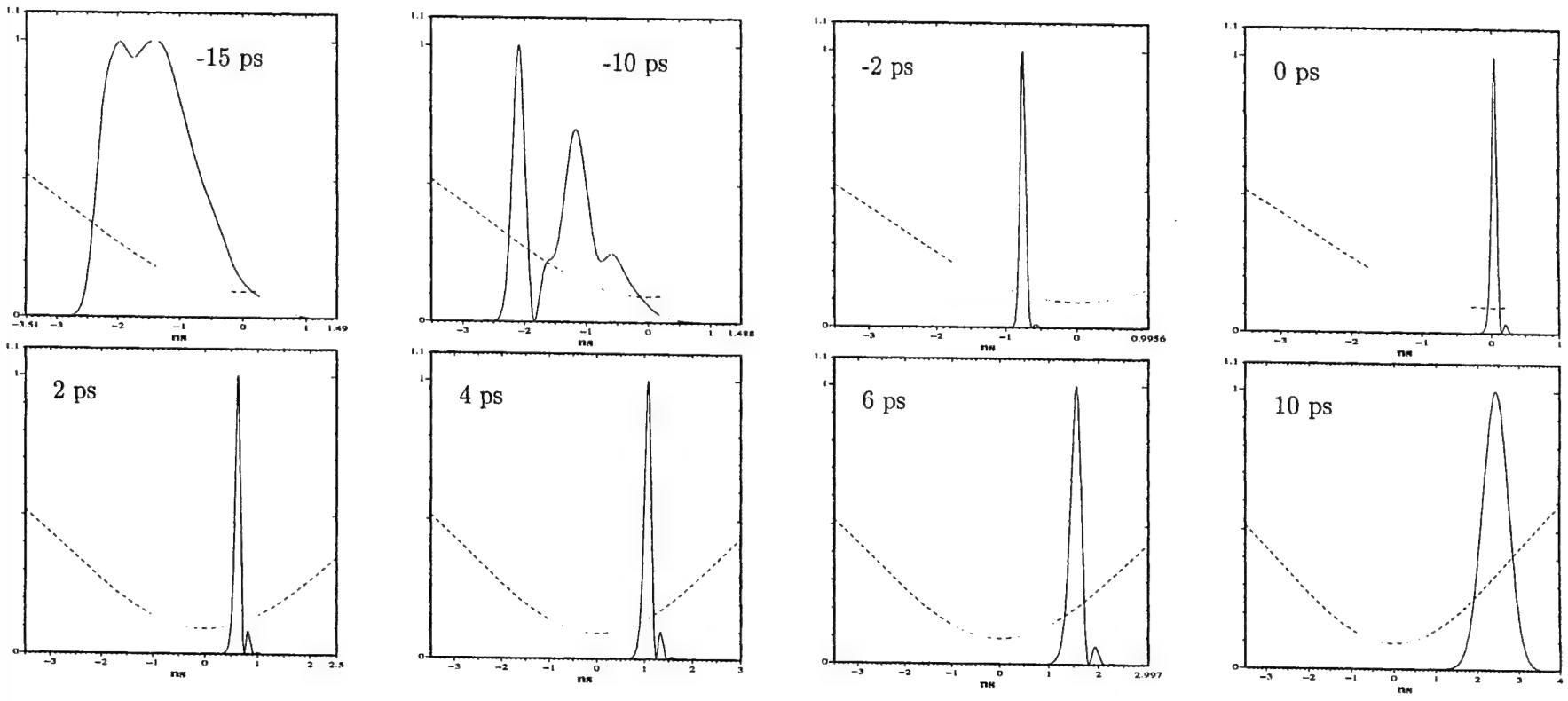

Fig. 2. Pulse shape evolution at different detuning values. The satellite is due to the short inversion recovery time in comparison with the mode-locker "window" width (dashed line). Averaging over 4000 pulses has been done. Afterpulses at the positive detunings are due to the coherence effects

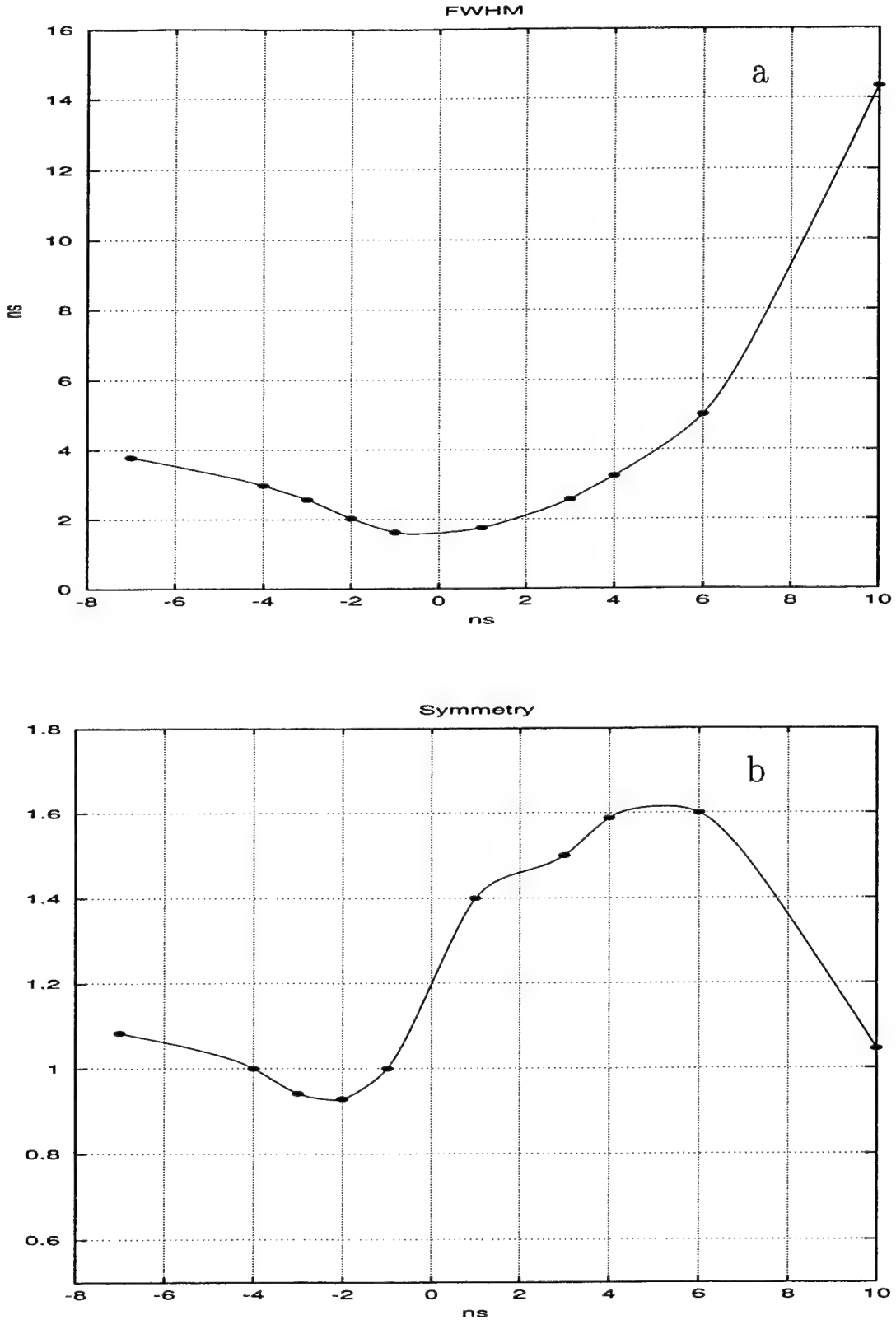

Fig. 3. The pulse duration (a) and its symmetry (b) at different positions in the mode-locker window

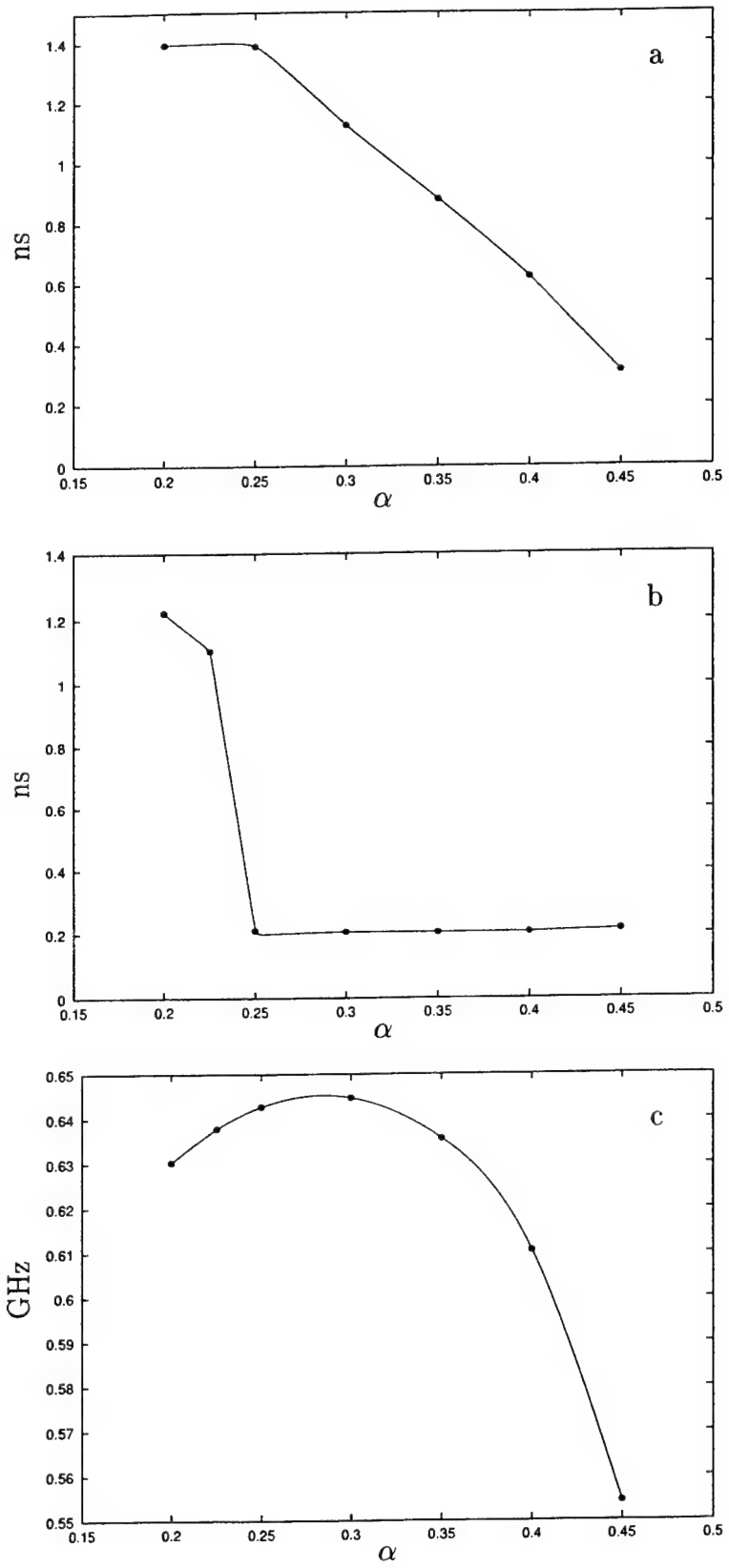

Fig. 4. The pulse parameters versus the modulation depth α: its position inside the mode-locker window (a, zeroth value is the center of the window); duration (b) and amplitude in the Rabi frequency units (c)

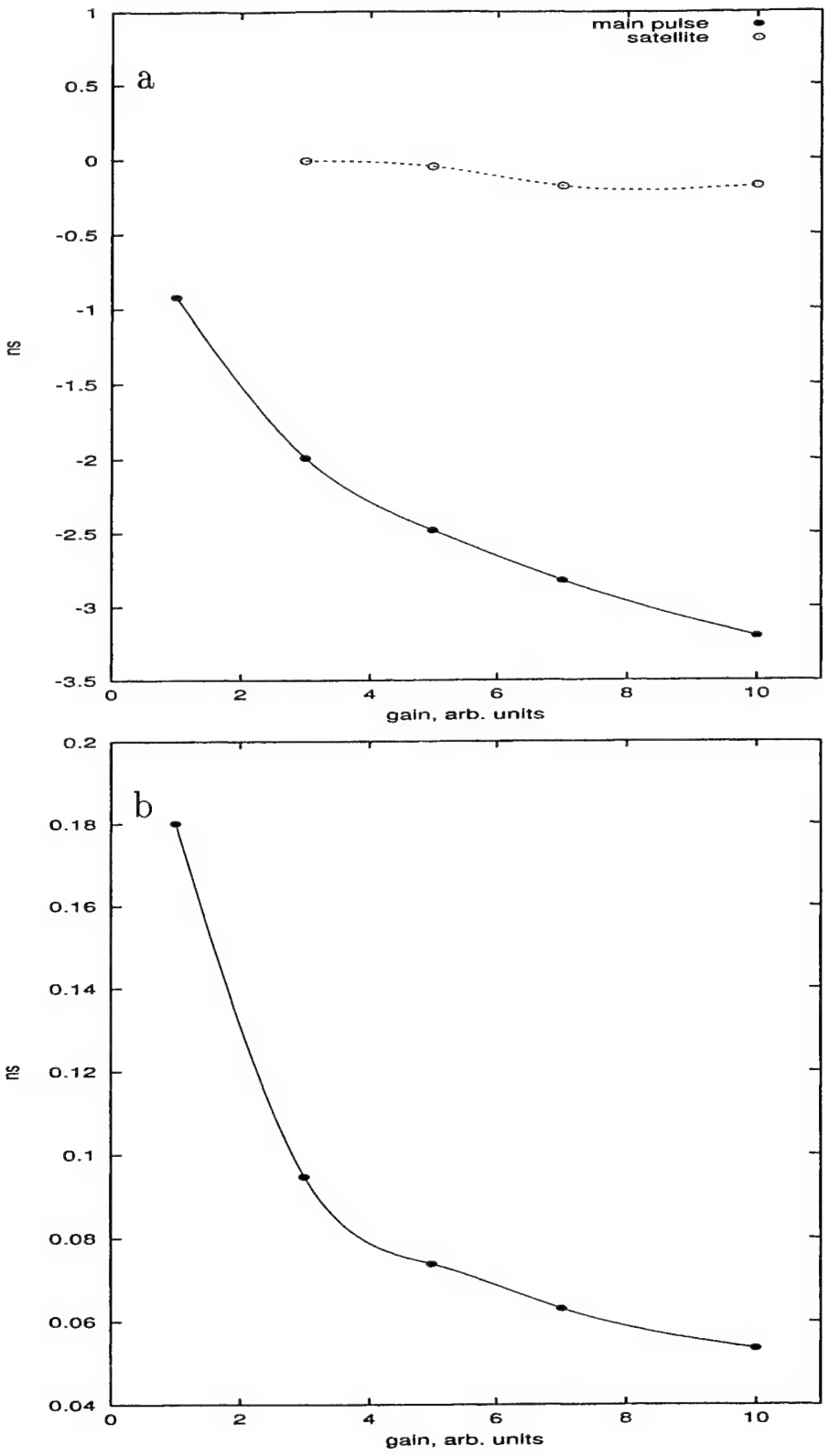

Fig. 5. The pulse/satellite positions inside the mode locker window (a) and the pulse duration (b) as a function of gain

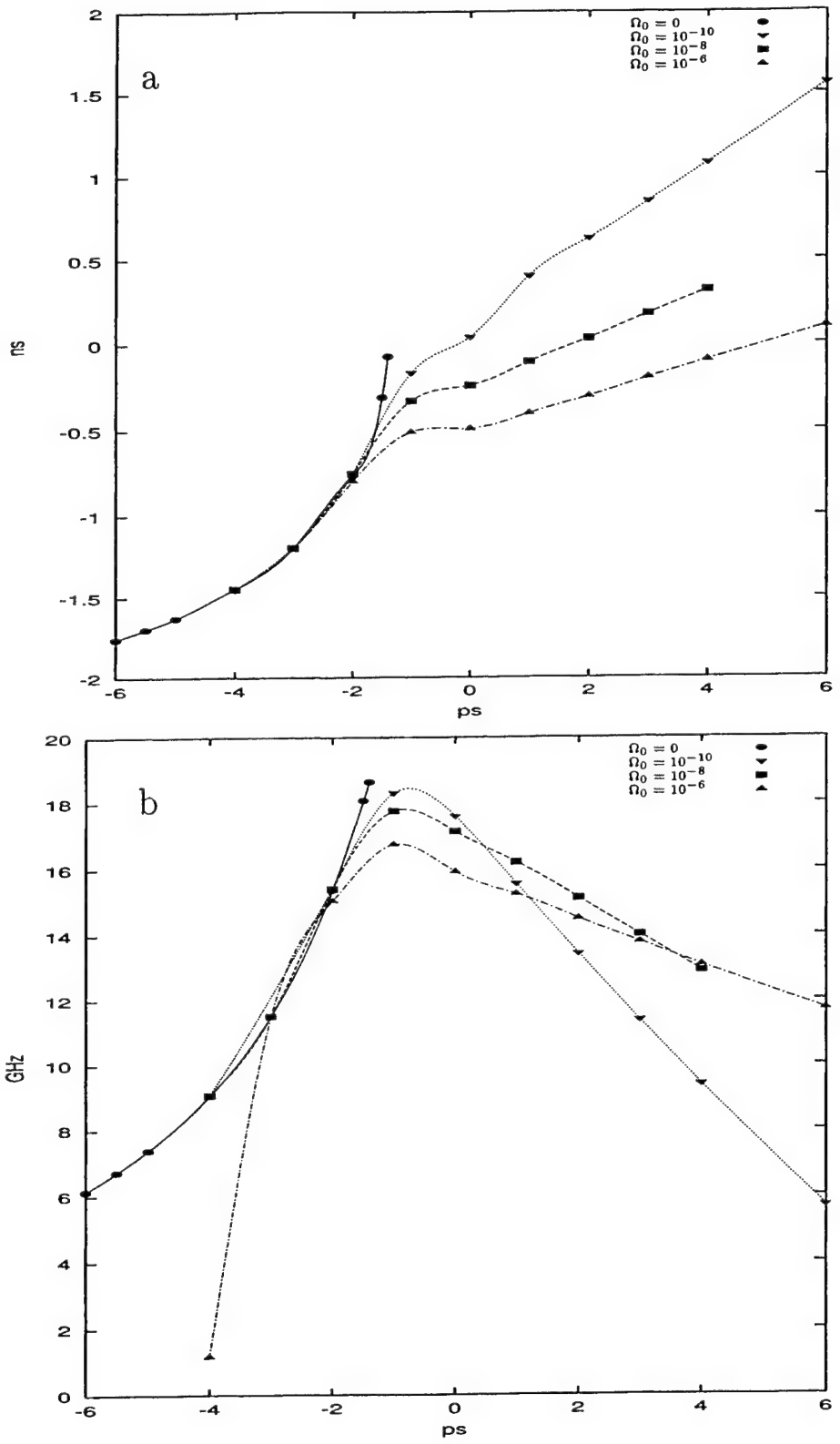

Fig. 6. The pulse position (a) and its amplitude (b) as a function of detuning at different values of "noise" Ω_0

A new high-bandwidth, all-solid-state pulse-shaping system for the OMEGA laser facility

A. V. Okishev, M. D. Skeldon, R. L. Keck, and W. Seka
Laboratory for Laser Energetics, University of Rochester
250 East River Road, Rochester, NY 14623
Phone: 716/275-5101
Fax:716/275-5960
e-mail: aoki@lle.rochester.edu

ABSTRACT

An all-solid-state pulse-shaping system based on a single-frequency master oscillator, preamplifier, and aperture-coupled-stripline electrical waveform generator has been developed and implemented in the OMEGA laser fusion facility.

Keywords: single-frequency, diode-pumped laser; diode-pumped amplifier; integrated optics modulator; aperture-coupled stripline; pulse-shaping; laser fusion.

I. INTRODUCTION

An integral part of the contemporary high-power laser system for inertial confinement fusion (ICF) research is a flexible pulse-shaping system that is able to produce a laser pulse temporal profile specified in advance and controlled to a high degree of accuracy. Temporally shaped optical pulses can be produced by applying shaped electrical waveforms to an integrated-optics (IO) modulator.[1,2] These shaped electrical waveforms are sent to the optical modulator synchronized with the passage through the modulator of a flat-top optical pulse from a single-frequency laser. The optical pulse exiting the modulator is then shaped in accordance with the voltage-dependent transfer function of the modulator. A pulse-shaping system has been in operation on OMEGA for several years.[3] Recently the performance of this pulse-shaping system was significantly improved by replacing the flash-lamp-pumped single-frequency laser with a diode-pumped, computer-controlled master oscillator.[4] Currently the pulse-shaping system uses an electrical-waveform generator based on the reflection of an electrical square pulse from a variable-impedance microstrip line. The electrical square pulse is generated by using a charge line with Si photoconductive switches activated by a single pulse from a laser system. The laser system includes a mode-locked cw timing laser, regenerative amplifier, SBS pulse compressor, and laser amplifiers. The complexity of this laser system motivated us to develop a simplified pulse-shaping system that meets all the pulse-shaping requirements for the OMEGA laser. This system includes a highly stable, diode-pumped, single-frequency master oscillator; a diode-pumped preamplifier; aperture-coupled striplines (ACSL); and commercially available electrical square-pulse generators, which make it a completely solid-state, computer-controlled system.

II. ALL-SOLID-STATE PULSE-SHAPING SYSTEM

The block diagram of OMEGA's new optical pulse-shaping system is shown in Fig. 1. The diode-pumped, single-frequency master oscillator[4] produces highly stable, 150-ns, *Q*-switched laser pulses at 300-Hz repetition rate. A high repetition rate allows us to use a high-bandwidth sampling oscilloscope for the pulse-shape measurement, which provides a higher temporal resolution than a single-shot digital oscilloscope. The flat-top portion of the master oscillator's 150-ns output pulse is used for pulse shaping. A high-repetition-rate slicer produces a 20-ns flat-top pulse from the 150-ns pulse, which eliminates unused energy from the pulse to avoid generating stimulated Brillouin scattering in our single-mode fiber. The diode-pumped, two-pass preamplifier boosts the flat-top pulse energy up to five times to meet OMEGA's pulse-shaping energy requirements (200 nJ per channel). The amplified pulse is launched into a single-mode, polarization-maintaining (PM) fiber, split into four fiber channels, and sent to the IO pulse-shaping modulators. Each pulse-shaping channel consists of two

Laser Optics 2000: Ultrafast Optics and Superstrong Laser Fields, Alexander A. Andreev,
Vladimir E. Yashin, Editors, Proceedings of SPIE Vol. 4352 (2001) © 2001 SPIE · 0277-786X/01/$15.00

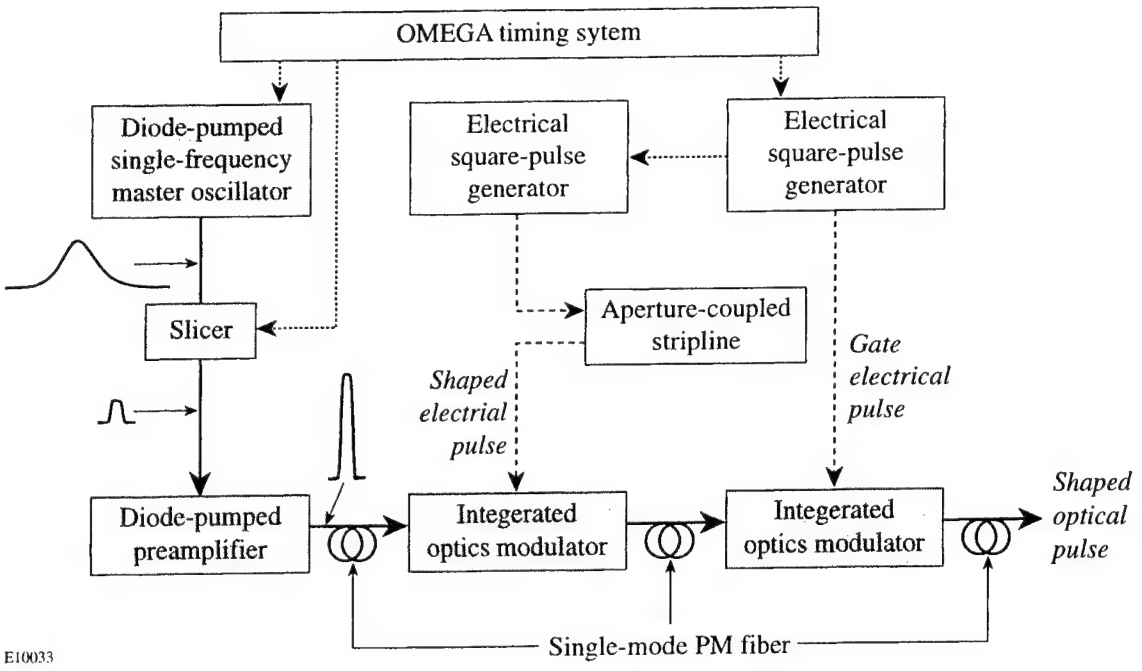

Figure 1. All-solid-state pulse-shaping system for the OMEGA laser system. A single-frequency sliced and amplified pulse from the master oscillator is shaped with a modulator driven by the aperture-coupled-stripline electrical-waveform generator and gated with a modulator driven by a square-pulse generator.

modulators: one shapes the optical pulse, and the other gates the shaped pulse, improving the overall bandwidth and contrast of the pulse. The output shaped optical pulse is sent via a single-mode PM fiber to a regenerative amplifier and then to the OMEGA laser system for amplification and frequency conversion.

III. ACSL-BASED ELECTRICAL WAVEFORM GENERATOR

The optical pulse exiting the modulator is shaped in accordance with the voltage-dependent transfer function of the modulator; hence, the electrical-waveform generator is an important component in any optical-pulse-shaping system incorporating optical modulators.

A square electrical waveform from a commercially available pulse generator is sent to the ACSL.[5] The ACSL generates a shaped electrical waveform that is sent directly to the IO modulator for pulse shaping (Fig. 1). An ACSL is a four-port device consisting of two 50-Ω striplines separated by a ground plane with an aperture to provide directional coupling as shown in Fig. 2. A square pulse propagating along one of the two 50-Ω striplines is coupled to the other stripline in the backward direction. Knowing the electrical coupling coefficient as a function of the aperture width, the ACSL model determines the exact aperture shape to be machined to generate the required electrical waveform.

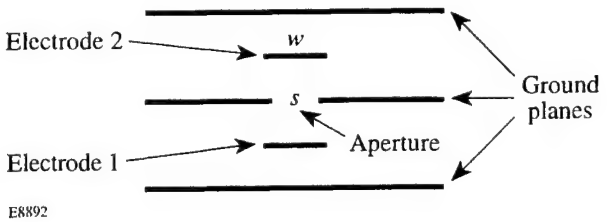

Figure 2. Cross-sectional view of an ACSL in the coupling region. The electrode width w is chosen to provide a 50-Ω impedance structure. The amount of electrical coupling from electrode 1 to electrode 2 depends on the aperture width s.

IV. PULSE-SHAPING SYSTEM'S PERFORMANCE

The temporal profile of the shaped pulse, when amplified and frequency tripled by the OMEGA laser system, must compensate for the temporal distortions caused by both the gain saturation in the amplifiers and the frequency-tripling process, and will produce the desired pulse shape on target. Figure 3 shows the IO modulator's output-pulse shape required to produce a reversed-ramp UV pulse on target. Good agreement is seen between the measured pulse shape and the design shape.

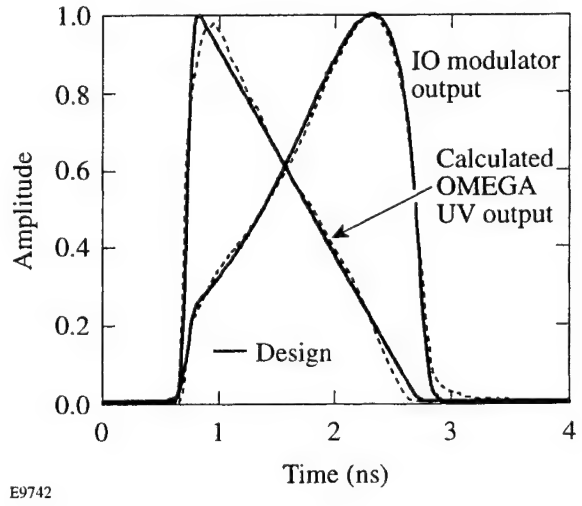

Figure 3. The OMEGA pulse-shaping system is able to produce precisely tailored optical waveforms (reversed ramp pulse shape is shown).

V. PULSE-SHAPING SYSTEM COMPUTER CONTROL

The new OMEGA pulse-shaping system is completely controlled from a computer (Fig. 4). The master oscillator is reset every half-hour and is maintained in a single-frequency regime between resets.[4] The modulator output using fiber splitters is directed to the OMEGA regenerative amplifiers (regens), to a modulator minimization channel, and to pulse-shape diagnostics (fast photodetector and sampling oscilloscope). To produce the required optical waveform each modulator must be reset (minimized), which means that a modulator has zero transmission in the absence of an electrical waveform at a modulator RF port. To accomplish this a computer disables the master oscillator's Q-switch trigger, turning the master oscillator into a truly cw laser.[4] Then using a motorized flipper mount, a half-wave plate is introduced between the slicer polarizers, providing propagation of cw radiation through the modulators. A computer scans the voltage applied to the modulator's dc port and measures the modulator transmission with a photodiode. After finding the voltage that provides zero modulator transmission, the computer sets this voltage at the modulator dc port. When the modulator reset (minimization) procedure is completed, a half-wave plate is removed from the slicer and the master oscillator's Q-switch trigger is restored.

The pulse-shaping system output optical waveform can be tuned to a design goal by using the interface shown in Fig. 5. It recognizes the installed pulse shape, controls the pulse shape in each of four OMEGA pulse-shaping channels, sampling oscilloscope, electrical gate timing and other adjustments. One can plot a modulator output design and on-line measured optical waveforms, regen output and OMEGA UV output design, and calculated optical waveforms. By making small adjustments to an electrical gate timing and modulator dc voltage, it is possible to adjust an optical waveform on-line to a designed goal.

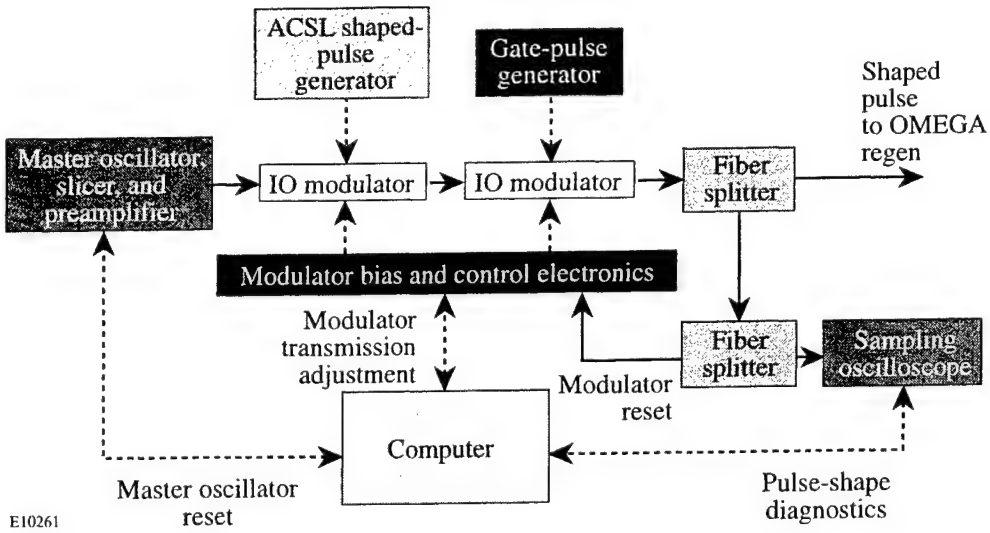

Figure 4. The OMEGA pulse-shaping system is completely controlled from a computer.

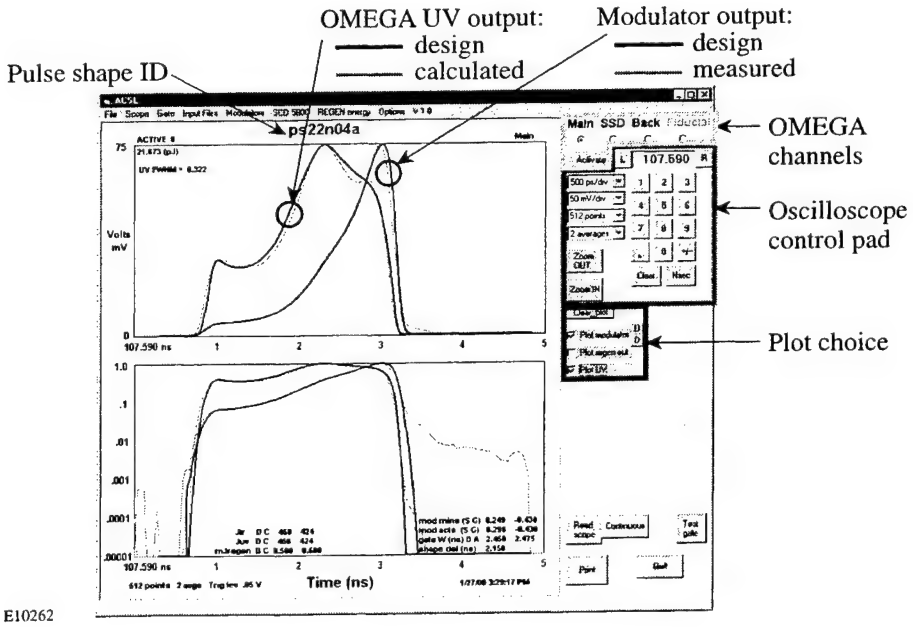

Figure 5. Pulse-shaping system diagnostics provide a possibility of making pulse-shape adjustments on-line.

VI. CONCLUSION

We have developed an all-solid-state, compact, computer-controlled, flexible optical pulse-shaping system for the OMEGA laser facility. This pulse-shaping system produces high-bandwidth, temporally shaped laser pulses that meet OMEGA requirements. The design is a significant simplification over existing technology with improved performance capabilities.

VII. ACKNOWLEDGMENT

This work was supported by the U.S. Department of Energy Office of Inertial Confinement Fusion under Cooperative Agreement No. DE-FC03-92SF19460, the University of Rochester, and the New York State Energy Research and Development Authority. The support of DOE does not constitute an endorsement by DOE of the views expressed in this article.

VIII. REFERENCES

1. R. B. Wilcox, "Pulse shaping with transmission lines," U. S. patent No. 4,667,161 (19 May 1987).
2. R. B. Wilcox, W. Behrendt, D. F. Browning, D. R. Speck, and B. M. Van Wontergem, "Fusion laser oscillator and pulse-forming system using integrated optics," in *Laser Coherence Control: Technology and Applications*, edited by H. T. Powell and T. J. Kessler (SPIE, Bellingham, WA, 1993), Vol. 1870, pp. 53–63.
3. A. V. Okishev, M. D. Skeldon, S. A. Letzring, W. R. Donaldson, A. Babushkin, and W. Seka, "The pulse-shaping system for the 60-beam, 30-kJ (UV) OMEGA laser," in *Superintense Laser Fields*, edited by A. A. Andreev and V. M. Gordienko (SPIE, Bellingham, WA, 1996), Vol. 2770, pp. 10–17.
4. A. V. Okishev, M. D. Skeldon, and W. Seka, "A highly stable, diode-pumped master oscillator for the OMEGA laser facility," in *OSA TOPS on Advanced Solid-State Lasers*, edited by M. M. Fejer, H. Injeyan, and U. Keller (Optical Society of America, Washington, D.C., 1999), Vol. 26, pp. 228–235.
5. M. D. Skeldon, A. V. Okishev, R. L. Keck, S. A. Letzring, and W. Seka, "An optical pulse-shaping system based on aperture-coupled striplines for OMEGA pulse shaping applications," in *Solid State Lasers for Application to Inertial Confinement Fusion*, edited by W. H. Lowdermilk (SPIE, Bellingham, WA, 1999), Vol. 3492, pp. 131–135.

On the threshold lowering of a injection seeding regime in presence of periodic losses modulation in the laser

Boris V. Anikeev, Rimma Sh. Zatrudina, Vladimir V. Rudov

Volgograd State University, Department of Laser Physics
30, 2-ya Prodol'naya St., Volgograd State University, 400062, RUSSIA

ABSTRACT

In development of a known method of an regenerative amplification of low-power picosecond pulses (the injection seeding method) its modification – the method of injection locking (IL) of master laser with the amplifying laser (laser with short-term resonance modulation of losses – STRML-laser) is offered. The use of the STRML-laser as the regenerative amplifier allows to lower a level of the laser - injector power on two – four order. For the neodymium laser with an output pulse energy 1–2 J this power can be lowered up to 1 W, and the reliable capture can be carried out with 5 W. It enables to realize the circuit of self-injection in the STRML-laser by adding a nonlinear passive modulator in a cavity. Thus at a beginning of linear stage it is possible to "sow" pulses resulting in generation of much more short on a comparison with realized in a STRML-regime with preservation of remaining positive qualities of this laser.

On experimental established optical properties of a passive modulator on base of computer model of the STRML-laser checked earlier by physical experiments a reality of a realization of this circuit numerically is confirmed. The experiments with film modulator convince of a possibility of a regenerative amplification of the picosecond ultra-short pulses (USP) in itself laser up to greatest possible (from reasons of optical durability) energies.

1. INTRODUCTION

The principle of the regenerative amplification of the picosecond USP is already realized in an injection seeding method [1–4]. Developed nowadays by some authors this method allows to be approximated to creation of the powerful compact laser source of pico- and femtosecond range. And complexity of a device, its dimensions and autonomy depend on a power and energy of a radiation of the laser-injector.

According to the method, in a cavity of the Q-switching laser on the initial generation stage the pulse is injected which forming of a laser radiation begins. From experiments [4] it is known that for an achievable amplification factor ~10^8 the threshold values of a power density of the single injected pulse for the Nd-glass laser with an output pulse energy 20–200 mJ makes ~10 kW/cm^2 at the pulse duration 3–9 pc. The same authors [5] have shown by experiments that the resonance excitation by injection of the limited (about 15 pulses) train reduces in lowering on approximately four order of a threshold power of pulses for amplifying Nd-laser in such condition with an pulse energy ~0.1 J. But there is additional hardness of capture conditions due to resonance character of interaction. The capture becomes feasible only in a narrow band of detuning.

The capture conditions in an injection seeding regime can be determined from positions of the fluctuation theory of USP forming at large exceeding by an amplification of a generation threshold similarly [6] for the laser with short-term resonance modulation of losses (STRML). According to this approach the USP forming in the beginning of a linear stage begins with one or several maximum (in the range of defined temporal sample) fluctuation field spike of a spontaneous radiation. Then the capture in the injection amplification methods can be presented as an result of a competition in forming between maximum fluctuation spike of a spontaneous radiation and injected USP from the outside.

It is shown that for STRML-laser the characteristic decreasing of duration of the spontaneous radiation sample in a cavity reduces sharply the amplitude of a maximum spike at the expense of slacking of capture conditions. Earlier [7] the analysis of a character of a power increase of a regenerated spontaneous radiation in a cavity of the STRML-laser after Q-switching was made. The stage of forming from the spontaneous radiation to the coherent field component in an amplifying laser contour is defined. It is established that on this stage the increase of an average field power does not happen practically. Below it is shown that thus the amplitude of a maximum noise spike is approximately proportional to duration of sample equal to duration of a stage. But then it is apparent that the reduction of temporal sample at the expense of creation of narrow temporal windows for the injected pulse forming can be an effective method of additional (and considerable) increase of an amplification factor of pulses injected in the Q-switching laser. Just such situation exists in the

Laser Optics 2000: Ultrafast Optics and Superstrong Laser Fields, Alexander A. Andreev, Vladimir E. Yashin, Editors, Proceedings of SPIE Vol. 4352 (2001) © 2001 SPIE · 0277-786X/01/$15.00

STRML-amplifier. But it is already new system for forming of high-energy picosecond pulses. Conceptually it is a modification of an injection seeding method, i.e. it is creation in the amplifier with deep Q-switching of narrow temporal windows on an axial period, in which one of is introduced the low-power USP. For injection the picosecond laser is used, and for an amplification the high-energy STRML-laser is used. The method can be quite submitted by the resonance injection excitation of the power amplification cascade. Let's name it as injection locking method (IL), and its experimental realization - accordingly the IL-system.

The investigations of STRML-lasers have shown [8] that they is easy synchronized by external electrical pulses and have temporal binding to an external signal approximately equal the generated pulse duration (less than 1 ns). They are also capable reliably and with high reproducibility of characteristics of pulses to work in a wide range of the modulation and intermodes frequencies detuning [9]. With use of STRML-lasers as the regenerative amplifier there is a necessity of hit of injected USP in one of temporal windows. I.e. the defined precision of a synchronization of work of lasers is required. If in an injection seeding method this precision equals some axial periods, in an offered method one equals units of percents from an axial period (i.e. ~0.1 ns). But with excitation of the power amplifier by limited USP-train [5] the precision incomparably higher is required.

2. INJECTION LOCKING REGIME

As in any generator the generation in the STRML-laser starts with a level of a spontaneous radiation. The developed model of a STRML-system [7] has allowed to study detailed the process of generation forming. In particular it was defined that on the initial stage (in limits 10–15 round trips) the average field intensity in a cavity practically does not increase. On this stage there is a USP forming from the noise field, exacter there is the spectrum contraction of a selectively amplified luminescence up to a spectrum width of lasing. Only then the real linear stage of generation starts.

The injection capture in a IL-method is most favorable on the first stage of transformation amplified luminescence in a laser radiation. It is much longer than for the Q-switching laser, agrees to fluctuation representations about dynamics of an establishment of generation in the STRML-laser [6]. Due to existence of a delay in forming of own pulse of the amplifying laser generation the injected USP at once begins to amplify intensively, essentially anticipating the natural increase of the luminescence field component.

Let's consider a device of a STRML-contour (Fig.1a). The method of pulse input from the outside is not critical. At first, in experimental practice the series of these circuits are known already. And secondly, optical circuit of the STRML-laser (and in particular, its special modulator) allow to offer the additional input circuits.

In the STRML-laser the used modulators are contrast ~10^3 [10], and the modulation is produced synchronously with each return of pulse in the modulator. The pulse not caught in "a temporal window" has extracted automatically from a cavity. As was established by many experiments [11], the requirements to the coordination of modulation frequency with intermode one are low – up to 2% of detuning. Let's consider that the cavity is formed by a 100% mirror R_1 and output mirror R_2. The temporal diagram of amplification process of injected pulse is submitted in Fig.1b. The STRML-laser in limits of a stage t_1 works in an expecting regime: USP is injected in one of temporal windows after fast Q-switching. In result at amplification more than in 1,6 times exceeding losses in a cavity and low Q-factor of a cavity the single high-contrast USP is radiated [11].

Let's consider correlation between amplitude of maximum spike of spontaneous noise on a time interval ΔT and width of this interval. This connection follows from a relation for the spike number n^+ of spontaneous noise with Rayleigh statistics exceeding the given level C [6]:

$$n^+ = \frac{C\omega_1}{<A_o^2>^{1/2}} \frac{\Delta T}{\Gamma^N(\alpha_o N+1)} \exp\left\{-\frac{C^2(1+\alpha_o N)}{2<A_o^2>\Gamma^{2N}}\right\}. \qquad (1)$$

Here ω_1 is half-width of the gain line, α_0 is the field unsaturated gain in active medium, $\langle A_0^2 \rangle$ is the average power of spontaneous noise, $\Gamma = \exp(\alpha_0 - \gamma)$ is the pulse gain for one round trip, γ is product of mirrors reflectivities, N is quantity of round trips. The required correlation in the implicit form $C_{\max}(\Delta T)$ will be defined from (1) for unique on an interval (i.e. maximum) spike. If Γ is great, at large spectrum width ω_1 the inequality $2(\alpha_o N+1)^3 / \omega_1^2 \Delta T^2 >> 1$ is true. Then the connection between parameters $C_{\max}$ and ΔT becomes approximately linear:

$$C_{\max} \approx 2\omega_1 \Delta T \Gamma^N <A_o^2>^{1/2} /(\alpha_o N+1)^2. \qquad (2)$$

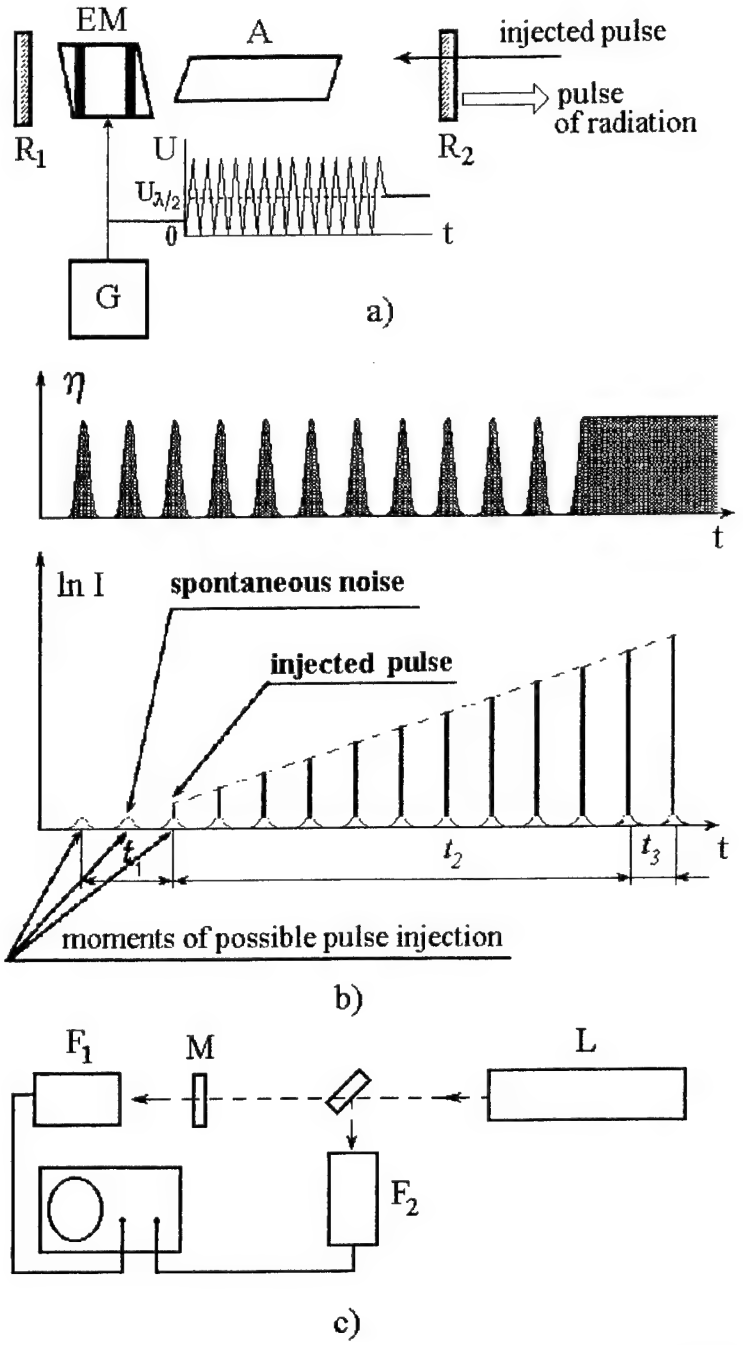

Fig.1. A principle scheme (a) and temporal diagrams of a condition of an electrooptical modulator *EM* and of generation process (b) of a STRML-contour and scheme of a modification of optical properties of a passive modulator. The pulse is injected in a cavity from a mirror R_2 (η is the transparency function of a modulator *EM*, *I* is power of a radiation. (c) – a scheme of measurements of optical characteristics of passive modulator.

It corresponds to the STRML-laser. And as the magnitude ΔT can achieve 10^{-2} from an axial period and Γ essentially more one, (2) reveals of principle difference of a IL-method on a comparison with the injection seeding circuits: intensity of a maximum spike and, accordingly, a power of the injected signal decrease more, than on two order. On evaluations, the average power of noise in axial modes for the Nd-laser with doubly exceeding of a self-excitation threshold with an output pulse energy ~1 J and with an average value of Q-factor equal ~0.1 W. A decrease of maximum spike amplitude in the STRML-laser in the correspondence with (1) gives in a reality also additional decrease of spike amplitude owing to narrow band of gain for regenerated part of a noise field.

The width of a "temporal window" is determined according to [12] as

$$\Delta T = \frac{2}{\Omega}\arcsin\left\{\frac{2}{\pi}\arccos\left(\frac{\lambda_n}{1+3\alpha_o/4-\gamma}\right)^{1/2}\right\}, \quad (3)$$

where $\Delta\Omega$ is intermodes interval, $\lambda_n = 1+\frac{3}{4}\alpha_o - \gamma - \left(\frac{\pi(n+1/2)}{\omega_1 \Delta T}\right)^2$.

Thus the width of a "temporal window" is connected with a line half-width ω_1 by relation:

$$\Delta T = \left(\frac{2}{\Omega\omega_1}\right)^{1/2}\left(1+3\alpha_o/4-\gamma\right)^{-1/4}, \quad (4)$$

and the expansion of an amplification spectrum narrows down additionally a "temporal window" reducing sample of spontaneous noise.

Thus the high-contrast modulation of losses reduces sharply the maximum spike amplitude of spontaneous noise in the beginning of a linear stage of generation according to (2).

3. CALCULATED TEMPORAL CHARACTERISTICS OF A SYSTEM IN THE INJECTION LOCKING REGIME

The numerical experiments for a broadband active medium – Nd-glass and for narrow-band – YAG: Nd^{3+} were carried out. As an example the computation is carried out for high Q-factor of a laser cavity ($R_1 \approx 100\%$, $R_2 \approx 95\%$). As will be shown below the excitation of IL-regime there is possible with a minimum power of injected USP.

There are the profiles of output pulses in Fig.2 with various exceeding by a peak power of injected pulse I_{inj} of an average power of a spontaneous radiation of an active medium in the STRML-contour $I_{sp} = \left\langle A_0^2 \right\rangle$ for a narrow-band active medium (Fig.2a, the duration of injected pulse equals 200 pc) and for broadband active medium (Fig.2b, the duration of injected pulse equals 20 pc). The time of round trips equals 10 ns. As against earlier carried out experiments with the STRML-laser (including numerical), the submitted below dependences show a temporal course of processes in a resonator with high Q-factor (the transparency of mirrors for full round trip is equal 0.95). As it is visible from Fig.2a, with a unsufficient ratio I_{inj}/I_{sp} (profile #1) the injected pulse is badly chosen on a background of spontaneous noise. With increase of a ratio I_{inj}/I_{sp} up to 50 (profile #2) the injected pulse keeps only insignificant tracks of a spontaneous initial field, which smooth out at a nonlinear stage (profile #3). With the same ratio for a broadband active medium (Fig.2b, profile #2 and #3) the part of a spontaneous radiation in the injected pulse will increase somewhat.

The constructed by a computer method at stochastic input conditions with not reproduced from flash to flash realizations of a spontaneous radiation dependences in Fig.2 correspond to oscillograms of laser generation in a IL-regime. These dependences, earlier for the STRML-laser obtaining confirmation in experiments, we use here for numerical experiments. On base of calculations with simulation of a real statistician is like [8] we has been obtained the various dependences of a modification of USP-duration during their forming. The scatter of data on these dependences is connected with not reproduced from flash to flash realizations of the spontaneous noise continuously accompanying process of an amplification injected USP.

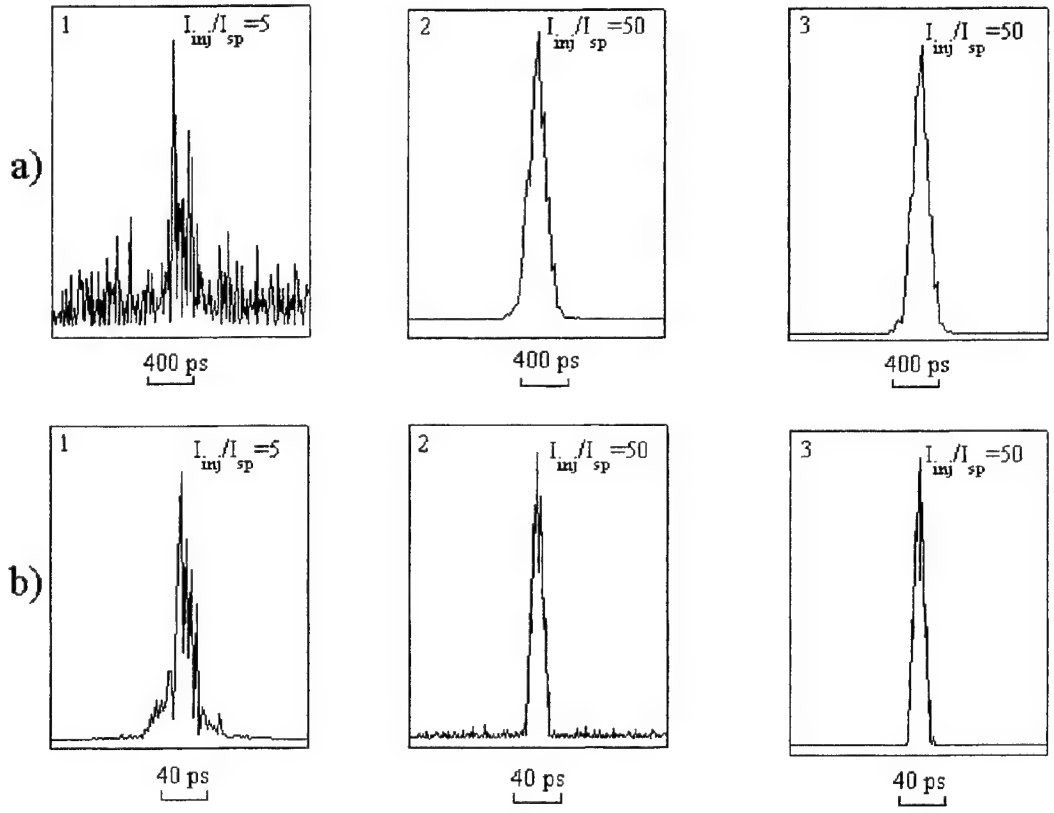

Fig.2. "Oscillograms" on a linear stage after 10 round trips of a STRML-contour for: (a) – narrow-band active medium (#1 – $I_{inj}/I_{sp} = 5$; #2 – $I_{inj}/I_{sp} = 50$; #3 - on a nonlinear stage); (b) – broadband active medium (#1 – $I_{inj}/I_{sp} = 5$; #2 – $I_{inj}/I_{sp} = 50$; #3 – on a nonlinear stage).

However realizing a principle of regenerative amplification in the STRML-laser, as has shown experiment, is possible and without introduction from the outside of USP with the above-stated power. For selection of separate spikes in a maxima of a temporal window it is possible to take advantage of an ordinary passive modulator.

4. TEMPORAL CHARACTERISTICS OF STRML-LASER WITH INTRACAVITY PASSIVE MODULATOR

The light characteristic dependence of a used modulator is necessary for their calculations. Below we used ordinary film modulator. Its optical characteristic was measured with use of a spike radiation of the CW YAG:Nd^{3+}-laser L (Fig.1c). The past through film modulator M radiation was measured by photometer F_1, and the incident radiation on a modulator was measured photodetector F_2. Simultaneously the spikes were photographed from a screen of the two-beam oscilloscope and on a known average power the power of spikes on an oscillogram was determined already. The obtained nonlinear dependence of the modulator transparency is shown in Fig.3.

A computer model of the STRML-laser, with use of which the shown above results were obtained, was supplemented by experimentally defined the transparency function of a passive modulator. There is submitted an USP profile in Fig.4, which is a result of action on the initial spontaneous radiation both passive filter and STRML-mechanism, i.e. of development of generation in conditions rather narrow, but limiting deep temporal windows. The duration of maximum pulse is 3 ps in end of linear stage that is more shorter than the pulse duration of itself STRML-laser. It is visible that as well as with external injection (Fig.2), the laser sharply has reduced the USP duration on a comparison with a usual STRML-regime in the correspondence with a line width of an active medium.

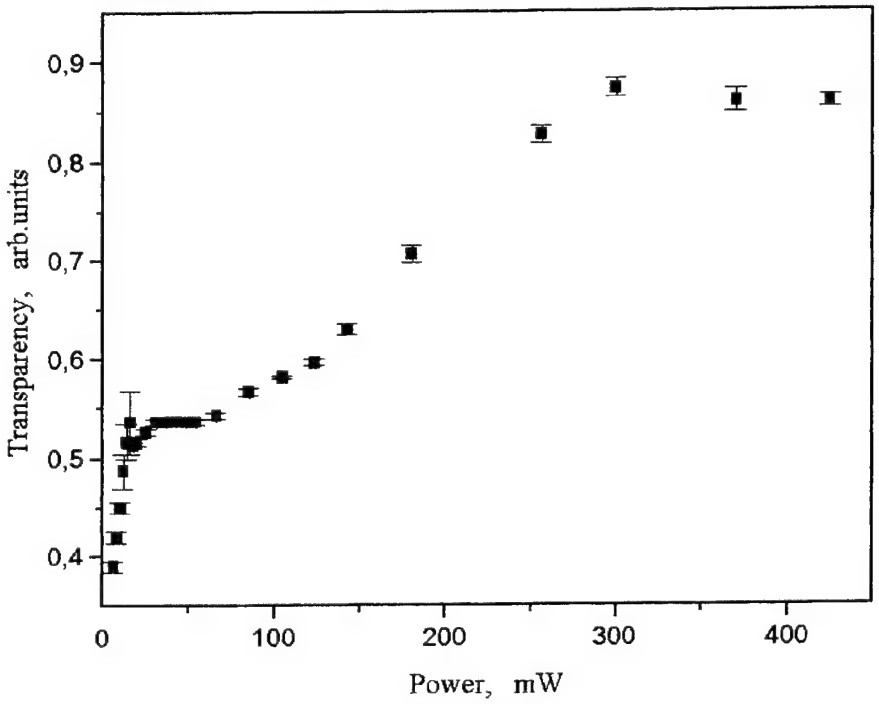

Fig.3. The dependence of a passive modulator transparency versus a spikes power of the CW laser.

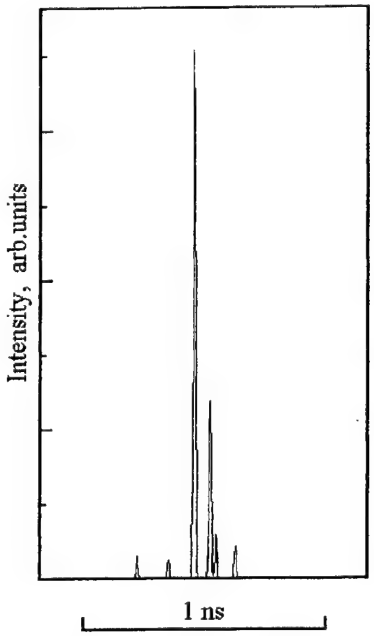

Fig.4. The calculated picture of USP in the Nd-glass STRML-regenerative amplifier with a intracavity passive modulator.

The experimental realization of this idea is made in the Nd-glass laser. In Fig.5a the usually poorly reproduced from flash to flash picture of generation of the laser with a passive mode locking is submitted. The laser with intracavity film modulator corresponded to Fig.1a, but to an electrooptical modulator EM any electrical signal did not apply. With switching of the STRML-circuit, i.e. with applying the appropriate signal to the modulator the picture sharply varied and had ~100%-s' reproducibility, and USP (see Fig.5b) were shortened in the correspondence with calculated in Fig.4. The

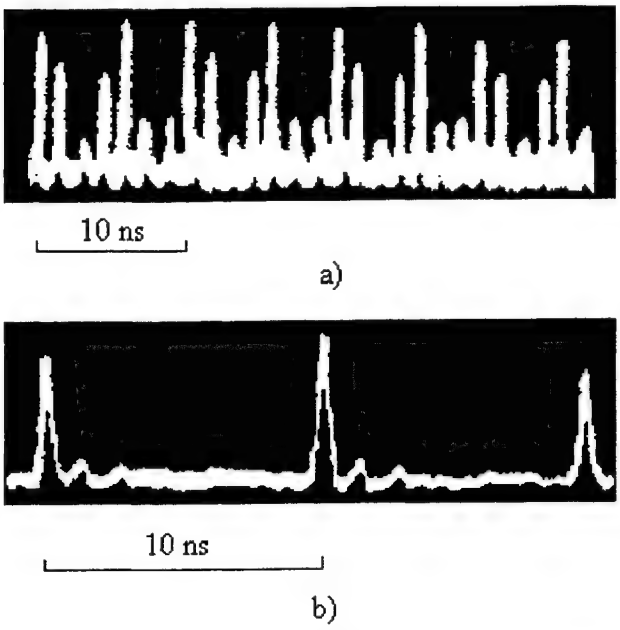

Fig.5. The USP shapes is obtained with use of a coaxial photocell: (a) – of passive mode locking laser; (b) – in that the laser, but with applied Q-switching on a STRML-principle.

additional pulses in Fig.5b are connected to oscillations in electrical circuits of photodetector with a time resolution not better $5 \cdot 10^{-10}$ s.

Thus the experiment convinces in perspective of the injection seeding idea.

5. REFERENCES

1. A.E. Siegmann, *Lasers*, Mill Valley CA, USA, University Science, 1986.
2. G. Basu, R.L. Byer, "Short Pulse Injection seeding of Q-Switched Nd: Glass Laser Oscillators - Theory and Experiment", *IEEE Journal of Quantum Electronics*, **26** (1), 149-157 (1990).
3. I.M. Bel'dyugin, M.V. Zolotarev, I.V. Shinkareva, "Statistical analysis of phase locking of optically coupled lasers with internal injection of low-noise radiation", *Kvantovaya Elektronika*, **24** (1), 37–41 (1997) (in Russian).
4. R.A. Ganeev, F.Sh. Ganikhanov, V.I. Redkorechev, T. Usmanov, "Investigation of the parameters of a high power picosecond feedback controlled chirp pulsed amplified Nd:glass laser with injection seeding", *Optical and Quantum Electronics*, **28**, 1747-1757 (1996).
5. R.A. Ganeev, F.Sh. Ganikhanov, Sh.R. Kamalov, V.I. Redkorechev, T. Usmanov, "Highly efficient neodymium glass and YAG picosecond pulse amplifiers", *Kvantovaya Elektronika*, **23** (12), 1065–1068 (1996) (in Russian).
6. B.V. Anikeev, A.I. Khizhnyak, "Pulse laser with short-term periodic modulation of losses", In: *Quantum electronics*, Naukova Dumka, Kiev, 38, 3–15, 1985 (in Russian).
7. B.V. Anikeev, R.Sh. Zatrudiva, "Numerical model of STPML-laser with narrow-band gain". In: *Diagnostic applications of lasers and fiber optics*, Saratov, SSU, 21–26, 1989 (in Russian).
8. V.N. Khramov, R.Sh. Zatrudiva, B.V. Anikeev, "Precision of the synchronization of subnanosecond laser pulses with brief periodic Q switching", **23** (7), 626–629 (1993).
9. V.N. Khramov, R.Sh. Zatrudiva, B.V. Anikeev, "Reproducibility of Parameters of Pulses Produced by Lasers with Short-Term Periodic Modulation of Losses", *Laser Physics*, **3** (3), 559–565 (1993).
10. B.V. Anikeev, "Investigation of Pockels double shutter in laser with active spectrum phasing", In: *Quantum electronics*, Naukova Dumka, Kiev, 17, 77–80, 1978 (in Russian).
11. B.V. Anikeev, V.N. Khramov, K.A. Levin, "Neodymium lasers with short-term periodic loss modulation", *Quantum Electronics*, **26** (1) 57–59 (1996).
12. B.V. Anikeev, R.Sh. Zatrudiva, V.N. Khramov, "Spectroscopy of Supermodes in an SPML Laser", *Laser Physics*, **4** (3), 457–466 (1994).

Theory of sub-10 fs generation in Kerr-lens mode-locked solid-state lasers with a coherent semiconductor absorber

V. L. Kalashnikov, I. G. Poloyko
International Laser Center, 65 Skorina Ave., Bldg. 17, Minsk, 220027 Belarus
tel./fax: /375-0172/ 326-286, e-mail: vkal@ilc.unibel.by

ABSTRACT

The results of the study of ultra-short pulse generation in continuous-wave Kerr-lens mode-locked (KLM) solid-state lasers with semiconductor saturable absorbers are presented. The issues of extremely short pulse generation are addressed in the frames of the theory that accounts for the coherent nature of the absorber-pulse interaction. We developed an analytical model that bases on the coupled generalized Landau-Ginzburg laser equation and Bloch equations for coherent absorber. We showed, that in the absence of KLM semiconductor absorber produces 2π– non-soliton pulses of self-induced transparency, while the KLM provides an extremely short soliton generation. 2π– and π– *sech*-shaped soliton solutions and variable-squared chirped solutions have been found. It was shown, that the presence of KLM loosens the stability requirements for ultra-short pulse generation removing the limitation on the minimal modulation depth in absorber necessary for the pulse stabilization. An automudulation stability and self-starting ability analysis is presented.

Keywords: ultrashort pulse, semiconductor absorber, self-induced transparency, soliton, Kerr-lens mode locking

1. INTRODUCTION

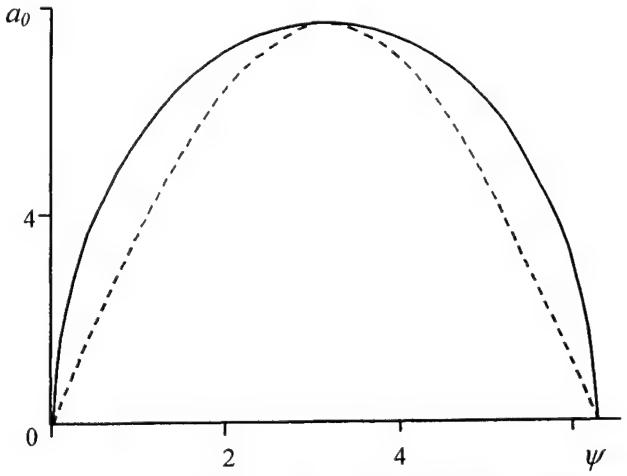

Fig. 1. 2π-pulse envelope in the coordinates "pulse amplitude – pulse square" as resulted from numerical solution of Eq. (5 (solid curve) and the *sech*-shaped pulse envelope (dashed curve) γ=0.04, γ_a=0.01, δ=0.042, t_f=2.5 fs.

A rapid progress in ultra-fast lasers has resulted in generation of sub-10 fs pulses, which is close to the fundamental limit defined by the light wave period in near-IR[1]. Today a basic technique for fs-generation is the Kerr-lens mode locking[2] in combination with a slow saturation of interband or excitonic transitions in semiconductor structure[3]. It was shown[4], that in both cases a soliton formation plays the key role. The soliton mechanism stabilizes an ultra-short pulse generation and works efficiently down to shortest possible pulse durations. Moreover, the soliton generation due to its highest stability and simple pulse form is of highest practical importance, which stimulates the investigations in this field.

It was shown in[5, 6], that the strong nonlinear effects in semiconductor absorbers, such as absorption linewidth enhancement and Stark effect, transform the condition for soliton formation, that leads to an additional pulse stabilization and compression. Since the pulse durations in modern ultrafast lasers are comparable or shorter than the absorber dephasing time t_{coh}, the coherent nature of the pulse-absorber interaction has to be taken into consideration. A coherent absorber mode locking has been analyzed in refs.[7-10]. In particular, it was shown in[7-9] that the dynamical gain saturation is essential for the coherent soliton generation in lasers. However, the latter is negligible in femtosecond solid-state lasers, where the dominating nonlinear factors are self-phase modulation (SPM) and self-focusing. Numerical simulations[10] have demonstrated the generation of fs-pulses of self-induced transparency in solid-state laser with semiconductor quantum-well absorber with no Kerr-lensing in the system. It was shown, however[11], that Kerr self-focusing is essential in fs time domain and should be taken into account in the analysis. Furthermore, an analytical solution for this problem is still lacking which might provide a new insight into the physics of fs-lasers and semiconductor optical devices.

Laser Optics 2000: Ultrafast Optics and Superstrong Laser Fields, Alexander A. Andreev, Vladimir E. Yashin, Editors, Proceedings of SPIE Vol. 4352 (2001) © 2001 SPIE · 0277-786X/01/$15.00

Here we present a study of fs-soliton generation in cw solid-state Kerr-lens mode-locked laser with semiconductor absorber. We developed an analytical model that accounts for coherent absorption in semiconductor, SPM, KLM, group-velocity dispersion and gain saturation by the full pulse energy. The condition of the soliton (*sech*-shaped pulse) formation is found and the contribution of Kerr-lensing to soliton formation is demonstrated. We showed that the generation of chirp-free 2π- and π- solitons and chirped quasi-solitons with variable square is possible. The solutions obtained are stable against laser noise with no limitation on the minimal necessary modulation depth introduced by absorber. An automodulational stability and self-starting ability of mode locking are estimated, too.

A rapid progress in ultra-fast lasers has resulted in generation of sub-10 fs pulses, which is close to the fundamental limit defined by the light wave period in near-IR[1]. Today a basic technique for fs-generation is the Kerr-lens mode locking[2] in combination with a slow saturation of interband or excitonic transitions in semiconductor structure[3]. It was shown[4], that in both cases a soliton formation plays the key role. The soliton mechanism stabilizes an ultra-short pulse generation and works efficiently down to shortest possible pulse durations. Moreover, the soliton generation due to its highest stability and simple pulse form is of highest practical importance, which stimulates the investigations in this field.

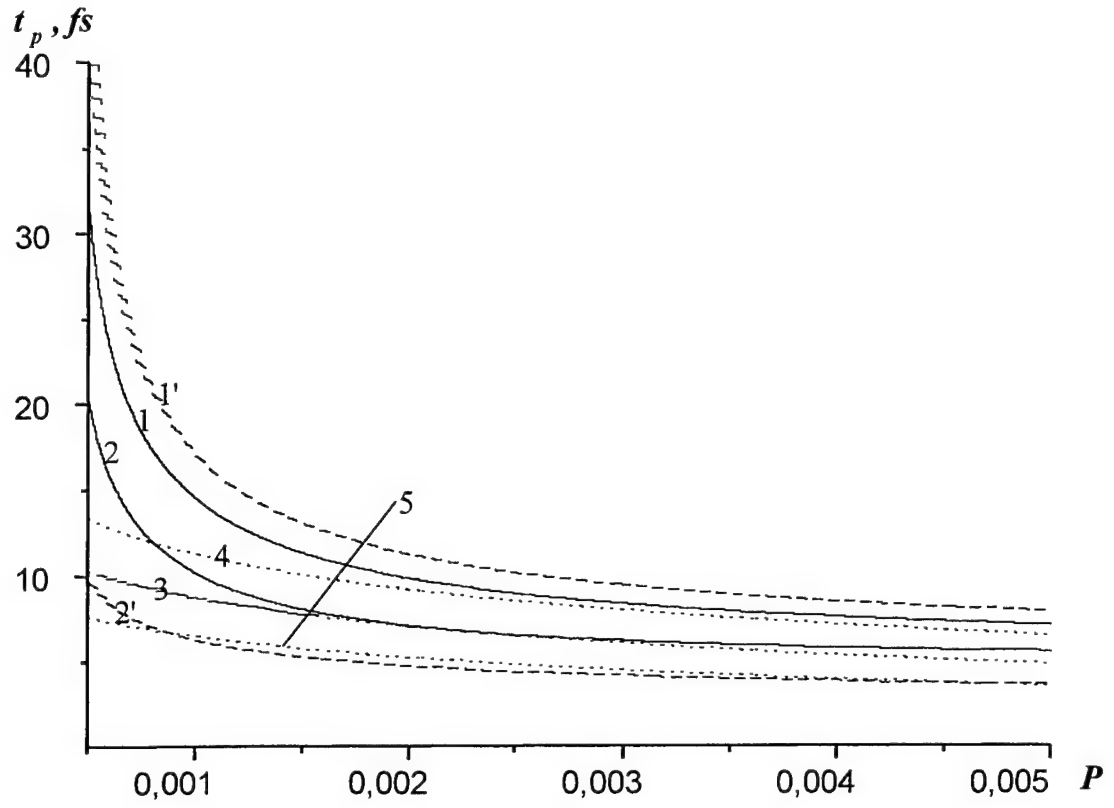

Fig. 2. Pulse duration t_p versus pump P. 2π-pulses (*1*, *2*) in the absence and (*1'*, *2'*) in the presence of SPM. (*2*, *2'*) – unstable against the noise solutions. (*3*) 2π-soliton; (*4*) π-soliton; and (*5*) chirped quasi-soliton (σ=0.14, β=0.26) with the KLM present in the system. α_{max}=0.1, T_r=3 μs, T_{cav}=10 ns, τ=6.25×10^{-4}, γ=0.01, η= 1 (*1*, *1'*, *2*, *2'*), 0.5 (*3*), 0.2 (*4*), 0.3 (*5*).

It was shown in[5, 6], that the strong nonlinear effects in semiconductor absorbers, such as absorption linewidth enhancement and Stark effect, transform the condition for soliton formation, that leads to an additional pulse stabilization and compression. Since the pulse durations in modern ultrafast lasers are comparable or shorter than the absorber dephasing time t_{coh}, the coherent nature of the pulse-absorber interaction has to be taken into consideration. A coherent absorber mode locking has been analyzed in refs.[7-10]. In particular, it was shown in[7-9] that the dynamical gain saturation is essential for the coherent soliton generation in lasers. However, the latter is negligible in femtosecond solid-state lasers, where the dominating nonlinear factors are self-phase modulation (SPM) and self-focusing. Numerical simulations[10] have demonstrated the generation of fs-pulses of self-induced transparency in solid-state laser with semiconductor quantum-well absorber with no

Kerr-lensing in the system. It was shown, however[11], that Kerr self-focusing is essential in fs time domain and should be taken into account in the analysis. Furthermore, an analytical solution for this problem is still lacking which might provide a new insight into the physics of fs-lasers and semiconductor optical devices.

Here we present a study of fs-soliton generation in cw solid-state Kerr-lens mode-locked laser with semiconductor absorber. We developed an analytical model that accounts for coherent absorption in semiconductor, SPM, KLM, group-velocity dispersion and gain saturation by the full pulse energy. The condition of the soliton (*sech*-shaped pulse) formation is found and the contribution of Kerr-lensing to soliton formation is demonstrated. We showed that the generation of chirp-free 2π- and π- solitons and chirped quasi-solitons with variable square is possible. The solutions obtained are stable against laser noise with no limitation on the minimal necessary modulation depth introduced by absorber. An automodulational stability and self-starting ability of mode locking are estimated, too.

2. MODEL

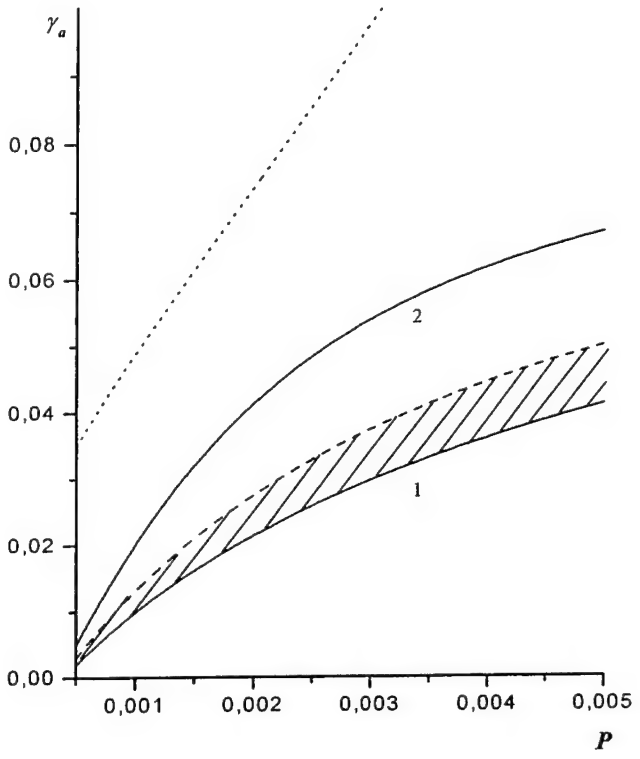

Fig. 3. Minimal modulation depth of absorber γ_a for (*1*) stable and (*2*) unstable 2π-pulse, (dashed curve) generation threshold and (dotted curve) maximal modulation depth for π-pulse. Dashed region is a stability zone. η=1 (*1*, *2*), 0.2 (dotted curve).

Based on the slowly varying envelope approximation for the field amplitude $a(t)$, we consider a distributed system including saturable gain α, linear loss γ, SPM β, Kerr-lens-induced fast saturable absorption with saturation intensity $1/\sigma$, group-velocity dispersion D and bandwidth limiting element with transmission band $1/t_f$. To account for the coherent interaction with the semiconductor absorber while staying in frame of analytic approach we adopted a two-level model of energy levels in semiconductor. This assumption is valid for quantum-confined semiconductor structures utilized in mode-locked fs-lasers.

When the pulse duration is much shorter than the dephasing time in absorber, $t_p \ll t_{coh}$ and the field intensity $|a(t)|^2$ is not enough for the Stark effect manifestation, the pulse-semiconductor interaction obeys the Bloch equations[12]:

$$\frac{du}{dt} = (\Delta - \frac{d\phi}{dt})v + qaw,$$
$$\frac{dv}{dt} = -(\Delta - \frac{d\phi}{dt})u, \qquad (1)$$
$$\frac{dw}{dt} = -qau,$$

where $u(t)$, $v(t)$ and $w(t)$ are the slowly varying envelopes of the polarization quadrature components and the population difference, respectively, $q=d/\hbar$, d= 0.28e Coulomb×nm is the dipole momentum, e is the elementary charge (in our calculations we used the parameters of GaAs/AlAs absorber, the saturation energy E_a=50 μJ/cm^2 and t_{coh}=50 fs), Δ is the mismatch between optical resonance and pulse carrier frequency, ϕ is the instant field phase. An initial saturable absorption $\gamma_a = 2\pi N d^2 \omega z_a t_{coh}/(c\hbar) = 0.01$ (ω is the field frequency) corresponds to the carriers density $N = \gamma_a E_d/(\hbar \omega z_a) = 2\times10^{18}$ cm^{-3} and the thickness of semiconductor absorber z_a=10 nm.

The laser part of the master equation is the generalized Landau-Ginzburg equation[2]. Then the master laser equation can be written as:

$$\frac{\partial a(z,t)}{\partial z} = \left[\alpha - \gamma + i\theta + \delta\frac{\partial}{\partial t} + (t_f^2 + iD)\frac{\partial^2}{\partial t^2} + \frac{\sigma - i\beta}{\eta^2}|a|^2\right]a + \frac{2\pi N z_a \omega d}{c}u - \frac{2\pi N z_a d}{c}\frac{dv}{dt}, \qquad (2)$$

where z is the longitudinal coordinate normalized to the cavity length, i.e. the number of the cavity round-trip, c is the light velocity, θ and δ are the phase and time field delay after the cavity round-trip, respectively. We neglected the spatial effects in the absorber. In what follows we shall consider only steady-state pulsed solutions, which allows to eliminate the dependence on z. We normalized the times to t_f and the field to qt_f. β and σ are normalized to $(2qt_f)^2/nc\varepsilon_0 = 5\times10^{-12}$ cm^2/W, where n is the index of refractivity, ε_0 is the permittivity and t_f=2.5 fs (Ti: sapphire laser). With this normalizations σ=0.14 corresponds to the saturation parameter of Kerr-lens induced fast saturable absorber of 10^7 W and 30 μm spot size in active medium. Dimensionless SPM parameter β is equal to 0.26 for 1 mm thick Ti: sapphire crystal. (Note, however, a

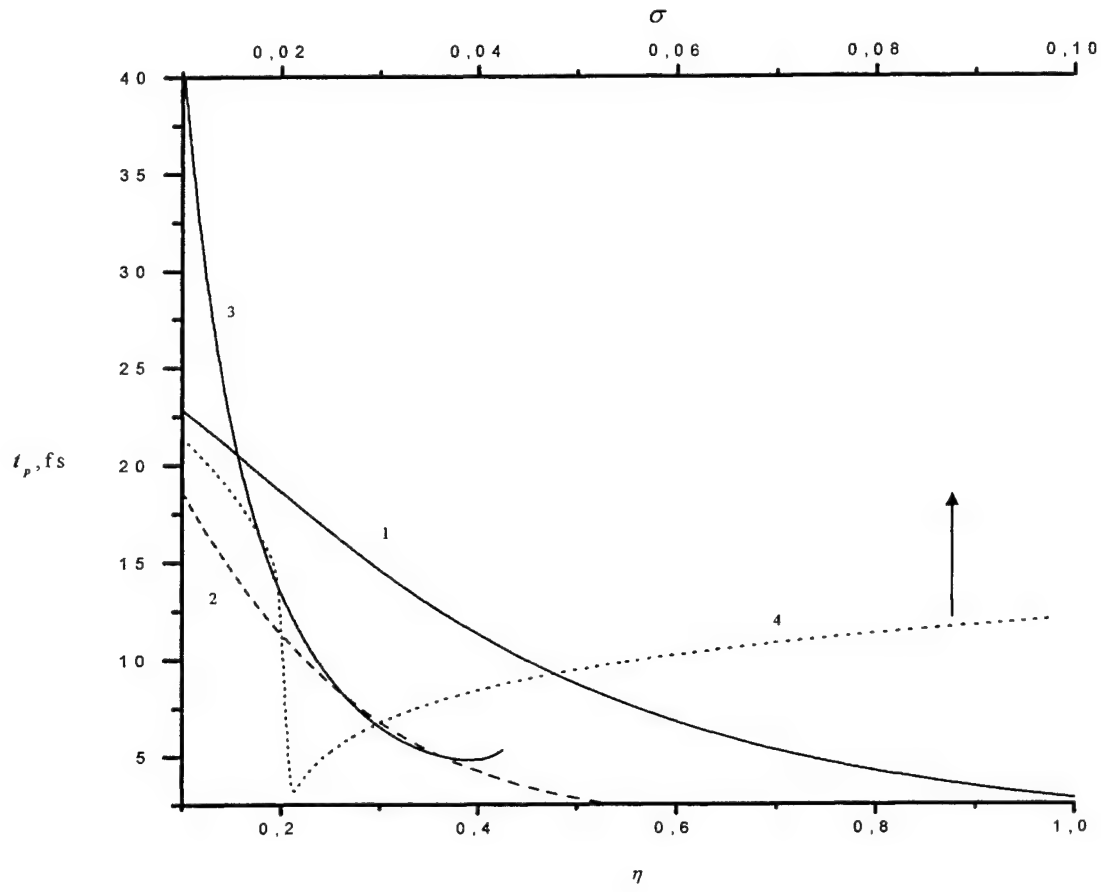

Fig. 4. Pulse duration t_p versus (solid and dashed curves) η and (dotted curve) σ in the presence of KLM for (*1*) 2π-soliton; (*2*) π-soliton; (*3*) chirped quasi-soliton for σ=0.14, β=0.26; (*4*) chirped quasi-soliton for η=0.2, β=0.26. P=0.001 for all curves.

dimensioned pulse duration in Figs. 2 and 4). Additionally, we introduced an important control parameter η, which is governed by 1) the ratio between the size of generation mode in active medium and in semiconductor absorber or by 2) the reflectivity of the upper surface of the semiconductor saturable device. Formally, the variation of η means the variation of relative contribution of SPM, Kerr-lens-induced saturable absorption or saturable gain with respect to the saturable absorption in semiconductor.

As we shall see later, the gain saturation by the full pulse energy is an important factor for the pulse stability and thus should be taken into account. The simplest way to do this is to use a quasi-two level model for active medium. After some calculations for the gain saturated by the full pulse energy E in the steady-state condition we have

$\alpha = \dfrac{P\alpha_{max}}{P + \tau E/\eta^2 + 1/T_r}$, where α_{max} is the gain for the full population inversion, T_r is the gain relaxation time normalized to the cavity period T_{cav}, $P = \sigma_{14}T_{cav}I_p/h\nu_p$ is the dimensionless pump intensity, ν_p is the pump frequency, σ_{14} is the absorption cross section of active medium, I_p is the pump intensity, τ=6.25×10^{-4} is the normalized inverse energy of the gain saturation.

Later we will consider the different simplifying realizations of our model aimed to investigation of the pulse solution of the system (1, 2).

3. PULSE OF THE SELF-INDUCED TRANSPARENCY IN THE ABSENCE OF KLM

We consider the case Δ=0 and restrict ourselves to the case of chirp-free solutions. After integration the equations (1) the master equation (2) reads:

$$\frac{\partial a(z,t)}{\partial z} = \left[\alpha - \gamma + i\theta + \delta\frac{\partial}{\partial t} + (1+iD)\frac{\partial^2}{\partial t^2} + \frac{\sigma - i\beta}{\eta^2}|a|^2\right]a - \frac{\gamma_a}{t_{coh}}\sin(\psi(z,t)), \qquad (3)$$

where $\psi(z,t) = \int_{-\infty}^{t} a(z,t')dt'$ is the pulse square (note, that the field and time are dimensionless quantities here). Under steady-state condition (the pulse envelope is independent on z), an integro-differential Eq. (3) transforms to the differential equation

$$\left[(\alpha - \gamma + i\theta)\frac{d}{dt} + \delta\frac{d^2}{dt^2} + (1+iD)\frac{d^3}{dt^3} + \frac{\sigma - i\beta}{\eta^2}\left(\frac{d\psi(t)}{dt}\right)^2\frac{d}{dt}\right]\psi(t) - \frac{\gamma_a}{t_{coh}}\sin(\psi(t)) = 0. \qquad (4)$$

In the absence of the lasing factors we have a well-known nonlinear equation of the Klein-Gordon's type with 2π-soliton solution in the form $a(t)=a_0 sech(t/t_p)$, where a_0 is the amplitude, t_p is the duration[12]. But this solution does not satisfy the full Eq. (4) in the absence of KLM (σ=0). Further we consider the Eq. (4) neglecting the KLM, SPM and GVD ($\sigma=\beta=D=\theta=0$).

The substitution $\psi(t) = x$, $d\psi(t)/dt = y(x)$ ("square-amplitude" representation) reduces the third-order Eq. (4) to the second-order one:

$$\left[\left(\frac{d^2y}{dx^2}\right)y + \left(\frac{dy}{dx}\right)^2 + \delta\frac{dy}{dx} + (\alpha - \gamma)\right]y - \frac{\gamma_a}{t_{coh}}\sin(x) = 0. \qquad (5)$$

We solved this equation numerically and found a nonsoliton (i.e. non-*sech*-shaped) 2π-solutions for it (see Fig. 1, where numerical solution is shown in comparison with the *sech*-shaped pulse). This clearly indicates on some additional nonlinear factors which are necessary for the soliton formation and which are absent in Eq. (5).

However, 2π- nonsoliton solution is worth more detailed investigation for it might be relevant mechanism for ultimately short pulse generation in real lasers. As is known[4], the main mechanism of destabilization of fs-pulses is the noise generation as result of loss saturation in absorber. In the case of 2π-pulse formation, the Rabi flopping of the absorber population suppresses the noise behind the pulse tail, thus stabilizing fs-generation[10].

To investigate the pulsed solutions of Eq. (5) analytically, we used a harmonic approximation: $y(x) = a_1 sin(x/2) + a_2 sin(x) + \ldots$. Retaining only the first term, in the "square-amplitude" representation, we arrive to the solution $a_1 = 2\sqrt{2(\alpha-\gamma)}$, $\delta = \gamma_a/(2(\alpha-\gamma)t_{coh})$, $t_p = 2/a_1$, which corresponds to *sech*-shaped solution in the "time-amplitude" representation. The relations between pulse parameters are analogues to that ones for 2π *sech*-shaped solution, except an additional relation arising between pulse amplitude and lasing factors α and γ.

Fig. 2 (curves *1* and *2*) presents the pulse durations for two physical solutions of Eq. (5). One can see, that the coherent absorber provides sub-10 fs pulse generation starting from some minimal pump. An important feature of this solution is the positive difference between saturated gain and linear loss $\alpha-\gamma > 0$, which imposes a requirement on the possible minimal saturable loss γ_a necessary for stable pulse generation, i.e. the minimal modulation depth of absorber that confines the region of the pulse stability against laser noise. As it was shown in[2], the pulse is stable if the net-gain outside pulse is negative that produces the condition $\alpha-\gamma-\gamma_a<0$, i.e. $\gamma_a>\alpha-\gamma$. The dependence of the minimal modulation depth on the pump is shown in Fig. 3 for two physical solutions of Eq. (5) presented in Fig. 2 (lower curve corresponds to the solution with larger duration, the dashed curve depicts the generation threshold, hatching shows a corresponding stability zone). As one can see, the pulse stabilization against laser noise is possible only for the solution with longer duration. The stability range widens in γ_a, however at the cost of pump growth, which is the obvious disadvantage of this regime.

Now we introduce into equations the SPM and the GVD terms, that corresponds to a real femtosecond lasers. Assuming a chirp-free nature of possible solution we can reduce Eq. (4) to the first-order equation making use of a pure real character of the field:

$$\left[\delta\frac{dy(x)}{dx}+\frac{\beta}{\eta^2 D}y(x)^2+(\alpha-\gamma-\frac{\theta}{D})\right]y(x)-\frac{\gamma_a}{t_{coh}}\sin x=0. \qquad (6)$$

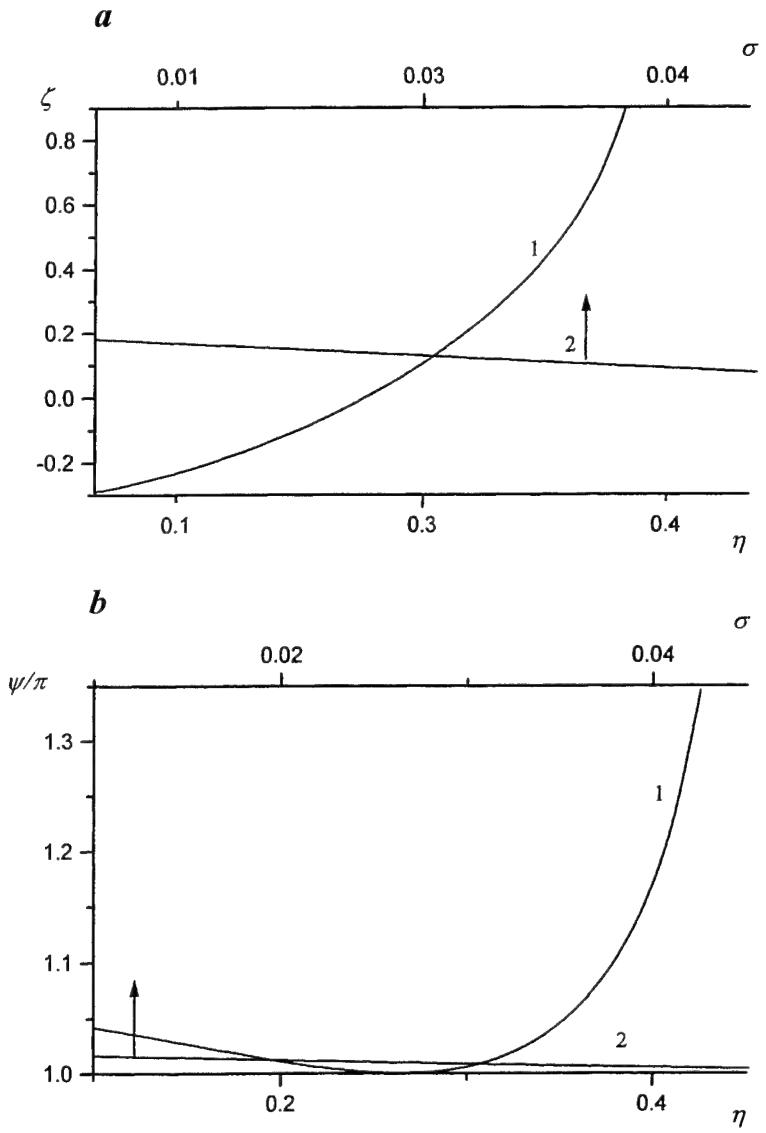

Fig. 5. *a*) chirp ζ and *b*) pulse square ψ/π versus η and σ in the presence of KLM: (*1*) σ=0.14; (*2*) η=0.2. β=0.26, P=0.001.

and η, so that $\sigma=\frac{\eta^2}{2}$. The *sech*-shaped solution has the following parameters:

$$a_0=\frac{2}{t_p}, t_p=\frac{1}{\sqrt{\gamma-\alpha}}, \delta=\frac{\gamma_a}{t_{coh}(\gamma-\alpha)} \qquad (7)$$

With the above described harmonic approximation we have the following solution: $\theta = 3\beta a_1^2/4\eta^2+D(\alpha-\gamma)$, $\delta=4\gamma_a/(t_{coh}a_1^2)$, $a_1=2\sqrt{3(\alpha-\gamma)}$, $t_p=2/a_1$ again for 2π-squared solution. The pulse duration is presented in Fig. 2 by curves *1'* and *2'*. The stable against the noise solution has a slightly longer duration than the unstable one.

Formally, the solution obtained is the solutions of the laser part of master equation that in the same time satisfies the Bloch equations. The stability of the solution results from the self-induced transparency in absorber, when the pulse propagates in the conditions of the positive net-gain and noise suppression due to Rabi flopping of the absorber population. We do not analyze the automodulational stability[13] of the solution since it has been testified directly by the numerical simulation in[10].

Thus we can conclude, that there is not the generation of coherent soliton in the absence of Kerr-lens-induced fast saturable absorption. But the generation of nonsoliton 2π-pulse takes place, which imposes a limitation on minimal modulation depth of the absorber with subsequent growth of generation threshold. In the next section we take into account the contribution of KLM.

4. COHERENT 2π-SOLITON IN THE PRESENCE OF KLM

The presence of KLM is described by the term $\sigma|a|^2$ in Eq. (3). In this case there is a 2π-soliton solution of Eq. (3), however for a strict relation between σ

There are two distinct features of 2π-soliton generation: 1) the condition $\alpha-\gamma<0$ is satisfied and, consequently, there is no limitation on the minimal modulation depth of the absorber; 2) the expression for the pulse duration is precisely the same as for the case of pure fast saturable absorber mode locking[2], that suggests that the KLM is the main mechanism determining the pulse duration. This conclusion corroborates with the results of ref.[11]. The action of the coherent absorber determines the pulse delay δ and imposes a restriction on the pulse square, i. e. the relation between pulse duration and amplitude. Pulse duration in the presence of KLM is shown in Fig. 2 by dotted curve *3*. As is seen, the pulse duration is much shorter than for the case with no KLM, especially for the small pump. As the contribution of semiconductor absorber is increased (η approaches 1, curve *1* in Fig. 4) the pulse duration is reduced down to the limit of the validity of the slowly varying envelope approximation.

An explanation of additional relation between the parameters of Kerr-lens-induced absorber and semiconductor absorber is as follows: a *sech*-shaped solution satisfies both pure laser equation and the Bloch equations, but the coherent interaction discriminates the special cases of nπ–squared pulses, in particular 2π–pulses, which are provided by $\sigma=\eta^2/2$ relation.

Let us study an automodulational stability of the laser coherent soliton, which we showed before to be very important factor in fs-lasers[13]. We used an aberrationless approximation, which assumes an unchanged form of solution and *z*-dependence for the pulse parameters. The substitution of the pulse envelope in Eq. (3) with following expansion into the time series yields:

$$\frac{da_0}{dz}=2\frac{(\alpha-\gamma)\eta^2 t_p^2-\eta^2+4\sigma}{\eta^2 t_p^3},\frac{dt_p}{dz}=4\frac{\eta^2-2\sigma}{a_0\eta^2 t_p^2},$$
$$\theta=\frac{2(D+4\frac{\beta}{\eta^2})}{a_0 t_p^3},\delta=2\frac{\gamma_a t_p}{t_{coh}a_0}. \tag{8}$$

Eqs. (8) were derived for a chirp-free solution with the dispersion $D=-2\beta/\eta^2$ exactly compensating for SPM. To be self-consistent the system (8) should be completed by additional relation between pulse duration and amplitude arising from the Bloch equations. After some calculations we have the explicit expressions, which determine the pulse stability. The pulse is stable if the Jacobean of the right-hand sides of first two Eqs. (8) has only non-positive eigenvalues. The condition for amplitude perturbation decay $-4(\gamma-\alpha)^2<0$ is satisfied automatically. For $\sigma=\eta^2/2$ the pulse possesses a marginal stability with respect to pulse duration. However for any $\sigma<\eta^2/2$ the pulse stability condition with respect to duration is satisfied.

Thus, we have analyzed the characteristics of 2π-solitons generated in fs KLM lasers with semiconductor coherent absorber. However, equations describing this physical situation allow yet another type of solutions.

5. COHERENT π-SOLITON AND CHIRPED QUASI-SOLITONS IN THE PRESENCE OF KLM

As one can see from the previous part of our work, the ultrashort pulse is the soliton for the both laser part of the master equation and the Bloch equations. Now we consider the complex ansatz describing a pulse with chirp ζ, $a(t)=a_0\,\mathrm{sech}(\frac{t}{t_p})^{1-i\zeta}$. It is known[12], that the Eqs. (1) have a *sech*-shaped solutions in form of chirp-free π-pulse or *sech*-shaped chirped solution, when the following relations hold:

$$u(t)=u_0\,\mathrm{sech}(\frac{t}{t_p}),v(t)=v_0\,\mathrm{sech}(\frac{t}{t_p}),w(t)=\tanh(\frac{t}{t_p}),\frac{d\phi(t)}{dt}=\frac{\zeta}{t_p}\tanh(\frac{t}{t_p}),\ \text{where}$$

$$a_0=\frac{\sqrt{1+\zeta^2}}{t_p},u_0=-\frac{1}{\sqrt{1+\zeta^2}},v_0=\frac{\zeta}{\sqrt{1+\zeta^2}}.$$

A chirp-free solution is a π-soliton, which is obviously unstable in the absorber since the full population inversion behind the pulse tail amplifies the noise. However, another nonlinear factors in KLM-laser can stabilize the pulse and this requires a corresponding consideration.

Parameters of the chirp-free π-soliton in KLM-laser are:

$$a_0=\frac{1}{t_p},t_p=\frac{1}{\sqrt{\gamma-\alpha}},D=-\frac{\beta}{2\eta^2},\theta=\frac{\beta(\gamma-\alpha)}{2\eta^2},\sigma=2\eta^2. \tag{9}$$

This is very similar to 2π-solution (7), however with some differences. As the pulse amplitude of the π-soliton is two times smaller than for the 2π-soliton, a KLM-parameter in order to produce the same effect and support soliton generation should be increased four times and the dispersion should be decreased accordingly.

Curve *4* in Fig. 2 depicts the pulse duration for π–soliton. As is seen, the pulse duration slightly differs from the duration for 2π-soliton (curve *2*) and is shorter in the region of small η (curve *2* in Fig. 4).

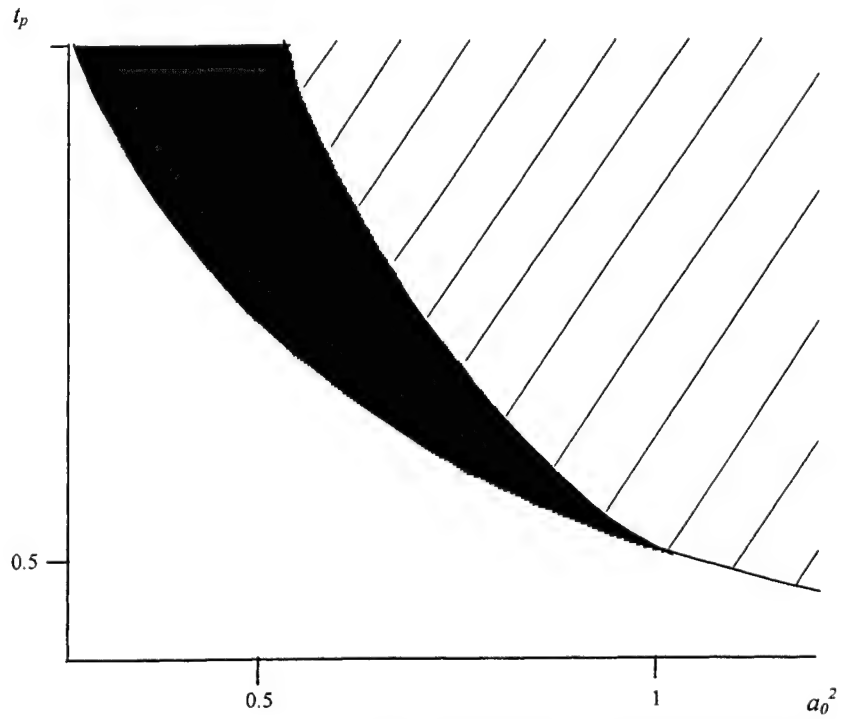

Fig. 6. Self-starting ranges on the plane "peak intensity of initial noise pulse – duration of initial noise pulse". Dark and hatched (together with dark) regions correspond to the self-starting for P=8.5×10^{-4} and 8.8×10^{-4},respectively. T_a=1 ps, γ=0.01, η=1, τ=6.25×10^{-5}.

As was said before, a π-soliton inverts the population difference in the absorber that causes the noise amplification behind the pulse tail. Hence, the laser pulse stabilization is possible if the condition $\alpha+\gamma_a-\gamma<0$ is satisfied. This defines the maximal initial loss in the absorber (dotted curve in Fig. 3). It is seen, that the maximal modulation depth exceeds the threshold (dashed curve) and, consequently, the generation of the stable π-soliton is possible.

When the condition $\eta^2 < \frac{3\sqrt{\sigma^2+\beta^2}-\sigma}{4}$ holds there are the physical chirped solutions with *sech*-shape. In this case, the expressions for D and pulse parameters are bulky and we do not write them here. The pulse duration is presented in Fig. 2 by curve *5*. As is seen, the chirped pulse duration can be very short even for the moderate value of P. There is a minimum in the dependence of the pulse duration on η (an optimal reflectivity of semiconductor absorber device, curve *3* in Fig. 4) and it does not coincide with the point of precise chirp compensation (curve *1* in Fig. 5, *a*). Additionally, the pulse square is variable for this type of solution (curve *1* in Fig. 5, *b*).

There is a sharp minimum in the dependence of the pulse duration on σ, also (curve *4* in Fig. 4). For our parameters a corresponding KLM-parameter is 7×10^7 W. As it was in the previous case, the minimum of the pulse duration does not coincide with the point of chirp compensation (curve *2* in Fig. 5, *a*). Unlike the case of variation of η, the variation of σ causes only a slight variation of the pulse square (curve *2* in Fig. 5, *b*).

Summarizing, the generation of *sech*-shaped π-pulses and chirped pulses with variable square is possible in KLM-lasers with coherent semiconductor absorber as a result of definite relation between KLM and saturable absorber's contribution. A larger KLM contribution (for a fixed η) is needed to produce the pulse as compare to the case of 2π-soliton.

6. SELF-STARTING ABILITY

Our results suggest that the pulse duration is determined rather by KLM, whereas a saturable absorber puts a limitation on the pulse square. But an important feature of KLM in the presence of semiconductor absorber is the self-starting ability. To estimate it in our model we analyzed an evolution of the initial noise pulse, which is much longer than the relaxation time of the excitation in absorber T_a=1 ps. For such a noise pulse an absorber is fast and the action of SPM and self-focusing is negligible. Using the normalization of the time, gain saturation energy and field intensity to T_{cav}, E_a and E_a/T_{cav}, respectively an evolution equation for the noise pulse is:

$$\frac{\partial a(z,t)}{\partial z}=\left(\frac{P\alpha_{max}T_r}{1+2\tau T_r a_0^2(z)t_p(z)/\eta^2+PT_r}-\frac{\gamma_a}{1+2a_0(z)t_pT_a}-\gamma+t_f^2\frac{\partial^2}{\partial t^2}\right)a(z,t), \qquad (10)$$

where all notations have the meaning as before, and field parameters refer to the noise pulse. To solve Eq. (10) we used, as before, an aberrationless approximation. The decay of the noise pulse (growth of the duration and decrease of the intensity) means in our model that the system will not self-start. An opposite situation with an asymptotic growth of the noise pulse testifies about ability of the system to self-start. After some calculations, the self-starting conditions are:

$$\begin{aligned}
&t_f^2(1+4T_aa_0^2+4t_f^2a_0^4)-\gamma_aT_aa_0^2t_p^2>0,\\
&-\gamma t_f^2t_p^2(PT_r\eta^2+2T_rT_aPa_0^2\eta^2+2a_0^2t_pT_r\tau+4a_0^4t_p\tau T_rT_a+\eta^2+2a_0^2t_p\eta^2T_a)+\\
&PT_r\eta^2(\alpha_{max}t_p^2+2\alpha_{max}a_0^2t_p^2T_a-t_f^2-2t_f^2a_0^2T_a)-2t_f^2a_0^2T_r\pi t_p(1+2a_0^2T_a)-\\
&t_f^2\eta^2(1+2a_0^2T_a)-\gamma_at_p^2(PT_r\eta^2+2a_0^2t_p\tau T_r+\eta^2)>0.
\end{aligned} \qquad (11)$$

Fig. 6 demonstrates the regions of the initial pulse parameters corresponding to the self-starting. The dark zone corresponds to the pump $P = 8.5\times10^{-4}$, which is close to the threshold of mode locking self-start. Lower pump cannot provide the self-starting while a higher pump ($P = 8.8\times10^{-4}$) causes an expansion of self-starting region.

7. CONCLUSION

In conclusion, we investigated the conditions of soliton formation in cw solid-state laser with coherent semiconductor absorber. It was found, that the mode locking in the absence of Kerr-lens-induced fast saturable absorption does not produce *sech*-shaped pulse. This 2π-pulse (pulse of self-induced transparency) has fs-duration and is stabilized by the defined minimal modulation depth of absorber. The stabilization results from the positive difference between saturated gain and linear loss and an increase of the threshold of sub-10 fs generation. A combined action of KLM and coherent absorption produces the *sech*-shaped soliton, which removes a requirement to the minimal modulation depth of semiconductor absorber. The pulse duration, which is close to the fundamental limit, is defined by KLM and the coherent absorber defines the pulse square. As result, there are 2π-, π-solitons and chirped quasi-soliton with variable square.

Our results can be useful for the development of high-efficient self-starting generators of extremely short pulses for fs spectroscopy, X-ray and THz generation.

All calculations in this paper were carried out in Maple V, the corresponding commented programs are presented at http://www.geocities.com/optomaplev.

8. REFERENCES

1. D. H. Sutter, G. Steinmeyer, L. Gallmann, N. Matuschek, F. Morier-Genoud, and U. Keller, "Semiconductor saturable-absorber mirror's assisted Kerr-lens mode-locked Ti:sapphire laser producing pulses in the two-cycle regime", *Opt. Lett.*, 24, 631-633 (1999).
2. H. Haus, J. G. Fujimoto, and E. P. Ippen, "Analitic theory of additive pulse and Kerr lens mode locking", *IEEE J. Quant. Electr.*, 28, 2086-2095 (1995).
3. U. Keller, K. J. Weingarten, F. X. Kärtner, D. Kopf, B. Braun, I. D. Jung, R. Fluck, C. Hönninger, N. Matuschek, and J. A. der Au, "Semiconductor saturable absorbers mirrors (SESAM's) for femtosecond to nanosecond pulse generation in solid-state lasers", *IEEE J. Selected Topics in Quant. Electr.*, 2, 435-451 (1996).
4. F. X. Kärtner, I. D. Jung, and U. Keller, "Soliton mode-locking with saturable absorbers", *IEEE J. Selected Topics in Quant. Electr.*, 2, 540-555 (1996).
5. V. L. Kalashnikov, D. O. Krimer, I. G. Poloyko, V. P. Mikhailov, "Ultrashort pulse generation in cw solid-state laser with semiconductor saturable absorber in the presence of the absorption linewidth enhancement", *Optics Commun.*, 159, 237-242 (1999).
6. V.L. Kalashnikov, D.O. Krimer, I.G. Poloyko, V.P. Mikhailov, "Stark induced contribution to mode locking in cw solid-state lasers with semiconductor saturable absorber", Proceedings of SPIE, v.3683, 225-231(1998).
7. V.V. Kozlov, E.E. Fradkin, "Theory of mode locking with a coherent absorber. 1. Generation of soliton-like 2π pulses", *JETP*, 80, 32-40 (1995).
8. V.V.Kozlov, "Theory of mode locking with a coherent absorber. 2. Transition processes and stability analysis", *JETP*, 107, 360-375 (1995) (in Rus.).

9. K.P. Komarov, V.D. Ugozhaev, "Steady-state 2π-pulses under passive mode locking", *Sov. J. Quantum Electronics*, 14, 787-792 (1984).
10. V. P. Kalosha, M. Muller, and J. Herrmann, "Theory of solid-state laser mode locking by coherent semiconductor quantum-well absorbers", *J. Opt. Soc. Am. B*, 16, 323-337 (1999).
11. I. P. Christov, V. D. Stoev, M. M. Murnane, H. C. Kapteyn, "Absorber-assisted Kerr-lens mode locking", *J. Opt. Soc. Am. B.*, 15, 2631-2633 (1998).
12. L. Allen, J.H. Eberly, *Optical resonance and two-level atoms* (Wiley, New York,1975).
13. V.L. Kalashnikov, D.O.Krimer, F.Mejid, I.G.Poloyko, V.P. Mikhailov, "Self-oscillations in cw solid-state ultrashort-pulse generating lasers with mode locking by self-focusing", *Quantum Electronics*, 29, 329-333 (1999).

About possibility of formation of shock electromagnetic waves on optical cycle due to generation of higher harmonics

Vitali E. Gruzdev *, Anastasia S. Gruzdeva
State Research Center «S.I.Vavilov State Optical Institute»
Birzhevaya Liniya 12, St.Petersburg, 199034, Russia

ABSTRACT

There is considered formation and propagation of shock electromagnetic waves (SEW) of visible spectral range as possible nonlinear optical phenomenon taking place at laser intensities characteristic of femtosecond laser interaction with transparent solids. Main regularities of SHEW formation are studied on the basis of 1D model of plane-wave propagation in isotropic dielectric with nonlinear optical response. Special attention is paid to influence of color dispersion and absorption on SEW formation and propagation. Necessary conditions for appearing of SHEW are obtained, in particular, threshold amplitude is estimated. There is presented a model for numerical study of SHEW formation and propagation influenced by dispersion of linear and nonlinear parts of refractive index. Using the simulation, we studied dynamics of SHEW formation on several optical cycles near leading edge of femtosecond laser pulse propagating in transparent medium. Important observed features of SHEW are discussed.

Key words: femtosecond laser pulses, transparent materials, shock electromagnetic waves, nonlinear propagation, femtosecond laser-induced damage

1. INTRODUCTION

Fast developing of femtosecond lasers and general trend in increasing of damage threshold with decreasing of pulse duration have resulted in new situation in the area of high-power nonlinear optics. Many nonlinear optical phenomena can be studied at laser intensity $10^{12} - 10^{13}$ W/cm^2 in transparent materials that cannot be reached for nano- and pico-second laser pulses. That results in revealing of new effects and strong changes of regularities for known nonlinear optical effects. On the other hand, characteristic intensities of laser-induced damage and ablation have exceeded 10^{14} W/cm^2 what, being combined with femtosecond pulse duration, gives possibility of new insight into process of laser-matter interaction.

Two main characteristic features of femtosecond laser pulses make nonlinear processes induced by them very different from similar processes induced by longer pulses: mentioned above possibility to reach very high laser intensity and very small pulse duration. Due to that, some traditional models of nonlinear processes cannot be applied to description of propagation of femtosecond pulses that requires more detailed and correct consideration. For this reason we come back to concept of shock electromagnetic waves (SHEW) which appeared in high-frequency electrodynamics some 45 years ago [1-4] and was not accepted in nonlinear optics some 35 years ago [5, 6]. New understanding and models of nature of nonlinear material response [7, 8] allow now more correct consideration of influence of two factors extremely important for SHEW appearing – dispersion of linear and nonlinear parts of refractive index and absorption.

Important reason to consider high-power nonlinear propagation of femtosecond pulses and possibility of SHEW formation is connected with one of main problems of femtosecond laser-matter interactions that is unclear mechanism of energy transfer from radiation to materials. That is especially true for the case of laser ablation and damage of transparent materials by femtosecond pulses. Any studying of femtosecond laser-matter interactions with transparent materials should start with consideration of nonlinear pulse propagation and accompanying optical phenomena because they determine conditions of energy deposition to electron and phonon systems and, thus, conditions of material modification. In spite of that obvious point many investigators of femtosecond interactions use simple models of pulse propagation (mainly, plane monochromatic wave model) suitable for linear propagation only.

Thus, the nonlinear optical phenomenon to be considered in this paper is formation and propagation of shock electromagnetic wave that occurs on optical cycle due to generation of higher harmonics. For the case of positive nonlinear addition to refractive index, brief picture of mechanism of SHEW formation is as follows. Radiation-induced nonlinear

* Phone: (81272) 246-22, Fax +7-81272-246-22, E-mail: gru@mailbox.alkor.ru

Laser Optics 2000: Ultrafast Optics and Superstrong Laser Fields, Alexander A. Andreev, Vladimir E. Yashin, Editors, Proceedings of SPIE Vol. 4352 (2001) © 2001 SPIE · 0277-786X/01/$15.00

response of the medium increases refractive index of the medium and results in slowing down the part of optical cycle corresponding to large electric or magnetic field strength (point 1 in Fig. 1). Bottom part of wave profile (2 in Fig. 1) moves with unperturbed speed of light in the material, i. e., faster than top part of wave profile. That process results in distortion of wave profile (Fig. 1) in such a way that top of the profile "falls down" onto the region of the profile where electric-field strength is small and which moves behind the top. That leads to appearing of very abrupt field variation within length much smaller than wavelength what looks like disruption and step of field strength. The step is referred to as SHEW front. In general, there is no exact disruption, and structure of SHEW front should be studied with taking into account complicated mechanism of dispersion and wave-energy dissipation near SHEW front [1-3, 7, 8]. Picture of SHEW formation is similar in case of negative field-induced variation to refraction: the top part of wave cycle moves faster and overtakes the nearest bottom part of the profile, then the top part falls onto the forth-going bottom part of wave cycle.

One should distinguish several types of SHEW referred to in literature [1-6, 9, 10]. Historically, SHEW of megahertz frequency range was the first to be revealed in late 50-s and was being intensively investigated in 60-s [1 - 3]. Mechanism of its formation is similar to that described above. Main feature of SHEW of MHz frequency domain is that nonlinear response for electromagnetic pulses of MHz frequency is nonlinear magnetic response in ferromagnetic [1 - 3] and many higher harmonics (HH) are inside transparency band.

Other type of SHEW that has been studied since late 60-s is self-steepening of slowly-varying amplitude of optical pulse (Fig. 2) [4, 6, 9, 10]. It has been observed for optical pulses propagating in fibers [9] and is now being intensively studied because it can account for many nonlinear optical effects in propagation of femtosecond laser pulses [10]. Its dynamics, mechanisms of formation and regularities are not so simple and obvious as for mentioned above SHEW of MHz frequency. Important feature of self-steepening is dominating contribution of dispersion of linear and nonlinear parts of refractive index in process of its formation [10].

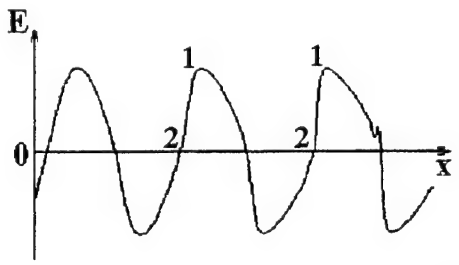

Fig. 1. Sketch of deformation of plane-wave profile during formation of shock electromagnetic wave in nonlinear medium with positive nonlinear addition to refractive index.

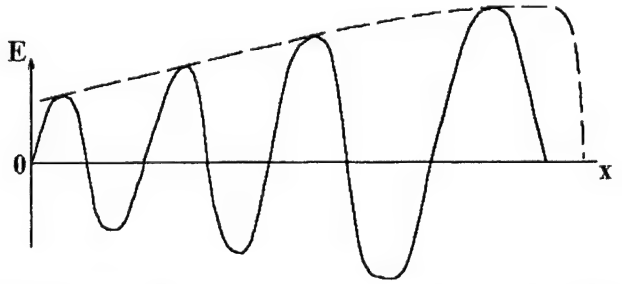

Fig. 2. Sketch of self-steepening process – formation of shock wave for slowly-varying amplitude of laser pulse.

This paper is devoted to formation of SHEW on optical cycle of high-power electromagnetic waves of optical frequency in transparent media that has structure similar to that in Fig. 1. Self-steepening of laser pulses is not considered below because of the following reason. Self-steepening of pulse envelope is observed in cases when material dispersion plays dominating role and small nonlinear distortions are incubated along long path in nonlinear medium. In such conditions threshold of SHEW is much larger than that of self-steepening. In turn, considered SHEW must have smaller threshold and dominate self-steepening in focal area for conditions typical of tight focusing of high-power laser beams in transparent materials [11-17] when laser intensity and laser-induced nonlinear distortions of refraction are large in focal area. On the other hand, path of effective nonlinear interaction in transparent material in this case is much smaller than dispersion length [10] and nonlinear distortions can dominate refractive-index dispersion. The SHEW under consideration is referred to as optical SHEW. Obtained estimation of SHEW threshold shows that this type of SHEW can appear near leading edge of femtosecond laser pulse. Because of that, we start with brief review of experimental facts connected with interaction of high-power femtosecond pulses with transparent materials. Then we consider general concept and specific features of optical SHEW. Key points are consideration of dispersion and absorption influence on SHEW and estimation of threshold for SHEW formation. Modeling of that process is considered also. We conclude with discussion of obtained results.

2. BRIEF REVIEW OF EXPERIMENTAL FACTS

All mentioned below experimental results to be used for estimations are concerned with processes induced by femtosecond laser pulses in transparent wide band-gap materials. *Characteristic parameters of laser radiation* are as follows:

- pulse duration τ_p=900 fs – 10 fs [11 - 17];
- laser wavelength in vacuum λ_0=10.6μm – IR [12] – 1.06 μm – 0.8 μm [11, 14] – 0.6 μm [17];
- energy of laser quantum $h\nu$ 0.117 eV - 1.17 eV - 1.55 eV - 2.07 eV;

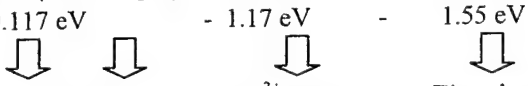

- type of laser FE lasers Nd^{3+}:glass Ti:saphpire
- intensity of laser radiation at focal plane 1) for self-focusing and white-light generation I^{*}_{TH}=10^{12} – 10^{13} W/cm^2 [10, 18], 2) for laser-induced damage and ablation I^{**}_{TH}=10^{13} – 10^{14} W/cm^2 [11 – 17];
- focal spot radius r_F = 1 μm – 10^2 μm [11 - 17], what allows estimating of beam path s in nonlinear material along which nonlinear interaction is the most effective: $s \cong 2z_c = \pi r^2_F/\lambda = (10 - 3\cdot10^4)\lambda$, typical value of s is (10 – 100)λ;
- repetition rate (for multi-pulse damage and ablation) from 10 Hz to 10^9 Hz (pulse trains [12]).

Materials used in experiments are wide band-gap semiconductors and dielectrics which typical band gap is 3 or more times larger than photon energy [11 - 17]: $E_g \geq 3h\nu$. Characteristic value of nonlinear coefficient of refraction is about $n_2 \cong 10^{-16}$ cm^2/W. Linear constant part of refractive index n_0 for most of considered materials varies between 1.45 and 3. Many of investigated materials are isotropic, for example, fused silica and glasses of various types. Looking through papers with experimental data, one can find that often used material for femtosecond laser-induced damage and ablation is fused silica which parameters are as follows: E_g = 7.5 eV [18], n_0 = 1.45, $n_2 = 2\cdot10^{-16}$ cm^2/W, absorption $\alpha \approx 10^{-3}$ cm^{-1}, group velocity dispersion coefficient β=385 fs^2/cm [10].

For further estimations we can use the following experimental data: length of effective nonlinear interaction path is no more than 100 λ what is 79 μm for laser wavelength 0.79 μm and 400 μm for laser wavelength 4.0 μm [12]. For pulse duration 100 fs effective dispersion length in glass BK-7 or fused silica [10] is about 6.5 cm. Thus, path of effective nonlinear interaction is at least 100 times less than dispersion length and group velocity dispersion can be neglected in the first approximation. Photon energy is 1.55 eV for the most typical laser wavelength 0.8 μm. Thus, five photons should be absorbed to ionize a center in fused silica. For wavelength 4.0 μm photon energy is 0.31 eV, thus, 25 photons should be absorbed to produce ionization.

Considering nonlinear optical effects, we concentrate on experimental data connected with effects of nonlinear laser-pulse propagation in transparent media and do not touch results on laser-induced heating and ablation that are considered in other our paper [19]. *Typical regularities of nonlinear femtosecond-pulse propagation in transparent materials* are as follows:

1. Very high damage threshold (10^{13} – 10^{14} W/cm^2) [11 - 17]. Such thresholds are observed practically for all tested materials, and they vary little for different materials. Laser-induced variations of refraction at laser fluences close to damage threshold are about $\Delta n_{NL} = n_2 I_{TH} \cong 0.1 - 0.01$.
2. White-light generation [10, 18] during propagation of femtosecond laser pulses in transparent materials. Spectrum analysis shows appearing of Stocks and anti-Stocks broadening of central laser line, and anti-Stocks wing of the spectrum of generated white light is about an order of magnitude longer than Stocks wing [18]. White-light generation is observed only for with materials band gap exceeding certain value showing threshold band-gap dependence [18].
3. Thresholds of self-focusing and white-light generation are the same in all transparent materials. [18]. That points at important connection between self-focusing and generation of white light that has not got clear explanation [18].
4. Most femtosecond interactions as well as propagation of femtosecond pulses are accompanied by generation of higher harmonics. In case of isotropic materials the harmonics are odd and can be of very high order (21-st – 27-th harmonics observed in [20]).
5. Detection of laser-induced damage is connected with one of important problems – what process should be taken as a signal of damage onset. Correct investigations [11, 13] shows that bulk laser-induced femtosecond damage of transparent solids includes several stages, each with its characteristic threshold. Formation of plasma comes before irreversible changes take place, and threshold of plasma formation is the lowest among all other thresholds. Next process is formation of invisible single-shot and multi-shot damage which threshold is higher than that of plasma formation. Appearing of visible laser-induced damage and irreversible fall of transparency have the highest threshold that is about 10 times higher than that for plasma formation. Electron plasma can appear at pulse tail and change its propagation sufficiently by specific dispersion [21]. For example, plasma formation results in conical emission effect [21], cut of self-focusing [18].

All those experimental facts are different parts of one universal process of nonlinear interaction of femtosecond pulse with

transparent materials and most of them have not got clear interpretation till now.

3. PHYSICAL AND MATHEMATICAL MODEL

2.1. General concept of optical SHEW

In general case, formation and propagation of SHEW is a self-consistent problem because high-power laser beam changes optical properties of the transparent material, where it propagates, and those changes result in variation of beam parameters in self-consistent manner. For example, ionization results in increasing of absorption by free electrons and color centers, while electron plasma also changes dispersion of refractive index. That is illustrated by the following scheme.

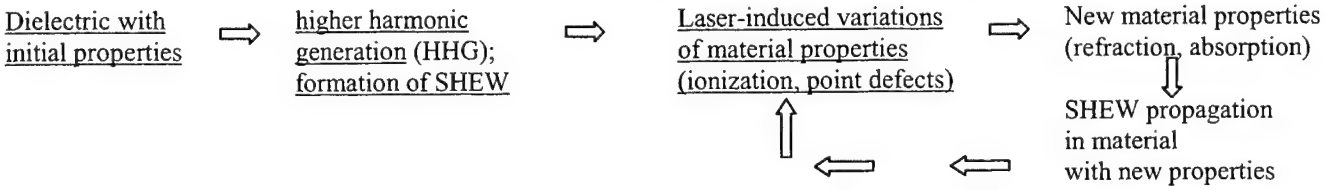

Analysis of that self-consistent problem should be based on solution to system of coupled nonlinear equations describing high-power wave propagation (nonlinear wave equation) and material response. Together with usual description of linear and nonlinear optical response, the correct material equations must describe possible phase transitions, laser-induced changes of material structure (e.g., excitation and relaxation of electron plasma and related processes, formation of vacancies and color centers) and variations of optical parameters resulting from those processes. Even deducing of correct material equations presents difficult problem, not to say about solving that system of coupled nonlinear equations.

To start, we reduce self-consistent problem to a couple of independent problems:

1) electrodynamical propagation problem - formation and propagation of SHEW in dielectric with constant properties to be studied in this paper;
2) interaction problem - processes induced by unperturbed SHEW (which space distribution and time evolution are results of solving of the first problem) in dielectric – to be studied in paper [19].

Several comments should appear in connection with this reducing to independent problems. First, that description can be applied to initial stage of SHEW formation and to a small leading part of laser pulse (first few periods of laser radiation only) where laser-induced variation of material parameters are small enough to be neglected. Duration of leading part of laser pulse to be considered is determined by characteristic time of laser-induced plasma excitation up to the level when it gives sufficient distortions to pulse propagation [21]. That time is about 15-20 fs. Plasma excitation is assumed to be the fastest process, other laser-induced processes of material parameters modification have longer excitation time and their influence on nonlinear processes at leading edge of laser pulse can be neglected. Thus, throughout this paper we consider only few (about 10) first cycles of femtosecond laser pulse.

Second, natural result of such reducing to independent problems is breaking of energy conservation law: energy transferred from SHEW to electrons (ionization and absorption by electrons) and crystal lattice (formation of point defects [19]) is not taken into account within this approximation. Thus, some energy appears in material and leads to it modification while nothing disappears from SHEW. On the other hand, neglecting of energy dissipation at SHEW front results in formation of non-steady SHEW. Two points should be mentioned in this connection: 1) the energy dissipating from SHEW to material is assumed to be small enough at leading part of laser pulse not to influence sufficiently on SHEW propagation; 2) presented consideration is the first approximation to exact solution while calculated in [19] absorption rate will be used to estimate energy dissipation in further approximations.

3.2. Basic equations for description of SHEW formation and propagation

Efficient formation of SHEW can take place at laser intensity close to 10^{13} W/cm^2, i.e., close to damage threshold. Thus, electric field strength is high enough to induce nonlinear electrodynamical effects in solids. On the other hand, generation of higher harmonics results in significant broadening of radiation spectrum. Thus, even the simplest model of polarization response of considered solid must take into account dispersion of polarization response and nonlinear optical properties. In this paper properties of SHEW and its formation and propagation are studied on the basis of the simplest model of 1D propagation of high-power plane homogeneous wave. Advantages of that 1D model are 1) relatively simple equations

describing considered below SHEW allowing to obtain rigorous solutions for some particular cases, 2) possibility to compare obtained results with some rigorous solutions to problems of 1D nonlinear wave propagation and shock wave formation [5 - 9], and 3) relatively low computational resources (in particular, computer memory) required for modelling of SHEW formation.

Nonlinear wave propagation is described by full wave equation including material polarization and linear frequency-independent absorption:

$$\frac{\partial^2 E}{\partial t^2} - c_0^2 \frac{\partial^2 E}{\partial z^2} = -4\pi \frac{\partial^2 P}{\partial t^2} - \frac{4\pi\sigma}{\varepsilon_0} \cdot \frac{\partial E}{\partial t}. \quad (1)$$

Wave equation (1) should be coupled with a system of nonlinear equations describing material response P to laser field consisting of fast P_e (electronic) and slow P_i (ionic) components:

$$P=P_e+P_i. \quad (2)$$

Each of them includes linear and nonlinear contributions. Considering input pulse of arbitrary wavelength range that can be close to vibrational absorption band (area of anomalous dispersion of refraction) or electronic absorption band (area of normal dispersion of refraction), one should also take into account frequency-dependent contributions to absorption.

Description of polarization variations in time must give correct dispersion law for both linear and nonlinear parts of refractive index in all considered spectrum range. One of the simplest and the most suitable models for that is phenomenological model of two parametrically coupled oscillators [7, 22] which gives the same functional form of dispersion as quantum-mechanical three-level model [22]. According to that model, laser-induced variations of polarization have contributions from linear and nonlinear vibrations of electrons and ions and are described by the following four equations:

$$\frac{\partial P_e}{\partial t^2} + \frac{2}{T_e} \cdot \frac{\partial P_e}{\partial t} + \omega_e^2 P_e = \alpha_e E + \beta_e (R_e + R_i) E \quad (3)$$

$$\frac{\partial P_i}{\partial t^2} + \frac{2}{T_i} \cdot \frac{\partial P_i}{\partial t} + \omega_i^2 P_i = \alpha_i E \quad (4)$$

$$\frac{\partial R_e}{\partial t^2} + \frac{2}{T_{e1}} \cdot \frac{\partial R_e}{\partial t} + \omega_{e1}^2 R_e = \gamma_e (P_e + P_i) E \quad (5)$$

$$\frac{\partial R_v}{\partial t^2} + \frac{2}{T_v} \cdot \frac{\partial R_v}{\partial t} + \omega_v^2 R_v = \gamma_v (P_e + P_i) E. \quad (6)$$

These equations describe polarization contributions from vibrations of optical electrons (3) and ions (4) excited straightly by laser electric field as well as contributions from secondary vibrations of valence electrons (5) and ions (6) excited by straight laser-induced vibrations of electrons and ions. Effective frequency ω_e corresponds to electron transitions between ground level and one of higher energy levels while ω_{e1} corresponds to forbidden transitions between ground level and the other higher energy level. Influence of laser electric field and secondary influences of valence electrons (term R_e) and ions (term R_v) which vibrations are excited by laser-induced vibrations of optical electrons and ions (equations (3) and (4)) are taken into account to describe electronic and electron-vibrational contributions to nonlinear optical response. That allows correct description of *inertia*-free Kerr and Raman nonlinear response. Two-photon absorption is also included into polarization response deduced from (3) – (6). With suitable parameters, dispersion law deduced from (3) - (6) describes real dispersion of linear part of refractive index of transparent materials with accuracy of 0.01% within full transparency band [7]. We do not touch further details of two-oscillator model for description of polarization dispersion, which can be found in papers [7, 22].

As it is well known, all processes of SHEW formation and evolution can be divided into two groups – slow processes and fast processes [1, 2]. Characteristic space and time scales for slow processes are much larger than laser wavelength λ_0 in vacuum and laser period T_0 while time and space scales of fast processes are much less than laser period and wavelength. Example of slow process is increasing of intensity of generated higher harmonics in space, slow accumulation of nonlinear distortions connected with generation of higher harmonics resulting in formation of abrupt SHEW front. That process takes from 10 to 100 of T_0 and develops within distances of (10 – 100) λ_0. Fast processes are connected with SHEW front evolution due to energy dissipation and interplay between higher harmonics which characteristic time is less than $T_0/6$ and space scale is less than $\lambda_0/6$. Making use of (3)-(6), one can estimate what contributions play key role in developing of

slow and fast processes. For both processes let us assume all frequencies ω giving sufficient contribution to SHEW formation to be between ionic and electronic absorption bands, i.e., the following condition must be satisfied:

$$\omega_i<\omega<\omega_e,\ \omega_v<\omega<\omega_{el}. \tag{7}$$

Applying Fourier integral transformation to (3) – (6), then applying perturbation technique to obtained expressions with respect to small parameters ω/ω_e, ω_i/ω, ω/ω_{el}, ω_v/ω, and then applying inverse Fourier transformation to obtained perturbation series [7], one can obtain the following expression for polarization:

$$\begin{aligned}P=&\frac{\alpha_e}{\omega_e^2}E-\frac{\alpha_e}{\omega_e^4}\cdot\frac{\partial^2 E}{\partial t^2}+\alpha_i\int_0^t d\tau\int_0^\tau E(\tau')d\tau'-\frac{2\alpha_e}{\omega_e^4 T_e}\cdot\frac{\partial E}{\partial t}-\frac{2\alpha_i\omega_i}{T_i}\int_0^t d\tau\int_0^\tau d\tau'\int_0^{\tau'}E(\tau'',x)d\tau''+\\&+\frac{\beta_e\gamma_e\alpha_e}{\omega_e^4\omega_{el}^2}\cdot E^3-\frac{\beta_e\gamma_e\alpha_e}{\omega_e^4\omega_{el}^2}\cdot\left(\frac{1}{\omega_e^2}+\frac{1}{\omega_{el}^2}\right)\frac{\partial^2 E^3}{\partial t^2}+\frac{\beta_e\gamma_e\alpha_i}{\omega_e^2\omega_{el}^2}\cdot E^2\int_0^t d\tau\int_0^\tau E(\tau')d\tau'+\\&+\frac{\beta_e\gamma_e\alpha_e}{\omega_e^4\omega_{el}^2}\cdot\frac{\partial^2}{\partial t^2}\left\{E^2\int_0^t d\tau\int_0^\tau E(\tau')d\tau'\right\}\end{aligned} \tag{8}$$

The first, the second and the third terms in (8) give linear contributions to refractive index describing *inertia*-free, normal dispersive and anomalous dispersive contributions respectively. The fourth and the fifth terms describe polarization decay due to absorption corresponding to electron and vibrational transitions respectively. The sixth term gives *inertia*-free nonlinear response, the seventh, the eighth and the ninth terms correspond to nonlinear laser-induced contributions to refractive describing their normal and anomalous dispersion. Omitted terms describe absorption appearing near vibrational and electronic absorption bands and high-order contributions to linear and nonlinear parts of refractive index. Each term in (8) can be estimated using the following parameters, corresponding to experimental data for fused silica [7]: $\omega_e=2.096\cdot10^{16}$ s^{-1}, $\omega_i=2.154\cdot10^{14}$ s^{-1}, $\alpha_e=3.862\cdot10^{31}$ s^{-2}, $\alpha_i=2.534\cdot10^{27}$ s^{-2}, $\omega_{el}=3.0\cdot10^{16}$ s^{-1}, $\omega_v=8.3\cdot10^{13}$ s^{-1}, $\beta_e=2.0\cdot10^{43}$ esu, $\gamma_e=2.9\cdot10^9$ esu, $\gamma_v=8.0\cdot10^3$ esu. According to these data [7] omitted terms give about 5% contribution to the value given by (8), and they can be neglected in the first approximation. Among all terms in (8) only the first and the sixth terms give non-dispersive linear part and Kerr electronic nonlinearity of refractive index respectively.

Bearing in mind that possible length of SHEW formation (an order of 100 λ) is much less than dispersion length [10-17] for most focusing geometries of experiments [11-17], one can estimate values of different polarization contributions for "slow" processes. Omitting small terms in (8), one derives the following form of polarization response for "slow" processes:

$$\begin{aligned}P=&\frac{\alpha_e}{\omega_e^2}E-\frac{2\alpha_e}{\omega_e^4 T_e}\cdot\frac{\partial E}{\partial t}+\frac{2\alpha_i\omega_i}{T_i}\int_0^t d\tau\int_0^\tau d\tau'\int_0^{\tau'}E(\tau'',x)d\tau''+\frac{\beta_e\gamma_e\alpha_e}{\omega_e^4\omega_{el}^2}E^3+\frac{\beta_e\gamma_e\alpha_i}{\omega_e^2\omega_{el}^2}\cdot E^2\int_0^t d\tau\int_0^\tau E(\tau')d\tau'+\\&+\frac{\beta_e\gamma_e\alpha_e}{\omega_e^4\omega_{el}^2}\cdot\frac{\partial^2}{\partial t^2}\left\{E^2\int_0^t d\tau\int_0^\tau E(\tau')d\tau'\right\}\end{aligned} \tag{9}$$

As it was shown in [7], the last two terms in (9) can be neglected for consideration of field evolution within time less than 15 fs from leading edge of femtosecond pulse, what means that near the leading front of femtosecond pulse within 15 fs one can neglect all dispersion terms in material response and consider only *inertia*-free absorption and linear and nonlinear responses in the first approximation:

$$P_{slow}=\frac{\alpha_e}{\omega_e^2}E+\frac{\beta_e\gamma_e\alpha_e}{\omega_e^4\omega_{el}^2}E^3-\frac{2\alpha_e}{\omega_e^4 T_e}\cdot\frac{\partial E}{\partial t}-\frac{2\alpha_i\omega_i}{T_i}\int_0^t d\tau\int_0^\tau d\tau'\int_0^{\tau'}E(\tau'',x)d\tau''. \tag{10}$$

In particular, estimations of threshold of SHEW formation can be done with neglecting dispersion. For the part of laser pulse which is more than 15 fs far from its leading edge one should take into account at least the last two terms in (9) describing dispersion of nonlinear material response. Thus, SHEW can appear near leading edge of femtosecond pulse where absorption and nonlinear response dominates influence of dispersion.

In case of "fast" processes connected with evolution of SHEW front, general expression (8) can be reduced to the following form by neglecting small contributions:

$$P=\frac{\alpha_e}{\omega_e^2}E-\frac{\alpha_e}{\omega_e^4}\cdot\frac{\partial^2 E}{\partial t^2}+\frac{\beta_e\gamma_e\alpha_e}{\omega_e^4\omega_{e1}^2}E^3-\frac{\beta_e\gamma_e\alpha_e}{\omega_e^4\omega_{e1}^2}\cdot\frac{\partial^2 E^3}{\partial t^2}-\frac{2\alpha_e}{\omega_e^4 T_e}\cdot\frac{\partial E}{\partial t}+\frac{\beta_e\gamma_e\alpha_e}{\omega_e^4\omega_{e1}^2}\cdot\frac{\partial^2}{\partial t^2}\left\{E^2\int_0^t d\tau\int_0^\tau E(\tau')d\tau'\right\}. \quad (11)$$

This expression includes two terms (the second and the fourth) describing dispersion of linear and nonlinear responses to be taken into account. Thus, slow process of SHEW formation is dominated by nonlinear Kerr electronic response while dispersion gives only small contributions (about 5% of inertia-free contributions to refractive index) which can be neglected in the first approximation. On the other hand, considering fast process of SHEW front evolution, one should take into account several terms describing dispersion of linear and nonlinear parts of refractive index.

3.3. Estimation of SHEW threshold

Estimating of threshold of SHEW formation is one of key problems because it allows to show applicability of proposed model to real situations. In case of dominating of nonlinear optical response one can neglect dispersion in the first approximation (section 3.2). Then that estimation can be obtained using the following simple consideration of field propagation in nonlinear isotropic medium with positive nonlinear index n_2.

Let us consider a part of instantaneous profile of electric field with amplitude E_0, propagating in nonlinear medium (Fig. 3a). Field disruption appears if point 1 of the profile with field value E_0 -ΔE has overtaken profile's top 2. That is possible because laser-induced addition to refractive index is larger at point 2 than at point 1, so, profile maximum slows down itself.

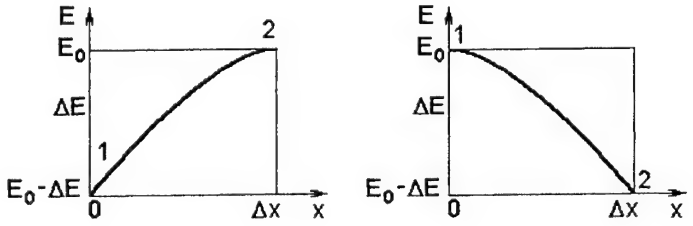

Fig. 3. A part of instant profile of laser wave near its maximum at the beginning of SHEW formation in nonabsorbing dielectric with positive (a) and negative (b) nonlinear coefficient of refractive index.

We consider not moving coordinate system which x-axis coincides with direction of wave propagation. If Δt is duration of moving of point 1 in nonlinear medium then coordinates of points 1 and 2 in the medium are respectively $x_1=\Delta t\cdot u_1$ and $x_2=\Delta x+\Delta t\cdot u_2$, where

$$u_2=\frac{c_0}{n_0+n_2E_0^2}, \quad u_1=\frac{c_0}{n_0+n_2(E_0-\Delta E)^2}, \quad (12)$$

c_0 - is light speed in vacuum, $n_0^2=\varepsilon_0$. According to the mentioned above $u_1=u_2+\Delta u$ and $u_1>u_2$. If field-induced addition to refractive index is smaller than n_0, we can apply perturbation technique to (12) and take into account only terms linear with respect to ΔE. The coordinates of points 1 and 2 will be the same at some moment $t+\Delta t$: $x_1=\Delta t\cdot u_1=x_2=\Delta x+\Delta t\cdot u_2$. Duration of disruption formation Δt can be estimated from the expression: $1/\Delta t=u/\Delta x$, which implies the following:

$$\frac{1}{\Delta t}=\frac{2n_2E_0}{n_0+n_2E_0^2}u_2\frac{\partial E}{\partial x}, \quad (13)$$

where $u_2=c_0/(n_0+\Delta n)$ - is speed of profile's maximum and $\Delta E/\Delta x \cong \partial E/\partial x$. Starting at moment t, the maximum have passed distance $s=u_2\Delta t$ in nonlinear medium by the moment $t+\Delta t$ that gives the following equation for E_0

$$E_0^2\frac{n_2}{s}-E_0\cdot 2n_2\frac{\partial E}{\partial x}+\frac{n_0}{s}=0. \quad (14)$$

Solution to the equation exists only if the following condition is satisfied

$$\left|\frac{\partial E}{\partial x}\right|\frac{s}{2}\geq\sqrt{\frac{n_0}{n_2}}. \quad (15)$$

This condition shows that field disruption cannot appear at arbitrary point of field profile, for example, at profile's top where derivative $\partial E/\partial x$ is about zero. At the same time the disruption cannot appear far from the top where field magnitude is too small. Integrating of (14) gives the following estimation for threshold field-amplitude of disruption formation:

$$E_{th} \approx \sqrt{\frac{n_0}{n_2}\left(\exp\left\{\frac{\Delta x}{s}\right\}-1\right)}, \tag{16}$$

where $\Delta x \leq s$. For example, disruption threshold is $I_{th} \leq 6 \cdot 10^{13}$ W/cm^2 for n_0=1.45, n_2=2·10^{-16} cm^2/W (fused silica), $s=z_c=30\lambda_0/n_0 << L_{DISP}$, $\Delta x=0.25\lambda_0/n_0$. Confocal parameter corresponds to focal spot radius $d_f=2.13\lambda_0$ (=1.71 μm, λ_0=0.8 μm).

Similar consideration is valid for negative nonlinear coefficient of refractive index. In this case top of field profile (Fig. 3b) can overtake a part of the profile moving at distance Δx in front of the top, i.e., geometry of this problem is reversed with respect to that depicted in Fig. 3a and point 1 corresponds to profile's. This implies the points 1 and 2 to move with the following speeds

$$u_1 = \frac{c_0}{n_0 - n_2 E_0^2}, \quad u_2 = \frac{c_0}{n_0 - n_2 (E_0 - \Delta E)^2}. \tag{17}$$

Similar consideration shows that disruption threshold can be estimated in the following way:

$$E_{th} \approx \sqrt{\frac{n_0}{n_2}\left(1-\exp\left\{-\frac{\Delta x}{s}\right\}\right)} \tag{18}$$

Obtained estimations (16) and (18) show that SHEW can appear at laser intensities ranging between 10^{13} W/cm^2 and 10^{14} W/cm^2 that are close to threshold of femtosecond laser-induced damage in transparent materials. That is very pessimistic estimation of SHEW threshold because 1) we considered formation of very hard SHEW corresponding to mesh of ¼ of initial optical cycle, 2) the path of nonlinear interaction s can be larger than the value used in numerical estimations. Optimistic estimation of SHEW threshold is about 10^{12} W/cm^2.

4. SIMULATION OF SHEW FORMATION AND PROPAGATION

4.1. FDTD technique for modeling

More detailed information on SHEW formation and propagation can be obtained from modelling and numerical calculations according to model (1)-(6). The most promising technique for that type of modelling is *finite-difference time domain technique* (FDTDT) [24-25]. A very brief description of calculation method used by the authors is given in this section because FDTDT has already been described many times [26, 27].

Simulation method used by the authors is based on dependence of field magnitude at fixed time-space point on field magnitudes at previous moments in neighboring points. The dependence is derived from nonlinear differential wave equation (1) by reducing it to a finite-difference equation in traditional way [26, 27]. So, the following updating finite-difference equation is obtained

$$E_x^t = 2E_{x-1}^{t-1} - E_{x-1}^{t-2} + \frac{(c_0 \cdot \Delta t)^2}{(\cdot \Delta x)^2}\left(E_{x+1}^{t-2} - 2E_x^{t-1} + E_{x-1}^t - \frac{4\pi}{c_0^2}\left((P_{x-1}^{t-1})^3 - 2(P_x^{t-2})^3 + (P_{x+1}^{t-3})^3\right)\right), \tag{19}$$

where Δx is period of regular spatial mesh, and Δt is corresponding time increment. The obtained dependence describes field evolution in medium with certain parameters if field source is given. Using of the model (2)-(6) to describe dispersion of refractive index allows to avoid the problem of appearing of field disruptions during SHEW formation because dispersion smoothens the disruptions and makes structure of SHEW front more complicated. The only problem is to take into account enough contributions from higher harmonics that is connected with problem of resolution discussed below.

Similar finite-difference equations can be derived from (3) – (6) and attached to (19) to solve a consequence of coupled equations. Field evolution is observed in the form of animation that can be stopped at any appropriate time. Outgoing waves are described by functions of the following type: $F(x-ct)$ at exit boundary of space grid and $E_s+F(x+ct)$ at entrance boundary. This allows to exclude artificial reflection and calculation mistakes at the boundaries. E_s is source field which is assumed to be as follows $E_s = E_0 \sin(2\pi t / \nu)$. This source describes normal incidence of plane linearly polarized monochromatic wave of amplitude E_0 and frequency ν onto plane surface of considered medium.

For stability of calculations to be obtained the calculation procedure is subjected to the following well-known criterion[28]

$$c \cdot \Delta t < \Delta x , \tag{20}$$

where Δx - is space grid period, and Δt - is corresponding time increment. This allows to exclude increasing of calculation mistakes. In our modeling we chose the ratio $\Delta x /(c\Delta t)$ to be 2 that implies number of time "cells" per laser period to be two times more than number of space "cells" per laser wavelength. Calculation stability was also controlled through energy conservation law by integrating of squared electric field over all calculation mesh and calculating of energy flows.

Space resolution of our calculations varied from 200 to 800 cells of spatial mesh per radiation wavelength in vacuum to give appropriate resolution. Development of field disruptions and SHEW is investigated with resolution 200 cells per wavelength. That resolution was chosen from the following estimations. Minimum number of space cells per wavelength to catch certain harmonic correctly is 5 that correspond to the following points of wave: zero point – point of maximum – zero point – point of minimum – zero point. Thus, space resolution allows to describe correctly harmonics of the order no higher than 200/5=40, i.e., the first higher harmonic we loose in modeling of SHEW formation and propagation is the 41-st harmonic. Its contribution to total field is similar to accuracy of our calculations (about 0.01% of field amplitude) and it can be neglected. That was also confirmed by calculations with space resolution of 400 cells (catching of upto 80-th harmonic) and 800 cells per wavelength (catching of upto 160-th harmonic). Full length of calculation space is 25 laser wavelengths in vacuum, i.e., 5000 calculation cells for resolution of 200 cells per wavelength.

To determine accuracy of developed simulation model, it has been tested in case of linear light propagation through boundary of two transparent dielectrics with different refractive indexes and plane dielectric layer (Fabri-Perout resonator). Results of calculations are in excellent agreement with well-known theoretical results [29] within accuracy of (±0.01%).

4.2. SHEW formation in transparent solids

First, process of SHEW formation was studied by numerical modelling. Fig. 4 depicts a snapshot of instant field profile in nonabsorbing medium. Appearing and evolution of SHEW is clearly seen from that figure. Large-scale variations of electric field are depicted in Fig. 5 as snapshot of instant field distribution in larger part of calculation mesh. Interesting point is relatively fast decay of total electric-field strength in nonabsorbing (!) medium. That is connected with energy transfer to higher harmonics and energy spreading due to dispersion.

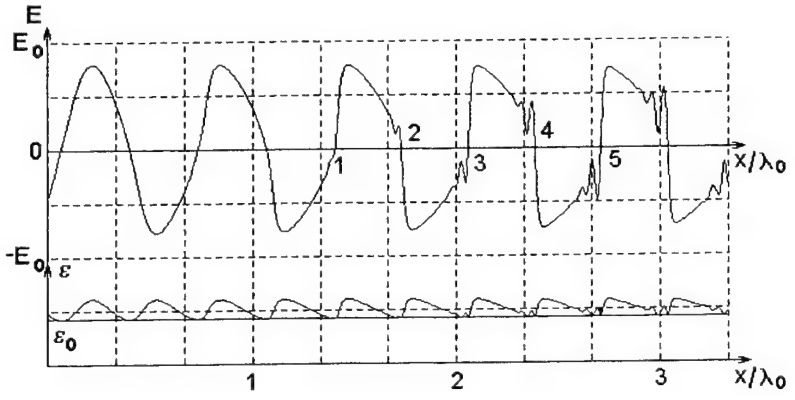

Fig. 4. Evolution of SHEW propagating in non-absorbing dielectric (fused silica, n_0=1.41). Points of interest: 1 – appearing of field disruption on wave profile (SHEW front); 2 – its evolution with formation of variations near SHEW front; 3, 4, 5 – developing of SHEW front and formation of high-frequency pulsation near SHEW front resulting from higher harmonics generation. A laser-induced variation of dielectric response is shown in the lower part of this figure. Input field amplitude is above damage threshold in order to obtain good illustrative picture with fast SHEW formation (high-frequency pulsations can not be made out in the picture otherwise).

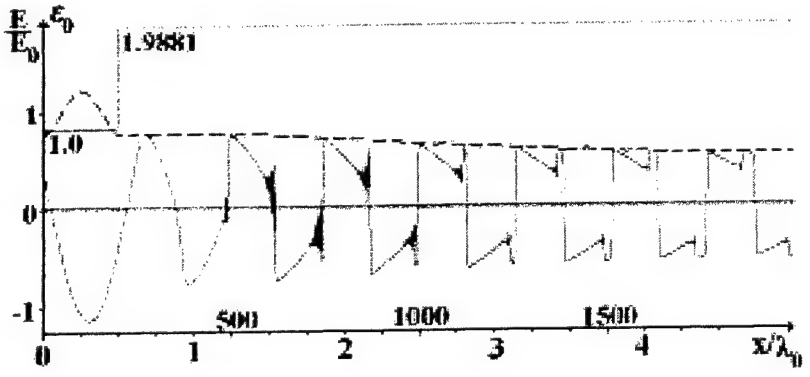

Fig. 5. SHEW formation and propagation in transparent non-absorbing dielectric (fused silica) with linear dielectric response ε_0=1.9881. Grey line in upper part of the figure depicts boundary between vacuum and the dielectric. Resolution 400 calculation cells per laser wavelength.

The last question to be considered in this paper is higher harmonic (HH) generation during SHEW formation in transparent materials. Calculations of radiation spectrum are based on straight Fourier transformation of field variations in time for selected space points. For example, Fig. 6 depicts spectrum of SHEW propagating in nonabsorbing dielectric with ε_0=1.9881 after it has passed 6-wavelength path in nonlinear medium (Fig. 6 is related to situation depicted in Fig. 5). One can see only odd harmonics that is characteristic of shock wave of arbitrary nature propagating in material with small energy dissipation and dispersion [1-4, 30, 31]. Characteristic features are also fast decreasing of amplitudes of low-order harmonics with increasing of their order and nonmonotonous decreasing of amplitudes of high-order harmonics – local maxima of harmonics amplitudes appear with period of 6 harmonics (Fig. 6). Spectrum structure has no steady form and varies within whole path of SHEW propagation. General trend of the variations is connected with dominating energy transfer back to main harmonics and fast decay of higher harmonics. Thus, there must be a path of SHEW propagation that corresponds to the most efficient excitation of higher harmonics.

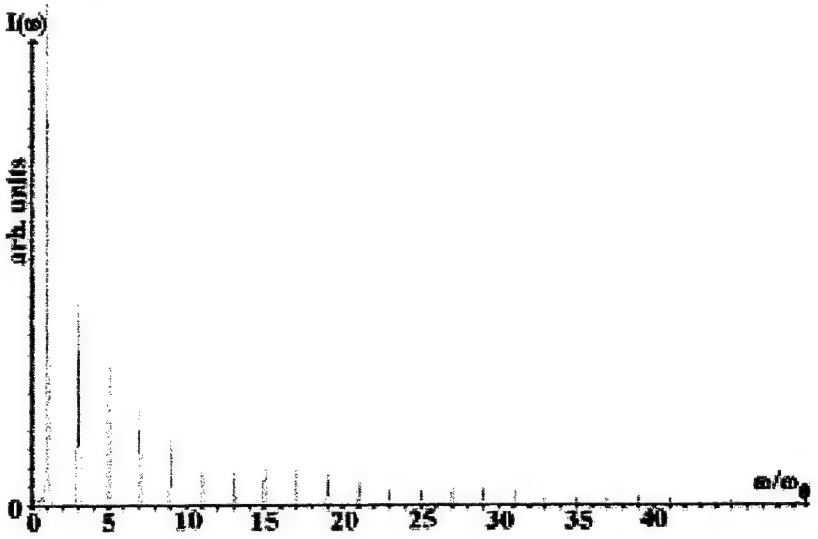

Fig. 6. Spectrum of SHEW propagating in non-absorbing dielectric (fused silica). Obtained after SHEW has passed 6-wavelength distance in the medium. Space resolution of modelling is 200 cells per wavelength, resolution of spectrum calculations is 10% of central frequency ω_0 of input laser pulse. That resolution is kept for all calculated spectra presented below.

5. CONCLUSIONS

Thus, we have shown that SHEW on optical cycle resulting from generation of higher harmonics can appear at certain conditions characteristic of femtosecond pulse propagation in transparent media. SHEW can appear only near leading edge of femtosecond laser pulse where influence of dispersion is minimal. This makes leading-edge form of the pulse of critical importance for process of SHEW formation. Presented results were obtained for rectangular pulses where this problem disappears but it can be critical for pulses with smooth leading front. Important point in this connection is self-steepening process resulting in sharpening of leading front [10] and making it closer to rectangular form. SHEW formation gives one of important examples of processes where exact wave equation (1) must be applied for investigation of nonlinear optical processes because of possible presence of backward moving waves reflected from laser-induced variations of reractive index. Possibly, being based on (1), analysis of high-power nonlinear optical processes induced by femtosecond laser pulses will give better agreement of theoretical results with experimental data.

Important result is also estimation of threshold of SHEW formation. It is interesting that SHEW can appear only at parts of wave front where space derivation of electric-field strength is above certain threshold even if pulse intensity is above SHEW threshold. Estimated SHEW threshold shows that it can appear at laser intensity between threshold of white-light generation and damage threshold. In particular, SHEW can be formed at initial stages of femtosecond laser-induced damage of transparent materials. Important point is that SHEW threshold does not depend straight on laser wavelength while there is strong dependence on refractive index, its nonlinear coefficient and focusing geometry through parameter *s*.

Important features of SHEW show at least two ways to detect SHEW in experiments. The first of them is connected with specific spectrum structure of HH appearing during SHEW formation (Fig. 6). One can expect appearing of odd harmonics (in isotropic materials) surrounded by Stocks and anti-Stocks wings at early steps of pulse propagation. Problem of the spectrum registration can be connected with developing of electron plasma which emission spectrum covers SHEW spectrum. Thus, pure SHEW spectrum can hardly be observed at times more than time of plasma formation (about 20 fs).

Other way of SHEW detection is connected with frequency shift of low-power probe beam [1-3] resulting from reflection at moving SHEW front. Nature of that shift is similar to well-known Doppler effect and can be calculated for two geometries of probe-beam reflection (Fig. 7) – when the beam propagates in the same direction as SHEW and when the probe beam propagates toward SHEW. In both cases transmitted and reflected parts of probe signal have different frequency shifts. For example, in case of probe beam propagating in the same direction as SHEW one can use the following formula for reflection at moving SHEW front

$$\frac{\omega^{refl}}{\omega_0} = \frac{v_2 - v_{SEW}}{v_2 + v_{SEW}} \tag{21}$$

and for transmission through SHEW front:

$$\frac{\omega^{trans}}{\omega_0} = \frac{1 + v_{SEW}/v_1}{1 + v_{SEW}/v_2} \tag{22}$$

where v_1 is light speed for probe signal in front of SHEW, and v_2 is light speed behind the SHEW (Fig. 7). Thus, detection of frequency shift of low-power probe beam reflecting at SHEW front allows both straight detection of SHEW and measurement of its speed. Having information about SHEW speed allows estimating value of field disruption at SHEW front.

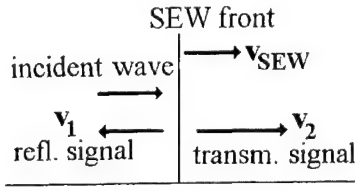

Fig. 7. Geometry of low-power probe beam reflection at SHEW front resulting in frequency shift which depends on SHEW speed.

Influence of SHEW can help to explain many observed regularities of nonlinear propagation of femtosecond pulses. In particular, SHEW concept is very promising for theoretical investigation of non-thermal mechanisms of femtosecond laser-induced damage of transparent materials [19]. Generation of higher harmonics of extremely high orders is other promising application of SHEW model. As one can see from estimation (16), the larger laser intensity, the smaller path is required to form SHEW front and to generate HH. Thus, HH can appear even during reflection if laser intensity is much above SHEW threshold what is typical for experiments on HH generation by femtosecond pulses.

6. ACKNOWLEDGEMENTS

Authors wish to thank Prof. M.N.Libenson (S.I.Vavilov State Optical Inst., Russia) and Prof. S.A.Kozlov (State Inst. of Fine Mechanics and Optics, St.Petersburg - Technical University, Russia) for fruitful discussions of various aspects of shock waves This work was partly supported by INTAS grant 97-31777 and grant of Russian Foundation for Basic Research N 00-02-16716-a.

7. REFERENCES

1. A.M.Beliantsev, A.V.Gaponov, G.I.Freidman, "Structure of shock electromagnetic wave front in transmission lines with nonlinear parameters", URSI Symposium, Delft, Nehterlands, 1965 in *Electromagnetic wave theory*, Pergamon Press, 1967.
2. A.V.Gaponov, L.A.Ostrovsky, M.I.Rabinovich, "Electromagnetic waves in non-linear transmission lines with active parameters", URSI Symposium, Delft, Nehterlands, 1965 in *Electromagnetic wave theory*, Pergamon Press, 1967.
3. G.B.Whiteham, "Nonlinear dispersive waves", *Proc. Roy. Soc.*, Ser. A, v. **283**, 1965, p. 238
4. L.A.Ostrovsky, "Propagation of modulated waves in nonlinear dispersive media", URSI Symposium, Delft, Nehterlands, 1965 in *Electromagnetic wave theory*, Pergamon Press, 1967.
5. G.Rosen, "Electromagnetic Shocks and the Self-Annihilation of Intense Linearly Polarized Radiation in an Ideal Dielectric Material", *Phys. Rev.*, v. **139**, N 2A, pp. A539-A543, 1965.
6. F.DeMartini, C.H.Townes, T.K.Gustafson, P.L.Kelley, "Self-Steepening of Light Pulses", *Physical Review*, v. **164**, N 2, pp. 312-323, 1967.
7. S.A.Kozlov, S.V.Sazonov, "Nonlinear propagation of optical pulses with a few light oscillation duration in dielectric media", *JETP (Sov. Physics - JETP)*, v. **111**, N 2, pp. 404-418, 1997.
8. N.R.Belashenkov, V.V.Bezzubik, S.A.Kozlov, S.V.Sazonov, "Nonresonant self-action of pulses with a few light oscillation duration", in *Ultrafast Processes in Spectroscopy*, Plenum Publishing Corp., New York, pp. 167-170,

1996.
9. J.E.Rothenberg, D.Grischkowsky, "Observation of the formation of an Optical Shock and Waves Breaking in the Nonlinear Propagation of Pulses in Optical Fibers", *Phys. Rev. Letters*, v. **62**, N 5, pp. 531-534, 1989.
10. J.K.Ranka, and A.L.Gaeta, "Breakdown of the slowly varying envelope approximation in the self-focusing of ultra-short pulses", *Opt. Letters*, v. **23**, N 7, pp. 534-536, 1998.
11. C.B.Schaffer, E.N.Glezer, N.Nishimura, and E.Mazur, "Ultrafast laser induced microexplosions: explosive dynamics and sub-micrometer structures", in *Commercial Applications of Ultrafast Lasers*, Proc. SPIE, v. **3269**, pp. 36-45, 1998.
12. H.K.Park, R.F.Haglund Jr., "Laser Ablation and Desorption from Calcite from Ultraviolet to Mid-Infrared Wavelengths", *Appl. Phys. A*, v. **64**, pp. 431-438, 1997.
13. C.B.Schaffer, A.Brodeur, N.Nishimura, and E.Mazur, "Laser-induced microexplosions in transparent materials: microstructuring with nanojoules", Proc. SPIE, v. **3616**, 1999, to appear.
14. D.Ashkenasi, A.Rosenfeld, H.Varel, M.Wahmer, E.E.B.Campbell, "Laser processing of sapphire with picosecond and sub-picosecond pulses", *Appl. Surface Science*, v. **120**, pp. 65-80, 1997.
15. E.E.B.Campbell, D.Ashkenasi, and A.Rosenfeld, "Ultra-short-Pulse Laser Irradiation and Ablation of Dielectrics", in *Lasers in Materials*, edited by R.P.Agarwal (Trans Tech Publ., 1998), Ch. 5.
16. R.F.Haglund, Jr., "Mechanisms of Laser-Induced Desorption and Ablation", in *Laser Ablation and Desorption*, eds. J.C.Miller and R.F.Haglund, Jr. (Boston, Academic Press, 1998), pp. 15-138.
17. D.von der Linde, H.Schuler, "Breakdown threshold and plasma formation in femtosecond laser-solid interaction", *JOSA B*, v. **13**, N 1, pp. 216-222, 1996.
18. A.Brodeur, S.L.Chin, "Band-Gap Dependence of the Ultrafast White-Light Continuum", *Phys. Rev. Lett.*, v. **80**, N 20, pp. 4406-4409, 1998.
19. A.S.Gruzdeva, V.E.Gruzdev, "Interaction of shock electromagnetic waves with transparent materials: classical approach", in *Laser Applications to Microelectronic and Optoelectronic Manufacturing-VI*, Proc. SPIE, v. **3933**, 2000 (to appear).
20. A.Bouhal, R.Evans, G.Grillon, A.Mysyrowicz, P.Breger, P.Agostini, R.C.Constantinescu, H.G.Muller, D. von der Linde, "Cross-correlation measurement of femtosecond noncollinear high-order harmonics", *JOSA*, v.**14**, pp. 950, 1997
21. O.G.Kosareva, V.P.Kandidov, A.Brodeur, C.Y.Chien, S.L.Chin, "Conical emission from laser-plasma interactions in the filamentation of powerful ultrashort laser pulses in air", *Opt. Lett.*, v. **22,** N 17, pp. 1332-1334, 1997.
22. S.A.Kozlov, «On classical dispersion theory of high-power light», *Optics and Spectroscopy*, v. **79**, N 2, pp. 198-200, 1995 (translated from Russian *Optica i Spectroscopia,* v.**79**, N 2, pp. 290-292, 1995).
23. R.V.Hohlov, "On the theory of shock radio waves in nonlinear lines", Radiotekhnika i Electronika, N 6, pp. 917-925, 1961 (in Russian).
24. V.E.Gruzdev, A.S.Gruzdeva, "Formation and propagation of shock electromagnetic waves in transparent solids", in *High-Power Ablation II*, Proc. SPIE, v. **3885**, 2000 (to appear).
25. V.E.Gruzdev, A.S.Gruzdeva, "Formation of shock electromagnetic waves during femtosecond pulse propagation in transparent solids", in *Optical Beam and Pulse Propagation*, Proc. SPIE, v. **3927**, 2000 (to appear).
26. K.S.Yee, "Numerical solution of initial boundary value problems in isotropic media", *IEEE Transactions on Antennas and Propagation*, **AP-14**, p.302, 1966.
27. S.J.Yakura, J.T.McGillivray, "Finite-Difference Time-Domain Calculations Based on Recusive Convolution Approach For Propagation of Electromagnetic Waves in Nonlinear Dispersive Media", Final Report PL-TR-97-1170, AF Research Laboratory, Kirtland AFB, NM, 30 October 1997.
28. N.N.Kalitkin, *Numerical Methods*, Nauka Publ., Moscow, 1978, Ch. XIII (in Russian).
29. M.Born, E.Wolf, *Principles of Optics*, 4-th ed. Pergamon Press, N.Y.,1968, Ch.1.6.
30. Ya.B.Zel'dovich, Yu.P.Raizer, *Physics of Shock Waves*, Academic Press, New York, v. I, 1966, v. II, 1968.
31. M.B.Vinogradova, O.V.Rudenko, A.P.Sukhorukov, *Theory of Waves*, Nauka, Moscow, 1990 (in Russian).

High-power laser plasma source of nuclear reaction

A.A.Andreev[1], A.V.Charukchev[2], V.E.Yashin[1]

[1] Institute for Laser Physics, St.Petersburg, Russia
[2]Institute for complex tecting of opto-electronic systems, Leningrad region, Sosnovy Bor.

ABSTRACT

During the interaction of picosecond laser pulse of intensity $5x10^{18}$ W/cm^2 with the target we observed a MeV energy proton beam, confined in a cone angle ~ 30° and directed normal to the target surface. Laser conversion efficiency into fast ions energy (at the front side of the target) was ~ 1 % (and near 5% at the rear). The simulations and optimisation of ion acceleration is discussed here. The laser intensity being ~10^{19} W/cm^2, nuclear reactions proceed in the target, particularly resulting in production of the γ-line radiation. In light materials irradiated by the laser beam the γ-photon yield reaches 10^{-4} number of fast ions. For nuclear excitation we used also X-ray pump from laser plasma to illuminate film mixture of KBr and Rb^{84}. Near 10^4, 200 Kev decay γ –photons from excited isomer nuclei can be produced per laser shot

Keywords: nuclear reaction, superstrong laser fields, high peak intensity, laser plasma

1. INTRODUCTION

It is well known already that high intensity laser pulse can produce nuclear reactions when interacting with different targets. To date, many applications call for using a source of γ -radiation, and the vast scope of applications range from non destructive gamma flaw detection to medical examinations[1]. It should be noted that, presently, the intensity of ordinary radioactive sources cannot be higher than 10-100 GBk, whereas much higher intensity is necessary for many applications.

Commonly, synchrotron radiation is used as a high-intensity γ -source, its activity being about PBk. However, significant success notwithstanding, the use of the synchrotron radiation as a γ -source has some essential drawbacks. First, it is impossible to obtain high intensity γ -radiation in a very narrow frequency range, because the synchrotron radiation spectrum is continuous. Hence narrow-frequency-band experiments with a high-power γ -source appear to be impossible, because the power of such a γ - radiation source drops as the frequency range narrows and it is difficult to cut a narrow MeV spectral range with any filters. The second reason is that synchrotron radiation source is a expensive for some applications.

In this paper, we consider two possibilities for laser excited monochromatic γ -source. First - using nuclear isomers as a high-intensity frequency-conversion γ -source. The nuclei are prepared in the isomeric state. Then the isomeric ground-state nuclei are pumped to an excited isomeric state, wherefrom an active γ -transition arises by the X -ray radiation from laser plasma produced by the action of high-intensity laser pulse on a solid-state target. The second method is laser-plasma acceleration of fast ions to generate nuclear reactions with high γ yield on interaction of fast protons with different targets.

2. BASIC CONCEPT OF A LASER TRIGGERING MONOCHROMATIC NUCLEAR γ - SOURCE

To produce MeV range energy photon emission we should use nuclear excitation instead of atomic excitation because even for high charge Z ions the energy of quanta estimated as RyZ^2 can not exceed 100 KeV.

As direct excitation of nuclear by laser field has very low efficiency we will consider some indirect processes whereby laser energy is transformed into electron energy effectively enough at first and then through another channels to cause nuclear excitation.

On Figure 1 we suggest for following analysis the different methods of γ – photon production involving high power laser radiation.

Laser Optics 2000: Ultrafast Optics and Superstrong Laser Fields, Alexander A. Andreev, Vladimir E. Yashin, Editors, Proceedings of SPIE Vol. 4352 (2001) © 2001 SPIE · 0277-786X/01/$15.00

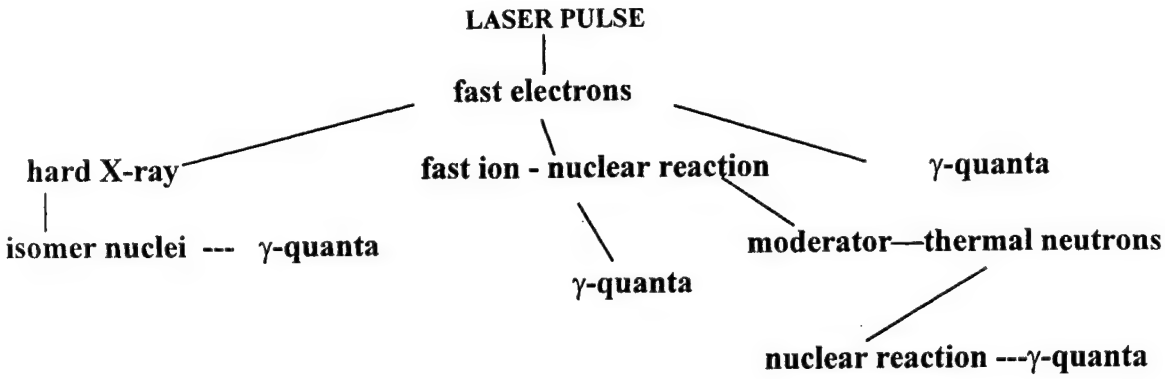

Figure 1. Laser γ-radiation conversion scheme

3. INDUCED γ - FLUORESCENCE OF ISOMERIC NUCLEI

If we have not very much laser intensity we can use the isomer nuclear method[2]. Let's first consider the main idea of a high-intensity γ - source using isomer nuclei (see Fig.2)

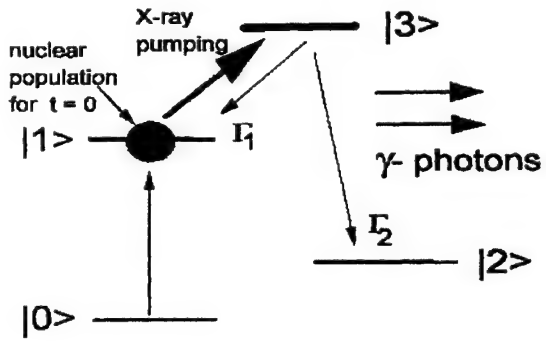

Figure 2. Three level scheme for isomer nuclei pumping X-ray

We assume that the |3>-|2> active γ -transition is pumped in two steps. First, atoms in the |1> nuclear isomeric state should be prepared. We can estimate the γ - radiation pulse power suppose that all isomeric nuclei in the target being pumped. We assume that the confinement region of the target is ~ 10^{-3} cm^{-3}, whereas the number of isomeric nuclei is $N_0 \approx 10^{12}$. Then the γ-radiation power, on condition that all isomeric nuclei in the target are pumped, is 10^{12} γ-photons during plasma lifetime $\tau_i \leq 1/\Gamma_0$ – lifetime of the |3> upper excited state. Nuclear level width Γ_0 can be estimated from matrix element of nuclear magnetic momentum:

$$\Gamma_0 = \Gamma_1 + \Gamma_2 \approx \frac{4\omega_{13}^3}{3\hbar c^3}\mu_{13},$$

where $\omega_{13} = \omega_x$ –frequency of X-ray pumping. Also the natural width of the |3> excited state, Γ_0, can be obtained from a one-partial Waiskopth's approximation as[5]: $\Gamma_0 = T(M1) = 1.76*10^{13}E_\gamma\ ^3B(M1)$, where $B(M1)=(7.5)^2/(10\pi)$ has to be taken in units $(eh/(4\pi Mc))^2$, while the γ-photon energy - E_γ in MeV, if we consider transition |3> - |2> as M1 [7]. Then the natural width value is $\Gamma_0 \approx 10^9$ s^{-1} for $\lambda_\gamma \approx 6*10^{-9}$ cm, $E_\gamma = \hbar\omega_\gamma$ =20 KeV. Then the total energy of the γ -radiation will be about $2*10^{-3}$ J.

At the same time, the width of the γ -radiation spectrum, which is emitted by the |3> - |2> transition, is governed by the Doppler effect caused the recoil during absorption of the X-ray pump. So Doppler shift of γ - line from recoil effect is the same for all nuclei $\Delta\omega_{\gamma D} = \hbar k_\gamma^2 / Am_p$ and Doppler width is $\Gamma_D = \hbar k_x k_\gamma / Am_p$ because nuclei obtain velocity $\hbar k_x / Am_p$ at absorption of pump X-ray quantum Where $k_{\gamma,x}$ is the wave vector of the γ, X -radiation, m_p -is the proton mass, and A is the atomic number. For the above values, the width of the γ -radiation spectrum is $\Gamma_D = 10^{13}$Hz. Line width is increased at isomer ionization from addition nuclear heating because all Z* ionized electrons with energy ~ $\hbar\omega_x$ give velocity to nuclei ~ $Z^*\sqrt{m_e\hbar\omega_x}/Am_p$ and it increases line width up to $(Z^*\sqrt{m_e c/\hbar k_x})\hbar k_\gamma k_x / Am_p$.

Finally ionized electrons heat nuclear by collisions, but in our case time of e-i collisions much more compare to γ - quantum generation time and line width does not increase up to $k_\gamma\sqrt{T_e / Am_p}$.

3.1. X-ray pumping of the isomeric nuclei

In this section, we discuss the conversion efficiency of emission from hot laser plasma of X-ray photons to produce γ - photons in isomeric nuclei confined in a target. Presently, the X-ray pumping with such high intensity (when the number of resonant X-ray photons is at least equal to the number of the isomeric nuclei in the target) can be obtained only when a laser radiation pulse with a high power acts on a solid-state target. We will consider laser plasma thus produced as a source of blackbody radiation.

Let us now estimate the number of the isomeric nuclei which are activated in a target when pumped by X-radiation of a laser plasma. The X-ray photon flux from a unit area on the surface of a hot plasma spot is equal to

$$(d N_x/dt\, d\omega_x\, dS) = (\omega_x^2 /\pi^2 c^2)/[\exp(h\omega_x/2\pi T) - 1] \qquad (1)$$

where T is the temperature of the laser plasma, and ω_x and N_x are the frequency and the number of X-ray photons, respectively. Assuming the plasma spot area to be S and the thickness of a cloud of the isomeric nuclei along the pump propagation direction to be a, it is possible to estimate the overall cross section for X - ray pump resonant absorption by an ensemble of nuclei with concentration n_i in a target by

$$\sigma_f = \Delta\Omega n_i S\, a\, \sigma_x, \qquad (2)$$

where $\Delta\Omega \approx 1$ – geometrical factor, $\sigma_x = 2\pi c^2/\omega_x^2$ is the X-ray resonant absorption cross section (we have assumed that the laser plasma, which is produced under the action of a sub-picosecond high-power laser pulse on a solid-state target, is near the region where the activated atoms are located). Then, during plasma lifetime τ_i, N_s isomeric nuclei in the volume of a target will rise to the $|3>$ upper active level

$$N_s = (d N_x/dt\, d\omega_x\, dS)\, \sigma_f \Gamma_0 \tau_i \approx \Delta\Omega(2/\pi)\, N_0 \Gamma_0 \tau_i /[\exp(h\omega_x/2\pi T) - 1] \qquad (3)$$

As can be seen from (3), only a small fraction of nuclei found in the target can be activated. For example, for $\tau_i \approx 10^{-11}$ sec, $\Gamma_0 = 10^9$ sec^{-1}, that is, the number of activated nuclei is about 10^{-4} of the initial number of nuclei N_0.

It should be emphasized that (3) defines the number of activated nuclei in a target without any losses. To determine the real concentration of the isomeric nuclei in the target, N_γ, it is necessary to take into account the X-ray photon loss via two main processes:

photo-effect in a continuous X-ray pump spectrum with cross section

$\sigma_{ph.eff.}(\omega_x) = 15.4\pi\, \alpha^4 Z^5 e^2/(m_e c^2)^2\, (2\pi m_e c^2/h\omega_x)^{7/2}$, at $h\omega > I_z$ – ionisation potential of atom;

$$\sigma_{ph.eff.}(\omega_x) \approx \pi R_{Bohr}, \text{ at } h\omega < I_z; \qquad \sigma_{ph.eff.}(\omega_x) \approx \pi \lambda_x^2, \text{ at resonance} \qquad (4)$$

and the absorption of X-ray photons at other nuclear and electronic levels.

Note that the atomic electron shells feature resonance absorption cross sections much larger than σ_x. Therefore, it is necessary to cut off the low-frequency portion of the pump spectrum. This can be done using a filter which cuts off pump frequencies lower than ω*. As a result, the actual concentration of activated isomeric nuclei can be found from the equation

$$N_\gamma = N_S/\{1 + \Sigma_i\, (\gamma_i/\Gamma_0)(\exp(E_x) - 1)/(\exp(E_i) - 1) + \int_{\omega^*} \sigma_{ph.eff.}(\omega_0)(\omega_0/c)^2)(\exp(E_x) - 1)/(\exp(E_0) - 1)\, d\omega_0/2\pi\Gamma_0\} \qquad (5)$$

Here $E_j = h\omega_j/2\pi T$ (j = 0, x, i), where both nuclear and electronic levels, which have frequencies lying in the pump spectral interval, are included in the sum over i from 1. Thus, each of such resonance has absorption cross section $\sigma_i = 2\pi c^2/\omega_i^2$ and width γ_i. If we assume the energy of pump photons to be $h\omega_j > T$, $h\omega^*$, then $\omega_i > \omega_x$ for all i ($\omega^* < \omega_x < \omega_i$), the terms in the sum in the denominator of fraction (5) will be exponentially small.

Next we estimate loss of pump photons due to ionisation. To this end, it is necessary to calculate the integral in the denominator of fraction (5). As a result, the condition for small losses of activated atoms due to ionization can be written as [4]:

$$K_I = 7.4\, Z^5 \alpha^6\, (2\pi m_e c^2/h\omega^*)^{3/2}(2\pi T/h\gamma_0))(\exp(E_x) - 1)\exp(-h\omega^*/2\pi T) \le 1, \qquad (6)$$

where $\alpha = 1/137$. By substituting $h\Gamma_0 = 10^{-6}$ eV ($\Gamma_0 = 10^9$ c^{-1}) $h\omega^* = 511$ eV, $h\omega_x - h\omega^* < T$ and $T = 400$ eV in (6), we obtain an estimate for the charge of the isomeric nuclei: $Z < 10$. Therefore, to obtain the nuclei with the charge much larger than Z=10, it is necessary to increase X-ray pumping by increasing laser pulse intensity. In another case we will have the decreasing of the number of active nuclei in K_I times.

3.2. Pumping by K_α line radiation.

We can increase X-ray yield at oblique incidence at angle θ of P-polarized laser radiation by resonant absorption, when fast electrons appear at temperature T_h and free path $l_{Th} \sim T_h^2/n_i$.
In this case X-ray yield in continuum can be estimated as:

$$I_x \approx I_{xT}(l_{Th}/l_T) \approx 10^{-3} z^3 I^{0.14} T_h^2 \approx 0.05 z^3 I^{1.64} (\frac{\lambda}{\cos\theta})^{1.5},$$

where $T_h \approx 50.0(\frac{I\lambda^2}{\cos\theta})^{\beta}, (\beta \approx \frac{1}{2} - 1)^{6,7}$

Anyway the spectral brightness of such X-ray pump in nuclear transition is not so high. From this reason we analyse the possibility of plasma line X-ray emission at energy approximately equal to nuclear transition energy. For this case the best candidate is K_α - line because the energy of such X-ray quanta can be very high.

Let's estimate the intensity of K_α - line emission from a flow of fast electrons interacted with over dense plasma at resonant absorption of laser radiation. For non-relativistic laser intensity according to equations: $mn_{eh}v_h^{3/2} = \eta_h I_L$, we can calculate the concentration of fast electrons $n_{eh} \approx \eta_h n_c I_{18}^{\beta/2}$, where n_c - electron concentration in critical point.

Then we obtain for $n_i^{(+1)}$ - ion concentration at charge +1: $n_i^{(+1)} = n_i[1 - \exp(-n_e^{(h)} v_i^{(z)} \tau)]$, *here* $v_i^{(z)} = 10^{-8}(Ry/I_z)A_i(\gamma^{-1/2} + \chi_i\gamma^{1/2})^{-1}\exp(-1/\gamma)$ - ionisation velocity of atom from ground level, $\gamma = T_h/I_z$, I_z - ionisation potential, $A_i = 60, \chi_i = 0.7, n_i = 6 \cdot 10^{22} cm^{-3}$.

Then we obtain for K_α - line intensity:

$$I_{k_\alpha} = \Delta E_{k_\alpha} n_i^{(+1)} A_{k_\alpha} l_{Th} \sim \Delta E_{k_\alpha} Z_{nu}^5 I_z^{-1/2} \lambda^{-2} T_h^{3/2} \tau, \quad here \quad A_{k_\alpha} \approx 5 \cdot 10^7 Z_{nu}^4 \text{ [s}^{-1}\text{]}$$

- probability of radiation decay, l_{Th} - free path of fast electron.

At $T_h \sim (I\lambda^2)^{\beta}$ we obtain $I_{k_\alpha} = \Delta E_{k_\alpha} I_z^{-1/2} Z_{nu}^5 (\frac{E_L}{s})^{3\beta/2} \lambda^{-2+3\beta} \tau^{1-3\beta/2}$

At $\beta = 2/3$: $T_h \sim (I\lambda^2)^{2/3}$ and the K_α line intensity is determined by the next approximation:

$$I_{k_\alpha} \approx 4 \cdot 10^8 \left(\frac{\Delta E_{k_\alpha}}{1keV}\right)\left(\frac{I_z}{1keV}\right)^{-1/2}\left(\frac{Z_{nu}}{10}\right)^5\left(\frac{E_L}{0.1J}\right)\left[\frac{W}{cm^2}\right]\left(\frac{d}{20\mu m}\right)^{-2}$$

Calculation according this formula line emission from Al plasma for data of [8] gives $I_{k_\alpha} = 7 \cdot 10^{12} W/cm^2$, and it has good agreement with experimental results.
We compare this formula with intensity of black-body radiation in the same band of quantum energies:

$$I_T \approx 2.5 \cdot 10^{11}\left(\frac{T}{1kev}\right)^4\left(\frac{\Gamma_{k_\alpha}}{T}\right)\left(\frac{\Delta E_{k_\alpha}}{T}\right)^3\left(\frac{1}{\exp(\Delta E_{k_\alpha}/T) - 1}\right)\left[\frac{W}{cm^2}\right]\left(\frac{d}{20\mu m}\right)^{-2},$$

where T-temperature, $\Gamma_{K\alpha}$ - a line width, estimated as $\Delta E_{K\alpha}(v_i/c)$.

For T=1 kev, E_L=1J, $\Delta E_{K\alpha}$ =3.4 kev, Z_{nu}=16, I_z =50, A=32 the ratio $I_{k\alpha}/I_T \approx 2.4 \cdot 10^2$. Thus we have magnification of pumping intensity of two orders of magnitude.
Why do we choose the element with Z_{nu}=16, A=32? (This is Sulphur - S). We can estimate an energy of the basic state for –hydrogen like spectrum $\Delta E_{K\alpha}$ = 3,482 KeV. It is closest to 3.4 KeV in the nuclei Rb^{86}. Besides the following statements are valid: the atom of sulphur in the target is partially ionized, therefore high atoms levels are free. At transition between these levels and ground state $E_{k_\alpha} = (3.482kev)(1 - 1/n^2)$. By selecting the number n of high level it

is possible to hit in a nuclear level. We can also remark, that Doppler width of X-ray pumping is about one electron volt at $\omega_x < \omega_i$ and it can help us to be very close near nuclear level. Another examples of such agreement is shown on this table [2]:

Table 1. Coincidences between the energies of nuclear transitions and the energies of characteristic emission lines

Nucleus	ΔE_n, keV	Element	X-ray line	ΔE, keV	Line width, ev
$^{159}Tb_{65}$	57.995	W_{73}	$K_{\alpha 2}$	57.982	43.2
$^{65}Ho_{67}$	94.699	U_{93}	$K_{\alpha 2}$	94.665	107
$^{169}Tm_{69}$	8.401	W_{73}	$L_{\alpha 1}$	8.398	5

It should be specially noted that such a γ -source has not substantial difficulties being faced in its experimental implementation. In experiments on observation of such a high activity of nuclei in the target, the ^{58}Co, ^{84}Rb, ^{93}Mo or ^{152}Eu nuclei could be used, because they feature the necessary scheme of nuclear transitions [9].
For example, it is preferable to take ^{84}Rb nuclei for the first experiment, because such atoms are very well known in respect of both laser pumping and trapping into Magnetic Trap [3]. As a result, a concentration of 10^{12} cm^{-3} can be readily obtained in MT. This number of cooled nuclei allows 10^6 resonance γ -photons to be emitted. At the same time, the noise of the natural γ -activity can be eliminated by using time-selective signal detection. For the above number of nuclei, the noise of the natural γ -activity of isomer nuclei with a half-life of one hour typically corresponds to 10^7 decays per second. However, during 10^{-6} sec, the number of naturally emitted γ -photons is 20, whereas the number of γ -photons produced by X-ray pumping of an active γ -transition will exceed 10^6. Therefore, signal-to-noise ratio of 10^6 can be readily observed in such a time-selective experiment.
We also analyse the possibility of nuclear excitation with help of solid target. In this case we use X-ray pump from laser plasma to illuminate solid film mixture of KBr and Rb^{84} (decay time 1 our). There is 10^9 total amount of Rb isomer nuclei in this target at the range of X-ray transparency. Geometrical loses of X-ray emission is near 0.1. 200 kev decay γ –photons from excited isomer nuclei can be registered by a detector with photomultiplier.

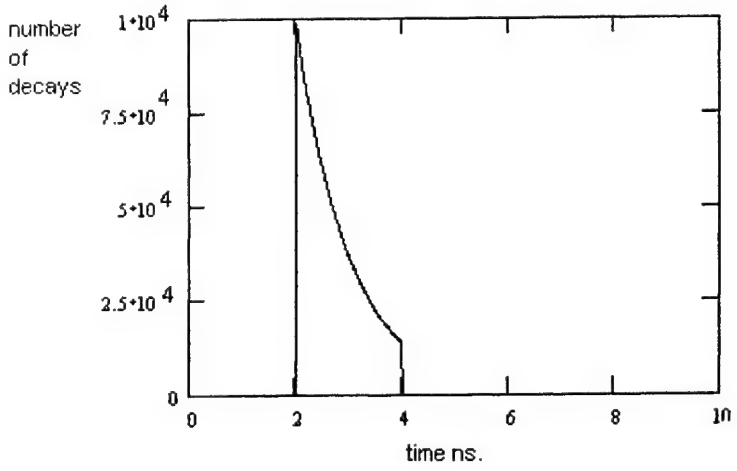

Fig.3. Time dependence of γ-emission detected signal for Rb target pumping by X-ray picosecond laser plasma radiation

In this figure there is expected signal of γ – detector which was switched on for 2 ns after laser shot. Time of life of excited level is 1 ns. We can see that approximately 10^4 γ –photons should be produced in this experiment and this is enough to be measured.

3.3.The possibilities of γ – laser effect for isomeric nuclear media

Let's mark that by using of narrow frequency pump of isomeric nuclei it is possible to find the way for solution of the γ – laser problem. The next conditions should be fulfilled to have laser effect in our activated media:
1. Amplification of γ – radiation in active media

$$G = (\lambda_\gamma^2 / 4\pi)(\Gamma_0 / \Gamma_D) n_{nu} L > 1$$

2. Losses of X-ray pump in laser media. The main losses are from photoionization in our case

$\sigma_{ph.eff.}(\omega_x) \le \pi \lambda_x^2 (\Gamma_0/\Gamma_D)$

3. Optimal thickness of laser media for X-ray pump

$a \le 1/(n_{nu} \lambda_x^2)$

4. Diffraction losses of γ - radiation

$L < k_\gamma a^2$

As $\Gamma_0 \approx \frac{4\omega_x^3}{3\hbar c^3} \mu_{13}$, where $\Delta\omega \approx \Gamma_D = \hbar k_x k_\gamma / Am_p$ we have two possibilities for active media and pump parameters:
1. $Z < 30$, $n_{nu} \le 10^{17}$ cm^{-3}, $d \approx 10^{-3}$ cm, $L < 100$ cm, $\lambda_\gamma \approx 10$ KeV, $\lambda_x \approx 1$ KeV;
it can be gas Co in "Magnetic Trap".
2. $Z \le 100$, $n_{nu} \le 10^{23}$ cm^{-3}, $d \approx 10^{-5}$ cm, $L < 10$ cm, $\lambda_\gamma \approx 1$ MeV, $\lambda_x \approx RyZ^2 \approx 100$ KeV;
it can be solid Ag[10]

4. Laser triggering nuclear reaction γ – source

According to Fig.1 we now consider fast electron generation by laser pulse, its conversion into fast ions and then nuclear reactions for γ - photon production with help of these ions:

4.1. Production of fast electrons by a high-power laser pulse

First, we estimate the number of high-speed electrons produced by a laser pulse. Numerical simulations show that, in the 10^{19}-10^{20}-W/cm^2 intensity range, the absorption coefficient becomes independent of the angle of incidence, and the absorption is about 10 % without pre-pulse. Laser pre-pulse increase scale of plasma inhomogenity L and absorption coefficient η. It has been shown[10] that, in the range 10^{18}-10^{20} W/cm^2 $\eta \propto L$. The same dependence was obtained in our paper[11], which considers the analytical model of pondermotive absorption. Below[11] we will use the scaling of $\eta(L,I)$ as:

$$\eta(L,I)=(0.1+0.01L)I_{18}/(30+I_{18})^{0.7},$$

where I_{18} - radiation intensity in units 10^{18} W/cm^2, $L = L\omega/c$. $L \approx c_s t_{pl}$. Here c_s - ion sound velocity and t_{pl} pre-pulse duration. At pre-pulse intensity 10^{12} W/cm^2 we have L=10 at t_{pl}=10 ps and we will use L = 0, 10 in our numerical simulations.
In our previous paper[12], we considered the physical mechanism of formation of high-speed electron jets due to the ponderomotive light pressure, whereby an electron oscillating in an electric field is transformed into plasma by the ponderomotive pressure force. Let suppose that $N_{ef}=K_e(I)\varepsilon_L/\varepsilon_e$ electrons will be accelerated during the laser pulse where ε_L is the laser pulse energy, $K_e(I)$ is the transformation coefficient of laser energy into fast electron energy, and ε_e is the energy of an electron. It has been shown[13] that for laser intensities more then 10^{20} W/cm^2, $K_e(I) \approx \eta$. This means that all the absorbed energy is assumed to be transferred to the motion of high-speed electrons. The energy of an individual electron is usually specified by laser wave field strength inside the skin-layer[14]

$$\varepsilon_e \approx mc^2[(1+(2-\eta)I_{18})]^{1/2}$$

Now we numerically estimate N_{ef} for the following plasma and laser pulse parameters: $I=10^2$, $\lambda=10^{-4}$ cm, τ_i = 100 fs, $n_{cr} = 10^{21}$ cm^{-3} (for materials with Z ~ 10, Z/A ~ 0.5, A- atomic number, Z-nuclear charge), and $S = 10^{-6}$ cm^2. For the chosen parameters N_{ef}= 1.3 10^{10} electrons.

It is well known[15] that the electron kinetic energy within the first part of a laser pulse at the vicinity of its maximum can be as high as $\varepsilon_e/mc^2 = (v_E/c)^2/2$ (here v_E is electron oscillation velocity) but the second part of this pulse will damp electron because it can not obtain any energy in vacuum from a plane wave if it was at rest initially. Anyway this electron can get energy from electromagnetic wave if it inertially penetrates a target and the laser pulse reflects from this target. Pre-plasma with a length approximately equal to the laser pulse length can significantly increase electron energy. If we have initial electron momentum in pre-plasma P_{e0} one can easily estimate its maximum energy

$$\varepsilon_e/mc^2 \approx (P_{e0}/mc)(v_E/c)^2 \approx (P_{e0}/mc)I_{18}$$

From this formula we see that electron energy can be tens of MeV level for relativistic electrons generated in pre-plasma by the Brunel effect for example.

4.2. Fast ion generation

In the case of a target with small Z, ions are vigorously accelerated under the action of ponderomotive pressure force. Moreover, at given energy the nuclear reaction cross section drops as Z increases; therefore, this channel works for light-atom elements. If we suppose that return current has a time to neutralize positive ion charge arriving from pondermotive pressure, then, from the low of pulse flow, characteristic ion energy takes the form[16]:

$$\varepsilon_{i_h} \approx Z(n_e/n_{cr})mc^2(2-\eta)I_{18}\,[1+(2-\eta)I_{18})]^{-1/2} \qquad (8)$$

When laser intensity $I_{18} = 10^3$, the ion energy amounts to 500 * A KeV. Here Z/A = 0.5, which holds true for most of light-atom elements. If A > 10, such energy is sufficient for nuclear reactions to proceed via ion-ion collisions.
Let's go now to the analysis of the physical mechanism of particles flying out from target to vacuum and inside dense plasma. Most fast electrons accelerates by pondermotive force inside plasma but electrons in under-dense plasma (transparent to laser radiation) fly out from the plasma in specular direction by reflected part of laser pulse action. The shape of pondermotive potential and laser pulse spatial profile influence the angle θ_e of fast electron movement into vacuum as considered in[17].
During laser pulse duration the relativistic electrons (at laser intensity $I \approx 10^{19}$W/cm^2) fly out from a target to distance greater than laser spot size on the target. As a result the boundary area of the target obtains a positive charge and ions are accelerated into target and in vacuum directions by the electrostatic field.
We analyse this process by simulations with help of kinetic relativistic code PM2D[17]. To check the simulation results for ion acceleration into target we also calculated the parameters for ions flying out into vacuum and compared these results with experimental results because in our experiments only this part of ions have been recorded [21]. Fig.6 shows spatial distribution of energy flux density of ions flying out into vacuum for laser intensity 10^{18} W/cm^2. In simulations as in experiments, ions fly out at angle diagram ~15° to normal to target surface. The difference between theoretical and experimental results is connected with collision-less simulation model.

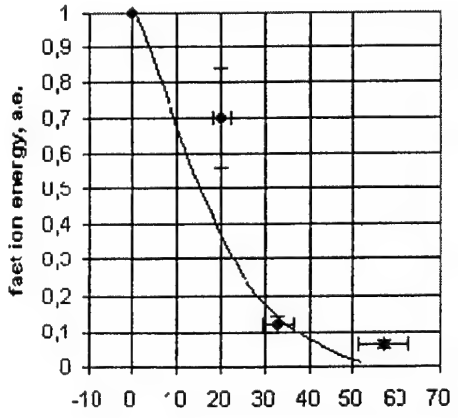

Fig.4 Spatial distribution of fast ion extension

According to our simulations, approximately the same (in angle distribution) ion beam propagates inside dense plasma from target boundary area with volume $V = \pi(d/2)^2 L$. This movement is connected with electrostatic potential from charge separation $e\varphi = \varepsilon_{eh}$ and this separation is connected with electrons of energy $\varepsilon_{eh} \approx \eta I/cn_{eh}$ going away from this target area. Suppose that fast ion takes energy equal to this potential $Ze\varphi \approx \varepsilon_{ih}$ and that fast electron energy exceeds electrostatic potential $\varepsilon_{eh} \geq e^2 n_{eh} \pi L d^2/(4L^2+d^2)^{1/2}$ we obtain the next formula for ion energy:

$$\varepsilon_{ih} \approx 3Z\, mc^2 (\eta I d L/\lambda^2)^{1/2}$$

This agrees with (8) and at $(d/\lambda)^{1/2} \approx n_e/n_{cr}$ we obtain the same result. This ion beam can be used for farther generation of nuclear reactions considered in [18].

To increase this energy much more we can use foil target with inhomogeneous plasma density. In this case shock wave which has been born in front side by laser pulse will accelerate ions according to (8) in main part of foil but when it propagates through decreasing plasma density profile on back side it accelerates ions much more[20] at least ten times in energy compare to homogeneous plasma slab.

4.3. Production of γ - photons via ion-ion collisions

As the result of laser ion acceleration there is some distribution in ion energy which depends on laser time and space profile. Nuclear reaction cross-sections have complicated behavior and depend on particle energetic distribution parameters. We model these cases by the next formula for the number of nuclear reactions:

$$N_{nur} = n_a \int_0^\infty d\varepsilon \frac{dN_i}{d\varepsilon} \int_0^\varepsilon d\varepsilon \sigma(\varepsilon) \left|\frac{d\varepsilon}{dx}\right|^{-1} \qquad (9)$$

here from Bete formula[19]:

$$\frac{d\varepsilon}{dx} = -\frac{m_a m_i}{m_a + m_i} \frac{2\pi e^4 Z_i^2 Z_a}{m\varepsilon} n_a \ln\left(4m\varepsilon \frac{m_a + m_i}{I_Z\, m_a m_i}\right),$$

where n_a, m_a, Z_a – concentration, mass and charge of target atoms, I_Z – their ionisation potential.

If fast ions leave skin depth area before laser pulse is finished we have stationary ion distribution in energy. In this case from ion kinetic equation we obtain the following equation for fast ion number:

$$F\frac{\partial N_i}{\partial \varepsilon} = \frac{\partial N_i}{\partial x} \approx n_{i0} S \text{, where } F \approx -Zmc^2 \frac{\partial}{\partial x}\sqrt{1+I_{18}} \approx \frac{1}{2l_s}\frac{\varepsilon(\varepsilon + 2Zmc^2)}{\varepsilon + Zmc^2} \text{ - force acting on ions.}$$

From these equations we obtain the next ion distribution:

$$\frac{\partial N_i}{\partial \varepsilon} \approx n_{i0} S l_s \frac{(\varepsilon + Zmc^2)}{\varepsilon(\varepsilon + 2Zmc^2)} \theta(\varepsilon - \varepsilon_m) \qquad (10)$$

Here $\theta(\varepsilon - \varepsilon_m)$ – step function and ε_m – maximum of ion energy from $\varepsilon_m \approx Z\, mc^2 [(1+\eta I_{max})^{1/2} - 1]$.

By way of example, we consider reaction $p + t = \gamma + {}^4He$, whose maximum cross-section is $\propto 2$ mbarn for a proton of 8-MeV energy and photon energy is near 5 MeV [8]. Such a reaction can proceed in a tritium target on a substrate. The number of photons produced in proton tritium nuclear collisions can be estimated from the equation (9):

$$N\gamma^{(t+p)} = N_p\, \sigma^{(t+p)}\, n_{nu}{}^t\, l^i_{ef},$$

where N_p is the total number of high-speed protons with energy ε and l^i_{eff} is their free path length

$$l^i_{ef} = \varepsilon^2 / 2\pi Z^t n_{nu}{}^t\, \varepsilon^4 \ln(4\varepsilon / I_Z)$$

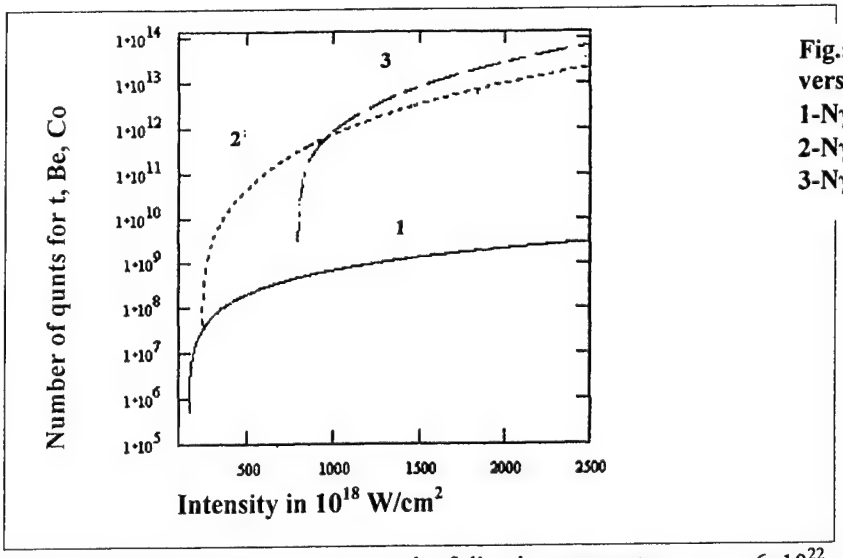

Fig.5. γ-quanta yeild versus laser intensity
1-$N\gamma^{(t+p)}$
2-$N\gamma^{(Be+p)}$
3-$N\gamma^{(Co+p)}$

For numerical estimates, we can use the following parameters: $n_{nu} = 6x10^{22}$ cm^{-3}, ionization potential $I_Z = 10$ eV. The thickness of the T- ice target is near 1 mm then $l_{ef} = 1$ mm and does not depend from energy. The number of fast protons $N_p \approx N_{he}$ - number of fast electrons from quasi-neutrality. The dependencies of photon number $N\gamma^{(t+p)}$ from laser intensity I are shown on Fig.5 for L=10.

On Fig.5 there are the number of γ-quanta for Be^{10} ($E_\gamma = 0.2$ MeV) and Co^{60} ($E_\gamma = 2$ MeV) targets with thickness greater

than l_{ef} in the following nuclear reactions: $p+Be^{10} \rightarrow B^{11}+\gamma$; $p+Co^{60} \rightarrow Ni^{59}+\gamma+2n$. In these targets the γ-quanta yield is more compare to T-ice target from reaction cross-section and more thickness, but the largest neutron yield has a higher laser intensity threshold because the high Z nuclei have higher Coulomb barrier.

5. PRODUCTION OF CONTINUUM γ-RADIATION BY A LASER PULSE.

Finally we consider the direct hardware component of the Bremsstrahlung radiation of fast electrons formed under the action of a laser pulse on a target, the quantum energy being higher than the rest energy of an electron. We estimate the energy of γ-quanta produced in spectral range for γ-photon registration ΔE_γ and laser energy - γ-quantum one conversion factor K_γ. The bremsstrahlung radiation energy is defined by the known Bete-Gaitler's equation[19]

$$\Delta E_\gamma = \frac{4e^6 Z^2 n_{nu} \tau_{ef}}{m^2 c^4 h} \int_0^{\varepsilon_2} dt \int_{V_{ef}} dV \int_{\varepsilon_1} d\varepsilon f(\varepsilon,t)\varepsilon[\ln(2\varepsilon/mc^2)-1/3], \qquad (11)$$

where the space integral of the distribution function f(ε, t) gives the total number of high-speed electrons at a given time t, and τ_{ef} is the effective lifetime of high-speed electrons, which comprises the laser pulse length and the time of free travel of the electrons produced $(n_{nu} c \sigma^{e}_{tot})^{-1}$, $(\varepsilon_2 - \varepsilon_1)$ – spectral range for γ-photon registration.
For electron energies of several mega-electron-volts, the time of free travel is substantially larger than the laser pulse duration. To calculate τ_{ef}, we use Bete-Bloch's equation[19]. Then we obtain the following simple expression for the conversion factor:

$$K_\gamma(I) \approx K_e(I) \frac{9 Ze^2 \varepsilon_e (\ln(\varepsilon_e/mc^2)+0.36)}{8\pi hc\, mc^2 \ln(\varepsilon_e^3/2I_Z^2 mc^2)} (\varepsilon_2 - \varepsilon_1)/mc^2 \qquad (12)$$

The laser radiation intensity enters in Eq. (12) through the characteristic electron energy ε_e and $K_e(I)$. Dependencies $K_\gamma = K_\gamma(I,L)$ from laser intensity for L=0,10 at Z = 10, I_Z = 50 KeV, $(\varepsilon_2 - \varepsilon_1)/mc^2 \approx 10^{-6}$ are shown on Fig.6

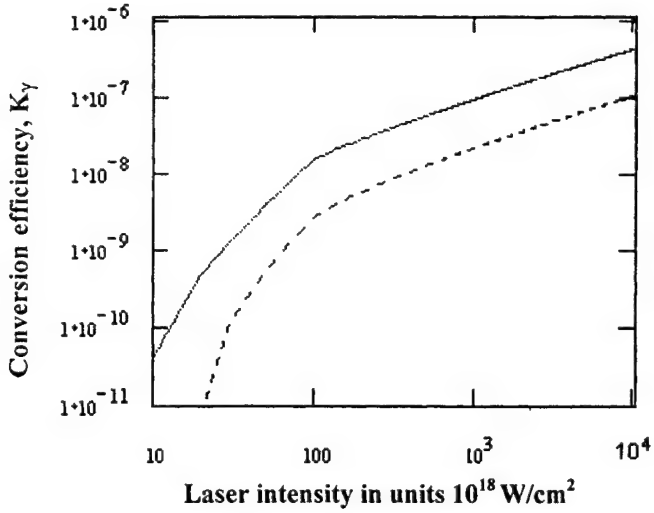

Fig.6. Conversion efficiency, K_γ as a function of efficiency for L=0 (dashed line) and L=10 (solid line)

With these parameters and radiation intensity I=100, $K_\gamma \approx 10^{-8}$ and the total number of γ-quanta appears to be $N_\gamma \sim 10^2$. From these calculations we can conclude that number of the MeV photons in the line spectral range is much less than for nuclear transition emission.

6. CONCLUSION

1. We have shown the feasibility of creating a pulsed monochromatic high-activity γ-source by X-ray pumping of active γ -transition of cooled isomeric nuclei confined in MT. The spectral brightness of such a radioactive source using isomeric nuclei in a magnetic trap is ~ 10^6 GBk/Hz.
2. The laser intensity being ~10^{19} W/cm^2, nuclear reactions proceed in a target, resulting in production of γ-line radiation. In light-atom materials irradiated by a laser beam with 10^{20} W/cm^2 intensity the γ-photon yield reaches 10^{-4} of the number of high-speed ions due to proton-triton collisions.
3. It has been shown, that the extension of fast ions has a preferred direction lengthways of target normal. The fraction of laser energy that is converted to energy of fast ions is 1-3 %. So high conversion coefficient confirms the feasibility of using lasers for ion acceleration and nuclear reaction generation.
4. The received acceleration rate (number of fast particle per unit time) exceeds another methods of acceleration.
Thus, a high-power laser pulse can be used as a γ photon-emitting source for investigating in physics of solids, for biology, and also for stimulating nuclear reactions.

REFERENCES

1. G.C.Baldwin and J.C.Solem Reviews of Modern Physics, v.69, No.4,1085 (1997)
C.B.Collins, F.W.Lee, D.M.Shemell, B.D.DePaola, S.Olariu, and I.Iovitzu Popescu J. Appl. Phys., 53, 4645 (1982)
2. V.S. Letohov . Kvantovaya Elektronika, p.125, 1974; C.B. Collins. Phys. Rev. C, v.37, p.2267, 1988; A.V Andreev., Vestn. Mosk. Univ., Ser.3, Fiz. V.35, p.4645, 1982.
3. D.Boiron, C.Triche, D.R.Meacher, P.Verkerk, and G.Grynberg Phys.Rev.A, v.52, N.5, R3425, 1995.
4. A.A. Andreev, K.Yu. Platonov, Yu.V. Rozhdestvenskii, JETP letters, v.68, no.9, p.704, 1998.
5. O.Bor and B.Mottelson - Atomic nuclear structure, v. 1, 1976.
6. A. A. Andreev, V.I.Bayanov, A.B.Vankov et.al. Quantum Electronics. v. 26, pp.884-887, 1996.
7. P. Gibbon, E. Forster. Plasma Phys. Control Fusion, v. 38, p. 769, 1996
8. V.Ienbner et. al. Proc. SPIE, v. 2700, p. 170, 1995.
9. Nuclear Data Sheets, 1989 - 1998.
10. E. Lefebvre, G. Bonnaud, Phys. Rev. E 55, p.1011,1997.
11. A.A. Andreev, K. Yu. Platonov, K. A. Tanaka, Proceedings of JAERI-Conf. 98-004, p. 37, 1997.
12. A.A. Andreev, M.N. Novikov, and.Platonov K.Yu., Proc. SPIE, vol.2770, p.153, 1995.
13. M.H. Key, M.D. Cable, et al., Phys. Plasmas 5, 1966 ,1998.
14. S.C.Wilks, Phys.Fluids B 5, p.2603, 1993.
15. L.D. Landau and E.M. Lifshits *Theory of Field* ,Moscow, Nauka, 1974.
16. S. C. Wilks, W. L. Kruer, M. Tabak, and A. B. Langdon, Phys. Rev. Lett. 69, 1383, 1992.
17. A.A. Andreev, I.A. Litvinenko, K.Yu Platonov, JETP, v.116, no. 4(10), p.1, 1999.
18. V.Yu Bychenkov, V.Tikchonchuk, S.V. Tolokonnikov JETP, no.6, 1999.
19. V.B. Berestetskii., E.M Lifshits., and L.P. Pitaevskii. *Quantum Electrodynamics,* Moscow, Nauka, 1980.
20. Ya.B Zeldovich., Yu.P. Raizer. Physics of shock wave and high temperature phenomena. M., Nauka, 1966.
21. A.A.Andreev, A.V. Charukchev et al. International Conference "Inertial Fusion Science and Applications", Bordoaux, France, September 1999.

Fast particles and hard photons generated by a ultra-intense laser pulse

G. Bonnaud, L. Gremillet[‡], E. Lefebvre, C. Toupin, F. Walraet, J.M. Rax[*]

Commissariat à l'Energie atomique, DIF/DPTA, 91680 Bruyères-le-Châtel, France
[‡]LULI, Ecole Polytechnique, 91128 Palaiseau, France
[*]LPGP, Univ. Orsay, 91405 Orsay, France

ABSTRACT

Two sets of computer results are discussed. By means of a 2-D Maxwell-Vlasov coupling code, the generation of MeV-range electrons and ions is addressed as well as the subsequent X-ray production and neutron production provided by post-processing the fast particle distribution. With a 3D MHD-fluid target-fast beam coupling code, the propagation of electrons in dense matter is discussed, with emphasis on the target heating.

Keywords: Laser-plasma interaction, Ultra-high intensity, fast particles

1. INTRODUCTION

As techniques for short laser pulse generation developed into a standard technique, the study of matter irradiated by ultra-high intensity (UHI) pulses has intensified the escalation in femtosecond laser-solid experiments over the world and simulations over the last five years. As a consequence, a lot of papers have tried to lay the milestones of the physics discovered in Mbar-pressure conditions. Now, this first phase of cognitive works is going to drive a renewed interest in this UHI field, stemming from the possibilities of each of these scenarii to be controled and optimized for various diagnostic or energetic applications: 100 MeV-range fast ions for medical purpose, hard photons for radiography of dense exploding matter, fast electrons to bring the spark for igniting a compressed fuel for thermonuclear fusion[1] and neutron bursts as a tool for nuclear physics.

In this paper, we will address the last results we got by means of kinetic simulations of the interaction of a laser-pulse with a solid-density target, more specifically the generation and transport of fast particle transport inside the target. After the presentation of the numerical codes, we will discuss and illustrate the heating of the electrons of the target surface and their subsequent transport in the target volume, then the associated hard Bremsstrahlung emission and finally the fast ion generation and the fusion neutron they can induce in the case of a deuterated target.

2. MODELING

A thick solid target remains inertially confined during the whole laser pulse. The area where the laser pulse and matter interact is a strongly-ionized plasma, with an axial extension of a few micrometers, imposed by the ion inertia: expansion of a 1-keV temperature plasma in vacuum and hole boring on the target side create a plasma transparent to the 1-μm laser wavelength. The plasma density stands below the so-called electron critical density n_c which is 10^{21} cm^{-3}. In this area, collisions are dominated by collective processes. The laser wave is screened along the skin depth $\lambda_0/(2\pi\sqrt{n_e/n_c})$, where n_e denotes the electron density of the target: the target is then opaque. The absence of predefined nature of the particle distribution and the permanent crossing of particle trajectories let the Maxwell-Vlasov model be the standard model. A few years ago, the standard simulations were 1-D but with a special transverse plasma boosting,[2,3] they were able to tackle oblique incidence light but wre limited to siatuations of permaently flat plasma surface. First 2-D PIC simulations[1] have exhibited clear corrugation of this surface and have streesed the stron influence of a second space dimension. With our present-day computers involving tenths of 1-GFlop processors, we have performed 2-D simulations with the code MANET on plasma as dense as 50 times the critical densities and during the whole laser pulse duration (one picosecond). The constraints of this type of simulation, which imposes use of parallel machines, is twofold: time step has to resolve the plasma period and the space mesh has to resolve the Debye length of the plasma bulk (1 keV electron temperature). No way to relax these constraints whenever the fast oscillations of the laser beam have to be modeled.

Laser Optics 2000: Ultrafast Optics and Superstrong Laser Fields, Alexander A. Andreev, Vladimir E. Yashin, Editors, Proceedings of SPIE Vol. 4352 (2001) © 2001 SPIE · 0277-786X/01/$15.00

The interaction of the laser beam with the plasma is a strong emitter of fast particles which flow into the target, whenever a return current can provide the surface region with fresh electrons: this actually defines the notion of thick target compared to thin target. The life of these particles is essentially controlled by beam currents and not space-charge forces. A model without fast dynamics of the plasma can then be used, which enables to relax drammatically the constraints on time step used in standard Vlasov-Maxwell coupling codes.[4]

Consequently, we have developped a code PÂRIS in order to simulate directly the 3-D motion of electrons which undergo the self-magnetic field and the axial field, as well as collisions; this code is a 3-D extension of the hybrid scheme presented by Davies et al.[5] At each time step, a group of macro-particles is injected inside the plasma and the whole set of macro-particles, injected so far, is moved with account of the collective electromagnetic fields via the Lorentz force calculated from the 8 nodes framing each particle (PIC method) and with account of the collisions with ions via a random rotation (Monte-Carlo method with multiple scattering via Molière's law). The ions are assumed to be fixed and compensate the electron charge everywhere: no space charge is considered. Losses are modelled by inelastic collision processes on bound electrons, and free electrons (via binary encounters and collective interaction). We use the continuous deceleration approximation according to the Bethe-Bloch cross section[6] The target is given an imposed density. The target electrons are characterized by 3 local quantities: the fraction of free electrons (ionization rate), the drift velocity and the temperature. Both isolating materials and conductors can be modelled. The ionization of the conductors is calculated by a Thomas-Fermi model fitted by More[7]; for insulating materials, SESAME table is used (only SiO_2 is available). The temperature is calculated by the energy deposition bound to the slowing down of the fast electrons and from a state law, via use of Sesame tables; perfect gas state law is also available. The resistivity is then inferred from the Lee and More model.[8] Initially, the target is given a zero temperature (for usual solid target) or a high one (for fast ignitor studies[9,10]). Such a code has been used to interpret an experiment of shawdography of a silicate target coated with a metal.[11]

3. ELECTRON HEATING AND TRANSPORT

In a previous work[12], the temperature of electrons have been determined within a 1-D geometry with a infinite mass ions (using the 1.5 D code EUTERPE). Three parameters have been seen to have an impact: the laser irradiance, the initial electron density and the sharpiness of the surface. Adding ion mobility creates a density ramp in front of the plasma, which increases the electron temperature up to the ponderomotive potential.[13] By means of 2-D kinetic simulations (code MANET), the electrons appear to be even hotter, as illustrated in Fig. 1. A combination of two factors can be put forward: the low density plasma area is enlarged via hole boring; moreover, the strong magnetic fields observed at the hole entrance can bend the electron orbits to reinject them into the laser-plasma area for new acceleration phase.

We report here on the penetration of an electron beam in Al target, as simulated by the code PÂRIS. The target is initialized with a 0.5 eV electron temperature. The electron beam is injected with a peak density at $4\ 10^{21}$ cm^{-3} and has a Gaussian profile with a 4 μm FWHM diameter along the transverse direction and 0.25 ps FWHM in time; the maximum is at time t = 0.3 ps. The initial distribution of the electrons injected in the box is Maxwellian with a peak temperature of 0.46 MeV; the temperature is time-space dependent and follows the density profile with FWHM equal to $\sqrt{3}$ times the density FWHM. 2 million of particles have been injected at the end of the simulation which consumed 12 h of one SUN 350 MHz CPU. In Fig. 2, the current density map of the beam shows self-focusing induced by the magnetic field self-generated by the beam, with a focal point around 10 μm. The target temperature reaches a peak temperature above 1 keV. From the temperature maps, we have estimated the volume of target with temperature above 0.5, 1 and 2 keV: we found 571 (i.e. 60x3x3), 187 (40x2x2) and 26 μm^3, respectively. The 2 keV area is concentrated around the pinching point. The current profile does not maximize at the beam center and tends to have a hollow shape. This observation could be correlated to a thermal process, as explained by Haines.[14] Initially, the energy deposition maximizes at the location of the peak current, that is at the beam center, causing a larger target heating and then a reduced resistivity. The return current is then prompted to use this minimum resistance way and via magnetic force repells the incident beam.

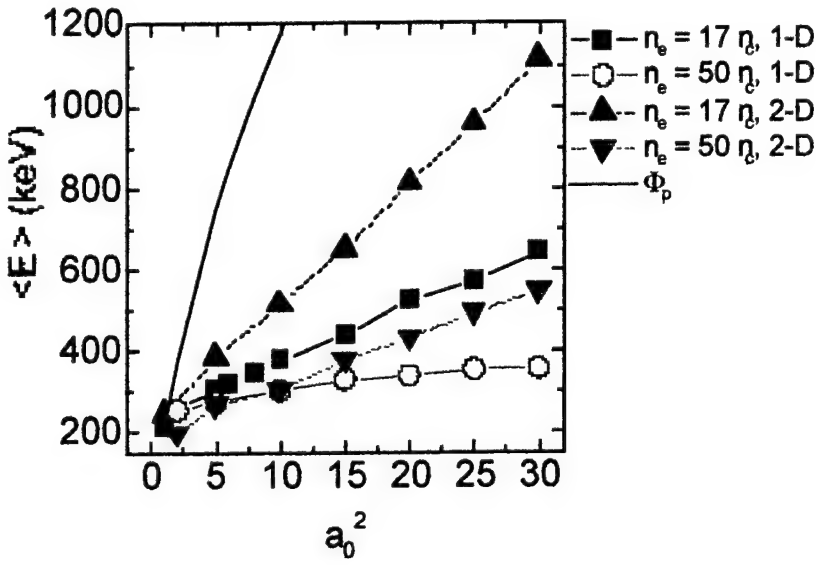

Fig. 1: Average kinetic energy of the population of electrons above 0.1 MeV as a function of the laser irradiance ($a_0^2 = 0.73 I_0\lambda_0^2$ in unites of 10^{18} W.μm^2/cm^2). The solid line shows the ponderomotive potential.

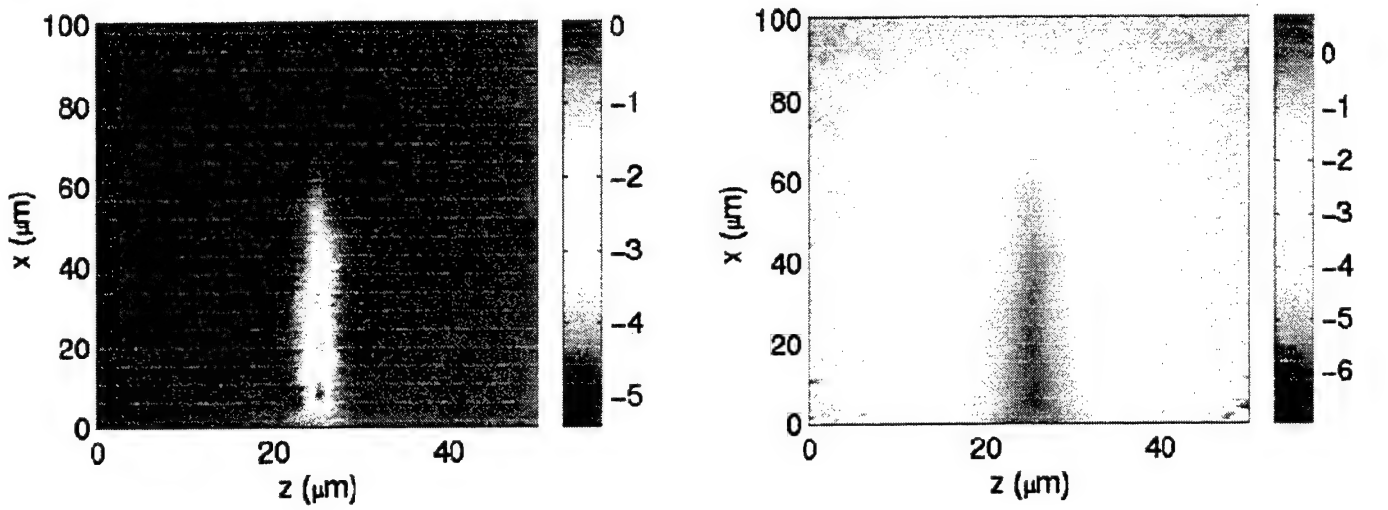

Fig. 2: (left) map of the electron current density, referred to $n_c ec = 5.4\ 10^{12}$ A/cm^2 for critical density n_c associated to 1 μm laser wavelength, (right) map of electron temperature $\log_{10}(T_e(keV))$ in a Al target as a function of the beam axis (x) and one transverse direction (z), through the central part of the beam. Time is 0.2 ps after the peak of the electron pulse.

4. HARD X-RAY EMISSION

In high intensity laser-plasma interaction, the electrons accelerated to high kinetic energy by the laser can emit Bremsstrahlung X-ray radiation when they slow down in the bulk of the target. Observation of this phenomenon has been reported, for instance, as early as 1992 by Kmetec et al.[15]. To investigate this process numerically, we need to couple a model for the electron source to one for the electron-photon converter. We compute the characteristics of the electron source with 2D PIC simulations in which the distribution of electrons leaving the interaction region towards the bulk of the target is calculated, as a function of energy and angle with respect to the laser direction. To compute the Bremsstrahlung emission of these electrons

through various depth of solid tungsten, we wrote a deterministic transport code that accounts for electron slowing down and scattering, X-ray emission by Bremsstrahlung, and uses the analytical fits given by Findlay for these phenomena[16].

As a result, we can compute the variations in Bremsstrahlung emission for various interaction conditions (such as target density, laser intensity)... An example is given in Figure 3, where we plot the distribution of x-ray photons emitted, through 0.12 cm of solid tungsten, by the hot electrons produced by a 1 μm, $5x10^{19}$ W/cm^2 laser pulse incident on a 4 n_c target. The left plot is colour-coded according to the log10 of the photon distribution, in photon/keV/sr. We note that the emission is very broad, reflecting the broad electron emission from the target surface. The right plot shows the photon distribution integrated in +/- 24° around the laser axis. Summing over the photons with energy above 500 keV, we find an x-ray energy of 0.2 J, compared to 4.8 J incident in the laser pulse. This amounts to a conversion officiency of a few percents, and supports the prospect of producing hundreds of Joules of hard x-rays with 10 kJ - 10 ps laser pulses in the future.

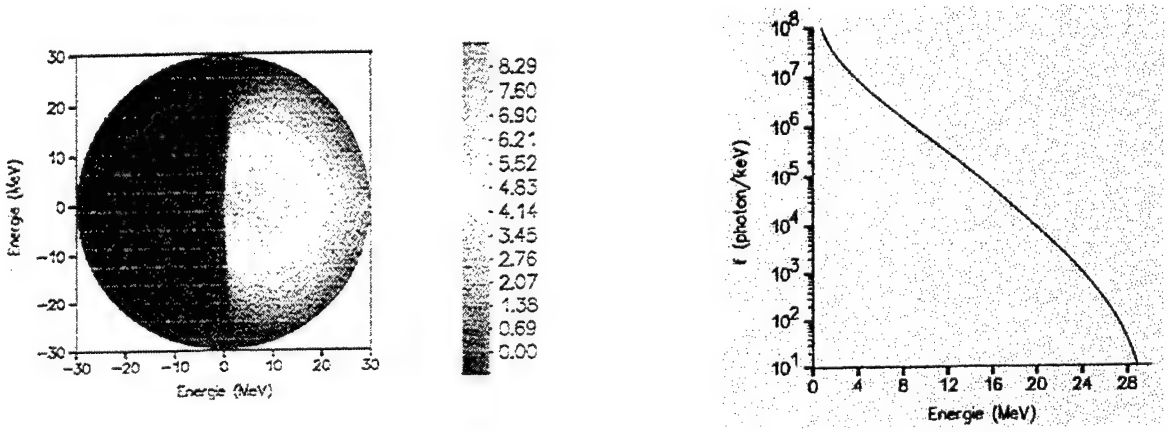

Fig. 3: (left) Energy distribution of the X emission and (right) emission pattern of the X-rays.

5. ION-INDUCED NEUTRONS

Ions are dragged radially of forwardly by the electrons which escape the laser beam, kicked by the laser ponderomotive force. The ion energy can then approach the electron energy, in the MeV range, and therefore in the case of deuterated targets can trigger fusion nuclear reactions. Production of neutrons has been quantified, in energy and angle, directly from the ion populations provided by the 2-D PIC simulations. The target is assumed to be a solid CD_2 target (1 g/cm^3) with 300 μm length at room temperature. During its slowing-down in the target, one ion will cause neutrons to be created according to the following angle distribution:

$$\frac{dN_n}{d\Omega_n}(\theta_n) = \int_0^{E_i} dE \frac{d\sigma(E,\theta_n)}{d\Omega} \frac{1}{\varepsilon(E)}$$

expressed as the ratio of the differential cross-section for neutron creation and the ion slowing down power ε. θ_n denotes the angle referred to the ion axis. Starting from the angle distribution of the D ions from the whole plasma at the end of the laser pulse, our model assumes that the ion distribution is axisymmetric around the laser propagation axis, with a 6 μm extension in the missing transverse direction (to get 3-D from 2-D) and integrates over the whole ion distribution to calculate the total neutron yield, the neutron spectrum and the angle distribution[$17,18]. Fig. 4 displays the ion distribution obtained from a 50 n_c density target and the corresponding neutron yield. Ions are beamed forward due to an electrostatic shock, strong enough to reflect ions at twice the velocity of the shock. Such a shock was identified by Denavit,[19] in results from 1.5-D PIC simulations; this type of scenario is therefore confirmed by our 2-D simulations. The anisotropy of the ion is clearly reproduced on the neutrons. This noticeable feature is much like the one observed in an experiment performed with a very high intensity contrast on P102 laser at frequency-doubled light.[20]

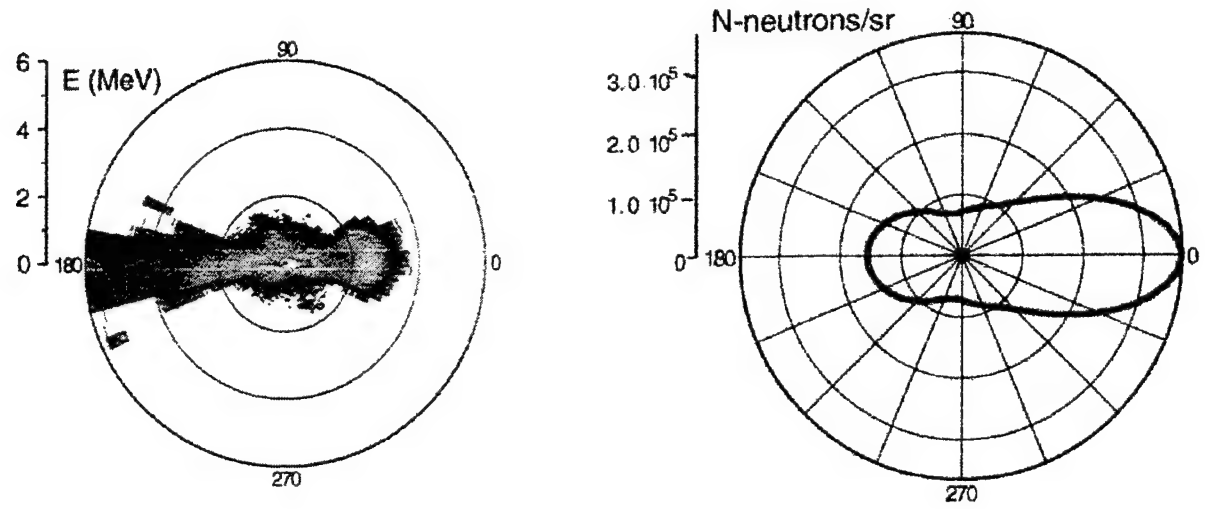

Fig. 4: (left) deuterium population as a function of energy and angle after the interaction of a 5 10^{19} W/cm^2, 0.5 ps laser pulse on a 50 n_c density plasma and (right) associated pattern of neutron emission. Angles refer to the laser light axis (0°).

We should note a large discrepancy about the absolute value of the forward yield, which is roughly 1000 times smaller in the calculation. The same feature is found in the experiment performed on Vulcan with a poorer contrast (only 10^{-4}) where our simulations let pronostic from the neutron number a radial ion distribution. Consistancy with the results from Pâris must be found: according to these simulations, a 200 μm long - 5 μm wide cigar - shaped volume of hot plasma is created by the MegaAmps of electrons. The deuterium ion slowing down is modified by the transformation of bound to free electrons. To be more precise, we have calculated the ion range as a function of the temperature (Fig. 4), following the Mehlhorn's paper.[21,22] Starting from zero temperature, the range decreases first when increasing the target temperature, by stronger friction from the free electrons, and then increases when the electron temperature is in excess of the ion energy. The slower the ion, the larger this last feature. Considering a 2 keV plasma temperature would make a 0.5 MeV (resp. 2 MeV) ion stop 28 (resp. 5) times further in the plasma. The previous expression let us infer that the number of neutrons, which is bound to the ion energy range [0-E_i] is increased by a factor which is larger than the factor got at the initial energy. We can anticipate that the neutron yield would approach the experimental figures, within a decade.

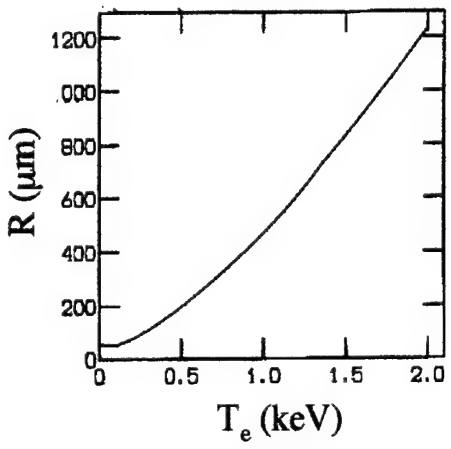

Fig. 5: deuterium range as a function of the target electron temperature, for a 2-MeV energy deuterium ion. The target is CD_2 with 7.5 10^{22} D atoms/cm^3.

6. CONCLUSION

This paper has emphasized four main results, based on 2-D PIC simulations: (i) the average kinetic energy of the fast electrons is larger in 2-D than in 1-D geometry and tends to be closer to the ponderomotive potential. (ii) the fast electrons are able to ionize and heat to keV level a 40-μm long plasma; (iii) the distributions of fast electrons post-processed with a general Bremsstrahlung emission model lead to 5 % laser to X-rays conversion efficiency, and 7 10^{10} hard photons / laser J at high irradiance (10^{21} W/cm^2); (iv) the angle distribution of neutrons is a clear sign of the underlying anisotropy of the deuterium ions but their number is too small compared to experiences, the discrepancy being partially resolved by ion stopping in a hot plasma heaten by the fast electrons.

In near term, we prospect to simulate within 3-D PIC simulations on Calder code[23] various scenarii studied in 2-D, by using the next generation to come of Tflop-crest cluster. High-energy Bremsstrahlung of the fast electrons will be specifically studied.

6. REFERENCES

1. M. Tabak *et al.*, "Ignition and high gain with ultrapowerful lasers", Phys. Plasmas **1**, 1626-1634 (1994).

2. P. Gibbon *et al.*, "Calibration of one-dimensional boosted kinetic codes for modeling high-intensity laser-solid interactions", Phys. Plasmas **6**, 947-953 (1999).

3. Th. Schlegel, S. Bastiani, L. Gremillet, J.P. Geindre, P. Audebert, J.C. Gauthier, E. Lefebvre, G. Bonnaud, and J. Delettrez, "Simulation of X-ray production by hot electrons in short-pulse laser-solid interaction at moderate intensities", Phys. Rev. E **60**, 2209-2217 (1999).

4. A. Pukhov and J. Meyer-ter-Vehn, "Relativistic magnetic self-channeling of light in near-critical plasma: three-dimensional particle-in-cell simulation", Phys. Rev. Lett. **76**, 3975-3978 (1996).

5. A.R. Bell, J.R. Davies and S.M. Guérin, "Magnetic field in short-pulse high-intensity laser-solid experiments", Phys. Rev. E **58**, 2471-2473 (1998).

6. V.V. Val'chuk, N.B. Volkov and P.A Yalovets, "Energy losses of fast electrons in a beam plasma", Plasma Physics Reports **21**, 159-164 (1995).

7. R. More, *Atomic physics of laser-produced plasmas*, A. Rubenchik and S. Witkowski Eds, p. 70 (North Holland, Amsterdam, 1991).

8. Lee and R. More, "An electron conductivity model for dense plasma", Phys. Plasmas **27**, 1273-1286 (1984).

9. C. Toupin, E. Lefebvre, C. Le Bourg, G. Bonnaud, J.M. Rax, L. Gremillet, "Energy and angle features of the accelerated electrons and ions in the interaction of a ultra-intense laser pulse with an overdense plasma", in Proceedings of the 25th European Phys. Society Conf. on Contr. Fusion and Plasma Physics, ECA vol. 22C pp. 914-917 (1998).

10. C. Toupin, G. Bonnaud, L. Gremillet, F. Walraet, E. Lefebvre, J.M. Rax, J. Robiche, "Penetration of relativistic electrons created by ultra-intense laser pulses in solid/overdense plasma", *Inertial Fusion Sciences and Applications 99*, C. Labaune, W.J. Hogan, K.A. Tanaka Eds., pp. 471-474 (Elsevier, Paris, 2000).

11. L. Gremillet *et al.*, "Time-resolved observation of ultrahigh intensity laser-produced electron jets propagating through transparent solid targets", Phys. Rev. Lett. 83, 5015 (1999).

12. E. Lefebvre and G. Bonnaud, "Nonlinear electron heating in ultrahigh-intensity-laser-plasma interaction", Phys. Rev. E 55, 1011-1014 (1997).

13. C. Toupin, E. Lefebvre and G. Bonnaud, "Hot particle generation in ultrahigh intensity laser-plasma interaction, *Superstrong fields in plasma*, M. Lontano *et al.* Eds., CP426, pp. 383-388 (AIP, 1998).

14. M.G. Haines, "Thermal instability and magnetic field generated by large heat flow in a plasma specially under laser fusion conditions", Phys. Rev. lett. **47**, 917-920 (1981)

15. J. D. Kmetec *et al.*, "MeV X-ray generation with a femtosecond laser", Phys. Rev. Lett. **68**, 1527-1530 (1992).

16. D. J. S. Findlay, "Analytic representation of Bremsstrahlung spectra from thick radiators as a function of photon energy and angle", Nucl. Instr. Meth. Phys. Res. A**276** 598-601 (1989).

17. C. Toupin, PhD dissertation (in french), Univ. Paris (1999).

18. C. Toupin, E. Lefebvre and G. Bonnaud, "Neutron emission from a deuterated solid target irradiated by an ultra-intense laser pulse", submitted to Physics of Plasmas (2000).

19. J. Denavit, "Absorption of high-intensity subpicosecond lasers on solid density targets", Phys. Rev. Lett. **69**, 3052-3055 (1992).

20. L. Disdier, J.P. Garçonnet, G. Malka and J.L. Miquel, "Fast neutron emission from a high-energy ion beam produced by a high-intensity subpicosecond laser pulse", Phys. Rev. Lett. **82**, 1454-1457 (1999); *Inertial Fusion Sciences and Applications 99*, C. Labaune, W.J. Hogan, K.A. Tanaka Eds., pp. 1026-1031 (Elsevier, Paris, 2000).

21. T.A. Mehlhorn, "A finite material temperature model for ion energy deposition in ion-drivzn inertial confinement fusion targets", J. Appl. Phys. **52**, 6522-6532 (1981).

22. J.F. Ziegler, *Stopping cross-sections for energetic ions in all elements*, Vol. 5 (Pergamon, NY, 1980).

23. E. Lefebvre, C. Toupin and G. Bonnaud, "Energetic particle and photon production with ultra-intense lasers", *Inertial Fusion Sciences and Applications 99*, C. Labaune, W.J. Hogan, K.A. Tanaka Eds., pp. 1020-1025 (Elsevier, Paris, 2000).

Forward Ion Acceleration and Nuclear Reactions on a Table-Top Driven by a High-Intensity Laser

A. Maksimchuk,[a*] K. Nemoto[b], V. Yu. Bychenkov,[c] K. Flippo,[a] S. Banerjee,[a]
D. Umstadter,[a] and G. Mourou[a]

[a] Center for Ultrafast Optical Science, University of Michigan, Ann Arbor, MI-48109-2099
[b] Central Research Institute of Electric Power Industry, Iwado-kita, Komae-shi, Tokyo, 201-8511 Japan
[c] P. N. Lebedev Physics Institute, Russian Academy of Science, Moscow 117924, Russia

ABSTRACT

The protons with the energy up to 10 MeV accelerated in the forward direction from the thin Mylar film by relativistically intense 10 TW, 400 fs laser pulse have been observed. When a deuterated polystyrene was deposited on the front surface of the film and a boron sample was placed behind the target the production of 10^5 atoms of positron active isotope ^{11}C from the reaction $^{10}B(d,n)^{11}C$ have been measured. The activation results suggest that ions (protons and deuterons) were accelerated from the front surface of the target.

Keywords: high-intensity laser, high-energy ions, activation technique, radioisotope

1. INTRODUCTION

Since their invention more than sixty years ago cyclotrons[1] have been the standard method used to accelerate protons and ions for experiments in nuclear physics and applications in nuclear medicine. The development of short-pulse high-intensity lasers[1] made it possible to accelerate protons and heavier ions to multi-MeV energies in the interaction of these lasers with solid targets[2-5] gas jets[6] and clusters.[7] Unlike traditional sources that generate proton pulses longer than several nanoseconds, the laser acceleration technique allows one to generate pulses that are a few orders of magnitude shorter with a peak current exceeding 1 kA. Therefore, such a technique offers a unique opportunity for fundamental research in the field of nuclear physics on ultrashort time scales. In particular, it becomes possible to study the decay modes of radioactive fission fragments right after the fission event and determine lifetimes of ultrashort-lived positron active isotopes.[8] We report in this paper a new technique for isotope preparation that makes use of light ions (protons and deuterons) accelerated to million-electron-volt energies by a powerful laser beam. This new technique permits the production of a much wider range of isotopes than have previously been produced by means of laser-induced photofission.[9,10] The results of this study shed new light on the mechanism and scaling of ion acceleration and imply that light-ion beams can also be used for advanced inertial confinement fusion research or as a high-current injector for linear accelerators.

2. EXPERIMENTAL RESULTS

The experiments were performed using a 10 TW hybrid Ti:Sapphire/Nd:phosphate glass laser, which is based on Chirped Pulse Amplification technique and able to deliver up to 4 J, 400 fs pulse at the fundamental wavelength of 1.053 μm with an intensity contrast 5.10^5:1. The p-polarized laser beam was focused on the surface of thin Mylar foil with a 6 μm thickness. The laser beam was incident at 45 degrees and focused down to a spot size of ~ 12 μm in diameter with an f/3 (f=16.5 cm) off-axis parabolic mirror. The maximum focused intensity was 6.10^{18} W/cm^2. In the previous studies[5] with the same laser system, 1.5 MeV proton beam was observed in the forward direction from aluminum targets using a high-intensity high-contrast 0.53 μm illumination. The protons were found to originate from H_2O contamination layer on the surface of Al foils. Proton acceleration was attributed to the electrostatic field of charge separation due to "vacuum heating",[12,13] when electrons are accelerated by the laser electric field at the sharp vacuum-target interface and deposit their energy inside the target.

* Correspondence: A. Maksimchuk, E-mail: tolya@umich.edu

Laser Optics 2000: Ultrafast Optics and Superstrong Laser Fields, Alexander A. Andreev, Vladimir E. Yashin, Editors, Proceedings of SPIE Vol. 4352 (2001) © 2001 SPIE · 0277-786X/01/$15.00

Acceleration field gradient ~ 10 GeV/cm have been inferred from a previous experiments. In current experiments we have used the Mylar ($H_8C_{10}O_4$) foil which contains more hydrogen than a contamination layer on a surface of Al target and is expected to be more dense proton source.

The maximum proton energy was measured with plastic nuclear track detectors, CR-39, placed parallel to the foil behind it at a distance ~ 20 cm. They were covered (depending on the expected maximum proton energy) with the steps of Mylar filters with thickness from 0 to 40 μm or from 25 to 525 μm and steps of Mg filters with thickness from 250 μm to 1500 μm. The projectile ranges were calculated using the program SRIM2000.[14] The maximum proton energy was found to vary linearly with the laser intensity (Fig. 1.) and reaches 10 ± 1 MeV at 6. 10^{18} W/cm^2. Proton energy given by the pondermotive potential of standing electromagnetic wave[15] is only 0.7 MeV, which is much less than the observed maximum proton energy. Estimation of proton energy from the mechanism of "vacuum heating"[5] is closer to observed value but also underestimate it by a few times. However, for the intensity contrast of 5.10^5:1 it is questionable to apply the latter estimation because a preplasma very likely appears before the maximum laser energy reaches the target. Thus, one may attribute such a preplasma as a reason for enhanced electron generation and, hence, enhanced electrostatic field which effectively accelerates the ions.

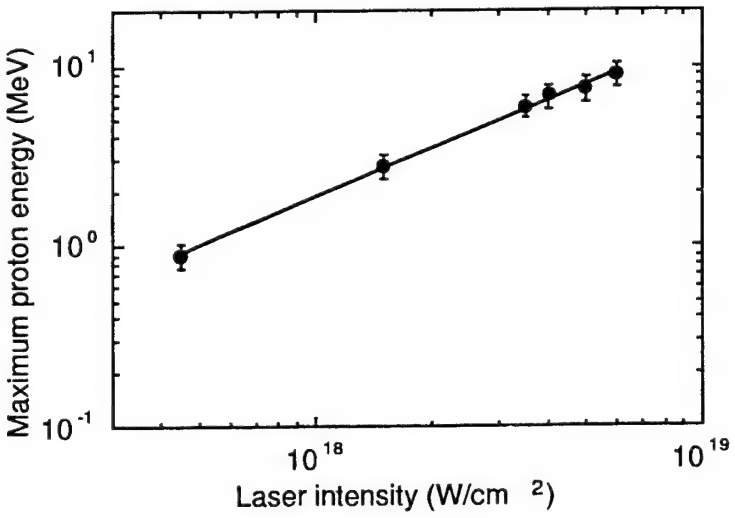

Fig. 1. Maximum proton energy in the forward direction as a function of laser intensity for 6 μm Mylar foil.

Electrons accelerated in an underdense (with density n_e less than critical) preplasma up to the energy ε_{max} can penetrate inside a solid target to their Debye length $l_{De} \sim \sqrt{\varepsilon_e / n_e}$ and accelerate ions forward from the skin layer. Since the skin depth is shorter than l_{De} a big number of ions should have an energy equal to the electrostatic potential and ion distribution function should demonstrate a plateau effect ("water bag" distribution) until energy cutoff Ze_{max}. Such an ion (proton, Z=1) distribution function has already been observed in previous experiments.[5]

Deuterons should be accelerated less because they are two times heavier than the protons, have less mobility and have higher energy losses. They follow behind the proton bunch and due to this experience a significantly lower accelerating electric field. Consequently their energy should be significantly lower than the proton's energy. Heavier ions, such as carbon ions, have little chance to be significantly accelerated without special surface cleaning of the light species. That is why only high-energy protons were observed in the experiments with Mylar or Aluminum foils.[5]

We performed an activation experiment on a boron sample with deuterons. The high-intensity laser beam was focused on the Mylar target covered by a deuterated polystyrene layer. The resultant ion beam was used to irradiate a ^{10}B enriched sample (enrichment 90%, purity 99%). A cylindrical shaped sample 10-mm in diameter, 5-mm thick was positioned on a CR-39 detector with a few steps of Mylar filters to monitor the energy of ion beam and its alignment. The deuterated polystyrene layer with a thickness ~ 1 μm was deposited on the front side of the 6 μm Mylar film by drying tetra-hydro-fluorine (THF) with deuterated polystyrene C_8D_8 dissolved in it. The experimental set up is shown in Fig. 2.

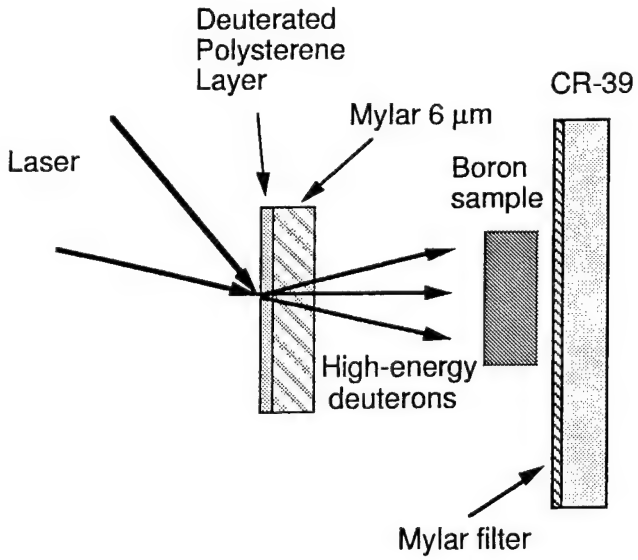

Fig. 2. The schematic diagram of the boron sample activation with high-energy deuterons.

The concentration of boron isotope ^{10}B in natural boron is 19.9%. Therefore, in an enriched boron sample the yield of isotope ^{11}C in the reaction $^{10}B(d,n)^{11}C$ is enhanced approximately by a factor of 4.5. Since the ion beam has a divergence angle ~ 40 degrees placing the boron target at 8-mm behind the Mylar foil ensures that most of high-energy ions are incident on the sample. Nuclear reactions are expected to occur only near the front surface of the sample, because even a 10 MeV deuteron has a projectile range of only 360 μm. Neutrons carry away most of the energy as kinetic energy released due to fusion, because they are much lighter than carbon nuclei. Thus, ^{11}C is produced with low energy and remains near the boron sample front surface. The yield of ^{11}C was measured by counting the number of positrons emitted. The coincidence measurements require a low background count rate to receive a good signal to noise ratio.

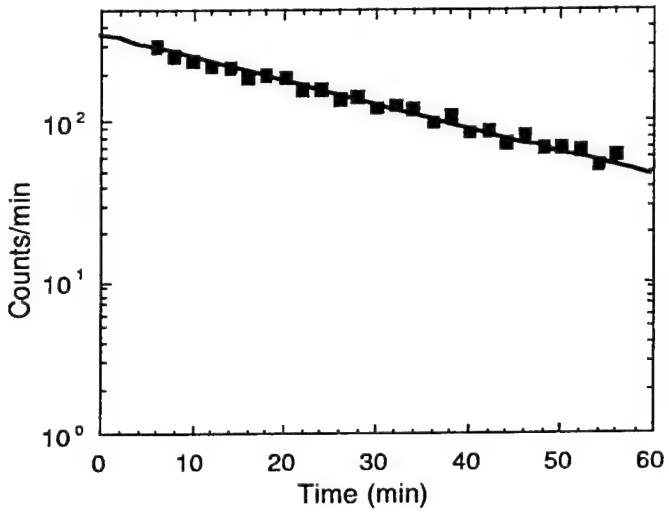

Fig. 3. Measured decay of radioactivity versus the time for the $^{10}B(d,n)^{11}C$ reaction (squares). The solid line corresponds to the theoretical result and demonstrates ~20 min half-life of ^{11}C.

Two 3-inch NaI detectors, placed opposite to each other, have been used to detect the coincidence signal resulting from the annihilation of electrons and positrons and the production of two gamma-quanta with energy of 0.511 MeV. The

detection efficiency was measured to be in the range 0.05-0.1 by using a ^{22}Na radioactive source with a precisely known activity of positron emission. The detection efficiency and background noise depend on the window width of the coincidence measurement and the detector separation. The background noise was found to be 1-5 count/min and a radioactivity detection limit was ~10 pCi.

Time dependence of a coincidence signal is shown in Fig. 3. We identified the source of this coincidence signal as the result of a positron decay of the carbon isotope ^{11}C with a half-life of 20.4 min. We measured a maximum of ~ 300 counts/min at 330 s after a laser shot. The total yield of ^{11}C is estimated to be ~ 10^5 which corresponds to ~ 2 nCi of radioactivity right after a shot. The laser was able to deliver shots with the time interval of about 7 minutes. Therefore, accumulation of several shots will increase radioactivity by only a factor of three. If a similar laser had a repetition rate of 10 Hz and the irradiation time is equal to the half-life of ^{11}C, a positron source with an activity of ~ 20 μCi can be produced.

We have observed a very sharp power dependence of ^{11}C yield as a function of the laser intensity (Fig. 4) indicating that deuterons energies are near the threshold of the ^{10}B(d,n)^{11}C reaction. A significant fluctuation of ^{11}C yield at the maximum focused intensity can also lead to this conclusion. Reaction yield (per one accelerated ion) produced by an ion with charge Ze and reduced mass M* in a reaction with atoms having a density n_a reads:

$$Y \equiv N/N_i = n_a \int_0^{\infty} d\varepsilon \frac{dN_i}{d\varepsilon} \varepsilon \int_0^{\varepsilon} d\varepsilon' \sigma(\varepsilon') \left| \frac{d\varepsilon'}{dr} \right|^{-1} , \quad (1)$$

where N is the total number of reactions, N_i is the number of accelerated ions, and bremsstrahlung losses are given by the Bete formula:

$$\frac{d\varepsilon}{dr} \approx -\frac{M^*}{m\varepsilon} 2\pi e^4 Z^2 Z^a n_a \Lambda , \quad (2)$$

Here m and e are electron mass and charge, $\Lambda = \ln\left(4m\varepsilon / M^* J\right)$, and Z_a and J are the atom charge and mean ionization potential of the medium atoms. We used the EXFOR data base[16] for the ^{10}B(d,n)^{11}C reaction cross section and water bag distribution function for deuteron energies to determine ^{11}C yield from equation (1).

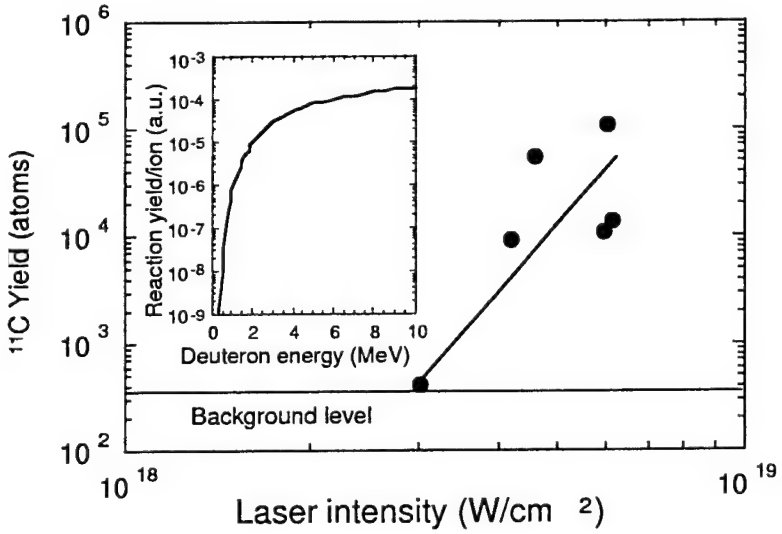

Fig. 4. Experimental yield of ^{11}C versus the laser intensity for the ^{10}B(d,n)^{11}C reaction. The inset shows calculated yield of ^{11}C per one deuteron as a function of maximum ion energy.

The inset of Fig. 4 shows that the threshold for this reaction is ~ 0.5 MeV. The comparison with the experimental data convinces one that the deuteron energy cutoff at the maximum laser intensity used is about 1-2 MeV.

To verify that high-energy ions are accelerated from the front side of the target, that agrees with Ref. [4] and contradicts to Ref. [6] we irradiated a 6 μm thick Mylar target with a layer of a deuterated plastic on a back side and performed the same experiment on activation of ^{10}B sample. In this case the activation signal was not above the background level. These results indicate unequivocally, that for the condition of our experiment light ions are accelerated indeed from the front side of the foil.

High-energy protons are also expected in the experiment with the layered deuterated target. They may participate in the $^{11}B(d,n)^{11}C$ reaction. The cross section of this reaction[16] has a higher threshold (above 3 MeV). Taking into account that the amount of ^{11}B in boron sample was only 10% we expect ^{11}C yield for this reaction to be much less that for deuterons. To verify that (p,n) reaction does not contribute sufficiently in ^{11}C yield we focused the laser at the highest intensity on a bare Mylar film with a boron sample behind. No activation signal was observed in this case. We eliminated also the reaction $^{11}B(d,2n)^{11}C$ because of (i) boron sample contains only 10% of ^{11}B; (ii) it requires energy of deuterons higher than 6 MeV; (iii) and the reaction cross-section is 10 times less than for the reaction $^{10}B(d,n)^{11}C$.

In summary, we have observed protons with energies up to 10 MeV and ~ 1 MeV deuterons in forward direction accelerated by tabletop laser focused on the thin films. The maximum proton energy is approximately proportional to the laser intensity and more than ten times higher than estimated from the pondermotive potential. We have also demonstrated the production of ~ 10^5 atoms of a positron active isotope ^{11}C from the $^{10}B(d,n)^{11}C$ reaction. The activation results have suggested that ions are accelerated in a plasma from the front surface of a Mylar target.

ACKNOWLEDGMENTS

The work of K. F. and A. M. and the laser facility were supported by the National Science Foundation. The work of V. Yu. B. was supported by the Russian Foundation for Basic Research and that of D. U, by the Office of Energy Research, US Department of Energy. S. B. is thankful for the support of CUOS Fellowship Program and K. N. would like to thank S. Akita, S. Sasaki and T. Suzuki for general support.

REFERENCES

1. E. O. Lawrence and N. E. Edlefsen, "On the production of high speed protons," *Science* **72**, pp. 376-377, 1930.
2. G. A. Mourou, C. P. J. Barty and M. D. Perry, "Ultrahigh intensity lasers: physics of the extremes on a tabletop," *Phys. Today*, **51** (1), pp.22- 28, 1998.
3. A. P. Fews, P. Norreys, F. N. Beg, A. R. Bell, A. E. Dangor, C. N. Danson, P. Lee, and S. J. Rose, "Plasma ion emission from high intensity picosecond laser pulse interactions with solid targets," *Phys. Rev. Lett.*, **73**, pp. 1801-1804, 1994.
4. E. L. Clark, K. Krushelnick, J. R. Davies, M. Zepf, M. Tatarakis, F. N. Beg, A. Machacek, P. A. Norreys, M. I. K. Santala, I. Watts, and A. E. Dangor, "Measurements of energetic proton transport through magnetized plasma from intense laser interactions," *Phys. Rev. Lett.*, **84**, pp. 670-673, 2000.
5. A. Maksimchuk, S. Gu, K. Flippo, D. Umstadter, and V. Yu. Bychenkov, "Forward ion acceleration in thin films driven by a high-intensity laser," *Phys. Rev. Lett.*, **84**, pp. 4108-4111, 2000.
6. S. P. Hatchett, C. G. Brown, T. E. Cowan, E. A. Henry, J. S. Johnson, M. H. Key, J. A. Koch, A. B. Langdon, B. F. Lasinski, R. W. Lee, A. J. Mackinnon, D. M. Pennington, M. D. Perry, T. W. Phillips, M. Roth, T. C. Sangster, M. S. Singh, R. A. Snavely, M. A. Stoyer, S. C. Wilks, and K. Yasuike, "Electron, photon, and ion beams from relativistic interaction of Petawatt laser pulses with solid targets," *Phys. Plasmas*, **7**, pp. 2076-2082, 2000.
7. G. S. Sarkisov, V. Yu. Bychenkov, V. N. Novikov, V. T. Tikhonchuk, A. Maksimchuk, S.-Y. Chen, R. Wagner, G. Mourou, and D. Umstadter, "Self-focusing, channel formation, and high-energy ion generation in interaction of an intense short laser pulse with He jet," *Phys. Rev. E*, **59**, pp. 7042-7054, 1999.
8. T. Ditmire, J. W. G. Tisoh, E. Springate, M. B. Mason, N. Hay, R. A. Smith, J. Marangos, and M. H. R. Hutchinson, "High-energy ions produced in explosions of superheated atomic clusters," *Nature*, **386**, pp. 54-56, 1997.
9. V. Yu. Bychenkov, V. T. Tikhonchuk, and S. V. Tolokonnikov, "Nuclear reactions triggered by laser-accelerated high-energy ions," *JETP*, **88**, pp. 1137- -1142 1999, translated from *Zh. Eksp. Teor. Fiz.*, **115**, pp. 2080-2090, 1999.
10. T. E. Cowan, A. W. Hunt, T. W. Phillips, S. C. Wilks, M. D. Perry, C. Brown, W. Fountain, S. Hatchett, J. Johnson, M. H. Key, T. Parnell, D. M. Pennington, R. A. Snavely, and Y. Takahashi, "Photonuclear fission from high energy electrons from ultraintense laser-solid interactions," *Phys. Rev. Lett.*, **84**, pp. 903-906, 2000.

11. K. W. D. Ledingham, I. Spencer, T. McCanny, R. P. Singhal, M. I. K. Santala, E. Clark, I. Watts, F. N. Beg, M. Zepf, K. Krushelnick, M. Tatarakis, A. E. Dangor, P. A. Norreys, R. Allott, D. Neely, R. J. Clark, A. C. Machacek, J. S. Wark, A. J. Cresswell, D. C. W. Sanderson, and J. Magill, "Photonuclear physics when a multiterawatt laser pulse interacts with solid targets," *Phys. Rev. Lett.* **84**, pp. 899-902, 2000.
12. W. L. Kruer and K. Estabrook, "JxB heating by very intense laser light," , *Phys. Fluids*, **28**, pp. 430-432, 1985.
13. F. Brunel, "Not-so-resonant, resonant absorption.," *Phys. Rev. Lett.*, **59**, pp. 52-55, 1987.
14. SRIM2000 by J. F. Ziegler, in: http://www.research.ibm.com/ionbeams/home.htm.
15. S. C. Wilks, W. L. Kruer, M. Tabak,and A. B. Langdon, "Absorption of ultra-intense laser pulses," *Phys. Rev. Lett.*, **69**, pp. 1383-1386, 1992.
16. Experimental Nuclear Reaction Data File, in: http://www.nndc.bnl.gov/nndc/exfor.

Effect of a laser pre-pulse on ion acceleration when an ultra intense laser pulse interacts with a foil target

Andreev A.A.[1)], Zhidkov A.G.[2)], Sasaki A.[2)], Platonov K.Yu.[1)], Tajima T.[3.2)]
1) Institute for Laser Physics, Russia
2) Advanced Photon Research Center JAERI, Japan
3) Lawrence Livermore National Laboratory, USA

PACS: 52.50.Jm; 52.40Nk; 52.25.Dg

Abstract

Upon the interaction of an ultra intense laser pulse with a solid target, generated fast electrons can produce MeV ions from laser plasmas. These fast ions can be used in different applications ranging from ion implantation to nuclear reaction stimulation. The most important point is the efficiency of this fast ion production. We analyze - with help of an analytical model and PIC code simulations - the different acceleration mechanisms and compare the efficiency of electrostatic ion acceleration, at the front and rear of a foil target, the ponderomotive mechanism and acceleration by the shock wave in detail. The optimal plasma density distribution, shaped by laser pre-pulse, is found.

1. Basic equations.

We consider acceleration of ions from a plasma layer with a thickness of several laser wavelengths. Such a plasma can be formed by laser illumination of a thin foil. To describe theacceleration of ions in laser plasma we formulate a set of equations. First we consider the given ion distribution and movement of an electron subsystem. The electron motion can be described with the help of kinetic or hydrodynamic equations. The electrons play the role of intermediary through which the energy of the laser pulse is converted to ion energy. Therefore, the purpose of describing of electron motion is to find a connection between the electrostatic field operating on the ions and the field of the laser pulse. In the kinetic approximation, plasma electron motion describe by a self-consistent set of equations consisting of a collision-less kinetic equation for a distribution function of electrons, and Maxwells equations for electromagnetic fields. The common solution of the kinetic equation in this case can be written as follows:

$$f(z;t;p_z;p_y) = \int \delta(\bar{p} - \bar{p}(z_0;\bar{p}_0;t))\delta(z - z(z_0;\bar{p}_0;t))f(\bar{p}_0;z_0)d\bar{p}_0 dz_0 \quad , (1)$$

Where $\bar{p}(z_0;\bar{p}_0;t)$; $z(z_0;\bar{p}_0;t)$: - result of solution of equations of electron motion

$$\bar{p}_\perp = \bar{p}_{0\perp} - e\bar{A}(z,t)/c$$

$$\frac{d}{dt}\dot{z}\sqrt{\frac{m^2 + (\bar{p}_{0\perp}/c - e\bar{A}(z,t)/c^2)^2}{1-\dot{z}^2/c^2}} = -e\frac{\partial\varphi(z,t)}{\partial z} - \frac{\partial}{\partial z}\sqrt{\frac{m^2c^4 + (\bar{p}_{0\perp}c - e\bar{A}(z,t))^2}{1-\dot{z}^2/c^2}} \quad , (2)$$

These equations define the phase trajectory of electrons with initial momentum $\bar{p}_0$ and coordinate z_0 in self-consistent electromagnetic fields.

In (2) A (z, t) - vector potential of the transverse (div$A$ = 0) electromagnetic fields, $\varphi(z, t)$ – the scalar potential of the longitudinal fields satisfying the Maxwells equations:

Laser Optics 2000: Ultrafast Optics and Superstrong Laser Fields, Alexander A. Andreev, Vladimir E. Yashin, Editors, Proceedings of SPIE Vol. 4352 (2001) © 2001 SPIE · 0277-786X/01/$15.00

$$\left(\frac{\partial^2}{\partial z^2}-\frac{\partial^2}{c^2\partial t^2}\right)\vec{A}(z,t)=-\frac{4\pi e}{c}\int\vec{v}f(z;t;p_z;p_y)d\vec{p}$$

$$\frac{\partial^2\varphi(z,t)}{\partial z^2}=-4\pi e(Zn_i-\int f(z;t;p_z;p_y)d\vec{p}) \qquad (3)$$

We assume spatial one-dimensionality of our task and it allows us to use the law of conservation of transverse canonical momentum to find $p_\perp(p_{0\perp},z_0,t)$.

The initial distribution function $f(\bar{p}_0;z_0)$ in (1) is the Maxwell – Boltzmann one:

$$f(\bar{p}_0;z_0)=\frac{1}{2\pi mT_e}\exp(-\frac{\bar{p}_0^{\,2}}{2mT_e})Zn_{i0}\exp(-\frac{e\varphi(z_0)}{T_e}), \qquad (4)$$

where the potential $\varphi(z_0)$ satisfies the Poisson equation:

$$\frac{\partial^2\varphi}{\partial z_0^2}=-4\pi eZn_{i0}[\exp(-\frac{e\varphi(z_0)}{T_e})-\frac{n_i(z_0)}{n_{i0}}]. \qquad (5)$$

In equations (4,5) we are using the analytical profiles of ion density $n_i(z)$. The derivated system (1-5) theoretically allows us to express a potential by the vector potential of a laser field and the density profile of ions, and thus to find a self-consistent force operating on the ions. For ion movement we have the next system of hydrodynamic equations

$$\frac{\partial n_i}{\partial t}+\frac{\partial}{\partial z}(n_iv_i)=0$$

$$\frac{\partial v_i}{\partial t}+v_i\frac{\partial}{\partial z}v_i+\frac{1}{Mn_i}\frac{\partial(T_en_e)}{\partial z}=-\frac{Ze}{M}\frac{\partial\varphi}{\partial z} \qquad (6)$$

However, it is impossible to solve analytically complete self-consistent system (1-6). Therefore, we simplify the situation and consider two approximate methods of finding a solution of the system. To check the used methods we also simulate the self-consistent problem by PIC-code simulations.

2. Approximation of a given electron distribution function.

As the first approximate method we set a given electron distribution function and investigate the acceleration of ions in this electron distribution. We describe the electron distribution function as a two-temperature Maxwell function:

$$f_{e0}=f_c\exp(-u^2/v_c^{\,2})+f_h\exp(-u^2/v_h^{\,2}), \qquad (7)$$

where

$$u^2=v^2-v_0^{\,2}-2e\varphi/m_e;\ v_{c,h}=(T_{c,h}/m_e)^{1/2}. \qquad (8)$$

Temperatures of hot and cold electrons is considered to be known. Selection of a such distribution function is natural and takes into account the basic groups of electrons, both accelerated in a skin layer, and cold electrons of background plasma [4].

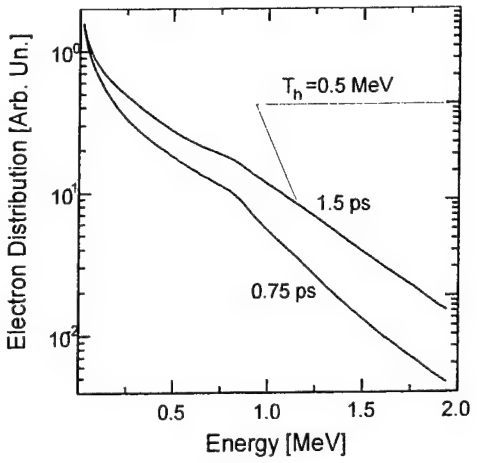

Fig.1

In Fig.1 show, calculated with the aid of PIC - code [2] simulations, electron distribution functions for the interaction of a laser pulse of duration 1 ps and intensity 510^{18} W/cm^2 with Al foil target. From this figure we see two reference slope angles of the distribution function, corresponding to the two indicated temperatures. Energy of hot electrons can be derived from laser intensity I_L as $T_h \approx mc^2(\sqrt{1+\eta I_{18}}-1)$, where η- absorption coefficient, I_{18} - intensity in terms of 10^{18} W/cm^2 [5]. The electron density is expressed by a distribution function:

$$n_e = 2\int_0^{v_{max}} f_{e0}(\sqrt{v^2 - v_0^2 - 2e\varphi/m_e})dv \qquad (9)$$

System (1-6) hydrodynamic equations of plasma motion transforms to:

$$\frac{\partial n_i}{\partial t} + \frac{\partial}{\partial z}(n_i v_i) = 0$$

$$\frac{\partial v_i}{\partial t} + v_i\frac{\partial}{\partial z}v_i + \frac{1}{Mn_i}\frac{\partial \sum_{j=e,h} T_{ej}n_{ej}}{\partial z} = -\frac{Ze}{M}\frac{\partial \varphi}{\partial z}$$

$$\frac{\partial^2 \varphi}{\partial z^2} = -4\pi e(Zn_i - \sum_{j=e,h} n_{ej}) \qquad (10)$$

where

$$n_{ej} = n_{0ej}\exp(-2e\varphi/m_e v_j^2) \qquad (11)$$

The system (10) is complete and allows to find n_i, v_i, φ. For analysis of the system we rewrite this in dimensionless variables:

$$\frac{\partial \eta}{\partial \tau}+\frac{\partial}{\partial \xi}(\eta\mu)=0$$

$$\frac{\partial \mu}{\partial \tau}+\mu\frac{\partial}{\partial \xi}\mu+\frac{1}{\eta}\frac{\partial}{\partial \xi}(\exp(-Z\psi))+p\frac{1}{\eta}\frac{\partial}{\partial \xi}(\exp(-Z\Lambda\psi))=-\frac{\partial \psi}{\partial \xi}$$

$$\delta\frac{\partial^2\psi}{\partial \xi^2}=\eta-Z\beta\exp(-Z\Lambda\psi)-Z\exp(-Z\psi) \qquad (12)$$

The dimensionless variables are selected as follows: $\eta = n_i / n_0$ - profile of ion density, normalized on density in over dense plasma, $\xi = z/L$ - coordinate, the scale of plasma inhomogenity $L = c_s t_L$, $\tau = t/t_L$ - time, normalized on duration of laser pulse, $\mu = v_i / c_s$ (where $c_s = \sqrt{ZT_{eh}/M}$) - Mach number of ions in relation to velocity of an ion sound, $\psi = Ze\varphi / Mc_s^2; \Lambda = T_h / T_c; \beta = n_{eh} / n_{ec}; p = n_{ec}T_c / n_{eh}T_h; \delta = r_D^2 / L^2$ - dimensionless Debye screening distance, Z - effective charge of the ions. Obviously, the following inequalities are true for the dimensionless variables:

$$\Lambda \approx 1, \beta \approx 1, \ \delta \le 1, p \approx 1 \qquad (13)$$

Quasi-neutrality is assumed for the solution of the Poisson equation. The quasi-neutral status is valid if the process time is great than the time of fast electron oscillation about the ion:

$$t_L[ps] \ge \left(\frac{m_e}{4\pi n_h e^2}\right)^{1/2} \sim (10^{-3} n_{cr}/n_h)^{1/2} \qquad (14)$$

In a quasi-neutral approximation $\delta = 0$. The maximum velocity of ions we present as [1]:

$$\mu_{max} = 1 + \varepsilon_{max} = 1 + \frac{m_e v_{e.max}^2}{2T_h} . \qquad (15)$$

By expansion of the dimensionless function Ψ into a series, the coordinates of the asymptotic values of these functions are found to be as follows [1]:

$$\Psi \approx 0.5(\xi-\xi_t)^2; \ \mu \approx 0.5(-\xi+\xi_t), \ \eta \approx (1/\sqrt{2\pi})(-\xi+\xi_t) , \qquad (16)$$

here coordinate ξ_t is defined from the requirement $\psi(\xi_t) = 0$.

There is the next physical picture: fast electrons carry away ions behind themselves; the average electron moves together with ions, however precise electron motion represents an oscillation about ions in an electric field during a time like (14). In the one-dimensional case the electrons can not leave the ions, since the potential increases ad infinitum. We define ε_{max} from the requirement that the time of an electron returning from vacuum is about the laser pulse duration:

$$t \simeq 2v_{e,max}(Lm_e / e\varphi_{max}) \ge t_L \qquad (17)$$

From here

$$\varepsilon_{max} \simeq v_h t_L / 2\sqrt{2}L \simeq \frac{A}{Z}\frac{m_e}{m_p}\frac{T_h}{T_c}\left(\frac{t_L}{t_p}\right)^2 \approx 10 , \qquad (18)$$

where t_p - duration of laser pre-pulse, producing an initial scale of plasma inhomogeneity. We can estimate in this case the ratio of ion velocity to speed of light as: $v_i / c \approx 6 \cdot 10^{-2}$. In a real situation the potential is restricted. We take for the estimation the potential of a charged disk of diameter 2r (about

the size of a laser spot) on the surface of the plasma, then

$$\varphi = \frac{2q}{r^2}(\sqrt{r^2+z^2} - z); q = e\pi r^2 l \cdot n_{h,max} \qquad (19)$$

where

$$n_{h,max} = \int_{v_{max}}^{\infty} \frac{dn_e}{dv} dv \qquad (20)$$

and l is the distance which fast electrons move out from the target during the laser pulse. The magnitude of this charge is estimated, thus, from the assumption of quasi-neutrality. Then $\varepsilon_{max} \simeq \ln\psi \simeq \ln(\omega_{p,h}{}^2 lr / v_{T_h}{}^2)$. The calculation for $T_h \approx 300$kev, $n_{e,h} \approx 10^{-3} n_{cr} \approx 10^{-18}$cm^{-3}, $r \approx 3\cdot 10^{-3}$ cm gives $\varepsilon_{max} \approx 6$ or $v_i/c \approx 3\cdot 10^{-2}$. Thus the one-dimensional model gives the same order of magnitude of ion velocity.

We consider now the estimations for very short pulses, when there is no time for quasi-neutrality to be reached: $t_L[ps] \le (10^{-3} n_{cr}/n_h)^{1/2}$. In this case [4]

$$v_{max} \simeq 2(1 + \ln(Z\omega_{pi} t_L))$$
$$\eta = \begin{cases} 4\varepsilon^2 + (1/\varepsilon)\exp(-\varepsilon^2/2), \xi < \xi_s \\ 0, \xi > \xi_s \end{cases}$$
$$\varepsilon = \exp(\xi - \xi_s); \mu = 1 + \varepsilon + \xi \qquad (21)$$

At distance, where the scale of plasma inhomogeneity is about the Debye screening distance, we assume that ion concentration is equal to zero. Then

$$r_D = c_s t_L; n_e = n_{0e}\exp(-\xi), \text{ from this } \xi_s = 2\ln(Z\omega_{pi} t_L)$$
$$v_{max} \simeq 2(1 + \ln(Z\omega_{pi} t_L)) \approx 10 \qquad (22)$$

for ion velocity $v_i/c \approx 6\cdot 10^{-2}$ again is obtained.

For plasma with a sharp boundary the value of velocity can be determined from the value of the ambipolar field

$$E_a \simeq T_h / r_D. \qquad (23)$$

Velocity of an ion then $v_i = \frac{Z}{M} E_a t_L$, and their energy

$$\varepsilon_{max} = T_h \frac{n_h}{2n_c}\frac{m_e}{M}(\omega_0 t_L)^2 \simeq 10 \qquad (24)$$

at $n_h = 10^{-2} n_c$ and t_L = 1.5 ps. Thus, within an order of magnitude, the same ion velocities are derived from the different models. The connection between ion velocity, duration of laser pulse and pre-pulse is determined by the following: for short pre-pulse (the initial scale of inhomogeneity is less than the Debye screening distance of fast electrons) ion energy does not depend on pre-pulse duration, but for longer pre-pulse the ion energies less than that given in (18). For short $t_L[ps] \le (10^{-3} n_{cr}/n_h)^{1/2}$ basic pulses the energy of an ion is weakly (see (21)) dependant on pulse duration. For longer pulses the energy of an ion starts to increase with $t_L{}^2$. This increase over the above is restricted by the fact, that the energy and number of fast electrons are limited by the finite duration of the laser pulse. The pulse duration, for which there is saturation, is much more than 1 ps, and pulses of such duration are not considered in this paper.

We compare these scalings with the results of our numerical simulations:

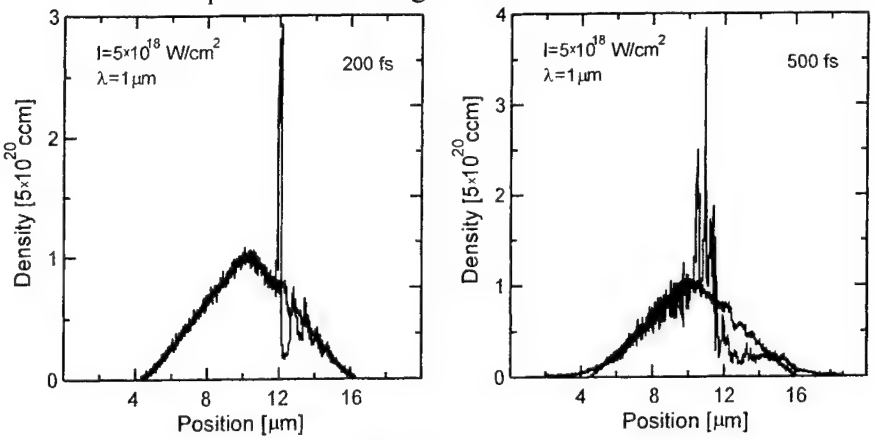

Fig.2

Figures 2, where plasma foil densities profiles are shown, illustrate that an intense laser pulse generates a shock wave with considerable of density 3-4 times that of foil density.

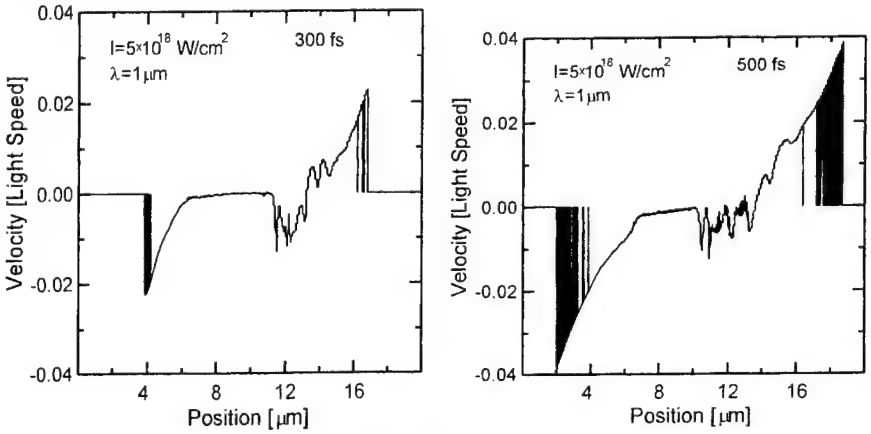

Fig.3

From figures 3, where are the ion velocity distributions, we see that the ions are accelerated by fast electrons on two surfaces of the thin foil, where the electrons leave this target and carry behind themselves ions. The acceleration happens also at a critical density $n = n_c$, where ponderomotive pressure forms the shock wave. Part of the ions take off into a vacuum in the opposite direction. The scalings from the given section are valid only for ions on the left-hand boundary, the opposite boundary we do not consider. From figures 2,3 we see that the values of ion velocity are in the interval 0.02-0.04 c, that well coincides with our scalings.

It also follows from the graphs, that the maximum velocity of ions increases with time. So at 300 fs and 500 fs the velocity increases from 0.02 till 0.04, that approximately corresponds to quadratic dependence (12,18) of ion energies from duration of laser pulse. We analyze also the dependence of ion energy from a scale of plasma inhomogeneity and now consider the results of simulations for plasma with a sharp density profile (such case is implemented without prepulse):

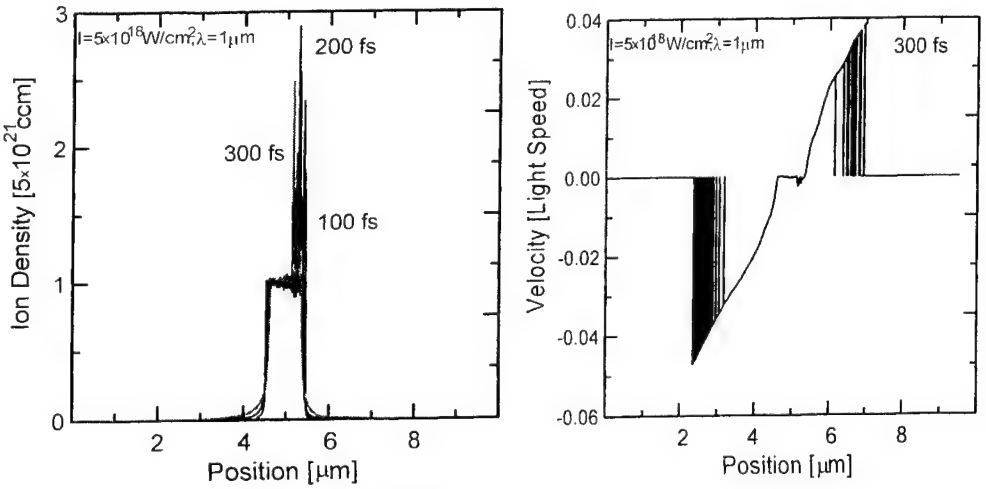

Fig.4

The graphs from Fig.4 of ion velocity for time 300 fs show: that on the back side of the foil the sharp plasma profile provides approximately twice as high ion speed compared with the smooth profile case. The explanation is as follows: on a sharp boundary, fast electrons travel a smaller distance from ions, as an ambipolar field is stronger. During the laser pulse the electrons make more cycles of oscillation about ions, and the rate of acceleration thus is higher. The scaling under the formula (24) gives magnitude of velocity of ions $v_i \sim 0.05c$, this agrees with numerical calculations.

So, the reason for ion acceleration on both target surfaces is the action of ambipolar field from fast electrons. The given electron distribution function approximation accurately describes the acceleration of ions on foil boundaries, but for an exposition of ion shock wave shaping inside plasma it is better to use hydrodynamic approximation.

3. Hydrodynamic approximation.

The hydrodynamic approach permits us to analyze processes inside dense plasma. It is valid for intense laser fields, when plasma electron velocity is increased by a field, and greatly exceeds thermal velocity. The electron distribution function in this approximation can be considered as a δ-function. As in the numerical simulations there is the following inequality between the temperature of cold and hot electrons $T_c << T_h$, we can use the hydrodynamic approximation, in which $T_c = 0$. We show, that in hydrodynamics there is an additional mechanism of acceleration of ions when propagating a shock wave in a nonuniform medium.

We find the solution of the self-consistent set of equations (1-6) by expansion on parameter v_T/v_E. In the zero order of approximation, we have instead of collision-less kinetics equation - hydrodynamic equations of motion of plasma electron component. The conservation law of transverse canonical momentum of electrons allows to reduce a system of hydrodynamic equations of electrons motion and Maxwells equations to two nonlinear partial equations for vector potential $\bar{A}(z;t)$ of electromagnetic

wave and longitudinal electric field $E(z;t)=-\partial\varphi(z,t)/\partial z$ in plasma [8]. Using the quasi-neutrality approximation, we have one equation for vector potential amplitude ($\bar{A}(z;t)=A(z,t)=A(z)e^{i\omega t}$):

$$(\frac{\partial^2}{\partial\xi^2}+\frac{\omega^2}{\omega_p{}^2})a(\xi)=(\eta(\xi)+\frac{\partial^2}{\partial\xi^2}\sqrt{1+a^2})\frac{a}{\sqrt{1+a^2}} \qquad (25)$$

and one equation, connecting longitudinal electric field with vector potential:

$$E=\frac{\partial}{\partial\xi}\sqrt{1+\bar{A}^2}+v_T{}^2\frac{\partial}{\partial\xi}\ln\eta(\xi) \qquad (26)$$

In a system (25-26) $\omega_p=(4\pi Zn_{i0}e^2/m)^{1/2}$- electron plasma frequencies and the following dimensionless variables are used:

$\xi=\frac{\omega_p}{c}z$; $a=\frac{e\bar{A}}{mc^2}$; $E=\frac{eE_z}{mc\omega_p}$; $v_T=(T_e/mc^2)^{1/2}$; $\eta(\xi)=\frac{n_i(\xi)}{n_i(\xi=\infty)}$ - dimensionless profile of ion density.

Now we return to system (6), by adding in the equations viscosity and by calculating an field E from (26). For the analysis of a strong shock wave parameters in plasma it is convenient to consider (6) in the following dimensionless variables: instead of velocity v_i we enter a Mach number $\mu=v_i/\sqrt{ZT_{ec}/M}$, ion time τ_i we measure in terms of $\frac{c}{\omega_p}\sqrt{\frac{M}{ZT_{ec}}}$, i.e. time an ion sound takes to transit a skin layer. Then the dimensionless hydrodynamical equations for ions havethe form:

$$\frac{\partial\eta}{\partial\tau_i}+\frac{\partial}{\partial\xi}(\eta\mu)=0$$

$$\frac{\partial\mu}{\partial\tau_i}+\mu\frac{\partial}{\partial\xi}\mu+\frac{\partial}{\partial\xi}\ln\eta(\xi)-\frac{1}{\eta(\xi)}\frac{\partial}{\partial\xi}\tilde{\eta}_i\frac{\partial}{\partial\xi}\mu=\frac{m_ec^2}{T_e}\frac{\partial\sqrt{1+A^2}}{\partial\xi}, \qquad (27)$$

where the dimensionless viscosity $\tilde{\eta}_i$ depends only on temperature of ions:

$$\tilde{\eta}_i=\frac{64}{L_c}\frac{Z^2T_e{}^2\omega_p}{e^4n_{0i}c}\left(\frac{T_i}{ZT_e}\right)^{5/2}, \qquad (28)$$

and L_c – Qulomb logarithm.

The system (27) is non-complete, and it is necessary to add an equation for temperature. We consider the process of shock wave propagation as adiabatic:

$$\frac{\partial}{\partial\tau_i}\left(\frac{T_i}{ZT_e}\right)\eta^{1-\gamma}+\mu\frac{\partial}{\partial\xi}\left(\frac{T_i}{ZT_e}\right)\eta^{1-\gamma}=0. \qquad (29)$$

The adiabatic exponent γ we take as equal 5/3, since the equation of plasma state differs a little from a ideal gas state.

If a laser pulse is shorter than $l_s/(ZT_e/M_i)^{1/2}$, then laser field pressure is equivalent to instantaneous shock, and the right side of the second equation of (27) is equivalent to the boundary conditions of the homogeneous system (27). The self-similar solution of the problem of strong shock is known [3]. From the second equation (27) the velocity of a fast ionis

$$\frac{v_i}{c} = \frac{u_w}{c} = \sqrt{\frac{Zm_e n_{cr}(\sqrt{1+A^2}-1)}{M_i n_e}}, \quad (30)$$

that coexists with [5]. The obtained formula gives the velocity of fast ions in the neighbourhood of a skin layer, i.e. behind the shock wave front. It is known that for a strong shock wave, the velocity of front and velocity of particles behind front connected by the factor 4/3, if an adiabatic exponent $\gamma = 5/3$.

$$\mu = \frac{4}{3} v_i \sqrt{\frac{M}{ZT_e}}.$$

Then a velocity of front we estimate as 4/3 u_w.

Thus, instead of a solution (27,29) in a medium with a given density profile, we divided the problem into two parts: first we found the parameters of a shock wave in the region of a skin layer, where it is shaped, and then we considered the exit of given shock wave in the region of low density (rear side of foil). In this region in (27) there is not a laser pulse force and it is possible to neglect viscosity.

Let's select the next law of plasma density dependence: $n_i(z) = bz^\delta = n_i(z_1)\left(\frac{z}{z_1}\right)^\delta$. Here z_1 is the distance at which the ion density starts to decrease. A density in this point is $n_i(z_1)$. At z=0 the density equals zero. Thus the shock wave goes from the position z_1 and at the position $z = 0$ goes out the rear side of the foil target. To get the solution of a homogeneous system (27) in this regionwe transfer to the self-similar variable $\chi = z/C(-t)^\alpha = z/X(t)$. Details of solution of equations (27) are described in [3]. For our purposes, we must know from [3] only one parameterα= 0.6 and after that, we get the velocity of a shock wave: $\dot{z} \sim |t|^{-(1-\alpha)} \sim X^{-(1-\alpha)/\alpha}$. On the surface at $z = 0$, velocity is going to infinity. Energy (per unit mass) $\varepsilon \sim \dot{z}^2 \sim X^{-2(1-\alpha)/\alpha}$, pressure $p \sim M_i n_i \dot{z}^2 \sim X^{\delta-2(1-\alpha)/\alpha}$. Thus the law of energy gain when a shock wave transits from a point z_1 to a point z is as follows:

$$\varepsilon(z) = \varepsilon(z_1)\left(\frac{z}{z_1}\right)^{-2(1-\alpha)/\alpha} \quad (31)$$

Further it is necessary to find a limit point z, wherethe ion (thermal ion before front) free path exceeds the width of plasma stratum, and plasma density becomes zero. After this point the hydrodynamic approximation is incorrect. The ion free path depends on its energy and density of plasma:

$$\Lambda_T(z) = \frac{12\pi^{3/2}T_i^2}{Z^4 e^4 n_i(z) L_c}. \quad (32)$$

We find this point z from the equation $z = \Lambda_T(z)$:

$$\frac{12\pi^{3/2}T_i^2}{Z^2 e^4 n_i(z_1) L_c z_1}\left(\frac{z}{z_1}\right)^{-\delta} = \left(\frac{z}{z_1}\right) \quad (33)$$

hence

$$\left(\frac{z}{z_1}\right) = \left(\frac{12\pi^{3/2}T_i^2}{Z^4 e^4 n_i(z_1) L_c z_1}\right)^{\frac{1}{1+\delta}} \quad (34)$$

Then ion's energy behind the front is:

$$\varepsilon(z) = \varepsilon(z_1)\left(\frac{12\pi^{3/2}T_i^2}{Z^4 e^4 n_i(z_1) L_c z_1}\right)^{\frac{-2(1-\alpha)}{\alpha(1+\delta)}} \quad (35)$$

In this formula $\varepsilon(z_1)$ - energy of an ion behind the front, which corresponds to velocity (30), $n_i(z_1)$ - ion concentration inside plasma, L_c- Culomb logarithm.
Coordinate z_1 is necessary to find the law of density dependence

$$bz_1^{\delta} = n(z_1) \quad (36)$$

Now the formula of energy gain can be presented as

$$\varepsilon(z) = \varepsilon(z_1)\left(\frac{z_1}{\Lambda_T(z_1)}\right)^{\frac{2(1-\alpha)}{\alpha(1+\delta)}} \quad (37)$$

In depth of plasma $\Lambda_T < z_1$, $\alpha < 1$ and the energy really grows.
From this formula we see that the energy gain is the ratio of the hydrodynamic scale to free path and varies as an exponent whose power is determined by the self-similar index α. The strong density dependence on coordinates reduces the rate of energy gain, for $\delta >> 1$, but at $\delta < 1$, i.e. for smoothly varying medium, the energy gain is much better, though it is necessary to understand that these two parameters not absolutely independent and $\alpha = \alpha(\delta)$. In the given model, the free path of a thermal ion in plasma is assumed as small in comparison with any hydrodynamic lengths.

Now we fulfil the numerical estimations. First we estimate free path of thermal ion, by expressing it in terms of laser wavelength:

$$\frac{\Lambda\omega}{c} \sim \frac{\omega}{Z^{*4} e^4 n_i L_c c}(T_i)^2 = \left(\frac{1}{Z^{*3} L_c}\right)\left(\frac{\omega}{\omega_{pe}}\right)^2\left(\frac{c}{\omega r_0}\right)\left(\frac{T_i}{m_e c^2}\right)^2, \quad (38)$$

where r_0 - classical radius of an electron. We choose $Z^* = 10$, $n_e = 10 n_{cr}$, then the free path is less than a wavelength at $T_i < 1.2$ keV.

The width of shock wave front is close to ion free path length because the viscosity of ions: $\eta_i = n_i T_i \tau_i$

$$l_\eta \sim \eta / m_i n_i v_{Ti} \sim \tau_i \frac{T_i / m_i}{v_{Ti}} \sim \Lambda_T$$

and typical scale of viscosity , from it width of front and ion free path, thus, are within one order of magnitude. At $\alpha = 0.6$, $\delta = 1$:

$$\varepsilon(z) = \varepsilon(z_1)\left(\frac{z_1}{\Lambda(z_1)}\right)^{\frac{2(1-\alpha)}{\alpha(1+\delta)}} = \varepsilon(z_1)\left(\frac{z_1}{\Lambda(z_1)}\right)^{2/3} \quad (39)$$

From this formula we see that a free path $\sim 0.1\lambda$ is necessary for raising ion energy for plasma width 3λ ($z_1 = 3$) and temperature of ions for this purpose should be less than 450 eV.

So parameters of plasma for ion acceleration can be as follows: $n_e = 10 n_{cr}$, scale of plasma density $z_1 = 3\ \lambda$, Ti = 450 eV. If we want to increase temperature k times more, scale should raise k^2 times. After laser pre-pulse plasma temperature decreases and scale of inhomogeneity grows - so this case is realizable.
Let's compare these results with PIC simulations. In the previous figures of numerical simulations, the shock wave propagates in the region of increasing density. Now we depict a shock wave in the plasma region with decreasing density.

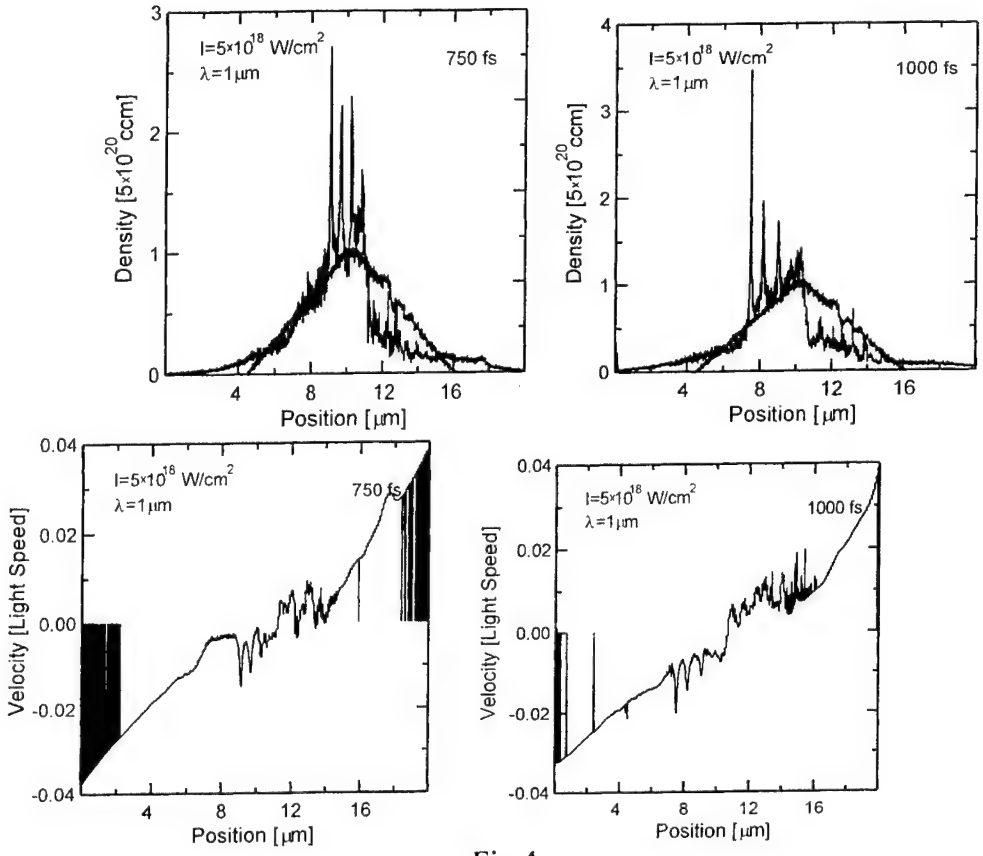

Fig.4

From these figures, we can conclude, that the shock front in plasma with decreasing density breaks up on some fronts (this is kinetic instability of shock wave front, when the wave top overtakes wave bottom). We compare the data of acceleration of a shock wave following from Figures 4 to the result of (39) . According to this law the shock wave velocity, on propagation from the point 9 microns to the point 8 microns increases by $\left(\frac{9-4}{8-4}\right)^{1-\alpha/\alpha} \simeq (1.25)^{0.66} \simeq 1.16$ times. (4 microns is the position, where the density is equals zero). Refering on Fig.4, from the graph of velocities in the vicinity of the shock front, we see the visual correspondence to this value. In the numerical calculations from Fig.4 we see thatthe ion free path is ~ 1 micron and the scalelength is z_l ~ 6мкм therefore, analytical coefficient of the ion velocity increase is ~ $6^{0.6}$ ~ 3 times as in the simulations.

4. Conclusion

We have discussed the process of ion acceleration from foil target by a laser.

1. The light pressure of a laser pulse is transmited to ions by means of electrons and ambipolar fields. A shock wave is formed in the vicinity of a critical density point (where the pressure is maximum) and propagates deep into the plasma. The hydrodynamic model gives adequate (confirmed by numerical calculations) exposure of this process. A characteristic shock wave velocity in Al target for intensity 510^{18} W/cm^2 and pulse duration 1.5 ps is about 0.02 the speed of light. Intensity of the shockwave and ion acceleration have a maximum in plasma with a scale of density gradient about a wavelength, as there are the maximum of absorption, amount of fast electrons and their energy in this

case.

2. A strong shock front disintegrates on several fronts, causing an order of decrease of their intensity when driving in inhomogeneous plasma from one surface of thefoil to other.

3. Ion velocity increases as plasma density decreases. It produces acceleration of ions, and magnification of their energy proportionaly tothe ratio of plasma density gradient to the length of ion free path. Gradient of rear side plasma density of the target should be smooth to a realize this effect.

4. Culomb mechanism of electron-ion acceleration from two surface, in contrary to that from a shockwave, is most effective in plasma with a sharp boundary and exceeds the acceleration of ions by a shockwave. At short initial scale of plasma inhomogeneity ion energy does not depend on this scale.For longer scale, ion energy decrease is inversely proportionally to square of plasma gradient. For short basic pulses the energy of an ion is weak (logarithmic) depending on pulse duration. For longer pulse, the energy of an ion begins to increase proportionally with the square of pulse duration down to a condition of saturation, at which energy flows of fast electrons and accelerated ions are comparable.

5. From the point of view of maximum ion acceleration, the optimal target should have a few micron thickness with smooth density gradient (scale of density inhomogenity about a wavelength) at rear and sharp density gradient front.

5. References

1. Y. Kishimoto et al. Phys. Fluids, v. 26, p.2308, 1983.
2. Zhidkov A. et al. Phys. Rev. E, v.61, p.2224, 2000.
3. Zeldovich Ya.B. Raiser Yu.P. Physics of shock waves and high-temperature hydrodynamic phenomena. M.: Science, 1966.
4. Pearlman J.S., and Morse R.L. Phys. Rev. Letters, v.40, p.1652, 1978.
5. Gibbon P. Forster E., Plasma Physics and Control Fusion, v.38, p.769, 1996.
6. Wilks S.C., Kruer W.L., Phys. Rev. Letters, 69, 1383 (1992).
7. Karpman V.I. Nonlinear waves in dispersive mediums. M.: Science, 1973.
8. A. A.Andreev, K. Platonov, K. Tanaka. JAERI-Conf 98-004 p.37, (1998).

Scattered light diagnostic of over-dense plasma cavity at ultra intense laser pulse interaction with solid target.

Andreev A.A[1)]., Zhidkov A.G.[2)], Sasaki A.[2)], Platonov K.Yu.[1)]

1) Institute for Laser Physics, Russia
2) Advanced Photon Research Center JAERI, Japan

PACS: 52.50.Jm; 52.40Nk; 52.25.Dg

Abstract

The light scattered backward from a target illuminated by ultra intense laser pulses carries important information about the nonlinear laser plasma interaction. We analyze the possibility of using this information with the help of developed analytical model and PIC simulations. The spectrum of scattered light is shown to be shifted, to be broadened and to be modulated, in comparison with the initial laser spectrum.

Introduction

The measurment of the spectrum of laser radiation scattered from a dense plasma is an important method of investigating laser plasma [1,2]. Reconstruction of plasma parameters by resuls of spectral measurements requires us at first to find the connection between these parameters and the spectrum. In the present paper we study the plasma dynamics in strong laser fields by a numerical simulations and analytical modeling. On the basis ofthe obtained velocity and density the nonlinear plasma oscillations are evaluated. Doppler shift and broadening of the spectrum of scattered radiation are obtained. At considered high laser pulse intensities the spectrum is explained not only by movementof the critical density surface that was obtained earlier but also generation of nonlinear sound oscillations in the plasma.

1. Basic equations.

First we consider plasma in a laser pulse field as an electron subsystem with a given ion distribution. The conservation law of conservation of electron transverse canonical momentum allows us to reduce a system of hydrodynamic equations of electron motion and Maxwell equations to two nonlinear differential equations for electromagnetic wave vector potential $\bar{A}(z;t)$ and longitudinal electric field $E(z;t)=-\partial\varphi(z,t)/\partial z$ in the plasma.

$$(\frac{\partial^2}{\partial\xi^2}-\frac{\partial^2}{\partial\tau^2})a=(\eta(\xi)+\frac{\partial E}{\partial\xi})\frac{a}{\sqrt{1+a^2}}\sqrt{1-v^2}\,, \qquad (1)$$

$$\frac{\partial}{\partial\tau}v\sqrt{\frac{1+a^2}{1-v^2}}=E-\frac{\partial}{\partial\xi}\sqrt{\frac{1+a^2}{1-v^2}}-\delta_i{}^2\frac{\partial}{\partial\xi}\ln(\eta(\xi)+\frac{\partial E}{\partial\xi}), \qquad (2)$$

Laser Optics 2000: Ultrafast Optics and Superstrong Laser Fields, Alexander A. Andreev, Vladimir E. Yashin, Editors, Proceedings of SPIE Vol. 4352 (2001) © 2001 SPIE · 0277-786X/01/$15.00

where $$v = -\frac{\partial E/\partial\tau}{\eta(\xi) + \partial E/\partial\xi} \qquad (3)$$

dimensionless (in terms of c) longitudinal hydrodynamic velocity of electrons, and $\omega_p=(4\pi Zn_{i0}e^2/m)^{1/2}$ – electron plasma frequency. In a system (1-3) the following dimensionless variables are used:

$\xi = \frac{\omega_p}{c} z$; $\tau = \omega_p t$; $a = \frac{e\bar{A}}{mc^2}$; $E = \frac{eE_z}{mc\omega_p}$; $\delta_T = (T_e/mc^2)^{1/2}$; here $\eta(\xi) = \frac{n_i(\xi)}{n_i(\xi=\infty)}$ - dimensionless profile of ion concentration of plasma. The equations (1,2) feature fast (in comparison with ions) oscillations of electronic density. We average on time (on scales of plasma oscillations times) the equation (2) or consider circular polarization of a laser wave (A^2 - slow function of time). Then, in an approximation of quasi-neutrality, the field E is connected with a by the equation:

$$E = \frac{\partial}{\partial\xi}\sqrt{1+\bar{A}^2} + v_T^{\,2}\frac{\partial}{\partial\xi}\ln\eta(\xi) \qquad (4)$$

After that, for amplitude of vector potential a from (1), the next equation is as follows:

$$\left(\frac{\partial^2}{\partial\xi^2} + \frac{\omega^2}{\omega_p^{\,2}}\right)a(\xi) = \left(\eta(\xi) + \frac{\partial^2}{\partial\xi^2}\sqrt{1+a^2}\right)\frac{a}{\sqrt{1+a^2}}, \qquad (5)$$

The knowledge of an ambipolar field (4) allows us to formulate equations of ionic component motion:

$$\frac{\partial n_i}{\partial t} + \nabla(n_i\vec{v}) = 0$$
$$\frac{\partial v}{\partial t} + v\,\nabla v + \frac{ZT_e + T_i}{M}\frac{\vec{\nabla} n_i}{n_i} = \frac{Zm\omega_p c}{M}\frac{\partial\sqrt{1+a^2}}{\partial\xi} \qquad (6)$$

If the laser pulse is shorter than $l_s / (ZT_e/M)^{1/2}$ (where l_s - length of the skin layer) the pressure of a laser field is equivalent to instantaneous shock on the plasma, and the right side of the second equation (6) is equivalent to the boundary conditions for a homogeneous system (6). The solution of a problem about such instantaneous shock for a system (6) is explained by an example in [5].

2. Under-critical plasma parameters.

The analytical solution (6) is difficult, however with the help of the second equation (6) it is possible to estimate the velocity of shock front. For this purpose we rewrite (6) as the dimensionless equation for the continuity of momentum flow:

$$\frac{\partial v_i}{\partial\tau} + \frac{\partial}{\partial\xi}\left(\frac{v_i^{\,2}}{2} + \frac{c_s^2}{c^2}\ln\eta(\xi) - \frac{Zm_e\sqrt{1+a^2}}{M}\right) = 0 \qquad (7)$$

Here $c_s = ((ZT_e + T_i)/M)^{1/2}$ -ion sound velocity and $v_i = v/c_s$

It is possible to omit the term containing plasma pressure, and also we assume that the laser field momentum flow is completely converted to ion momentum flow (by means of fast electrons), then from (7) we obtain the following ion velocity behind shock waves front

$$v_i = \left(\frac{2Zm_e}{Am_p}\sqrt{1+a^2}\right)^{0.5} \qquad (8)$$

We take Z/A = 0.5, m_e/m_p = 0.0005, therefore $v_i \simeq 0.02(1+a^2)^{1/4}$. For example for laser intensity $5\cdot10^{18}$ W/cm^2 (a^2 = 5) ion velocity is v_i~0.03. We emphasize that the expression (8) approximates a ion velocity near a position $n = n_{cr}$, where the ponderomotive pressure is applied. If we want to estimate

the velocity inside over-dense plasma, the conservation law of momentum flow produces a factor n_{cr}/n inside brackets in (8). For such a case, the formula (8) has been represented in [3]. These estimates of ion velocity are confirmed by our PIC simulations:

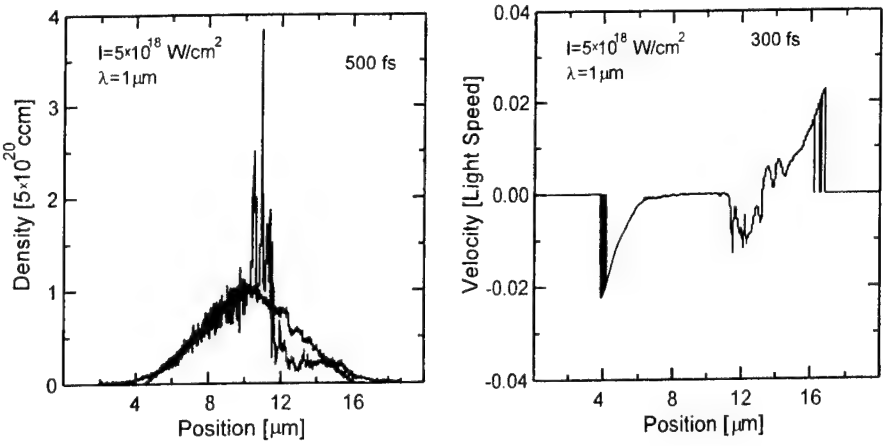

Fig.1

We see in Fig.1 that numerical simulation gives magnitude of the shock front velocity as $v \sim 0.014$. The estimates based on Eqs.(8) agree well with these numerical results.

3. Shock wave of a small amplitude.

The analytical solution (6) is possible for laser fields of small intensities ($a < 1$). In this case, the shock wave is feeble, and it is possible to use perturbation theory for solution of the equations (6). We substitute $n_i = n_{0i} + \delta n_i$ and expand (6) into a series of δn_i. For the first order perturbation theory, we obtain the sound equation for δn_i. For the second order the density perturbation $\delta\eta$ is described by KdW equation[4]:

$$\frac{\partial\delta\eta}{\partial\tilde{\tau}} + \frac{\partial\delta\eta}{\partial\xi} + \delta\eta\frac{\partial\delta\eta}{\partial\xi} + \beta\frac{\partial^3\delta\eta}{\partial\xi^3} + \frac{\alpha}{\pi}P\int_{-\infty}^{+\infty}\frac{\partial\delta\eta}{\partial\xi'}\frac{d\xi'}{(\xi-\xi')} = \frac{mc^2}{4T_e}\frac{\partial A^2}{\partial\xi} \qquad (9)$$

where

$$\delta\eta = -\frac{\delta n_i}{n_0}, \tilde{\tau} = \tau\sqrt{\frac{ZT_e}{Mc^2}}, \quad \beta = \frac{v_{Te}^2}{2c^2}\frac{\omega_{pe}}{\omega}, \alpha = \sqrt{\frac{\pi m_e}{8M}}\frac{\omega_{pe}}{\omega}. \qquad (10)$$

The term that contains an integral describes damping of nonlinear ion-sound oscillations, and the term containing parameter β, describes dispersion of plasmons.
The equation (9) together with the equation for a vector potential a:

$$\left(\frac{\partial^2}{\partial\xi^2} + \frac{\omega^2}{\omega_p^2}\right)A(\xi) = (\eta_0(\xi)(1 - A^2/2) + \delta\eta(\xi) + \frac{\partial^2}{\partial\xi^2}\frac{A^2}{2})A \qquad (11)$$

gives a system describing generation of a weak shock wave. For Al plasma and actual experimental data we substitute $\omega_{pe}/\omega = 10, v_{Te}/c = 0.1$, then $\beta = 0.05$ and $\alpha = 0.03$. The equations (9,11) are valid for $\delta\eta < 1$, therefore we can use the expansion in a in the equation (11). The restriction on amplitude of

a field in plasma, for which the perturbation of ion density in (9) remains weak, is s follows:

$$\frac{mc^2}{4T_e}A^2 \le 1 \qquad (12)$$

The scale length of ion-sound oscillations in (9) is about the length of a skin layer, the velocity is about the velocity of ion sound, so we can conclude that ion-sound frequency is equal to the ratio of these parameters for this case.
For a solution of a system (9,11) and for definition of plasma density profile in a shock wave it is necessary to set boundary conditions along ξ and initial conditions at $\tilde{\tau}$ also.

4. Solution of the boundary problem.

To determine the boundary conditions, we integrate (9) over ξ at the left-hand boundary of plasma:

$$\delta\eta + \frac{(\delta\eta)^2}{2} + \beta\frac{\partial^2\delta\eta}{\partial\xi^2}\bigg|_{\xi=0} = \frac{mc^2}{4T_e}A^2(\xi=0,\tilde{\tau}) \qquad (13)$$

At the right boundary we set boundary conditions for function and derivative to zero. The initial conditions also we put as: $\delta\eta|_{\tilde{\tau}=0} = 0$. Thus the mathematically problem about excitation of a shock wave has been completely formulated.
First, we qualitatively explore parameters of a shock wave in a homogeneous equation (9) using the following method. We search for a solution of form $\delta\eta(\xi - \tilde{\tau} - w\tilde{\tau})$, where w - velocity of a shock wave in a system moving with a velocity of an ion sound. Without a dissipative term theequation (12) becomes the Newton's law equation with an effective potential:

$$\beta\delta\eta'' = -\frac{\partial}{\partial\delta\eta}(\delta\eta^3/6 - w\delta\eta^2/2) \qquad (14)$$

The potential has a maximum at $\delta\eta = 0$ and minimum at $\delta\eta = 2w$. Dissipation reduces the effective driving force from the maximum represented by the potential to a minimum. Thus, the rarefaction wave moves to the right, and the Mach number is connected with density perturbation by a relation which is well known for a weak shock waves: $M_s = 1 + w = 1 + \delta\eta/2$. To construct the density profile for a shock wave we solve the equation:

$$\delta\eta'(\delta\eta - w) + \beta\delta\eta''' + \frac{\alpha}{\pi}P\int_{-\infty}^{+\infty}\delta\eta'\frac{d\mu'}{(\mu-\mu')} = 0 \qquad (15)$$

Far to the left of the front, where $\delta\eta(\mu) = 2w + \varepsilon(\mu)$, by linearizing (15), we obtain a linear integral equation for ε:

$$w\varepsilon' + \beta\varepsilon''' + \frac{\alpha}{\pi}P\int_{-\infty}^{+\infty}\varepsilon'\frac{d\mu'}{(\mu-\mu')} = 0 \qquad (16)$$

We search for a solution (16) as $\varepsilon(\mu) = \exp(i(k - i\gamma)\mu)$. The density oscillations thus have a scale k^{-1} and exponentially rise with an increment γ. Such oscillatory character of a density in a plasma shock wave was noted in [2]. The dispersion equation following from (16) has a simple form coinciding with the well known dispersion law for an ion sound:

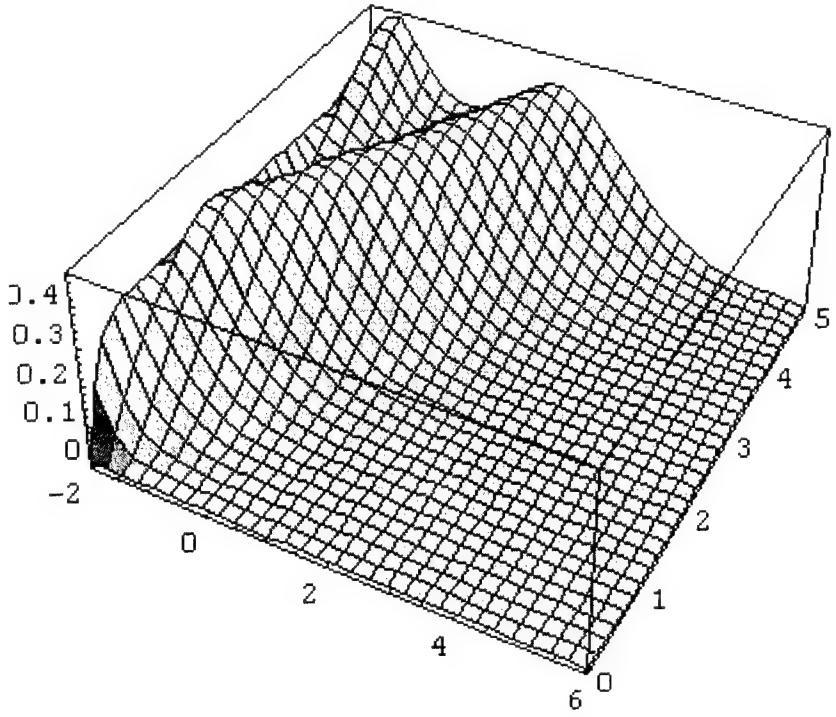

$$\beta(k-i\gamma)^2 - w + i\alpha\frac{\sqrt{k^2+\gamma^2}}{k-i\gamma} = 0 \qquad (17)$$

and is solved easily:

$$\gamma = \sqrt{\frac{-w+\sqrt{w^2+4\alpha^2}}{8\beta}}$$

$$k = \sqrt{\frac{5w+3\sqrt{w^2+4\alpha^2}}{8\beta}} \qquad (18)$$

Near to the shock front, the solution (9) can be found only numerically. We calculated this numerical solution with the above mentioned boundary conditions, by taking $\beta = 0.05$, $\alpha = 0$, $\frac{Zmc^2}{4T_e}A^2(\xi=0,\tilde{\tau}) = 4\tilde{\tau}\exp(-8\tilde{\tau}^2)$. In a figure 2, illustrating the numerical simulation, the spreading shock front and oscillating structure behind are shown (at $\tilde{\tau}=5$). At a later time the structure described above should be generated.

Fig.2

5. Analysis of laser pulse reflection from plasma density modulated by a shock wave.

As was shown before, upon action of the laser pulse on plasma, there is a shock front following by the oscillation of density. We can linearize the hydrodynamic equations because laser field, inside over dense plasma with sharp density gradient, is attenuated in $(\omega_p/\omega)>>1$ times. Then we consider joint solution of the equation for *a*:

$$\left(\frac{\partial^2}{\partial\xi^2} + 2i\frac{c_s}{c}\frac{\partial}{\partial\tilde{\tau}} + \frac{\omega^2}{\omega_p{}^2} - \eta_p + \delta\eta(\tilde{\xi},\tilde{\tau})\right)A(\xi,\tilde{\tau}) = 0 \qquad (22)$$

where $\tilde{\xi} = \xi - \tilde{\tau}$, and equation KdW for $\delta\eta(\tilde{\xi},\tilde{\tau})$:

$$\frac{\partial\delta\eta}{\partial\tilde{\tau}}+\frac{\partial\delta\eta}{\partial\xi}+\delta\eta\frac{\partial\delta\eta}{\partial\xi}+\beta\frac{\partial^3\delta\eta}{\partial\xi^3}=\frac{Zmc^2}{4T_e}\frac{\partial A^2}{\partial\xi} \quad (23)$$

We consider vector potential also as $a_0 + a_1$. We restrict this to terms of the second order, as the equation KdW is written to within the second order. As a result we obtain the next system:

$$(\frac{\partial^2}{\partial\xi^2}+2i\frac{c_s}{c}\frac{\partial}{\partial\tilde{\tau}}+\frac{\omega^2}{\omega_p{}^2}-\eta_p)A_0(\xi,\tilde{\tau})=0 \quad (24)$$

$$(\frac{\partial^2}{\partial\xi^2}+2i\frac{c_s}{c}\frac{\partial}{\partial\tilde{\tau}}+\frac{\omega^2}{\omega_p{}^2}-\eta_p)A_1=-\delta\eta(\tilde{\xi},\tilde{\tau}))A_0(\xi,\tilde{\tau})-\delta\eta(\tilde{\xi},\tilde{\tau}))A_1(\xi,\tilde{\tau})$$

(25)

$$\frac{\partial\delta\eta}{\partial\tilde{\tau}}+\frac{\partial\delta\eta}{\partial\xi}+\delta\eta\frac{\partial\delta\eta}{\partial\xi}+\beta\frac{\partial^3\delta\eta}{\partial\xi^3}=\frac{Zmc^2}{4T_e}\frac{\partial}{\partial\xi}(A_0{}^2+2A_0A_1+A_1{}^2) \quad (26)$$

Let's select plasma geometry relevant to a figure of the numerical simulations.

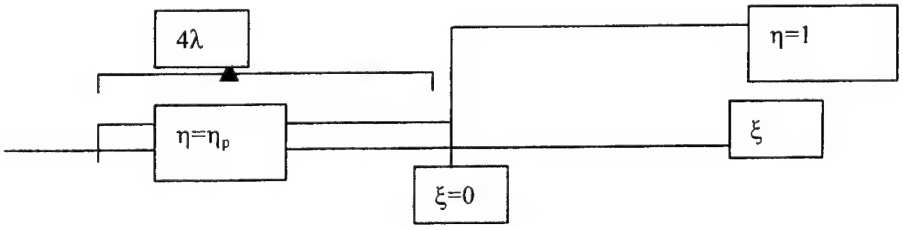

Field a_0 from (24) take as

$$A_0(\xi,\tilde{\tau})=A_0\sin(\sqrt{\omega^2/\omega_p{}^2-\eta_p}\,\xi) \quad (27)$$

We show at first, that the system (25,26) in under-dense plasma slab, with η=const, describes connected electromagnetic and sound waves and generation of sound harmonics. We search for a solution of the equations (25), (26) using a series expansion. A linear approximation gives the following coupled equations:

$$(\frac{\partial^2}{\partial\xi^2}+2i\frac{c_s}{c}\frac{\partial}{\partial\tilde{\tau}}+\frac{\omega^2}{\omega_p{}^2}-\eta_p)A_1=-\delta\eta(\tilde{\xi},\tilde{\tau}))A_0(\xi,\tilde{\tau}) \quad (28)$$

$$\frac{\partial\delta\eta}{\partial\tilde{\tau}}+\frac{\partial\delta\eta}{\partial\xi}-\frac{Zmc^2}{2T_e}\frac{\partial}{\partial\xi}A_0A_1=\frac{Zmc^2}{4T_e}\frac{\partial}{\partial\xi}A_0{}^2 \quad (29)$$

For solution of homogeneous equations we take:

$$A_1=A_1\exp(i(\omega_1-\omega)\tilde{\tau}-ik_1\xi)$$

$$\delta\eta=\delta\eta\exp(-i\omega_3+ik_3\xi) \quad (30)$$

Then from (28), (29) the following conservation laws for the interacting waves are obtained:

$$\omega - \omega_1 = \omega_3$$

$$k + k_1 = (\omega + \omega_1)\sqrt{1 - \eta_p \frac{\omega_p^2}{\omega^2}} = k_3 = \frac{\omega_3}{c_s} \quad (31)$$

From (31) the frequency of a sound and scattered waves can be determined:

$$\omega_3 = 2\omega \frac{c_s}{c}\sqrt{1 - \eta_p \frac{\omega_p^2}{\omega^2}}$$

$$\omega_1 = \omega(1 - 2\frac{c_s}{c}\sqrt{1 - \eta_p \frac{\omega_p^2}{\omega^2}}) \quad (32)$$

Taking finite length $L = 3l$ of plasma slab we see that a narrow frequency line is broadened and δ – function transforms to:

$$\delta(\Omega - \omega_1) \to \frac{\sin\left(\frac{3(\Omega - \omega_1)}{\omega}\right)}{\pi(\Omega - \omega_1)}, (\Omega - \omega_1) << \omega \quad (33)$$

Next iteration gives this system:

$$(\frac{\partial^2}{\partial \xi^2} + 2i\frac{c_s}{c}\frac{\partial}{\partial \tilde{\tau}} + \frac{\omega^2}{\omega_p^2} - \eta_p)A_{12} = -\delta\eta(\tilde{\xi}, \tilde{\tau}))A_1(\xi, \tilde{\tau}) - \delta\eta_2(\tilde{\xi}, \tilde{\tau}))A_0(\xi, \tilde{\tau}) \quad (34)$$

$$\frac{\partial \delta\eta_2}{\partial \tilde{\tau}} + \frac{\partial \delta\eta_2}{\partial \xi} - \frac{Zmc^2}{2T_e}\frac{\partial}{\partial \xi}A_0 A_{12} = \frac{Zmc^2}{4T_e}\frac{\partial}{\partial \xi}A_1^2 \quad (35)$$

The conservation laws for fields give the next frequency conditions:

$$\omega_{32} = \omega - \omega_1 + \omega_3 = 2\omega_3 \quad (36)$$

It means that a spectral line is shifted on the second harmonics of ion sound. It is broadened as given by Eq.(33) and has amplitude about the first harmonic $\sim \delta\eta/\eta_p$. Thus in a scatter spectrum there are harmonics of ion sound frequency determined by Eq.(32).

Obviously, the solutions of equations (30) are valid for homogeneous plasma and this rough approximation is good enough. To satisfy initial and boundary conditions it is necessary to use a self similar solution of the equation KdW (23) from a selfsimilar variable $\delta\eta(\tilde{\xi}, \tilde{\tau}) = \delta\eta(\beta\tilde{\xi}/\tilde{\tau}^{1/3})$. As shown in [4], solutions in this case are expressed through Airy functions. Such density profile, containing downward peaks, is qualitatively similar to numerical calculation results.

For the analysis of the spectrum of scattered radiation we use perturbation theory for (2):

$$(\frac{\partial^2}{\partial \xi^2} + 2i\frac{c_s}{c}\frac{\partial}{\partial \tilde{\tau}} + \frac{\omega^2}{\omega_p^2} - \eta_p(\xi))A^{(1)}(\xi, \tilde{\tau}) = -\delta\eta(\tilde{\xi}, \tilde{\tau}))A^{(0)}(\xi, \tilde{\tau}) \quad (37)$$

In under dense plasma $\eta(\xi) = \eta_p << 1$ and this plasma is transparent to laser pulse, but deep in plasma $\eta_0(\xi) > 1$ and laser pulse does not propagate inside this region.

Solution (37) we present through a Green function. Let's take into account, in the Green function the point of reflection $\xi_0(\tau)$ (boundary between over and under dense plasma), where the function equals zero. From the law of motion of a point of reflection we select $\xi_0(\tau) = -v_i \tau$, then this function has the form:

$$G(\xi,\xi';\tilde{\tau},\tilde{\tau}') = \sqrt{\frac{c_s}{2\pi i c(\tilde{\tau}-\tilde{\tau}')}}\left(\exp\frac{ic(\tilde{\tau}-\tilde{\tau}')(\omega^2/\omega_p{}^2-\eta_p)}{2c_s}\right)$$

$$\left(\exp\frac{ic_s(\xi-\xi_0(\tilde{\tau})-\xi'+\xi_0(\tilde{\tau}'))^2}{2c(\tilde{\tau}-\tilde{\tau}')}-\exp\frac{ic_s(\xi+\xi'-\xi_0(\tilde{\tau})-\xi_0(\tilde{\tau}'))^2}{2c(\tilde{\tau}-\tilde{\tau}')}\right). \quad (38)$$

This function is correct for slow dependence of $\xi_0(\tau)$, as from homogeneous equation (37) it is not satisfied precisely. Further we create a zero order approximation of the solution (24). Take as this approximation a laser standing wave:

$$A^{(0)}(\xi,\tilde{\tau}) = A_0\sin(\sqrt{\omega^2/\omega_p{}^2-\eta_p}\,(\xi-v_i\tilde{\tau})) \quad (39)$$

Thus we neglect the broadening of a spectral distribution of the laser pulse, connected with its duration, considering effects of sound generation more essential. For the correction to a field we get the following expression:

$$A^{(1)}(\xi,\tilde{\tau}) = -\int_{-\infty}^{\tilde{\tau}} d\tilde{\tau}' \int_{\xi_0(\tilde{\tau}')}^{\infty} d\tilde{\tau}' G(\xi,\xi';\tilde{\tau},\tilde{\tau}')\delta\eta(\xi',\tilde{\tau}')A^{(0)}(\xi',\tilde{\tau}') \quad . (40)$$

As perturbation of density, we substitute the following solution of the equation KdW– where Ei is Airy function.

$$\delta\eta(\xi,\tilde{\tau}) = \delta\eta_0 Ei(\beta\frac{\tilde{\tau}+\xi-\xi_0(\tilde{\tau})}{\tilde{\tau}^{1/3}})$$

The picture of the scattering looks like the following:

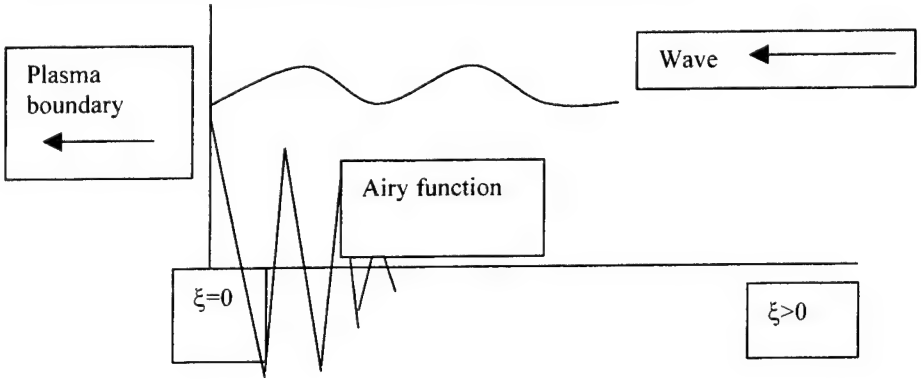

For the spectral distribution we have the next expression:

$$A^{(1)}{}_\Omega(\xi) = \frac{1}{2\pi}\int A^{(1)}(\xi,\tilde{\tau})\exp(i\Omega\tilde{\tau})d\Omega \quad (41)$$

We take a limited big interval ξ , where the field has the form of a propagating wave. For further evaluations we insert the new variable to integrate over and interchange the order of the integration. Then for (41) we obtain the following expression:

$$A_{\Omega}^{(1)}(\xi) = -A^{(0)}\delta\eta_0 \frac{1}{4\pi^{3/2}} \int_0^{\infty} d\xi'' \int_{-\infty}^{+\infty} d\tilde{\tau}' \int_0^{\infty} d\tilde{\tau}'' \sin((\sqrt{\frac{\omega}{\omega_p} - \eta_p})\xi'') \exp(i\Omega(\tilde{\tau}' + \tilde{\tau}''))$$

$$\int dk d\Omega_1 \exp(ik\xi'' - i\Omega_1\tilde{\tau}') \frac{i\Gamma(1/3)\sigma}{\sqrt{3}(2\pi)^2(\sigma^3 k^3 + k(1-u) + \Omega_1)^{4/3}}$$

$$\sqrt{\frac{c_s}{2\pi i c\tilde{\tau}''}} \left(\exp \frac{ic\tilde{\tau}''(\omega^2/\omega_p{}^2 - \eta_p)}{2c_s} \right) \left(\exp \frac{ic_s(\xi - \xi'' + u\tilde{\tau}' + u\tilde{\tau}'')^2}{2c\tilde{\tau}''} - \exp \frac{ic_s(\xi + \xi'' + u\tilde{\tau}'' + u\tilde{\tau}')^2}{2c\tilde{\tau}''} \right) \tag{42}$$

The integral on τ' can be easily taken, as it represents the Poisson integral. After that the integrals on τ'' and ξ'' are evaluated. These integrals give δ - functions relevant to the laws of conservation of energy and momentum for generation of sound by a laser pulse:

$$\Omega - \Omega_1 = -u\sqrt{\frac{\omega^2}{\omega_p{}^2} - \eta_p}$$

$$k = 2\sqrt{\frac{\omega^2}{\omega_p{}^2} - \eta_p} \tag{43}$$

With the help δ - functions from (43) it is possible to fulfil the next integrations on k and ω_1. As result, the vector potential of scatter radiation for large ξ becomes:

$$A_{\Omega}^{(1)}(\xi) = A_0\delta\eta_0 \exp(i\sqrt{\frac{\omega^2}{\omega_p{}^2} - \eta_p}\,\xi) \frac{\Gamma(1/3)\sigma}{\sqrt{3}64\pi^{7/2}(\sigma^3(\frac{\omega^2}{\omega_p{}^2} - \eta_p)^{3/2} + (\frac{\omega^2}{\omega_p{}^2} - \eta_p)^{1/2}(2-u) + \Omega)^{4/3}} \tag{44}$$

From this formula we see that:

The correction really is a plane wave propagating from a boundary.

Doppler shift is to the red side and has a large value at negative ω, where ω is related to the optical frequency. The spectrum is almost symmetrical about the maximum. The spectrum is shifted, broadened and its amplitude decreases as $\sim\omega^{-4/3}$. For the shift we have the following expression:

$$\Delta\omega = \omega_p \frac{c_s}{c}(\sigma^3(\frac{\omega^2}{\omega_p{}^2} - \eta_p)^{3/2} + (\frac{\omega^2}{\omega_p{}^2} - \eta_p)^{1/2}(2-u)) \tag{45}$$

There is frequency ω^* at which (44) converts to infinity. It has taken place because for the evaluation of Fourier components (43) we used this solution during all time. The introduction of an integral with cuttoff at some time removes this limitation. But it is obvious that (46) is valid while $A^{(1)} << A_0$. Thus, near to maximum of the spectrum our description is inapplicable, but wings of the spectrum we circumscribed correctly.

Let's compare the obtained results and our numerical simulation which we have shown in Fig.4

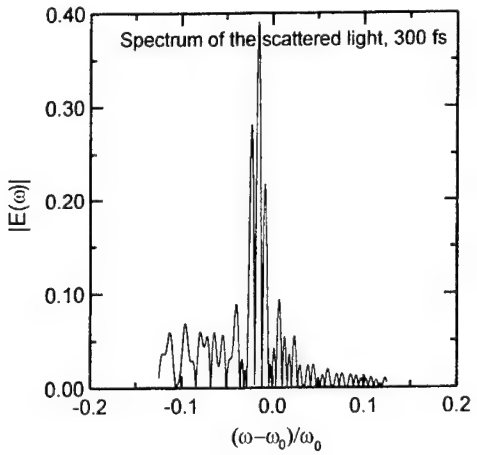

Fig.4

As we know from Fig.2 the calculated plasma boundary velocity is 0.014 c. It gives a shift $\frac{\omega-\omega_0}{\omega_0}$ to the laser spectral line which is also equal to 0.014. It approximately corresponds to the maximum on this graph. From the graph, we see that this peak is broadened and located in the interval of frequencis up to 0.02-0.025. To explain this broadening we should also take into account the generation of sound harmonics in under dense plasma. For this purpose we compare the spectrum from (45) and the simulation data. In the numerical simulation $\omega_{pe}/\omega = 2, v_{Te}/c = 0.1$ $c_s/c = 1.510^{-3}$, then $\sigma = 10$ and from (45) it follows that $\Delta\omega/\omega = 0.05$, which is close result to the simulation result.
Finally we discuss the modulation, observed in simulation of the spectrum. Finite time of Fourier transformation is- 300 fs. It corresponds in Fourier spectrum to dimensionless frequency $\frac{\lambda}{c\times 300\phi c} = 0.011$. This is approximately the modulation of the spectrum in figure 4. Thus, by experimentally measuring shift and width of spectrum on experiment wecan estimate under dense plasma parameters .

7. Conclusion

This theoretical analysis of short high power laser pulse reflection from a dense plasma resulted in the following conclusion:
1. Ponderomotive pressure of laser light near critical density produces a shock wave which propagates deep into plasma. This process changes the profile of plasma density and creates two areas: transparent under-dense plasma and above-critical dense plasma. The critical density surface separating these areas moves with supersonic speed deep into the plasma together with the front of the shock wave at ultra high laser intensity. In under- critical and above-critical areas intensive nonlinear ion sound waves generate. In the transparent area the degree of non-linearity is higher, due to higher field amplitude.
2. The indicated processes affect the spectrum of scattered radiation in the following way:
i) Critical surface movement produces Doppler red frequency shift of scattered light.
ii) Scattered radiation has a border peak of spectrum with wide spectral baseline from ion sound oscillations in over dense plasma.
iii) The nonlinear ion sound in under-dense plasma produces harmonics in the spectrum of the scattered radiation, widen and modulate it. This process forms a spectrum central peak also.
3. Low frequency modulation of a scattered light spectrum is produced by finite duration of a laser

pulse.
4. The measurements of the spectrum of reflected radiation thus allow us to determine the speed of critical surface, and the density in under-dense plasma.

References

1. R.Lichters, J.Meyer-ter-Vehn, A.Puchov, Phys. Plasmas, Vol.3, No.9, 3425 (1996)
2. P.Gibbon, Phys. Rev. Lett. 76, 50 (1996).
3. Wilks S.C., Kruer W.L., Phys. Rev. Letts, 69, 1383 (1992).
4. Karpman V.I. Nonlinear waves in dispersive mediums. M.: science, 1973
5. Zeldovich Ya.B. Raiser Yu.P. Physics of shock waves and high-temperature hydrodynamic appearances. M.: Science, 1966.

Interaction of super strong electromagnetic pulse with dense plasma layer.

Vladimir A. Cherepenin[1], Anton S. Il'in[1] and Victor V. Kulagin[2]

[1] Institute of Radio-Engineering and Electronics RAS, Mokhovaya 11, Moscow, Russia
[2] Sternberg Astronomical Institute, Moscow State University,
Universitetsky prospect 13, Moscow, 119899, Russia.*

ABSTRACT.

An interaction of a super strong linear-polarized electromagnetic wave with a dense plasma layer is investigated with the help of a self-consistent method of the analysis. It is shown that at falling a powerful harmonic wave at thin plasma layer the reflected field can be in the form of ultrashort pulses of radiation with amplitude considerably larger than an amplitude of an incident wave. A process of interaction of a plasma layer with a standing electromagnetic wave is considered also and a generalization of classical results about character of an electron motion in an electromagnetic field is obtained for a case of a strong field and large radiation friction. In a strong field a minimum of an effective potential splits into two new that results in violation of mirror symmetry of plasma layer radiation.

Keywords: Ultrashort pulse, plasma layer, laser-plasma interaction, radiation friction, radiation field

INTRODUCTION.

Recently large attention is given to the problems of generation of powerful ultrashort pulses and coherent electromagnetic radiation of high (up to x-ray) frequency through an interaction of a super strong laser radiation with a solid target [1-6]. The reason for occurrence of high harmonics in a spectrum of reflected wave is the following: at falling a powerful electromagnetic wave with intensity $10^{18}-10^{19} Wt/cm^2$ on a target the electron plasma with large density (about the order of $10^{22}\ cm^{-3}$) is formed on its boundary, the electrons of this plasma layer move not only in transversal direction but also commit the longitudinal vibrations at a double frequency under the action of magnetic component of the incident wave. There are two approaches now to the solution of such problems. First is based on a direct numerical simulation of Maxwell equations for process of interaction of plasma and powerful electromagnetic wave by a particle-in-cell method [2,4] and has all known lacks intrinsic to numerical experiments of such kind: technical complexity, difficulty of interpretation and selection of the physical solutions etc. In the second approach the simplified description permitting to receive analytical expressions is used. The model of an oscillating mirror is usually considered [1], in which the high harmonics in the reflected wave arise due to the periodic modulation of its phase: $E_R \propto \cos(\omega t+\varphi_0+\psi(t))$, $\psi(t)=\psi_0 \sin 2\omega t$, where ω - is a frequency of an incident wave and φ_0 is its initial phase. The incompleteness of such approach is due to the facts that, at first, the mirror is supposed to be absolutely reflecting, secondly, the time dispersion and dynamic relativistic effects are omitted. Besides the form of mirror oscillations in such approach is supposed to be harmonic that, generally speaking, does not correspond to the precise solution of self-consistent equations of motion for the plasma layer. At the same time at ultra relativistic amplitude of an external field when the work of a field on the wavelength becomes considerably larger than the rest energy of the electron (accelerating parameter $\alpha_0 = eE_0/m\omega c >> 1$), the indicated effects should play an essential role. Actually at reflection of a wave from a mirror moving towards with constant speed the reflected amplitude is proportional to the factor $A=(1+\beta)/(1-\beta)$, where β is the ratio of mirror speed to the speed of light in vacuum c [7]. In essentially relativistic regimes of interaction of the electromagnetic wave with the plasma layer ($\alpha_0 >> 1, |\beta| \sim 1$) the form of the reflected field can evidently has a strong dependence on the amplitude factor A.

The essential results describing the process of reflection of the powerful (ultra relativistic) electromagnetic wave from the plasma layer can be obtained within the framework of electron sheets model [8]. This model gives the consistent microscopic description of plasma layer interaction with electromagnetic waves and allows to solve many self-consistent problems about interaction of fields with charged medium. Especially simple equations of motion can be obtained in the

*Correspondence: V. V. K.; E-mail: kul@sai.msu.ru; V.A.C.; E-mail: cher@cplire.ru.

Laser Optics 2000: Ultrafast Optics and Superstrong Laser Fields, Alexander A. Andreev, Vladimir E. Yashin, Editors, Proceedings of SPIE Vol. 4352 (2001) © 2001 SPIE · 0277-786X/01/$15.00

case of small width of the plasma layer (considerably less than the wavelength of the incident radiation) when in the model it is possible to use one sheet only. Just this case will be considered in the present paper.

In particular it will be shown that at ultra relativistic amplitudes of the external field the reflected wave has essentially nonharmonic character: there is a synchronous radiation of harmonics of the incident wave frequency. Namely the sinusoidal incident wave can be converted into a sequence of short pulses of electromagnetic radiation with large amplitude. Thus due to the enrichment with the harmonics the decrease of each pulse duration takes place and the amplitude of pulses can essentially exceed the amplitude of the incident wave. The process of interaction of the plasma layer with a standing linear-polarized electromagnetic wave will be considered also and the generalization of the classical results about the character of electron motion in electromagnetic field [9] for the case of the strong field and large electron concentration (large radiation friction) will be obtained. It appears that in the strong electromagnetic field ($\alpha_0 > 2$) each minimum of an effective potential splits into two new minima. It results in violation of mirror symmetry of plasma layer radiation and dependence of the stationary state on the initial conditions due to essentially non-linear character of electron's oscillations.

For simplicity in the following analysis we shall consider that an ion background is fixed and electron concentration in plasma is large enough, so that the frequency of an external field will be much less than plasma characteristic frequency. Besides we shall consider that the initial velocity of the electrons is zero (approximation of a cold plasma).

1. MODEL AND MAIN EQUATIONS.

Let consider a charged medium homogeneous in directions perpendicular to Oz axis. In this case the densities of charge $\rho(z,t)$ and current $\vec{j}(z,t)$ depend only on z and are independent on x and y. Formal solutions of Maxwell equations can be in this case obtained by a method of a Green function and look like [8]:

$$\vec{E}(z,t)=2\pi\int_{-\infty}^{+\infty}\int_{-\infty}^{+\infty}dt'\,dz'\delta\left(t-t'-\frac{|z-z'|}{c}\right)sign(z-z')\rho(z',t')\vec{e}_z$$
$$-\frac{2\pi}{c}\int_{-\infty}^{+\infty}\int_{-\infty}^{+\infty}dt'dz'\delta\left(t-t'-\frac{|z-z'|}{c}\right)\vec{j}(z',t') \qquad (1)$$
$$\vec{H}(z,t)=\frac{2\pi}{c}\int_{-\infty}^{+\infty}\int_{-\infty}^{+\infty}dt'dz'\delta\left(t-t'-\frac{|z-z'|}{c}\right)sign(z-z')\left[\vec{j}(z',t'),\vec{e}_z\right]$$

Here [,] is the sign of a vector product.

Let now consider a thin layer of electrons extended in x and y-direction with the width considerably smaller than the wavelength of the incident radiation. In this case the layer is equivalent to an infinitely thin charged sheet the dynamics of which can be described by 3 + 1 functions of time: three components of speed $\vec{v}=\vec{v}(t)$ and one space coordinate $z=Z(t)$ (fig.1). The densities of charge and current of such sheet have the form:

$$\rho(z,t)=\sigma\delta(z-Z(t));\ \vec{j}(z,t)=\sigma\vec{v}(t)\delta(z-Z(t)), \qquad (2)$$

where σ is the surface density of charge.

Substituting now expressions (2) in equations (1) and integrating over z' and t', one can obtain the following expressions for the components of electromagnetic field:

$$E_z(z,t)=2\pi\sigma\,sign(z-Z(t'))$$

$$E_\perp(z,t)=-2\pi\sigma\frac{\beta_\perp(t')}{1-\beta_z(t')sign(z-Z(t'))}, \qquad (3)$$

$$H(z,t)=2\pi\sigma\,sign(z-Z(t'))\frac{[\beta_\perp(t'),e_z]}{1-\beta_z(t')sign(z-Z(t'))}$$

where $\vec{E}_\perp = E_x \vec{e}_x + E_y \vec{e}_y$, $v_\perp = v_x e_x + v_y e_y$, $\beta = v/c$ and the "delaying" time t' is determined from the equation $c(t-t') = |z - Z(t')|$.

It is worth to mention that the expressions (3) are one dimensional (or, more precisely, 3 + 1 dimensional) analogues of the classic Lienar-Wihert solutions [7] and give the exact expressions for the field created by the infinite plane. Here the component E_z can be interpreted as a near field and component $E_\perp$ as a field of radiation.

Let consider an expression for a spectral component of the radiation field $\vec{E}_{\perp\omega}(z)$. Substituting into equation

$$\vec{E}_{\perp\omega}(z) = \int_{-\infty}^{+\infty} dt\, \vec{E}_\perp(z,t) \exp(-i\omega t) \tag{4}$$

the expressions for the field (1), one can receive

$$\vec{E}_{\perp\omega}(z) = \frac{2\pi}{c} \int_{-\infty}^{+\infty}\int_{-\infty}^{+\infty} dt\, dz'\, \vec{j}_\perp(z', t) \exp\{-i(\omega t + kR)\}, \tag{5}$$

where $R = |z - z'|$ and $k = \omega/c$. Then using expression for the current density according to (2) one can obtain:

$$\vec{E}_{\perp\omega}(z) = 2\pi\sigma \int_{-\infty}^{+\infty} dt\, \vec{\beta}_\perp(t) \exp\{-i(\omega t + kR)\} \tag{6}$$

For periodic (with period $T = 2\pi/\omega$) motion of the plane the spectral decomposition of the radiation field contains only components at frequencies $n\omega$ with values

$$\vec{E}_{\perp n}(z) = 2\pi\sigma \frac{1}{T} \int_0^T dt\, \vec{\beta}_\perp(t) \exp\{-in(\omega t + kR)\} \ . \tag{7}$$

Let consider now an influence of the radiation field (3) on the motion of the electron sheet. It follows from expressions (3) that the interaction of the electron sheet with the own radiation field results in appearance of a specific self-action force [8]:

$$\vec{\Phi}_{sa\perp} = -2\pi\sigma^2 \beta_\perp \ , \ \Phi_{saz} = -2\pi\sigma^2 \beta_\perp^2 \frac{1}{1-\beta_z^2} \beta_z, \tag{8}$$

I.e. there is effective viscous force (8) with a constant coefficient of viscosity $\eta_\perp = \frac{2\pi\sigma^2}{c}$ for transversal motion and non-linear coefficient of viscosity $\eta_{||} = \frac{2\pi\sigma^2}{c} \frac{\beta_\perp^2}{1-\beta_z^2}$ for longitudinal motion.

The equations of motion for a separate electron of the sheet in homogeneous along x and y fields look like:

$$\frac{d\vec{p}}{dt} = e\vec{E} + e\left[\vec{\beta}, \vec{H}\right] + \vec{F}_{sa},$$

$$\vec{F}_{sa\perp} = -2\pi\sigma e \vec{\beta}_\perp \ , \ F_{saz} = -2\pi\sigma e \beta_\perp^2 \frac{1}{1-\beta_z^2} \beta_z \tag{9}$$

Here p is the relativistic momentum of the electron and e is its charge.

2. GIVEN LONGITUDINAL MOTION OF THE PLASMA SHEET.

Let at first consider a given longitudinal motion $z = z(t)$ of the sheet. For transversal motion of the sheet in a field $E_y = E_0 \cos(\omega t - kz + \varphi_0)$ (normal falling of the linear-polarized wave at the plasma layer) one has from equations (9):

$$\frac{dp_y}{dt} = eE_0 \cos(\omega t - kz(t) + \varphi_0)(1 - \beta_z(t)) - 2\pi\sigma e\beta_y \quad . \tag{10}$$

Let for simplicity the surface density of charge σ is large enough. In this case the sheet is practically an ideal mirror and, as was shown in Ref. [8], it is possible to neglect the inertial (dispersion) term dp_y/dt in equation (10) (strictly speaking, the larger β_z the greater should be the surface density σ for the sheet be the ideally reflecting mirror). Under these conditions the expression for the reflected wave has according to (3) the following form:

$$E_{Ry} = -E_0 \frac{1 - \beta_z(t')}{1 + \beta_z(t')} \cos(\omega t + kz - 2kz(t') + \varphi_0) \tag{11}$$

Note that the expression for the amplitude Doppler factor $A = (1 - \beta_z)/(1 + \beta_z)$ in this case appears valid not only for uniform motion but also for arbitrary dependence $\beta_z = \beta_z(t)$ with replacement of t by the delaying time t'.

Let now the dependence of the longitudinal velocity on time is determined by an expression $\beta_z = \beta_0 \sin 2\omega t$ (a phase difference between the mirror oscillations and electromagnetic wave is determined by the value φ_0). From (11) it follows that for $\beta_0 \to 1$ the function A has a form of infinitely high pulses at the double frequency. The amplitude modulation of the reflected field due to the factor A (cf. (11)) essentially enriches for $\beta_0 \to 1$ the radiation spectrum so the shape of the reflected wave considerably differs from a sine wave. In fig. 2 the time dependence of the reflected field is displayed for different values of β_0. There is a large number of odd harmonics of base frequency ω in the reflected wave and the closer is β_0 to unit the more harmonics is involved in the formation of the reflected wave. The principle point is the rigid binding for the phases of all harmonics to the phase of the incident wave. As a result all harmonics are added synchronously and the reflected field has the form of short pulses of radiation following with frequency ω with the amplitude directly proportional to the number of harmonics and with duration inversely proportional to that number. For relative complex amplitude of 2p + 1 harmonic one can obtain substituting the solution (11) into the spectral decomposition of the radiation field (7)

$$\tilde{E}_{R\,(2p+1)}/E_0 = -\exp\left(i\frac{\pi}{2}p\right)\left[A_p(\beta_0)\exp(i\varphi_0) + iB_p(\beta_0)\exp(-i\varphi_0)\right] \tag{12}$$

where the coefficients A and B are defined by the following expressions:

$$A_p(\beta_0) = \sum_{n=-\infty}^{+\infty} [1 + 2(-n+p)] J_n\left((2p+1)\frac{\beta_0}{2}\right) J_{-n+p}\left(\frac{\beta_0}{2}\right)$$

$$B_p(\beta_0) = \sum_{n=-\infty}^{+\infty} [1 + 2(n-p-1)] J_n\left((2p+1)\frac{\beta_0}{2}\right) J_{n-p-1}\left(\frac{\beta_0}{2}\right),$$

Here $J_n(x)$ is the Bessel function of the n-th order. Thus the expression (12) gives the precise analytical solution to the problem of reflection of the sine wave with frequency ω from the ideally reflecting mirror oscillating in the longitudinal direction with arbitrary amplitude β_0 and frequency 2ω. It is worth to mention that similar formulas can be obtained for the general case with dispersion.

The analysis of expression (12) gives not only a numerical value for a conversion coefficient of the incident wave power into harmonics, but also displays its strong dependence on the phase difference between the oscillations of the electron sheet and the wave.

3. RADIATION OF THE SHEET IN THE FIELD OF MONOCHROMATIC WAVE.

Let proceed now to the self-consistent analysis of the reflected field in the case when the sheet moves under the action of the linear-polarized incident wave $E_y = E_0 \cos(\omega t - k z + \varphi_0)$. Here contrary to the case considered in section 2 the dispersion of electron medium (inertial term) and highly nonharmonic character of electron oscillations will be taken into account. The trajectory of the electron sheet in this case can be presented as the sum of three components:

1). Transversal oscillations at the frequency of the incident wave.

2). Longitudinal oscillations at the double frequency of the incident wave.

3). Longitudinal drift under the action of a radiation pressure force.

At relativistic intensities the radiation pressure force acting on the sheet will be very large that will cause fast longitudinal acceleration of the sheet to about the speed of light; after that the sheet practically will stop to reflect the incident radiation. Therefore it is necessary to compensate the mean radiation pressure by, for example, an external electrostatic field $E_z = -E_{ext}$ (in real experiment such field can be produced by positive charge of heavy ions, for example. Actually for $2\alpha^2 \geq \alpha_0^2$, where $\alpha = 2\pi\sigma e/m\omega c$, the force of the electrostatic attraction from the ionic background appears to be larger than the force of light pressure, and the steady state regime is possible in the system). At $\alpha >> 1$ for the full compensation of the radiation pressure force it is necessary to put $E_{ext} = (\alpha_0 / 2\alpha) E_0$ [8]. In this case equations of motion (3) for the electron sheet have the following form:

$$\frac{d}{dt}\left(\frac{\beta_y}{\sqrt{1-\beta^2}}\right) = \alpha_0\omega\cos(\omega t - kz(t) + \varphi_0)(1-\beta_z) - \alpha\omega\beta_y$$
$$\frac{d}{dt}\left(\frac{\beta_z}{\sqrt{1-\beta^2}}\right) = \alpha_0\omega\cos(\omega t - kz(t) + \varphi_0)\beta_y - \alpha\omega\frac{\beta_y^2}{1-\beta_z^2}\beta_z - \omega g, \qquad (13)$$

where $g = eE_{ext}/m\omega c$ is a dimensionless compensatory force. A numerical analysis of the system (13) displays that the longitudinal oscillations of the electron sheet have essentially nonharmonic character for large α_0 that differs from the usually supposed sinusoidal law of motion. Besides there are parts of trajectory where the mirror moves towards to the incident wave with the speed close to the speed of light. According to expressions (3) just from these parts there is the radiation of large amplitude pulses (generation of high harmonics).

The most effective increase of reflected pulses' amplitude and enrichment by harmonics occur according to (3) for the motion of the sheet towards the incident wave with the speed close to c. For the oncoming acceleration of the electron sheet a swinging wave with frequency considerably smaller than the frequency of the incident radiation can be used in addition to the constant compensating field. Then the constant electrostatic field compensates the radiation pressure force of the incident wave and the swinging field provides at some moments the counter speed of the sheet close to the speed of light. Let, for example, the external field is selected in the form $E_{ext} = \frac{\alpha_0}{2\alpha} E_0 k(1+\sin(0.1\omega t))$, where the factor $k \approx 1$ is introduced for the regime to be quasistationary. For this case the shape of the reflected field E_R is shown in fig. 3 for $\alpha = 100$ and different values of α_0 and k. The reflected field represents a set of trains following with frequency of the swinging wave (0.1ω in fig. 3) and each train consists of the short pulses with large amplitude which are radiated from the parts of trajectory where $\beta_z \approx -1$. The duration of each train is about the half of the swinging field period and there is a nonuniform effective compression of the train due to the Doppler conversion of the frequency. Distance between different trains in the set practically does not change because these segments correspond to the instants when $|\beta_z| < 1$ and the Doppler frequency conversion is inessential. Note that here contrary to the approximation utilized in section 3 (fig. 2) accounting the inertial term results in the two-polar shape of each pulse.

4. RADIATION OF THE SHEET IN THE FIELD OF TWO COUNTER PROPAGATING WAVES.

It was already noted that the electron sheet commits finite oscillations in the field of the powerful electromagnetic wave when the radiation pressure force is compensated. In the previous section the force of radiation pressure was compensated by the homogeneous electrostatic field. However for the interaction of the electron sheet with the high-power electromagnetic wave the realization of such field in real experiment can be impossible. A more attractive scheme exists in which there are two waves of equal amplitudes running towards one another. Thus the problem of interaction of the electron sheet with a standing electromagnetic wave arises.

For electric and magnetic components of the standing linear-polarized wave one has:

$$E_y = 2E_0 \cos\omega t \cos kz\,;\; H_x = -2E_0 \sin\omega t \sin kz \qquad (14)$$

The equations of motion (9) will be recorded now in the following way:

$$\frac{d}{dt}\left(\frac{\beta_y}{\sqrt{1-\beta^2}}\right) = 2\alpha_0 \cos t \cos z - 2\alpha_0 \beta_z \sin t \sin z - \alpha\beta_y$$
$$\frac{d}{dt}\left(\frac{\beta_z}{\sqrt{1-\beta^2}}\right) = 2\alpha_0\beta_y \sin t \sin z - \alpha\frac{\beta_y^2}{1-\beta_z^2}\beta_z \qquad (15)$$

The normalized dimensionless variables $\omega t \to t; kz \to z$ are introduced here.

Let at first $\beta_y, \beta_z << 1$. In this case equations (15) become:

$$\frac{d}{dt}\beta_y = 2\alpha_0 \cos t \cos z - 2\alpha_0\beta_z \sin t \sin z - \alpha\beta_y$$
$$\frac{d}{dt}\beta_z = 2\alpha_0\beta_y \sin t \sin z - \alpha\beta_y^2\beta_z \qquad (16)$$

In the equation for β_z the term $-\alpha\beta_y^2\beta_z$ should be taken into account despite of the smallness of longitudinal and transversal velocities of the electron sheet because the factor $\alpha >> 1$ and this term can be about the order of remaining terms in the second equation of the system (16).

One can conclude that equations (16) belong to the well known type of particle's equations of motion in a high frequency electromagnetic field when the force of the sheet self-action (radiation friction) described by the last term in (16) is neglected. The classical result [9] is that in the absence of radiation friction the longitudinal motion of particles represents fast oscillations at frequency 2ω and slow drift in an effective Gaponov-Miller potential $U(z) = \left(e^2/2m\omega^2\right)\left\langle E^2\right\rangle \sim \cos 2kz$ (here character $\langle\ \rangle$ means time-averaging operation). It is natural to suppose that if there is a dissipation of energy due to the radiation the particles after some time will occur in a minimum of the potential energy $kz = \pi/2 + q\pi$ $(q = 0, \pm1, \ldots)$, i.e. in a node of the wave. At this points the electric field is equal to zero so the particles will stay at rest and will not radiate. Rigorous analysis of the system (16) displays that the inclusion of the non-linear radiation friction terms can essentially change the situation.

Let, for example, the condition $\varepsilon = 4\alpha_0^2/\alpha << 1$ is valid (this condition does not limit the analysis to a case of small amplitudes, since for any accelerating parameter α_0 it is possible to take rather large density for the sheet charge so that the condition $\varepsilon << 1$ remains valid). Retaining in equations (16) the terms of the first and second order in ε one can obtain for the slow longitudinal drift Z the following equation (see Appendix):

$$\frac{d^2}{dt^2}Z = -\frac{2\alpha_0^2}{\alpha}\frac{d}{dt}Z - \frac{\alpha_0^2}{\alpha^2}\sin 2Z\left(1 + \frac{\alpha_0^2}{4}\cos 2Z\right), \qquad (17)$$

and for an effective potential energy and effective friction coefficient the expressions:

$$U(z) = \frac{\alpha_0^2}{2\alpha^2}\cos 2z + \frac{\alpha_0^4}{32\alpha^2}\cos 4z, \qquad \gamma = \frac{\alpha_0^2}{\alpha}. \qquad (18)$$

The first term in (18) corresponds to the Gaponov-Miller potential, the second one describes the effect of non-linear radiation friction. It can be shown that at $\alpha_0 < 2$ the drift corresponds to the motion in the Gaponov-Miller potential: the steady state equilibrium position is in the node of the standing wave electric component ($z = \pi/2 + q\pi$). However for $\alpha_0 > 2$ the former equilibrium position becomes unstable, each effective potential minimum splits into two adjacent minima which for large α_0 tend to $\pi/4 + q\pi/2$ (fig. 4). Comparing for Z an effective oscillation frequency near the

minima of the potential energy with damping (cf. (18)) one can conclude that the drift of the sheet has a character of aperiodic motion to a new equilibrium position. At new equilibrium positions the amplitudes of electric and magnetic fields of the standing wave are nonzero so the electron sheet commits intensive oscillations at frequency ω in transverse direction and at frequency 2ω in longitudinal direction radiating the electromagnetic waves. Thus the effective radiation of the plasma layer in the field of standing wave is possible only for powerful enough fields ensuring $\alpha_0 > 2$ (note that the analytical solution is obtained under condition of $\varepsilon << 1$). The numerical analysis for the complete set of equations of motion displays that taking into account the relativistic factors in the system (15) does not change qualitatively the character of the longitudinal drift. For large enough intensity of the standing wave the amplitude of the relativistic velocity β_z of fast longitudinal anharmonic oscillations at frequency 2ω aims to unit and the radiation takes the form of a sequence of powerful pulses following at the double frequency of the wave. The shape of the radiation field is shown in the fig. 5 and 6. The essential point here is the dependence of the radiated field on the initial conditions. Actually if the initial value of the longitudinal coordinate is close to the equilibrium position then the steady-state amplitude of the radiation field is achieved practically during one-two periods of the incident wave. If initial position is far from equilibrium then at first one or two pulses are radiated with amplitude larger than the steady-state values (fig. 5) then a long period follows when the pulses have rather small amplitude and further the steady-state regime is achieved. Last case can be interesting to a problem of generation of ultra broadband single optical pulse.

Let mark another interesting effect arising due to a bifurcation in the considered system. For $\alpha_0 > 2$ the radiation of the plasma layer acquires an asymmetrical character (fig. 6), i.e. fields radiated to the left and to the right are different. In this case not only the transient process of steady-state achievement but also the stationary state itself becomes dependent on the initial conditions. In fig. 7 the steady-state trajectories of an electron in the ultra relativistic case ($\alpha_0 = 5$ and $\alpha_0 = 150$) are shown for some initial position of the layer. The asymmetry of the curves indicates asymmetry of radiation in the positive and negative directions of z axis. For other initial conditions the trajectory can be mirror reflected with regard to the node of electric component of the standing wave. The parameters of the layer radiation in this case change to the opposing.

5. DISCUSSION OF RESULTS.

Above considerations show that during interaction of the powerful electromagnetic wave with the dense plasma layer the sequence of ultrashort pulses with amplitude much greater than the amplitude of the incident wave can be generated.

Let estimate the value of acceleration parameter which can be realized experimentally now. From expression (8) one has $\alpha_0 \approx 50$ for a power density of an incident radiation $5 \cdot 10^{21}$ W/cm^2 and a wavelength of 2 microns. The increase in the amplitude of the reflected pulses with regard to the amplitude of the incident wave is more than 15 times (see fig. 3a). Further advance in super-power laser pulses generation will allow to increase the acceleration parameter. For values $\alpha_0 \approx 200$ (fig. 3b) the intensity of the pumping wave about $8 \cdot 10^{22}$ W/cm^2 is necessary that does not seem inaccessible. An alternative way for the increase of efficiency of powerful ultrashort pulses generation during the reflection from the plasma layer can be the usage of cascaded reflection process that will be considered elsewhere.

Let estimate the value of parameter α accessible in modern experiments. The surface density σ is determined by a volume concentration of electrons N and by a thickness of the sheet. Let the wavelength of radiation falling at the sheet is λ. Then for the thickness of the sheet smaller than $\lambda/4$ all points of the sheet will move practically along the same trajectories. For such case all expressions obtained for indefinitely thin sheet are valid (if the width of the medium is larger than $\lambda/4$ then for the correct solution of the problem it is necessary to take into account the difference of velocities for different layers inside the sheet so the set of equations becomes more complicated though the proposed method is still usable). Thus for the electron concentration N of the order of 10^{22} cm^{-3} and the sheet width equal to $\lambda/4$ one can obtain for parameter α the value from 10 to 100 depending on the wavelength. It is obvious that for more thin sheets the value of α can be made smaller.

In the present paper the perpendicular falling of the electromagnetic wave at the plasma sheet is considered. The obtained results can be easily generalized for the case of oblique falling using the method considered in Ref. [3]. Besides the proposed technique allows to find not only the reflected field but also the transmitted wave. For example in Ref. [8] the expression up to the third order in parameter α_0 is analytically retrieved for radiation passing through the thin plasma sheet.

For simplicity the ionic background was not considered in the above calculations. However one can easily take into account the effects of ions with the help of the approach used here for electrons. This is valid also if there is nontrivial initial distribution of electrons with velocity - for each value of velocity it is necessary to use the separate electron sheet with partial charge density, in this case the effective force of radiation reaction can be calculated by integrating over the velocity distribution function.

In experiment the thin plasma sheet model can be realized by evaporation of the freely suspended thin (about several microns or less) film by the powerful laser radiation. Probably this problem can be solved most naturally in the field of two counter propagating waves. It is necessary to note that the analogue of longitudinal low frequency swinging of the sheet considered in section 3 is evidently the case when one of the waves or both are modulated.

It is worth to mention in conclusion that the experimental confirmation of a capability of electromagnetic pulses' generation can be obtained in interferometric experiments, for example, using the division of a wave front [11] already for a moderate value of incident radiation power. Also the optical nonlinearities can be used for demonstration in the scheme based on the effects of two-photon (multiphoton) luminescence [12,13].

APPENDIX.

In this appendix the analytical results concerning the character of the electron sheet motion in the field of two counter propagating waves used without proof in section 4 will be justified.

The equations (16) can be written as the system of three first order equations:

$$\begin{aligned}
&\frac{d}{dt}\beta_y = 2\alpha_0 \cos t \cos z - 2\alpha_0\beta_z \sin t \sin z - \alpha\beta_y \\
&\frac{d}{dt}\beta_z = 2\alpha_0\beta_y \sin t \sin z - \alpha\beta_y^2\beta_z \\
&\frac{d}{dt}z = \beta_z
\end{aligned} \tag{A.1}$$

Let introduce the following dimensionless parameter (hereinafter we shall suppose that it is small): $\varepsilon = \frac{4\alpha_0^2}{\alpha}$. Then the equations (A.1) can be written in the following way:

$$\begin{aligned}
&\frac{d}{dt}\beta_y = 2\alpha_0 \cos t \cos z - 2\alpha_0\beta_z \sin t \sin z - \frac{4\alpha_0^2}{\varepsilon}\beta_y \\
&\frac{d}{dt}\beta_z = 2\alpha_0\beta_y \sin t \sin z - \frac{4\alpha_0^2}{\varepsilon}\beta_y^2\beta_z \\
&\frac{d}{dt}z = \beta_z
\end{aligned} \tag{A.2}$$

The solution of the first equation of a system (A.2) can be obtained with the method of sequential approximations, using for the transversal velocity the series expansion $\beta_y = \sum_n \varepsilon^n \beta_y^{(n)}$ and equating factors with identical powers of ε. For the solution to within $O(\varepsilon^3)$ one has

$$\beta_y = \frac{\varepsilon}{2\alpha_0}(\cos t \cos z - \beta_z \sin t \sin z) + \frac{\varepsilon^2}{8\alpha_0^3}\left(\sin t \cos z + O(\beta_z) + O\left(\frac{d}{dt}\beta_z\right)\right) + O(\varepsilon^3) \tag{A.3}$$

For the second bracket in the r.h.s. one can omit all terms proportional to $\varepsilon^2 O(\beta_z)$ and $\varepsilon^2 O\left(\frac{d}{dt}\beta_z\right)$. Substituting equation (A.3) into the system (A.2) one can obtain two equations of the first order:

$$\frac{d}{dt}\beta_z = \varepsilon \sin t \sin z\,(\cos t \cos z - \beta_z \sin t \sin z) +$$
$$+ \frac{\varepsilon^2}{4\alpha_0^2}\sin t \sin z\left(\sin t \cos z + O(\beta_z) + O\left(\frac{d}{dt}\beta_z\right)\right) -$$
$$-\varepsilon \beta_z\,[\cos t \cos z + O(\beta_z) + O(\varepsilon)]^2 + O(\varepsilon^3) \qquad \text{(A.4)}$$
$$\frac{d}{dt}z = \beta_z$$

Introducing $\beta_z = \varepsilon w_z$ one has

$$\frac{d}{dt}w_z = \frac{1}{4}\sin 2t \sin 2z + \frac{\varepsilon}{8\alpha_0^2}\sin^2 t \sin 2z$$
$$-\varepsilon w_z\left(\sin^2 t \sin^2 z + \cos^2 t \cos^2 z\right) + O(\varepsilon^2). \qquad \text{(A.5)}$$
$$\frac{d}{dt}z = \varepsilon w_z$$

The equations (A.5) can be solved by the averaging method [14,15], for what it is necessary to write them in a canonical form: $\frac{d}{dt}X = \varepsilon F(X,t,\varepsilon)$. With this purpose we shall make a change of variables $w_z = \overline{w}_z + K(z,t)$, where the function K is choosen so that to compensate in the first equation of the system (A.5) the term $\frac{1}{4}\sin 2t \sin 2z \sim 1$. It is easy to test that for this purpose it is enough to put $K(z,t) = -\frac{1}{8}\cos 2t \sin 2z$.

The system (A.5) in new variables has the form:

$$\frac{d}{dt}\overline{w}_z = \frac{\varepsilon}{8\alpha_0^2}\sin^2 t \sin 2z + \frac{\varepsilon}{8}\cos 2t \sin 2z\left(\sin^2 t \sin^2 z + \cos^2 t \cos^2 z\right) -$$
$$-\frac{\varepsilon}{32}\cos^2 2t \sin 2z \cos 2z -$$
$$-\varepsilon \overline{w}_z\left(\sin^2 t \sin^2 z + \cos^2 t \cos^2 z\right) + \frac{\varepsilon}{4}\overline{w}_z \cos 2t \cos 2z + O(\varepsilon^2) \qquad \text{(A.6)}$$
$$\frac{d}{dt}z = \varepsilon\left(\overline{w}_z - \frac{1}{8}\cos 2t \sin 2z\right)$$

Making now in (A.6) time-averaging operation one can obtain for the drift component of the longitudinal coordinate the following equation:

$$\frac{d^2}{dt^2}Z = -\frac{\varepsilon}{2}\frac{d}{dt}Z + \frac{\varepsilon^2}{16\alpha_0^2}\sin 2Z\left(1 + \frac{\alpha_0^2}{4}\cos 2Z\right), \qquad \text{(A.7)}$$

whence equation (17) directly follows. According to the averaging theorem [15] the error due to the replacement of the solutions of equations (A.6) by the solution of the average equation (A.7) have the order of $O(\varepsilon)$ evenly for the times of the order of $0 < t < 1/\varepsilon$.

REFERENCES

1. D .Von der Linde, K. Rzazewski, "High-order optical harmonic generation from solid surfaces", *Appl. Phys. B.*, **63,** pp. 499-506, 1996.
2. R. Lichters, J. Meyer-ter-Vehn, A. Pukhov, "Short-pulse laser harmonics from oscillating plasma surfaces driven at relativistic intensity", *Phys. Plasmas* , **3**, pp.3425-3437, 1996.
3. A. Bourdier, *Phys. Fluids*, **26**, pp. 1804-1813, 1983.

4. P. Gibbon, "Harmonic generation by femtosecond laser-solid interaction: a coherent "water-window" light source?", *Phys. Rev. Lett.*, **76**, pp. 50-53, 1996.
5. S. V. Bulanov, A. Macchi, F. Pegogaro, "On the theory of ionization of a thin foil by a laser pulse", *Phys. Lett. A.*, **245**, pp. 439-444, 1998.
6. D. Bauer, R. R. E. Salomaa, P. Mulser, "Generation of ultrashort light pulses by a rapidly ionizing thin foil", *Phys. Rev. E*, **58**, pp. 2436-2440, 1998.
7. L. D. Landau, E. M. Lifshitz, *Theory of the Field*, Science, Moscow, 1967 (in russian).
8. A. S. Il'in, V. V. Kulagin, V. A. Cherepenin, "Radiation effects in the model of electron sheets", *J. of Comm. Tech. and Electronics*, **44**, pp. 389-400, 1999.
9. A. V. Gaponov, M. A. Miller, *Sov. Phys. JETP*, **34**, pp. 242-251, 1958.
10. V. L. Bratman, S. V. Samsonov, "Radiation and radiative damping of a charged plane, oscillating with a relativistic velocity", *Phys. Lett. A*, **206**, pp. 377-382, 1995.
11. M. Born, E. Wolf, *Principles of Optics*, Pergamon Press, L-N.Y., 1968.
12. S. A. Akhmanov, Yu. E. Diakov, S. A. Chirkin, *Introduction to Statistical Radiophysics and Optics*, Science, Moscow, 1981 (in russian).
13. S. A. Akhmanov, V. A. Vysloukh, S. A. Chirkin, *Optics of Femtosecond Laser Pulses*, Science, Moscow, 1988 (in russian).
14. N. N. Bogolubov, Yu. A. Mitropolsky, *Asymptotic methods in theory of non-linear oscillations*, Science, Moscow, 1974 (in russian).
15. V. I. Arnold, *Additional chapters of the theory of ordinary differential equations*, Science, Moscow, 1978 (in russian).

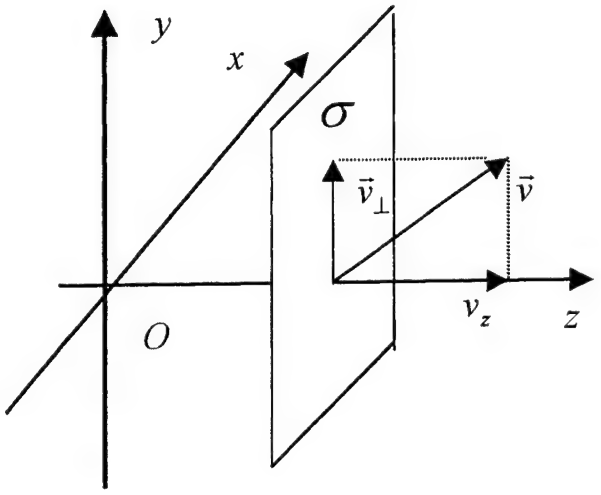

Figure. 1. (3 + 1) - model of electron

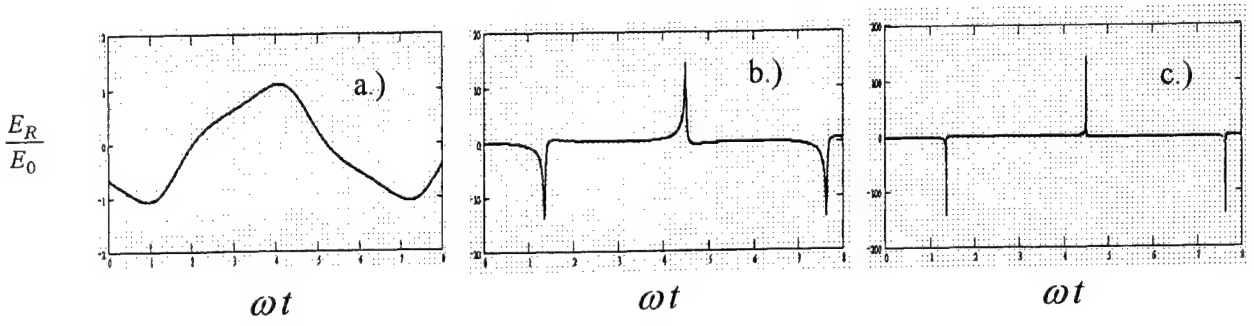

Figure. 2. Reflected field E_R for $\beta_0 = 0.1$ (a) ; 0.9 (b); 0.99

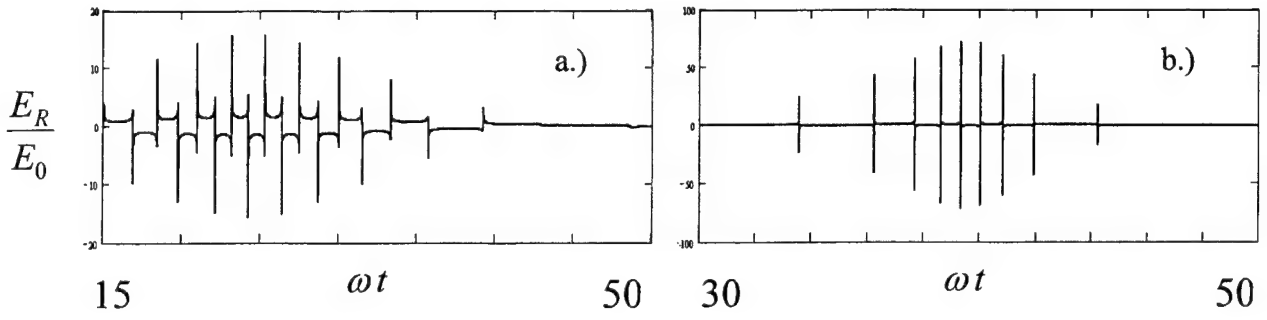

Figure. 3. Radiation field of the plasma layer at the presence of the swinging field for $\alpha = 100; \alpha_0 = 50; k = 1.5$ (a) and $\alpha = 100; \alpha_0 = 200; k = 0.3$ (b).

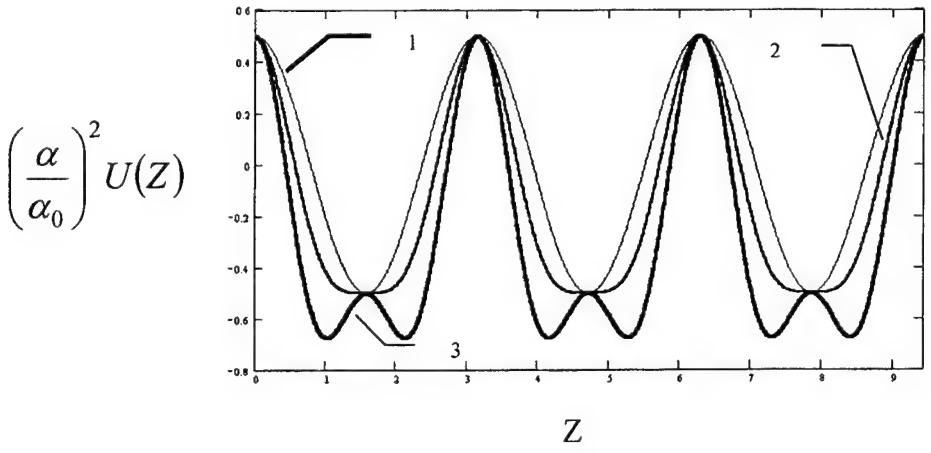

Figure. 4. Dependence of the normalized effective potential energy of the slow drift on longitudinal coordinate for different values of acceleration parameter: curve 1 - $\alpha_0 \to 0$; curve 2 -

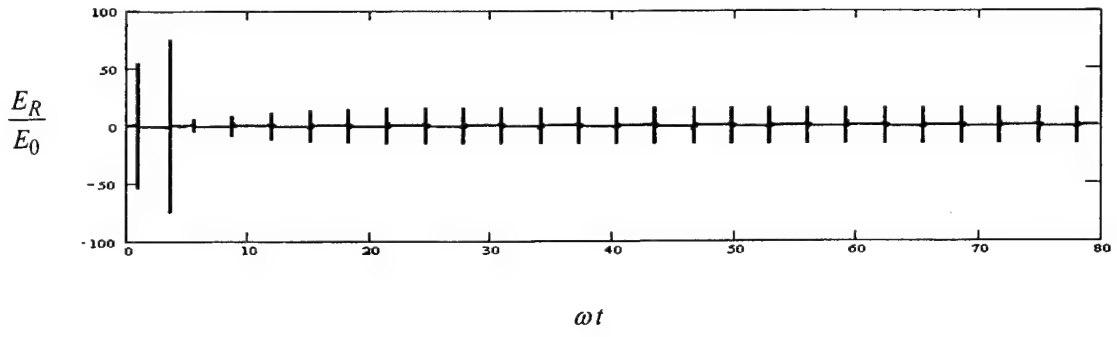

Figure. 5. Non-stationary radiation field of the plasma layer in the transient regime: $\alpha = 100; \alpha_0 = 150$; normalized initial coordinate of the layer $z_0 = 0.3$.

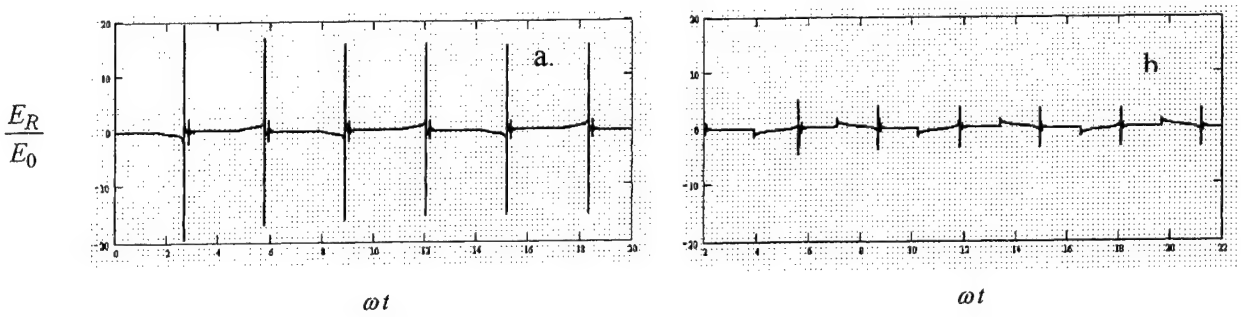

Figure. 6. Radiation field of the plasma layer in positive (a) and negative (b) directions of Oz axis for $\alpha_0 = 150, \alpha = 100$. The motion is near the left equilibrium position (with regard to the node of electrical component of standing wave).

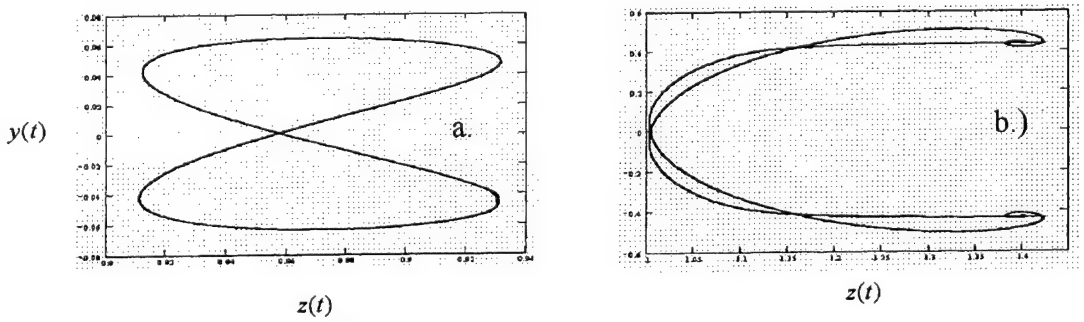

Figure. 7. Stationary trajectories of the plasma layer motion for $\alpha_0 = 5$ (a) and 150 (b). The motion is near the left equilibrium position.

Back Scattering of Ultra Short High Intensity Laser Pulses from Solid Targets at Oblique Incidence.

A. A. Andreev[1], K. Yu. Platonov[1], R. R. E. Salomaa[2]

[1]Institute for Laser Physics SC "Vavilov State Optical Institute"
12 Birzhevaya Line, St.Petersburg 199034, Russia
[2]Helsinki University of Technology, Department of Engineering Physics
and Mathematics, P.O.Box 2200, FIN-02015 HUT, Finland

PACS: 52.50.Jm; 52.40Nk; 52.25.Dg

Abstract: Back reflection of short, intense laser pulses at oblique incidence on solid targets is explained with a model where a periodic electron density modulation acts as a diffraction grating. The pump and reflected electromagnetic waves drive through the ponderomotive force the grating and the overall system becomes parametrically unstable. The basic equations governing this system are given. A linearized stability analysis yields the instability growth rate for a homogeneous plasma and the convective gain coefficients for the inhomogeneous case. The results support the feasibility of the suggested mechanism. An absolute instability is predicted to set on at a typical threshold intensity 10^{16} W/cm^2, laser pulse length 100 fs, and spot size 30 μm. The instability is shown to saturate at a level of a few percent, because the higher harmonics in the electron density modulation turn the diffraction more diffuse thus reducing both the sustaining ponderomotive force and the back reflection coefficient.

1. Introduction.

The interaction of super-intense ultra-short laser pulses with solid targets is presently actively investigated both experimentally and theoretically (for a review see, e.g., [1] . The hot, solid-density plasma formed is a unique physical object the study of which represents fundamental physical interest. Basic research methods of such plasmas include excitation and interpretation of emitted secondary radiation. Various diagnostics in a range of intensities has been proposed and demonstrated experimentally for short pulse interactions. For instance, the mechanisms of back reflection from low density plasmas due to the onset of electronic parametric instabilities has been discussed in detail in [2]. Theoretical studies of similar processes at a reflection of a pair of laser pulses from an overdense plasma surface are carried out in [3]. In experiments where laser pulses of relativistic intensity impinge on a solid target at an oblique incidence, back scattering may reach the level of the order of a few percent [4,5]..

In this paper, a possible mechanism explaining the origin of the back reflection of intense short laser pulse from a plasma surface is suggested and studied theoretically. The basic idea is that a periodic electron density modulation acts as a grating that diffracts the incident laser field into the backward direction in addition to the specular reflection. All the electromagnetic waves together form a ponderomotive force that under proper phase matching conditions drives the initial perturbation. The system presents a parametric instability with a characteristic threshold behaviour, growth rates and saturation at higher pump intensities.

The hydrodynamic equations governing the motion of the electron plasma in the laser and secondary electric fields are given in Sec. 2. Due to the short laser pulse length, ion motion is negligible. A stability analysis of the model system in Sec. 3 shows that in a underdense homogeneous

Laser Optics 2000: Ultrafast Optics and Superstrong Laser Fields, Alexander A. Andreev,
Vladimir E. Yashin, Editors, Proceedings of SPIE Vol. 4352 (2001) © 2001 SPIE · 0277-786X/01/$15.00

plasma slab an instability involving the excitation of a longitudinal electron plasma wave and backreflected electromagnetic waves develops once the pump intensity exceeds a well defined threshold. These considerations support qualitatively the idea that the same mechanism could also be operational in a more realistic situation of an inhomogeneous plasma. In Sec. 3 we, therefore, also estimate the convective gain of longitudinal wave propagating along the target surface. The calculated value turns out to be large enough so that an absolute instability could set on within the focal spot area encountered in actual experiments. For a linear density profile the threshold intensity, according to our calculations in Sec. 4, is of the order of 10^{16} W/cm^2 at a pulse duration of about 100 fs. In Sec. 5 the nonlinear evolution of the instability is discussed: the saturation is mainly caused by density profile steepening due to the ponderomotive pressure and density modulations due to the instability. Modulational effects can be described by diffraction involvingonly the two lowest order waves. This simplified model yields a nonlinear equation for the reflection coefficient. Its solution turns out to be in good agreement with the experimentally observed coefficients ofback reflected laser energy.

2. *Basic equations*

We consider the interaction between a short laser pulse and a solid target. Ion motion can be neglected during the interaction time when the laser pulse length is of the order of 100 fs or less. Electron motion must treated relativistically because of the high laser intensity. Maxwell equations together with the fluid equations form the basic set:

$$\begin{aligned}
&\frac{d}{dt}\frac{m\vec{v}}{\sqrt{1-v^2/c^2}} = -\frac{e\partial\vec{A}}{c\partial t} + e\vec{E} + \frac{e}{c}[\vec{v}[\vec{\nabla}\vec{A}]] - T\frac{\vec{\nabla}n}{n} \\
&\frac{\partial n}{\partial t} + \nabla(n\vec{v}) = 0 \\
&\nabla\vec{E} = 4\pi e(n - n_i) \\
&\Delta\vec{A} - \frac{\partial^2\vec{A}}{c^2\partial t^2} = -\frac{4\pi}{c}en\vec{v} - \frac{\partial\vec{E}}{c\partial t}
\end{aligned} \qquad (1)$$

The vector potential $\mathbf{A}'$ describes the transverse electromagnetic field comprising of the incident laser beam and the scattered waves; the field $\mathbf{E}'$ is the longitudinal field originating from charge separation in the plasma. The density, velocity, and temperature of electrons is denoted by n, v, and T, respectively, and n_i stands for the background ion density.

We assume an s-polarized electromagnetic wave with an amplitude $A_I\mathbf{e}_x$ and a wave vector $\mathbf{k}_0$ at oblique incidence on a plasma surface. At reflection both a specular component ($A_{r0}\mathbf{e}_x$, $\mathbf{k}_r$) and a backreflected component ($A_{r1}\mathbf{e}_x$, $\mathbf{k}_b$) are formed (see Fig. 1). For small reflected intensities we can expand Eqs. (1) in the parameter eA/mc^2 and we obtain the two coupled equations

$$\begin{aligned}
&\frac{\partial^2\vec{E}}{\partial\tau^2} + \frac{\omega^2{}_p}{\omega^2}\eta(\vec{\xi})\vec{E} = \frac{\omega^2{}_p}{2\omega^2}\eta(\vec{\xi})\frac{\partial A^2}{\partial\vec{\xi}} + \frac{v_T{}^2\omega^2{}_p}{c^2\omega^2}\eta(\vec{\xi})\frac{\partial}{\partial\vec{\xi}}\left(\frac{1}{\eta(\vec{\xi})}\frac{\partial E}{\partial\vec{\xi}}\right) \\
&\Delta\vec{A} - \frac{\omega^2}{\omega_p{}^2}\frac{\partial^2\vec{A}}{\partial\tau^2} = (\eta(\vec{\xi})(1 - \vec{A}^2/2) + \frac{\partial\vec{E}}{\partial\vec{\xi}})\vec{A}
\end{aligned} \qquad (2)$$

The upper equation describes the longitudinal plasma wave driven by the ponderomotive force (~ $\nabla\mathbf{A}^2$)

caused by the laser fields. The second equation describes the electromagnetic wave propagation under the influence of plasma oscillations. The fields are written in a normalised form, $\mathbf{A}=e\mathbf{A}'/mc^2$ and $\mathbf{E}=e\mathbf{E}'/mc\omega_p$, the dimensionless time and space coordinates are $\tau = \omega t$ and $\xi=\omega_p \mathbf{r}/c$, respectively; v_{th} is the thermal velocity, $\omega_p=[4\pi Z n_i(\infty)e^2/m]^{1/2}$ is the plasma frequency and $\eta(\xi) = n_i(\xi)/n_i(\infty)$ describes the frozen ion density profile normalized to the bulk ion density $\eta(\infty)$. The physics behind the coupling is simple: the laser field excites by the ponderomotive action density oscillations which, in turn, scatter the laser field. The spatially and temporally varying density grating diffracts transverse electromagnetic waves into new directions and oscillation frequencies. We shall show, that in a plasma that is transparent to the pump wave this process is unstable and leads to generation of electronic density perturbations at a wave length $\lambda_0/2\sin\theta$ where λ_0 is the incident laser wave length and θ is the angle of incidence. Such a diffraction grating scatters the incident laser beam not only into the specular but also into the back direction. A completely analogous parametric instability, Double Stimulated Brillouin Scattering (DSBS) (see, e.g., [6]), occurs for longer laser pulses, say one picosecond or more. In DSBS ion sound waves can be excited and consequently the ion density modulations introduce the corresponding diffraction grating. In the presently considered process, the ions are assumed immobile.

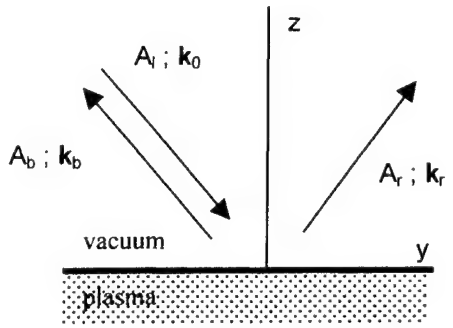

Fig.1: Incoming s-polarized (along x-axis) pump wave (A_l, $\mathbf{k}_0$) diffracts from the grating formed onto the plasma surface and generates specular (A_r, $\mathbf{k}_r$) and backreflected (A_s, $\mathbf{k}_s$) waves.

3. *Linear Stability Analysis*

When the density inhomogeneity scale L of the plasma exceeds the skin depth l_s, i.e., $L > l_s$, Eqs. (2) simplify to:

$$\frac{\partial^2 N}{\partial \tau^2} - \varepsilon^2 n_0 \Delta N + n_0 \eta(\vec{\xi}) N = \frac{n_0}{2} \eta(\vec{\xi}) \Delta A^2$$
$$\frac{1}{n_0} \frac{\partial^2 \vec{A}}{\partial \tau^2} - \Delta \vec{A} + \eta(\vec{\xi}) \vec{A} = N \vec{A} \qquad (3)$$

Here $n_0 = (\omega_p/\omega)^2$ is the relative density given in terms of the critical density and $\varepsilon = v_{th}/c$ is the normalized thermal velocity. Instead of the longitudinal field $\mathbf{E}$ we have used the relative electron density perturbation, $N = (n-n_i)/n_i = \nabla_\xi \cdot \mathbf{E}$, which reveals more transparently the scattering of transverse electromagnetic waves from density perturbations in the inhomogeneous plasma.

In the derivation of (3) we have neglected the derivatives $\nabla_\xi \eta$, because $L > l_s$. Assuming s-polarized waves, $A = (A, 0, 0)$, writing $A = A_0 + A_1$ and $N = N_0 + N_p$ where A_1 and N_p are small perturbations, we obtain from (3):

$$\frac{\partial^2 N_p}{\partial\tau^2} - \varepsilon^2 n_0 \Delta N_p + n_0(\eta(\varsigma) - \Delta A_0{}^2/2)N_p = n_0\eta(\varsigma)\Delta(A_0 A_1)$$
$$-\Delta A_1 + \frac{1}{n_0}\frac{\partial^2 A_1}{\partial\tau^2} + (\eta(\varsigma) - N_0)A_1 = N_p A_0 \qquad (4)$$

where the spatial coordinate $\xi = (\xi,\varsigma)$ is split into in-plane and perpendicular components ξ and ς components with respect to the the surface. The lowest order electron density N_0 is modified by the intense pump field A_0, and is obtained from

$$\frac{\partial^2 N_0}{\partial\tau^2} - \varepsilon^2 n_0 \Delta N_0 + n_0\eta(\bar{\xi})N_0 = \frac{n_0}{2}\eta(\bar{\xi})\Delta A_0{}^2 \qquad (5)$$

Equation (4) describes the following physical processes: 1) changing of the plasma density profile under the action of the ponderomotive pressure and 2) the generation of surface plasma waves in the planar interaction region. In more detail the generation of a plasma wave by a ponderomotive forcehas been investigated in Ref. [7] where also Eq. (5) was first derived.

If the plasma is uniform along the surface, the plasma wave (5) is independent of the coordinate ξ and, therefore, no back reflection of the pump wave occurs. It is also worth pointing out the problem of boundary conditions related to the plasma spot on the surface: It is artificial to assume reflection of plasma waves on the spot boundaries. In this case there appears a standing plasma wave able to reflect the laser pump wave in the back direction and no plasma instability would be required. In the present paper we shall neither consider the effects of two-dimensional plasma inhomogeneity in which case the average density, $N_0 = \frac{1}{2}\nabla^2 \langle \mathbf{A}_0{}^2 \rangle$, is taken as a solution for (5). Then in Eqs. (4) one can simply introduce a new density profile $\eta(\varsigma) - N_0 \rightarrow \eta(\varsigma)$ and the model reduces to that described by the original equations (3).

As discussed above, the instability develops in the transparent plasma region where the fields have their largest amplitudes. To demonstrate the onset of the instability, we shall first consider a uniform, underdense plasma layer which lies in front of a reflecting surface. The solution of Eqs. (4) can be written as

$$A_0 = A_{0i}\exp[i(-\chi_{0\varsigma}\varsigma + \chi_{0\xi}\xi - \Omega_0\tau)] + A_{0r}\exp[i(\chi_{0\varsigma}\varsigma + \chi_{0\xi}\xi - \Omega_0\tau)]$$
$$A_1 = A_{1i}\exp[i(-\chi_{1\varsigma}\varsigma - \chi_{1\xi}\xi - \Omega_1\tau)] + A_{1r}\exp[i(\chi_{1\varsigma}\varsigma - \chi_{1\xi}\xi - \Omega_1\tau)] \qquad (6)$$
$$N_p = n_{pi}\exp[i(-\chi_{p\varsigma}\varsigma + \chi_{p\xi}\xi - \Omega_p\tau)] + n_{pr}\exp[i(\chi_{p\varsigma}\varsigma + \chi_{p\xi}\xi - \Omega_p\tau)]$$
$$\chi_j(\Omega_j) = k_j/k_0, \quad \Omega_j = (\omega_j + i\gamma)/\omega_0$$

where $\chi_j(\Omega_j) = k_j/k_0$ and $\Omega_j = (\omega_j + i\gamma)/\omega_0$ for $j = 0, r, p$; the projections of the wave vectors are denoted by $\chi_{j\varsigma} = \chi_j \cos\theta$ and $\chi_{j\xi} = \chi_j \sin\theta$. These formulas describe the reflection of the pump wave at $\varsigma = 0$ from the overdense plasma ($\eta > 1$ when $\varsigma < 0$). At $\varsigma > 0$ there is an underdense ($\eta < 1$) plasma layer with a thickness of a few wave lengths.

Figure 2 illustrates the wave vectors of the incident and scattered laser fields and the plasma wave described by Eqs. (6). Momentum and energy conservation, i.e., spatial and temporal phase

matching, imply that

$$k_{0y} = k_{ry} + k_{py}$$
$$k_{0z} = k_{rz} + k_{pz} \qquad (7)$$
$$\omega_0 = \omega_1 + \omega_p$$

The absolute values of the wave vectors and frequencies are obtained from the dispersion relations:

$$2\sin\theta = \chi + (1/\varepsilon)\tan\theta\,(\,\delta^2 - n - \chi^2\varepsilon^2\,)^{1/2}$$

$$(\cos^2\theta - n)^{1/2} = [\,(1-\delta)^2 - n - (\sin\theta - \chi)^2\,]^{1/2} + 0.5(\,\delta^2 - n - \chi^2\varepsilon^2\,)^{1/2} \qquad (8)$$

where $\chi = k_{py} / k_{0y}$, $\delta = \omega_p / \omega_0$, and $n = (\omega_{pe} / \omega_0)^2$, ω_p is the plasma frequency in the transparent underdense region, ω_{pe} is that in the dense bulk plasma.

The growth rate of the instability γ is obtained by inserting (6) into (4):

$$\gamma = (\eta/8)(\chi_p^2/\mathrm{Re}\Omega_1\,\mathrm{Re}\Omega_p)|A_0|^2 . \qquad (9)$$

By calculating χ and δ from (8), we get an estimate for γ. Let us consider the parameter range $\delta < 2$ and $(2\sin\theta\,\varepsilon)^2 < n < 4$. Equation (8) gives $\chi \approx 2\sin\theta\,(1 - 0.5n^{1/2})$ and $\delta \approx n^{1/2}$ leading to an approximation γ_0 for γ:

$$\gamma_0 \approx \omega_0\,(n_e / 4n_c)^{1/4}\sin\theta\,(eA_0/mc^2). \qquad (10)$$

For a laser intensity $I=10^{17}$ W/cm^2, unperturbed plasma density $n_e = 0.02n_c$, and angle of incidence $\theta = 30^0$, the growth time γ_0^{-1} is approximately 30 fs according to (10). Thus in a transparent plasma the instability will have enough time to develop during the laser pulse.

The growth rate calculated above using a plasma model consisting of homogeneous slabs is, of course, only indicative, because in actual conditions we have a spatially inhomogeneous plasma density distribution. In that case we may have either convective amplification or an absolute instability. In the convective case the waves grow exponentially along the surface with a gain coefficient [8]

$$G = \gamma_0^2\, l^2 / v_{1y}\, v_{py} \qquad (11)$$

The inhomogeneity due to density gradients resides in the parameter $l^{-2} = (\partial/\partial y)(\,k_{0y} - k_{1y} - k_{py})$; $\mathbf{v}_i = \partial\omega_i/\partial\mathbf{k}_i$ denotes the group velocity of the wave i. Using the dispersion relations (8) and approximating the density gradient scale length by L_y, we find the following expression for the convective gain coefficient

$$G \approx k_0\, L_y \sin^2\theta\,(eA_0/mc^2)^2 \geq 30 \qquad (12)$$

for the same parameters as used in connection with Eq. (10) and for a laser spot size L_y=30 microns. Thus, in an extended laser formed plasma a convective instability generating a back reflected wave can develop. As is known, already at $G > 1$ also an absolute instability can be exited. Therefore, we shall continue to analyse the conditions for an absolute instability in inhomogeneous plasmas with and

inhomogeneity scale length $l_s << L_z << \lambda$ along the perpendicular direction z.

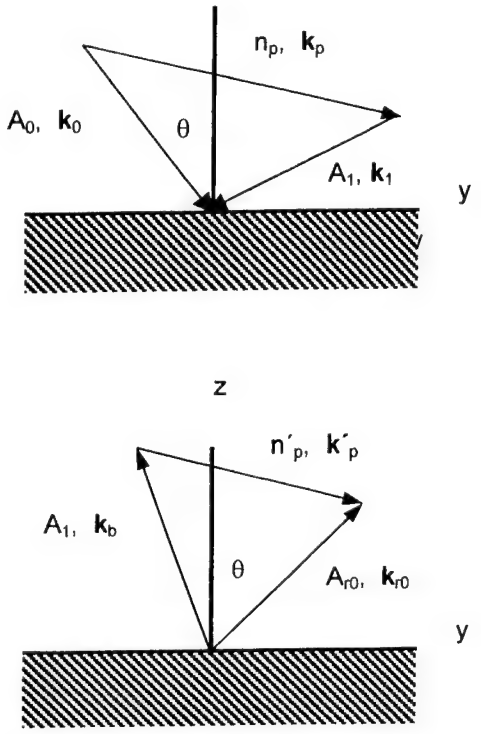

Fig. 2: In the upper frame the incoming pump wave decays parametrically into a plasma wave and a reflected EM wave; in the lower frame the specularly reflected pump wave experiences a similar decay. When the plasmon is along the plasma surface the two processes become coupled as shown in Fig. 3.

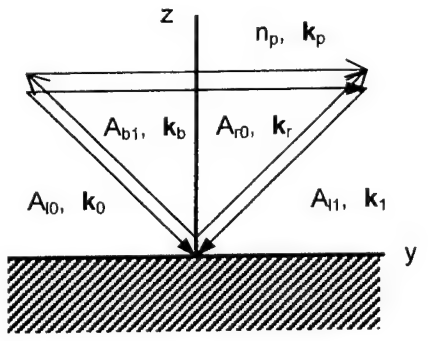

Fig. 3: An absolute instability can be excited when the plasma wave is along the surface.
The two decay instabilities $A_{l0} \rightarrow A_{l1} + n_p$ and $A_{r0} \rightarrow A_{b1} + n_p$ become coupled because of the common plasma wave and the specular reflections $A_{l0} \rightarrow A_{r0}$ and $A_{l1} \rightarrow A_{b1}$.

4. Absolute Instabilities

We shall consider a linear plasma density profile $\eta(\varsigma) = \alpha\varsigma = (c/\omega_p L_z)\varsigma$. An analytical solution of Eqs. (4) will be given below for that particular case. We assume a surface plasmon, which propagates as shown in Fig. 3. This configuration enables energy exchange between incident, back and specularly reflected waves. Above a threshold intensity of the pump wave, the wave amplitudes can grow exponentially inside the focal region and an absolute instability develops.

Let us calculate the threshold for this process. For this purpose we Laplace transform Eqs. (4) with respect to ζ, the normalized z-coordinate along the normal of the surface, and find

$$
\begin{aligned}
&(-\alpha\frac{\partial}{\partial p} - \varepsilon^2\chi^2{}_{p\xi} + \hat{\Omega}^2{}_p + \varepsilon^2 p^2)n_p = a_0\alpha\frac{\partial}{\partial p}(p^2 - \chi^2{}_{1\xi})a_1 \\
&(-\alpha\frac{\partial}{\partial p} - \chi^2{}_{1\xi} + \hat{\Omega}^2{}_1 + p^2)a_1 = n_p a_0{}^*
\end{aligned}
\qquad (13)
$$

The Laplace transforms

$A_1(\varsigma) = \int a_1 \exp(-p\varsigma)dp \qquad N_p(\varsigma) = \int n_p(p)\exp(-p\varsigma)dp$ have the same temporal and spatial variation along

the surface coordinate ξ as in (5). When performing the transformation we have neglected the spatial dependence of A_0, although the inhomogeneity scales *of* A_0 and A_1 are comparable. It is standard approximation, although relative corrections may be of the order of unity [8]. As a result, equations (13) reduce to an ordinary second order differential equation for $a_1(p)$

$$
\begin{aligned}
&\alpha^2\frac{\partial^2 a_1}{\partial p^2} - \alpha b(p)\frac{\partial a_1}{\partial p} + f(p)a_1 = 0, \\
&b = p^2(1+|a_0|^2) + \hat{\Omega}_p{}^2 + \hat{\Omega}_1{}^2 - \chi^2_{1\xi}(1+|a_0|^2) \\
&f = \hat{\Omega}_p{}^2 p^2 - 2\alpha p(1+|a_0|^2) + \hat{\Omega}_p{}^2(\hat{\Omega}_1{}^2 - \chi^2_{1\xi})
\end{aligned}
\qquad (14)
$$

where $\hat{\Omega}_1^2 = \Omega_1^2 / n_0; \hat{\Omega}_p^2 = \Omega_p^2 / n_0$. We have omitted some small terms in (13) to obtain (14).

To solve Eq. (14) we shall transform it into a Schrödinger equation with zero energy with the help of the transformation

$$
a_1(p) = a(p)\exp(\int\frac{b(p)}{2\alpha}dp) \qquad (15)
$$

and obtain

$$
\alpha^2\frac{\partial^2 a(p)}{\partial p^2} - U(p)a(p) = 0 \qquad (16)
$$

The effective potential U (p) in the Schrödinger equation (16) is given by

$$U(p)=\frac{1}{4}(1+|a_0|^2)^2 p^4+\frac{1}{2}p^2((1+|a_0|^2)(\hat{\Omega}_1^{\,2}-\chi_{1\xi}^{\,2}(1+|a_0|^2))-\hat{\Omega}_p^{\,2}(1-|a_0|^2))$$
$$+\alpha p(1+|a_0|^2)+\frac{1}{4}(\hat{\Omega}_p^{\,2}-\hat{\Omega}_1^{\,2}+\chi_{1\xi}^{\,2}(1-|a_0|^2))^2-(\hat{\Omega}_1^{\,2}-\chi_{1\xi}^{\,2})\chi_{1\xi}^{\,2}|a_0|^2 \qquad (17)$$

Using the methods described in [8] we obtain the threshold intensity for the absolute instability in the following fashion. The discrete energy eigenvalues Ω_l can be determined with the aid of semiclassical quantization rules, i.e., by requiring that

$$\int_{p_1}^{p_2}\sqrt{-U(p)}\,dp=\pi(2n+1), \qquad (18)$$

where $p_{1,2}$ are solutions of the equation U (p) =0 (turning points). The instability develops only if there are the regions, where U (p) < 0. The potential (17) is a fourth order polynomial in A_0 which can attain negative values. At a_0=0 $U(p)=\frac{1}{4}(p^2+\hat{\Omega}_1^{\,2}-\hat{\Omega}_p^{\,2}-\chi_{1\xi}^{\,2})^2+\alpha p$ which has no positive roots. At normal incidence, when $\chi_{1\xi}$=0, real roots are also missing. Accurate to a factor about unity the first root occurs, when

$$a_{0th}=(\frac{eA_0}{mc^2})_{th}\approx\left(\frac{\omega}{\omega_p}\right)^2\frac{\lambda}{L_z}\frac{1}{\sin\theta} \qquad (19)$$

This gives an estimate for the instability threshold. At $\omega/\omega_p \approx 0.1$, $L \approx 0.2\lambda$, $\theta = 30^o$ we obtain a threshold of about 10^{16} W/cm^2 which agrees with experimental data.

5. Analysis of the Nonlinear Behaviour

We shall next consider the saturation properties of the instability. The ponderomotive pressure will steepen the plasma density profile which influences the scattering from the surface and consequently the total electromagnetic field. As the electromagnetic field, on the other hand, is responsible of the ponderomotive force, the feedback loop is thus established. To begin the analysis, we shall assume a given value of the reflection coefficient and from this basis evaluate the electron density profile. A stable operating point is found when the reflection caused by the grating due to the density modulation is consistent with the force sustaining the grating.

Let us study the neighborhood of the plasma surface around the operating point of fully developed instability. From Poisson equation we obtain for the electron density perturbation

$$\frac{\delta n}{n}=\frac{c^2}{\omega_p^2}\Delta(\varphi/mc^2)<1. \qquad (20)$$

In a steady state situation, the electrostatic force must compensate the pondermotive pressure

$$\varphi/mc^2\approx\sqrt{1+A^2} \qquad (21)$$

So the grating amplitude is approximately given by

$$\frac{\delta n}{n} = \frac{c^2}{\omega_p^2}\Delta\sqrt{1+A^2} \qquad (22)$$

where the time-averaged potential A^2 includes both the incident and back reflected waves

$$A^2 = A_0{}^2 e^{-2z/ls}(1 + R^2 + 2R\cos(2y\sin\theta)). \qquad (22)$$

The diffraction efficiency, and consequently also the reflection coefficient R, of the induced grating can be calculated as a function of the density profile $\delta n/n$.

Figure 4 shows, as an example, the constant density contours $< \delta n/n > = 0.5$ for two values of back reflection coefficient, R=0.4 (broken line) and R=0.8 (solid line), and for two pump amplitudes $A_0 = 1$ (lower pair of curves) and 7 (upper curves). The ordinate axis denotes the perpendicular direction into the plasma and the abscissa the transverse direction both in units of $l_{s0}=c/\omega_p$. In the unperturbed situation the plasma-vacuum boundary is at z=0. We have assumed an angle of incidence $\theta = 45^o$, and plasma density such that $l_{s0}/\lambda=0.2$ where $l_{s0}=c/\omega_p$ (note that the effective skin-layer depth, $l_s=l_{s0}(1+A_0^2)^{1/4}$, depends on the pump field amplitude A_0). From Fig. 4 we can conclude that: 1) The plasma deformation clearly increases with A_0 . 2) At small pump amplitude values A_0 and reflection coefficients R, the induced density profile modification is rather insensitive to R, and its shape is nearly harmonic. A good approximation is obtained by expanding Eq. (22) in power series of A_0. 3) At large pump amplitudes the profile shape is more sensitive to the level of back reflection R and it exhibits higly anharmonic features.

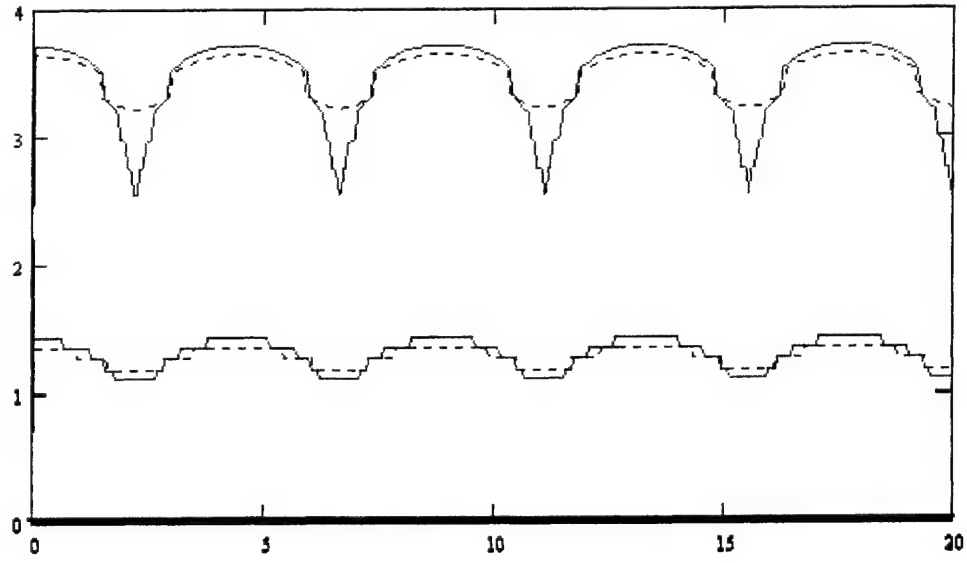

Fig. 4: Constant density contours $<\delta n/n>=0.5$ for R=0.4 (broken lines) and R=0.8 (solid lines); in the upper pair of the curves the pump amplitude is $A_0=7$ and in the lower ones $A_0=1$. The ordinate is the distance into the plasma (down the z-axis) and the abscissa the spatial coordinate along the input surface; both are given in units of $l_{s0}=c/\omega_p$. The unperturbed plasma vacuum surface is at z=0.

The introduction of higher harmonics into the density profile modification makes the reflections from the grating more diffuse and can thus lead to a saturation of the instability. We shall estimate the

value of the reflection coefficient under saturation conditions taking into account the incident and both of the reflected waves (in the back and specular directions). Such approximation corresponds to the two-wave theory of a diffraction, i.e., to a model where the incoming wave diffracts from a purely sinusoidal perturbation, sin(qy), with $k_y=k_{y0}\pm q$. This model is valid for lowest order expansion in A. At A>>1, higher harmonics sin(Nqy) appear introducing new diffraction orders with $k_y=k_{y0}\pm Nq$. The simple two-wave model is a reasonable approximation even close to the saturation level where A is of the order of unity. Instead of the vector potential A_x, it is more convenient to use the wave electric field E_x. In the vacuum region, the total electric field is of the

$$E_x = E_i \exp(ik_y y + ik_z z) + \sum_q E_q \exp(i(k_y - q)y + \Gamma_q z) + \kappa.c.$$
$$\Gamma_q{}^2 = -\omega^2/c^2 + (k_y - q)^2 \quad , \qquad (24)$$

The first term stands for the incident field and the sum term contains the reflected components. Within the plasma region we have.

$$E_x{}^p = \sum_q E'_q \exp(i(k_y - q)y - \gamma_q z) + \kappa.c.$$
$$\gamma_q{}^2 = -\omega^2\varepsilon(\omega)/c^2 + (k_y - q)^2 \qquad (25)$$

We shall assume a high dielectric permeability of the plasma, so that

$$\gamma_q^2 \cong -\omega^2\varepsilon(\omega)/c^2 = \gamma^2 \qquad (26)$$

The amplitudes of the spatial harmonics of the fields are determined by the usual boundary conditions on the plasma-vacuum surface. Since the depth of the surface modulation, as also the scale length of the plasma inhomogeneity, are less than the wave length, we actually apply these conditions at the critical surface inside the plasma:

$$E_x = E_x{}^p\Big|_{z=f(y)}$$
$$\frac{\partial E_x}{\partial z} = \frac{\partial E_x{}^p}{\partial z}\Big|_{z=f(y)} \qquad (26)$$

The equation of the plasma surface (rippled by the instability) z = f(y) is expanded in spatial harmonics

$$f(y) = \sum_q \xi_q \exp(-iqy) + \kappa.c. \,. \qquad (28)$$

The amplitudes ξ_q are assumed smaller than the relevant vacuum wave lengths, but they can be comparable to the width of the plasma skin-layer. An estimate of the depth of modulation ξ is obtained by equating the ponderomotive and ambipolar forces, i.e., $\ln\xi = \frac{\partial}{\partial z}\sqrt{1+A^2}$, from which we find

$$k_z\xi \le (\omega/\omega_p)A_0^2 \le 1 \qquad (29)$$

We have assumed above the width of the skin layer to be of the order of c/ω_p.

The boundary conditions (27) involve an infinite set of equations for the amplitudes E_q. We shall

truncate this system to contain only the wave numbers $q = 0$ and $q = 2k_y$ which is consistent with the two-wave approximation of the diffraction theory. The equation of the surface is thus of the form

$$f(y) = \xi_0 + \xi_2 \cos(2k_y y - \varphi_2) \tag{30}$$

where $\xi_{0,2}$ are the modulation amplitudes and φ_2 the relative phase. When substituting (24) and (25) into (27) we shall check that the depth of modulation of the surface is less than a wave length (in agreement with (29)), although it can exceed the skin-layer depth, i.e., $k_z\xi \le 1$, $k_z\gamma \le 1$ which also follows from (29) at $A_0 \sim 1$.

In the vacuum region, the electric field which is consistent with (30) is given by

$$\begin{aligned} E_x = {} & E_i(\cos(k_z z + k_y y - \omega t) - \cos(-k_z z + k_y y - \omega t) + \\ & + 2k_z(\xi_0 + 1/\gamma)\sin(-k_z z + k_y y - \omega t) + 2k_z\xi_2 \sin\varphi_2 \cos(k_z z + k_y y + \omega t) - \\ & - 2k_z\xi_2 \cos\varphi_2 \sin(k_z z + k_y y + \omega t) \end{aligned} \tag{31}$$

Accordingly, the amplitude back reflection coefficient equals $2k_z\xi_2$. For its determination we need the fields in the plasma. Their general form within the two-wave approximation is as follows:

$$E_x{}^p = \exp(-\gamma z)(E_0' \cos(k_y y - \omega t + \alpha_0') + E_2' \cos(k_y y + \omega t + \alpha_2')) \tag{32}$$

Substituting (31) into (26), we find:

$$\begin{aligned} E_0' \exp(i\alpha_0') &= 2E_i \exp(\gamma\xi_0 + 2i\phi - i\pi/2)\frac{(k_z/\gamma)(I_0 \exp(-i\phi) + 2\xi_0 I_0 \sin(\phi) + \xi_2 I_1 \sin(\phi))}{I_0{}^2 - I_1{}^2} \\ E_2' \exp(i\alpha_2') &= 2E_i \exp(\gamma\xi_0 + 2i\phi + i\varphi_2 - i\pi/2)\frac{(k_z/\gamma)(I_1 \exp(-i\phi) + 2\xi_0 I_1 \sin(\phi) + \xi_2 I_0 \sin(\phi))}{I_0{}^2 - I_1{}^2} \\ \phi &= arctg(k_z/\gamma) << 1 \end{aligned} \tag{33},$$

where $I_0 = I_0(\gamma\xi_2); I_1 = I_1(\gamma\xi_2)$ are modified Bessel functions of order 0 and 1, respectively.

It is worth emphasizing that the system depends in an essentially nonlinear manner on the amplitudes ξ. If the second wave amplitude ξ_2 is zero, i.e., =0, the surface is planar, and we obtain the standard Fresnel formulas:

$$\begin{aligned} E_0' &= 2(k_z/\gamma)E_i \\ E_2' &= 0 \\ \alpha_0 &= 2\phi - \pi/2 \end{aligned} \tag{34}$$

The nonlinearity starts to appear, when the surface oscillation amplitude becomes of the order of skin layer depth, $\gamma\xi_2 \sim 1$, that is when the arguments of the Bessel functions reach the value of about unity. From that observation it is possible to deduce the amplitude back reflection coefficient (which is equal

to $2k_z\xi_2$) to be of the order of k_z/γ. Also it is obvious, that for large modulation amplitudes ξ_2 ($\gamma\xi_2 > 1$) the electric field amplitudes decreases. The back reflected wave disappears both when $\xi_2 \to 0$ and when $\xi_2 >> 1/\gamma$, reaching a maxima at about $\xi_2 \sim 1/\gamma$.

The electron density in the plasma is determined by the average plasma wave intensity:

$$n(z,y) = Zn_i\left(H(z) + \frac{1}{\gamma^2}\frac{\partial^2\sqrt{1+<E_x^{\,p}(z,y,t)>^2}}{\partial z^2}\right) \tag{35}$$

Where Zn_i is the background density of electrons and $H(z)$ is the Heaviside step function. From (35) we get the constant density contours. In particular, the reflecting surface $z = f(y)$ is determined by the critical density contour $n(z,y) = n_{cr} = m\omega^2/\varepsilon_0 e^2$. Inserting the plasma field from (32), we find

$$f(y,\xi_0,\xi_2) = \frac{1}{2\gamma}\ln\left(\frac{E_0'^2 + E_2'^2 + 2E_2'E_0'\cos(2k_y y + \alpha_0' + \alpha_2')}{n_{cr}/Zn_i - 1}\right) \tag{36}$$

We again decompose f (y) into spatial harmonics and keep only the two first terms of the ensuing series. Thereafter we compare the result to the initial assumption made for the surface profile:

$$f(y,\xi_0,\xi_2) \approx \frac{1}{2\gamma}\left(\ln\left(\frac{E_0'^2}{n_{cr}/n - 1}\right) + 2\frac{E_2'}{E_0'}\cos(2k_y y + \alpha_0 + \alpha_2)\right) = \tag{37}$$

$$= \xi_0 + \xi_2\cos(2k_y y - \varphi_2)$$

As a result we find for $\xi_{0,2}$ and for φ_2 the expressions:

$$\begin{aligned}
&\frac{1}{2\gamma}\ln\left(\frac{E_0'^2}{n_{cr}/n - 1}\right) = \xi_0 \\
&\frac{E_2'}{\gamma E_0'} = \xi_2 \\
&\alpha_0' + \alpha_2' = -\varphi_2
\end{aligned} \tag{38}$$

As was pointed out before, the amplitude back reflection coefficient $R = 2k_z\xi_2$ is determined by ξ_2. By inserting the second equation of (38) into (33) we obtain

$$\begin{aligned}
&1 + \frac{k_z\xi_2}{2}\sin(2\phi)\frac{(I_0^{\,2}(\gamma\xi_2) - I_1^{\,2}(\gamma\xi_2))}{I_1(\gamma\xi_2)I_0(\gamma\xi_2)} = \frac{\gamma\xi_2 I_0(\gamma\xi_2)}{2I_1(\gamma\xi_2)} \\
&\phi = arctg\frac{k_z}{\gamma}
\end{aligned} \tag{39}$$

which can be used for solving ξ_2. The amplitude of the incident field does not enter in (39) (although it appears in (38)). This is connected to the expansion in E_0 used in the derivation of Eqs. (38): The fields

are proportional to the incident amplitude (as we have a linear boundary conditions), and as a result the ratio E_2'/E_0' is independent of E_0 . The dependence on E_0 enters only in higher order terms.

Equation (39) has a solution

$$\gamma\xi_2 = 0.4; R_{0r} = 2.5(k_z/\gamma)^2 = 0.025\cos^2\theta \qquad (40)$$

at ω/ω_p=0.1. Physically it is clear, that in the diffraction grating a nonlinear anharmonic profile develops, when the amplitude of perturbations becomes comparable with those caused by E_0, i.e., when the modulation amplitude ξ_2 becomes of the order of the depth of the skin layer. In that case the profile of the surface looses its harmonic structure (field is inhomogeneous along z), and higher harmonics at the expense of ξ_2 . Note that the amplitude ξ_0 describes a global shift of the surface into the plasma and is not connected with a saturation from unharmonic behavior. Thus the back reflection coefficient approaches zero both at small pump intensities, when the surface modulation is small, and at large intensities, $A_0 > 1$, when the surface modulation acquires higher harmonics resulting in a diffuse scattering of a radiation on them. The maximum backreflection is reached at $A_0 \leq 1$. We shall further elaborate on this by writing an approximate analytical expression for the reflection coefficient R as a function of the pump intensity: R(I). According to Eqs. (11) and (12), for small values of the pump amplitude a_0, the amplitude of the back reflected back increases exponentially the gain factor being dependent on the pump intensity. From (39) it follows that saturation at a level R_r occurs when the pump intensity is further increased. Beyond $I > 1$, the magnitude R_r should decrease, because according to (33) the amplitude E_2 decreases exponentially, when $\gamma\xi_2 > 1$. Thus a reasonably good approximate expression for R (I), in the range $I > I_{th}$, can be written as:

$$R(I) = \frac{\exp(G(I)) - \exp(G(I_{th}))}{1 + \frac{1}{R_r(I)}\exp(G(I))} \qquad (41)$$

where G (I) is given by (12) and the threshold value I_{thr} by Eq. (18). From (33) one obtains for $R_r(I) = R_{0r}\exp(-2I/I_{18})$ where the reference intensity I_{18} corresponds to the value A_0=1 (the subscript 18 follows from the approximate numerical value $I_{18} \approx 10^{18}$W/cm^2 . A plot of the amplitude reflection coefficient R(I) is given in Fig. 5 for a numerical values G, I_{th}, and R_{0r}, taken from (12), (18), and (40), respectively.

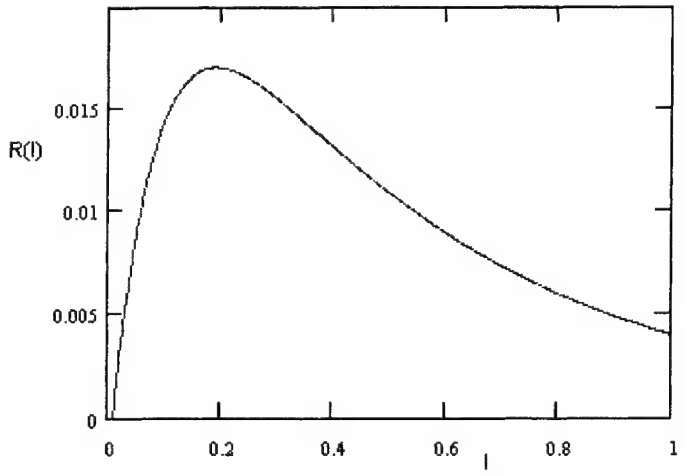

Fig. 5: The approximate reflection coefficient R(I), according to the fit (41),.versus laser intensity I in units of 10^{18} W/cm^2

6. *Summary and Conclusions*

We have discussed the possibility of inducing of grating structure on the surface of plasma by high intensity oblique incident and reflected laser beams.
The absolute instability conditions in inhomogeneous plasma are found, so at intensity of laser pulse more 10^{16} W/cm^2 and the duration near 100 fs the instability should develop.
The constructed profile of plasma surface becomes essential anharmonic at relativistic laser intensity and the reflection coefficient in back direction becomes saturated.
It was shown that reflection coefficient of back scattered light can be some percents and it correlates with experimental date.
ACKNOLEDGEMENTS: This work was partly supported by a NORDIC Grant.

REFERENCES

1. M.Perry, G.Mourou, Science v.264, p.917 (1994).
2. D.Umstadter, Science v.273, p.472 (1996).
3. L. Plaja, L. Roso, Phys. Rev. E. v.56, p.7142 (1997)
4. T.Miyakoshi, K.A.Tanaka, R.Kodama et al. AHPLA'99, HPL02, 3886-68, p.80, Osaka Univ., Japan, November 1999.
5. A.A.Andreev, V.I.Bayanov, A.B.Vankov et al., AIP Conference Proceedings 426Int. Conf. "Superstrong Field in Plasma", Varenna, Italy, August 1997, p.61.
6. A. A. Zozulya, V. P. Silin, and V. T. Tikhonchuk, "Theory of double stimulated Mandel'shtam Brillouin scattering in a plasma with a reflecting boundary", Sov. Phys. JETP**59**, 756-763 (1984); T. J. H. Pättikangas and R. R. E. Salomaa, "Double Stimulated Brillouin Scattering", Physica Scripta **40**, 99-108 (1989); A. A. Andreev V.I.Bayanov, A.B.Vankov et al. "Kvantovaya Electronica", v.24, no.2, p.99 (1997)
7. A. A.Andreev, K. Platonov, K. Tanaka.JAERI-Conf 98-004 p.37, (1998).
8. A.A.Andreev. Dr. of Sci. Theses, Vavilov State Optical Institute, Leningrad, (1990)

X-ray short pulse generation from femtosecond laser-produced plasmas and its application in pump-probe spectroscopy

Hidetoshi Nakano, Peixiang Lu*, Tadashi Nishikawa, and Naoshi Uesugi†

NTT Basic Research Laboratories, 3-1 Morinosato Wakamiya, Atsugi, Kanagawa 243-0198, Japan

ABSTRACT

High-density plasmas created near a solid surface by a femtosecond laser pulse emit ultrashort x-ray pulses that are synchronized to the laser pulse. In the first part of this paper, the spectral and temporal properties of the x-ray emitted from plasma created on aluminum film by a femtosecond laser pulse are shown. The minimum pulse duration was <3 ps as measured by an x-ray streak camera. The energy conversion efficiency, from laser pulse into soft x-ray at 14 ± 0.05 nm, was 10^{-6}–10^{-5}. More than a 30-fold enhancement in soft x-ray emission was achieved by fabricating an array of nanoholes on an alumina surface. In the latter half, we demonstrate time-resolved absorption measurement in the soft x-ray region by means of pump-probe spectroscopy. Using a 10-ps x-ray pulse, we measured time-resolved absorption of optically-pumped silicon near its $L_{II,III}$ edge. We found that laser-pulse irradiation caused a more than 10% increase in soft x-ray absorption near the edge, which means that the transition of electrons in inner shells was rapidly modulated by excitation of valence electrons. The absorption change recovered within 20 ps.

Key words: x-ray source, ultrafast, laser-produced plasma, x-ray spectroscopy

1. INTRODUCTION

The recent development of high-power ultrafast laser technologies has made laser-produced plasmas more attractive for their potential use as bright x-ray sources.[1,2] High-density plasmas created near a solid surface by femtosecond laser pulses emit short x-rays pulses in the energy range from sub-keV to MeV. These x-rays are also synchronized to the incident laser pulse. Therefore, they are extremely important as diagnostic probes in pump-probe type experiments for observing the dynamic response of optically excited materials. From this point of view, efforts have been made to demonstrate time-resolved diffraction[3,4] and absorption measurements[5–7] using femtosecond laser-produced plasma x-rays. To date, more attention has been paid to diffraction measurements, since x-ray diffraction provides direct information on atomic positions and molecular structure. However, x-ray absorption measurements are also important in material study. From the x-ray absorption spectrum, we can extract microscopic information on a material, such as the electronic states of atoms, chemical bonds, and local structures. In addition, pump-probe absorption spectroscopy using short x-ray probe pulses is expected to be able to reveal the dynamics of electrons in inner shells in optically-excited materials, as opposed to that of valence electrons, which have been well studied by laser spectroscopy.

In the first part of this paper, we will describe x-ray emission properties from femtosecond laser-produced plasmas and our recent experimental results showing enhanced soft x-ray emissions.[8–13] Using a nano-structured target, we achieved more than a 30-fold enhancement in soft x-ray emission while keeping pulse duration less than 20 ps. The latter half demonstrates time-resolved absorption measurements in the soft x-ray region by mean of pump-probe spectroscopy.[7] We observed, for the first time, a rapid absorption change induced by femtosecond laser pulse irradiation in silicon membrane near its $L_{II,III}$ absorption edge.

2. X-RAY EMISSIONS FROM FEMTOSECOND LASER PLASMA CREATED ON METAL SURFACE

For practical use, intense x-ray pulses are needed. From this point of view, we tried several ways to improve the efficiency of conversion into x-rays. There are basically three approaches to improving conversion efficiency. One is modifying the conditions of the laser pulse to create plasma. Using a prepulse to form gaseous plasma before incidence of the intense laser pulse is the most powerful and controllable scheme,[8,9,15–18] though there is the drawback of pulse broadening. Using a pre-

* Present address: Advanced Photon Research Center, Kansai Research Establishment, Japan Atomic Energy Research Institute, 8-1 Umemidai, Kizucho, Souraku-gun, Kyoto 619-0215, Japan.

† Present address: Tohoku Institute of Technology, 35-1 Yagiyama Kasumicho, Taihaku-ku, Sendai, Miyagi 982-8577, Japan.

Laser Optics 2000: Ultrafast Optics and Superstrong Laser Fields, Alexander A. Andreev, Vladimir E. Yashin, Editors, Proceedings of SPIE Vol. 4352 (2001) © 2001 SPIE · 0277-786X/01/$15.00

pulse scheme, we can adjust the pulse duration, photon flux, and emission spectrum by selecting appropriate prepulse conditions.[9, 18] Another way is choosing appropriate target materials or modifying them. Metals with higher atomic number Z, composite materials such as metal-doped glasses,[10, 11] and nano-structured targets[12–14, 19] are examples. In the following sections, we will describe the properties of x-ray emission from plasma on metal surface created by a femtosecond laser pulse and the enhanced emission properties we obtained by fabricating a nanohole array on an alumina target surface.

2.1. X-ray emissions from Al-plasma

The light source was a Ti: sapphire laser system consisting of a passively mode-locked Ti: sapphire laser, a pulse stretcher, a regenerative amplifier, a 3-pass linear amplifier, and a pulse compressor. It operates at 10 Hz, and provides 100-fs, 100-mJ optical pulses at the wavelength of 790 nm. The extinction ratio between the main pulse and undesirable satellite pulses that preceded it by more than 1 ns is better than 10^6, which is high enough to ignore the influence of the satellites as prepulse. The laser pulses were focused on the target at normal incidence with a 200-mm focal length MgF_2 lens. The spot size was about 30 μm, and the peak intensity was 1.6×10^{16} W/cm^2. As a target, we used a 4-μm thick aluminum film deposited on a silicon wafer. Targets were mounted on a motorized stage and scanned to expose a fresh surface for each laser shot. To measure soft x-rays in the sub-keV region, we used a grazing incidence flat-field spectrograph and a single-shot time-resolved spectrograph.[9] A spherically bent mica crystal ($2d$ = 1.994 nm) with bending radius of 100 mm was used to measure x-ray emission spectra in the keV region.[20]

Figure 1 shows time-integrated x-ray emission spectra in the sub-keV and keV regions. The unit of the vertical axis in Fig. 1(b) was of the order of 10^8 photons/Å/sr. In both regions, one can find fine structures corresponding to line emissions, which are dominated by emissions from Al^{0+}–Al^{5+}, on a broad continuum-like pedestal. We estimated the electron density of the plasma at the emitting zone to be 8×10^{22} cm^{-3} from the intensity ratio among Li-like dielectric satellite lines. The efficiency of conversion into soft x-rays at a wavelength of 14 nm was measured to be 4×10^{-5} %/Å/sr using a multi-layered mirror combined with a microchannel plate (MCP) detector. The temporal evolution of soft x-ray emission is shown in Fig. 2. This shows that soft x-ray emission at 4–10-nm wavelengths started almost simultaneously and lasted almost the same amount of time. The duration of the soft x-ray pulse was 3.0 ps, which is almost the instrumental limit. Due to a small source size (< 100 μm) and short pulse duration (< 3 ps), the peak brightness exceeds 10^{22} ph/s/mm^2/sr/0.1%BW when the input energy of the 100-fs laser pulse is 20 mJ.

2.2. Dependence of soft x-ray emissions on atomic number of target material

Figure 3 shows soft x-ray emission spectra from femtosecond laser-produced plasmas created on Si, Ti, Sn, and Au. In all cases, the intensity of the laser pulse on the target surface was 1.6×10^{16} W/cm^2. These graphs show that the emission spectrum becomes less structured with increasing atomic number due to numerous transitions that give emissions in this energy range.[17] Figure 4 summarizes the dependence of the conversion efficiency into soft x-rays on the atomic number of the target materials. We measured conversion efficiencies at 8 and 14 nm using the multi-layered mirrors and MCP detector. At both 8

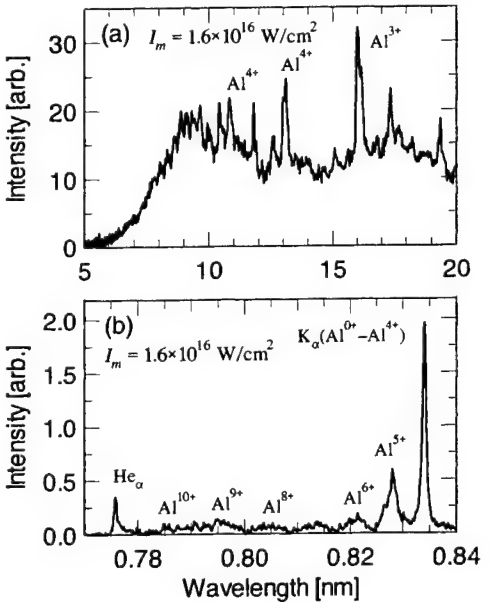

Fig. 1. Time-integrated spectra of x-ray emitted from Al-plasma.

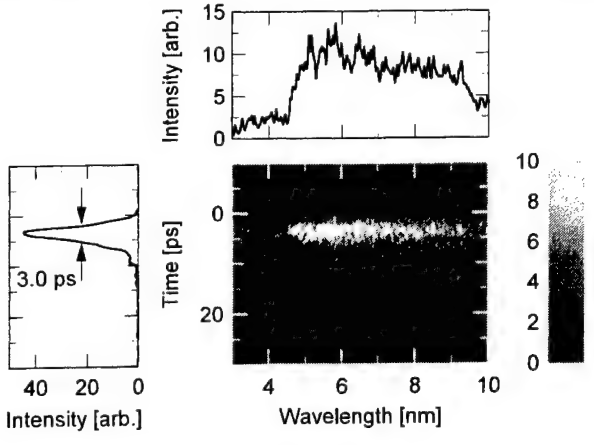

Fig. 2. Temporal evolution of soft x-rays emitted from Al-plasma.

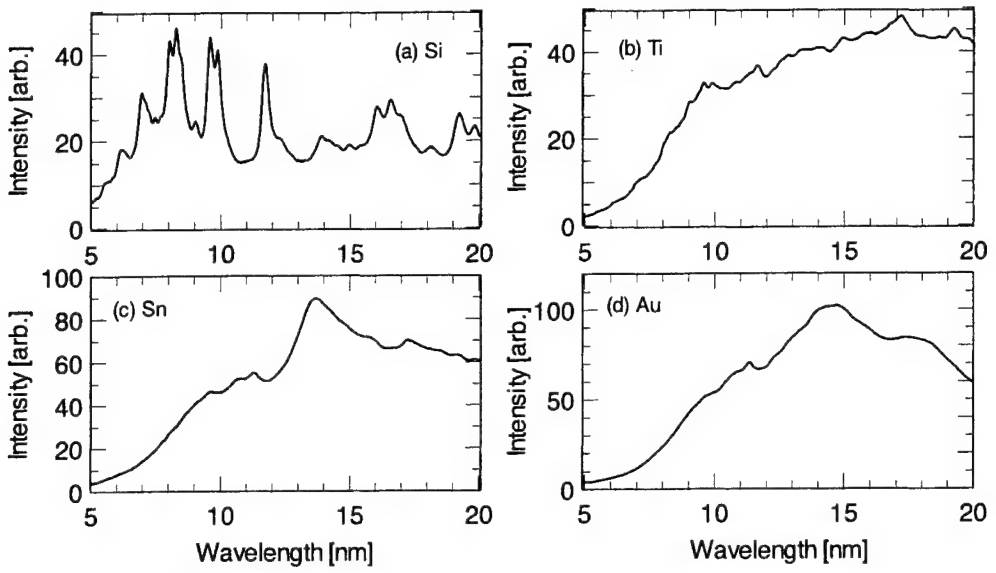

Fig. 3. Time-integrated spectra of soft x-rays in sub-keV region emitted from (a) Si, (b) Ti, (c) Sn, and (d) Au. In all cases, the intensity of a laser pulse was 1.6×10^{16} W/cm^2.

and 14 nm, the efficiency increased gradually with some undulation with increasing atomic number. This trend is the same as that seen in ns-laser plasma x-rays. The humps in Fig. 4 correspond to maximum emissivity for *L*-, *M*-, *N*-, and *O*-shell ions. We can select the target material that will provide intense soft x-ray emissions in the wavelength range suitable for specific applications. For example, for x-ray absorption spectroscopy, broadband x-rays without fine structures are required. Therefore, a high-*Z* target material should be used. For all materials, the duration of soft x-ray pulses was 3–10 ps, which is close to the instrumental limit. In the case of pulse broadening, which was observed at higher pumping intensity, particularly in high-*Z* materials, soft x-ray emission at longer wavelength stayed a longer period of time.

2.3. Enhanced soft x-ray emission from plasma created on nano-structured target

We found that by fabricating an array of nanoholes perpendicular to the surface of an alumina target, as shown in Fig. 5, soft x-ray emission from laser-produced plasma is enhanced and the pulse duration is kept short.[14] A nanometer structure on a target surface, such as a porous or nanohole structure, is expected to realize a low average density with a high local density. Low average density is a favorable for overcoming the tiny interaction volume of the material with an intense femtosecond laser pulse, which results in a limited efficiency of conversion into soft x-ray emission. High local density is required in order to maintain the relatively high cooling rate of plasma created near the target surface.

The targets were made by the anodic oxidation of an aluminum plate. In Fig. 6, soft x-ray emission spectrum from plasma created a 100-fs laser pulse on an anodic alumina target with mean nanohole diameter and cell size of 90 nm and

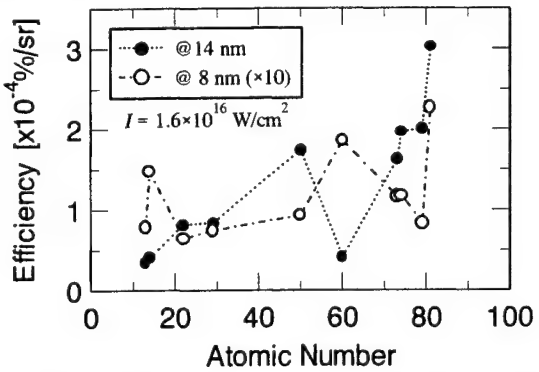

Fig. 4. Dependence of efficiency of conversion from a femtosecond laser pulse into soft x-rays on atomic number Z of target materials.

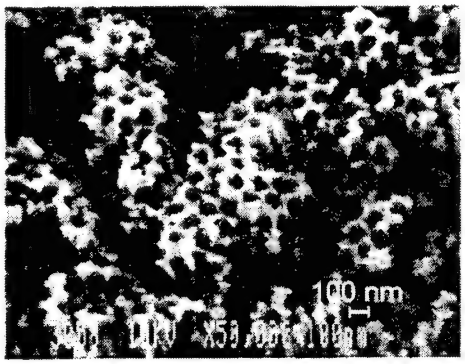

Fig. 5. SEM image of an anodic-alumina structure.

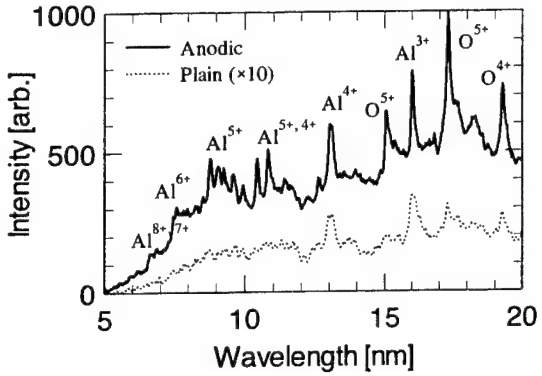

Fig. 6. Time-integrated soft x-ray spectra emitted from anodic alumina and plain alumina targets. The intensity scale on the plain target is expanded by a factor of ten.

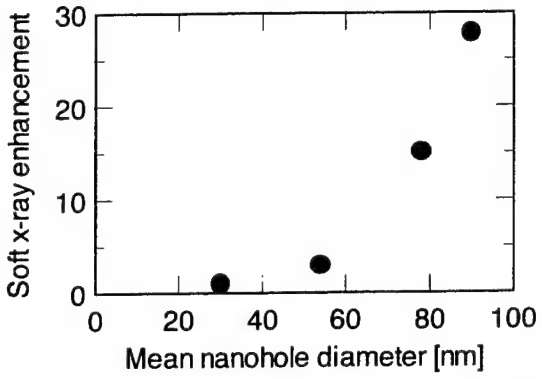

Fig. 7. Enhancement of time- and wavelength- (5–30 nm) integrated soft x-ray emission as a function of the mean diameter of nanoholes on an anodic-alumina target.

100 nm, respectively. The intensity of the laser pulse was 1.5×10^{16} W/cm^2. In the figure, the soft x-ray emission spectrum from plasma on a plain alumina target is also shown (dotted curve). The intensity scale on a plain target is expanded by a factor of ten. Comparing Fig. 6 with Fig. 1, one can see that additional groups of line emissions due to oxygen ions appeared in the case of alumina targets. Figure 6 shows that soft x-ray emission over the entire wavelength region was enhanced about 30 fold when using a target with an array of nanoholes on its surface. Further enhancement of soft x-ray emission was observed at the shorter wavelengths corresponding to the emission from highly ionized species (Al^{7+}–Al^{9+}). The measured pulse durations of soft x-ray emitted from anodic and plain alumina targets were 17 and 5 ps, respectively. The lower heat conductivity of the anodic alumina target might have affected the pulse duration. Figure 7 shows that further enhancement was achieved by using a target with larger pore diameter, which means a lower average density to interact with laser pulse. By fabricating nanometer-sized structures perpendicular to the surface, similar enhancement of soft x-ray emission is expected for other target materials.[21]

3. TIME-RESOLVED ABSORPTION SPECTROSCOPY OF OPTICALLY EXCITED SILICON USING FEMTOSECOND-LASER PLASMA X-RAY PULSES

We have demonstrated time-resolved measurement of soft x-ray absorption in optically-excited silicon membrane by means of pump-probe spectroscopy.[7, 17] The dynamic change in the soft x-ray absorption near the $L_{II,III}$ edge induced by a 100-fs laser pulse was probed by synchronized soft x-ray pulses emitted from femtosecond laser-produced plasma. A block diagram of the setup is shown in Fig. 8. The 50-mJ laser pulses were sent into a beam splitter, where 80% of the energy was reflected. Reflected light was focused onto a flat target using a 200-mm focal length MgF_2 lens at the normal incidence to generate soft

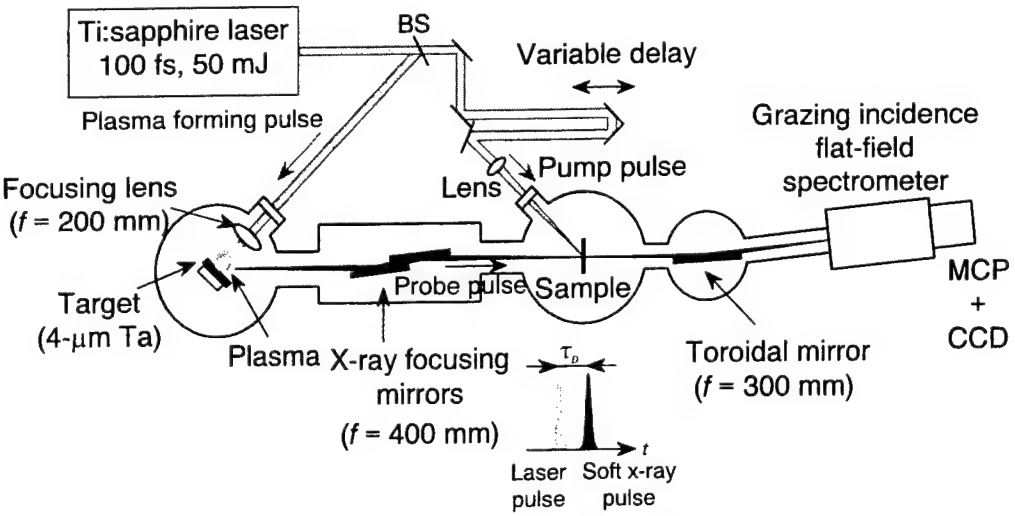

Fig. 8. Experimental setup for time-resolved soft x-ray absorption measurements by means of pump-probe spectroscopy.

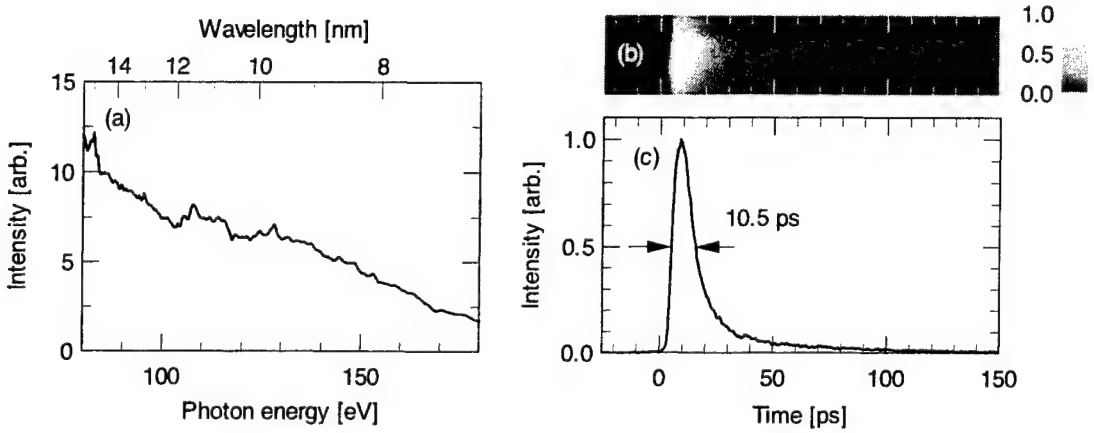

Fig. 9. Time-integrated spectrum (a), streak image (b), and line trace of the streak image (c) of the soft x-ray pulse emitted from Ta-plasma created by a 100-fs Ti: sapphire laser pulse.

x-ray pulses. To obtain a broadband soft x-ray pulse without fine structures in a spectrum, we used a 4-μm-thick Ta film as a target to create plasma. Figure 9 shows the emission spectrum and shape of the probe soft x-ray pulse, which indicate that the temporal resolution of the system was ~10 ps. The emitted soft x-rays were focused by a set of grazing incidence concave mirrors onto a 100-nm-thick silicon membrane. The sample was set on a pinhole with a radius of 100 μm. Soft x-ray, which transmitted through the sample, was again focused onto the entrance slit of a flat-field grazing incidence spectrograph. The spectrograph had an unequally grooved grating with a nominal groove number of 1200 mm^{-1}. To detect soft x-rays (10–15 nm), we used a MCP detector coupled with a cooled CCD. The sample was a 100-nm-thick silicon membrane without any supporting structures. The remaining 10 mJ of laser light was sent into an optical variable delay line and a variable attenuator, and then focused onto the sample by a 500-mm focal length lens. To ensure spatial overlapping, the diameter of the spot size of the laser beam focused on the sample was set at 5 mm. The estimated photon flux on the detector was ~ 1000 photons/Å in each pulse. The spectral resolution was higher than 400 (in $\lambda/\Delta\lambda$) near 100 eV.

3.1. Change in soft x-ray transmission by femtosecond laser pulse irradiation

Figure 10 shows typical transmission spectra with and without laser pulse irradiation. In this case, the laser and the soft x-ray pulses arrived simultaneously on a sample. Curve (b), the thick dotted one, shows the transmission spectrum of the sample when the pumping pulse was blocked. Curve (a), the thick solid one, was obtained when the sample was irradiated by a laser pulse. The intensity of the pumping pulse on the sample was 3×10^{10} W/cm^2, which was well below the damage threshold (~ 0.1 J/cm^2). In the figure, a slight downward shift of the absorption edge is observed with laser pulse irradiation. Curve (c) shows the normalized difference between curves (a) and (b). The differential transmittance T_D is defined as $T_D = (T_p - T_u)/T_u$, where T_p and T_u represent the transmittance with and without laser pulse irradiation, respectively. Curve (c) shows that a sharp change in transmission only appeared near the $L_{II,III}$ absorption edge. The most significant dip in the differential transmittance appeared at 99.5 eV, which corresponds to the energy difference between the $L_{II,III}$ level and the top of the valence band.

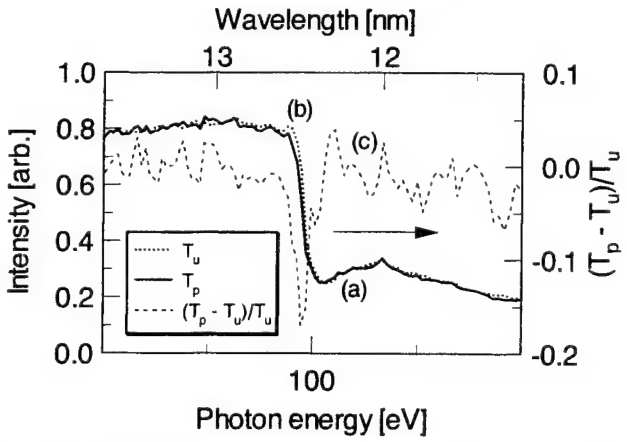

Fig. 10. Transmission spectra of Si membrane near the $L_{II,III}$ absorption edge. The thick solid and dotted curves, (a) and (b), represent transmission spectra observed with and without laser pulse irradiation, respectively. The thin broken curve, (c), is the differential transmission spectrum, which shows the difference induced by the femtosecond laser pulse irradiation.

Figure 11(a) shows the differential transmission spectra at various time delays between pump and probe pulses when the intensity of the pump pulse was 3×10^{10} W/cm^2. The delay step was 6.6 ps. Change in transmission is clearly observed only at -10 ps $< \tau_D <$ 20 ps, where τ_D represents the time lag between the arrival of the probe pulse and that of the pump pulse at the sample surface. In obtaining these curves, we confirmed at each step that there was no big difference among the transmission spectra

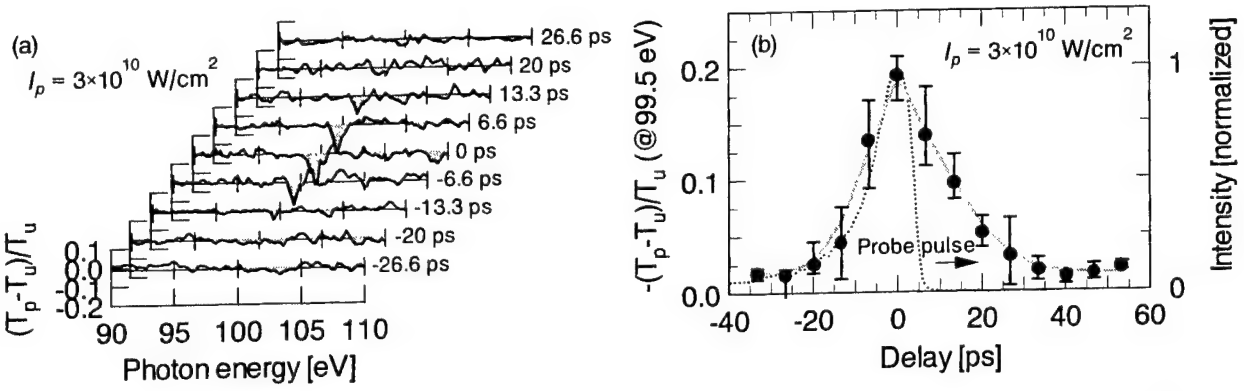

Fig. 12. (a) Differential transmission spectra of Si membrane induced by laser pulse irradiation at various soft x-ray probe pulse delays. (b) Depth of differential transmission at 99.5 eV as a function of soft x-ray pulse delay time. The dotted curve represents the temporal profile of the soft x-ray probe pulse, which was observed with an x-ray streak camera.

measured in case of no pumping laser pulse. Therefore we can exclude the possibility of irreversible processes induced by strong laser pulse irradiation on the sample, such as melting and destruction. In Fig. 11(b), the depth of the dip at 99.5 eV is plotted as a function of time delay τ_D. The dependence of the relative increase in absorption on the time delay at $\tau_D < 0$ ps fits the pulse shape of the soft x-ray within the error bars. This means that the absorption change built up almost instantaneously (< 10 ps). On the other hand, on the positive delay side, one can clearly see the recovery of the absorption change. By fitting the result to an exponential function, we obtained the recovery time constant of about 20 ps.

3.2. Dependence of soft x-ray absorption change on pumping laser intensity

In Fig. 12(a), transmission spectra of the silicon membrane are shown for three different laser pulse intensities (I_p = 3×10^9, 1×10^{10}, 3×10^{10} W/cm^2). In all cases, the probe soft x-ray and the pumping laser pulses arrived on the sample simultaneously. From the spectra, one can see that the amount of $L_{II,III}$-edge downward shift increased with increasing pumping intensity I_p. However, the spectral resolution of our system does not allow us to quantitatively discuss the amount of absorption edge shift. In all cases, significant change in differential transmittance only appeared near the absorption edge. The most significant dip appeared near 99.5 eV. In Fig. 12(b), the dip in differential transmittance at 99.5 eV is plotted as a function of arrival time delay of the probe soft x-ray pulse to the pumping laser pulse τ_D. Although the SNR was not high enough, the recovery time constant seems to increase with decreasing pumping laser pulse intensity I_p. The recovery time constant at the intensity of 3×10^9 W/cm^2 was about 35 ps, while it was about 20 ps at 3×10^{10} W/cm^2

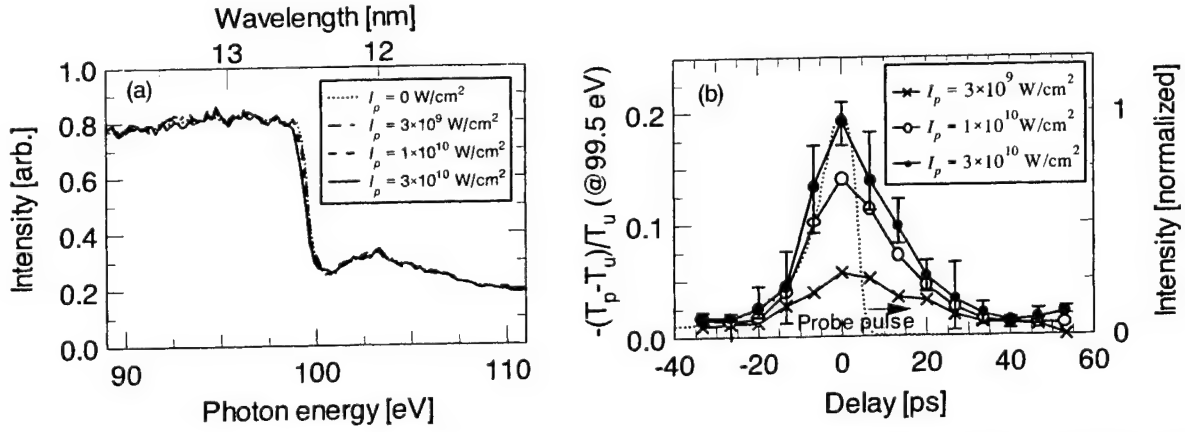

Fig. 11. (a) Change in soft x-ray transmission spectrum of silicon membrane by irradiation of a 100-fs laser pulse. Spectra are shown for four different laser intensities. In all cases, the laser pulse and probe soft x-ray pulse reached the sample simultaneously. (b) Dependence of the depth of the dip in differential transmittance at 99.5 eV on probe soft x-ray pulse delay τ_D at various pumping pulse intensities I_p.

3.3. Discussions

The most probable reason for the absorption change is the modification of the energy structures across the band gap due to high-density electron-hole pairs created by the strong field of the pumping laser pulse. We observed an absorption edge shift of about 0.2 eV toward the lower energy side when the sample was pumped by a laser pulse with an intensity of 3×10^{10} W/cm^2. However, this amount of shift was close to the resolution of our system. The estimated initial density of photo-induced carriers is 10^{20} cm^{-3}, which is high enough to modify the band energy. It is well known that the band gap energy shifts downward due to renormalization of the band energy.[22] By using an empirical formula given in Ref. 22, the amount of band gap shift is estimated to be 0.15 eV when the density of induced carriers is 10^{20} cm^{-3}. This estimation supports our assumption that the $L_{II,III}$ absorption edge downward shift is related to the band gap renormalization in a highly excited semiconductor. The smaller shift at lower pumping intensity [Fig. 12(a)] is consistent with the formula given in Ref. 22. From the results described in Ref. 23, high-density electron-hole pair plasma decays within tens of picoseconds. In our case, soft x-ray absorption change was observed within this decay time. Reference 23 also indicates that the recombination rate of induced carriers increases with increasing carrier density. Our result in Fig. 12(b) qualitatively agrees with this. When high-density electron-hole pair plasma exists, the electronic structure of the silicon is modified. As a result, the L-absorption edge corresponding to ionization potential could have shifted when the plasma existed. To make the origins of the absorption change clear, further studies are required.

4. SUMMARY

In summary, femtosecond laser-produced plasmas are attractive ultrashort x-ray sources for time-resolved spectroscopy. They emit x-rays covering the sub-keV to keV energy region with durations of less than 10 ps. Due to a small source size and short pulse duration, the peak brightness exceeds 10^{22} ph/s/mm^2/sr/0.1%BW. We found that the photon flux of soft x-ray emission can be enhanced more than 30 fold by making an array of nanoholes on an alumina surface and the duration of emission kept to less than 20 ps. Even greater enhancement was achieved at the shorter wavelengths corresponding to emission from highly ionized species. By using a femtosecond laser-produced plasma x-ray, we demonstrated time-resolved absorption measurement of optically excited silicon by means of pump-probe spectroscopy. As a result, we found that a more than 10% increase in soft x-ray absorption near the $L_{II,III}$ absorption edge in silicon was induced by a 3×10^{10}-W/cm^2-femtosecond-laser pulse irradiation. This absorption change recovered within 20 ps. The origin of this observation is most likely the modification of the energy structures across the band gap due to high-density electron-hole pairs created by the strong field of the pumping laser pulse.

Potential applications of ultrafast x-ray pulses from femtosecond laser-produced plasmas are expected to open a new class of material studies, such as dynamics of electrons in inner shells, photo-induced phase change, chemical change, and structural change, with high temporal resolution.

ACKNOWLEDGEMENT

The authors thank Dr. Hisataka Takenaka of NTT Advanced Technology Corp. for providing the multilayered soft x-ray mirrors.

REFEREMCES

1. M. M. Murnane, H. C. Kapteyn, S. P. Gordon, and R. W. Falcone, "Ultrashort x-ray pulses," Appl. Phys. B **58**, 261–266 (1994).
2. J. C. Kieffer, M. Chaker, J. P. Matte, H. Péppin, C. Y. Côté, Y. Beaudoin, T. W. Johnston, C. Y. Chien, S. Coe, G. Mourou, and O. Peyrusse, "Ultrafast x-ray sources," Phys. Fluids B **5**, 2676–2681 (1993).
3. C. Rischel A. Rousse, I. Uschmann, P.-A. Albouy, J.-P. Geindre, P. Audebert, J.-C. Gauthier, E. Förster, J.-L. Martin, and A. Antonetti, "Femtosecond time-resolved x-ray diffraction from laser-heated organic films," Nature **390**, 490–492 (1997).
4. C. W. Siders, A. Cavalleri, K. S.-Tinten, Cs. Tóth, T. Guo, M. Kammler, M. H. von Hoegen, K. R. Wilson, D. von der Linde, and C. P. J. Barty, "Detection of nonthermal melting by ultrafast x-ray diffraction," Science **286**, 1340–1342 (1999).
5. M. H. Sher, U. Mohideen, H. W. K. Tom, O. R. Wood II, G. D. Aumiller, and R. R. Freeman, "Picosecond soft x-ray pulse-length measurement by pump-probe absorption spectroscopy," Opt. Lett. **18**, 646–648 (1993).
6. J. Workman, M. Nantel, A. Maksimchuk, and D. Umstadter, "Application of a picosecond soft x-ray source to time-resolved plasma dynamics," Appl. Phys. Lett. **70**, 312–314 (1997).

7. H. Nakano, Y. Goto, P. Lu, T. Nishikawa, and N. Uesugi, "Time-resolved soft x-ray absorption spectroscopy of silicon using femtosecond laser plasma x rays," Appl. Phys. Lett. **75**, 2350–2352 (1999).
8. H. Nakano, T. Nishikawa, H. Ahn, and N. Uesugi, "Effects of an ultrashort prepulse on soft x-ray generation from an aluminum plasma produced by femtosecond Ti:sapphire laser pulses," Appl. Phys. B **63**, 107–111 (1996).
9. H. Nakano, T. Nishikawa, H. Ahn, and N. Uesugi, "Temporal evolution of sot x-ray pulse emitted from aluminum plasma produced by a pair of Ti:sapphire laser pulses," Appl. Phys. Lett. **69**, 2992–2994 (1996).
10. H. Nakano, T. Nishikawa, and N. Uesugi, "Soft x-ray pulse generation from femtosecond laser-produced plasma with reduced debris using a metal-doped glass target," Appl. Phys. Lett. **70**, 16–18 (1997).
11. H. Nakano, T. Nishikawa, and N. Uesugi, "Strongly enhanced soft x-ray emission at 8 nm from plasma on a neodymium-doped glass surface heated by femtosecond laser pulses," Appl. Phys. Lett. **72**, 2208–2210 (1998).
12. T. Nishikawa, H. Nakano, H. Ahn, N. Uesugi, and T. Serikawa, "X-ray generation enhancement from a laser-produced plasma with a porous silicon target," Appl. Phys. Lett. **70**, 1653–1655 (1997).
13. T. Nishikawa, H. Nakano, N. Uesugi, and T. Serikawa, "Porous layer effects on soft x-ray radiation emitted from a plasma generated by 130-fs laser pulses irradiating a porous silicon target," Appl. Phys. B **66**, 567–570 (1998).
14. T. Nishikawa, H. Nakano, N. Uesugi, and M. Nakao, and H. Masuda, "Greatly enhanced soft x-ray generation from femtosecond-laser-produced plasma by using a nanohole-alumina target," Appl. Phys. Lett. **75**, 4079–4081 (1999).
15. D. Kühlke, U. Herpers, and D. von der Linde, "Soft x-ray emission from subpicosecond laser-produced plasmas," Appl. Phys. Lett. **50**, 1785–1787 (1989).
16. U. Teubner, G. Kühnle, and F. P. Schäffer, "Detailed study of the effect of a short prepulse on soft x-ray spectra generated by a high-intensity KrF* laser pulses," Appl. Phys. B **63**, 493–499 (1992).
17. H. Nakano, P. Lu, T. Nishikawa, and N. Uesugi, "Generation of short x-ray pulse from femtosecond laser-plasma and its application," in "*Frontiers of Laser Physics and Quantum Optics*," edited by Z. Xu, S. Xie, S.-Y. Zhu, and M. O. Scully (Springer-Verlag, Berlin, 2000), 139–148.
18. H. Nakano, T. Nishikawa, N. Uesugi, J. Limpouch, and A. A. Andreev, "Femtosecond laser-produced plasmas as x-ray sources," paper presented at XXVI European Conference on Laser Interaction with Matter (ECLIM 2000), Prague, Czech Republic (2000), paper Fr/O3/1.
19. S. P. Gordon, T. Donnelly, A. Sullivan, H. Hamster, and R. W. Falcone, "X rays from microstructured targets heated by femtosecond lasers," Opt. Lett. **19**, 484–486 (1994).
20. A. Y. Faenov, I. Y. Skobelev, S. A. Pikuz, G. A. Kyrala, R. D. Fulton, J. Abdallah Jr., and D. P. Kilcrease, "High-resolution x-ray spectroscopy of a subpicosecond-laser-produced silicon plasma," Phys. Rev. A **51**, 3529–3533 (1995).
21. T. Nishikawa, H. Nakano, N. Uesugi, M. Nakao, K. Nishio, and H. Masuda, "X-ray generation from femtosecond-laser-produced plasma on nanostructure-array targets," paper presented at 7th International Conference on X-ray Lasers (ICXRL2000), Saint-Malo, France (2000).
22. P. Vashishta and R. K. Kalia, "Universal behavior of exchange-correlation energy in electron-hole liquid," Phys. Rev. B **25**, 6492–6495 (1982).
23. M. C. Downer and C. V. Shank, "Ultrafast heating of silicon on sapphire by femtosecond optical pulses," Phys. Rev. Lett. **56**, 761–764 (1986).

Energy distribution of charged particles in laser erosion plume on ablation of solid metallic targets with excimer laser

O.A.Novodvorsky, E.O.Filippova, O.D.Khramova, A.K.Shevelev

Institute on Laser and Information Technologies, Russian Academy of Sciences, (ILIT RAS)
Svyatoozerskaya st. 1, 140700 Shatura, Moscow Region, Russia

ABSTRACT

The Langmuir probe was used to study erosion plume resulting from ablation of a tantalum target in vacuum with excimer laser (308 nm) radiation. The spatial and temporal dependencies of electron and ion probe currents were obtained in real time. Relying upon a series of dependencies of electron probe currents on the value of probe potential, electron temperature of different plume regions was taken at various distances from the target. It was established that the plume electron temperature is non-uniform. The ion concentration in the plume determined at various distances from the target.

Key words: erosion plume, Langmuir probe, ion scatter velocity, electron temperature.

INTRODUCTION

The process of ablation of solid targets has long been the subject of a large body of research. This is related both to complexity of involved processes and to possibility of wide practical applications [1,2]. One major application of solid target ablation by laser beam is the process of thin film deposition with pulsed laser.

Practical applications, especially the processes of laser-plasma deposition, require the information on characteristics of erosion plume. The energy spectra of ions are known to play an essential role in deposition of thin films by physical methods [3], particularly in laser-plasma deposition [4]. Of great importance in these processes is the possibility of ion energy spectrum control, which has a pronounced effect on deposited film characteristics (type of crystal structure, crystal size, adhesion, etc.) [4]. Determination of the plume energy parameters (energy spectrum of ions, electron temperature, density), their dependence on laser pulse energy, spatial evolution and angular dependence are of special importance in pulsed laser deposition of thin metal films. The resolved in time and space measurements made in the course of plume motion from target to substrate yield information on kinetics and velocity of different particles.

The investigations of laser erosion plume in ablation of metals, semiconductors, ion crystals, ceramics widely involve the probe methods [5,6-9]. It is typical of laser ablation of metals that the target evaporation threshold approaches the threshold of plasma generation [10]. Thus, in pulsed laser deposition, erosion plume of metal is largely ionized [5,11]. In highly ionized plume plasma the Langmuir probe makes records of charged particles, which present a considerable share of the plume particles, and provides therewith for high local accuracy of measurements. The Langmuir probe was used to take the plume electron temperature [7-9], to measure the velocity distribution [6,9] and energy spectrum of ions [5].

This paper reports the investigation of erosion plume in ablation of tantalum target by excimer laser radiation (308 nm) using the Langmuir probe. The spatial and temporal dependence of electron and ion probe currents was obtained in real time. The measurements were taken of ion velocity, of electron temperature and ion density distribution in the plume, and of their dynamics.

EXPERIMENT

The experiments were run in the vacuum chamber which was evacuated by diffusion pump to $p \leq 10^{-5}$ mm Hg. Laser erosion plasma was generated by XeCl excimer laser. Pulse half-height duration made 20 ns, pulse energy was regulated between 2 to 25 mJ. The beam was focused by two-lens objective and directed to the target at 50° to the normal. The targets were made as discs from tantalum foil of 0.5 or 1 mm thickness, 99.9% purity (Alfa, Asohnson Mattey Comp.). The discs

*Correspondence: Email: onov@laser.nictl.msk.su; Telephone:09645 22214; Fax 09645 22532

Laser Optics 2000: Ultrafast Optics and Superstrong Laser Fields, Alexander A. Andreev, Vladimir E. Yashin, Editors, Proceedings of SPIE Vol. 4352 (2001) © 2001 SPIE · 0277-786X/01/$15.00

were fixed on electric drive axis and rotated at 10 Hz frequency. The focus spot had an ellipsoidal shape and 0.5 mm^2 area at the target. The target and vacuum chamber walls were earthed. The Langmuir probe of 5 mm length was made from tungsten wire of 0.2 mm diameter, which was placed into ceramic tube. The probe potential could be varied within ±18 V. The controlled voltage at the probe was supplied by a bank of accumulators which was connected to the probe by one pole through a potentiometer, and was earthed by the other pole through a load resistor. To stabilize the probe potential when current was flowing, the source of controlled voltage was bypassed by 2.5 μF capacitor. The value of load resistance could be discretely varied from 10 to 1000 Ω. The signal from the load resistor was processed by high-speed ADC and stored by IBM PC computer. The ADC digitization period made 0.1 μs. The range of measured ADC voltages was ±5 V. The time of charge arriving to the probe was counted from the moment of generation of laser pulse recorded by photodiode sending the signal to the ADC trigger input. The probe was placed in the vacuum chamber with its axis parallel to the target plane and was moved parallel with the normal to the place of radiation focusing at the distance of 3 to 160 mm from the target surface. For the purpose of running angular measurements, the probe could be deviated from the normal by ±80°. To study the particles scattering over the target surface, the probe was moved within 3 mm above the target plane up to 45 mm away from the irradiated area. In all measurements the probe axis was kept parallel to the target plane, and the probe was held with its side parallel to ablation area.

RESULTS AND DISCUSSION

The performed experiments yielded more than a thousand of time-of-flight curves (TFC) of probe current in ablation of tantalum at different probe-to-target separations and probe potentials and at different energies of laser incident radiation. Changing the sign of probe potential, we obtained TFC both for ions and for electrons. For the characteristic points of TFC volt-ampere probe curves were generated; their electron branches served to determine electron temperature, and the potential of ion current saturation was found from the ion branch.

The times of leading ion groups arrival were measured for several probe-to-target separations. The time of arrival was determined by the delay of probe signal front edge measured at the amplitude half-height relative to laser pulse. The time of signal front edge arrival was found to be proportional to the probe-to-target separation. The ion scatter velocity was determined from the probe curves as the ratio between the probe-to-target separation and the time of corresponding current value delay relative to laser pulse onset.

For the leading group of Ta ions the scatter velocity does nod depend on probe-to-target separation and makes $1.9 \cdot 10^4$ m/s. This value of velocity obtained by us satisfies the dependence $v \sim (M)^{-1/2}$, where M is molecular weight of the element; this dependence was observed by the other authors for ions of barium, yttrium and copper [12] when the experiments were conducted at laser radiation density 2 J/cm^2. In this paper the experiments were run under similar conditions.

The probe time-of-flight curves of tantalum ions differ considerably at different probe-to-target separations. The evolution of TFC of tantalum ions with the distance for 2 J/cm^2 radiation flux is shown in Fig. 1. The signal amplitude is reduced as the probe-to-target separation increases, so for convenience the TFC in Fig. 1 are not scaled. Al the curves were obtained for the range from 0 to 100 μs, it was reduced to 30 μs in order to gain higher resolution. As seen from the curves given in Fig. 1, the delay of signal front edge is proportional to the probe-to-target separation.

When the probe is moved to 10 mm (Fig. 1, curve 1) away from the target, the time-of-flight signal presents a smooth curve that has one maximum with steeply sloping front edge and more flattened back edge falling off to zero within 10 μs. If we assume that this curve corresponds to some smooth distribution by ion velocities, then it should retain its smooth shape even at further scatter. Though, the time-of-flight signal exhibits more complicated behavior as the probe-to-target separation increases. With the probe moving away from the target several maximums can be observed on TFC, which become even more pronounced as the distance increases. As seen in Fig. 1, TFC has two maximums at the distances of 23 mm and 75 mm. At 113 mm, three maximums can be distinguished, and at 133 mm four maximums are already observed. It turned out that velocity distribution in the group of particles corresponding to an individual maximum on curves 4 and 5 can be described by Maxwell distribution [13,14]

$$I(t) = K \cdot L \cdot t^{-4} \cdot \exp(-(L/t)^2 / v^2 \qquad (1)$$

or by shifted Maxwell distribution[15]

$$I(t) = K \cdot L \cdot t^{-4} \cdot \exp(-((L/t) - v_o)^2 / v^2). \qquad (2)$$

where K is proportionality factor, $v=(2k \cdot T/M)^{1/2}$ is most probable velocity, L is probe-to-target separation, v_o is velocity of mass center of ion group moving away from the surface in collision mode. These distributions were used to describe the

obtained experimental data. After mathematical processing of the experimental data it turned out that each of curves 1-5 (Fig. 1) presents a sum of four Maxwell curves having different locations of maximums; that is, at negative probe potential four groups of positively charged particles are observed in the plume through TFC for all the studied distances. For illustration, Fig. 2 (a, b) presents TFC for L=23 mm and 113 mm, respectively. Though one can see two maximums on the first curve and three of them on the second curve, both the curves are approximated with a high degree of accuracy by four Maxwell curves. When the probe is located at 23 mm from the target, TFC is described by the curves with maximums in the points of 1.1, 2.1, 4.0, 16.7 μs which correspond to particle velocities 21, 11, 6, 1.4 km/s. The curve obtained at the distance of 113 mm in the region below 30 μs with four distinct peaks is well approximated by three curves which are described by Maxwell distribution. To describe the curve in the region with scatter time more than 30 μs, one more approximation should be used, i.e. shifted Maxwell distribution with relatively low mean velocity. The maximums of these distributions are in the points of 5.3, 10.2, 17.7, 49 μs with most probable velocities 21, 11, 6, 2.5 km/s. It can be seen from velocity values obtained for the distances 23 and 113 mm to the probe that velocities of the first three groups of ions are constant, and the velocity of the fourth group increases with the distance from the target. An increase in velocity of the fourth ion group is also confirmed by TFC approximation at all the studied probe-to-target separations (10-133 mm). Two- and three-mode distributions of ions by velocities were noted previously by the other authors for multi-component targets of ion crystals [16] and HTSC ceramics [17].

It has been established in our earlier studies that in ablation of Ta, ion probe current saturation is achieved at probe potential ≈10 V [18]. The probe current value in ion current saturation mode is found by the formula

$$I_i = 0,5 \cdot S \cdot e \cdot n \cdot V, \qquad (3)$$

where S is probe area, e is electron charge, n is ion density, V is ion velocity at the boundary of probe collision-free layer [19]. The ion time-of-flight signal can be point-by-point transformed to distribution of charge density in the flying plume

$$n(t) = I(t)/(0,5 \cdot S \cdot e \cdot V) = I(t) \cdot t/(0,5 \cdot S \cdot e \cdot L) \qquad (4)$$

where t is arrival time of recorded ions, L is probe-to-target separation. Relying upon these relationships we evaluated the concentration of particles in the plume at different distances from the target using the obtained TFC. It has been found that maximum concentration of ions in the plume varies from $3.3 \cdot 10^{13}$ cm^{-3} at the distance L=10 mm to $1.4 \cdot 10^{11}$ cm^{-3} at L=133 mm.

The first groups of ions moving with constant velocity are formed at the start of ablation process in the mode of free collisionless release. For these ion groups amplitudes of signals reduce with the distance as L^{-2} [18], corresponding to spherical layer scatter. More slower groups of ions are resulting from the release process characterized by the presence of Knudsen layer when a backward flow of particles emerges having an effect upon further evaporation conditions [14]. The time of evaporation of atoms from the target surface can far exceed laser pulse duration as the result of radiation heating of the target surface by plume plasma and backward flow of particles from plasma. As the hydrodynamic scatter model [20] shows, when a cloud is scattered to the distance of several centimeters the density of neutral particles retains its maximal value at the target surface. It is well known that neutral particles in the plume have lower scatter velocities than charged particles [12]. Though, their leading part that moves faster than the "tail" of fast ion groups can be ionized as the result of resonance recharging, that will lead to increase in scatter velocities of slow ion groups. A long "tail" on probe TFC can also be formed during ionization as the result of neutral particle flow overlapping the back front of electron cloud of the plume charged part [8].

The emergence of "hot" electrons in plasma can be caused by the processes of multi-photon absorption, by backward retarding absorption [2], by build-up of Langmuir vibrations [21]. As a consequence of Coulomb interaction with external layers of erosion plume, these electrons form a high-energy leading part of ions, their energy reaching several hundred electron-volt, which is observed in the experiment [5,18,22]. Though, due to low depth of external field penetration into the plume plasma, a portion of these ions in the whole mass of plume ions is rather small and makes several per cent their overall amount [18,22].

The time dependencies of electron probe current are complicated similarly to time-of-flight ion curves. They are also considerably varied with the probe-to-target separation. At long distances they have several maximums which are close in their temporal location to the maximums on time-of-flight curves of ion current. A typical view of electron current curve with the probe placed at the plume axis is shown in Fig. 3. The probe-to-target separation is 23 mm. Relying upon dependence of the amplitudes of TFC maximums on the probe potential, electron temperature T_e was determined in the plume parts corresponding to these maximums.

The electron temperature was found from the plot illustrating the dependence of logarithms of peak amplitudes on the electron current time-of-flight curve upon the probe potential. The slope of this plot in the region below electron saturation current is equal to $e/(k \cdot T_e)$, where e is electron charge, k is Boltzmann constant, T_e is electron temperature in electron-volt terms. This follows from the probe equation

$$I_e \propto \exp(e \cdot V/k \cdot T_e),$$

where $V = V_p - V_s$ is probe-to-space voltage, V_p is probe potential, V_s is plasma potential that can be different from zero by the value of $(k \cdot T_e)/e$, I_e is probe current. The probe equation is valid when positive voltage at the probe is above $(k \cdot T_e)/e$; below this value ion current is comparable with electron current, and the relationship $\ln I_e(V)$ is shifted from the linear one [19].

The value of T_e was determined for the probe-to-target separations 23 mm, 75 mm and 133 mm using three observed maximums, the temporal location of which was varied with the probe-to-target separation. The results are presented in Table 1. The temperature appeared to be different at all the three maximums. The tend is toward temperature lowering to the last peak, i.e. to the tail part of the plume. Though the obtained temperatures apply to electron clouds related to different groups of ions scattering at different velocities. If, by analogy with ion TFC, we ascribe to the maximums on the electron curves the obtained scatter velocities, then, relying upon temporal location of TFC maximums for different probe-to-target separations, it is possible to distinguish the temperatures corresponding to the electron cloud which is related to a specific ion group and moves form the target at a constant velocity. These are, for example, the first maximum at the distance of 22 mm, the second one – at 75 mm, and the third maximum – at 133 mm, each of them being associated with an electron temperature, correspondingly, 6.4 eV, 5.9 eV, 5.3 eV. Thus, the temperature in the electron bunch moving at a constant velocity falls with distance from the target. The formula [23]

$$T_e = 2.98 \cdot 10^4 \cdot A^{1/8} \cdot (Z+1)^{-5/8} \cdot Z^{3/4} \cdot (I \cdot \lambda)^{1/2} \cdot \tau^{1/4} \cdot K,$$

where A is atomic weight of an ion, Z is average charge of ions in the cloud, I is laser radiation intensity (W/cm^2), λ(cm) is radiation wavelength, τ(c) is laser pulse duration, gives an estimate of electron temperature for tantalum atoms with single ionization (Z = 1) as T_e = 4.8 eV, and for Z = 1.5 (tantalum atoms with single and double ionization) as T_e = 5.6 eV, which is in a good agreement with the obtained results. In measurements of electron temperature in the plume by probe method on ablation of ion crystals with excimer laser [16] a drop in temperature T_e with the distance from the target surface was also observed.

At the start of scaling a short pulse is seen on the electron current probe curves, the temporal location of which does not depend on the probe-to-target separation at 0.1 μs resolution. It is produced by photoelectrons released from the target surface under laser radiation even before intense ablation. A similar pulse of photoelectrons was recorded in ablation of dielectrics [8,16]. The amplitudes of these pulses are also dependent on the probe potential. T_e measured for them at the distance of 75 mm is 11.5 eV, and it makes 7.35 eV at the distance of 133 mm.

The electron TFC were studied when the probe was moved over the target surface at the distance of 3 mm from the surface. In this case three maximums are also observed on TFC. A typical view of the electron current at the probe placed near the target surface is given in Fig. 4. It is seen that the shape of the signal is considerably different from the probe current curve located at the plume axis. The relationships of amplitudes of different peaks are also different. The absence of a peak of photoelectrons engages one's attention. The initial part of scaling shows an individual peak that is slightly seen or is lacking when the probe is set on the normal to the target. This peak is produced by the electrons scattering outside the ion cloud, but held by Coulomb forces. Due to high concentration of charges in the cloud propagating along the normal this peak is not discernible. In the direction along the surface concentration of charges in the ion cloud is much lower (diagram of ion scatter $\sim\cos^6\theta$ [18,22]), and the peak is clearly seen. The values of electron temperature were taken from the maximums of electron TFC. The dependencies of signal amplitudes on the probe potential were obtained by moving the probe from the normal to the plume at the distances of 15 mm, 30 mm and 45 mm. Table 2 presents the obtained values of T_e. The first and second maximums on TFC correspond to ion groups propagating at constant velocities. We notice that the temperature falls with the distance from ablation area, as well as in the direction to the plume tail. It should be noted that all the three values of temperature in different parts of the plume along the surface are lower than those noted along the normal to the surface.

CONCLUSION

The distribution of ions by scatter velocities in the erosion plume on ablation of tantalum targets in vacuum is not smooth in its nature. The velocity distributions in individual groups of ions are well described by Maxwell one-dimensional distribution. The leading groups of plume ions propagate at constant velocities. Slow groups of ions are accelerated in scatter. This can be caused by variation in ion concentration as the result of chemi-ionization and recombination processes, as well as by variation in ion scatter velocity due to second-kind collisions. The accelerated motion of electrons in slow modes exhibits the dominant role of processes of electron and ion collisions with neutral particles in the tail part of the charged area of the plume in the studied range of distances. Plasma here does not yet reach the state of free flight condition. The electron temperature in different parts of the plume has been taken at various distances from the target relying upon series of electron

probe current dependencies on the probe potential. It has been established that the plume temperature is not uniform. Concentration of ions in the plume has been determined at different distances form the target.

REFERENCES

1. Heinrich Hora, "Physics of Laser Driven Plasmas", *John Wileg and Sons*, New York, 1981.
2. Arutyunyan R.V., Baranov V.Yu., Bolshov L.A. et al. "Action of laser radiation on materials".
3. (M.: *Nauka.* 1989, 367 p.).
4. Roy R.A., Catania P., Saenger K.L., Cuomo J.J., Lossy R.L."Role of energetic atoms and ions in Ta films grown by different physical vapor deposition methods" *J. Vac. Technol.* **B 11**, N 5, 1921 (1993).
5. Saenger K.L. J. *Appl. Phys.*, 70, 5629 (1991).
6. Jordan R., Cole D., Lunney J.G., Mackay K., Givord D, "Pulsed laser ablation of copper" *Appl. Surf. Sci.* 86, 21 (1995).
7. Dyer P.E., Greenough R.D., Issa A., Key P.H.,"Spectroscopic and ion probe measurements of KrF laser ablated Y-Ba-Cu-O bulk samples", *Appl. Phys. Lett.*, 53(6), 534 (1988).
8. Von Gutfeld R.J. and Dreyfus R.W.,"Electronic probe measurement of pulsed copper ablation at 248 nm", *Appl. Phys. Lett.*, 54, N 13, 1212 (1989).
9. Ermer D.R., Langford S.C. and Dickinson J.T., "Interaction of wide band gap single cristals with 248 nm excimer laser radiation" J. Appl. Phys., **81** 1495 (1997).
10. Lubben D., Barnett S.A., Suzuki K., Gorbatkin S. And Greene J.E.,"Laser-induced plasmas for primary ion deposition of epitaxial Ge and Si films", *J. Vac. Technol.*, **B3,** N 4, 968 (1985).
11. Ready J.F. "Effects of high power laser radiation", (*Academic London*, 1971).
12. Witke T., Ziegele H., Surf. And Coat. Technol., 97, 414 (1997).
13. Marine W., Gerri M., Scotto d'Anielo J.M., "Analysis of the plasma expansion dynamics by optical time-of-flight vtasurements",Appl. Surf. Sci., 54, 264 (1992).
14. Anisimov S.I. "Metal vaporization by laser beam", JETP, **54**, N 1, 339 (1968).
15. Kelly R. And Dreyfus R.W.,"On the effect of knudsen-layer formation on studies of vaporization, sputtering, and desorption", Surface Science, **198**, 263 (1988).
16. Otis C.E., Goodwin P.M.,"Internal energy distribution of laser ablated species from Y-Ba-Cu-O", J. Appl. Phys., **73**, N 4, 1957 (1993).
17. Chin J.J., Ermer D.R., Langford S.C., Dickinson J.T.,"The role of photoelectronic processes in the formation of a fluorescent plume by 248-nm laser irradiation of single cristal $NaNO_3$", Appl. Phys. A, **64**, 7 (1997).
18. Boyarkin O.V., Burimov V.N., Golubev V.S., Zherikhin A.N., Popkov V.L.,"Velocity distribution of Ba^+ ions in a plasma formed by laser ablation" Izvestiya AN. Ser. Fizicheskaya, **52**, N 12, 90 (1993).
19. Novodvorsky O.A., Khramova O.D., Shevelev A.K., Filippova E.O. Proc. SPIE, 3885, 471 (1999).
20. Demidov V.I., Kolobkov N.V., Kudryavtsev A.A. "Probe methods of low-temperature plasma investigation" (M.: *Energoatomizdat*, 1996, 240 p.).
21. Leboenf J.N., Chen K.R. et al.,"Modeling of dynamical processes in laser ablation", Appl. Surf. Sci., **96-98**, 14 - 23 (1996).
22. Gorbunov L.M., Kirsanov V.I. JETP, 96, N 2(8), 583 (1989).
23. Novodvorsky O.A., Khramova O.D., Filippova E.O., Wenzel C., Bartha J.W. Optics and lasers in engineering, 32 (5), 449 (1999).
24. Phipps C.R., Turner Jr.T.P., Harrison R.F. et al.,"Impulse coupling to targets in vacuum by KrF, HF, and CO_2 single-pulse lasers" J. Appl. Phys., **64**, 1083 (1988).

Table 1. Values of erosion plume electron temperature (eV) at different probe-to-target separations taken vertically.

	Distance from probe to target, mm		
Number of maximum on TFC	23	75	133
1	6,4	6,25	5.8
2	5,7	5,9	5,3
3	4,8	5,0	4,7

Table 2. Values of erosion plume electron temperature (eV) at different probe-to-target separations taken horizontally

	Distance from probe to normal, mm		
Number of maximum on TFC	15	30	45
1	4,2	3,9	2,90
2	4,0	3,65	1,85
3	3,3	2,6	1,80

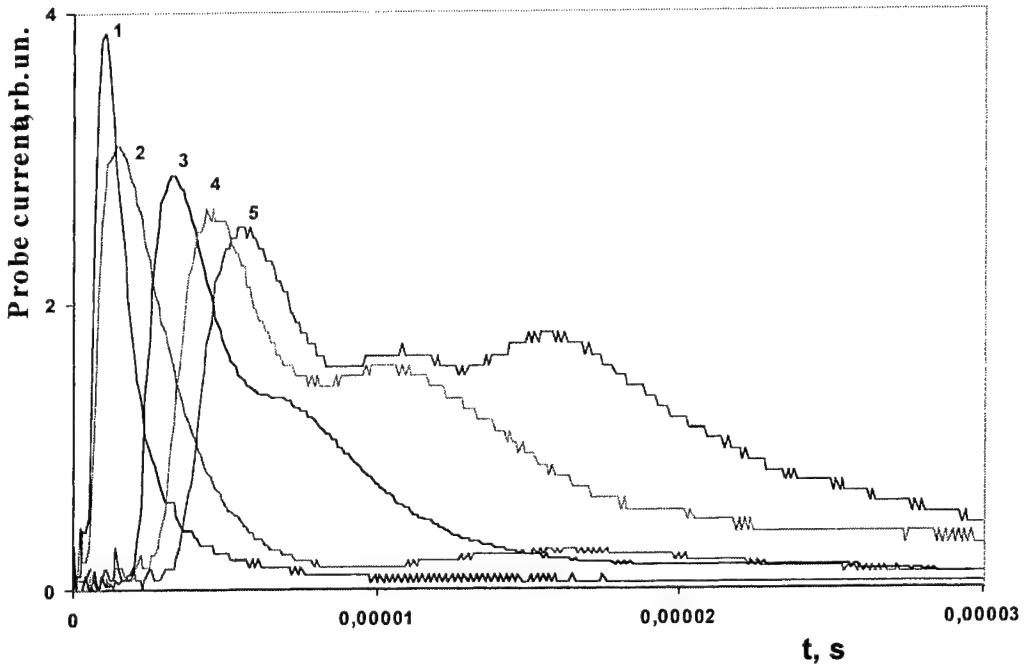

Fig. 1. Dependence of shape of probe time-of-flight curves on probe-to-target separation. For convenience the curves are not scaled, and the scanning time is shortened.

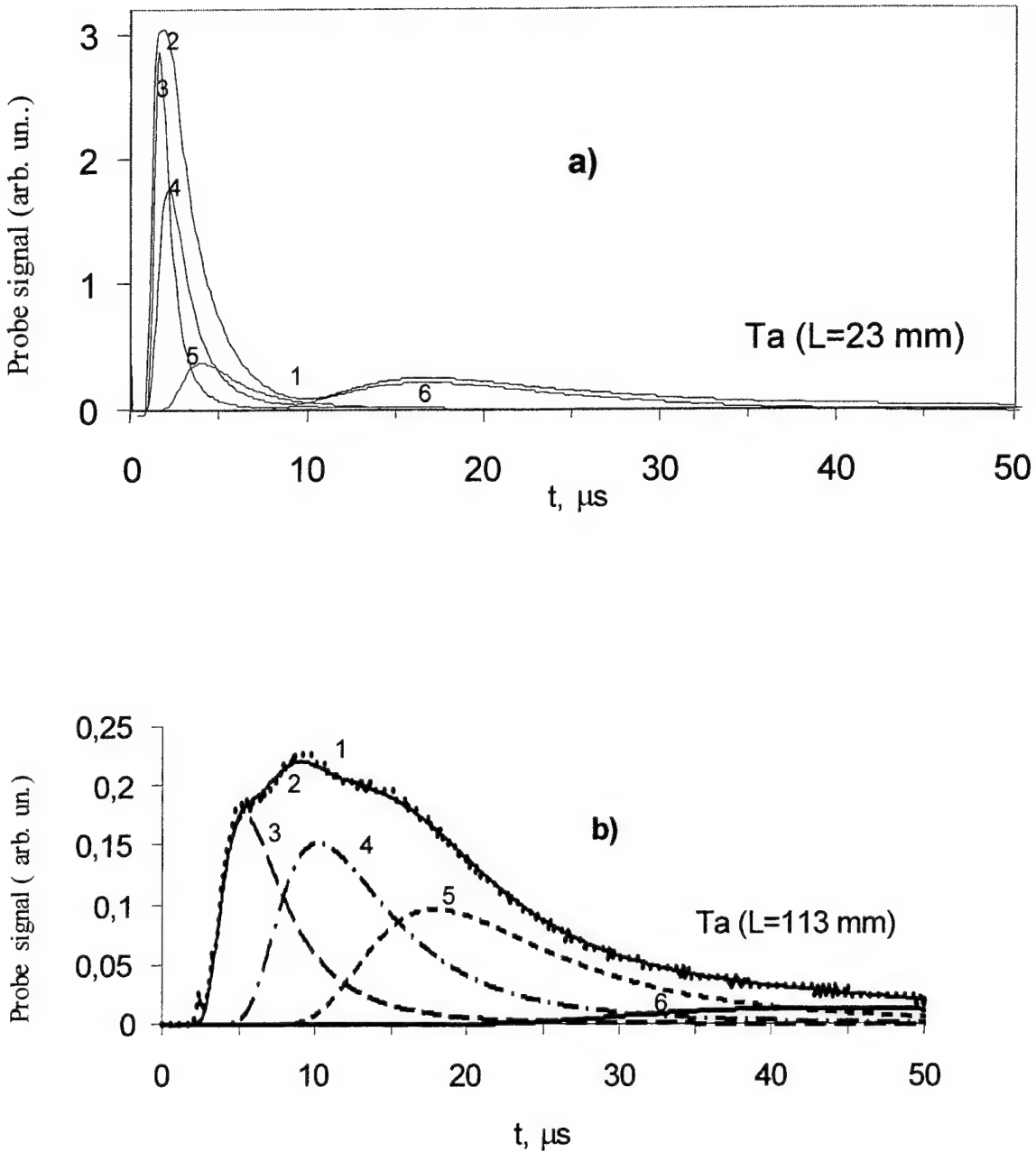

Fig.2. Approximation of time-of-flight curves by Maxwell distributions: a – by 23 mm, b – by 113 mm (1 – experimental curves, 2 – their approximations by sum of Maxwell curves 3 – 6).

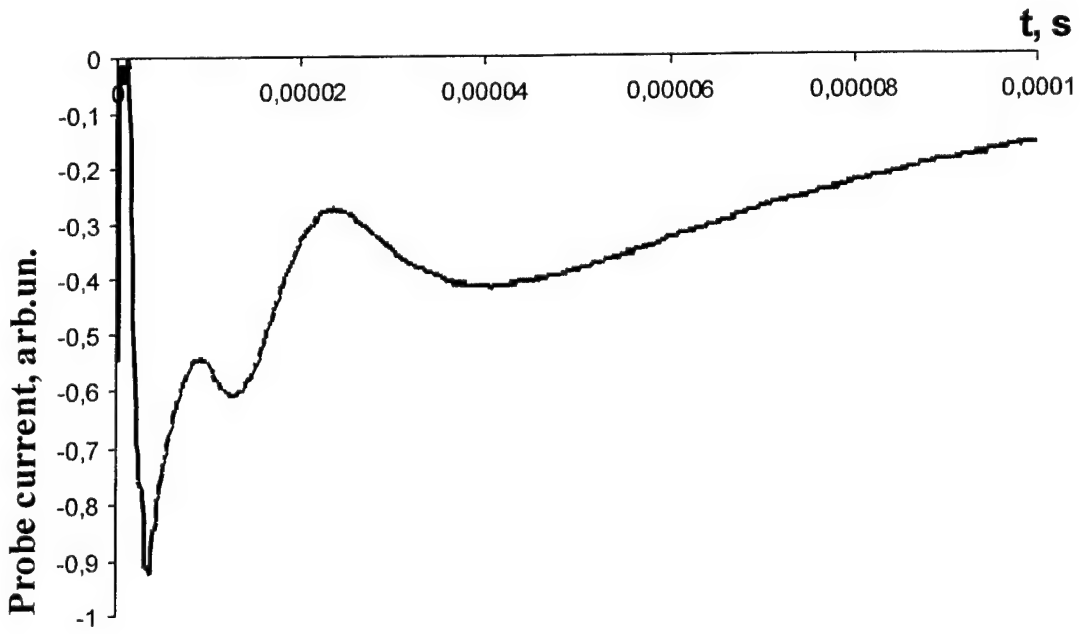

Fig. 3. Curve of electron probe current; the probe is located at 23 mm along the normal to the target. Probe potential is +8 V.

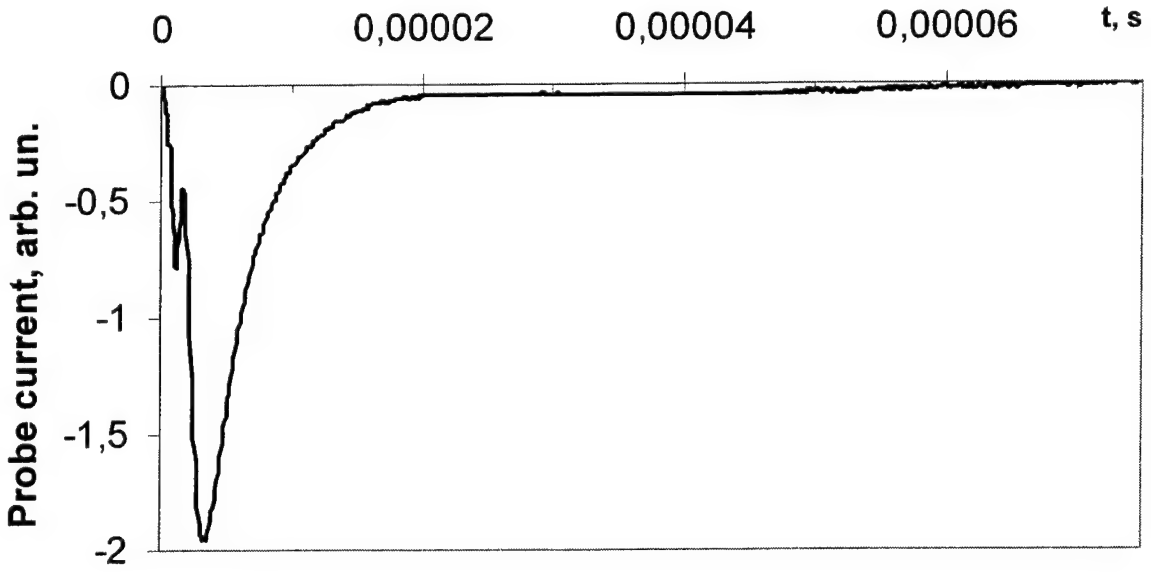

Fig. 4. Curve of electron probe current; the probe is located at 3 mm from the target surface and moved to 30 mm from the plume axis.

Laser plasma source for highly charged ions

N.E. Andreev, M.V. Chegotov
Institute for High Energy Densities, Associated Institute for High Temperatures
of Russian Academy of Sciences,
Izhorskaya st. 13/19, 127412 Moscow, Russia
E-mail: andreev@ips.ras.ru, chegotov@hedric.msk.su

ABSTRACT

A production of large amount of ions with low temperature (less than 100 eV), low momentum spread and narrowed charge state distribution by petawatt-class short-pulse laser is under consideration. Residual ion energy as the least unavoidable ion energy after ionization of gases by a short intense laser pulse is calculated as a function of laser pulse parameters. Electron thermal energy coupling to the ions is estimated taking into account a multi-group structure of free electrons produced by optical field ionization.

1 INTRODUCTION

The progress achieved over the past decade in the generation of intense femtosecond laser pulses[1] made it possible to extend substantially the area of theoretical and experimental research on the interaction of highly localized intense electromagnetic fields with matter (see, e.g.,[2]). Many applications based on the interaction of short intense laser pulses with gases and plasmas, such as laser particle acceleration,[3,4] X-ray laser,[5] harmonic generation,[6] and fast ignitor scheme for inertial confinement fusion,[7] are discussed intensively.

A possibility to produce highly-charged low-temperature ions by optical field ionization (OFI) of gases under the action of short intense laser pulses opens a new attractive approach to create an ion source with a low ion momentum spread and a charge state distribution that can be narrowed down to essentially a single charge state.[8]

In the present paper we calculate the residual ion energy (RIE) as the least unavoidable energy of ions produced by OFI, estimate the restrictions on the extraction time of ions due to recombination and collisional heating, and also estimate the laser pulse power necessary to

Laser Optics 2000: Ultrafast Optics and Superstrong Laser Fields, Alexander A. Andreev,
Vladimir E. Yashin, Editors, Proceedings of SPIE Vol. 4352 (2001) © 2001 SPIE · 0277-786X/01/$15.00

produce highly charged ions without their substantial energy spread due to ponderomotive laser acceleration.

2 RESIDUAL ION ENERGY

Meaning comparatively wide laser beam we assume one-dimensional geometry with the electromagnetic pulse propagating in z direction. Electric field $\mathbf{E}$ in the pulse has the following form

$$\mathbf{E} = \{E(t - z/c), 0, 0\} \cos(\omega_0(t - z/c)$$

We discuss the motion of ions in nonrelativistic limit because of their large masses M:

$$\frac{\partial \mathbf{V}_i(t, t_k^*)}{\partial t} = \frac{|e| k \mathbf{e}_x}{M} E(t) \cos(\omega_0 t) \tag{1}$$

which leads approximately (as an expansion with parameter $(\omega_0 \tau_{imp})^{-1}$) to the

$$\mathbf{V}_i(t, t_k^*) = \mathbf{V}_i(t_k^*, t_k^*) + \frac{|e| k \mathbf{e}_x}{M\omega_0} \left(E(t) \sin(\omega_0 t) - E(t_k^*) \sin(\omega_0 t_k^*)\right) \tag{2}$$

Here t_k^* is the moment of time when an ion of the ionization degree k was born, $\mathbf{e}_x = (1, 0, 0)$. Further we have to take into account that $\mathbf{V}_i(t_k^*, t_k^*)$ is the result of regular motion of ion with ionization degree $k - 1$ in quiver electric field after it's birth at the moment $t = t_{k-1}^*$:

$$\mathbf{V}_i(t_k^*, t_k^*) = \mathbf{V}_i(t_{k-1}^*, t_{k-1}^*) + \frac{|e|(k-1) \mathbf{e}_x}{M\omega_0} \left(E(t_k^*) \sin(\omega_0 t_k^*) - E(t_{k-1}^*) \sin(\omega_0 t_{k-1}^*)\right) \tag{3}$$

As a result of (2) and (3) one gets

$$\mathbf{V}_i(t, t_k^*) = \mathbf{V}_i(t_{k-1}^*, t_{k-1}^*) + \frac{|e| \mathbf{e}_x}{M\omega_0} \left(kE(t) \sin(\omega_0 t) - E(t_k^*) \sin(\omega_0 t_k^*) - (k-1) E(t_{k-1}^*) \sin(\omega_0 t_{k-1}^*)\right) \tag{4}$$

Processing the recurrent relation (3) one can generalize formula (4)

$$\mathbf{V}_i(t, t_k^*) = \mathbf{V}_{i0} + \frac{|e| \mathbf{e}_x}{M\omega_0} \left(kE(t) \sin(\omega_0 t) - \sum_{j=1}^{k} E(t_j^*) \sin(\omega_0 t_j^*)\right) \tag{5}$$

where $\mathbf{V}_{i0}$ is the velocity of the neutral. The residual velocity of the particular ion of k-th degree ionization is a limit of (5) at $t = +\infty$:

$$\mathbf{V}_i(t, t_k^*) = \mathbf{V}_{i0} - \frac{|e| \mathbf{e}_x}{M\omega_0} \sum_{j=1}^{k} E(t_j^*) \sin(\omega_0 t_j^*) \tag{6}$$

This expression leads to the following formula for RIE

$$RIE = \frac{1}{2} M \mathbf{V}_{i0}^2 + \frac{e^2}{2M\omega_0^2} \sum_{j=1}^{Z} \frac{1}{N_j(+\infty)} \int_{-\infty}^{+\infty} N_{j-1}(t) W_j(t) E^2(t) \sin^2(\omega_0 t) dt \tag{7}$$

where $N_j(t)$ is the density of ions with j - th degree of ionization, $W_j(t)$ the rate of ionization of the ion with ionization degree k - 1 to the ion with ionization degree k, Z the nuclear charge. Here we use for $W_j(t)$ so called ADK formula[9] which implies tunnel mechanism of ionization. This formula is valid for ionization by laser pulses with relativistic intensities if the typical energy of ejected electrons during ionization (which is equal to residual electron energy REE (see for example[10])) is less than electron rest energy mc^2.[11] Calculations below give $REE < 100$ keV which justifies application of ADK formula in our consideration.

The most important consequence of (7) is the dependence of RIE on the highest degree of ionization k at the assigned parameters of laser pulse and gas. For the first glance relation (2) gives $RIE = k^2(m/M)REE$ but the precise final formula (7) predicts $RIE = (m/M)REE$. For $k >> 1$ this is much less than "naive" consideration of (2).

3 COLLISIONAL HEATING and RECOMBINATION TIMES

One of the channel to couple an electron energy to ions is the collisional one. During an action of the laser pulse this channel is efficiently suppressed by large value of the electron-ion relative quiver motion velocity in strong laser pulse electric field. After the laser pulse an energy exchange between electrons and ions becomes more effective. For this exchange we have to take into account the group structure of the electron velocity distribution function.[10] Namely every emerging group of electrons during the ionization of k-th shell has the temperature $T_{e,k}$ which differs from the temperature $T_{e,k-1}$ corresponding to the electron group emerged during the ionization of previous $k-1$-th shell. The characteristic time of the Coulomb collisions between ions and electrons of k-th group can be estimated with the help of formula (see for example[12])

$$\tau_{ei,k} = \frac{m^2 w_k^3}{4\pi k^2 e^4 n_{\mathrm{at}} \Lambda}, \tag{8}$$

where Λ is the Coulomb logarithm ($\Lambda \sim 10$), n_{at} the density of atoms. By virtue of small velocity of ions we estimate the typical velocity of relative motion of electrons of k-th group with respect to ions w_k by the formula

$$w_k = \sqrt{<(\mathbf{v}_k)^2>} = \sqrt{<(\mathbf{v}_k - \mathbf{V}_e)^2> + (\mathbf{V}_e)^2} = \sqrt{\frac{3}{m} T_{e,k}},$$

where $\mathbf{V}_e$ is the electron quiver velocity which is equal 0 with the absence of laser pulse. As a result we obtain for $\tau_{ei,k}$ the estimated formula ($T_{e,k}$ is measured in eV and n_{at} is in cm^{-3})

$$\tau_{ei,k} = 10^5 \times \frac{T_{e,k}^{3/2}}{k^2 n_{\mathrm{at}}} \ (\mathrm{s}). \tag{9}$$

The time for electron-ion energy exchange $\tau_{ei,k,E}$ is determined by $\tau_{ei,k}$ with the help of well known relation[12]

$$\tau_{ei,k,E} = \frac{M}{2m}\tau_{ei,k} = 10^8 \times \frac{A}{k^2}\frac{T_{e,k}^{3/2}}{n_{\rm at}} \ [\rm s], \tag{10}$$

where A is the atomic number of the gas in use. Notice that the value $\tau_{ei,k,E}$ gives the typical time for electron of k-th group to deliver it's kinetic energy to ions until $T_{e,k}$ becomes equal to the ion temperature. Instead of this we have to estimate the typical time for electron to deliver the kinetic energy equal to ε_{ion} to ions. To estimate this time we have to multiply $\tau_{ei,k,E}$ by the ratio $\varepsilon_{ion}/T_{e,k}$

$$\tau_{ei,k,E}^{\varepsilon_{ion}} = \frac{\varepsilon_{ion}}{T_{e,k}}\tau_{ei,k,E} = 10^8 \times \frac{A}{k^2}\frac{\varepsilon_{ion}T_{e,k}^{1/2}}{n_{\rm at}} \ [\rm s]. \tag{11}$$

All $T_{e,k}$ could be calculated by formulas of.[10]

Ionization of Xe from Xe^0 until Xe^{+26} ($A = 131$, $U_{26} = 890$ eV is the energy of ionization of Xe^{+25} to Xe^{+26}) by laser pulse with wave length $\lambda_0 = 1.053$ μm, peak intensity $I_{max} = 10^{19}$ W/cm^2, duration $\tau_{imp} = 100$ fs leads to

$$REE \approx 36.5 \text{ keV}, \ RIE \approx 0.15 \text{ eV}, \ T_{e,26} \approx 27 \text{ keV} .$$

The ionization $Xe^0 \rightarrow Xe^{+1}$ occurs in the vicinity of $I = I_{th,1} = 1.3 \times 10^{14}$ W/cm^2 and the ionization $Xe^{+25} \rightarrow Xe^{+26}$ occurs in the vicinity of $I = I_{th,26} = 3.7 \times 10^{18}$ W/cm^2. The set of $T_{e,k}$ enables to estimate electron-ion collisions and energy exchange times by (9) and (11). Except times $\tau_{ei,k,E}^{\varepsilon_{ion}}$ at $k = 1, 2, 3$ (which are larger than at $k = 4, 5, \ldots 26$) all $\tau_{ei,k,E}^{\varepsilon_{ion}}$ are near the same

$$\tau_{ei,k,E}^{\varepsilon_{ion}} \approx 3 \text{ mks}$$

at atomic density $n_{\rm at} = 10^{17}$ cm^{-3} and $\varepsilon_{ion} = 100$ eV. It means that the effectiveness to couple the electron kinetic energy to ions is about 23 times higher than for any single electron group and the typical collisional time to heat ions up to $\varepsilon_{ion} = 100$ eV is

$$\tau_{ei,k,E}^{\varepsilon_{ion}} \approx 0.1 \text{ mks}.$$

Besides the ion heating discussed above the recombination is undesirable process which could destroy the sharp charge states distribution. Here we estimate the typical collisional three-body and electron-ion radiative recombination times. For collisional three-body (α_3) and electron-ion radiative (α_r) recombination rates we use the following formulas,[13,14] which should be applied to different electron groups

$$\alpha_3 = 8.75 \times 10^{-27} T_{e,k}^{-4.5} \text{ cm}^6/\text{sec} ,$$

$$\alpha_r = 5.2 \times 10^{-14} Z \left(\frac{U_k}{T_{e,k}}\right)^{1/2} \left[0.43 + \frac{1}{2}\ln\left(\frac{U_k}{T_{e,k}}\right) + 0.469 \times \left(\frac{U_k}{T_{e,k}}\right)^{-1/3}\right] \text{ cm}^3/\text{sec},$$

where U_k is the energy of ionization of the ion in $k-1$ charge state to the ion in k charge state. Collisional three-body (τ_3) and electron-ion radiative (τ_r) recombination times are the smallest ones for $k = 1$ and are equal to ≈ 1 mks and ≈ 2 mks correspondingly ($n_{\rm at} = 10^{17}$ cm^{-3}). Thus for considered parameters the typical collisional heating time is about one order of magnitude shorter than any recombination times and equals to ≈ 0.1 mks.

4 PONDEROMOTIVE ACCELERATION and LASER POWER ESTIMATIONS

The radial inhomogeneity of the laser pulse intensity will push out electrons by the ponderomotive force

$$\mathbf{F}_{pond} = mc^2 \nabla_\perp \sqrt{1 + a^2/2},$$

where the normalized laser strength a is related to the intensity I_L of a linearly polarized laser pulse (of wavelength λ) by the relation

$$a = \left(2e^2\lambda^2 I_L/\pi m^2 c^5\right)^{1/2} \simeq 8.6 \times 10^{-10} \lambda\,[\mu\mathrm{m}] \sqrt{I_L\left[\mathrm{W/cm^2}\right]}. \tag{12}$$

In a relatively dense plasma, when the electron plasma frequency $\omega_p = (4\pi e^2 n_e/m)^{1/2}$ is in excess of the inverse laser pulse duration ($\omega_p \tau_{imp} >> 1$) and the laser spot size r_0 is higher than the plasma skin depth c/ω_p, the space charge separation field will act on an ion of k charge state by the force $F_k = kF_{pond}$. If the laser pulse duration τ_{imp} is smaller than the maximal time of ion acceleration $\sim r_0/V_k$ than the velocity of an ion of k charge state due to ponderomotive action of laser pulse can be estimated as[15]

$$V_k \approx F_k \tau_{imp}/M,$$

and consequently the maximum kinetic energy of ions equals to[16]

$$\varepsilon_k = \frac{MV_k^2}{2} \approx \frac{1}{32}\frac{mk^2}{M}\left(\frac{c\tau_{imp}}{L_\perp}\right)^2 \frac{a^4}{1 + a^2/2} mc^2, \tag{13}$$

where $L_\perp \approx r_0$ is the characteristic transverse scale of the laser pulse intensity.

The above estimated ion energy (13), which determines the momentum spread of produced ions due to ponderomotive acceleration, will be smaller than the claimed ion energy ε_{ion} only when the laser pulse radius ($L_\perp$) will be comparatively large:

$$L_\perp > L_k \approx \frac{1}{4\sqrt{2}} k \sqrt{\frac{m}{M}} \frac{a^2}{\sqrt{1 + a^2/2}} \left(\frac{mc^2}{\varepsilon_{ion}}\right)^{1/2} c\tau_{imp}. \tag{14}$$

»From the other side the maximum laser pulse intensity I_{max} has to be high enough to produce charge state with required degree of ionization. As a result the laser power P_L has to exceed a minimum value P_k in order to produce ions with the required degree of ionization k and the energy spread lower than ε_{ion}:

$$P_L = \frac{\pi}{2} r_0^2 I_{\max} > P_k \approx L_k^2 I_{th,k} \approx \frac{1}{32} k^2 \frac{m}{M} \frac{a_{th}^4}{1 + a_{th}^2/2} \frac{mc^2}{\varepsilon_{ion}} (c\tau_{imp})^2 I_{th,k} \tag{15}$$

where $I_{th,k}$ is the threshold intensity to produce the charge state with required degree of ionization k and a_{th} is the corresponding normalized laser strength (see (12)).

For deep shells of Xe ionized by the laser pulse with wavelength $\lambda_0 = 1.053$ μm, $\tau_{imp} = 100$ fs, the threshold intensity $I_{th,26}$ is of order $4{\times}10^{18}$ W/cm^2 that for $\varepsilon_{ion} = 100$ eV leads to $L_{26} \approx 42$ μm and $P_{26} \sim 70$ TW in accordance with Eqs. (14) and (15).

5 CONCLUSIONS

Here we made estimations of residual ion energy, electron-ion collisional energy coupling time, and recombination times in a homogeneous gas (Xe) ionized by a short intense laser pulse. Our results show that such estimations are not in conflict with parameters of the scheme[8] and can be accessible at present time to produce highly charged ions with low ion temperature and narrow (essentially a single) charge state.

To avoid substantial transverse momentum spread of produced ions due to ponderomotive laser acceleration, the laser pulse power should exceed the minimum value that is of order 100 TW for considered example of Xe^{+26} ion source. It should be noted that a special attention has to be paid for the processes of laser pulse self-focusing, filamentation and self-modulation,[3,4] which can cause the ion momentum spread to increase.

Acknowledgments

The work was partially supported by the Russian Foundation for Basic Research, grant No 98-02-16263.

6 REFERENCES

[1] D. Strickland, G. Mourou, Opt. Commun. **56,** 219 (1985); P. Maine et al., IEEE J. Quantum Electron. QE-**24**, 398 (1988).

[2] Proceedings of ICONO'98:Ultrafast Phenomena and Interaction of Superstrong Laser Fields with Matter: Nonlinear Optics and High-Field Physics, Moscow, 1998, Proceedings of SPIE, **3735** (1999).

[3] E. Esarey et al., IEEE Trans. Plasma Sci., **24,** 252 (1996).

[4] N.E. Andreev, L.M. Gorbunov, Physics-Uspekhi, vol. 42, pp. 49-53, 1999.

[5] P.V. Nickles et al., Phys. Rev. Lett., **78**, 2748-51 (1997).

[6] Atoms in Intense Laser Fields, M. Gavrila, ed., Academic Press, Boston (1992); I.P. Christov et al., Phys. Rev. Lett., **77**, 1743 (1996).

[7] M. Tabak et al., Phys. Plasmas, **1**,1625 (1994).

[8] PHELIX Petawatt High-Energy Laser for Heavy-Ion Experiments, GSI-REPORT 98-10, Gesellschaft fur schwerionenforschung, Darmstadt, December 1998.

[9] M.V. Ammosov, N.V. Delone, V.P. Krainov, Zh. Eksp. Teor. Fiz., **91**, 2008 (1986).

[10] N.E. Andreev, M.V. Chegotov, M.E. Veisman et al., JETP Lett., **68**, 592 (1998); Proceedings of SPIE, **3735**, 234 (1999).

[11] N.V. Delone, V.P. Krainov, Usp. Fiz. Nauk, **168**, 531 (1998)

[12] N.Krall and A.Trivelpiece, Principles of Plasma Physics, Academic Press, New York, 1973 [Russian translation, Mir, Moscow, 1975].

[13] M.J. Seaton, Mon. Not. Roy. Astron. Soc., **119**, 81 (1959).

[14] Ya.B. Zel'dovich, Yu.P. Raizer, Physics of Shock Waves and High-Temperature Hydrodynamic Phenomena, Academic Press, New York (1966).

[15] G.S. Sarkisov et al., JETP Lett., **66**, 828 (1997); **69**, 20 (1999).

[16] S. Dobosz et al., JETP Lett., **68**, 485 (1998); JETP, **88**, 1122 (1999).

On the effect of electron plasma waves with relativistic phase velocity on large-angle stimulated Raman scattering of modulated short laser pulse in plasmas

N.E.Andreev, S.Yu.Kalmykov
Institute for High Energy Densities, Associated Institute for High Temperatures, RAS,
Izhorskaya street 13/19, 127412 Moscow, Russian Federation

ABSTRACT

Suppression of a large-angle stimulated Raman scattering (LA-SRS) of a short modulated (two-frequency) laser pulse in a transparent plasma in the presence of a linear long-wavelength electron plasma wave (LW EPW) having relativistic phase velocity is considered under the conditions of weak and strong coupling. The laser spectrum includes two components with a frequency shift equal to the frequency of the LW EPW. The mutual influence of different spectral components of a laser on the SRS under a given angle in the presence of the LW EPW is examined.

1 INTRODUCTION

The stimulated Raman scattering through large angles of laser radiation in plasmas[1–3] is known to have a significant effect on a propagation of a short (< 1 ps) intense laser pulse in plasmas,[4,5] and, hence, on operation of various schemes of laser-plasma particle accelerators.[6] In order to optimize these schemes, one must clarify the conditions under which the detrimental pulse errosion due to the LA-SRS could be minimized.

We have shown previously[7–9] that certain nonlinear processes of a laser pulse evolution in a rarefied plasma can suppress the backward and near-backward SRS. Namely, when an amplitude modulation of a pulse occurs with a spatial period close to $\lambda_p = 2\pi c/\omega_{pe}$, where $\omega_{pe} = \left(4\pi e^2 n_0/m_e\right)^{1/2}$ is an electron plasma frequency corresponding to the electron background density n_0 (which is the case under the conditions of resonant self-modulation[10] of a pulse), the resonant suppression of the LA SRS of higher-frequency spectral components of the modulated pulse occurs.[8] We noted[7,8] that the self-modulation of a pulse is accompanied by the excitation of a large amplitude long-wavelength electron plasma wave with a phase velocity close to the group velocity of a pulse, hence, to ignore the influence of the LW EPW on the scattering process would be incorrect in many cases. We found[9] that the features of the LA-SRS of a monochromatic pulse (we denote its frequency ω_0, $\omega_0 \gg \omega_{pe}$) in the presence of the LW EPW whose phase velocity coincides with a group velocity of a laser radiation are follows:

- The Stokes band of the weakly coupled SRS [$a_1 = eE_1/(m_e\omega_0 c) \ll (\omega_{pe}/\omega_0)^{1/2}$, where a_1 is a normalized amplitude of the laser electric field] undergoes a suppression when a normalized amplitude of a density perturbation $N_{LW} \equiv \delta n_{LW}/n_0$ in a LW EPW becomes of order or exceeding the ratio ω_{pe}/ω_0; under the same condition the anti-Stokes branch appears.

Laser Optics 2000: Ultrafast Optics and Superstrong Laser Fields, Alexander A. Andreev, Vladimir E. Yashin, Editors, Proceedings of SPIE Vol. 4352 (2001) © 2001 SPIE · 0277-786X/01/$15.00

- For the limit of strong coupling $[(\omega_{pe}/\omega_0)^{1/2} < a_1 < 1]$, the density perturbation amplitude must be as large as $N_{LW} > (a_1\omega_{pe}/\omega_0)^{2/3} \gg \omega_{pe}/\omega_0$ to approximately halve the maximum increment of the LA SRS.

The suppression of the LA-SRS in the presence of the LW EPW is caused by the multi-wave nature of the process. In an unperturbed plasma, the weakly coupled LA-SRS is a three-wave resonant process, in which a pump EM wave $(\omega_0, \mathbf{k}_0)$ decays into a scattered EM wave $(\omega_0 - \omega_{pe},\ \mathbf{k}_s)$ and a plasma natural mode $(\omega_{pe},\ \mathbf{k}_e)$, where $\mathbf{k}_e = \mathbf{k}_0 - \mathbf{k}_s$. In a plasma perturbed by a LW EPW the phase modulation of scattering Langmuir waves[9,11] occurs. Then, the complex spectrum of scattering plasma waves $(\omega_{pe} + n\omega_{LW}, \mathbf{k}_e + n\mathbf{k}_{LW})$[11] participates in the scattering process. The sidebands (which are not natural plasma modes) are shifted to integer multiples of a frequency $\omega_{LW} \approx \omega_{pe}$ and wavenumber $k_{LW} \ll k_e$ of the LW EPW, and can exist only at the expense of the original natural Raman mode $(\omega_{pe}, \mathbf{k}_e)$, whose energy can be completely exhausted for $N_{LW} \sim \omega_{pe}/\omega_0$.[11] Hence, in the presence of a LW EPW, the transfer of the energy of the unstable plasma oscillations to a great number of satellites, which are not natural modes, dramatically decreases the growth rate of the instability.[9]

The results reported in the present paper substantially supplement the earlier investigations.[7–9] We have examined the spectral features of the LA-SRS of a modulated (two-frequency) laser pulse in a rarefied plasma in the presence of a given linear LW EPW with a phase velocity close (not necessarily equal) to the phase velocity of a laser pulse. In order to describe the LA-SRS of a laser pulse under the conditions of resonant self-modulation, the two-frequency pulse is considered with a frequency difference equal to the frequency of the LW EPW, which is close to the electron plasma frequency. Since the frequency difference of the laser spectral components (pump waves) is close to ω_{pe}, resonant suppression of the SRS of the higher-frequency pulse component[7,8] does not occur, because such effect necessitates the frequency difference of the pump waves close to $2\omega_{pe}$. In the presence of a given linear LW EPW, the convective amplification of the unstable modes in the frame of reference co-moving with the pulse is studied in the approximations of weak and strong coupling. In the regime of weak coupling, the dispersion analysis of the instability has shown that the Stokes components of scattered radiation from spectral components of the pulse are both suppressed provided $N_{LW} > \omega_{pe}/\omega_0$. The latter condition fulfilled, the anti-Stokes bands from both components of a pulse appear in the spectrum of scattered light (however, the anti-Stokes increments remain small if compared with the increments of the instability in a non-perturbed plasma). We have found that the LA-SRS of a higher-frequency pump wave undergoes more severe suppression in the presence of the LW EPW than the scattering of the lower-frequency one (it is notable that the increment of the latter even increases until $N_{LW} \leq 0.5\,\omega_{pe}/\omega_0$, and for larger N_{LW} the decrease occurs). The phenomenon of suppression is found to be almost independent on the detuning $\Delta\omega_{LW} \equiv \omega_{LW} - \omega_{pe}$ of a frequency of the LW EPW, which can occur in the process of the resonant self-modulation (in such case, $|\Delta\omega_{LW}| \ll \omega_{pe}$[12]). Under the conditions of strong coupling, when the scattering process is nonresonant in character, and its spectrum is much wider than the electron plasma frequency,[1,2] the instability experiences suppression for $N_{LW} > (a_1\omega_{pe}/\omega_0)^{2/3} \gg \omega_{pe}/\omega_0$ rather than for $N_{LW} \sim \omega_{pe}/\omega_0$.

2 BASIC EQUATIONS

To describe the LA SRS of a laser radiation in rarefied plasmas we represent a high-frequency (HF) electric field in a plasma as a sum of two components with close frequencies

$$\mathbf{a}(\mathbf{r},t) = \frac{1}{2}\left\{\mathbf{a}_0(\mathbf{r},t)e^{-i\omega_0 t + ik_0 z} + \mathbf{a}_s(\mathbf{r},t)e^{-i\omega_s t + i(\mathbf{k}_s,\mathbf{r})}\right\} + c.c., \tag{1}$$

where the dimensionless amplitudes of a laser pulse $\mathbf{a}_0 = e\mathbf{E}_0/(m_e\omega_0 c)$ and scattered radiation $\mathbf{a}_s = e\mathbf{E}_s/(m_e\omega_s c)$ are assumed to vary slowly in time and space on the scales $\omega_{0(s)}^{-1}$ and $k_{0(s)}^{-1}$, respectively. In the present report we consider the nonrelativistic electron motion in the electromagnetic field, so $|\mathbf{a}_{0(s)}| \ll 1$. Both incident and scattered radiation obey the dispersion relation for electromagnetic (EM) waves in plasmas $\omega_{0(s)}^2 = \left(k_{0(s)}c\right)^2 + \omega_{pe}^2$. Hence, in the case of strongly rarefied plasma $(\omega_{0(s)} \gg \omega_{pe})$, one can let, without loss of generality, $\omega_0 = \omega_s$ and

$|\mathbf{k}_s| \equiv k_s = k_0$ thus including possible deviation of a frequency and wave number of scattered radiation from ω_0 and k_0 in the spatio-temporal dependence of the envelope $\mathbf{a}_s(\mathbf{r},t)$. Hence, the wave vector of the scattered field is determined as $\mathbf{k}_s = (\mathbf{k}_{s\perp}, k_0\cos\alpha)$, where $|\mathbf{k}_{s\perp}| \equiv k_{s\perp} = k_0\sin\alpha$, and $\alpha \leq \pi$ is a scattering angle reckoned from the direction of a pulse motion. Since now, we consider the case of the linearly polarized laser light and analyze the SRS through a given angle in the plane orthogonal to the plane of the laser polarization ($\mathbf{k}_{s\perp} \perp \mathbf{a}_0$), where the coefficient of amplification of waves achieves a maximum.[5,9] Ponderomotive force at the beat frequency of incident and scattered EM waves excites an electron density perturbation with a chatacteristic wave vector $\mathbf{k}_e = \mathbf{e}_z k_0 - \mathbf{k}_s$ [so that $k_{ez} = 2k_0\sin^2(\alpha/2)$ and $k_e \equiv |\mathbf{k}_e| = 2k_0\sin(\alpha/2)$], which is responsible for the stimulated Raman scattering through an angle α:

$$\delta\tilde{n}_s(\mathbf{r},t) = \frac{1}{2}\,\delta n_s(\mathbf{r},t)e^{i(\mathbf{k}_e,\mathbf{r})} + c.c. \tag{2}$$

Assuming that the scattering angle is not small [$\sin(\alpha/2) \sim 1$], we suppose that the envelope of the scattering plasma waves $\delta n_s(\mathbf{r},t)$ is also slowly varying on the laser time and space period. Apart from the short-wavelength plasma waves, which participate in the scattering process, the short laser pulse can create a long-wavelength electron plasma density perturbations.[10,13] These long-wavelength electron plasma waves possess a relativistic phase velocity close to the group velocity of a laser pulse, and can be utilized in various schemes of plasma-based particle accelerators.[6] The electron density perturbations related with such waves may have an amplitude of order tens per cent of the background electron density.[14]

We will describe the SRS of a laser radiation under a given angle in a time scale short compared to the ion plasma period $\tau_i = 2\pi/\omega_{pi}$ [where $\omega_{pi} = (4\pi e^2 n_0/m_i)$ is an ion plasma frequency], using nonrelativistic hydrodynamic equations for a cold electron fluid with the immobile ion background and the Maxwell equations for scattered radiation. Apart from the scattering plasma waves (2), we account for the presence of a LW EPW in a plasma. We arrive at a pair of linear coupled equations for the amplitudes $\mathbf{a}_s$ and $N_s \equiv \delta n_s/n_0$, in which the electron quiver velocity $\tilde{\mathbf{v}}_{LW}(\mathbf{r},t)$ of the LW EPW enters ($\tilde{\mathbf{v}}_{\mathrm{LW}}$ known, corresponding long-wavelength electron density perturbation $\delta\tilde{n}_{\mathrm{LW}}(\mathbf{r},t)$ can be retrieved using the continuity equation):

$$i\left(\frac{\partial}{\partial t} + (\mathbf{v}_g,\nabla)\right)\mathbf{a}_s = \frac{\omega_{pe}^2}{4\omega_0}\mathbf{a}_0 N_s^*, \tag{3}$$

$$\left(\left(\frac{\partial}{\partial t} + (\tilde{\mathbf{v}}_{LW},\nabla) - i(\mathbf{k}_e,\tilde{\mathbf{v}}_{LW})\right)^2 + \omega_{pe}^2\right) N_s^* = -\frac{1}{2}(k_e c)^2(\mathbf{a}_0^*,\mathbf{a}_s). \tag{4}$$

In Eq. (3), $\mathbf{v}_g = c^2\mathbf{k}_s/\omega_0$ (as the limit of strongly rarefied plasma is under consideration, we set $|\mathbf{v}_g| = c$). The functions $\mathbf{a}_0(\mathbf{r},t)$ and $\tilde{\mathbf{v}}_{LW}(\mathbf{r},t)$ may be determined self-consistently, or be given in a certain form. In the latter case, Eqs (3) and (4) form the basis of a linear theory of the LA SRS in plasmas. Eq. (4) is linear in the amplitudes of the decay waves, and nonlinear in $\tilde{\mathbf{v}}_{LW}$. Generally, the LW EPW might be nonlinear wave, and $\tilde{\mathbf{v}}_{LW}$ may be represented as a row expansion in harmonics of ω_{LW} and k_{LW} whose amplitudes are expressed through powers of a normalized amplitude of the density perturbation $N_{LW} = \delta n_{LW}/n_0$ in a linear wave[11,15] [The connection between N_{LW} and $\tilde{\mathbf{v}}_{LW}$ in a linear wave is given by Eq. (9)]. In the present report we presume the LW EPW to be the linear wave. This is possible when the effect of the LW EPW nonlinearity on the scattering process is negligible, which necessitates the following limitation of the amplitude of the density perturbation[9]

$$N_{LW} < \left(\frac{\omega_{pe}}{\omega_0}\right)^{1/2}. \tag{5}$$

Throughout the present report, we meet the condition (5) and omit the term $(\tilde{\mathbf{v}}_{LW},\nabla)$ in the second-order operator of Eq. (4).[9] Further, for the sake of simplicity, we exclude the variable coefficient $\tilde{\mathbf{v}}_{LW}$ from Eq. (4) by means of a unitary replacement

$$\{\mathbf{a}_s, N_s^*\} = \left\{\hat{\mathbf{a}}_s, \hat{N}_s^*\right\}\exp\left(-i\tilde{\Psi}\right), \tag{6}$$

$$\tilde{\Psi} = -\int_0^t (\mathbf{k}_e,\tilde{\mathbf{v}}_{LW})\,d\tau,$$

which accounts for the phase modulation of the decay waves in the presence of the LW EPW. Since the transformation (6) preserves the absolute value, the instability onset may be studied in terms of the amplitudes $\left\{\hat{\mathbf{a}}_s, \hat{N}_s^*\right\}$. Instead z and t, it is convenient to use variables $\xi = z - ct$ and $\eta = t$ of the frame of reference co-moving with the pulse ($\mathbf{r}_\perp$ remains the same in both frames). When the change of variables is made, the equations for the amplitudes of the modulated waves read

$$i\left(\frac{\partial}{\partial\eta} + (\tilde{\mathbf{v}}_g, \tilde{\nabla})\right)\hat{\mathbf{a}}_s + \hat{\mathbf{a}}_s\left(\frac{\partial\tilde{\Psi}}{\partial\eta} + (\tilde{\mathbf{v}}_g, \tilde{\nabla})\tilde{\Psi}\right) = \frac{\omega_{pe}^2}{4\,\omega_0}\mathbf{a}_0\hat{N}_s^*, \tag{7}$$

$$\left(\left(\frac{\partial}{\partial\eta} - c\frac{\partial}{\partial\xi}\right)^2 + \omega_{pe}^2\right)\hat{N}_s^* = -\frac{1}{2}(k_e c)^2(\mathbf{a}_0^*, \hat{\mathbf{a}}_s). \tag{8}$$

Here, $\tilde{\mathbf{v}}_g = \left(c^2\mathbf{k}_{s\perp}/\omega_0, -2c\sin^2(\alpha/2)\right)$, $\tilde{\nabla} = (\partial/\partial\mathbf{r}_\perp, \partial/\partial\xi)$.

We consider below a given shape of both laser pulse and LW EPW thus neglecting their evolution on time scales of interest. The LW EPW is given to be one-dimensional, linear and free, with the electron quiver velocity

$$\tilde{\mathbf{v}}_{LW} = \mathbf{e}_z v_{ph\,LW} N_{LW}\cos\phi, \tag{9}$$

$$\phi = k_{LW}z - \omega_{LW}t + \varphi_0, \tag{10}$$

where $\varphi_0 = \text{const}$ is a constant phase shift of the LW EPW, and $v_{ph\,LW} = k_{LW}/\omega_{LW} \approx c$ is its phase velocity. We account for the possible deviation of a wave number and frequency of the LW EPW from the plasma wave number $k_p = \omega_{pe}/c$ and plasma frequency,[12] so that in Eq. (10) $k_{LW} \equiv k_p + \delta k_{LW}$, and $\omega_{LW} \equiv \omega_{pe} + \delta\omega_{LW}$. In order to make a dispersion analysis of the SRS instability of the laser pulse subjected to the resonant self-modulation, we consider a laser pulse which consists of two spectral components (pump waves) shifted to the frequency and wave number of the LW EPW:

$$a_0 = a_1 + a_2 e^{i\phi}, \tag{11}$$

where a_1 and a_2 are the constant amplitudes of the pump waves in the region $-L_{pulse} < \xi < 0$ (L_{pulse} is a longitudinal pulse length) and are zero outside this interval. The laser pulse with the envelope (11) consists of the components with a carrier frequency ω_0 and blue-shifted (anti-Stokes) frequency $\omega_0 + \omega_{LW}$. The representation (11) of a laser envelope corresponds to the three-dimensional regime of the self-modulation of a laser pulse with a power which is near critical for a relativistic self-focusing[14] and describes the on-axis structure of the pump field in that 3D regime (see Fig. 2 of Ref.[14]).

The pump field with an envelope (11) represents a pair of one-dimensional quasi-plane waves. As applied to the problem of scattering through large angles, such choice of the pulse envelope can be substantiated as follows. It was shown[3] that the LA-SRS of a laser pulse, which is bounded in two dimensions, enters the regime of steady-state spatial amplification in the co-moving variables as the time $\tau_0 = \max\left\{L_{pulse}/c, L_{pulse}/[2c\sin^2(\alpha/2)]\right\}$ passes since the pulse entered the plasma. It can be shown,[3,16] that the one-dimensional regime of spatial amplification dominates in a plasma, if the transverse dimension $L_\perp$ of a pulse is large enough to satisfy the inequality

$$L_\perp/L_{pulse} \gg \cot(\alpha/2). \tag{12}$$

Throughout this report we meet the condition (12), which supports the choice of the one-dimensional geometry of a pump field. In the one-dimensional regime, we will find the increments of spatial amplification of the unstable modes in the co-moving variables. These increments determine the maximum possible amplification of the unstable waves in the co-moving frame, rather than an exact structure of the scattered EM field, which depends on both shape of the laser pulse and boundary-value conditions at the pulse side boundaries.[16]

3 DISPERSION EQUATION

We substitute (9) and (11) into Eqs. (7) and (8) and make the Fourier transformation of the envelopes $\hat{\mathbf{a}}_s$ and $\hat{N}_s^*$ with respect to the transverse spatial variable

$$\left\{\hat{\mathbf{a}}_s, \hat{N}_s^*\right\}_{(\mathbf{r}_\perp,\xi,\eta)} = \int \left\{\hat{\mathbf{a}}_s, \hat{N}_s^*\right\}_{(\mathbf{k}_\perp,\xi,\eta)} e^{i(\mathbf{k}_\perp,\mathbf{r}_\perp)}\, d\mathbf{k}_\perp, \tag{13}$$

where $\mathbf{k}_\perp$ is a real vector, and represent the Fourier transformants in the Floquet form

$$\left\{\hat{\mathbf{a}}_s, \hat{N}_s^*\right\}_{(\mathbf{k}_\perp,\xi,\eta)} = \sum_j e^{-i\omega\eta + ik_j\xi} \sum_{n=-\infty}^{n=\infty} \left\{\hat{\mathbf{a}}_s^{(n)}, \hat{N}_s^{*(n)}\right\}_{(\mathbf{k}_\perp,k_j,\omega)} e^{in\phi}, \tag{14}$$

from which the recurrent relation for the ampliudes $\hat{\mathbf{a}}_s^{(n)}$ follows:

$$-Y^{(n-1)}\hat{\mathbf{a}}_s^{(n-1)} + X^{(n)}\hat{\mathbf{a}}_s^{(n)} - Y^{(n)}\hat{\mathbf{a}}_s^{(n+1)} = 0. \tag{15}$$

The dispersion equation for the infinite set of the coupled equations (15) is expressed through continued fractions

$$X^{(n)} = \frac{\left(Y^{(n)}\right)^2}{X^{(n+1)} - \dfrac{\left(Y^{(n+1)}\right)^2}{X^{(n+2)} - \ldots}} + \frac{\left(Y^{(n-1)}\right)^2}{X^{(n-1)} - \dfrac{\left(Y^{(n-2)}\right)^2}{X^{(n-2)} - \ldots}}. \tag{16}$$

Solution to the Eq. (16) $k_j(\omega, k_\perp)$ is a complex number; its positive imaginary part is an increment of spatial amplification, which corresponds to the solution growing towards the pulse trailing boundary. The functions, which enter (16), are defined in the following way:

$$\begin{aligned}
X^{(n)} &= D_1^{(n)} + \frac{\omega_{pe}^3}{2}\left(\frac{\beta_1}{D_{2(n)}^{(+)}D_{2(n)}^{(-)}} + \frac{\beta_2}{D_{2(n-1)}^{(+)}D_{2(n-1)}^{(-)}}\right), \\
Y^{(n)} &= \frac{\omega_{pe}}{2}\left[\mu\left(\frac{v_{ph\,LW}}{c} - \cos\alpha\right) - \frac{\omega_{pe}^2\sqrt{\beta_1\beta_2}}{D_{2(n)}^{(+)}D_{2(n)}^{(-)}}\right], \\
D_1^{(n)} &= \omega + ck_j - \Delta\omega_d + n\left(\omega_{LW} + \frac{\delta\omega_{LW} - c\delta k_{LW}}{1-\cos\alpha}\cos\alpha\right), \\
D_{2(n)}^{(\pm)} &= \omega_{pe} \pm (\omega + ck_j + n\omega_{LW}),
\end{aligned}$$

where $\Delta\omega_d \equiv (ck_\perp \sin\alpha - \omega\cos\alpha)/(1-\cos\alpha) = \omega_d - \omega_0$ is a frequency shift of the scattered light detected in the lab frame, $\beta_{1(2)} = \left(a_{1(2)}^2/2\right)(\omega_0/\omega_{pe})$ are the coupling coefficients of the waves, and $\mu = (\omega_0/\omega_{pe})N_{LW}$ is a normalized amplitude of the density perturbation in a given linear LW EPW. There is a principal difference in the behavior of the instability under the conditions of weak ($\beta_{1(2)} \ll 1$) and strong ($\beta_{1(2)} \gg 1$) coupling. These limits are investigated in the two following Sections.

4 LIMIT OF WEAK COUPLING

4.1 Frequency domains of the instability

In the limit of weak coupling ($\beta_{1(2)} \ll 1$), the instability onset is due to the resonant interaction of waves, which are close to the natural modes. This regime implies that the spatial growth rate remains much smaller than

the plasma wavenumber k_p. As the equations $D_1^{(n)} = 0$ and $D_{2(n)}^{(\pm)} = 0$ are the dispersion equations (written in the co-moving frame) for normal EM and electron plasma modes, the domains of parameters, in which the complex solutions $k_j(\Delta\omega_d)$ of Eq. (16) are to be searched for, are determined by the solutions to the following four sets of equations: (*a*) $D_1^{(0)} \approx 0$, $D_{2(0)}^{(+)} \approx 0$, (*b*) $D_1^{(0)} \approx 0$, $D_{2(0)}^{(-)} \approx 0$, (*c*) $D_1^{(1)} \approx 0$, $D_{2(1)}^{(+)} \approx 0$, (*d*) $D_1^{(1)} \approx 0$, $D_{2(1)}^{(-)} \approx 0$. Eq. (*a*) gives $\omega_d \approx \omega_0 - \omega_{pe}$ — the Stokes domain for the "red" (ω_0) pump wave; Eq. (*b*) gives $\omega_d \approx \omega_0 + \omega_{pe}$ — the anti-Stokes domain for the "red" pump wave; Eq. (*c*) gives $\omega_d \approx \omega_0 + \omega_{LW} - \omega_{pe}$ — the Stokes domain for the "blue" ($\omega_0 + \omega_{LW}$) pump wave; Eq. (*d*) gives $\omega_d \approx \omega_0 + \omega_{LW} + \omega_{pe}$ — the anti-Stokes domain for the "blue" pump wave.

4.2 Limit of small μ

For $\sqrt{\beta_{1(2)}} \ll \mu \ll 1$, one can retain in the expansion (14) the fundamental terms ($n = 0$) and a pair of additional terms, corresponding to $n = \pm 1$. With the account for those terms, the dispersion equation becomes

$$X^{(0)} = \frac{\left(Y^{(0)}\right)^2}{X^{(1)}} + \frac{\left(Y^{(-1)}\right)^2}{X^{(-1)}}. \tag{17}$$

While $\mu \ll 1$, there is no complex roots of (17) in the anti-Stoke regions, whereas in the Stokes domains the imaginary parts $\mathrm{Im}\, k \equiv \kappa(\Delta\omega_d)$ read as follows:

$$\kappa(\omega_d \approx \omega_0 - \omega_{pe}) = \frac{1}{2c}\sqrt{\tilde{\beta}_1\omega_{pe}^2 - [\omega_d - (\omega_0 - \omega_{pe})]^2}, \tag{18}$$

$$\kappa(\omega_d \approx \omega_0 + \delta\omega_{LW}) = \frac{1}{2c}\sqrt{\tilde{\beta}_2\omega_{pe}^2 - [\omega_d - (\omega_0 + \omega_{LW} - \omega_{pe})]^2}, \tag{19}$$

where $\tilde{\beta}_1 = \beta_1 R_1^{(+)}$, and $\tilde{\beta}_2 = \beta_2 R_2^{(-)}$. Here, $R_{1(2)}^{(\pm)}(\mu, \delta\omega_{LW}, \delta k_{LW})$ are the renormalizing functions for the coupling coefficients in the presence of the LW EPW:

$$R_{1(2)}^{(\pm)} = \frac{1 \pm \mu\sqrt{\dfrac{\beta_{2(1)}}{\beta_{1(2)}}}\left(\dfrac{v_{ph\,LW}}{c} - \cos\alpha\right)\left(1 + \dfrac{\delta\omega_{LW}}{\omega_{pe}} + \dfrac{\delta\omega_{LW}\cos\alpha - c\delta k_{LW}\sin\alpha}{\omega_{pe}(1-\cos\alpha)}\right)}{1 + \dfrac{\mu^2}{2}\left(\dfrac{v_{ph\,LW}}{c} - \cos\alpha\right)^2}. \tag{20}$$

As it follows from (20), with the increase in μ the monotonic decrease of the coupling coefficient $\tilde{\beta}$ occurs in case the pulse is monochromatic (when either β_1 or β_2 equals zero); the correction quadratic in μ reduces the maximum of the increment. In the case of the two-frequency pulse an asymmetry appears in the dependence on μ of the coupling coefficients $\tilde{\beta}_1$ and $\tilde{\beta}_2$. That is, on the contrary to the case of a monochromatic pulse, the coupling coefficient $\tilde{\beta}_1$, which corresponds to the "red" pump wave, grows with μ when $\mu \ll 1$, and in the presence of the "blue" pump wave the increment (18) increases due to the linear correction in μ. On the other hand, the increment (19) of the SRS from the "blue" pump wave decreases even faster than in the case of the monochromatic pulse; that is, the negative correction to this increment is also linear in μ rather than quadratic. Note that the angular dependence of the increments (18) and (19) emerge only in the presence of the LW EPW; in a non-perturbed plasma (i. e. in the absence of LW EPW) the increment of the spatial growth in the one-dimensional regime of the LA-SRS is independent on scattering angle.[3,9,16]

4.3 Numerical solutions of the dispersion equation for arbitrary μ

In the case of arbitrary μ restricted from above by the value $(\omega_0/\omega_{pe})^{1/2}$ [see (5)], the dispersion equation (16) is solved numerically, and its complex solutions are searched for in both Stokes and anti-Stokes regions defined

above in the Subsection 4.2. Previously,[9] for the LA-SRS of a monochromatic pulse in the presence of a given linear LW EPW with a phase velocity equal c (namely, $\omega_{LW} = \omega_{pe}$, and $k_{LW} = k_p$), the suppression of a Stokes and generation of the anti-Stokes branches of the instability were established. As is already noted in the Introduction, the suppression of the instability is connected with the participation in the scattering process of new short wavelength satellites $(\omega_{pe} + n\omega_{LW}, \mathbf{k}_e + n\mathbf{k}_{LW})$, $n \neq 0$, which appear as a consequence of periodic spatio-temporal phase modulation (6) of scattering plasma waves in the presence of a LW EPW. The satellites (which are not natural plasma modes) gain the energy from the original eigenmode $(\omega_{pe}, \mathbf{k}_e)$, which is resonantly driven by the ponderomotive force at the beat frequency $(\approx \omega_{pe})$ of incident and scattered EM waves. Therefore, the energy, which in in the absence of LW EPW would be transfered to the single mode of plasma oscillations, is expended in excitation of a large number $(n \sim \mu^2 \gg 1)$ of plasma modes (*not* natural modes), which causes the dramatic decrease in the increment.

We investigate first how the phenomenon of suppression is affected by the additional component in the pulse spectrum. Numerical solution to the Eq. (16) yields the dependence on μ of the spatial increments, corresponding to the Stokes and anti-Stokes bands from both spectral components (ω_0 and $\omega_0 + \omega_{LW}$) of a pulse. These dependencies corresponding to the central frequencies of both Stokes and anti-Stokes bands are shown for $v_{ph\,LW} = c$ and $\alpha = \pi$ (direct backscatter) in Fig. 1 ("red" pump wave) and Fig. 2 ("blue" pump wave). In these Figures suppression of the Stokes branches of the instability as well as generation of the anti-Stokes branches are clearly seen for $\mu > 1$. The anti-Stokes branches are, in turn, suppressed for $\mu > 2$. In the case of a two-frequency pump, the Stokes increment of the "red" pump wave increases until $\mu < 0.5$ and then drops [see Fig. 1(a)]. The Stokes increment of the "blue" pump wave experiences more severe suppression than in the case of the monochromatic pulse [compare Fig. 1(a) and 2(a) for $\beta_1 = \beta_2$]. The linear growth with μ of the "red" pump wave increment and linear decrease in the increment of the "blue" pump wave for small μ are discussed in the previous Subsection and described by formulas (18)-(20).

The self-modulation of the laser pulse can be accompanied by shifts in frequency and wave number of the LW EPW from the resonant values ω_{pe} and k_p,[12] which can also exert some influence on the scattering process. We have considered the effect of the frequency detuning $\delta\omega_{LW}$ on the increments of backward SRS ($\alpha = \pi$) of a single pump wave ($\beta_2 = 0$). The increments corresponding to the centers of the Stokes and anti-Stokes lines are shown in Fig. 3. The curves shown in Fig. 3 correspond to small frequency shifts ($\delta\omega_{LW} \ll \omega_{pe}$), as in most regimes of a pulse self-modulation these shifts are indeed small if compared to the electron plasma frequency in the rarefied plasmas. In particular, an electron plasma should be too dense ($n_0 \approx 0.2 n_c$) to make the frequency shift $\delta\omega_{LW} = (\omega_{pe}/2)(\omega_{pe}/\omega_0)^3$ (which corresponds to the 1D-2 regime of the self-modulation[12]) equal the quite moderate value $\delta\omega_{LW} = 0.05\omega_{pe}$ used in the calculation of Fig. 3. As is clear from Fig. 3, the influence of a frequency shift $\delta\omega_{LW} \ll \omega_{pe}$ on the suppression of the SRS-instability does not produce significant changes in the effect of suppression.

The effect of suppression of the SRS-instability also depends on the angle between $\mathbf{k}_e$ and $\tilde{\mathbf{v}}_{LW}$ [in the geometry accepted in the present paper, this angle coincides with the scattering angle – see Eq. (4)]. Reduction of the scattering angle (then, $|\mathbf{k}_e|_{\alpha \to 0} \to 0$) makes the influence of the LW EPW on the scattering process less pronounced, as is seen in Fig. 4. Thus, the fraction of the energy losses due to the side-scattering becomes more pronounced in the presence of a LW EPW.

To conclude the discussion of the limit of weak coupling, let us consider a certain regime of the laser pulse self-modulation in which the discovered effect of suppression of the LA SRS would be observed. That is, in the known 3D regime of the self-modulation of a laser pulse with a power close to the critical power for the relativistic self-modulation,[14] the laser spectrum consists of the component with the carrier frequency and the anti-Stokes component blue-shifted to the plasma frequency [the on-axis pulse structure is described approximately by the dependence (11)]. For such regime of the self-modulation instability, the numerical modelling[14] performed for a plasma and laser parameters such that $\omega_0/\omega_{pe} = 20$, $\beta_1 = 0.256$, and $\kappa L_{pulse} \approx 13.5$ (hence, the LA SRS of such pulse is in the weakly coupled regime and is far from the nonlinear saturation) gives the maximum amplitude of the electron density perturbation $N_{LW} \approx 0.1$ {under the parameters of modelling,[14] N_{LW} remains less than $(\omega_{pe}/\omega_0)^{1/2} \approx 0.22$ [see Eq. (5)], which yet allows us to use the linear approximation (9) for the LW EPW}. The

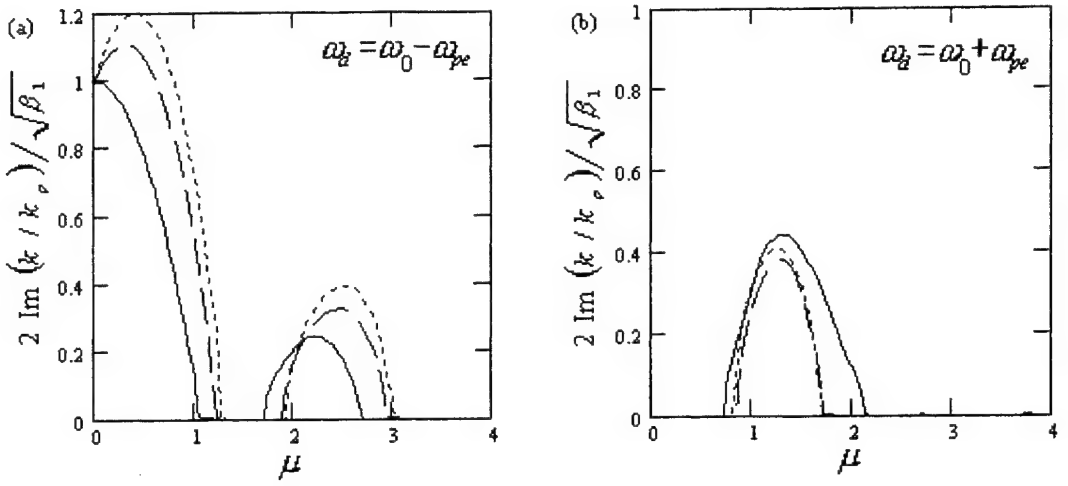

Figure 1. Maximum increments of the Stokes (a) and anti-Stokes (b) bands of backscatter ($\alpha=\pi$) of the "red" spectral component of a pulse (ω_0) versus $\mu=(\delta n_{LW}/n_0)(\omega_0/\omega_{pe})$. The amplitude of the "blue" pulse component ($\omega_0+\omega_{pe}$) is such that $\beta_2=0$ (monochromatic pulse, solid line), $\beta_2=0.5\beta_1$ (dashed line), $\beta_2=\beta_1$ (dotted line).

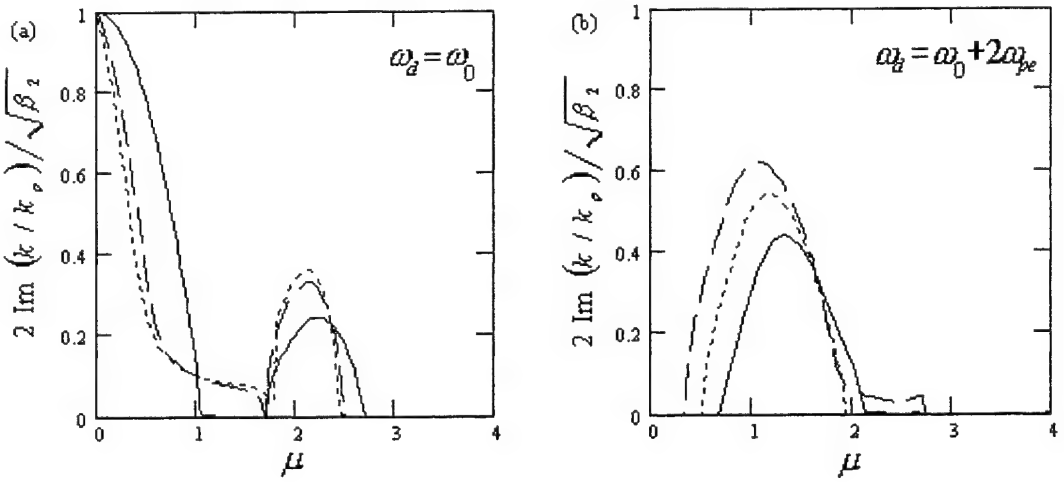

Figure 2. Maximum increments of the Stokes (a) and anti-Stokes (b) bands of backscatter ($\alpha=\pi$) of the "blue" spectral component of a pulse ($\omega_0+\omega_{pe}$) versus $\mu=(\delta n_{LW}/n_0)(\omega_0/\omega_{pe})$. The amplitude of the "red" component (ω_0) is such that $\beta_1=0$ (monochromatic pulse, solid line), $\beta_1=0.5\beta_2$ (dashed line), $\beta_1=\beta_2$ (dotted line).

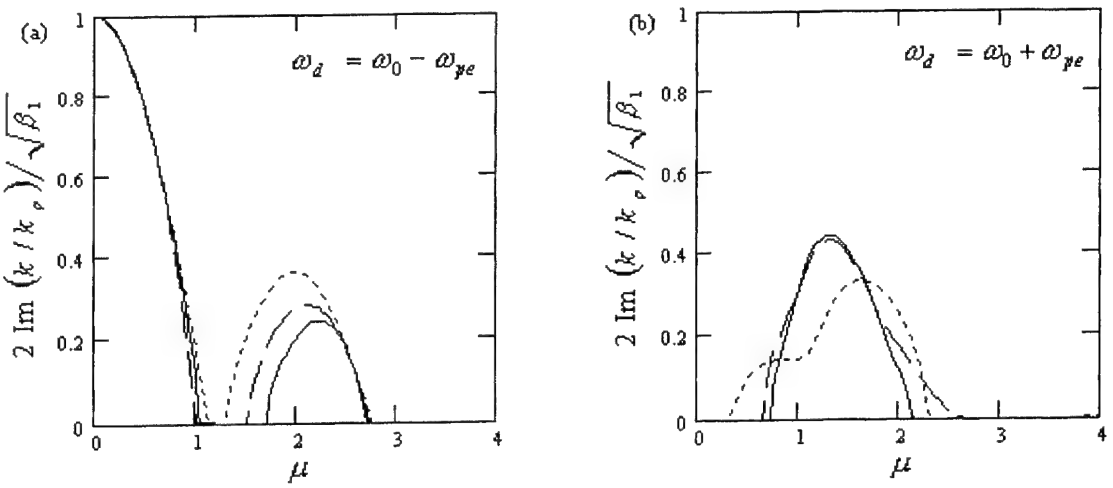

Figure 3. Maximum increments of the Stokes (a) and anti-Stokes (b) bands of backscatter ($\alpha=\pi$) of a single-frequency pulse versus $\mu=(\delta n_{LW}/n_0)(\omega_0/\omega_{pe})$. The detuning of a frequency of the LW EPW from the resonant value ω_{pe} equals zero (solid line), $0.01\omega_{pe}$ (dashed line), $0.05\omega_{pe}$ (dotted line).

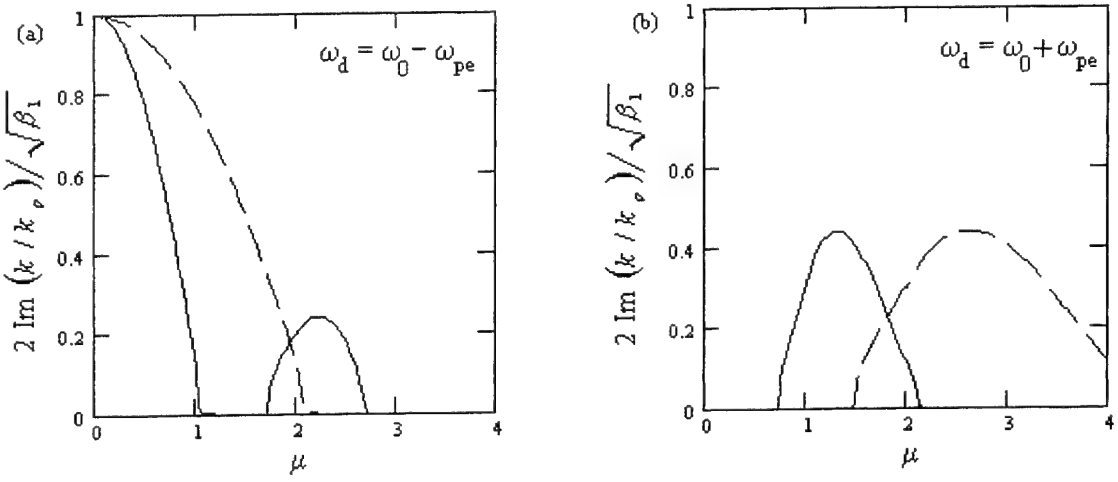

Figure 4. The influence of the reduction of the scattering angle ($\alpha=\pi$- solid line, $\alpha=\pi/2$- dashed line) on the SRS of a monochromatic pulse in the presence of the LW EPW. The normalized amplitude of the density perturbation $\mu=(\delta n_{LW}/n_0)(\omega_0/\omega_{pe})$, which corresponds to the first vanishing of the Stokes increment, grows with the decrease in the scattering angle.

maximum value of the density perturbation achieved in the considered regime of the laser pulse self-modulation yields $\mu \approx 2$, and it is evident that the suppression of the LA SRS is possible under such conditions.

Let us sum up the basic features of the LA-SRS of a two-frequency pulse in the presence of a LW EPW having a phase velocity close to the group velocity of a pulse.

- The most significant effect of the LW EPW on the scattering process in the limit of weak coupling is the suppression of the Stokes and generation of the anti-Stokes branches of the instability provided the normalized electron density perturbation N_{LW} in the LW EPW exceeds the value ω_{pe}/ω_0; in strongly rarefied plasmas $(n_0/n_c < 10^{-2})$ the suppression occurs for a quite moderate density perturbation $N_{LW} < 0.1$.
- The mutual influence of the spectral components of the pulse shifted to the frequency close to ω_{pe} leads to the asymmetry of the suppression of the SRS of different components: The maximum of the Stokes increment of the lower-frequency pump component slightly grows for $N_{LW} < 0.5\,\omega_{pe}/\omega_0$, and for larger N_{LW} the suppression follows (for $N_{LW} > \omega_{pe}/\omega_0$); the maximum of the Stokes increment of the higher-frequency pump component undergoes mononotonic decrease with N_{LW} for $\mu < 1$ and more severe suppression than in the case of the monochromatic pulse.
- The effect of suppression is almost independent on the detuning of a phase velocity of the LW EPW from the group velocity of a pulse if $\left|v_{ph\,LW} - c\right| \ll c$.
- Reducing the scattering angle makes the effect of suppression less pronounced, and the density perturbation amplitude N_{LW}, at which the Stokes increments vanish for the first time, grows.

5 LIMIT OF STRONG COUPLING

In the limit strong coupling ($\beta_{1(2)} \gg 1$), scattering plasma waves are not natural modes. In the case of a single-frequency pulse ($\beta_2 = 0$), the scattered radiation in a plasma without LW EPW has a wide-spread (if compared to ω_{pe}) spectrum, which is extended to the blue side: $\omega_0 - (3/2)\sqrt[3]{\beta_1}\omega_{pe} \le \omega_d \le \omega_0 + (1/2)\beta_1\omega_{pe}$. The maximum value of the increment $\kappa_0 = (\sqrt{3}/2)k_p(\beta_1/2)^{1/3}\left[1 - (2\beta_1^2)^{-1/3}\right] \gg k_p$,[5,9] which can be obtained from the dispersion equation $X^{(0)} = 0$, corresponds to the frequency $\omega_d = \omega_0$. For a two-frequency pulse with a frequency difference small compared to $\sqrt[3]{\beta_1}\omega_{pe}$, and close amplitudes of the spectral components, the spectral width and maximum increment can be described by the above dependencies with β_1 replaced by $\left(\sqrt{\beta_1} + \sqrt{\beta_2}\right)^2$.

When a plasma is perturbed by a small-amplitude LW EPW such that $\mu \ll \beta_{1(2)}^{1/6}$, one may obtain from Eq. (17) the correction to the increment κ_0 which accounts for the influence of the LW EPW on the strongly coupled LA-SRS. In the case of a monochromatic pulse the corrected increment reads

$$\kappa = \kappa_0 - \mu^2 \frac{3\sqrt{3}}{8} k_p \left(\frac{\beta_1}{2}\right)^{-1/3}. \tag{21}$$

Eq. (21) proves to be useful for estimation of the effect of a LW EPW on the strongly coupled LA SRS even far beyond its strict validity region. So, expression (21) predicts a decrease in $\kappa(\omega_d = \omega_0)$ when $\mu \approx \sqrt[3]{\beta_1}$, or $N_{LW} \sim \left(a_0\omega_{pe}/\omega_0\right)^{2/3}$. This prediction is confirmed in part by the results of numerical solution to the general dispersion equation (16). The increments were calculated using (16) for both single-frequency (ω_0) and two-frequency ($\omega_0 + \omega_{pe}$) pulses. The dependencies $\kappa(\omega_d = \omega_0)$ versus μ, which are drawn for a direct backscatter ($\alpha = \pi$), are seen in Fig. 5. The curves shown in Fig. 5 demonstrate the reduction in the increment of the strongly coupled SRS for both single- and two-frequency pulse. Although the complete suppression of the SRS of a single-frequency pulse does not occur, the decline by nearly one half of the growth rate of the SRS-instability is the case, in accordance with the approximate expression (21), for $\mu \approx \sqrt[3]{\beta_1}$, or $N_{LW} \sim \left(a_1\omega_{pe}/\omega_0\right)^{2/3}$.

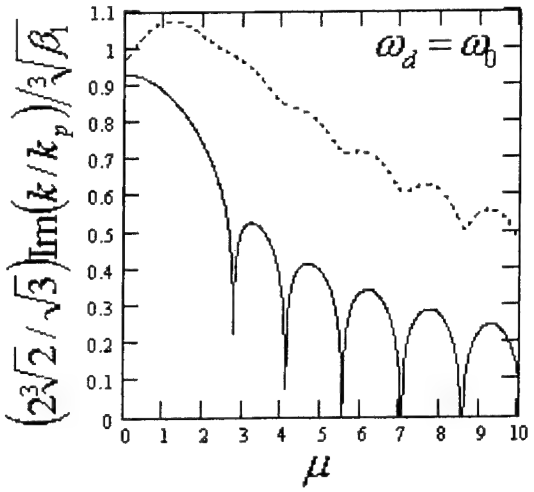

Figure 5. The spatial increment $\kappa(\omega_d = \omega_0)$ of the direct backscattering ($\alpha=\pi$) under the conditions of strong coupling, which correspond to β_1=20, β_2=0 (monochromatic pulse, solid line), and $\beta_1=\beta_2$=20 (two-frequency pulse with a frequency difference equal to ω_{pe}, dashed line), versus the normalized amplitude of the density perturbation $\mu=(\delta n_{LW}/n_0)(\omega_0/\omega_{pe})$.

To illustrate the effect of suppression of the LA SRS under the condition of strong coupling, let us consider the long laser pulse ($L_{pulse} > \lambda_p$) with a sharp leading edge ($L_{front} < 0.5\lambda_p$), which excites in a plasma a LW EPW whose amplitude is approximately equal to $N_{LW} = (a_1/2)^2$.[13] Leaving aside the fact that such a plasma wave can itself seed a laser pulse self-modulation, we consider first an influence of this wave on the LA SRS of a monochromatic laser pulse with a given rectangular envelope (this is valid on time scales larger than a pulse duration, but small enough for the development of the self-modulation, and corresponds to the early stage of the self-modulation instability). The normalized amplitude of density perturbation $N_{LW} = (a_1/2)^2$ gives $\mu = \beta_1/2$, which, under the conditions of strong coupling, is significantly larger than that is necessary to halve the maximum increment [i.e. $\mu \approx \sqrt[3]{\beta_1}$ and $N_{LW} \approx (a_1\omega_{pe}/\omega_0)^{2/3}$]. Using the dependencies plotted in Fig. 5, we find that the increment of direct backscattering $\kappa(\omega_d = \omega_0, \alpha = \pi)$ takes at $\mu = \beta_1/2 = 10$ the value equal to approximately one fifth of its value in an unperturbed plasma. Now it is clear that the strongly coupled LA SRS of a pulse with a sharp leading edge can be suppressed at the very beginning of the self-modulation process. However, the important requirement of linearity of the LW EPW (5) should be met, which limits the density perturbation amplitude $N_{LW} < (\omega_{pe}/\omega_0)^{1/2}$, and, hence, the amplitude of the laser $a_1 < 2\,(\omega_{pe}/\omega_0)^{1/4}$. In the case of more intense laser, one must account for the effect of harmonics of a nonlinear LW EPW on the scattering process along with the effect of the linear component (9) of the LW EPW excited by the front edge of the laser pulse. This can drastically modify the suppression of the scattering process. As is seen in the results of modelling[17] of the LA-SRS of a short ($L_{pulse} \sim \lambda_p$) relativistically strong ($a_1 \sim 1$) laser pulse generating a strongly nonlinear LW EPW, significant variations of a spectral shape of LA-SRS were established[17] depending on a pulse length and intensity in the parameter regions $\beta > 50$ (hence, $\mu > 25$), and $\omega_0/\omega_{pe} > 20$ rather than suppression of the instability.

6 CONCLUSION

The results reported in the present paper clearly point to the fact that in the presence of a linear LW EPW the LA-SRS of a two-frequency laser pulse acqires new specific features. That is, under the conditions of weak coupling the instability undergoes suppression when a density perturbation in the LW EPW exceeds the value, which for rarefied plasmas ($n_0/n_c \approx 10^{-2}$) represents about ten per cent of the background electron plasma density. Mutual

influence of diffrent spectral components of a laser pulse shifted to approximately ω_{pe} retains the common features of the suppression effect the same as in the case of monochromatic pulse, except the somewhat asymmetry in the behavior of the increments of different pump components at $N_{LW} \ll \omega_{pe}/\omega_0$. As the scattering angle reduces, the suppression becomes less pronounced in comparison with the case of direct backscatter (thus, in the presence of the LW EPW the fraction of the energy losses due to the side-scatter increases). Besides, in the anti-Stokes ranges corresponding to each pump spectral component new branches of the instability appear (however, with an increment small in comparison to the conventional increment of the LA-SRS in a non-perturbed plasma). Under the condition of strong coupling the complete suppression of the instability is not the case; though, the significant reduction of the increment is the case for $N_{LW} \sim (a_1\omega_{pe}/\omega_0)^{2/3}$. In the case of the wake-field excitation by the sharp leading edge of a pulse [then, $N_{LW} = (a_1/2)^2$], when the condition of strong coupling fulfulled, the increment of the SRS falls approximately to one fifth of the value corresponding to an unperturbed plasma. This work was supported in part by the Russian Foundation for Basic Research under Grant no. 98-02-16263.

7 REFERENCES

[1] N. Bloembergen and Y. R. Chen, Phys. Rev. **141**, 298 (1966); N. E. Andreev, Sov. Phys. JETP **32**, 1141 (1971); D. W. Forslund, J. M. Kindel, and E. L. Lindman, Phys. Fluids **18**, 1002 (1975).

[2] T. M. Antonsen Jr. and P. Mora, Phys. Fluids B **5**, 1440 (1993); P. Mounaix, D. Pesme, W. Rosmus, and M. Casanova, Phys. Fluids B **5**, 3304 (1993); P. Mounaix and D. Pesme, Phys. Plasmas **1**, 2579 (1994).

[3] C. J. McKinstrie, R. Betti, R. E. Giacone, T. Kolber, and E. J. Turano, Phys. Rev. E **51**, 3752 (1995); C. J. McKinstrie, and E. J. Turano, Phys. Plasmas **4**, 3347 (1997).

[4] A. S. Sakharov and V. I. Kirsanov, Phys. Rev. E **49**, 3274 (1994).

[5] N.E. Andreev, V.I. Kirsanov, and L.M. Gorbunov, Phys. Plasmas 2 (1995) 2573.

[6] E. Esarey, P. Sprangle, J. Krall, and A. Ting, IEEE Trans. Plasma Sci. **PS-24**, 252 (1996).

[7] N. E. Andreev and S. Yu.Kalmykov, in *Laser Optics'95 and ICONO'95: Superintense Laser Fields*, A. A. Andreev and V. M. Gordienko, Editors, Proc. SPIE **2770**, 53 (1996).

[8] N. E. Andreev and S. Yu.Kalmykov, Phys. Lett. **227**A, 110 (1997); Plasma Phys. Rep. **24**, 862 (1998).

[9] N. E. Andreev and S. Yu.Kalmykov, IEEE Trans. Plasma Sci. **PS-28**(4) (2000).

[10] N. E. Andreev, L. M. Gorbunov, V. I. Kirsanov, A. A. Pogosova, and R. R. Ramazashvili, JETP Lett. **55**, 571 (1992); T. M. Antonsen Jr. and P. Mora, Phys. Rev. Lett. **69**, 2204 (1992); P. Sprangle, E. Esarey, J. Krall, and G. Joyce, Phys. Rev. Lett. **69**, 2200 (1992).

[11] M. J. Everett, A. Lal, C. E. Clayton, W. B. Mori, T. W. Johnston, and C. Joshi, Phys. Rev. Lett. **74**, 2236 (1995); Phys. Plasmas **3**, 2041 (1996).

[12] N. E. Andreev, V. I. Kirsanov, L. M. Gorbunov, A. A. Pogosova, and A. S. Sakharov, Plasma Phys. Rep. **22**, 379 (1996).

[13] L. M. Gorbunov and V. I. Kirsanov, Sov. Phys. JETP **66**, 290 (1987); in *Proceedings of the Lebedev Physics Institute*, vol. 213, O. N. Krokhin, Ed. New York: Nova Science Publishers, Inc., 1993, pp. 1-86.

[14] N. E. Andreev, V. I. Kirsanov, and A. S. Sakharov, Plasma Phys. Rep. **23**, 270 (1997).

[15] E. A. Jackson, Phys. Fluids **3**, 831 (1960); C. J. McKinstrie and D. W. Forslund, Phys. Fluids **30**, 904 (1987).

[16] S. Yu. Kalmykov, Plasma Phys. Rep. **26**(11) (2000).

[17] A. S. Sakharov, N. M. Naumova, and S. V. Bulanov, Plasma Phys. Rep. **24**, 818 (1998); A. S. Sakharov, Plasma Phys. Rep. **26**(8), 657 (2000).

Study of efficiency of the thermonuclear burning in laser targets with fast ignition

Aleksey A. Levkovskii*[a], Aleksandr A. Andreev[b], Dmitrij V. Il'in[a], Vladimir E. Sherman[a], Oleg B. Vygovskii[a] , Vladislav B. Rozanov[c], Sergei Yu. Gus'kov[c]

[a]St.-Petersburg Institute of Machine Building, Department of Physics, 14, Polustrovsky, St.-Petersburg, 195108, Russia

[b]S.I. Vavilov State Optical Institute, 12, Birzhevaja, St-Petersburg, 199034, Russia

[c]P.N.Lebedev Physical Institute RAS, 53,Leninsky prospect, Moscow B-333, 117924, Russia

ABSTRACT

By means of Monte-Carlo modeling of thermonuclear (TN) burn wave propagation in isochoric spherical laser deuterium-tritium targets criteria of fast ignition are elaborated and corresponding energy gain is evaluated. It is shown that the target thermonuclear (TN) burning is independent on ignitor presence if the ignitor areal density and temperature are lower than the critical ones. In the opposite case TN flash results in effective burning with the gain $G\sim10^3$, and the TN energy release is practically independent on the further increase of ignitor parameters. The critical ignitor parameters are calculated for targets with different parameters of main fuel The overcritical target gain is practically independent on ignition origin and may be evaluated with a good accuracy by the simple asymptotic expression. It is shown that the energy coupled to ignitor with critical ignitor parameters tends to some minimum value in the limit of small ignitor mass. The corresponding values of energy are obtained as a function of the temperature of the main fuel. Under these optimum ignition conditions the parameters of extra laser pulse are evaluated taking into account the fast ions energy transport mechanism.

Keywords: laser fusion, spark ignition, fast ignition, thermonuclear burning, energy gain

1. INTRODUCTION

The Fast Ignitor concept is widely discussed recently as one of the most perspective way to produce effective laser confinement fusion (LCF)[1]. Deuterium - tritium capsule is imploded by the main driver to assemble high density configuration as in the conventional approach but with relatively low temperature. The ignition of the fuel is due to extra ultrashort laser pulse of ultrahigh intensity with an energy of several or few tens of kilojoules. The mechanism of conversion the ignition laser energy into the energy of target fast ions is expected to be sufficiently effective to deliver the ignition energy to the fuel[2]. If successful, the fast ignition scheme drastically reduces the difficulty of the compression and can possibly lead to high gain with relatively small energy of implosion driver.

In the present report we consider some aspects of the gain model describing the fast ignition approach to inertial fusion. The study of thermonuclear (TN) burning of inhomogeneously heated targets gives the possibilities to calculate the ignitor parameters setting off high TN gain and as a result to evaluate the required laser pulse parameters both of main driver and of ignition laser.

2. PHYSICAL-MATHEMATICAL MODEL

In the fast ignition scheme the ignition energy is suggested to deliver sufficiently rapidly and the gain can be calculated with isochoric (uniform density) model, where the hot spot and main fuel are out of pressure equilibrium[1,3]. In original scheme[1] the other parameters of ignitor and main fuel were chosen in the following way. An average temperature T_f and areal density $(\rho r)_f$ of hot spot were determined by well-known criterion of TN flash corresponding to isolate plasma self-heating by α particle energy: $T_f \sim 5$ keV; $(\rho r)_f \sim 0.3\text{-}0.4$ g/cm^2 . (Here and all through the report the values relating to the ignitor are indicated by the subscript f). The internal energy of ignitor E_f at fixed $(\rho r)_f$ is inversely proportional to ρ^2 . The cold main fuel was suggested to be in the state near to degenerate one and to be approximately ten times as large as ignitor. The energy of the main fuel was dominated by the electron Fermi-energy: $E \sim \rho^{2/3} M$, where M is the mass of the fuel. By means of

Laser Optics 2000: Ultrafast Optics and Superstrong Laser Fields, Alexander A. Andreev, Vladimir E. Yashin, Editors, Proceedings of SPIE Vol. 4352 (2001) © 2001 SPIE · 0277-786X/01/$15.00

density variation the gain was maximized for fixed energy coupled to the target[1]: $G = 3*10^4 (E_0)^{0.4}$, $\rho = 33(E_0)^{-0.5}$ (E_0 in MJ). The target TN energy gain G is determined in the presented paper as $G = E_{tn}/E_0$, where E_{tn} is the released TN energy.

Both parameters of the ignitor and of the main fuel should be revised from our point of view. Firstly, conditions of plasma self-heating are not the same for an isolate plasma and for the hot spot in cold plasma because ignitor is cooled by contact with surrounding plasma due to electron heat conductivity. So, for example, the qualitative estimations of the isobaric ignitor parameters obtained in our previous papers[4, 5] in the frame of semianalytical approaches give for minimum ignitor temperature T_f the value greater by several fold as that giving in the paper[1]. On the other hand the increase in ignitor temperature T_f at initial moment is not the necessary condition of TN flash. Numerical calculations[6,7] show that a burn wave under certain initial conditions goes through two stages. The initial "subsonic" stage is characterized by a dropping or slightly rising temperature behind the wave front. The dimensions of "smoldering" ignitor are increased preparing the conditions of the second "supersonic" stage of intense burning which give rise to the TN flash. It is quite sufficiently for the spark ignition if the duration of "subsonic" stage would be far less than the target hydrodynamic lifetime. The critical minimum ignitor parameters depend on the parameters of main fuel. One of the main purpose of this paper is to obtain these dependencies.

Secondly, on the assumption that the energy of the main fuel is dominated by the electron Fermi-energy, the density dependence of the total internal energy in compressed target takes the form: $E_0 = A\rho^{-2} + B\rho^{2/3}$. It easy to see[1] that if the gain is optimized then ignitor energy ($E_f = A\rho^{-2}$) and energy of the main fuel are comparable i.e. an extra laser pulse energy is of the same order that the energy of the main driver in contradiction with fast ignition concept. Besides, realization of the target implosion with degenerate final state is very questionable. In the present work the main fuel is supposed to be in the non-degenerate state which temperature T_0 is one of the free parameters of problem. The gain is reduced in compare with optimized value but the ignitor energy is limited by a few percent of total energy. We consider these conditions as more realistic.

The theoretical analysis of TN burning in non-degenerate fuel is drastically different from that of original scheme[1]. In spite of appearance the additional parameter (main fuel temperature) the situation is in some sort more simple. It is just obvious that in this case at fixing areal densities and temperatures of ignitor and fuel the target density ρ plays a role of the scale for other physical quantities only. For example the mass is proportional to $(\rho r)^3/\rho^2$; the target lifetime $\Delta t \sim r/v \sim (\rho r)/\rho T^{1/2}$ where v is a mean speed of sound; $E_0 \sim MT \sim \rho^{-2}$ and so on. The process of TN burning is approximately scale invariant in terms of variables: $r^* = \rho r$; $t^* = \rho t$; $E^* = \rho^2 E$; $M^* = \rho^2 M$. In particular at given areal densities and temperatures the target gain is approximately independent on ρ and hence on initial target energy E_0 in contrast to original scheme[1]. The exact scale invariance is violated only by density dependencies of Coulomb logarithms. Our numerical calculations are in good agreement with this conclusion.

The calculations of energy gain are carried out by means of TN burning simulation from the moment of isochoric hot spot generation up to the target destruction. The similar results for isobaric and volume ignition were presented in preceding papers[8,9]. Mathematical model of the TN burning of inhomogeneous spherical target is described by equations system of motion, energy balance, continuity, state and kinetic equations for fast TN particles[10,11]. The single-fluid, two-temperature plasma approximation with allowance made for ion-electron energy exchange and for electron and ion heat conductivity is used in the solution of hydrodynamic equations.

The kinetic processes with fast TN particles and thermal X-rays are characterized by sharp gradients of density and temperature with the scales of the order of particle range, by substantially anisotropy of particles angle distribution, by complicated energy dependence of charged particles energy loss, and by presence of a set of correlated channels of primary and secondary TN reactions. Under the conditions the Monte-Carlo method for the kinetic processes simulation seems to be more convenient than other standard computational schemes. As the characteristic time of target hydrodynamic processes is much more than the TN particle transit time, the plasma parameters may be considered as a constant under kinetic process simulation on each time step of a well-known difference non-stationary scheme for medium equations. These approximations are realized in TERA code using in presented paper for self-consistent solution of kinetic and hydrodynamic equations system. For detailed description of the physical-mathematical model see[6-9,11].

The target at the end of implosion is supposed to be homogeneous with the exception of a relatively small central hot spark (ignitor). The initial conditions of isochoric ignitor are described by two parameters: characteristic dimension (areal density) ρR_f and temperature T_f. (Let's make arrangement to consider product ρR as separate physical value marked by two letters, then $\rho_f R_f = (\rho R)_f = \rho R_f$ and so on) It turns out in agreement with [8,9] that the target gain is practically independent on ignition origin if the TN flash takes place. As a consequence the analysis of burn efficiency is reduced to determination of the critical

(minimum) values of ignitor parameters. As for initial parameters of the main fuel ρR_0, T_0 we suppose that there is no TN flash in homogeneous target. In the opposite case the concept of fast ignition has no physical meaning. Preliminary calculations carried out for different homogeneous targets make it possible to establish the upper bound for target temperature and dimension.

3. RESULTS OF THE NUMERICAL CALCULATIONS.

3.1. Thermonuclear burning of homogeneous target.

The study of homogeneous target TN burning is not only the starting point to obtain the limits of initial target parameters in fast ignition problem. It may be supposed that in the case of effective TN flash the process of burning is self-regulated and the target gain is practically independent on the ignition origin. The results of calculations setting forth below confirm this prediction. That's why TN burning of homogeneous target may be used as a point of reference in analytical treatment of burn efficiency of targets with arbitrary temperature and density distributions.

The general measure of target TN burning efficiency is the TN gain $G = E_{tn}/E_0$, where E_{tn} is the released TN energy, E_0 is the initial internal energy coupled to the target. The results of TERA calculations of the gain of homogeneous targets with different ρR_0, T_0 are presented in figure 1. The sharp increase in the gain within narrow interval of target temperature T_0 corresponds to generation of self-sustaining TN burning. If the TN flash takes place the released energy depends weakly on the initial temperature T_0, as a result at further temperature increase the gain varies in inverse proportion to temperature: $G \sim 1/T_0$.

The most interesting result consists in the fact that the TN flash of thick targets with a great areal density ($\rho R_0 > 1 g/cm^2$) may occur at initial temperatures $T_0 \sim$ 3-5 keV far lower than the temperature of maximum TN reaction rate ($T \sim$ 15-20 keV). As a result the energy gain G ranges into the hundreds. It is due to the target heating by the α particle thermalization on the initial stage of burning. (The cold plasma with $\rho R_0 > 1 g/cm^2$ is impenetrable to fast TN particles). The transparency of thin targets with $\rho R_0 < 1 g/cm^2$ leads to high values of critical temperature $T_0 \sim$ 15-20 keV and as a consequence to low values of the gain ($G \leq 1$).

Let us consider the energy gain of volume ignited targets as a function of ρR_0, T_0 in detail. By definition the value of G may be presented in the form:

$$G = E_{tn} / E_0 \sim \langle \sigma v \rangle \rho \Delta t / T_0 \quad , \tag{1}$$

where $\langle \sigma v \rangle$ is a time-averaged TN fusion rate , Δt is a characteristic target hydrodynamic lifetime. The TN fusion rate as a function of temperature shows a pronounced maximum at $T \sim 20$ keV and changes relatively slightly with further temperature increase up to $T \sim 1000$ keV [12]. As a result the value of $\langle \sigma v \rangle$ in the range of active TN burning is approximately independent on the target initial parameters. The target lifetime may be presented as the ratio of target radius and mean speed of sound $v \sim \langle T \rangle^{1/2}$: $\Delta t \sim R_0/\langle T \rangle^{1/2}$. Our calculations show that in the process of active TN burning of thick target with $\rho R_0 > 1$ g/cm^2 temperature runs into hundreds of keV. The corresponding lifetime reduction decreases the index of a power in ρR_0 dependence of the gain. Really, during the thick target TN flash the fraction of released TN energy caused plasma self-heating is getting essentially greater than initial energy E_0 , so the TN flash mean temperature $\langle T \rangle$ and target lifetime Δt are determined by target gain: $\langle T \rangle \sim E_{tn} \sim G T_0$, $\Delta t \sim G^{-0.5}$. As a result the energy gain may be presented in the form:

$$G = F(\rho R_0, T_0)\ \rho R_0^{2/3} / T_0 \tag{2}$$

where the coefficient F weekly depends on ρR_0, T_0.

The function $F(\rho R_0, T_0)$ may be obtained from the data presented in figure 1 (see figure 2). It is seen that the value of coefficient F is approximately constant with the accuracy of the order of 10% provided that the conditions of volume ignition are satisfied ($G \gg 1$). Under the conditions the TN energy gain may be evaluated as:

$$G = 370 \rho R_0^{2/3} / T_0 \tag{3}$$

In eq. (3) T_0 and ρR_0 are measured in keV and g/cm^2 , respectively.

As may be seen from its derivation, equations (2), (3) are applicable only if $G >> 1$. There is another factor limiting the application field of these equations. During the TN burning the density ρ changes not only by hydrodynamic processes but partially due to the fuel depletion. If significant fraction of the fuel is burned out the effective density in eq. (1) as well as mean temperature $<T>$ depends on the target gain. Let us introduce the burn efficiency g as the fraction of depletion fuel: $g = \Delta M/M$. The released TN energy can be expressed in terms of a number of deuterium and tritium nuclei undergoing the reactions of DT fusion ΔN: $E_{tn} = \Delta N<E>/2$, where $<E> \cong 17.6$ MeV. The initial energy E_0 is connected with total number of D- and T-nuclei N: $E_0 = 3NT_0$. Taking into account that $g = \Delta M/M = \Delta N/N$, eq. (3) may be rewrite in terms of burn efficiency:

$$g = 6GT_0 / <E> = \rho R_0^{2/3} / 7.9 \qquad (3a)$$

The real value of depletion fuel is approximately ten percent greater than one giving by eq.(3a) due to the contribution of DD fusion reactions and so on. In spite of this it is convenient to use eq. (3a) as a specific measure of efficiency of DT burning. In accordance with the above mentioned reasons eq.(3) is valid only at relatively small values of the burn efficiency g. The results of TERA numerical calculations of the gain of homogeneous targets with different ρR_0 being converted to that in terms of DT burn efficiency g are presented in figure 3. Comparing these results with the values given by eq.(3a) we obtain the range of applicability of eq.(3a): $g \le 0.4$. In the light of foregoing arguments the eqs. (2), (3) may be used under the conditions: $G >> 1$, $g \le 0.4$. The corresponding range of areal density and temperature (1 g/cm$^2 \le \rho R_0 \le 5$ g/cm^2 ; $T_0 < 100$ keV) is rather appropriate to the fast ignition targets.

If the effect of lifetime reduction due to target self-heating is neglected (it is correct for thin targets with $\rho R_0 < 1$ g/cm^2) the same reasons results in the linear ρR_0 dependence of the gain and burn efficiency: $G \sim \rho R_0 / T_0^{3/2}$, $g \sim \rho R_0 / \sqrt{T_0}$. With allowance for depletion effect the expression of burn efficiency takes the form[10]: $g = \rho R_0 / (\rho R_0 + A\sqrt{T_0})$. In the case of thin target only the temperature of TN flash ($T_0 \sim$ 15-20 keV) is a matter of interest. That is why the temperature dependence of g is not considered as a rule and corresponding expression is extended to the range of $\rho R_0 > 1$ g/cm^2 . It should be noted that TN fusion rate and α particle energy losses in deuterium - tritium plasma are combined in such a way that considerable depletion is accompanied by considerable self - heating. Both depletion and self - heating affect the burn efficiency in similar way. Because the constants in expressions of g are treated as fitting parameters no wonder that the well-known evaluation of burn efficiency[1,10] obtained without allowance for target self - heating: $g = \rho R_0 / (\rho R_0 + 7)$ is in a good agreement with eq.(3a) (see figure 3). The temperature dependencies of the gain presented in figure 2, however, show that the effective TN flash represents the self-regulated process which if have been initiated is independent on the initial temperature. Therefore the approach based on the allowing for the self-heating effect and leading to eqs.(3), (3a) is more suitable in the range under consideration. As a matter of fact the fuel depletion affect the energy gain considerably and should be taken into account simultaneously with the self-heating effect only in the range of large areal density $\rho R_0 >> 1$ g/cm^2 .

The same reasons remain in force and rise in importance in the case of ecologically cleaner fuel with a small number of neutrons among the products of its burning (for instance a mixture of deuterium with He^3). In this case the fraction of TN energy responsible for target self-heating increase considerably and as a result the relative contribution of fuel depletion in the ρR_0-dependence of the gain is reduced.

3.2. Fast ignition criteria.

There is no heating by α particles and as a consequence no burn wave in rather thin targets with $\rho R_0 < 1$ g/cm^2 . For thick targets with $\rho R_0 > 1$ g/cm^2 the TN combustion wave being initiated by a spark makes it possible to produce the effective TN flash at initial temperature substantially below the critical temperature of volume ignition. Fixing the value of T_0 in this range we consider a set of model isochoric target with different ignitor parameters T_f and ρR_f at given ρR_0. For every target the energy gain G is obtained by means of TERA code simulation of TN burning. The total number of the targets under consideration exceeds 500.

Consider the typical results of the calculation for targets with $\rho R_0 = 2$ g/cm^2 . The obtained values G as a function of ignitor dimension ρR_f at different T_0 and T_f are presented in figure 4. It may be seen that for every value of ignitor temperature T_f there are some critical values of ignitor dimension, corresponding to the sharp increase in the gain within relatively narrow range of ρR_f . The similar behavior of the gain-dimension dependencies is obtained at the other ρR_0 , and the range of critical ρR_f narrows with increase of ρR_0 . The same results may be presented in terms of gain-temperature dependencies at

fixing ρR_f. In this case the range of critical temperature T_f corresponding to the sharp increase in the gain is less than 0.5 keV.

From the physical point of view this increase is associated with a fact that the time of TN burn extension over the whole target under the conditions near to the critical is of the order of the target lifetime. Up to the critical ignitor parameters the low energy gain corresponds to the "smoldering" of homogeneous target with temperature T_0 and is independent on ignitor presence. There is no spark ignition. In the opposite case TN flash results in effective burning with $G \sim 10^2 - 10^3$. If the TN flash takes place the energy release is practically independent on the history of ignition. The calculated values of energy gain in the limit of overcritical ρR_f , T_f tend to ones given by Eq.(3) with the obvious correction on the additional ignitor energy:

$$G = G_H / (1 + \Delta_E),$$

where G_H is the energy gain of homogeneous target with the same ρR_0, T_0; Δ_E is a dimensionless ratios of energy coupled to ignitor due to an extra laser pulse E_f to the total energy of corresponding homogeneous target with the same ρR_0, T_0.

Thus the values of critical ignitor parameters are only the matter of interest. As for the parameters of the main fuel we intend to obtain the condition under which the gain is maximized. As it is resulted from eq.(3), it is necessary for this aim to reduce the target temperature as possible. On the other hand, as was argued above plasma is supposed to be in non-degenerate state whereas in the dense DT plasma with $\rho \sim 10^2$ g/cm^3 the Fermi energy runs into hundred of eV ($E_F \cong 14\ \rho^{2/3}$ eV, where ρ is measured in g/cm^3). Therefore, the initial temperatures T_0 are chosen in the range $T_0 \sim 0.5 - 1$ keV.

We carry out the numerical calculations of critical ignitor parameters ρR_f, T_f for targets with areal density ρR_0 equals to 3, 4 and 6 g/cm^2 . For targets with $\rho R_0 = 1$ and 2 g/cm^2 and $T_0 > 1$ keV the same values were calculated in our previous paper[13] both for the case of isobaric and of isochoric ignitors. The aim of that paper was to compare the possibilities of two way of spark ignition with each other. This accounts for the choice of initial target parameters and for the presentation of the results in terms of dimensionless variables $\Delta_r = R_f/R_0$ and $\Delta_t = T_f/T_0$.

Our calculations show that the critical ignitor parameters are practically independent on the target areal density ρR_0 in the range under consideration. The obtained values of ρR_f, T_f for targets with different T_0 are presented in figure 5. It is just obvious that the critical ignitor temperature increase with the reduction of ignitor areal density in agreement with the curves in figure 5. More interesting is the behavior of the corresponding additional thermal energy E_f coupled to ignitor because it is connected immediately with an energy of the extra laser pulse. It was noted in our previous paper[13] that for relatively large value of ρR_f this energy is in a straight dependence on the ignitor mass m_f whereas for small value of ρR_f when m_f is less than or equal to one percent of total mass the critical value of E_f is practically independent on the ignitor mass. In other words for every target there is a minimum value of additional absorbed extra pulse energy corresponding to some optimum ignitor.

The presence of optimum ignitor may be consistently explained taking into account the temperature behavior of TN fusion reaction rate. Until the critical temperature reaches the values corresponding to the maximum $\langle\sigma v\rangle$ at $T \sim 15 - 20$ keV the considerable reduction in critical ignitor dimension is compensated by a small variation of critical temperature due to the sharp increase of $\langle\sigma v\rangle$ with temperature. As a result the critical value of E_f is reduced in this range. The further reduction of ignitor dimension and increase of ignitor temperature gives no additional advantage in energy because TN fusion reaction rate remains approximately invariable and the electron heat conductivity extends the absorbed energy over the optimum ignitor size corresponding to the temperature of maximum $\langle\sigma v\rangle$. For illustration, the critical ignitor parameters giving in figure 5 are presented in figure 6 in terms of Δ_E , T_f ($\rho R_0 = 3$ g/cm^2). As may be seen Δ_E tends to the constant in the range $T_f > 12$ keV with accordance to above-stated arguments. The minimum values of ignitor energy E_f run about a few percent and under of the total target internal energy E_0 .

We calculate the values of minimum absorbed energy under fast ignition for targets with different temperature T_0. As was mentioned above these values depend on the density ρ whereas the values of $E_f^* = \rho^2 E_f$ are approximately scale-invariant. To verify this statement the calculations were carried out at ρ equal to 10 and 100 g/cm^3 . At tenfold change in density the corresponding change in scaling critical ignitor energy E_f^* is less than five percent. The calculated values of minimum additional absorbed extra pulse energy E_f corresponding to optimum ignitor are presented in figure 7 in the form of energy - temperature dependencies for targets with $\rho = 316$ g/cm^3 . This choice of ρmakes it easy to change the scale of densities ($\rho^2 = 10^5$ g^2/cm^6). With account for scale invariance the presented curves give a possibility to evaluate the minimum extra laser pulse energy at arbitrary condition of basic driver implosion and may be used under examination the fast ignition scheme of ICF.

The scale of the ignition laser E_L is set by coupling efficiencies η and required ignition energy: $E_L = E_f / \eta$. One of the possibly coupling mechanism is the recently proposed scheme[2] of laser energy conversion into the energy of accelerated ions

produced at critical densities. The corresponding coupling efficiencies η may be evaluated as $\eta \sim 10\%$ in relatively wide range of parameters. Taking into account the values of E_f presented in figure 7 we may conclude that the required parameters of ultrashort laser pulse with ultrahigh intensity lie in the limits of the modern experimental possibilities.

4. CONCLUSIONS.

Summing up the results it should be emphasized the following features of laser target TN burning:

The sharp increase in the TN gain of homogeneous targets caused by generation of self-sustaining TN burning is found within narrow interval of target temperature T_0 at given $\rho R_0 > 1$ g/cm^2 . If the volume ignition takes place the released energy depends weakly on the initial temperature T_0, so at further temperature increase the gain varies in inverse proportion to temperature. The values of critical (minimum) temperature T_0 of thick target volume ignition are of the order of a few keV and corresponding values of maximum target gain reach hundreds.

The spark ignition is possible at temperature less than 1 keV and the corresponding gain runs into 10^3 . The effective TN flash takes place provided that the time of TN burn wave extension over the whole target is of the order or less than the target hydrodynamic lifetime. This process is accompanied by the sharp increase in the gain within relatively narrow range of ignitor areal density ρR_f and temperature T_f . The critical ignitor parameters depend on the temperature but not on the areal density of the main fuel. The calculated values of these parameters are presented in figure 5.

The energy of the extra laser pulse is connected immediately with an additional thermal energy E_f coupled to ignitor. The critical (minimum) value of E_f is a simple function of critical parameters ρR_f, T_f. It is shown that if ignitor is small, the critical value of E_f is practically independent on ignitor mass being the function only of the main fuel parameters. The corresponding dependencies are presented in figure 7.

The overcritical burn efficiency and target gain are practically independent on the ignition origin and may be evaluated with the reasonable accuracy by the simple asymptotic expression:

$$g = \rho R_0^{2/3} / 7.9 \qquad , \qquad . G = 370 \rho R_0^{2/3} / T_0$$

These relations are valid both for volume and for spark ignition.

ACKNOWLEDGMENTS

We are grateful to Academicians N.G.Basov and A.A.Samarsky for support this work and Prof. N.V.Zmitrenko for fruitful discussions.
These work is partially supported by the Grant RFFI 99-02-16100 , by Russia Dept. of Education Grant "Thermonuclear and nuclear reactors-1997" (Investigation in nuclear technique Field) and by the Program 015 "Russia Universities" 03.01.05.

REFERENCES

1. M.Tabak, J.Hammer, M.E.Glinsky et al., "Ignition and high gain with ultrapowerful lasers," *Preprint UCRL-JC-114425* (Livermor, LLNL, 1993), *Physics of Plasmas* **1**, pp.1626-1634,1994.
2. S.Atzeny, *Physics of Plasmas* **6**, p.3316, 1999.
3. R. Kidder, *Nucl. Fusion* **16**, p.405, 1976.
4. O.B.Vygovskii, S.Yu.Gus'kov, D.V.Il'in., A.A Levkovskii, V.B.Rozanov, V.E.Sherman, " Criterion of formation of a thermonuclear burn wave in deuterium-tritium targets," *J.Sov.Las.Research*,**14**, pp.85-91, 1993.
5. S.Yu.Gus'kov, D.V.Il'in, A.A.Levkovskii, V.B.Rozanov, and V.E.Sherman, "Study of ignition criteria in inhomogeneously heated laser target," *Proc.SPIE-Int.Soc.Opt.Eng.(USA)* **2770**, pp.182-189, 1996. (Laser Optics'95 and ICONO'95 Superintense Laser Fields, St.-Petersburg, Russia, 27 June - 1 July 1995.)
6. N.G.Basov. S.Yu.Gus'kov, D.V.Il'in, A.A.Levkovskii et al.,*Fizika plazmy (Sov. J. of Plasma Phys.)* **12**, pp. 916-928, 1986; A.A.Levkovskii, "Mathematical simulations of thermonuclear flash in laser target," *Preprint FIAN 73*, Moscow, 1990. (in Russian)

7. N.V.Zmitrenco, D.V.Il'in, A.A.Levkovskii V.B.Rozanov, V.E.Sherman, "Physics of a two-temperature thermonuclear burning wave in an inertial confined plasma," *Zh.Eksp.Teor.Fiz.* **106**, pp.1069-1088, 1994.(in Russian); Engl.transl.,*JETP* **79(4)**, pp.581-590, October 1994
8. A.A.Andreev, D.V.Il'in, A.A.Levkovskii et al., "Study of efficiency of TN burning in laser targets with spark ignition", *Proc.SPIE-Int.Soc.Opt.Eng.(USA)* **3684** , pp.170-179, 1999. (Laser Optics'98 , St.-Petersburg, Russia, June 22-26, 1998).
9. S.Yu.Gus'kov, D.V.Il'in, A.A.Levkovskii, V.B.Rozanov, and V.E.Sherman, "Particle diagnostic of laser targets", *Laser and Particle Beams* **16**, pp.129-151,1998.
10. J.J.Duderstadt & G.A.Moses, *Inertial Confinement Fusion*, John Wiley & Sons, New York, 1982.
11. A.A. Levkovskii, "Mathematics modeling of dynamic laser target plasma TN burning on basis of Monte-Carlo method', *Authoreferat*, Institute Mathematics modeling RAN, Moscow, 1993.
12. G. Cauglan, W. Fowler, M. Harris, B. Zimmerman, *Atomic Data and Nucl. Data Tabl.* **32,** p.197, 1985.
13. A. Levkovskii, A. Andreev, D. Il'in, et al., "Conditions for initiation of effective thermonuclear burning of laser targets", *Proc.SPIE-Int.Soc.Opt.Eng.(USA)* **3886,** pp. 448-456, 2000

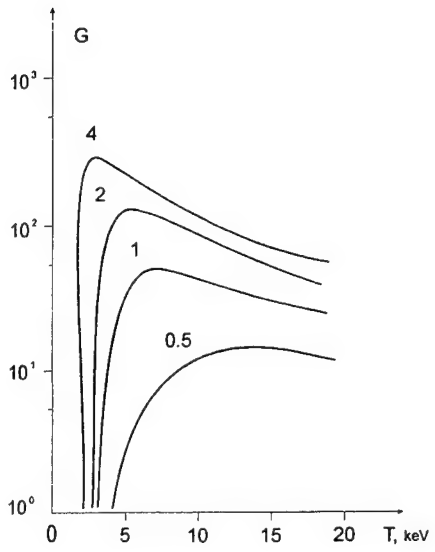

Fig. 1 The energy gain of homogeneous target as a function of temperature T_o at different ρR_o. The curves are marked by corresponding values of ρR_o in g/cm^2.

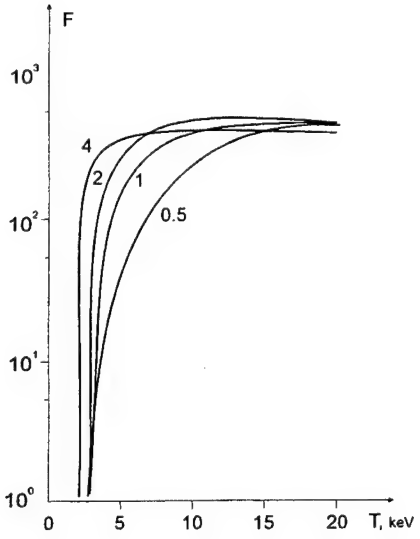

Fig. 2 Normalized energy gain F as a function of temperature T_o at different ρR_o. The curves are marked by corresponding values of ρR_o *in* g/cm^2.

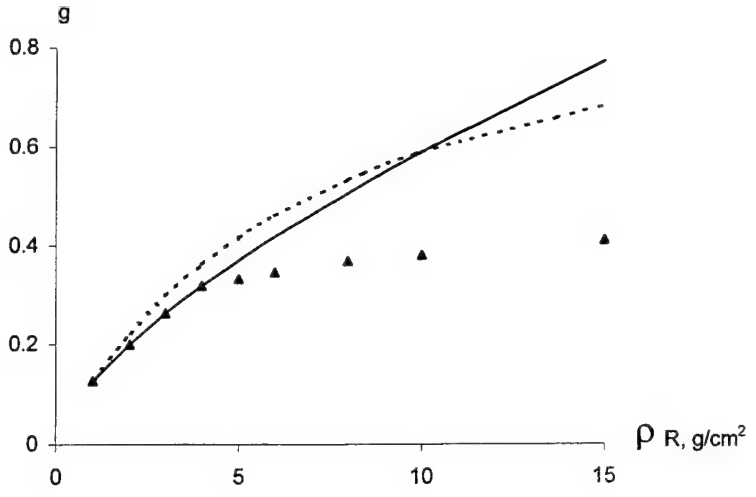

Fig. 3 The DT burn efficiency g of homogeneous target as a function of ρR_o Solid and dashed lines correspond to $g = \rho R_0^{2/3} / 7.9$ and $g = \rho R_0 / (\rho R_0 + 7)$ respectively. Markers present the results of TERA numerical calculations.

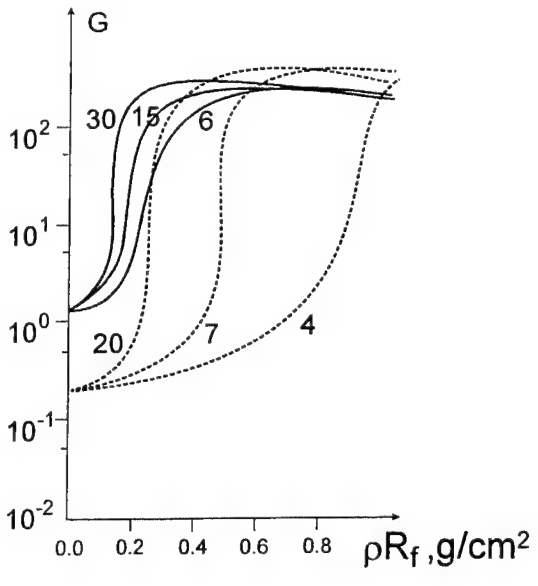

Fig. 4 The energy gain G as a function of the ignitor areal density ρR_f at different ignitor temperature T_f (indicated in the figure) for target with $\rho R_o = 2$ g/cm^2. Solid and dashed lines correspond to To = 3 and 2 keV respectively

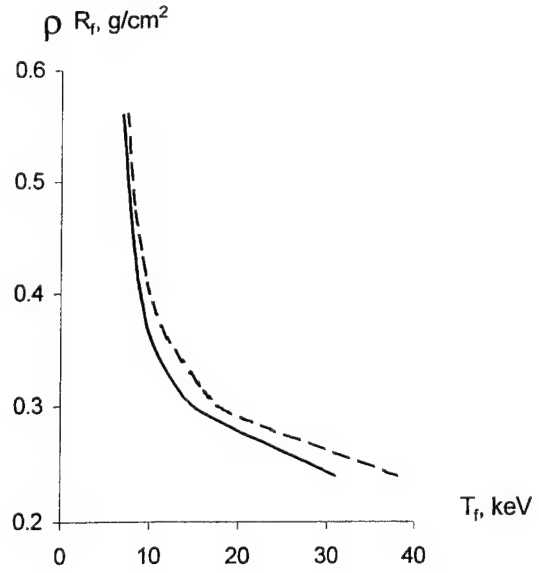

Fig. 5 The critical ignitor parameters for targets with the main fuel temperature $T_0 = 1$ keV (solid line) and $T_0 = 0.6$ keV (dashed line).

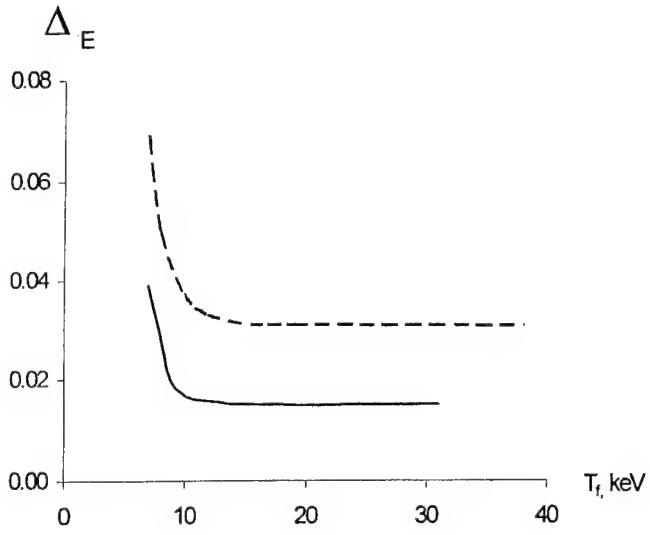

Fig. 6 The relative value of energy $\Delta_E = E_f / E_0$ corresponding to the critical parameters of ignitor as a function of ignitor temperature. Solid and dashed lines correspond to the main fuel temperature $T_0 = 1$ keV and $T_0 = 0.6$ keV respectively.

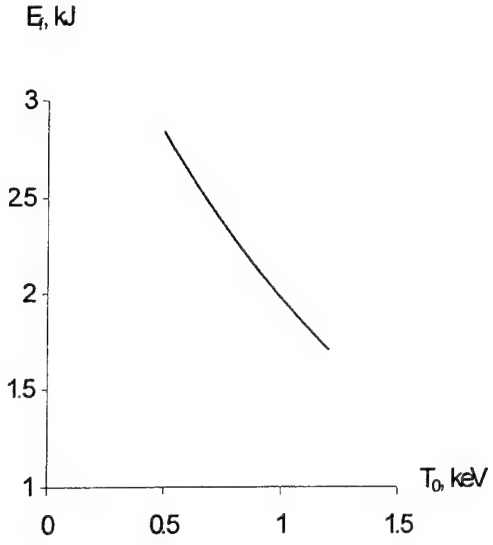

Fig. 7 The minimum value of the energy coupled to the ignitor E_f as a function of temperature of isochoric target with $\rho = 316$ g/cm^3 ($\rho^2 = 10^5$ g^2/cm^6).

Status of gamma-laser problem on current moment'2000: ranging analysis and screening of gamma-laser schemes on their feasibility

S.V.Karyagin

Semenov Institute of Chemical Physics, RAS. Prospect Kosygina 4, 117997 (GSP-1), Moscow, GSP-1, Russia
e-mail: chaika@chph.ras.ru ; fax: (095)-137-8318

ABSTRACT

Joint theory of gamma-generation (GG) and radiation-heat regime (GG&RH) in active medium (AM) of γ-laser (GL) is applied for the analyses of total world experience in the GL-problem in order to choose those nuclei-candidates, active media, GL-schemes which are indeed actual for the GL-creation. The classification of GL over a degree of the «comfortable conditions» for the GG is given. The GL-schemes could be "residential(Rsd)" (creation of excited laser-active nuclei, ELAN, from its parents directly in the site of AM) or "nonresidential(Nrsd)" (creation of ELAN out off the AM). It has been turned out that all "residential" part of the world experience does not fit for the realization of GL and can be considered only as a museum-piece. Any Rsd AM on the short-lived isomers must be inevitably blasted before the beginning of the GG. That "museum" part includes a lot of ideas: GG on long-lived isomers; line narrowing by radio-frequency or optical fields; creation of γ-gain in the inversionless mixture of the excited and de-excited nuclei (amplification without inversion); super-dilution of work-nuclei in a matrix via multi wave Borrman effect; non-Moessbauer active media in plasma, gas or beam with its optical laser cooling, a lot of schemes (one-stage, two-stage, two-phase, two-step, two-photon, etc.). The exception could be only Rsd GL pumped by another GL. But the Nrsd part of world experience had stood yet all strict tests of that joint theory.

Keywords: gamma-laser; quantum nucleonics; gamma-generation (induced, super-radiant, in plasma, in beam, in solid); laser cooling of atomic beam; amplification without inversion; Borrmann effect; Shpol'skii effect; Moessbauer effect; hyper fine structure; laser selection (separation) of excited nuclei, isomers, isotopes; radiation-heat regime of active media of gamma-laser; anomalous superdilution

INTRODUCTION

The most advanced non residential (Nrsd) GL (see ABSTRACT) is based on the use of the short-lived isomers (10^{-4} - 10^{-7} *s*) produced under nuclear pulse radiation in a special "converter"[28] (alias multibeam emitter, MBE[34-36]) and delivered into the AM by the method SPTEN (Soft Prompt Transplantation of Excited Nuclei) with use of the complex of measures for well generation and cooling of AM[27-36]. The enriched bunch with 90% of the Excited Laser-Active Nuclei (ELAN) is delivered into the site of AM just before the GG. Hence the Nrsd GL could be characterized by the removal from the site of AM absolutely all processes for the nuclei activation and for the inverted population creation. Only the GG and the cooling are acting in such Nrsd AM. Hence the Nrsd GL could do without use of any methods for the creation of gain in the inversionless medium because the Nrsd AM is strongly inverted before its creation, at "beam-study", out off the AM's site. Owing to such circumstance the ideas developed in works[27,28-36] allow to obviate the most weak flows of the GL-schemes. One such weak flow was pointed in Refs.[9,10,12,32,35]. It may be any process or device based on use of the hyperfine structure (HFS) directly in the AM (*in situ*). The ideas of works[27-36] do not at all use any HFS inside of the AM (in situ).

The Nrsd GL[27,28-36] could generate almost parallel γ-beam with the length of coherence ~ 10^3 - 10^6 *cm*, the intensity averaged over pulse duration ~ 10^{12} - 10^{14} W/cm^2, the pick intensity ~ 10^{14} - 10^{20} W/cm^2, the brightness ~ 10^{20} - 10^{23} W/cm^2rad^2, the energy 0.01 - 1 *J per pulse*. Such beam could be practically applied in micro-lithography, in micro-holography, in microtomography of the alive albumen molecules, etc. It is possible to reanimate some "museum" schemes through their hybridization with the SPTEN. But the main its application is the triggering of a more powerful residential GL. In that application the nonlinear interaction of the combined "strong GL field + strong optical laser field" with the stored resonant long-lived nuclei is very important. The adequate theory[17] must be improved. Such "nonresidential-residential" γ-laser is an exception from above rule about unfitness of Rsd GL. More complex " Many-Section Nrsd-Rsd" γ-lasers could be more powerful by many orders than the simple SPTEN GL. But it needs to remind that even the simple SPTEN γ-laser is sufficiently powerful for the plural applications, the super-powerful GL included[49,50].

At last the new direction "Multi Beam Laser Separation of Nuclei" was arisen as a result of the SPTEN development. This direction leads to the essential, by many orders, acceleration of the laser separation of atoms, molecules, isotopes, isomers, radionuclides, etc.

1. Joint "Gamma-Generation and Radiation-Heat" theory (GG&RH) and criteria for the screening of the nuclei-candidates and schemes for the GL.

The principal steps for the screening of nuclei-candidates and schemes for the GL creation on base of single theory were the following:
1. - Revision of the recent theories for the GG and the radiation-heat regime (GG&RH) in AM. Creation of new "Joint GG&RH theory". Formulation of exact criteria of GG&RH for the fast screening of nuclei-candidates, active media and schemes for the GL realization.
2. - Application of the general GG&RH criteria and the special screening to the GL based on the solid aggregate state of the AM.
3. - The screening of the GL based on the different non-solid aggregate states of the AM: plasma, gas and atomic beam.
4. - The screening of the GL over total amount of nuclear γ-transitions in all known manifold of the isotopes.

Laser Optics 2000: Ultrafast Optics and Superstrong Laser Fields, Alexander A. Andreev, Vladimir E. Yashin, Editors, Proceedings of SPIE Vol. 4352 (2001) © 2001 SPIE · 0277-786X/01/$15.00

5. - The screening of the overall manifold of GL for the choice of the GL feasible in a near future.
That direction is reflected in works[34-36] and its status is fixed on the 2000 in seven works A(GL status), B(GL design), C-D(theory), E(nuclei-candidates), F(use of mega-Ampere source), G(optical HFS in GL) which are reported on "LO'2000" (see its Program).

1.1. Revision of the recent theories for the GG and the radiation-heat regime (GG&RH) in the AM. Creation of new "Joint GG&RH theory". Formulation of exact criteria of GG&RH for the fast screening of nuclei-candidates, active media and schemes for the GL realization.

1.1.1. The revised GG theory and its coordination with the Radiation-Heat (RH) theory. Such RGGT accounts total complex of conditions for the real experiment: the decay of the excited work level, the lethargy of the induced processes, the influence of the competing channels (other transitions), the resonant and non-resonant losses, the diffraction, the line broadening, the wave dephasing (e.g., at the GG beginning, see above, the influence of the detector, etc.), the initial ELAN concentration, the form and the sizes of AM.

The super-fluorescent GG (alias super-radiant, SR) theory is developed on base of the almost-correct solution of the Bloch equations at the length of the Bloch vector strongly variable in time. Such approximation is absolutely original because there are no more correct Bloch's approximations in a world.

The initial ELAN concentration n_+, the form and sizes of AM **are coordinated with the RH theory.** E.g., for the solid AM the crucial heat condition (5) for the GG, see section 1.1.2., is used. The more delicate relation between the super-radiant (SR) and induced thresholds

$$p_{SR} > p_{ind} \qquad (1)$$

is proved also with use of the RH theory which shows that the relation $p_{SR} < p_{ind}$ is achieved only in the regime of the AM's blast. The computer calculations show also that in case of the RH-regime beneficial for the GG the SR-contribution in GG is much smaller versus the Induced contribution. In that reason **the main criterion for the nuclei-candidates choice, active media and schemes for GL is**

$$p/p_{ind} > 1 \qquad (2)$$

where the formulas for the parameters p , "Reserve of Amplification", and p_{ind} , "Induced Threshold" are given in the paper [C].

1.1.2. The revised Radiation-Heat (RH) theory and its coordination with the GG theory. Exact criteria RH theory for the GL realization. The theory of the radiation-heat regime of the active medium of GL is developed in the series of works [27-29,32,35] and in the work [D] which is represented at this conference "LO'2000". The RH-theory begins with the energy-release **coordinated with the GG-theory:**

$$q = n_+ E_\gamma (\alpha/1+\alpha)/\tau_+ \qquad (3)$$

Here n_+ is density of ELAN in AM, E_γ is the energy of work γ-transition, α is the internal conversion coefficient, τ_+ is the ELAN time-life. The use of the Anomalous Super Dilution (ASD, see[23,27]) on base of the Multi Wave Borrman Effect[26] (MWBE) is unreal (see below point 1.5.3.). But without the ASD the optimal concentration $n_+ = 10^{21}$ cm^{-3} even in the very beneficial case of the SPTEN γ-lasing. Hence at $E_\gamma \sim 10 - 100$ keV, $\alpha \sim 10$, $\tau_+ \sim 10^{-5}$s ones have

$$q \sim 10^{11} - 10^{12} \text{ W/cm}^3. \qquad (4)$$

It is clear that the cooling of the AM at such high energy-release is not a simple thing. The first deep analyses of this heat problem and the first recommendations are given in [27-29]. Particularly it was shown the unfitness of old suggestion "needle in the liquid helium bath" owing to the adiabatic isolation of the AM by the gaseous bubble. But this origin variant [27-29] of RH theory was based on the classical thermodynamical conceptions of the "heat capacity" and "heat conductivity". Their nonlinear behavior at low temperatures $T<T_D$ (T_D is the Debye temperature) was accounted. The conception of the quasi temperature instead of the temperature was introduced in that first variant. But there were revealed some contradictories in that origin theory, especially in the interesting case of the small diameter of the active medium $a_1 \sim \Lambda_{ph}$ (the free path for the phonon).

The next stage of the RH-theory overcame that contradictories by the transition from the thermodynamics to the non equilibrium kinetic theory of two linked non-equilibrium subsystems: electrons-holes and phonons. The temperature dependence of the parameters of that theory (including the parameter of coupling between that subsystems $\tau_{e\text{-}ph}(T)$, the free path for the electrons and holes $\Lambda_e(T)$, and the free path for the phonons $\Lambda_{ph}(T)$) are gotten from the experiments. Hence this is a half phenomenological quasi temperature theory. The equations of that theory contain the fields of the energy densities Q_e (for electrons-holes) and Q_{ph} (for phonons) of that subsystems. That fields $Q_e(t,r)$ and $Q_{ph}(t,r)$ are the functions of the time t and the space point r. The quasi temperature field $T(t,r)$ is a certain function of field $Q_{ph}(t,r)$. Hence the parameters $\tau_{e\text{-}ph}(T)$, $\Lambda_e(T)$, $\Lambda_{ph}(T)$ also are the fields $\tau_{e\text{-}ph}(t,r)$, $\Lambda_e(t,r)$, $\Lambda_{ph}(t,r)$. Hence it is a task with the infinity variables and infinity number of equations. Such task could be resolved only approximately.

The zero approximation of quasi-free exit of carriers from AM into the adjacent cooler is represented in [32,35]. That zero approximation could not to give the sharp transition from the stationary heat regime to the blast. It is very fishily. The next quasi diffusion approximations (see work [D] reported at this conference "LO'2000") give that sharp transition in a reasonable region of the quasi temperatures T ~ 100 - 200 K. The computer calculations of different cases of the active medium with different nuclei and other different parameters gives the following approximate **crucial condition (criterion) for the stationary low temperature radiation-heat regime**

$$\Theta_{reg} = (q\, a_1^{27/11})/5 < 1 \text{ W cm}^{-6/11} \qquad (5)$$

The case of the heat blast for the AM takes place if the regime parameter $\Theta_{reg} > 1$. This criterion (4) together with the criterion (2) are the main exact criteria for the valid and fast screening of nuclei-candidates, active media and schemes for the GL realization. Another criteria are discussed below in the next point of this section 1.

1.2. Application of general GG&RH criteria and special screening to the GL based on the solid aggregate state of the AM.

1.2.1. The application of the general GG&RH screening to the GL based on the solid aggregate state of the AM. In accordance (4) and (5) the AM is not blasted at the heat release ~ 10^{11} -10^{12} W/cm^3 if the diameter of the AM is less than

$$a_1 < (5/q)^{11/27}\, W^{-11/27}\, cm^{20/9} \sim 7\ 10^{-5} - 3\ 10^{-5}\ cm \qquad (6)$$

A lot of computer calculations for the various nuclei and AM in case of the SPTEN GL verify this rule and give the quasi-temperature T < 100 K. **The solid AM had stood the total test of the Joint GG and RH theories**[32,35], see also the works[C,D] presented at "LO'2000".

1.2.2. The application of the special screening to the GL based on the solid aggregate state of the AM. The SPTEN is the most stable (against different trammels) model among all manifold of GL, solid GL included. It is a reason for additional tests for the SPTEN which were not applied to any its competitors. All that competitors were rejected already on stage of the general screening (see points below). The special screening was applied to SPTEN γ-laser by the wide front in each its device element[28-36], see also the works [B,C,D,E,F, G] presented at "LO'2000". The especial attention is devoted to the central device of the SPTEN which holds twelve title: it is the <<converter nuclear radiation ⇒ ELAN>> specially for the GL and it is the <<multi beam emitter>>, "MBE", in case of more broad circle of the tasks from the gene engineering up to the industrial separation of rare isotopes for the ecologically safe nuclear energetics.

1.3. The screening of the GL based on the different non-solid aggregate states of the AM: plasma, gas and atomic beam.

It is shown[34,35] that the condition of the generation could not be fulfilled if the AM is plasma, gas and atomic beam owing to the strong longitudinal dispersion of the velocity which lead to very strong Doppler line broadening.

It is shown also[34.35] that the laser methods[82] are unfitted for the longitudinal cooling of the beam with the short-lived ELAN. The main reason is the heating and the ionization of the gas or the beam by the secondary electrons in a result of the internal conversion. Each act of the internal conversion creates more than 1000 secondary electrons and ions. The time of the ions with the opposite signs in a beam is much more than the work isomer time-life. It lads to the accumulation of the ion concentration. The forces between ion and other ion, between atom and ion are very strong and could not be suppressed by the cooling optical fields (COF). The value of COF needs be extremely big, much more than the value of the disruption.

The two-photon GL[52,53] (decay into two contrary directed quanta when linear Doppler effect broadening is suppressed) is too romanced because the very strong decay channel of the long-lived isomer is omitted in Refs.[52,53]. This channel is the electron conversion which could carry away practically any angle momentum with big coefficient conversion α ~10^3 - 10^6. Hence the big values of the ignition laser field ~ 10^{12} W cm^{-2} (see [52,53]) must be increased up to the values ~ 10^{15} - 10^{18} W cm^{-2}. The total ionization in such field is fatal. Hence the strong heterogeneity of the Stark-effect on the different atoms or ions in the microfields must be created by the stochastically distributed ions. It must give the line broadening of the order ~ 10^7-10^9 s^{-1}. It gives the suppression factor ~ 10^{-10} - 10^{-15} . So the two-photon scheme is only a delusion which is fit for the "museum" but not for the indeed GL realization.

The reader. There are no any active medium for GL composed of the plasma, the gas or the atomic beam. Hence *all manifold of the GL on the nuclear transitions* is reduced towards to the more compact manifold of the GAMMA-RAY SOLID LASER. On that reason "GAMMA-RAY SOLID LASER" is the first title of all last works of the author after 1995 ([29-36] and all his seven works at the present conference "LO'2000") as a certain challenge to the backing of the non-solid GL.

1.4. The screening of the GL over total amount of nuclear γ-transitions in all known manifold of the isotopes.

The γ-radiation spectra of all available nuclear data-banks, e.g., [59-65,80,] were researched in order to find the tentative nuclei candidates with the work transitions fit for the GL realization without use of Borrman effect[26] (trammels of this effect application see in 1.5.3.). All that origin tentative candidates (more than 200) were screened by the tests of Joint GG & RH theory (see 1.1). The results of that screening are placed in the tables of the work [E] presented at this conference "LO'2000". The brief results are given below.

1.4.1. Candidates of the first short-lived diapason τ_+~ 10^{-4} - 10^{-6} s for both, Nrsd and Rsd, GL realization. There are 19 candidates for the Rsd and Nrsd GL realization (e.g., for SPTEN). Each that candidate fits the main criteria (2) and (5) of the Joint GG&RH theory. These candidates are:

Table1. Isomers of the first short-lived diapason τ_+~ 10^{-4}–10^{-6} s for Nrsd GL and Rsd GL. All they get $p/p_{ind}>1$ without use of Borrman effect

Isomer (E_γ, keV)	$^{46}Sc_{21}$(52.01)	$^{58}Co_{27}$(28.1)	$^{56}Co_{27}$(53.0)	$^{65}Ni_{28}$(86.9)	$^{65}Zn_{30}$(53.96
Isomer (E_γ, keV)	$^{67}Zn_{30}$(93.32)	$^{74}Ga_{31}$(56.5)	$^{69}Ge_{32}$(85.0)	$^{76}As_{33}$(46.04)	$^{92}Nb_{41}$(90.2)
Isomer (E_γ, keV)	$^{107}Pd_{46}$(115.7)	$^{110}Ag_{47}$(1.113)	$^{122}Sb_{51}$(61.45)	$^{154}Eu_{63}$(68.2)	$^{165}Tm_{69}$(80.3)
Isomer (E_γ, keV)	$^{172}Lu_{71}$(67.5)	$^{173}Lu_{71}$(123.7)	$^{177}Re_{75}$(84.7)	$^{179}Re_{75}$(65.6)	–

Three candidates $^{58}Co_{27}$(28.1), $^{74}Ga_{31}$(56.5), $^{76}As_{33}$(46.04) hold high work-ratio p/p_{ind}: ~29 for ^{58}Co; ~20 for ^{74}Ga; ~24 for ^{76}As. The champion $^{58}Co_{27}$(28.1) was first announced in[34,35] and its properties are well known. Other 18 candidates will be researched more completely in near future. The optical isomer shifts for $^{58}Co_{27}$(28.1) and $^{154}Eu_{63}$(68.2) are given in work[E] on "OL'2000". The existence of such big grope of very effective nuclei-candidates gives the great hope for the GL creation, especially SPTEN.

1.4.2. **The absence of long-lived candidates of "minute" diapason $\tau_+ \sim 10^{+2} - 10^{-3}$ s fit for the GL creation without the Borrman effect.** No one among the following 24 isomers of the "minute" diapason does not fit the crucial condition (2) if the Borrman effect is absent:

Table 2. Isomers of "minute" diapason $\tau_+ \sim 10^{+2} - 10^{-3}$ s get only $p/p_{ind} < 1$ without use of Borrman effect. They could not be used in near future for GL.						
Isomer (E_γ, *keV*)	$^{43}Sc_{21}$(151.7)	$^{45}Sc_{21}$(12.4)	$^{46}Sc_{21}$(142.5)	$^{74}Ga_{31}$(59.7)	$^{75}Ge_{32}$(139.7)	$^{77}Ge_{32}$(159.7)
Isomer (E_γ, *keV*)	$^{77}Se_{34}$(162.0)	$^{79}Se_{34}$(95.7)	$^{79}Kr_{36}$(130.0)	$^{83}Rb_{37}$(42.3)	$^{105}Rh_{45}$(129.6)	$^{103}Ag_{47}$(134.3)
Isomer (E_γ, *keV*)	$^{107}Ag_{47}$(93.1)	$^{109}Ag_{47}$(88.03)	$^{111}Ag_{47}$(59.8)	$^{116}Ag_{47}$(81.0)	$^{118}Ag_{47}$(127.7)	$^{120}Ag_{47}$(203.0)
Isomer (E_γ, *keV*)	$^{116}In_{49}$(162.4)	$^{116}In_{49}$(138.0)	$^{126}Sb_{51}$(22.7)	$^{134}Cs_{55}$(11.3)	$^{141}Eu_{63}$(96.4)	$^{157}Er_{68}$(156.0)

The natural line-width $\Gamma_0 = 1/\tau_+$ was supposed for all tentative long-lived nuclei at the calculation of the "probe-work ratio" $p/p_{ind} \sim$ 0.5 - 0.01 placed in this table. Hence the real work ratio, at the account of the real line-width $\Gamma >>> \Gamma_0$, must be less by some orders: $p/p_{ind} \sim (0.5 - 0.01)\,\Gamma_0/\Gamma \sim 10^{-3} - 10^{-8}$. The other (out of the Table 2) isomers of the "minute" diapason with $E_\gamma > 200$ keV, or a mass number A<40, or a coefficient of internal conversion $\alpha > 10^3$ have the "probe-work ratio" $p/p_{ind} << 10^{-3}$. Thus they were rejected previously. The lines with $\tau_+ >> 100$ *s* could not be narrowed [8]. Hence the unfitness for the GL of the above 24 long-lived "minute" isomers means the unfitness of all long-lived isomers as a work-nuclei *) for the GL without use of the Borrman effect[26]. Hence there are no long-lived nuclei for the GL creation without the Borrmann effect. Below it is shown that the realization of the Borrman effect for the GL creation could be feasible only at very far future. Hence the GL could be realized in a near future only on the short-lived isomers.

*) Note: Some long-lived isomers could be used as the parents of the short-lived isomers, e.g., in the two-step methods[11,39-45].

The reader: The long-lived ELAN, fit for the GL realization at near future without use of Borrman effect, are not reveled **as yet** in spite of the careful search for the such type of ELAN. The word **as yet** means some feeble hope that the Author could be wrong*.[1*]) Hence, at account of point 1.3.,

overall manifold of the GL REALIZABLE AT A NEAR FUTURE is reduced **as yet** to ITS SUB-MANIFOLD "GAMMA-RAY SOLID LASER BASED ON THE SHORT-LIVED ISOMERS".

1.5. The screening of the overall manifold of GL for the choice of the GL feasible in a near future.

By the points 1.3., 1.4.2. such manifold is reduced to the SOLID GL with the SHORT-LIVED isomers WITHOUT USE of Borrman effect.

1.5.1. **Hot microplasma in a cold solid AM as a tool of the screening.** In such case the Joint GG&RH theory predicts[32,34,35,D] the existence of the hot (T_{plasma}>30000 K) light (non-equilibrium secondary electrons and holes) microplasma with a big density (10^{17} - 10^{19} *pairs per cm*^{3}) in the cold lattice ($T_{lattice} \sim$ 30 - 100 K) of the host matrix in the site of the AM, see [32,34,35] and the work [D] presented at this conference "OL' 2000". This result gives the quite new sight on the active medium of GL because there was no a word about microplasma in the active medium during all period from 1961 up to nowadays in all works on GL problem. Soon this microplasma turned into a powerful tool of the screening in the GL problem, see below.

1.5.1.1. **Collapse of the hyperfine structure (HFS) by the movement of the light carriers of the hot microplasma.** Each act of the electron internal conversion give the avalanche of ~ 10^3 secondary light charged carriers: electrons and holes. The work centers with the ELAN could be regarded as like as the traps for that carriers. The traps could be deep or fine. All deep traps must be transformed into the fine traps after the absorption of one or two light charged carriers. Such transformation is realized for the short time ~ $10^{-3}\,\tau_+$.
After that time the form of the Moessbauer spectrum in the AM is governed by the dynamics of that fine traps in the flux of the charged light carriers. It is shown that due to that dynamics the charge-state of the work centers is fast altered between "plus", "zero" and "mines". In a result the HFS parameters are altered too.
In case of the heterogeneous traps it leads usually to the transformation of Moessbauer spectrum into very broad band. The total width of that band is $\Gamma \sim 10^3 - 10^4\ 1/\tau_+$. The GG in that case is surely absent.[32,33,34]
But the Moessbauer spectrum could be constricted into the single line of the natural width in case of the homogeneous traps. [32,33,34]
In both cases the HFS is destroyed or alias is "collapsed".

1.5.1.2. **Fiasco of methods based on the use of HFS in the AM.** The following methods are based on the use of the HFS in the AM:
a. – The use of the HFS in order to selectively pump nuclei through one HFS transition but to use the other HFS transition for the generation in so called "fluorescent" variant of the Two-Stage pumping. [22,23]
b. – The line narrowing by the radio-frequency (r-f) or *optical* methods. [4,5,8,9,17,19,27,48,51,71,72]
c. – The creation of the high ~ 90% inversion by the action of the r-f fields, or the *optical* laser fields, or their mixture on the Inversionless Mixture (IM) of the Excited and De-excited Nuclei. [23,27,68]
d. – Creation of gain ~ 90% in IM due to the creation of frequency shift between γ-emission and γ-absorption by *optical* field [23,27].
e. – Λ and V schemes for "γ-amplification without inversion" and " inversionless gain" via nuclear coherence by *optical* driving[24-25].
All that methods are destroyed via the collapse of HFS in Moessbauer, optical and r-f spectra.

1.5.1.3. **Plus trammels in case of the use of the optical HFS in AM.** Too small widths ~ $10^3 - 10^6$ s^{-1} for the lines in the optical HFS of solid are necessary for the realization in GL of the optical methods b, c, d, e mentioned above. Such narrow lines exist only in a rarefied well cooled gas. But the achievement of such narrow lines in a solid as like as ones in a rarefied cooled gas is very difficult problem.

1.5.2. Residential (Rsd) and Nonresidential (Nrsd) categories of solid GL with short-lived ELAN.

1.5.2.1. **The first objection on the Residential Solid GL with Short-Lived ELAN (RS-GL-SL).** The active medium of the RS-GL-SL must be prepared from the inversionless mixture of the excited and non-excited work nuclei. Because only such inversionless mixture could be created at any pump except the fluorescent selective two-stage pump[22,23] and some types of the two-step pump[11,39-44].

1) The Author pleases to be wrong in that negative reader because he had devoted the significant efforts for the line-narrowing problem[8,19,48].

But all that exceptions could not be realized nowadays and at near future. Hence the RS-GL-SL could do only with use of the methods c, d or e mentioned above in the point 1.5.1.2. But all that methods are inevitably destroyed by the microplasma and by the heating. Hence **nothing** RS-GL-SL could be realized.

IT IS "THE FIRST OBJECTION" AGAINST THE RESIDENTIAL SOLID GL WITH SHORT-LIVED ELAN (RS-GL-SL)

1.5.2.2. The second objection against the Residential Solid GL with the short-lived ELAN (RS-GL-SL). The RH theory of the heat blast[34,35,D] gives the next objection against the RS-GL-SL. In short the substantiation of this, second, objection is following:

Selective resonant pumping by the monochromatic radiation[22,23,27] is the most soft type of the pump for the RS-GL-SL. The flux of that selective radiation Φ_{sel} *per pulse* must provide a sufficient relative concentration of the ELAN $C_{elan} \sim \Phi_{sel}\ 0.1\ \sigma_0$. Here σ_0 is the asymptotic value of resonant cross section[35,C], $0.1\ \sigma_0$ is the approximate real value of resonant cross section averaged over the time of pump $t_{pump} \sim \tau_+/10$. At $\sigma_0 \sim 10^{-18}$ cm^2 ones have the energetic pump flux $\Phi_{sel}\ E_\gamma \sim 10\ E_\gamma/\sigma_0 \sim 1.6\ 10^3\ E_\gamma\ J\ cm^{-2}\ keV^{-1}$. So the integral heat release in the *host* matrix *per pulse* is $Q_h \sim \Phi_{sel}\ E_\gamma\ /\ l_{pen}$ where $l_{pen} = (n'\ \sigma'_{abs})$ is the penetration depth, $n' = 1.76\ 10^{23}$ cm^{-3} is the density of the number of host atoms (e.g., for a diamond), σ'_{abs} is the photo-effect's cross-section at the host atoms. This cross section depends on the energy as like as it is shown in the Table 3 below (see ref.[80]). The other values in that table are: q_h is the instant heat release in host matrix via the action of the selective pump radiation on the host; T_h is the temperature of the host

Table 3. Real radiation-heat regime at the selective resonant pumping[22,23,27].

$E_{sel} \sim E_\gamma (keV)$	1	3	10	30	100
σ'_{abs} (*barn*)	$4\ 10^4$	$1.7\ 10^3$	38.1	1.15	0.42
l_{pen} (*cm*)	**$1.4\ 10^{-4}$**	**$3.3\ 10^{-3}$**	0.15	4.9	13.5
$\Phi_{sel}\ E_\gamma (J/cm^2 imp)$	$1.6\ 10^3$	$4.8\ 10^3$	$1.6\ 10^4$	$4.8\ 10^4$	$1.6\ 10^5$
$Q_h (J/cm^3 imp)$	10^7	$1.5\ 10^6$	10^5	10^4	10^4
$q_h\ (W/cm^3)$	10^{13}	$1.5\ 10^{12}$	10^{11}	10^{10}	10^{10}
T_h (*K*)	10^6	10^5	10^4	10^3	10^3
$Q_{self}\ (J/cm^3)$	$2\ 10^5 < Q_h$	$5\ 10^5 > Q_h$	$2\ 10^6 > Q_h$	$5\ 10^6 > Q_h$	$2\ 10^7 > Q_h$
$q_{self}\ (W/cm^3)$	$2\ 10^{10}$	$5\ 10^{10}$	$2\ 10^{11}$	$5\ 10^{11}$	$2\ 10^{12}$
$Q_h + Q_{self}\ (J/cm^3)$	$10^7 \sim Q_h$	$5\ 10^5 \sim Q_{self}$	$2\ 10^6 \sim Q_{self}$	$5\ 10^6 \sim Q_{self}$	$2\ 10^7 \sim Q_{self}$
$T_{AM\ adiab}$ (*K*)	$\sim 10^6$	$\sim 5\ 10^4$	$\sim 2\ 10^5$	$\sim 5\ 10^5$	$\sim 2\ 10^6$
$T_{AM\ adiab;\ ioniz\ account}$ (*K*)	$\sim 10^5$	$\sim 2\ 10^4$	$\sim 10^5$	$\sim 10^5$	$\sim 10^5$
Regime	Heat Blast	Heat Blast	Heat Blast	Heat Blast	Heat Blast

near the AM; Q_{self} is the integral self heat release in AM; q_{self} is the instant self heat release in AM; $T_{AM\ adiab}$ is the "adiabatic" temperature evaluated without account of the ionization; at the last accounting the temperature must be decreased by factor ~ 0.5 - 0.1 because the most part of energy-release is distributed among free electrons. Below some other types of pamp radiation are compared:

1. - **The characteristic X-rays** have the line width $\sim 10^{15}\ s^{-1}$ i.e., by many orders more than the selective radiation's width $\sim 10^4 - 10^{10}\ s^{-1}$. Hence the heat release and temperature of the AM at pump by the Roentgen radiation[17] must be much more than in the Table 3.

2. -**The bremsstrahlung** (Brmstr) is more (~ by 6 orders) than Roentgen radiation and hence is much more dangerous for active medium. Besides the ELAN creation at use of Brmstr is realized via high excited interim state ($E_{interim} > 10$ MeV). Part of that energy, less than ~ 90%, is carried away (via cascade γ-quanta) but the rest part, more than ~10%, gives the contribution into heat release

$$Q_{interim} > 0.1\ E_{interim}\ n_+ / W > 10^9\ J/cm^3 \quad (7)$$

$$\textit{In very deed}\ Q_{interim} \sim 10^{10}\ J/cm^3 \quad (7')$$

Here W ~ 0.1 - 0.01 is the branching coefficient, i.e., it is the probability to create the ELAN from the interim excited state $E_{interim}$.

3. - **The pump by the neutrons**[6] gives also three parts of the contribution into the total heat release:
- The first part is as like as above the self "interim" heat $Q_{interim} > 10^9\ J/cm^3$. This part acts even in the case of cold neutrons;
- The second part is the heat release in the host matrix by the neutrons' scattering

$$Q_{scat\ host} \sim \Phi_n\ \sigma_{scat\ host}\ n'\ E_n / A_{host} \sim 10^9\ J/cm^3 \quad (8)$$

Here the neutron integral flux is $\Phi_n \sim (\sigma_{n\ exc}\ \xi)^{-1} > 10^{23}/cm^2$; the value $\sigma_{n\ exc}\ \xi$ is the cross section of the inelastic scattering with the creation of the ELAN, the cross-section for the neutron scattering on the host matrix is $\sigma_{scat\ host} \sim 10^{-24}$ cm^2; $E_n \sim 10$ *MeV* is the neutron's energy, $A_{host} \sim 10$ is the mass number of the host atoms.

- The third part Q_{self} is the same as like as in the Table 3 above.

! ! !Note: The parts Q_h and $Q_{scat\ host}$ do not depend on the concentration of the work nuclei. ! ! !

See Table 4 (point 1.5.3) as the illustration to this note.

These values are the same both for the normal 0.5% dilution ($n_+ \sim 10^{21}$ cm^{-3}) and for the anomaly super dilution[23,27] (e.g., for $n_+ \sim 10^{14}$ cm^{-3}). It needs to remember that the any anomalous wave (γ-radiation or neutron wave) is directed in very tight interval. Hence it is the ungrounded fantasy to propose the pumping of the GL by the anomalous gamma-wave(as it is supposed in [24a]) or by the anomalous neutron wave(as it supposed in [17]).

Reader of the point 1.5.2.2.: Radiation-heat conditions in the residential short-lived AM are much more hard than in SPTEN-case. The most soft radiation heat conditions are represented in the Table 3.
Hence the residential short-lived AM must be blasted inevitably at any residential type of the pump.
IT IS THE SECOND OBJECTION AGAINST THE RESIDENTIAL SOLID GL WITH SHORT-LIVED ELAN (RS-GL-SL).

1.5.2.3. The third objection against the Residential Solid GL with the short-lived ELAN (RS-GL-SL). Let suppose that the parts Q_h and $Q_{scat\ host}$ could be decreased (via some unknown as yet mechanism) so that $T_h \sim 200 - 300\ K$. Nevertheless it turns that this normal temperature of the host matrix around the AM is not yet sufficiently low. At such temperature the free paths Λ_e, Λ_h, Λ_{ph} of the carriers (electrons, holes, phonons) are less than the diameter a_1 of the active medium:

$$\Lambda_e, \Lambda_h, \Lambda_{ph} < a_1 \tag{9}$$

Such condition is very adverse for the cooling of the AM. Indeed, at this relation the adiabatic isolation of the AM is beginning via the back scattering of the carriers. It leads to the acceleration of the quasi-temperature growth in the AM and hence to the further decrease of the free paths Λ_e, Λ_h, Λ_{ph}. Such self acceleration quasi-temperature growth is finished for the very shot time by the heat blast. In order to get the meaning of the blast appearance it needs to represent the regime parameter Θ_{reg} in some more general form

$$\Theta'_{reg} = (q\ (a_1 + \delta_e)^{27/11})/5 \tag{10}$$

Here $a_1 + \delta_e$ is a mean radius ρ weighted over AM and irradiated host with the heat-release distribution $q(\rho,\phi)$. Addition δ_e is increased via the action of pump radiation. Before the blast $\Theta_{reg} \sim 1$ and small $\delta_e \sim a_1$ is sufficient to get $\Theta'_{reg} > 1$ when the blast is inevitable.
IT IS THE THIRD OBJECTION AGAINST THE RESIDENTIAL SOLID GL WITH SHORT-LIVED ELAN (RS-GL-SL).

OVERALL READER ON THE RESIDENTIAL SHORT-LIVED ACTIVE MEDIA:
ALL RESIDENTIAL SHORT-LIVED ACTIVE MEDIA WITH THE COOLING VIA THE HEAT-CONDUCTIVITY ARE BLASTED AT ANY TRANSVERSAL PUMP.
There is only one exclusion: the pumping by the longitudinal selective radiation (LSR). That LSR needs be formed as like as very narrow parallel beam with a diameter $a_1 < \Lambda_e, \Lambda_h, \Lambda_{ph}$. At $T_{host} < 100\ K$ it needs be $a_1 < 10^{-4}\ cm$. Such narrow beam of LSR must travel inside of AM. Such beam needs to have the intensity more than $\Phi_{sel} E_\gamma/(0.1\ \tau_+) \sim 10^{10} - 10^{12}\ W\,cm^{-2}$, see Table 3. Such intensive parallel and narrow beam could be given only by another γ-laser. Such "another" prime γ-laser could be the SPTEN γ-laser.

1.5.3. Residential (Rsd) active media with short-lived ELAN cooled by the Anomalous Super Dilution (ASD) on base of the Multi Wave Borrman Effect (MWBE). There are two different ways for the cooling of the active medium:
1. - The cooling by Anomalous Super Dilution (ASD) of the ELAN in the light host matrix via the use of the Multi Wave Borrman Effect (MWBE).(1980-83, Karyagin, [23,27]) This 1st way was discarded and replaced long ago by the more useful 2nd way(1983, Karyagin[27]).
2. - The cooling by use of the heat conductivity via the free or quasi-free removal of the non-equilibrium "hot" energy carriers (secondary electrons, holes and high frequency phonons).[27,29,32,34,35] This 2nd way was used in all items which were discussed above in 1.5.2.
Now it would be appropriate to remember some flaws of ASD based on the MWBE.
In case of the MWBE the formal balance GG equation holds the form

$$n_+ \sigma_0 k_0 = (n_+ \sigma k + n' \sigma' k' + n'' \sigma'' k'')\, p \tag{11}$$

Here k_0, k, k', k'' are the coupling coefficients of the anomaly wave correspondingly with the ELAN (see k_0), the electrons' shell of the work nucleus (see k), the host atom (see k') and the unwonted mixture (see k''). At very high perfection of host lattice (not achieved as yet) the MWBE could be realized. Let the number of the waves-components is $n_B \sim 100$. Then is possible to have $k_0 \sim k \sim k'' \sim n_B \sim 100$, $k' \sim 10^{-5}$. Let $\sigma'' \sim \sigma$. Let all mixed atoms are fixed at the interstitials of the host lattice. Then the value p, so called "reserved amplification" (see [23,27,30,34,35,C]), is

$$p \sim (\sigma_0/\sigma)/[1 + (n'\sigma'/n_+\sigma)\ (k'/k) + (n''/n_+)]. \tag{12}$$

Let $n'' < 0.1\ n_+$. Then at the diamond $(n'\sigma'/n_+\sigma)\ (k'/k) < 0.1$ ones have

$$(n_+/n') \sim 10\ (k'/k)\ (\sigma'/\sigma) \sim 10^{-6}\ (\sigma'/\sigma) \tag{13}$$

then $p \sim (\sigma_0/\sigma)$ as like as at usual 0.5% dilution (see [C,D]). In case of the AM "Co^{58} *in diamond*" ($E_\gamma = 28.1\ KeV$) [34,35,E] ones have $n' = 1.76\ 10^{23}\ cm^{-3}$, $\sigma' = 5.63$ b, $\sigma = 1200$ b and $(n_+/n') \sim 5\ 10^{-9}$. In that case the integral self energy-release is $Q_{self} \sim 3.6\ J/cm^3$. The low-temperature capacity is $C(T) = C_0\ (T/T_D)^3$. In case of diamond $T_D = 1860\ K$, $C_0 = 568\ J/cm^3K$. Hence the temperature "only by the self-heat" is $T_{AM\,self} = (4Q\ T_D^3/C_0)^{1/4} = 113\ K$. But the value $Q_{self} \sim 3.6\ J/cm^3$ is only small part contribution into the total heat release, see point 1.5.2.2. and the table 3 with the account the note at the end of that point. In according with that note the following table is created:

Table 4. Real radiation-heat regime at the selective resonant pumping[22,23,27] **in case of ASD** $n_+/n_e \sim 5\ 10^{-9}$.		
$E_{sel} \sim E_\gamma (keV)$	ASD and MWBE could not change this result	30
$\Phi_{sel}\ E_\gamma (J/cm^2 imp)$	ASD and MWBE could not change this result	$4.8\ 10^4$
$Q_h (J/cm^3 imp)$	ASD and MWBE could not change this result	10^4
$q_h (W/cm^3)$	ASD and MWBE could not change this result	10^{10}
$T_h\ (K)$	ASD and MWBE could not change this result	10^3
$Q_{self}\ (J/cm^3)$	**Only this result is changed by use of the ASD and MWBE**	$3.6\ J/cm^3$

Q_h+Q_{self} (*J/cm³*)	ASD and MWBE could not change this result	10^4
$T_{AM\ adiab}$ (*K*)	ASD and MWBE could not change this value	10^3
Result for GG	Any r-f or optical schemes with use of HFS, see1.5.1.2., could not do at such high temperature	**No GG**

1.5.3.1. The pump by the super cold neutrons. In case of the pump by the super cold neutrons it needs to account only the result (7) which gives $Q_{self} \sim Q_{interim} \sim (n_+/n')\ (10^{10}/(0.005))\ J/cm^3 \sim 10^4\ J/cm^3$ and quasi temperature

$$T_{AM\ self} = (4Q\ T_D^3/C_0)^{1/4} = 82\ (Q)^{1/4}\ K\ (\ J/cm^3\ )^{-1/4} \sim 800\ K \qquad (14)$$

The optical schemes with use of HFS, see1.5.1.2., could not do at such high temperature. The action of the r-f schemes could be hardly possible at such temperature[23,27] but see point 1.5.3.2. below.

1.5.3.2. The microplasma in the residential AM at the ASD. The ASD is linked with the MWBE and hence is possible only for the much high perfect big crystal. But in the perfect big crystal the centers for the pairs annihilation are absent. Hence the time relaxation for the pairs' density must be more than the time life τ_+. It means that the pairs' concentration in the perfect dielectric crystal could be

$$n_{e\ perf\ diel} \sim 10^3\ n_+ \sim 10^{18}\ cm^{-3} \qquad (15)$$

This result corresponds to the above ASD ratio $n_+/n_e \sim 5\ 10^{-9}$. The crystal needs be big (see below), it could be only dielectric in order to be transparent for the radio-frequency or optical waves. **The reader: The microplasma has very high density in case of the ASD in the residential AM. Hence all methods specified in the point 1.5.1.2. are destroyed by microplasma.**

1.5.3.3. The natural limit for the ASD ratio $(n_+/n') \sim 10\ (k'/k_B)$ (σ'/σ) depends on two factors. The values σ'/σ could be evaluated as $\sigma'/\sigma \sim$ **0.03 - 0.001**, see data for different six work isotopes in the Table 5 taken from the Ref.[E].

Table 5. To the evaluation of the ratio interval $\sigma'/\sigma \sim 0.01 - 0.001$						
Work Isotope	$^{92}Nb_{41}$	$^{122}Sb_{51}$	$^{152}Eu_{63}$	$^{65}Zn_{30}$	$^{69}Ge_{32}$	$^{58}Co_{27}$
σ'/σ	0.014	0.0027	0.0015	0.014	0.031	0.0047

The limit for the factor (k'/k_B) must be depend on the mosaic structure of the crystal. In deed the crystal is divided into a big amount of the quite perfect blocks (QPB) with the sizes ~ 10^{-4} - 10^{-1} cm. But the directions of the main crystallographic axes of one QPB are slightly deviated from the directions of the another QPB. Let denote the dispersion of that deviation (in the radians) as $(\delta\theta)^2_{Avarige}$. In case of a good crystal that value is ~ $|\delta\theta|_{Average} \sim 10^{-3}$ *rad*. Let the amount of the partial waves in the MWBE is $k_B >> 1$. The sum of the polarization vectors $\vec{P}_k$ of that waves must be zero at the point-like node of the perfect crystal

$$\sum_{1\le k\le k_B} \vec{P}_k = 0 \qquad (16)$$

The square of that sum is

$$[k_B + 2 \sum_{1\le k<k'\le k_B} Cos\theta_{kk'}] = 0 \qquad (17)$$

That square is changed in case of small deviations $\delta\theta_{kk'}$ of the fixed angles $\theta_{kk'}$ between the wave-components of the MWBE:

$$I_{node} = (\sum_{1\le k\le k_B} \vec{P}_k)^2 = [k_B + 2 \sum_{1\le k<k'\le k_B} Cos(\theta_{kk'} + \delta\theta_{kk'}]P^2 \approx P^2 k_B (\delta\theta)^2_{Average} \qquad (18)$$

The relation (17) is accounted in the equation (18). The right part of the eq.(18) is averaged over the crystal-lattice. The physical sence of the left part of eq. (18) is the intensity of the anomalous wave at the lattice node. The value P^2 is the intensity of the ordinary wave. Hence the coupling coefficient k' for the MWBE in case of the small deviations $\delta\theta_{kk'}$ is following

$$k' = I_{node}/P^2 \approx k_B\ (\delta\theta)^2_{Average} \qquad (19)$$

Hence the natural limit for the ASD ratio is the following

$$(n_+/n')_{ASD} \sim 10\ (k'/k_B)\ (\sigma'/\sigma) \sim 10\ (\sigma'/\sigma)\ (\delta\theta)^2_{Average} \sim (0.3 - 0.01)\ (\delta\theta)^2_{Average} > 10^{-8} \qquad (20)$$

E.g., the real estimation $(n_+/n')_{ASD} \sim 10^{-6}$ was used in Refs.[23,27]. It is a reason for very cautious supposition about $(n_+/n')_{ASD} \sim 10^{-8}$ as probable only at a far future[28-36]. But the possibility of the value $(n_+/n')_{ASD} \sim 10^{-9}$ as surely achievable[24a] could be regarded only as a mere assertion. **The reader: In deed the real achievable value of the anomalous super-dilution $(n_+/n')_{ASD}$ on base of the MWBE can't be less than 10^{-8}. All values $(n_+/n')_{ASD} < 10^{-8}$ must be regarded only as a mere assertion or as a wanton fantasy.**

1.5.3.4. The too <u>overmuch hope on the Anomalous Super Dilution</u> (ASD) [23,27] with the factor $k'/k_B < 10^{-6}$ <u>on the bases of the Many Wave Borrman Effect</u>[26] (MWBE). In deed at such ASD the longitude of AM must be $L_{ASD} > 0.1\ k_B/k' > 1000\ cm$ in order to achieve the amplification of the normal AM (without ASD, at normal dilution ~ 0.5%, $L_{AM} \sim 0.1\ cm$). It needs also to have the diameter of the active medium $D_{ASD} > 10^{-2}\ k_B/k' > 100$ cm in order to avoid the losses linked with the transversal diffusion[88] of the anomalous Borrman mode. It needs to have the relative accuracy $\sim (k'/k_{Borr})^{1/2} < 10^{-3}$ for the amplitudes and directions of the polarization vectors $\vec{P}_k$ for all k_B partial waves in MWBE in the volume of the active medium $V_{ASD} > 10'000$ *liters*. Such big crystal needs be high perfect and almost without any mosaic. The creation of such big very perfect crystal is unsolvable task even at very far future[34,35]. Besides the MWBE is sensitive to very slight deviations of the micro-tensions in the crystal. But that deviations are inevitable at any fixation of such big crystal. The temperature of such big crystal would be also heterogeneous and it leads also to the destroying of MWBE and ASD. The too big mass (~30 *tons*) of AM don't allow to achieve some desirable low temperatures (see [C-D]) during a short time ~ 0.1 τ_+.

ADDENDUM to 1.5.2. The fluorescent selective two-stage pump[22,23] is based on the use of the HFS in the AM. This method is included in a list of methods which are inevitably destroyed by the microplasma or by the heating, see point **1.5.1.2.a.** At pump by the bremsstrahlung even at use of so called "Texas resonance" [11,41-44] both work levels are populated via manifold of the more high interim levels. Such population gives only the inversionless mixture. The selective pump by method[39,40] is possible in case of the pump by the monochromatic γ-radiation generated by another γ-laser. See below the Classification Table. But our task is to find that origin GL which cold do without use of another GL.

2. Gamma-Lasers' Classification on Base of the Plural Characteristic «Adverse Overwork».

2.1. Adverse Overwork (AOW): the degree of total adverse influence on *active medium* (AM) from all processes in *it*.

In a result of direct or indirect *adverse influence* (sec.1.2) the totality of all functions, beneficial and adverse processes *in situ* (in site of active medium) *adversely do* on the active medium. I.e., **the mentioned totality adversely do on active medium**, on its host structure (through damages and other heterogeneity), on its radiation and temperature regimes, on its parameters (Moessbauer factor, heat capacity, heat conductivity, line width), on its conditions for the gamma-lasing. This total adverse influence on the active medium is analogous as like as the excruciating for a man. The degree for that excruciating for the active medium is named here as **Adverse Overwork (AOW)**. In deal AOW is a many-parameter's value. But the AOW's *qualitative* account can be given in terms of a specification for the main elements and parameters of AOW. The very main components of AOW are the nuclear fluxes, the heat release, the quasi-temperature T_{AM}, the degree of irradiation (number of charges per cm^3) in Active Medium (AM) and the necessary over-threshold density of ELAN (number of ELAN per cm^3).

2.2. The γ-Lasers' Classification based on the comparison of γ-lasers over their Adverse Overwork.

Table 6. Γ-lasers (GL) on nuclear transitions. Classification over active medium's Adverse Over Work.
Analysis of different ways for GL creation, their merits and flaws with use of joint γ-lasing and radiation-heat regimes theory.

The ways to the GL creation in blind-alley are labeled by its number against dark field as like as on the right. ⇒	13a
The remote, dim or too spurious ways are labeled against shadow as like as on the right. ⇒	13b

Manifold «Γ-Lasers on nuclear transitions (GLNT)»

Non-Moessbauer GL based on plasma, on gas or on beams of free nuclei[77,78] are infeasible[34,35]. Hence a big Manifoldf "GLNT" is reduced to the less Manifold "Gamma-Ray Solid Lasers"

Manifold «GLNT» ≡ Manifold «Gamma-Ray Solid Lasers»

All total manifold of GLNT is divided into *residential* and *non-residential* manifolds. In *residential* GL the ELAN are inserted in active medium (AM) *long before* the starting of γ-generation (GG). In *non-residential* GL the ELAN are inserted in AM *just before* the starting of GG.

CATEGORY «LONG LIVED (LL)» ≡ \SOLID\LL

Active medium (AM) on LL isomers could be only solid[34,35]. AM in lasing study consists of the long-lived ELAN diluted in the solid cold matrix. LINE NARROWING IS EXTREMELY NECESSARY. Category «LL» is divided into the Residential and Non-residential Subcategories.

SUBCATEGORY «LONG LIVED (LL) *NON-RESIDENTIAL*» ≡ \SOLID\LL\NONRES

Non-residential AM could be located only at surface layers of solid and so has no well developed Borrman effect. At this adverse condition, BUT AT BENEFICIAL HYPOTHESIS OF ACHIEVEMENT OF A QUITE PERFECT LINE NARROWING, AS LIKE AS A NATURAL LINE WIDTH, **the LL nuclei-candidates with time-life $\tau_+ \sim 10^{+2} - 10^{-3}$ s fit for GL are not revealed as yet.**

HENCE THIS *NON-RESIDENTIAL* SUBCATEGORY *REMAINS AS YET EMPTY*

Subcategory«Long Lived (LL) *RESIDENTIAL* with use of Multiwave Borrman Effect (MWBE)» ≡ \SOLID\LNG\RSD\MWBE

Residential AM needs be fixed in deep part of volume of crystal where well developed Multiwave Borrman Effect is probable. At this beneficial condition many LL **nuclei-candidates with time-life $\tau_+ \sim 10^{+2}$-10^{-3} s could be used in GL** even if they are not used in non-residential schemes. Some ways for the realization of such \LL\RES\GL are discussed in[34,35].

Many ideas on pumping first arose in «Long Lived» and are used now in other category «Short Lived». E.g., an idea on laser selection of «middle-lived» isomers[7] was transformed afterwards into the ideas of SPTEN for the «short-lived» isomers[27-37]. The Category LL is divided also into the classes *over ways for line narrowing*.[8] First works were the **«radio-frequency narrowing»** methods[5, 31] and the magnetic «one-parametric» compensation of **«monopole»** broadening[48]. The main difficulty for the narrowing consists in the **dependence of Hyper-Fine Structure from a lot of chancy parameters varied independently**[18,19]. This main difficulty is partly overcame in the **«diamagnetic super-anomalous-dilution»** methods[25,27] on base of the Borrmann effect[26] and is totally overcame in the **«multiparametric»** methods **with** exterior action (by laser, etc.)[19,8] and **without** one[8]).

**«FLAW DESIGN SPECIFIC (FDS)» CLASSES IN «LONG LIVED *RESIDENTIAL*» ≡ *\LL\RSD\FLAW DES SPEC **

*\FDS-1\ based on **dubious interpretation** of a certain low-temperature effect for the γ-transition from the long-lived top level to the short lived one[73]. This effect is *not reproduced* in other laboratories[79].

*\FDS-2\ based on **spurious hypothesis** of screen's influence on rate of nuclear γ- ray decay[74-76]

*\FDS-3\ based on **remote canal** of two-photon nuclear generation ignited by powerful $\sim 10^{13}$ *W/cm²* laser beam[52,53]. Such GL *perhaps* could be realized *but only by means of hybridization* with the SPTEN. See the 8^{th} lines.

CATEGORY «SHORT LIVED» ≡ «SOLID PULSE» PUMPING ≡ \SLD\PLS

Active medium on short-lived isomers could be only solid[34,35].

Active medium in lasing study consists of the short-lived ELAN diluted in solid cold matrix

LINE NARROWING IS NOT NECESSARY. «Solid Pulse» pumping could do without any exterior device for line narrowing
Category «Short Lived» is divided *over the means for pumping* into Residential and Non-residential Subcategories.

«RESIDENTIAL SHORT LIVED» SUBCATEGORIES ≡ «RESIDENTIAL - SOLID - PULSE» PUMPING ≡ \RSD\SLD\PLS

Residential Subcategory «One-Stage Pumping» or alias «SOLID DIRECT PULSE» PUMPING ≡ \RSD\SLD\DRCT\PLS\
Nuclear parents of ELAN are located *in AM* long before the start of γ-generation. ELAN are created as a result of nuclear reaction immediately before the start of γ-generation. Nuclear reaction in AM is executed by radiation from a certain exterior powerful source

№	1	Main Parameters of Adverse Over-Work (AOW) 2	3	4	5	6	7
	Type or class of γ-laser and its lineal branch on family tree	Heat release	T_{AM}	Irradiation degree in AM	ELAN's density	Necessary exposition Φ	Exposed target
	Dimension unit	W/cm³	°K	charges/cm³	cm⁻³	particles or quanta/cm²	
1	One-Stage Simple (1Stg'S) :*\1stg\smp\	10^{14}	10^{8}	### 10^{22}	10^{21}	10^{27} neutrons[21,22]	Active Medium

Scheme[6]: Source of Nuclear Radiation (SNR) ⇒ [Filtered or Moderated nuclear radiation] ⇒ [Active Medium (AM)] ⇒ **γ-generation**
♦ Active Medium (AM) according to [6] may be needle dipped in liquid helium. Such AM is blasted inevitably[28]. ♦ Pump 1Stg'S needs in nuclei with big «isomer ratio» $\xi >> g$ for population of work levels where $g = (2j_+ + 1)/(2j_- + 1)$ is the degeneration's ratio for top work level and lower one[9,30]. Such nuclei are absent [9-12]. At $\xi \sim g$ a value of pump exposition ~ 10^{27} neutrons/cm² is unfeasible[20,21]. [9,29,32,35]
γ-generation (GG) for 1Stg'S *is not feasible* because its AM is blasted owing to high overheating.

2	**One-Stage Generalized (1Stg'G) ≡ ≡ One-Stage⊗Two-Phase⊗ASD ≡ ≡ *\1stg\2phs\asd**	10^{8}	350	$0 \div 10^{20}$ subject to crystal	10^{14}	10^{21} cm⁻² of slow neutrons[23,27]	Active Medium

Only so low temperatures $T_{AM} > 350$ *K* could be hardly achieved at very beneficial parameters $E_n \sim 0.01$ *eV*, $k_0 \sim k_B \sim 100$, $k' \sim 10^{-5}$, $n/n' \sim 10^{-9}$. Such parameters could be realized in very far future. However, the creation of gain in excited inversionless nuclear mixture could be feasible only at much less temperatures: $T_{AM} \leq 5 \div 10$ *K* in case of the optical two-phase methods[23,27] or $T_{AM} < 50 \div 100$ *K* in case of the radio-frequent two-phase methods[23,27].
Scheme[23,27]: SNR ⇒ [Filtered selective or Moderated nuclear radiation] ⇒ [Non-inverted Excited Mixture ≡ ELAN+ de-excited nuclei] ⇒ [Creation of gain in originally inversionless excited nuclear mixture by optical or r-f methods + ASD] ⇒ GG
♦ Optical schemes for Amplification Without Inversion and r-f schemes for the creation of gain in originally inversionless excited nuclear mixture + ASD are suggested[23,27] 20 years ago. ♦ Special construction of AM supply its cooling[23,27,29,32,35]. Doppler-broadening by AM heat expansion is averted by special construction[27,29] of work body. ♦ 1Stg'G could do without big isomer ratio *at* $\xi < g$[23,27]
But 1Stg'G *is not feasible* owing to contradictory demands to size of AM for the cooling and ASD. [23,27,29,32,35]

Further development of residential GL idea lies in the creation of special powerful sources or converters for the creation of the more soft radiation which is effective in pumping and is not destructive for the AM. This way leads to the subcategory «Indirect Pulse Pump».

RESIDENTIAL Subcategory «SOLID INDIRECT PULSE» PUMP ≡ \RSD\SLD\INDRCT\PLS
The «Indirect Pump» is less destructive for active medium than the «Direct Pump».
Parents (in long lived state or stable) of ELAN are located in AM long before the start of γ-generation
ELAN are created by the way of parents' excitation immediately before the start of γ-generation.
Excitation of parents into ELAN needs be executed by more soft type of radiation than in case of «Direct pump».

TWO-STAGE CLASS

CLASS «RESIDENTIAL SOLID INDIRECT PULSE TWO-STAGE» PUMP ≡ 2Stg ≡ \RSD\SOL\INDR\PUL\2STG\ ≡ *\2STG\.
The *resonant γ-radiation for the ELAN creation in active medium* is less destructive than any rigid nuclear radiation.

	Type or class of γ-laser and its lineal branch on family tree	Heat release	T_{AM}	Irradiation degree in AM	ELAN's density	Necessary exposition Φ	Target under pump exposition
	Dimension unit	W/cm³	°K	charges/cm³	cm⁻³	particles, quanta/cm²	
3	Two-Stage Simple ≡ 2Stg'S ≡ ≡ *\Rsd\2stg\sim\ [22]	10^{21}	10^{5}	### 10^{22}	10^{21}	10^{27} neutrons [20,21] 10^{24} reson. γ-quanta[23]	Input of Converter Active Medium

Scheme[22]: SNR ⇒ filter or moderator (F, M) ⇒ 1st stage: converter «neutrons - resonant γ-quanta» creates selective resonant γ-radiation ⇒ 2nd stage: selective excitation of ELAN in AM ⇒ No γ-generation
♦ 2Stg'S needs in a big isomer ratio $\xi >> g$. ♦ 2Stg'S *is not feasible* because its AM is blasted owing to high overheating.[29,32,35]

	Dimension unit	J/cm³	°K	charges/cm³	cm⁻³	particles, quanta/cm²	
4	**Two-Stage - Fluorescent'2ASD :: 2Stg'F⊗2ASD::*\RSD\2STG\FLU\2ASD**	1	100	$0 \div 10^{20}$	10^{21}	10^{22} neutrons [23] 10^{19} res. γ-quanta[23]	Input of Converter Active Medium

Scheme[22]: SNR ⇒ (F,M) ⇒ 1st stage: converter «neutrons - resonant γ-quanta» creates selective resonant γ-radiation ⇒ ⇒ 2nd stage: selective excitation of ELAN in AM with very remote «Double ASD» ⇒ **very feeble γ-generation**
♦ Selective excitation begins from one HFS-level of ground state but γ-lasing transition finishes on another HFS-level[22]. **2StgSel'F** could do without big isomer ratio *even at* $\xi < g$.[23,27]. But the pre-γ-lasing strongly decreases the inversion in **2StgSel'F**[17,23].
♦ «Double ASD» is a pair of ASD: The 1st ASD is assigned for the selective pumping γ-radiation. The 2nd ASD is assigned for the γ-lasing. Such «Double ASD» is very remote. Type **2StgSel'F could do (but very hardly) only at realization of ASD-**

conditions (it is utterly hard task even at far future)[23,27,32]

Dimension unit	J/cm^3	°K	charges/cm^3	cm^{-3}	particles, quanta/cm^2	
5 2Stg Generalized ≡ 2Stg'G'2ASD ≡ Two-Stage⊗Two-Phase⊗Two-ASD ::\2stg\2phs\2ASD\	1	100	0 - 10^{20}	10^{21}	10^{20} neutrons[23] 10^{17} reson. γ-quanta[23]	input of Converter Active Medium

Scheme[23,27]: SNR ⇒ F,M ⇒ 1st stage {converter «neutrons-resonant g-quanta» ⇒ Selective Resonant Filter Þ Selective G-resonant Radiation} ⇒ 1st phase of 2nd stage {Selective Excitation of ELAN in AM, i.e., creation of Non-inverted Excited Mixture (NEM) of ELAN and de-excited nuclei} ⇒ 2nd phase of 2nd stage {ASD + optical or r-f scheme's action[23,27] for Gamma-Resonant Self-Absorption's Suppression (GRSAS)+ Double ASD } Þ very remote γ–generation

"Special construction of AM for its cooling Doppler-broadening by AM's heat expansion is prevented owing to special measures. "Type 2Stg'G is feasible in future *at remote Double «Anomalous Super-Dilution*, ASD»[23,27] ~ one work nucleus per 10^9 atoms of high perfect host on base of Many-Wave Borrmann Effect (MWBE).[26,32,34,35] At such case 2Stg'G could do with a small isomer ratio x and is free from a parasitic leakage through the pre-γ–lasing.[23] 2Stg'G has ~ 90% inversion at use of Two-Phase «Radio-Frequency Pulse Separation» methods.[23,27,32,35,36] It has Amplification Without Inversion at use of Two-Phase «Optical Pulse Separation» methods.[32,35,36] Without the Double ASD creation, its action is destroyed by migration of charges in microplasma[32,35,36]. 2Stg'F and 2Stg'G are not deprived of its merits and are not bad as like as the 2Stg's only with use of remote Double ASD[23,27] ~10^{-9}. Other ways for realization of 2Stg'G add up to some variants of hybridization 2Stg'GASPTEN. See some types below.

Two-Step class ≡ \RSD\SLD\INDR\PLS\2STP\ ≡ *\2STP\

So called «Two-Step» class of γ-lasers, predicted many years ago[11,39-45] is well known nowadays. Work nuclei of that class arise in a result of sudden transformation of long lived high excited nuclei into the short-lived ones. It is the 2nd step. The 1st step is a preparation and the storage of long lived high excited nuclei in work-body of γ-laser. The last analysis[11] of both that steps contains only nuclear reaction problems. But the radiation-heat regimes of AM for such γ-laser are practically without sufficiently total analysis. The main results of general jointed γ-generation and radiation-heat regimes theory are used below for the analysis of Two-Step class.

CLASS «RESIDENTIAL SOLID INDIRECT PULSE TWO-STEP» PUMP ≡ 2Stp ≡ \RSD\SLD\INDR\PLS\2STP\ ≡ *\2STP\[11,39-45]

First Step: Storing of long-lived parent isomer (LLPI). Second Step: Turning of stored LLPI into the short-lived ELAN by a triggering pulse.[39-43]

Type or class of γ-laser and its lineal branch on family tree	Heat release	T_{AM}	Irradiation degree in AM	ELAN's density	Necessary exposition Φ	Exposed target
Dimension unit	W/cm^3	°K	charges/cm^3	cm^{-3}	particles or quanta/cm^2	-
6 Two-**Step** Simple ≡ 2Stp-S	10^{16}	10^9	10^{24}	10^{21}	$\Phi_{tr}E_{tr}>10^{10}$ J/cm^2	Active Medium

Scheme: 1st step: Long-Lived Excited Nuclei (LLEN) are stored in solid host⇒2nd step: Transfer of LLEN into Short-Lived Interim State (SLIS) by triggering action of pulse non-resonant radiation *in a transversal geometry*. ⇒Spontaneous transition (or chains of transitions) of SLIS into the ELAN-state.⇒Generation of AM on that ELAN.

The type Two-Step Simple is not feasible due to the heat explosion of its AM before the γ-lasing.

	Unite of instant release is W/cm^3	W/cm^3	°K	charges/cm^3	cm^{-3}	particles, quanta /cm^2	
6A	Two-Step⊗Two-Phase ≡ *\RES\2- STEP\2-PHAS\	10^{16}	10^9	## 10^{24}	10^{21}	$\Phi_\gamma E_\gamma>10^{10}$ J/cm^2	Interim beam

Scheme: Second step includes the r f or optical methods for creation of gain in inversionless excited nuclear mixture[23,27].

Type 6A is destroyed by the heat explosion of AM before the generation. [32]

	Unite of heat release per pulse is J/cm^3	J/cm^3	°K	charges/cm^3	cm^{-3}	particles, quanta /cm^2	
6B	**Two-Step⊗Two-Phase⊗ASD** ≡ *\RES\2- STEP\2-PHAS\ASD\	10^5	10^4	10^{23}	10^{14}	$\Phi_\gamma E_\gamma>10^{10}$ J/cm^2	**Active Medium**

Scheme: Scheme 6A modernized by introducing of ASD (Anomalous Super Dilution[23,27]) for pumping γ–radiation and for γ-lasing simultaneously. Note: the creation of ASD for the pumping radiation is more problematic than ASD for only g-lasing alone.

Supposed Super Modernized Two-Step (Type 6B) is INFEASIBLE too [32,34,35]

CATEGORY «SHORT LIVED *NONRESIDENTIAL*» ≡ «PULSE PUMPING *NONRESIDENTIAL*» ≡ \NRSD\SOLID\PULSE\

NONRESIDENTIAL Category «Soft Prompt Transplantation of Excited Nuclei» ≡ SPTEN ≡ \NRSD\SOLID\PULSE\INDIRECT\SPTEN\

many Unfeasible Classes of GL could be turned into Feasible Classes through the Hybridization with SPTEN

Soft Prompt Transplantation of Excited Nuclei(SPTEN)[28-36] is much less destructive for the active medium than any radiation (e.g., γ–resonant) in residential pump which penetrates in the host in order to create the ELAN. It leads to more low quasi-temperature T ~ 30 K in active medium during a total γ–lasing circle.[32,35,36] The ELAN for SPTEN are creating in a «converter» of type «nuclear or another radiation ⇒ ELAN» called as «Multi-Beam Emitter» (MBE). At *SPTEN* a high relative inversion more than 90% arises in the active medium (in situ). But the process of the inverting is located *ex situ* . Hence SPTEN γ-laser can do without use of any processes in situ (i.e., in active medium) for the inversion creation or for the «amplification without inversion». Besides SPTEN γ-laser can do without use of any line narrowing devises because this γ–laser uses the short-lived isomers as all classes of the General Category «Pulse Pumping». Hence SPTEN γ-laser can do without use of any HFS. The last, the heterogeneous HFS of ELAN is collapsed owing to the existence of a hot microplasma in a cold host-lattice[32,35,36]. Hence all possible work transitions are cumulated only in one narrow line without any parasitic branches. It is very beneficial for γ-lasing. All above results are connected with the utter least loading on the active medium (in situ). Indeed in case of SPTEN the active medium has only one simple load, viz., γ-lasing. In the SPTEN ALL OTHER LOADS ARE TRANSFERRED *from the* in situ *into* THE EXTERIORITY OF ACTIVE MEDIUM (i.e., into the *ex situ*[30]). In a result the complexity in the exteriority turns into the utter simplicity and feasibility of conditions for γ-lasing[30].

Class «Soft Prompt Transplantation of Excited Nuclei» ≡ SPTEN

	W/cm^3	K	charges/cm^3	cm^{-3}	per cm^2

7	SPTEN-simple \SLD\PLS\INDRCT\RSD\SPTEN\	10^{11}	30	10^{17}	10^{20}	10^{15} neutrons[28] 10^{14} ELAN[28]	Input of MBE Active Medium

Scheme[27-36]: Power Source of Nuclear Radiation (PSNR)⇒ nuclear radiation ⇒ Multi Beam Emitter (MBE) ⇒ flux with mixture of ELAN ⇒ fast laser selection of ELAN ⇒ their soft prompt focusing on cooled host crystal in place of AM ⇒ γ-lasing

"PSNR[28-30]: nuclear explosions(neutrons)[6]; aperiodical pulse reactors(neutrons)[37]; mega ampere electron accelerators (γ-bremsstrahlung)[56]; power storage-rings for ~100 GeV heavy nuclei (part of them is excited at their passing through material of MBE) [28-30]. "Special cooling of AM[27-30,32,34,35]. "Doppler-broadening by AM's heat expansion is prevented[27-30]. "Nouadays 19 nuclei-candidates are fit for γ–laser with time life in first short-lived interval 10^{-4}-10^{-6} s without MWBE and 22 nuclei-candidates are fit for GL with time life in the 2nd short-lived interval 10^{-6}-10^{-7} s without MWBE. It is very important because the sufficiently effective MWBE is very remote thing. "SPTEN-simple is really feasible after creation of MBE. MBE are necessary in many fields out of GL problem and could be realized before their application in GL. It is the best guarantee for soon realization of MBE and hence SPTEN.

SPTEN-simple is FEASIBLE on existing technical base

Hybridized pumping systems[29,30] with SPTEN
(Soft Prompt Transplantation of Excited Nuclei) *\IND\SPTEN\HYBR\

SPTEN-Simple acts at many types of ELAN creation[27-36]: at many nuclei-candidates, at many reactions and processes for ELAN creation, at many types of sources for primary radiation, etc. The SPTEN construction is utter variable. These properties of SPTEN make a lot of possibilities for the hybridization of SPTEN with many other γ-laser types. Perhaps, in such manner could be realized many projects of γ-laser[9-12,17,41,42,47] (including some projects, e.g., two-photon γ-lasers[52,53], considered at revision as «no go»[34]).

8A	**TWO-STEP⊗SPTEN** *\RSD\INDRCT\2STP\SPTEN\	10^{11}	30	10^{17}	10^{20}	$\Phi_\gamma E_\gamma$~**10** J[28] 10^{14} ELAN[28]	Input of MBE Active Medium

Scheme: The parents of the two-step are triggered into the short-lived work isomers. In a result of high temperature the triggered nuclear mixture is blasted and as a hot plasma penetrate into the grating of Multi-Beam Emitter (MBE). That plasma is fast cooled in MBE and transformed into the Multi-Beam on the output of MBE. Further the system works as like as SPTEN without problems.

Hybrid «Two-Step⊗SPTEN» is FEASIBLE in principle. Here the residential type «Two-Step» is transformed with use MBE into the nonresidential type «SPTEN»

		W/cm^3	K	charges/cm^3	cm^{-3}	per cm^2	
8 B	**SPTEN⊗2Stg'G⊗2ASD** ⇒\spten\2Stg'G\2ASD\	10^{11}	50	10^{17}	10^{20}	10^{18} ELAN [23] 10^{17} res. γ-quanta[23]	Input of Converter Active Medium

Scheme: Powerful Source of Nuclear Radiation⇒Multi Beam Emitter⇒Fast Laser Selection of ELAN from nuclear mixture ⇒ Focusing of well enriched nuclear mixture on Converter «Excited nuclei - Selective resonant γ–radiation» ⇒ **2Stg'G⊗2ASD** (which is feasible in far future on base of Double Many-Wave Borrmann Effect. It has energy output ~10^8 J/imp[49,50]) ⇒ **γ-lasing**

In case 8B the SPTEN is used in unusual manner: the nuclei from MBE come to the input of converter «ELAN → resonant γ-radiation» which is a certain «antipode» for the MBE. This hybrid is feasible only in a far future on base of «anomalous super-dilution»[23] ~ 10^{-9} (one heavy nucleus per 10^9 light atoms of host) or some another use of a Many-Wave Borrmann Effect (MWBE)[26] in a converter. The active medium uses Double MWBE (for γ-pump and for γ-lasing). In such case active medium can have a big diameter at low quasi-temperature and hence can give a big output energy per impulse of γ-lasing[23,35,49,50].

Hybrid «SPTEN⊗2Stg'G⊗2ASD» is FEASIBLE in principle **in a far future**. Here only part of SPTEN scheme, viz., MBE is used in order to supply the action of the source of the selective radiation for the residential active medium of the two-phase GL with a Double ASD.

SPTEN-HYBRIDS[34,36]

on ELAN Creation by Strong Laser Field in Plasma[46,47,90], ECSLFP⊗SPTEN, see 8C,
and on ELAN Promotion (Ignition) for Two-Photon γ-Lasing[52,53], EPTPGL⊗SPTEN, see 8D

		W/cm^3	K	charges/cm^3	cm^{-3}	in volume of AM	–
8 C	**ECSLFP⊗SPTEN**	10^{11}	30	10^{17}	10^{20}	$N_0 = 10^{11}$	High temperature laser plasma

Short Scheme 8C: Phase «**ELAN Creation** by Strong Laser Field in Plasma[46,47,90], **ECSLFP**» ⇒ Phase for preparation of AM by the «SPTEN-method» ⇒ Active Medium ⇒ Stimulated γ-generation.

Detailed Scheme 8 C: Super Strong Laser Field in laser plasma transforms the parent nuclei (in isomer or in stable state) into ELAN ⇒ Hot plasma-mixture with the promoted ELAN ⇒ input of MBE⇒ The transformation of that hot plasma-mixture into the cooled atomic mixture-flux formed as like as a Multi Beam ⇒ laser selection of ELAN ⇒ their soft prompt focusing in place of AM ⇒ γ-lasing

8 D	**EPTPGL⊗SPTEN**	10^{11}	30	10^{17}	10^{20}	$N_0 \sim 10^8 \div 10^{11}$	High temperature laser plasma

Short Scheme 8D: Phase «Promotion of 2-photon γ-decay»⇒ Phase «SPTEN-preparation of AM from promoted ELAN» ⇒ ⇒Stimulated 2-photon γ-generation.

Detailed Scheme **8D**: Super Strong Field of power optical laser promotes the 2-photon γ-decay for the Long-Lived ELAN ⇒ Hot temperature plasma-mixture with the promoted ELAN ⇒ input of MBE⇒ The transformation of hot plasma-mixture into a cooled atomic mixture-flux as like as a Multi Beam ⇒ laser selection of the promoted ELAN ⇒ their soft prompt focusing in place of AM ⇒ 2photGG

Note: ♦Ratio ρ = «induced signal/spontaneous noise» < 1 or ~ 1 at $N_0 \sim 10^8$ - 10^{10}; ρ ~ 1 or ρ > 1 at $N_0 > 10^{10}$, see sec.6 of the present work. ♦ Nowadays the achieved experimental amounts of the excited nuclei created in a power laser focus $N_{in\ focus} \sim 10^3$ - 10^5 are by many orders less than the necessary amount $N_0 \sim 10^8$ - 10^{11}. ♦The state of the promoted ELAN[52,53] is seems to be the non-stationary mixture of the top state and the lower state of the work nucleus. Hence the HFS of the promoted ELAN needs be differ from the HFS of the non-promoted ELAN. It is the base for the selection of the promoted ELAN by the SPTEN-method. ♦ By[52,53], some significant time-delay t_{del} exists between the promotion (ignition) moment and the rise moment of the stimulated 2-

photon γ-decay. By[52,53], the high ionized and high temperature plasma does not destroy the ability of the promoted ELAN to the stimulated 2-photon γ-decay after that time-delay t_{del}. The conditions in all chain of the SPTEN-phase are more soft than in the Promotion phase. Hence the SPTEN-phase of duration $t_{SPTEN} < t_{del}$ could not to destroy the rise of the stimulated 2-photon γ-generation too. ♦The use of the INVENTIONS[23,27] is supposed: ♦Special cooling of AM ♦ The prevention of the Doppler-broadening linked with the heat expansion of the AM [23,27].

SPTEN-HYBRIDS[34,36] on ELAN Creation by Strong Laser Field in Plasma[46,47,90], ECSLFPÄSPTEN, line **8C**, and on ELAN Promotion (Ignition) for Two-Photon γ–Lasing[52,53], EPTPGLÄSPTEN, line **8D** are FEASIBLE in principle in a far future.

MIXED CATEGORY «RESIDENTIAL -NONRESIDENTIAL» ≡ \RSDÄNONRSD\SOLID\PULSE\	
9	Class SPTEN with Transformation of Driving Frequency (TDF)
9a	Class Two-Step γ-laser Triggered by Another Gamma-Laser (TSTAGL). Active medium of TSTAGL could be cooled in two variants: by «Heat Conductivity»[27] at strong bounded transversal size of active medium r by «Anomalous Super Dilution»[23] at unbounded transversal size and hence at big output energy. Class TSTAGL (as like as SPTEN) also could do without of any r/f or optical methods based on any use of the HFS inside of the active medium[4,5,8,17,19,24-25,27,48,68].
10	Class SPTEN with Combination Gamma-Amplification (CGA). Class SPTENACGA is FEASIBLE in principle in two variants of the cooling: «By Heat Conductivity» at strong bounded transversal size of active medium and «By Heat Capacity» at unbounded transversal size and hence at big output energy.
11	AUXILIARY CATEGORY «FILIAL SPTEN» ≡ FIL SPTEN
FIL-SPTEN as a filial category «MBE for the auxiliary researches in frames of γ-laser Creation Program» \FIL-SPTEN\MBE\AUX\. **E.g.:**	
11a	**\FIL-SPTEN\MBE-AUXIL\PARENTS** MBE FOR THE PRODUCTION OF PARENT NUCLIDES IN THE CLASS above *\SPTEN\HYBR\2-STEP\ — Production and storing of parent nuclides for γ-lasers of all types could be accelerated by a factor ~ 10^9 with a distinct use of MBE[34,36]: particularly in the cumulation of the long-lived isomers for the Two-Step γ-lasers.
Construction: Volume with nuclear reaction ⇒ gas of nuclear mixture with goal nuclei⇒input of MBE⇒laser separation⇒storage	
11b	\FIL-SPTEN\MBE-AUXIL\PRECIS-ANALYS\ USE of MBE in GL and other trials for the analysis and detection of rare and short-lived nuclides arising at different processes. — New much precision and together efficacious methods with high quality collimated and big flows of analyzed atoms or molecules could be created on the base of the hybridization of known methods with MBE [34,36].
Construction: gas of nuclear mixture with different goal nuclei⇒input of MBE⇒laser separation on groups ⇒ detectors	
12	Category «Distinct MBE's Applications» to the Other (Non-Gamma-Laser) Problems. \fil-spten\MBE distinct\non-γ-laser\
The Categories «Filial SPTEN» and «Distinct MBE's Applications» ARE THE MUCH MOST FEASIBLE IN THE NEAR FUTURE	
Note: Semenov Institute of Chemical Physics RAS has an experimental basis, know-how and takes the lead for the formation of the International Cooperation "Project MBE" on the development and creation of MBE for the various goals (e.g., γ-laser) on base of the modern physical and chemical micro and nano-technologies [34,36]	

This Table 6 is one of the main results of the *Single Theory of γ-laser creation in the 1st SPTEN-approach.*

This Classification is developing and will be gradually time and again revised.

It could be regarded as a compressed status on a γ-laser problem at a doorstep of the third millennium.

CONCLUSION

The last 40 years are characterized as the period of the «romanticism» in gamma-laser problem, as the period of the search of relatively light ways. The main features of that "romantic" period are a belief in a row of light ways instead of a knowledge, fantasy about that light ways without their strict checking and many delusions. It needs very big efforts in order to show that they are fit only for a museum.

The 1st delusion is the opinion that the simple Shawlov-Towns relation is sufficient for the quality substantiation of any gamma-laser's model. It is not so. It needs use much more strict conditions, e.g., the criteria of the 1st approximation of the joint gamma-generation and radiation-heat regime theory with the account of many very important different effects and trammels[9,10,12,17,28-30,35].

The 2nd delusion is the overmuch hope on the super-radiation (alias superfluorescence)[41,51,73,77,87,88]. The joint theory shows[34,35,87-89,{B},{C}] that the super-radiation (SR) contribution is much less than the induced contribution when the generated wave is much more than the spontaneous radiation in the generation mode. The SR contribution could be comparable with the induced one only in case of very slow total generation comparable with the spontaneous radiation in generation mode.

The 3rd delusion is the old belief about feasibility of the γ-laser on the long-lived isomers[1-17]. Now it is the fact that this idea is like as a generalissimo without his army. This idea has as yet no one isomer candidate from the indeed realizable minute interval $10^2\ s > t_+ > 10^{-3}\ s$ fit for the SPTEN GL, see [E].

The **4th** delusion is the belief about feasibility of the Non-Moessbauer active media: plasma, gas or beam on base of Marcuse induced process or on the two-photon induced decay.[15,17,39,40,41,52,53,77,78] The laser cooling could not be applied in that tasks because the heat release from the secondary processes of the internal electron conversion is too much big[34,35].

The **5th-a** delusion is too overmuch hope on the Anomalous Super Dilution (ASD) [23,27] with factor $k'/k_{Borr} < 10^{-6}$ on base of the Many Wave Borrman Effect (MWBE)[26]. See sec.1.5.3.

The **5th-b** delusion (linked with 5th-a) is the overmuch hope to avoid very high density of ELAN in solid AM (see, e.g., [24,24a]). In a reality (at least in a near future, see 1.5.3.) only normal active medium without Borrman effect could be realized[34,35]. Hence the density of ELAN in the AM **must be** $n_+ \sim 10^{21}$ *ELAN/cm*^{3}. In the demonstration trials the parameters of AM at such density are: diameter $a_1 \sim 3\ 10^{-5}$ *cm*, the length $L \sim a_1^2/\lambda \sim 1$ *cm*, the total volume $V \sim a_1^4/\lambda \sim 10^{-9}$ *cm*, the total number of ELAN is $N_+ \sim V n_+ \sim 10^{11}$.

The **6th delusion** is the overall mention[1-27] that the cold active medium for the gamma-laser (GL) is similar qualitatively to the ordinary Moessbauer media. It is not so. The cold solid AM of gamma-laser with $T_{AM} \sim 50$ *K* is replete with the hot secondary electrons and holes with density $n_e \sim 10^{17} - 10^{18}$ pairs/cm^3 and quasitemperature $T_e > 30000$ *K* [35, D].

The **7th delusion** is the overall mention[1-27] that the Moessbauer spectrum in the AM of γ–laser is similar to the spectra of ordinary media. It is not so. In deed any HFS in active medium is collapsed[34,35], see also , see 1.5.3 and [A,C-D].

The **8th delusion** is the mention about the feasibility of some gropes of methods based on the use of the resolved HFS inside of the AM[4,5,8,9-27]. In deed the collapse of HFS leads to the infeasibility of that methods[34,35]. Particularly the following groups of methods for the GL-creation are infeasible **in case of the short-lived isomers:**

(1) The selective pumping methods of the simple fluorescent type;[22]
(2) All radiofrequency and optical methods for the line narrowing;[4,5,8,9,17,19,48,51]
(3) All radiofrequency and optical methods for inversion of the inversionless excited nuclear mixture;[23,27,41,68]
(4) All radiofrequency and optical methods for the Amplification Without Inversion (AWI) creation.[23,27,24,24a]

The **9th delusion** is the mention about the feasibility of the gamma-lasers with the two-stage selective pumping of both simple and generalized types;[22,23,27], see present work about this delusion.

The **10th delusion** is the mention about the feasibility of the γ–lasers with the two-step pumping.[11,13-16,39-44], see present work[A].

The **11th delusion** is to think that all other types of GL are in all right e.g., [73-78]. In deed some other types of gamma-lasers are not as yet strictly analyzed on their feasibility. Only some origin arguments against that types are as yet published. [34,35]

The **12th delusion** is the talk about very soon experimental realization of gamma-laser. Sometimes in some papers, at some disclosures the words about very soon GL experiment arise. In deed the most realizable SPTEN γ–laser is a very complex thing. This complexity is enhanced by the fact that the creation of SPTEN is based in turn on the creation of the Multi Beam Selection (MBS). The MBS must be realized. But the SPTEN gamma-laser (based surely on MBS) could be realized only after the MBS creation.

It is shown in the works [A,B,C,D,E,F,G] that some types of active media, isomers-candidates and schemes for the GL stand as yet all tests, see, e.g., in [35] the SPTEN γ–laser on the isomer ^{58}Co (28.1 *keV*) in diamond host -matrix. The SPTEN γ–laser cold give at its development the following main results:

(1) Demonstration γ–laser with high ratio (*generation signal*/*spontaneous radiation in the generation mode*) >> 1;
(2) The γ–π-pulse with output energy $E_{out} \sim 1$ *J*, intensity ~ $10^{15} - 10^{17}$ *W*/*cm*^{2} and brightness ~ $10^{24} - 10^{26}$ *W*/*cm*^{2}rad^2;
(3) The residential Two-Step GL triggered by the longitudinal selective γ–ray pulse from the SPTEN γ–laser.

The main question is how to realize that ideas? The strict common theory of γ-laser creation reveals that the way is only one. It is the SPTEN way and not any other. The strict theory shows that all other ways give one and the same inevitable result, viz., the heat-blast of the active medium. The way pointed by the strict theory GG&RH is very rich with the different nuclei-candidates and the means for their creation. One of such means, the SPTEN-pumping by neutrons is much more effective[28-36]. Another mean, the photo-nuclear reactions, suggested in [28-30] too, are regarded in[F]. But all plenty of SPTEN-pumping (on neutrons, γ-quanta, or other particles) is based on the use of the special device «Multi Beam Emitter» (MBE). The MBE is the carefully designed joint ion-optical and laser-optical system. This Project MBE now is in its further development. This Project has twice goal: the effective pumping of γ-laser and the essential acceleration (by many orders!) of the selection of atoms, molecules, isotopes, isomers and radionuclides. This Project needs be developed by the specialists in different fields. Semenov Institute of Chemical Physics of RAS has an experimental basis, know-how and takes the initiative for the formation of the International Cooperation "Project MBE" on development and creation of MBE for various goals (e.g., γ-laser) on the basis of the modern physical and chemical micro and nano-technologies [34,36] The real significant result as yet is the formation of a Single Theory of γ-Laser Creation in SPTEN Approximation which is a quite suitable tool for the GL creation.

ACKNOWLEDGMENTS

The Author expresses his gratitude to V.I.Gol'danskii, Y.M.Kagan, R.V.Khokhlov, Yu.A.Il'inskii, L.A.Rivlin, G.C.Baldwin, V.S.Letokhov, Yu.B.Khariton, A.A.Rukhadze, V.G.Minogin, J.J.Carroll, C.B.Collins, A.N.Starostin, V.Yu. Baranov for the discussions in divers times to I.A.Kondurov (Petersburg's Nuclear Center) and V.V.Varlamov for the giving the possibility to get acquainted with the nuclear data-banks.

REFERENCES

1. Rivlin L.A. \\ 1961, USSR Patent Disclosure № 709714 from 10.01.1961.
2. Baldwin G.C., Neissel J.P. and Tonks L. \\ 1962, General Electric Co. Report № 62GL22.
3. Vali V. and Vali W. \\ 1963, Proc.IEEE, V.**51**, P.182-184; **ib.** P.1248.
4. Khokhlov R.V. \\ 1972, ZhETF Pis'ma, V.**15**, P.580-583; Sov.Phys.-JETP Lett., V.**15**, P.414-416.
5. Il'inskii Yu.A., Khokhlov R.V. \\ 1974, ZhETF, V.**65**, 1619-1625; Sov.Phys-Jetp, V.**38**, P.809-812;
6. Gol'danskii V.I., Kagan Yu. \\ 1973, ZhETF, V.**64**, P.90-107; Sov.Phys. - JETP, V.**37**, P.49-52.
7. Letokhov V.S. \\ 1973, JETP, V.**64**, P.1555-1557; Sov.Phys.- JETP, V.**37**, P.787-793.
8. Karyagin S.V. \\ 1977, "On the Ways of Suppression of Heterogeneous broadening of Moessbauer spectral lines", inv. lect. (Russ), Proc. Int. Conf. Moessb. Spectr., ed. by D. Barb and D. Jarina, Bucharest, Vol.**2**(1977), P.1-34.
9. Baldwin G.C., Solem J.C. and Gol'danskii V.I. \\ 1981, "Approaches to the development of gamma-ray lasers", Rev.Mod.Phys., V.**53**, P.687- 698.
10. Baldwin G.C., Solem J.C. \\ 1995, "Resent proposals for gamma-ray lasers", Laser Physics, V.**5**, P.231-239.
11. Collins C.B. and Carroll J.J. \\ 1995, "Progress in the pumping of a gamma-ray laser", Proc. 1-st Int. Gamma-Ray Laser Workshop (GARALAS'95), Predeal, Romania, 19-23 August 1995, ed. by C.B.Collins - L.A.Rivlin, in **Ref.[14]**, P.3-41.

12. Baldwin G.C., Solem J.C. \\ 1997, "Recoilless gamma-ray lasers", Rev.Mod.Phys., V.**69**, P.1085-1117.
13. Laser Physics, V.**5**(1995)
14. Hyperfine Interactions **107**(1997)
15. Proc. SPIE (Intern. Soc. for Optical Engineering), ed. by N.N.Rosanov, vol. **3685**(1999).
16. Induced gamma-emission (IGE). Proc.1st Int. IGE'97 Workshop, Predeal, Romania, August 1997. Ed. by I.I.Popescu and C.A.Ur. Bucharest - Magurele, Romania, 1999.
17. Vysotskii V.I., Kuz'min R.N. \\ 1989, "Gamma-Lasers", Moscow State University, 176 pp., (in Russian).
18. Elton R.C. \\ 1990,"X-Ray Lasers", Academic Press, INC, Boston - New York - Toronto, 287 pp..
19. Karyagin S.V. \\ 1976, "On Possibility of Regulation of Hyper-Fine Structure Over Many Parameters", Pis'ma v Zh. Tekh. Fiz., V.**2**, P.500-504; Sov.Tech.Phys.Lett., V.**2**, P.196-198.
20. Baldwin G.C. and Solem J.C. \\ 1979, Nuc. Sci. and Eng., V.**72**, P.281 - 289; **ib.** P.290 -292.
21. Baldwin G.C. and Solem J.C. \\ 1980, J. App. Phys., V.**51**, P.2372-2380.
22. Gol'danskii V.I., Kagan Yu. and Namiot V.A. \\ 1973, ZhETF Pis'ma, V.**18**, P.34-35; Sov.Phys. - JETP Lett., V.**18**, P.34-35.
23. Karyagin S.V. \\ 1980, "On Possibility of Low-Temperature Gamma-Laser", Zh. Eksp. Teor. Fiz., V.**79**, P.730-750.
24. Rostovtsev Yu., Kolesov R., Kocharovskaya O. \\ 1997, "Inversionless gain at gamma-ray transition via nuclear coherence created by optical driving", ref.[16], P.222-234.
24a. Kocharovskaya O., Kolesov R., Rostovtsev Yu. \\ Phys.Rev.Lett., 1999, V.**82**, P.3693.
25. Kocharovskaya O. \\ 1995, "Lasing Without Inversion: Problems and Prospects", Laser Physics, V.**5**, P.187- 196.
26. Hutton J.T., Trammell G.T. and Hannon J.P. \\ 1987, AIP Conf.Proc., Adv.in Laser Science-II, V. **160**, P.55.
27. Karyagin S.V. \\ 1983, "On the possibility of generation in the short-wavelength (Moessbauer) range at low temperatures", available from VINITI, Moscow, **no.2797-83**, May(1983), P.1- 61.
28. Karyagin S.V. \\ 1995, "Low-temperature gamma-ray lasers with combined pulse pumping from an aperiodic reactor", Laser Physics, V.**5**, P.343-354.
29. Karyagin S.V. \\ 1995, "Gamma-ray solid laser: the heat problem and means of solution", Proc. 1-st Int.Gamma-Ray Laser Workshop (GARALAS'95), Predeal, Romania , *19-23* August 1995, ed. by C.B. Collins – L.A. Rivlin in Hyperfine Interactions, V.**107**(1997), P.449-463.
30. Karyagin S.V. \\ 1995, "Gamma-ray solid laser: realization of pumping", **ib.**, P.465-480.
31. Sysoev A.A., Shcheckina I.V. and Karyagin S.V. \\ 1995, "Gamma-ray solid laser: ion-optical system for fast high-quality focusing of powerful non-paraxial ion beams of large format enriched with excited nuclei", **ib.**, P.481-492.
32. Karyagin S.V. \\ 1997, "Gamma-ray solid laser: line narrowing in self micro-plasma, steadiness against both the self-radiation defects and self-heating", 1st International Induced γ-Emission Workshop, Predeal, Romania, August 16-20, Techn. Digest(1997)97. Published in Ref.[16], p.p.120-137.
33. Karyagin S.V. \\ 1998, "Atomic multibeam emitters with oriented microrelief for laser isotope (isomer) separation", in "Program and Abstracts" of VI int. conf. "Industrial Lasers & Laser Applications'98", ed. by V.Panchenko, V.Golubev, Shatura, NICTL RAN, 1998, P.72.
34. Karyagin S.V. \\ 1998, "Solid gamma-laser", The transactions of the 2nd scientific and technical sector conference "*Laser-systems'98*", town Raduzhnii (Rainbow) (in Russian), P.15-125.
35. Karyagin S.V. \\ 1998, "Gamma-ray solid laser: amplification without inversion and microplasma of an active medium. Some results in substantiation for a feasible gamma-lasing experiment." - Intern. Conf. "Fundamental Problems of Laser Optics (Laser Optics'98)" , 22 - 26 June 1998, St. Petersburg, Russia, published in Proc. SPIE (Intern.Soc. for Optical Engineering), ed. by N.N.Rosanov, V.**3685**, P.167-176.
36. Karyagin S.V. \\ 1999, «Multi Beam Emitters for the Cardinal Acceleration of Selection Processes», Proc. of IV All-Russian (International) Scientific Conference «Physical Chemical Processes at Selection of Atoms and Molecules», October 4 - 8, 1999, Zvenigorod; ATOMINFORM, P.187-192.
36A. Karyagin S.V. \\ 1999, «Multi Beam Emitters for the Cardinal Acceleration of Selection Processes» Theses of IV Russian International science conference «Physical Chemical Processes at Selection of Atoms and Molecules», October4 - 8, 1999, Zvenigorod, ATOMINFORM, P.60.
37. Khariton Yu.B., Voinov A.M., Kiseliov V.F. etc. \\ 1984, "Aperiodic pulse research reactors". Problems of Modern experimental and theoretical physics, ed. by A.P. Alexandrov, Leningrad, Nauka (in Russian).
38. Dyer P., Baldwin G.C., Sabbas A.M., et al. \\ 1985, J. Appl. Phys., V.**58**, P.2431.
39. Baklanov E.V., Chebotaev V.P. \\ 1975, ZhETF Pis'ma, V.**21**, P.286-289; Sov.Phys-Jetp Lett., V.**21**, P.131-132.
40. Baklanov E.V., Chebotaev V.P. \\ 1976, Kvant. Elektr., V.**3**, P.634-636; Sov.J.Quant.Elect., V.**6**, P.345-347.
41. Program 1st Int. laser science Conference, Dallas, Texas; 18-22 Nov. 1985. Bulletin of the American Physical Society, V.**30**, Number 10, 1985.
42. Arad B., Elieser S. and Paiss Y. \\ 1979, Phys.Lett, V.**74A**, P.395.
43. Collins C.B., Olariu S., Petrascu M. and Popescu I. \\ 1979, Phys.Rev.Lett. 42, 1397-1400;
44. Collins C.B., Olariu S., Petrascu M. and Popescu I. \\ 1979, Phys.Rev.C., V.**20**, 1942-1945.
45. Carroll J.J. \\ 1977, "Prospects for triggered gamma-emission as a precursor to a gamma-ray laser", in Ref. [16], 48-59.
46. Vysotskii V.I. \\ 1977, "Pumping of gamma-laser by nonthermal action of optical laser", in Ref. [16], 192-198.
47. Andreev A.V., Gordienko V.M., Savel'ev A.V. \\ 1977, "Nuclear transition excitation in high-temperature near-surface plasma: feasibility of γ–lasing", in Ref. [16], P.291 - 302.
48. Gol'danskii V.I., Karyagin S.V., Namiot V.A. \\ 1974a, ZheTF Pis'ma **18**, 61-62; 1974b, Jour de Physique **35**, C 6,192-196; 1974c, Fiz. Tverd. Tela. **16**, 2517 - 2520.
49. Karyagin S.V., Gol'danskii V.I. \\ 1996, "Gamma-Lasers", Proc. Nauch. Tech. Conf. Las. Syst., GNILS, "Rainbow'96", Russian, P.39-43.
50. Karyagin S.V. \\ 1996, "Feasibility of Gamma-Laser Based on the Modern Technology and the Existing Technique", **ib.**, P.43-44.
51. Andreev A.V., Il'inskii Yu.A., Khokhlov R.V. \\ 1974, ZhETF, V.**67**, P.1647-1650; Sov.Phys-Jetp, V.**40**, P.819-820.
52. Rivlin L.A. \\ 1995, "Inducing nuclear gamma-ray emission by strong-field ignition without a total population inversion", in Ref.[14], P.297 - 300.
53. Zadernovsky A.A. \\ 1997, "Two-quantum Doppler-free induced gamma-emission", in Ref.[16], P.42 - 47
54. Osad'ko I.S. \\ 1979, Usp. Fiz. Nauk, V.**128**, P.31- 46. (The results[54] on the Shpol'skii effect are used in Ref.[27])
55. Moiseev S.A. \\ 1997, "About Optical Modeling of Moessbauer Gamma-Ray Laser Generation", in Ref.[16], P.375 - 393.
56. Forrest J. Agee \\ 1995, "Radiation machines for gamma-ray laser research", **ib.**, P.69-79.
57. Lehmann Chr. \\. 1979, "Interaction of Radiation with Solids and Elementary Defect Production". North-Holland Publishing Company. Amsterdam-New-York-Oxford. 1977. Atomizdat (Russia) 1979, 296 pp.
58. Balko B., Kay I.W., Silk J.D., Sparrow D.A. \\ 1995, "Pumping Requirements for Achieving Nuclear Super-fluorescence", in Ref.[13], 355-362.

59. Lederer C.M., Shirley V.S. \\ "Table of isotopes". New-York. 1978.
60. Storm E., Israel H. \\ "Photon cross-sections". Los Alamos. 1967.
61. Band I.M., Trjaskovskaia M.B. \\ 1978, Tables for Coefficients of the Internal Conversion. Leningrad.
62. E.G.Fuller, H.Gerstenberg. Photonuclear Data Index 1973-1981. NBSIR 82-2543-1,1983.
63. Fuller E.G., Gerstenberg H. \\ 1983, Photonuclear Data-Abstract Sheets 1955-1982/ NBSIR 83-2742,1983.
64. Dietrich S.S., Berman B.L. \\ 1988, Atomic Data and Nuclear Data Tables, V.38, P.199.
65a. Varlamov V.V., Sapunenko V.V., Stepanov M.E. \\ 1996, «*Photonuclear data*». Index 1976-1995.Institute of Nuclear Physics of Moscow State University. Centre for Photonuclear Experiments Data (CDFE). Moscow State University. Moscow.1996
65b. Varlamov A.V., Varlamov V.V., Rudenko D.S., Stepanov M.E. \\ 1996, Web Site: **http://depni.npi.msi.su/cdfe** . Institute of Nuclear Physics of Moscow State University. Centre for Photonuclear Experiments Data (CDFE). Moscow State University. Moscow.1996.
65c. Varlamov A.V., Varlamov V.V., Rudenko D.S., Stepanov M.E. \\ 1999, «*Atlas of Giant Dipole Resonances. Parameters and Graphs of Photonuclear Reaction Cross Sections*». January 1999. IAEA nuclear data section, Wagramerstrasse 5, A-1400 Vienna, pp. 1-311.
66. Blatt I.M., Weisskopf V.A. \\ "Theoretical Nuclear Physics", New York. 1952.
67. Zvelto O. \\, 1979, "Laser Physics". In the Russian translation. The publishing house MIR, Moscow,1979, chapter 9.
68. Zaretskii D.F. and Sazonov S.B. \\ 1997, "The Coherent Repopulation of Hyperfine Levels and Induced Gamma-Emission", The 1st Int. Induced Gamma-Emission Workshop, Predeal, Romania, August 16-20, Technical Digest(1997)69. This work is printed in Ref.16, 1999, P.287 - 290.
69. Vavilov V.S., Gippius A.A., Konorova E.A. \\1985, "Electronic and optical processes in diamond", Nauka, 120 pp., (Russian).
70. Potylitsyn A.P. \\ 1997, "Compton Backscattering of Coherent Diffraction Radiation as an Intense X-Ray Source", in Ref.16, 1999, P. 212-221.
71. Gol'danskii V.I., Karyagin S.V., and Namiot V.A.\\ 1974, Pis'ma Zh. Eksp. Teor. Fiz., V.19, P.625-627.
72. Gol'danskii V.I., Karyagin S.V., and Namiot V.A.\\ 1974, Fiz. Tverd. Tela, V.18, P.2517- 2522.
73. Skorobogatov G.A., Dzevitskii B.E.\\ 1998, Proc. IX Conf. Laser Optics'98, Techn.Progr., Quant.Nucleon., St.Petersburg, June22-26(1998), P.71.
74. Vysotskii V.I. \\ 1998, ib., P.69.
75. Vysotskii V.I., Reiman S.I. \\ 1998, ib., P.71.
76. Godovikov S.K. \\ 1998, ib., P.71.
77. Samartsev V.V., Andrianov S.N. \\ 1998, ib., P.73.
78. Rivlin L.A. \\1998, ib., P.69.
79. Belier G. \\ Inv. rep., X Conf. on Laser Optics'2000, S.-Petersburg, 26-31 June 2000, section «Super Strong Laser Fields». To be published in special issue of Proc.SPIE, ed. by A.A.Andreev.
80. Storm E., Israel H.\\ «Photon cross sections from 0.001 to 100 MeV for elements 1÷100», LASL, New Mexico, 1967 June.
81. Chirikov B.V. \\ 1963, ZhETF, V.44, P.2016-2022; Sov. Phys. - JETP, V.17, 1355-1359.
82. Balykin V.I., Letokhov V.S., Minogin V.G. \\ 1985, Usp. Fiz. Nauk., V.147, P.117.
83. Baranov V.Yu., Kolesnikov Yu.A. \\ 1999, «Preamble», Proc. of the IV All-Russian (International) Scientific Conference «Physical Chemical Processes at Selection of Atoms and Molecules», October 4 - 8, 1999, Zvenigorod; ATOMINFORM, Pages 3, 4.
84. Heidemann A., Kaindl G. et al.\\ 1976, Phys. Rev.Let.V.36, P.213.
85. Lynch F.J., Holland R.E., Hamermesh M. \\ 1960, Phys.Rev., 120, No.2, P.513-520.
86. Marcuse D. \\ 1963, Proc. IEEE, V.51, P.849.
87. Bonifacio R. and Lugiato L.A. \\ 1975, Phys.Rev.V.A11, P.1507; V.A12, P.587.
88. Andreev A.V. \\ 1977, ZhETF, V.72, P.1397-1406; Sov. Phys.-JETP, 45, P.734-739.
89. Letokhov V.S. \\1983, "Nonlinear selective photo processes in atoms and molecules", M.: Nauka, 408 pp.
90. Kazantsev A.P., Surdutovitch G.I., Yakovlev V.P. \\ 1991, "Mechanical Action of Light on Atoms", M.: Nauka,190 pp.
91. Andreev A.V., Il'inskii Yu.A. \\ 1975, ZhETF Pis'ma, V.22, P.422-465; Sov. Phys.-JETP Lett., V.22., 223-224.

Papers reported at the X Conference "LO'2000" and sent to the present volume of the Proceeding SPIE:

[A]. Karyagin S.V. \\2000, "Status of gamma-laser problem on current moment'2000: ranging analysis and screening of gamma-laser schemes on their feasibility". Corresponds to the report TuB1-8 at the X Conference "Laser Optics'2000", St.-Petersburg, June 26-30, 2000, Technical Program, p. 16.

[B]. Karyagin S.V.\\2000, "Multi beam emitters as joint optical laser complex and ion-optical system for laser selection of atoms, molecules, isotopes, isomers, long-lived and short-lived radionuclides in different spheres from γ-laser and atomic energetics to the medicine and gene engineering." Corresponds to two reports TuB1-8 (partially) and FrB1-p05 (total) at the X Conference "Laser Optics'2000", St.-Petersburg, June 26-30, 2000, Technical Program, pp. 16, 66.

[C-D]. Karyagin S.V. \\ 2000, "Joint gamma-generation and radiation-heat regime (GG&RH) theory for gamma-lasers' screening in the first approach of "Soft Prompt Transplantation of Excited Nuclei" (SPTEN)." Corresponds to two reports FrB1-p06 and FrB1-p07 at the X Conference "Laser Optics'2000", St.-Petersburg, June 26-30, 2000, Technical Program, p. 66.

[E]. Karyagin S.V. \\2000, "Gamma-ray solid laser: variety of work nuclei and host-matrixes in Mendeleev Table screened with use of system of criteria based on joint GG&RH theory." Corresponds to Technical Program of X Conference "Laser Optics'2000", St.-Petersburg, June 26-30, 2000. Report FrB1-p08, p. 66.

Papers reported at the X Conference "LO'2000" and sent to the other publishing outfits:

[F]. Karyagin S.V. \\ 2000, "Possibility of straight gamma-lasing experiments based on nuclei-candidates activated by a rigid bremsstrahlung". Technical Program of the X Conference "Laser Optics'2000", St.-Petersburg, June 26-30, 2000. Report FrB1-p08, p. 66.

[G]. Karyagin S.V., Khristenko S.V., Adamson S.O, Dement'ev A.I., Khafizov R.U., Kuz'menko N.K., Saperstein E.E., Zverev M.V. \\2000, Gamma-Laser: optical isomer shifts for three main groups of nuclei-candidates. Technical Program of the X Conference "Laser Optics'2000", St.-Petersburg, June 26-30, 2000, p.16.

Multi beam emitters as joint optical laser complex and ion-optical system for laser selection of atoms, molecules, isotopes, isomers, long-lived and short-lived radionuclides in different spheres from γ-laser and atomic energetics to the medicine and gene engineering.

S.V.Karyagin

Semenov Institute of Chemical Physics, RAS, Prospect Kosygina 4, 117997, Moscow, GSP-1, Russia
e-mail: chaika@chph.ras.ru ; fax: (095)-137-8318

ABSTRACT

The SPTEN-γ-laser's development leads to the essentially new principles for the effective converting of the nuclear radiation (neutrons, gamma, etc.) into the well controlling and focusing broad formatted atomic (ionic, molecular, etc.) beams which are fit for the creation of the active medium of the γ-laser and for the other aims, e.g., for the acceleration by many orders of the selection of atoms, molecules, isotopes, isomers, radionuclides, for high precision methods in the spectroscopy-chromatography of the macromolecules, etc.. The appropriate Multi Beam Emitter systems, MBE, are based on the dividing of the broad formatted beam of nuclei into a big amount ~ 10^6-10^9 of the collinear microbeams with use of the especial deeply engraved gratings together with *ad hoc* ion and laser optics. MBE will be realized in a non-γ-laser sphere before the first direct γ-lasing demonstration experiments.

Keywords: quantum nucleonics; gamma-generation (induced, super-radiant in plasma, in beam, in solid); amplification without inversion, Borrmann effect, hot microplasma in cold solid; collapse of HFS by motion; soft prompt transplantation of excited nuclei; multi-beam laser selection; heat blast of active media) of gamma-ray laser (residential, non-residential); optical pressure on atoms; laser cooling and acceleration of beams

1. Introduction. The difficulties in a problem of gamma-laser (*GL*) creation[1-27] can be overcome only if the adequate cardinal innovations will be introduced into technique of experiment. Hence the investigations of the ways for *GL*-creation necessarily must be accompanied with the generation of some new technical directions which can be useful not only for *GL*. The *GL*-investigations of the beginning period led to a row of directions (e.g.,[1-7,23,27]) which at that period were considered as mutually incompatible. E.g., the low temperatures are needs in the methods of line-narrowing [4,5,8,19,23,28,71,72] . But low temperatures are impossible at the pulse pumping [6-7,23,27]. The short-lived nuclei which are necessary for pulse methods [6-7,23,27] can not be used in the methods for a laser selection of excited nuclei [7,89].The work on overcoming of the inconsistency between different ways of the *GL*-creation was began in works [23,27] and it resulted in a discovery of a *GL*-class *SPTEN* (*soft prompt transplantation of excited nuclei*)[28,30,31,34,35] which in deed conjoins the merits of all three aforecited directions[5-7] but without their flaws.

For a *GL* of *SPTEN*-class a time-life of excited laser-active nuclei (*ELAN*) is less than 10^{-4} *s* and a relative inverse population in active medium is more than *90%*. Owing to these beneficial conditions a *GL* of *SPTEN*-gamma-laser can do without methods based on use of *HFS* (*hyper fine structure*) [8-11,13-17] (e.g., methods of line narrowing, methods amplification without inversion). Hence the *GL*-schemes of *SPTEN*-class are free from a demerit of many modern *GL*-models - just namely from an instability to fluctuations and disruption of *HFS* (*hyper-fine structure*) at the inevitable powerful radiation-heat impact on active medium of *GL*[9,10,12].

The *SPTEN*-schemes are based on use of so called «softening complex» (*SC*) of measures in order to soften threshold and radiation-heat regimes in *GL*. One of the elements of *SC* is a laser selection of *ELAN specially elaborated for SPTEN*. A function of input device for a transforming nuclear radiation (neutrons, γ-quanta, etc.) into a beam previously enriched by *ELAN* (due to *Szilard-Chalmers effect*) is a «converter» named in more wide than *GL* employment as a «*multibeam emitter*» (*MBE*). *MBE* in complex with selection and transport-focusing systems (*STFS - selection and transport focusing system*) are the most complicated (among all multibeam (*MB*)-systems) just in case of *GL* owing to concurrent superposition of five rather rigid conditions:

I -a high relative inverse population $\varpi \equiv 1 - \chi \geq 0.9$ on the output of *STFS*;
II - a big amount of *ELAN* ~ 10^{12} - 10^{13} on the output of *STFS* with a good reserve which is by 1 - 2 orders more than a threshold value;
III - a short total time (less than 10^{-6} *s*) for pulse action of *STFS* in its entirety;
IV - a soft transplantation of *ELAN* into substratum at a kinetic energy of atoms less than *500 eV*;
V - a high (more than 10^6) compression of a large format beam with a cross-section ~ 10^3-10^4 cm^2 into a tight strip with a cross-section ~ 10^{-4} $cm \times 1$ *cm*.

However the conditions for use of *MBE* are more softer for a lot of many other goals (e.g., a selection of stable and long-lived nuclei) which are not linked directly with a *GL*-pumping. For that cases a creation of *MBE* is more simple problem than in case of *GL*. A realization of MBE in simple cases can be considered as a simulation of more complex *MBE*-schemes because the general designation of all *MBE-types* (simple and compound) - it is a preparation of a beam for an effective selection (with use of laser or in other methods).

2. Structure of multibeam emitter (*MBE*). In its external form a working body of MBE resembles a diffraction grating used in optical diffraction spectrometers. The more near analogy could be the microchannel plate. The working body of MBE is represented at the distinct list at the end of this paper. But the MBE-grating for the improvement of selection needs to have a more deep (by 1 - 2 orders) «thread» (alias the "riffle" or "groove") and a more big density of «grooves» ~ 10^3 cm^{-1}. The external working surface of *MBE*

Laser Optics 2000: Ultrafast Optics and Superstrong Laser Fields, Alexander A. Andreev, Vladimir E. Yashin, Editors, Proceedings of SPIE Vol. 4352 (2001) © 2001 SPIE · 0277-786X/01/$15.00

can be both concave (e.g., spherical) or plane [28,30,31]. Let the MBE is constructed as a plane rectangular grating of external dimensions $D_1 \times D_2 \times (l_0 + l_1)$, where l_0 is a depth for a cell of *MBE*, l_1 is a thickness for a bottom of emitter (see below), $D_1, D_2 >> l_0 + l_1$. Along side $\boldsymbol{D_1}$ a distance between adjacent *directing* cells (the 1st period of grating) is $d_1 + d_0$, where d_1 is inner size of a cell, and d_0 is a thickness of a wall between the cells. Let in another (orthogonal) direction $\boldsymbol{D_2}$ a distance between adjacent cells (the 2nd period of grating) is $d_2 + d_0$, where d_2 is another inner size of a cell. Let $d_0 \cong d_1 << d_2 << l_0 << D_1, D_2$. Such relation between the sizes of *MBE* is near an optimal one in many cases. Each cell has inner volume $d_1 \times d_2 \times l_0$. The initial values of divergence angles for micro-beams are $\beta_1 \cong 2 d_1 / l_0$ and $\beta_2 \cong 2 d_2 / l_0$. Characteristic sizes of MBE: $d_0 \cong d_1 \cong 0.001cm$; $d_2 \cong 0.1cm$; $l_0 = 1cm$; $D_1, D_2 \sim 30 - 100$ *cm*; $\beta_1 \cong 0.002$ *rad*; $\beta_2 \cong 0.2$ *rad*. Such MBE forms a multibeam (*MB* - *multibeam*) composed of $N_{\mu B} \approx D_1 \times D_2 / (d_1 + d_0)(d_2 + d_0) \approx 10^8 - 10^9$ *micro-beams* (μ*B*). The cell of *MBE* can be created [27-31,34,35] or in a through form (without bottom), or in a form of cell closed with a bottom. *MBE with through cells creates a multibeam* (*MB*) *in a transmission regime. MBE with bottom (closed cells)* creates *MB*, as a rule, in a regime of scattering ("reflection") in plains parallel with a directing plains of the cells. *MBE with bottom* are using[27-31,34,35] also: I - in case when the goal nuclei are born in a substance of cells; II - in case of Coulomb excitation of nuclei with initial kinetic energy ~ 10^{10} *eV* at its passing through the substance of *MBE* (including a blind bottom); III - in cases when the separating mixture is previously stored (adsorbed or congealed) in cooled cells. In this last case the stored mixture is then heated and then is going into *MB* with a time-dependence and duration corresponding to a heat-cell-regime (impulsive, continuous, etc.). The "bottom" of closed cell has a thickness $l_1 \sim 0.001 - 1$ *cm*. For the layout of electrodes and traps (see below points 7-10) within the *MB* the last is divided into compact blocks of microbeams with necessary gaps between these blocks.

3. Working conditions for MBE. The coefficient of penetration of atoms through the grating

$$\varsigma \approx (d_1 d_2 / l_0^2 4\pi) + 0.3 \exp(-\theta l_0 / d_1) \qquad (1)$$

is near a maximal one if an atomic adhesion coefficient θ for the walls of directing cells is very small $\theta << d_1/l_0$ and $d_2 >> d_1$.[27-31] In eq. (1) the first term has a geometric (aperture's) nature, the 2nd term is linked with a multiple atomic scattering by the walls of the directing cells. Eq. (1) approximates the numerical modeling results. In order to decrease θ it was recommended [27-31]: I. - To use some monoatomic coatings with small absorption coefficient for the directing walls; II - To heat the walls of MBE up to the temperature $T \sim 1000$ *K*. Besides absolutely there are need both: a vacuum $10^{-10} - 10^{-11}$ *Torr* and a careful cleaning of the system from the sorbed atoms and molecules. At $T = 1000$ *K*, atomic (molecular) weight $A = 200$, the initial prolong mean velocity of atoms in *MBE* is

$$V_s \cong 1.57\ 10^4\ (T/A)^{1/2}\ cm/s \cong 3.5\ 10^4\ cm/s\ . \qquad (2)$$

A ***boundary layer*** (*BL*) of thickness $h \sim 1$ *cm* arises along the output surface of emitter for a time $t_1 = h/V_s \sim 3\ 10^{-5}$ *s*. The selective excitation of atoms in this layer is created by laser beam of band-like profile with a cross section $D_2 \times h$. The wave vector $\boldsymbol{k}$ of that beam is parallel with the output plane of *MBE* and a side $\boldsymbol{D_1}$, and is orthogonal to a side $\boldsymbol{D_2}$.

4. The recharging in a boundary layer (*BL*). The recharge (charge exchange) leads to big difficulties in the extraction of ions with goal nuclei: as a rule the goal ions lose its charges due to recharge at the insufficient high degree of vacuum depression in a beam or in a cell for selection and selection experiments finalize in failure even for the stable isotopes[10,38]. In deed, the condition for a ***resulting*** relative concentration (content) of the goal ions $\varpi_{res} = 1 - \chi_{res} \sim 1$, ($\chi_{res} << 1$) is

$$h\ n_{mix}\ \sigma_{rech} < \chi_{res} \qquad (3)$$

The left part of inequality (3) is a probability of a recharge (*with cross-section* σ_{rech}) for a goal ion at the extracting of ions from the boundary layer (*BL*) of thickness h; n_{mix} – is the total initial concentration of all atoms (goal and non-goal) of mixture in *BL*. In case of one-beam *LIS* the term "boundary layer" (*BL*) needs be changed into a more correct term "initial volume of a mixture at the beginning of beam". A recharge is the most risky on a stage of a goal ion extraction from BL because a vacuum in the rest part of selecting system is more depressed and hence the recharge probability is essentially less. The other parasitic processes in BL are suppressed also at carrying out the condition (3) if the cross-sections of that processes are not more than or of the same order as a value σ_{rech}. Let the relative content of the goal isotope in the ***initial*** mixture is $v_0 = n_0/n_{mix} << 1$, where n_0 – is the initial concentration of goal nuclei in *BL*. Then from (3) it follows

$$h\ n_0 < \chi_{res}\ \varpi_0 / \sigma_{ex}\ . \qquad (4)$$

A typical example $h = 1cm, \sigma_{rech} \sim 10^{-15}\ cm^2, \varpi_0 \sim 10^{-4}, \chi_{res} \sim 0.1, \varpi_{res} = 1 - \chi_{res} \sim 0.9$ (*90%* of goal atoms at output of system) gives the next value for the initial (before selection) density-flux of goal atoms (molecules)

$$h\ n_0 \sim 10^{10}\ cm^{-2}\ . \qquad (5)$$

5. Necessity of transition to multibeam (*MB*) systems. Hence in a typical case only so small flux of goal selecting atoms $h\ n_0 \sim 10^{10}\ cm^{-2}$ can be given into the entrance of selection device. In order to increase amount of atoms at the entrance it needs to increase the input cross-section of a monobeam in *LIS*-system (e.g., in common *AVLIS-schemes*) significantly more than $10\ cm \times 10\ cm$ but without degradation of a beam collimation. In common systems it is possible only if one increase a length of «entrance» above *100* meters. A transition to *MB*-systems takes off this problem.

6. Complex of selfconsistent conditions for *MBE*-action. The *MBE*-action is effective at the abidance of the next complex of selfconsistent conditions:

I. - Conditions (3),(4) in a common case, or the condition (5) in typical case;

II. - The condition for a big active section of *MBE*

$$S = D_1 \times (d_1/(d_1+d_0)) \times D_2 \times (d_2/(d_2+d_0)) >> 1cm^2 ; \quad (6)$$

III.- A minuteness of aperture $\beta_1 = 2\, d_1/l_0 \sim 0.002$ *rad*, at which a Doppler-width (hindering to *selective laser ionization, SLI*) $\Delta\omega_D \sim (\beta_1 V_s \omega_{opt}/c) \sim 4\ 10^6\ s^{-1}$ is less than natural width of optical transition $\tau_{1opt}^{-1} \sim 10^7\text{-}10^8\ s^{-1}$. Here $\omega_{opt} \sim 1.5\ 10^{15}\ s^{-1}$ is a frequency of optical transition with energy $E_{opt} \sim 1\ eV$; $c = 3\ 10^{10}\ cm/s$ is the light velocity. The wave-vectors $\boldsymbol{k}$ of *SLI*-photons are parallel to the side $\boldsymbol{D}_1$ and orthogonal to axis of MB.

IV.-The acceptable total length of MB-device for LIS is about one meter [27-31].

7. Production of selection for the systems of multibeam (MB) and monobeam types. If G_i is a coefficient of selective ionization and η is a coefficient of conveyance of goal atoms onto substrate then a full number of goal atoms at output selected after one circle is

$$N_0 = (1 - \chi_{res}) S\, G_i\, h\, n_0\, \eta \quad (7)$$

Let $S \cong 500\text{–}5000\ cm^2$, $hn_0 \cong 10^{10}\ cm^{-2}$, $G_i \cong 0.5$, $\chi_{res} \cong 0.1$, $\eta \cong 0.5$, then $N_0 \sim 10^{12} - 10^{13}$. (8)

A boundary layer (BL) of a thickness $h \cong 1\ cm$ is filled by atoms after the time $t_1 = h/V_s \cong 3\ 10^{-5}\ s$. A total time of a pulse *SLI* and a conveyance of goal atoms onto substrate[31] is $t_{SLI+conv} < 10^{-6}\ s$. A time for cleaning of BL from non-goal atoms, ions and molecules is less than $10^{-5}\ s$. At such conditions a period of selection t_{sel} and a frequency of selection-cycle n_{sel} are

$$t_{sel} \cong 4\ 10^{-5}\ s\ , \quad \nu_{sel} = 1/t_{sel} \cong 2.5\ 10^4\ Hz\ . \quad (9)$$

As a result the production of MB-system after day ($t = 86400\ s$) is

$$N(t) = N_0\, \nu_{sel}\, t\, f_3 \cong (2.5\ 10^{21} - 2.5\ 10^{22})\, f_3 \quad (10)$$

of goal atoms, e.g., $\sim (1 - 10) f_3$ *grams of goal isotope* (at atomic mass $A \sim 100 - 200$ *a.e.*) after day, where the factor $f_3 \approx 1 - 10^{-3}$ is linked with an uncertainty in evaluation of a selection period. The input part of a beam in usual (monobeam) *LIS*-systems needs have a length $\sim 10^3\ cm$ (instead of $\sim 1\ cm$ in MB-systems) in other to form a collimation angle $\beta_1 \sim 0.001\ rad$ at a diameter of a beam $\sim 1\ cm$. At such conditions the time for a rebuilding (cleaning) of system in case of a monobeam LIS- system amounts $\sim 10^{-3} - 10^{-2}\ s$. In a result at $S' \sim 1\ cm^2$ one has

$$N_0' \sim 3\ 10^9,\ \nu_{1sel} \sim 10^3 - 10^2\ Hz,\ N'(t) \sim (10^{16} - 10^{17})\, f_3'\ per\ a\ day. \quad (11)$$

The parameters of a monobeam is marked here *with a dash* ('). A comparison with (10) is pointing on a cardinal growth of goal atoms production at transition monobeam selection systems to *MB*-systems. This result is based on two features of a multibeam (*MB*):

I.-The *MB* has a transversal cross-section S which is more by a factor $f_1 \sim 10^3 - 10^4$ than a cross-section S' of a monobeam with the same collimation angle.

II.- The *MB* could be divided (see sec. 2) into the blocks of a small width $\sim 10^{-1}\ cm$. In the gaps between the blocks the traps for impurities (e.g., the thorium wires or grids) could be inserted. Owing to it the time for the cleaning of a multibeam (*MB*) from the impurities can be decreased by a factor $f_2 \sim 10^2 - 10^3$ in comparison with case of a monobeam of a blind cross-section $\sim 1cm^2$. It is apparent that $f_3 \approx f_3'$. Thus the transition from a monobeam selection to multibeam one leads to acceleration of selection by factor f_{ac} which amounts

$$f_{ac} = N(t)/N'(t) \approx f_1 \times f_2 \times f_3/f_3' \approx f_1 \times f_2 \sim 10^5 - 10^7 \quad (12)$$

i.e. the production of multibeam (*MB*) selection systems is by *5-7* orders more than monobeam ones.

8. Multibeam (*MB*) emitter as a part of ion-beam system. *MB*-systems with repeat of selection process. *MB*-emitter is the anode of the ion-optical system (*IOS*). *IOS* is the most complex in case of *GL* when at first the goal ions accelerates and then its retards and softly transplants into a micro-target of small dimensions which are by many orders less than the anode. If it needs (see below p.10) one can to create *MB*-systems with a repeat (two- or more-fold) of the main selection process (e.g., selective laser ionization) in some few parts of a transport-focusing track [27,28]. For the extraction, acceleration, correction, retardation and focusing of ion-beams practically all methods of ion-optics can be used (with stationary, pulse and running wave type electric and magnetic fields, a feedback, etc.). A high directionality of microbeams leads to a special modification of ion-optics[31] which is used in *IOS*[27-31] for the increasing of a laser ionization effectiveness, for an acceleration of a conveyance of goal ions, for the increase of its compression and for decrease of its transport leakage. In case of GL the transport's leakage can be decreased below *90%*. The main reasons of transport's leakage are linked with strong retardation and edge focusing (for *GL*) of *MB*. The transport's leakage of goal ions is small in case of more simple (than *GL*) *MB*-systems in which the retardation and (or) the edge focusing are needless.

9. Selective laser ionization (*SLI*) in a regime of saturation or induced transparency. A selective laser ionization (*SLI*) could be[7,34-36,38,89] one-resonant (the first transition is selective-resonant, but the second is a broad ionizing transition); two-resonant (two first transitions are selective-resonant, but the third is a broad ionizing transition) or *n*-resonant (n > 2; the first *n* transitions are selective-resonant, but the last is a broad ionizing transition). Each subsequent transition moves upward from the level which was excited in a previous transition. The more amount of resonant selective transitions the higher a selectivity of SLI and the higher order of relative inverse population can be achieved (e.g., at the selective laser separation of isomers). At $n \geq 2$ a selectivity does not depend on the value of a Doppler broadening. At $n > 2$ the use of *SLI* is technically more hard. Hence $n = 2$, as a rule, is enough and optimal.

Let us consider a density flux of photons for a laser radiation $\Phi_{1SLI}(x, \omega_{opt1}) \equiv \Phi(x)$ of a band profile dependent on a path length x along a boundary layer *BL* at the direction $\boldsymbol{D_1}$ (see sec.2). This flux excites the first selective transition on a frequency ω_{opt1} in goal atoms (molecules) of *BL*. The second selective transition on a frequency ω_{opt2} must be excited by a flux $\Phi_{2SLI}(x, \omega_{opt2})$ of a laser radiation of a band profile along a boundary layer *BL* at the direction which is opposite to a vector $\boldsymbol{D_1}$. A Doppler breadth is minimal at such orientation of selective flows. The ionizing flow with a broad bandwidth needs be directed also along the boundary layer *BL* but orthogonal to the line $\boldsymbol{D_1}$ (i.e., parallel to $\boldsymbol{D_2}$). A Doppler width at this direction is by factor d_2/d_1 more than at the direction $\boldsymbol{D_1}$. But it is not sufficient for the ionizing transition with a broad bandwidth. The moments of cut-in and lasting of the laser pulses of different carrier frequencies (ω_{opt1}, ω_{opt2}, ω_{opt3}) need be synchronized in case of the pulse *SLI*-regime. In some cases it is helpful to use the mirrors: an effective pathway x_{max} in *BL* becomes longer, the *SLI* becomes more fast and homogeneous. But it needs to attend in order that the reflected beams would be parallel to the incident ones. Otherwise the reflecting would increase a Doppler breadth and would lead to a marked disturbance of a pulse synchronization. The conditions for a propagation of selecting radiation have a big account for a quality of *SLI*. A resonant cross-section is $\sigma_{res} \sim 10^{-9}\ cm^2$ for the transitions of energy $E_{opt} \sim 1\ eV$. A path-way of resonant absorbing for a weak signal is $L_{res} \sim 0.1\ cm$ at $n_0 \sim 10^{10}\ cm^{-3}$. Hence a propagation of laser resonant beam along a boundary layer *BL* after distance $D_1 \sim 10 - 100\ cm >> L_{res} \sim 0.1\ cm$ is possible only in the saturation or induced transparency regimes. Below is shown that at $E_{opt} \sim 1\ eV$ the surface density of power $\Phi E_{opt} \sim 10\ W/cm^2$ is sufficient for the realization of such regimes. Indeed, let here Φ is a surface density of photons' amount. In deed in a stationary regime in a saturating flow Φ the population difference in *BL* amounts

$$\Delta = n_- - n_+ = n_0/(1 + 2(\Phi/\Phi_{sat})). \tag{13}$$

Here $\Phi_{sat} \equiv (\tau_{1opt}\sigma_{res})^{-1} \sim 10^{16}\ photons\ cm^{-2}s^{-1}$ is an adopted "scale" for the saturating flux,

$$\sigma_{res} = \lambda^2/((1+(\tau_{1opt}\Delta\omega_D)^2)4\pi) \sim 10^{-9}\ cm^2 \tag{14}$$

is a cross-section for an induced absorption (emission), $\Delta\omega_D \sim \omega_{opt}\beta V_s/c \sim 4\ 10^6\ s^{-1}$ is a Doppler breadth, $\lambda \sim 10^{-4}\ cm$ is a wave-length; $\omega_{opt} = 2\pi\nu_{opt} \sim 1.5\ 10^{15}\ s^{-1}$ is a photon's frequency, $\tau_{1opt} \sim 10^{-7}\ s$ is a time-life of an optically excited state. The equation for the dependence of Φ from a coordinate x along $\boldsymbol{D_1}$ is

$$d\Phi/dx = \Phi\,\sigma_{res}\,\Delta = \sigma_{res}\,n_o\,\Phi/(1 + 2(\Phi/\Phi_{sat})) \tag{15}$$

and it has an exact decision in an implicit form:

$$\varphi = \varphi_0\,exp(-\xi + 2(\varphi_0 - \varphi)), \tag{16}$$

where $\varphi_s = \Phi/\Phi_{sat}$, $\varphi_0 = \Phi_0/\Phi_{sat}$, $\xi = x/L_{res}$, $L_{res} = (\sigma_{res}\,n_0)^{-1} \sim 0.1\ cm$, $\Phi_0 \equiv \Phi(0)$ is an initial flux density. Explicit approximate decision is:

$$\varphi_s/\varphi_0 = \Phi/\Phi_0 \cong 1 - \xi/(1 + 2\varphi_0). \tag{17}$$

Numeral example: At $D_1 = 100\ cm$ and $d_1 = d_0$ one has $x_{max} = D_1/2 = 50\ cm$, $\xi_{max} = x_{max}/L_{res} = 500$. At demand $\Phi/\Phi_0 > 0.9$ one has $\xi_{max}/(1+2\varphi_0) < 0.1$. Hence $\varphi_0 = \Phi_0/\Phi_{sat} > 2500$, $\Phi_0 > 2500 \times \Phi_{sat} \sim 3\ 10^{19}\ cm^{-2}\,s^{-1}$, $\Phi(0)\,E_{opt} \sim 10\ W/cm^2$. Hence a longitudinal homogeneity of a light flux along a layer BL $\Phi(x_{max})/\Phi(0) \sim 0.9$ is achieved in a saturating regime at the energy flux $\Phi(0)\,E_{opt} \sim 10\ W/cm^2$. A transversal size of a light flow amounts $\sim D_2 \times h \sim 100\ cm^2$. Hence the necessary power from a dye laser is $P \sim 1000\ W$. The energy of *SLI*-pulse at *SLI*-pulse lasting $t_{sli} < 10^{-6}\ s$ amounts $P \times t_{sli} < 10^{-3}\ J$ and is more than the excitation energy for a total amount of the goal atoms (molecules) in the BL. The *SLI*-realization demands simultaneous or alternate action of some few good synchronized pulses at different carrier frequencies[7,36,38,89]. All that pulses can penetrate through *BL* (along $\boldsymbol{D_1}$) practically without a resonant absorption if a decision of equations (14)-(17) satisfies the condition $\Phi(x_{max}) \sim \Phi(0)$. At enough big input flux $\Phi(0)$ the tandems of π- or 2π-pulses propagate through the resonantly absorbing medium. In this case the attenuation of SLI-field is still less than at a saturation and the equations (14) – (17) are applicable only for the quality account of the transparency in the *BL*.

10. LASER SYSTEMS FOR THE CORRECTION OF THE MBE ACTION.

10.1. The correction of the microbeams' angle divergence. The laser radiation is not capable to create the sufficiently low longitudinal temperature in the atomic beams as like as the active medium for the realization the gamma-laser [34,35]. However the transversal laser cooling for the atomic beams in SPTEN is rather useful and feasible[34,35]. The guarantee for that feasibility is a rather low $\sim 10^{10}$–$10^{14}\ cm^{-3}$ atomic concentration of the atoms in beams and a fine directionality of their movement ~ 0.1 angular degree.

The methods for the transversal lasing cooling (collimation) of the atomic beams had been realized and checked in a big amount of the experiments. The analyzing of that experiments is placed, e.g., in the survey [82]. The estimations below are based on data of that survey. The transversal laser cooling use the recoil of the atoms at the absorption by them of the photons from the laser waves with wave-vector orthogonal to the beam. Besides the frequency of that photons ω needs be shifted into a red side relatively to the atomic transition frequency ω_0. At that red shift, $\delta = \omega - \omega_0 < 0$, the force of the light pressure F is directed against a transversal speed v of the atom. Hence the light pressure F is a force of friction. In a linear on a velocity approximation ones have the following formula for the friction force $F = -M\beta_D v$. Here $\beta_D = 8\varphi_S\omega_{rec}(|\delta|/\gamma)/(1+\delta^2/\gamma^2)^2$ is a friction coefficient, $\omega_{rec} = \hbar k^2/2M$ is a recoiling frequency (a recoiling energy divided by Plank constant). The rest terms are: M is a mass of atom, γ is a width of the atomic transition, $k = \omega/c$ is a wave number, $\varphi_S = \Phi/\Phi_S$ is a saturation degree, i.e., a ratio of the laser radiation intensity Φ to the saturation intensity Φ_S. The Φ - values were used in the previous sec.9. The spread of the transversal speed could be decreased to the value

$v_{min} \sim (2\hbar\gamma/M)^{1/2}$ at the transversal Doppler's cooling of the atomic beam. The parameters $\gamma = 10^7\ s^{-1}$, M = 50 *atomic units* are character for the atomic selection. At such parameters the minimal velocity spread is about $v_{min} \sim 30\ cm/s$. But the same spread $V_{transv1} \sim 30\ cm/s$ *needs be* given at the MBE's output, see sect.2. Such coincidence could be very beneficial for the joining of MBE with the transversal laser cooling[34-36]. A part of the cooled atoms resulted in the transversal Doppler cooling lies near the unity for a beam with a low density [82]. The deceleration time

$$\tau_{ret} \sim (1/kv_{rec})(kv_0/\gamma)^3/3\varphi_S \tag{18}$$

and the deceleration path

$$l_{ret} \sim \lambda(\gamma/kv_{rec})(kv_0/\gamma)^4/12\varphi_S \tag{19}$$

are need for the deceleration of the spread from the original value v_0 to the end minimal one v_{min}. Here $\lambda = 2\pi/k$ is a wave length of the laser radiation, $v_{rec} = \hbar k/M$ is a speed of the recoiled atom, M is a mass of the atom, γ is a natural half width of line for the atomic transition. A numerical example : $M \sim 50$ *atomic units* $\sim 8\ 10^{-23}$ *gram* ; $E_{opt} \sim 1eV = 1.6\ 10^{-19} J$; $\omega \sim 1.5\ 10^{15}\ s^{-1}$; $k = \omega/c \sim 5\ 10^4 cm^{-1}$; $\lambda \sim 10^{-4}\ cm$; $\gamma \sim 10^7\ s^{-1}$; $\sigma_{res} \sim$ 10-9 cm2; $\Phi_S = \gamma/\sigma_{res} \sim 10^{16}\ cm^{-2}s^{-1}$; $\hbar = 10^{-27}\ erg\ s$, $v_{rec} = \hbar k/M \sim 2\ cm/s$, $\Delta v_{min} \sim (2\hbar\gamma/M)^{1/2} \sim 20$ cm/s, $v_0 \sim 10^3\ cm/s$. Hence

$$l_{ret} \sim 0.5\ cm/\varphi_S,\ \tau_{ret} \sim 5\ 10^{-4}\ s/\varphi_S. \tag{20}$$

It is a case of a bad initial transversal velocity spread $v_0 \sim 10^3\ cm/s$ which is more by a factor ~ 20 than it needs ($v_{0\ necessary} \sim 50\ cm/s$ in the accordance with the sec.2). At these conditions the deceleration time is $\tau_{ret} \sim 5\ 10^{-4}\ s/\varphi_S$. The atom is excited in schemes of [82]-type through one canal (induction by laser wave) and is de-excited through two canals (spontaneous decay and induced emission). In present work on owing to the analyzing of such scheme action the following additional «cinematic» condition (demand) is revealed

$$\tau_{ret} > 2v_0/v_{rec}\gamma \tag{21}$$

This condition gives with account of (20) the restriction on the saturation parameter

$$\varphi_S < 5 \tag{21'}$$

Hence ones have in given example:

$$\Phi < 5\Phi_S\ ;\ \Phi E_{opt} < 5\Phi_S E_{opt} \sim 0.1 W/cm^2\ ;\ \tau_{ret} > 10^{-4}\ s\ ;\ l_{ret} > 0.1\ cm. \tag{21''}$$

That case corresponds to the difficulties of a real experiment with a real, non-perfect MBE-grating and with a real non-perfect ionic optics [28-31,36].

10.2. The previous forming of a sharp directional movement in the atomic mixture for its effective propagation through the grating of the MBE. Let the atoms of the separating mixture are accelerated up to the velocity $\sim 10^5\ cm/s$ before the intrusion of these atoms into the grating of the MBE. Let such accelerated atomic flux is collimated by the laser as like as in sec.10.1. The atoms of such formed flux will penetrate into the grating of the emitter almost in parallel with the walls of the directive slits. The estimation (1) of the penetration coefficient ς (see sec.3) was made at the suppose of the isotropic distribution of atoms over the velocity's direction before the penetration into the grating. But that distribution will become sharply anisotropic in case of the previously accelerated and collimated beam. Hence the outlined above procedure of the previous laser action on the separating mixture could give the significant growth of the penetration coefficient ς in a comparison with the formula (1). Any decrease of longitudinal velocity spread is not necessary in that case. This fact is beneficial for this experiment realization. The violet shift $\delta = \omega - \omega_0 > 0$ and the fulfillment of conditions as like as ones in the section 10.1 are necessary in order to accelerate the atoms of mixture up to the speed $v_{end} \sim 10^5\ cm/s$ for the time t_{acc} The main equations are like as above in sec.10.1. The acceleration time

$$\tau_{acc} \sim (1/kv_{rec})(kv_0/\gamma)^3/3\varphi_S \tag{22}$$

and the acceleration path

$$l_{acc} \sim \lambda(\gamma/kv_{rec})(kv_0/\gamma)^4/12\varphi_S \tag{23}$$

are need for the deceleration of the spread from the original value $v \sim 0$ to the end maximal one v_{end}.
A numerical example: $M \sim 50$ *atomic units* $\sim 8\ 10^{-23}$ *gram*; $E_{opt} \sim 5eV = 8\ 10^{-19} J$; $\omega \sim 7.5\ 10^{15}\ s^{-1}$; $k = \omega/c \sim 2.5\ 10^5 cm^{-1}$; $\lambda \sim 2.5\ 10^{-5}\ cm$; $\gamma \sim 10^9\ s^{-1}$; $\sigma_{res} \sim 5\ 10^{-11}$ cm^2; $\Phi_S = \gamma/\sigma_{res} \sim 2\ 10^{19}\ cm^{-2}s^{-1}$; $\hbar = 10^{-27}\ erg\ s$, $v_{rec} = \hbar k/M \sim 10\ cm/s$, $\Delta v_{min} \sim (2\hbar\gamma/M)^{1/2} \sim 200$ cm/s, $v_{end} \sim 10^5\ cm/s$. Hence

$$l_{acc} \sim 330\ cm/\varphi_S,\ \tau_{acc} \sim 2\ 10^{-3}\ s/\varphi_S. \tag{24}$$

The atom is excited in schemes of [82]-type through one canal (induction by laser wave) and is de-excited through two canals (spontaneous decay and induced emission). In present work on owing to the analyzing of such scheme action the following additional «kinematics» condition (demand) is revealed

$$\tau_{acc} > 2v_0/v_{rec}\gamma \tag{25}$$

This condition gives with account of (20) the restriction on the saturation parameter

$$\varphi_S < 100 \tag{25'}$$

Hence ones have in given example:

$$\Phi < 100\Phi_S\ ;\ \Phi E_{opt} < 100\Phi_S E_{opt} \sim 1.6\ 10^4 W/cm^2\ ;\ \tau_{acc} > 2\ 10^{-6}\ s\ ;\ l_{ret} > 3\ cm. \tag{26''}$$

Besides the synchronous increasing of the frequency shift $\delta = \omega - \omega_0 > 0$

$$from\ \delta\omega_{min} = 0 \quad up\ to \quad \delta\omega_{max} = \omega_0\, v_{end}/c \sim 3\ 10^{10}\ s^{-1} \tag{27}$$

needs be used in order to compensate the Doppler shift's increasing. Also other measures discussed in [82] could be used for this aim. All that measures correspond to the difficulties of a real experiment with a real, non-perfect MBE-grating and with a real non-perfect ionic optics [28-31].

The laser collimation task in mixture flux forming could be solved at the same conditions (the intensities included) as like as ones in the section 10.1. It is seen that a problem of the formation of the sharp mixture intrusion in the grating of the emitter (sec.10.2) is not more complex than the task for the transversal laser cooling (collimation) of beams which are emerged from the MBE (sec.10.1).

10.3. The decrease of the atom's «sitting time» and adhesion on the directive walls of the MBE-grate. The special covers and the high-temperature heating ($\sim 1000\ K$) were suggested in the early works on the MBE [27-31] in order to decrease the atom's «sitting time» and the adhesion on the directive walls of the MBE-grate. In the late works [34-36] that suppositions against the «sitting» and adhesion were refilled with the suggestion of the laser resonant (and hence selective) cleaning of the surface from the «sitting atoms». The frequency of laser radiation needs be resonant with the oscillations of atom attached to the surface by the elastic forces. In a result of the multi-photon resonant cascade transitions the bind «surface - atom» will be broken. This measure leads to the significant additional decrease of the effective adhesion coefficient θ. Besides the resonant character of the laser beam action saves from the emergence of the unwanted atoms which hinders the selection.

All above (sections 9, 10) give only small part of the possible auxiliary applications of laser radiation apart from its main application in MBE, viz., the selective laser ionization. All this in toto points on the unlimited amount of different variants on the way of the development and the creation of the Multi Beam systems of the selection.

11. Selection of short-lived isomers and radio-nuclides. Anti-decay effects (*ADE*).

For a selection of short-lived isomers and radio-nuclides one needs of a converter[27-30] combining the properties of a nuclear target and *MBE*. The goal isotopes (isomers) are arisen in a substance of target with a concentration less than 10^{-7}–10^{-11} at the exposure of nuclear radiation (neutrons, photons of the big and middle energies or other particles) even from the most strong pulse reactors. Hence to evaporate irradiated (by nuclear radiation) target and after that to selectively separate the resulted mixture[7,10,38,89] for a short time-life of a radio-nuclide 10^{-4} - $10^{-7} s$ is a practically unfeasible problem. But in case of a solid unvaporized target (i.e., a converter-*MBE*) a boundary layer (*BL*) filled up with atoms **only of two types**:

I type - the recoiled atoms *(Szilard-Chalmers effect)* and

II type - the other atoms which are knocked out the walls of the converter by the recoiled atoms. So a relative concentration of goal nuclei in *BL* at the output of *MBE*-converter ($C_0 \sim 10^{-2} - 10^{-4}$) is more by *5 – 7* orders[27-30] than in the gas cloud evaporated from the irradiated target (in methods[7,19,17]) and this concentration. This concentration $\tilde{N}_0$ at the output of converter does not depend on the volume pulse radiation dose in the target-converter[27-30].

A big amount of the secondary electrons activated by the internal electron conversion (*IEC*) arises in a multibeam (*MB*). The many of these electrons recombines with a positive charged ions or vanishes at the touching with the walls of the LIS-system. But in case of short-lived isomers a significant part of secondary electrons ~ 0.001 – 0.1 "glues" to the neutral atoms and hence forms the negative ions [35]. So a *BL* contains a notable portion ~ 0.001 – 0.1 of positive and negative ions (labeled below as "side" ions (*SI*)), which arise *non-selectively* in a side result of *IEC*. Hence if there are no the especial measures for the cleaning from *SI* then the hindrances of two types will arise:

1. - A lot of *SI* are undistinguished from goal ions arisen at *SLI*. Hence the goal ions are focusing together with *SI* and so the relative content of the goal isotope at outlet of *LIS* decreases.

2.- The goal ions are scattering on the *SI* and this reason something complicates the task of *MB*-focusing. But at time-life of a radionuclide $\tau_1 > 10^{-6}$ *s* and at a summary duration $t_{sum} = t_{SLI} + t_{extr} < 10^{-7}$ *s* the system for cleaning from *SI* could be created without the insurmountable difficulties. So both types of hindrances above are removed. Here t_{SLI} is a time of *SLI*-pulse, t_{extr} is a time for an extraction of goal ions from *BL*. During the time t_{extr} the cleaning from *SI* needs be interrupted.

Let regard the case of edge focusing of goal ions into a micro-target. Let ρ is the probability that the de-excited nuclei will hit in the focus (into the microtarget). Let after goal ions extraction from *BL* in some of them an act of *IEC* arises and their nuclei become de-excited. Such ions with de-excited nuclei will change charge and will be: (A) – defocused and (or) (B) – captured into traps. So at such conditions the probability ρ will become small: $\rho << 1$. So the relative concentration of goal nuclei in beam Ψ will decrease with a time of passing t more slow than a usual exponent[34] $exp(-t/\tau_1)$, namely

$$\Psi(t/\tau_1) \equiv exp(-t/\tau_1)/(exp(-t/\tau_1) + \rho'\,(1 - exp(-t/\tau_1))) \equiv 1/(1-\rho' + \rho'\,exp(t/\tau_1)), \tag{28}$$

where *t is a time for residence of nucleus in a beam* (a passing-time), $\rho' = (1+\alpha\rho)/(1+\alpha)$, α is a coefficient of *IEC*. So owing to "cleaning" action of focused multibeam system the relative concentration of short-lived radionuclide in a beam becomes less dependent

on *IEC*-decay. I.e., a special **"anti-decaying effect"** (*ADE*) arises. *ADE* is provided: **(1)** - by the edge focusing ($\rho < 0.1$) and **(2)** - by the cleaning-traps-system. *ADE* is big ($\Psi(t/\tau_1) \sim 1$) at $\rho << 0.1$ and $\alpha >> 1$. *ADE* vanishes, i.e., $\Psi(t/\tau_1) \equiv exp(-t/\tau_1)$, at $\alpha = 0$ *and* (or) $\rho = 1$.

Numeral example: At $\alpha = 50$, $\rho = 0.01$, $t/\tau_1 = 4$ one has $\Psi(t/\tau_1) = 0.388$, in contrast with $\varpi_{dec} = exp(-t/\tau_1) = 0.0183$, i.e. the decay-decreasing of the relative inverse population is retarded by the factor $\Psi(t/\tau_1)/\varpi_{dec} \cong 21.2$. *ADE is possible also for a row other nuclear processes (not only IEC) which are accompanied by the change in a charge of electronic shell.* Also another mechanism ADE, more strong than above, is possible. It consists of a repeat of the main selection process (e.g., *SLI*) in two or more places of a transport-focusing track (see p.8).[27,28] Such mechanism complicated a MB-system but it supply the high relative concentration of goal atoms (molecules) [27,28] which by some orders exceeds the "decay" value $\varpi_{dec} = exp(-t/\tau_{dec})$ at a big passing-time $t >> t_{dec}$ on the outlet of *MB*-system.

SUMMARY

Multibeam emitters (MBE) with high oriented developed microrelief are suggested to create more effective multibeam (*MB*) selection systems (e.g., laser selection). A general function of *MBE* is a preparation of a beam for an effective selection. A beam of a big transversal format is splintered into ~10^6-10^9 parallel microbeams on the outlet of *MBE*. As a result it becomes possible to increase a number of atoms at input gate of device for selection and at a time to decrease the next parameters: Doppler dispersion, aberrations at focusing of broad beam on a microtarget, a time for the renovation of selection cycle, a density of amount of atoms and, as a sequence, *to decrease* a probabilities for a lot of parasitic processes, e.g., for a recharging of goal ions. Hence in principle *MBE* are capable to exceedingly (by some orders) accelerate the laser selection of molecules, atoms, isotopes (*LIS - Laser Isotope Selection, AVLIS - Atomic Vapor LIS*), the stable and short lived isomers, radionuclides. At realization in the microrelief of *MBE* of nuclear reactions for creation of goal radionuclides *the relative concentration of the last* at the input gate of *LIS* becomes *by 5-9 orders more* than in case of evaporation of irradiated nuclear targets in *AVLIS*-method. The mechanisms for conservation along beams of relative inversion for the short lived nuclei (*ADE – antidecaying effects*) are suggested. The ideas of *MBE* and *MB*-systems (e.g., the ideas of *SPTEN - Soft Prompt Transplantation of Excited Nuclei*) arose in the bosom of *GL*-problem and they are material for the *GL*-realization. But *MBE* are useful in decision of more wide circle of problems than only *GL* (*GL*, laser and electromagnetic selection of molecules, atoms, isotopes, isomers, radionuclides; precision beam chromatography-spectroscopy of macromolecules in biochemistry, etc.). Semenov Institute of Chemical Physics of RAS has an experimental basis, know-how and takes the lead for the formation of the *International Cooperation "Project MBE"* for the development and creation of *MBE* for various goals on base of modern physical-chemical (e.g., laser) micro and nano-technologies.

ACKNOWLEDGMENTS

The Author expresses his gratitude to V.I.Gol'danskii, Y.M.Kagan, R.V.Khokhlov, Yu.A.Il'inskii, L.A.Rivlin, G.C.Baldwin, V.S.Letokhov, Yu.B.Khariton, A.A.Rukhadze, V.G.Minogin, J.J.Carroll, C.B.Collins, A.N.Starostin, V.Yu.Baranov for the discussions in divers times.

REFERENCES

All references cited at present work could be found in the paper labeled here as [A]:

[A]. Karyagin S.V. \\ 2000, "Status of gamma-laser problem on current moment'2000: ranging analysis and screening of gamma-laser schemes on their feasibility". Corresponds to the report TuB1-8 at the X Conference "Laser Optics'2000", St.-Petersburg, June 26-30, 2000, Technical Program, p. 16.

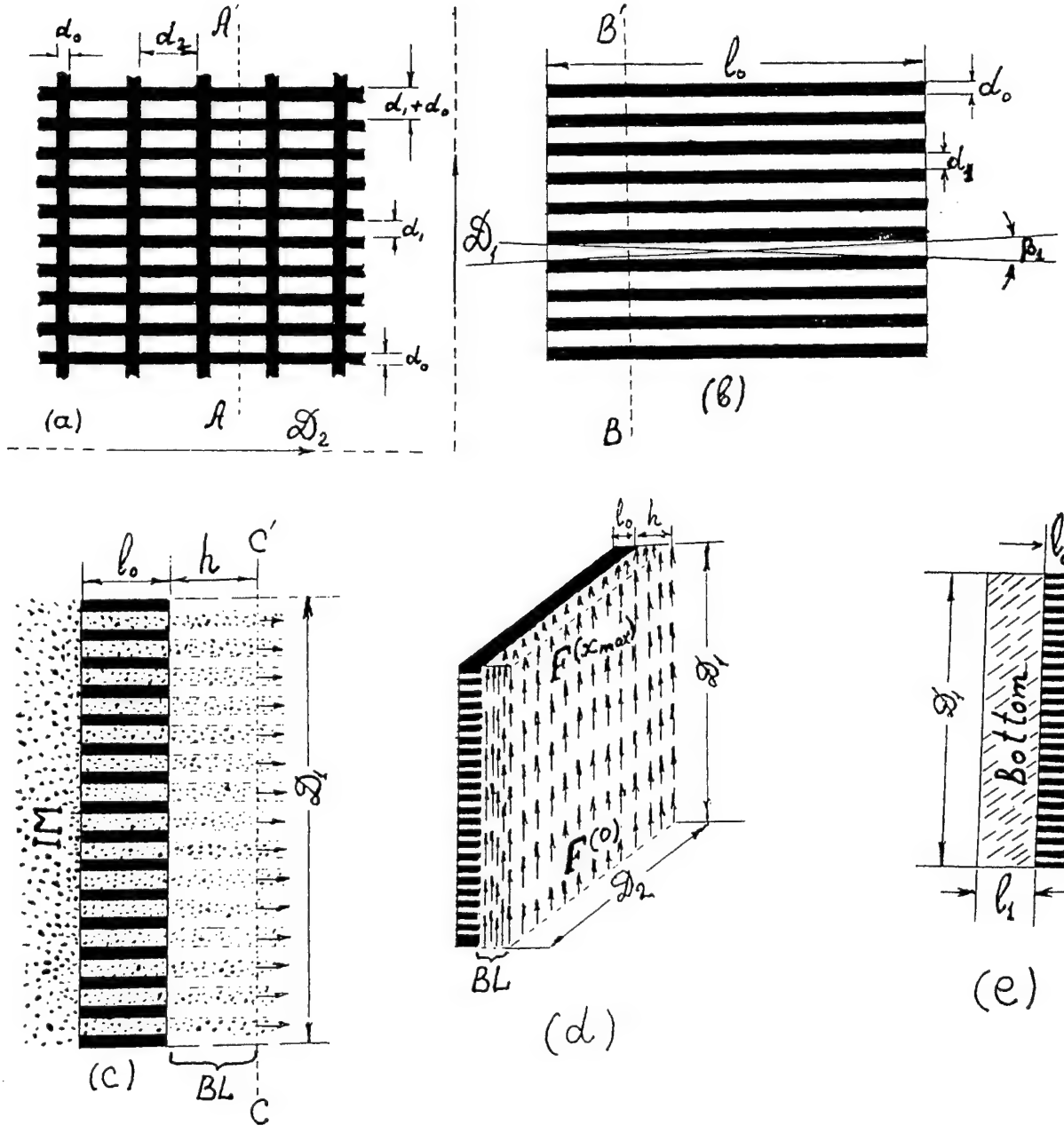
A
B
C
(a)
(b)
(c)
(d)
(e)
BL
Bottom

Joint gamma-generation and radiation-heat regime (GG&RH) theory for gamma-lasers' screening in the first approach of "Soft Prompt Transplantation of Excited Nuclei"

S.V.Karyagin

Semenov Institute of Chemical Physics, RAS, Prospect Kosygina 4, 117997 (GSP-1), Moscow, GSP-1, Russia
e-mail: chaika@chph.ras.ru ; fax: (095)-137-8318

ABSTRACT

Joint theory of gamma-generation (GG) and radiation-heat regime (GG&RH) in active medium (AM) of γ-laser (GL) was created and applied for the analyses of the total world experience in the GL-problem in order to choose those nuclei-candidates, active media, GL-schemes which are indeed actual for the GL-creation.

Keywords: quantum nucleonics; gamma-generation (induced, super-radiant in plasma, in beam, in solid); amplification without inversion, Borrmann effect, hot microplasma in cold solid; collapse of HFS by motion; soft prompt transplantation of excited nuclei; multi-beam laser selection; heat blast of active media) of gamma-ray laser (residential, non-residential)

PART 1. GAMMA-GENERATION THEORY.

The γ-generation theory with account of a big hindrances' complex is developed and checked on the example of big amount of different work nuclei. The real conditions for the γ-generation are much rigid, more rigid than the relatively soft Shawlov-Towns conditions for the induced radiation or the conditions for the super-fluorescence (super-radiance) which are deduced without the appropriate accounting of the hindrances. At the calculation of the real active medium (AM) for the γ-generation it needs to account an absence of the good reflecting mirrors, the stochastic character of the origin initiating γ-wave, the lethargy of AM relatively the resonant processes, the surplus of the spontaneous decay's rate above the rate of the exit of AM from the lethargy, the amplification of the γ-radiation phase's damping owing to the non-resonant absorption of γ-quanta and the heat regime. The real AM and the appropriate radiation-heat regimes accept the γ-generation only in a solid and bind a number of the nuclei-candidates and the hosts. The conditions for the generation are quite different between the «nonresidential» active media and the «residential» ones. Hence they are different also between the first «fuse» γ-lasing section and the subsequent more powerful sections of the compound γ-lasers.

1. Real threshold conditions (*RTC*) for induced gamma-oscillation

The parameter p of "Reserved Amplification" (*RA*) is introduced through a formal balance equation[23-32,34,35,49,50] in the most favorable case of 100% inverted population and at the supposition that the maximal value of the resonant cross-section is reached

$$n\sigma_0 \tau_2/\tau_1 = p\,(n\,\sigma + n'\,\sigma'), \qquad (1)$$

where $n = n_+ + n_-$ is a total density of working nuclei amount (*DWNA*) averaged over tooth volume; n_+ is *DWNA* for a level "+", and n_- is *DWNA* for a level "-". Here the level "-" is considered as a stable or almost stable one when $\tau_- >>> \tau_+$. Here τ_-, τ_+ are the live-times of levels "-" and "+" correspondingly. It is so for the majority of nuclei candidates. The seldom case when $\tau_- \sim \tau_+$ will be regarded especially in another paper. But here it is adopted only the relation $\tau_- >>> \tau_+$. And hence $\tau_1 = \tau_+$. At this condition a formula (1) is a certain formal definition of *RA*. The value

$$L_0 = (n\sigma + n'\sigma')^{-1} \qquad (2)$$

is length of non-resonant losses in tooth. Appropriate value in *DOCLMP* equals $2L_0$. The Reserved Amplification (RA) is a formal «gain»

$$RA \equiv p = (\tau_2/\tau_1)\, n\sigma_0 L_0 \qquad (3)$$

on the photon's free path length L_0 in a continuous substance of tooth. The definitions (1) and (3) for $RA \equiv p$ are only a handy combination of basic values and the equation (1) isn't a real balance equation because $n_+ < n$ and the induced cross-section could reach its maximal limit $(\tau_2/\tau_1)n\sigma_0$ only at the time $t >> \tau_2$.[9,81]. The necessary for the γ-generation value RA is estimated from a complex of conditions below. According to (1) the value *RA* has a maximum $p_m = p_0\, \tau_2/\tau_1$ where $p_0 = \sigma_0/\sigma$. For ^{58}Co ones have $p_0 = 888$.

Another basic value is a density n' of host-atoms. For a diamond $n' = 1.76\ 10^{23}\ cm^{-3}$. The relative impurity concentration n/n', a value ψ, total length L of *DOCLMP*, relative length $\nu = L/2L_o$, amount of diffraction modes $\boldsymbol{m}$, all these data are used as the input values for the chain of the subsequent estimations in the special algorithm[34,35]. Then the *interim values* are derived: the reserved amplification RA; the cross-size $\boldsymbol{d}$ (diameter) of active medium AM; volume of AM $\boldsymbol{V \sim d^2 L}$ (this formula is exact for a square form of *AM*-cross-section); solid angle $\boldsymbol{\Omega \sim d^2/L^2}$ of diffraction mode; total number $\boldsymbol{N_0 = nV/2}$ of working nuclei (ones need to account that half of comb-like AM is empty); resonant cross section $\boldsymbol{\sigma_0}$ (averaged on HFS, polarization, wave-vector direction at frequency maximum) i.e.

Laser Optics 2000: Ultrafast Optics and Superstrong Laser Fields, Alexander A. Andreev, Vladimir E. Yashin, Editors, Proceedings of SPIE Vol. 4352 (2001) © 2001 SPIE · 0277-786X/01/$15.00

$$\psi = (n/n')/((n/n')+(\sigma'/\sigma)); \; L_0 = (1-\psi)/(n'\sigma'); \; L=2yL_0; \; p = \psi p_0 \tau_2/\tau_1; \; d = (m\lambda L)^{1/2}; \; V = 4\,(L_0 y)^2\, m\lambda; \; \Omega = m\lambda/L; \quad (4)$$

$$N_0 = 2\,(m\lambda/n'\sigma'\sigma)\;\psi\,(1-\psi)\,y^2; \quad (5)$$

$$\sigma_0 = (\lambda^2/2\pi) f' w/(1+\alpha). \quad (6)$$

The number of γ-quanta arisen in the amplification of stimulated emission (*ASE*) at account of width-path effects (sec.2.0) is

$$N_{ASE}(p) = (N_S/y)\int_0^{\infty} exp(-x')\,dx'\,[exp[[\,pG(x')-2\,]\,y] - 1]\,/\,[pG(x')-2]. \quad (7)$$

In usual case of a non-resonant detector the negative part «-2 » of the «gain» **(pG−2) contains two parts: the first ordinary part «−1 »** owing to the direct non-resonant losses and **the second equal but unusual part «−1 »** owing to the non-direct influence of the same non-resonant losses but through the introduced above «Width-Path Effects» (WPE) which particularly decrease the resonant cross-section. Without WPE the «gain» equals to (pG−1). Here $x=t/\tau_1$ is a «normalized» time; $N_S = (m/4)\gamma p(\tau_1/\tau_2)\,\exp(-x_1)$ is a number of spontaneous γ-quanta emitted for all generation time in m modes in a spectral interval τ_2^{-1}; $exp(-x_1) = n_+(0)/n$; $n_+(0)$ is *ELAN*-amount density at momentum $t = 0$; the value $n = n_+ + n_-$ is independent on time (at the condition $\tau_- >> \tau_+$). A value $pG(x)/L_0$ is a generalized induced gain for the time x. The cross-section of induced emission $\sigma_i(t)$ equals to zero at the start momentum $t = 0$, when a resonant interaction (of *ELAN* and γ-radiation field) is switched[9,10,12,17,81]. *The value of* $\sigma_i(t)$ asymptotically grows up to its limit $\sigma_i(\infty) = \sigma_o$ during time ~ τ_2. Any correct formula for $\sigma_i(t)$ is not yet derived because of difficulties in transforming of complicated non-linear decisions of Maxwell-Bloch equations to cross-section concept. The next simple approximate formula which contains all properties marked above was suggested and used in Refs.[28-35] as a compromise:

$$\sigma_i(t) = (1-exp(-t/\tau_2))\;\sigma_i(\infty). \quad (8)$$

Hence a stationary form $p/L_o = (n_+ - g\,n_-)(\tau_2/\tau_1)\sigma_o$ for the induced gain need be transformed to the non-stationary form

$$pG(t)/L_o = n_+(t)\;\sigma_{+-}(t) - [n_-(0)\;\sigma_{-+}(t) + \int_0^t n_+(t')\;\sigma_{-+}(t-t')\;d(t'/\tau_1)\,]. \quad (9)$$

Here $\sigma_{+-}(t) = \sigma_{+-}(\infty)\;(1 - exp(-t/\tau_2))$ is $\sigma_i(t)$ for emission from "+" nuclear quantum state to "-" state; $\sigma_{+-}(\infty) = (\tau_2/\tau_1)\sigma_o$ is a limit for $\sigma_{+-}(t)$ at infinity great time. By analogy $\sigma_{-+}(t) = \sigma_{-+}(\infty)\;(1 - exp(-t/\tau_2))$ is $\sigma_i(t)$ for the transition from "-" to "+" state; $\sigma_{-+}(\infty) = (\tau_2/\tau_1)g\sigma_o$ is a limit for $\sigma_{-+}(t)$ at infinity time. In common case a value g can be different from $(2j_+ +1)/(2j_- +1)$. E.g., $g = 0$ in case of ideal *AWI* (see[A]); $g = 1$ in case of non-degenerated working levels. The nuclei arisen spontaneously in a lower state "-" at momentum t' are dephased at this time-point t'. So at $t > t'$ a phasing time t_ϕ of these nuclei (or time of growing of its absorption cross-section) is $t_\phi = t - t'$. The value $n_+(t')\;d(t'/\tau_1)$ is a number of "new" nuclei in state "-" in the time-interval dt'. In case of weak generation the populations $n_+(t)$ and $n_-(t)$ are

$$n_+(t) = n_+(0)\;exp(-t/\tau_1), \quad n_-(t) = n_-(0) + \int_0^t n_+(t')\;d(t'/\tau_1). \quad (10)$$

A time-dependent factor $G(t)$ of induced gain function is transferred to the form (12) at a formal denoting (11):

$$exp(-x_1) = n_+(0)/n; \; n = n_+ + n_- = const; \; n_-(0) = (1-exp(-x_1))n\,; \quad (11)$$

$$G(t) = (1 - exp(-x\tau_1/\tau_2))\;(exp(-x_1 - x) - g) + g\,exp(-x_1)\;(e^{-x} - exp(-x\tau_1/\tau_2))\;/\;(1-(\tau_2/\tau_1)); \quad (12)$$

or else (see below) at denotations $\mu = e^{-x}$ and $\zeta = (\tau_1/\tau_2)$ ones have

$$G(t) = G(\mu) = (1 - \mu^{\zeta})\;(\mu\,\mu_1 - g) + g\,\mu_1\,(\mu - \mu^{\zeta})/(1 - (1/\zeta)) \quad (12')$$

Note that the limit of $G(t)$ at $\zeta = (\tau_2/\tau_1) \to 1$ is a function $\mathrm{Lim}\{G(t)\;at\;\tau_1/\tau_2 = 1\} = G_{lim}(t)$ estimated as

$$G_{Lim}(t) = (1 - e^{-x} + gx)\;exp(-x_1 - x) - g\,(1 - e^{-x}). \quad (12'')$$

Here (12") corresponds to a particular case $\tau_1 = \tau_2$. The decisions (12), (12") satisfy for all initial and limit conditions. The further analysis is based on the approximation of $G(t)$ by a quadratic form $G(\mu) \approx G_m - (\mu - \mu_o)^2 K$, where $\mu = e^{-x}$. The values G_m, μ_o, K depend on the basic parameters $\zeta = (\tau_1/\tau_2)$, $g = (2j_+ +1)/(2j_- +1)$, $exp(-x_1) \equiv n_+/n|_{\,at\,t=0}$. The Poisson's formula leads to

$$N_{ASE}(p) \approx (\pi p/yK)^{1/2}\;(m/4)\;(\tau_1/\tau_2)\;exp(-x_1)\;\{\{\,exp[(pG_m - 2)y] - 1\,\}\,/\,(pG_m - 2)\}, \; p > p_{thr} = 2/G_m. \quad (13)$$

Here the negative part «- 2 » of the «gain» $(pG_m - 2)$ contains two parts: the part «- 1 » owing to the direct non-resonant losses and the another equal part «- 1 » owing to the non-direct influence of the same non-resonant losses but through the introduced above «width-path» effect action. Eq.(13) is approximately valid at $(pG_m - 2)y > 0.5$ and contains threshold condition for *ASE*: $p > 2/G_m$. The more precision expression at $(pG_m - 2) \le 5$ is derived from (12), (12') with use of a serial expansion of the exponential on the «generation's interval» $\mu_- < \mu < \mu_+$:

$$N_{ASE} \equiv N_A \approx (N_S/y)\int_{\mu-}^{\mu+} d\mu\,[exp[[pG(\mu)-2]\,y] - 1]\,/\,[pG(\mu)-2] \approx 2N_s\,(v/pK)^{1/2}\,[1+(5/6)(vy)+(19/45)(vy)^2+(87/280)(vy)^3] \quad (13')$$

with the relative error less than 20% at $vy<3$. Here $v \equiv (pG_m - 2)$ and μ_+, μ_- are the roots of *equation* $G(\mu) = 2/p$: $\mu_+(p) = \mu_0 + \Delta(p)$, $\mu_-(p) = \mu_o - \Delta(p)$, where $\Delta(p) = [(G_m - (2/p))/K]^{1/2}$. The factors «**2**» *instead of* «**1**» in (26) are due to the above Width-Path Effects. The start-time for γ-lasing is $t_+ = -\tau_1 ln\mu_+$. The end-time for γ-lasing is $t_- = -\tau_1 ln\mu_-$. At $t < t_+$ and at $t > t_-$ γ-lasing is absent. Time-interval of *ASE*-generation is $t_+<t<t_-$ with duration $t_G(p) = t_- - t_+ = \tau_1 ln(\mu_+/\mu_-)$ and with a maximum of intensity at $t = t_m = -\tau_1 ln\mu_o$. Eqs.(13), (13') with $p = \psi p_0 \tau_2/\tau_1$ give an upper limit of N_A. The substitution of decision p' *of equation* $p' = p\, t'_G /2\tau_2$ (instead of p) to (12), (13) gives a lower limit for N_A. Here $t'_G = t_G(p')$. Factor $t'_G/2\tau_2$ **over-accounts** a frequency band $\sim 2(t'_G)^{-1}$ of γ-pulse. The real value N_A is inside the interval $N_A(p') < N_A < N_A(p)$. A peak energy flow I_p equals (at appropriate p or p') to the integrand of (13') multiplied by $E_\gamma/(d^2\tau_1)$. A peak saturation parameter $P_s = \tau_2\sigma_o I_p/E_\gamma$ is also used below. At big $vy>28$ the formula (13') needs be replaced by a *π-pulse* asymptotic approximation formula

$$N_{ASE\ asympt} \approx N_{\pi\text{-pulse}} \approx d^2\,(p\text{-}1)/\sigma_0 \qquad (13'')$$

This formula is based on the Zvelto's theory[67] which was generalized and corrected in works [23,27].

Numerical examples. According to data of **1.1** there are the next values: $\zeta = \tau_1/\tau_2 = 1.1$; $exp(-x_1) = 0.9$; $n/n' = 5\ 10^{-3}$; $\sigma'/\sigma = 4.7\ 10^{-3}$; $\psi = 0.515$; $L = 0.321$ *cm*; $y = 0.329$; $d = 3.8\ 10^{-5}$ *cm*; $p = 416.5 >> p_o = 2/G_m = 14.5$, p_o is a threshold. So it is a super-threshold γ-lasing. Note, that necessary short period $t_i \sim 10^{-8}$ *s* of *ELAN*-implantation is in touch in SPTEN-method[27-35]. Besides, the prompt shatters with $t_i \sim 10^{-12}$ *s* could be created[23,27]. Other parameters are: $G_m = 0.138$; $\mu_o = 0.705$; $K = 1.586$; $\Delta = 0.290$; $\mu_+ = 0.995$; $\mu_- = 0.415$; $t_+ = 5\ 10^{-3}\tau_1 = 7.6\ 10^{-8}$*s*; $t_- = 0.879\tau_1 = 1.33\ 10^{-5}$*s*; $t_m = 0.35\ \tau_1 = 5.3\ 10^{-6}$*s*; $t_G = 0.874\tau_1 = 1.32\ 10^{-5}$*s*; $p' = 200$. The γ-lasing pulse characteristics are: $10^3 < N_A < 1.3\ 10^7$; $5\ 10^{12} < N_A E_\gamma < 6\ 10^8$ *J*; flux $F = N_A/d^2$: $10^{12} < F < 10^{16}$ *cm*$^{-2}$; $3\ 10^{-3} < FE_\gamma < 40$ *J/cm*^{2}; mean energy flow $I = FE_\gamma/t_G$: $230 < I < 3.0\ 10^6$ *W/cm*^{2}; $2\ 10^3 < I_p < 4\ 10^7$ *W/cm*^{2}; solid angle of mode is $\Omega = \lambda/L = 1.37\ 10^{-8}$ *rad*^{2}; brightness: $1.5\ 10^{10} < I/\Omega < 2\ 10^{14}$ *W/cm*^{2}*rad*^{2}; $2\ 10^{11} < I_p/\Omega < 3\ 10^{15}$ *W/cm*^{2}*rad*^{2}; $10^{-5} < P_s < 0.2$; $16 < N_S < 34$. The ratio "signal to noise": $60 < N_A/N_S < 4\ 10^5$ is more than sufficient for the experimental demonstration *of* γ-lasing.[27,30] A total number of working nuclei in *AM* is $N_o = 2\ 10^{11}$, i.e., less by 2-3 orders than amount of *ELAN*, which can be put into AM owing to SPTEN-method. Efficiency of γ-lasing in this case: $10^{-8} < N_A/N_o < 10^{-4}$. More effective results are at further increasing of concentration **n/n'**. E.g., at $n/n' = 0.01$ and the same $N_o = 2\ 10^{11}$ the values are: $L = 0.227$*cm*; $y = 0.352$; $d = 3.2\ 10^{-5}$ *cm*; $p = 549.5$; $t_G = 0.884\ \tau_1$; $p' = 265$; $4\ 10^4 < N_A < 3\ 10^{10}$; $4\ 10^{13} < F < 3\ 10^{19}$ *cm*$^{-2}$, that is less than its π-pulse limit[23,27,67] $F_{lim} = (p\text{-}1)/(\sigma_0\,\tau_2/\tau_1) \approx 5\ 10^{20}$ *cm*$^{-2}$; $0.2 < FE_\gamma < 10^5$ *J/cm*^{2}; $10^4 < I < 10^{10}$ *W/cm*^{2}; $2\ 10^5 < I_p < 2\ 10^{11}$ *W/cm*^{2}; $10^{13} < I_p/\Omega < 10^{19}$ *W/cm*^{2}*rad*^{2}; $10^{-3} < P_s < 660$, and I_p needs be decreased; $26 < N_S < 53$; $1.5\ 10^3 < N_A/N_S < 5\ 10^8$; $2\ 10^{-7} < N_A/N_o < 0.13$, i.e. a high efficiency could be gotten. It is very difficult to keep $\tau_1/\tau_2 \cong 1.1$, because at $n/n' > 0.005$ clustering of atoms leads to a strong line-broadening. These results could be corrected by accounting of noise, saturation, etc.

2.Real threshold conditions for the super-fluorescent (super-radiant) gamma-oscillation on base of the approximate theory for the strong varied length of Bloch's vector.

The decision[87] for the projection R_3 of Bloch's vector R had been generalized (1995,1998, Karyagin) for non-keeping R: [34,35]

$$R_3 = R\,(R - e^{\varphi+\varphi'})/(R + e^{\varphi+\varphi'}). \qquad (14)$$

Here $R = R'\,D_{ph} - (\tau_{mod}/\tau_2)$ is the length of *effective time-dependent Bloch's vector*, $R' = (ze^{-x} - g)N_o$ is a time-dependent ordinary inverse population in AM generalized on common case of arbitrary nuclear state degeneration, sec.**1**. Value R' depends on $x = t/\tau_1$ and $z = (1 + g)\exp(-x_1)$. Factor $D_{ph} = 1 - (1 + y)e^{-y} = (\beta/y^2)$ is an effectively phased relative part of all nuclei in the active medium at the totally reliable event that the spontaneously emitted γ-quanta are emitted in one axial generation mode, here $y = l/2L_0$. Values p, w, f', α, τ_1, τ_2, y, x, etc., see in **1**. Time τ_2 depends on length L', see «Width-Path Effect» in[34,35] and in the next paragraph below. The factor D_{ph} accounts the loss of photons from phasing process. That loss is owed to *scattering* or *non-resonant absorption* in AM. The speed of transitions $\tau_{mod}^{-1} = (1/2)\,(\Omega/4\pi)wf'(\tau_2/\tau_1)/(1+\alpha)\tau_1$ is the probability (in s^{-1}) of the event above that the γ-quantum is spontaneously emitted just into the axial generation mode. The factor 1/2 accounts two polarizations. The solid angle of the first diffraction mode is $\Omega = \lambda/L$. The length $L = 2L_0\,y$ in case of a dispersed active medium is twice in a comparison with the usual active medium. The resonant cross-section averaged over all polarizations, directions and HFS-components is $\sigma_0 = (\lambda^2/2\pi)$ (w f' / $(1+\alpha)$) (τ_2/τ_1). The «reserved amplification» p is a formal gain factor $p = n\sigma_0 L_0\,(\tau_2/\tau_1)$, sec.**1**. In case of one-mode generation the square of the transverse section of the active medium is $a_1^2 = \lambda L$. The volume of the active medium is $V = a_1^2\,L$. The total number of work nuclei (exited and non-exited ones together) is $N_0 = (1/2)nV$ because the dispersed active medium is a half-empty one. The accounting of all relations above leads to the simple equivalent form $(1/\tau_{mod}) = (y\,p\,/\,4\,N_0\,\tau_1)$. Hence $\tau_{mod} = (4N_0\tau_1/yp)$ is the time of the spontaneous emission per one nucleus into the generation mode. Note that $\tau_{mod} >> \tau_1$. The selection of photons for phasing into tight band width $1/\tau_1$ is accounted in τ_{mod}^{-1} by the factor τ_2/τ_1. *Such factor is absent in more simple old formulas* [17,88]. *Because of it that old simple formulas overestimate SF-part in the γ-lasing.* The main term of dephasing loss τ_{mod}/τ_2 is introduced in accordance with work[88]. It is necessary to fulfill the threshold condition $R'|_{t=0} > \tau_{mod}/(\tau_2 D_{ph})$, which at $D_{ph}=1$ coincides with Andreev's condition[17,88]. A number of effectively phasing "priming" photons for a time t is

$$\varphi = \int_0^t (R/\tau_{mod})\,dt = \int_0^t ((R'D_{ph}/\tau_{mod}) - \tau_2^{-1})\,dt. \qquad (15)$$

The "feedback" phasing addition from the super-fluorescent pulse in axial mode is

$$\varphi' = \int_0^t (\tau'/\tau_0)\, I_{SF}\, dt \;=\; \int_0^t (I_{SF}/\tau_0)^{1/2}\, dt, \qquad (16)$$

where width τ^{-1} is a logarithmic derivation of function I_{SF} and $\tau_0^{-1} \equiv w/(1+\alpha)\tau_1$ is a radiation width. So $\tau^{-1} \approx (\tau/\tau_0) I_{SF}$ and the integrand in (29) is proportional to $I_{SF}^{1/2}$. This procedure (1995,1998,Karyagin) is approximate equivalent of averaging of resonant interaction "radiation-ELAN" over a time-depending frequency distribution of γ-pulse, evaluated as a Fourier from pulse-form cut after momentum t. In a derivation $dR_3/dt = C_1 + C_2 + C_3$ the term $C_1 = -R\,(R^2 - R_3^2)/(2\tau_{mod})$ coincides with a right part of standard Bloch's equation. By analogy with[87] it gets

$$I_{SF} = (R^2 - R_3^2)/(2(g+1)\tau_{mod}) = 2R^3\, e^{\varphi+\varphi'}/\,[(g+1)\,(R + e^{\varphi+\varphi'})^2\, \tau_{mod}\,]. \qquad (17)$$

The term $\mathbf{C_2 = dR/dt \equiv dR'/dt}$ is a natural addition to C_1 from inverse population decay and needs to be adopted in generalized Bloch's equation. Term $C_3 = -(1/2)\,(1 - (R_3/R))^2\, dR/dt$ has no apparent nature and can be understood as a deflection from exact equation $\mathbf{dR_3/dt = -(R^2 - R_3^2)\, R/(2\tau_{mod}) + dR/dt}$. At $x < x_c$ a relation $|C_1 + C_2| > |C_3|$ is valid; $\mathbf{x_c}$ is *a root of equation* $\mathbf{R'(x) = 0}$. An approximate decision (14) satisfies *to initial condition* $R_3(0) = R(0)$ *and to asymptotic condition* $R_3(\infty) = -R(\infty)$. A *maximum* of function I_{SF} is achieved in point $x = x_m$, in which $\mathbf{R(x) = e^{\varphi(x) + \varphi'(x)}}$. The analysis leads to the next algorithm in order to estimate the amount of γ-quanta in a super-fluorescent (super-radiant) pulse.

I. To introduce the parameters which are independent on the relative length $y = L/2L_0$

$\mathbf{A_1 = (p/4)\, z\ ;\ A_2 = (p/4)\, g\ ;\ A_3 = 4\, N_{00}/p}$ where $\mathbf{N_{00} = N_{00}/y^2} = 2(m\lambda/n'\sigma'\sigma)\psi\,(1-\psi)$, sec. 1.

II. To estimate the argument y and its functions

$\mathbf{(\beta/y) = [1 - (1+y)e^{-y}]/y\ ;\ G_1 = (\beta/y)\, A_1;\ G_2 = (\beta/y)\, A_2 + (\tau_1/\tau_2)\ ;\ K' = y\, A_3.}$

Note that $K' = (4N_0/yp)$ but $N_0 = y^2\, N_{00}$.

III. To introduce the argument $x = t/\tau_1$ and its functions $R(x) = K'\,[G_1 e^{-x} - G_2]$; $\varphi(x) = G_1\,(1 - e^{-x}) - x\, G_2$; $\xi_1(x) = e^{\varphi}$. The region of x in which $R(x)>0$ and $\varphi(x)>0$ is determined by the conditions $x < \mathbf{x_c} \equiv \mathbf{ln(G_1/G_2)}$ and $(G_1/G_2)(1-e^{-x}) > x$

IV. The majorant for the formula (29) $\varphi'_{maj} = 2\ln[1 + (R/\xi_1))/2e] - 4(\xi_1/R) > \varphi'$ leads to the simple approximate results

$\xi_2(x_m) < e^{\varphi'(x_m)maj} \cong 31.5;\ R(x_m) < R(x_m)_{maj} \cong \xi_1(x_m)\, 31.5;\ \xi_1(x_m) \cong \xi_1(x_c);\ x_m = \mathbf{ln[G_1/(G_2+(R/K))]}$;

$$N_{SF} < N_{SF\,maj} \equiv N_{00}\, \xi_1(x_m)\, \xi_2(x_m) \equiv (1 - e^{-y})\, y^{-1}\, (1+g)^{-1}\, \xi_1(x_m)\, \xi_2(x_m). \qquad (18)$$

Numerical example for Co^{58}: E_γ=28.1 *KeV*; g=9/11; $\exp(-x_1) = 0.9$; τ_1/τ_2 =1.1; z = 1.636; p= 416; $N_{00} = 1.85\ 10^{12}$; A_1 =170; A_2= 85.1; $A_3 = 1.78\ 10^{10}$. *In case* $n/n' = 0.005$, $n=8.8\ 10^{20}\ cm^{-3}$; $N_o = 3\ 10^{11}$; y = 0.402; $\beta/y = 0.154$; give: G_1= 26.3; G_2=14.2; $\mathbf{K'}$= $7.16\ 10^9$; x_c=0.616'326'97; $x_c - x_m < 10^{-8}$; $\xi_1 = 28.5$; $\xi_1\xi_2 = R = 900$; $N_{SF} < N_{SF\,maj} = 400$; $N_{ASE} = 9.6\ 10^8$; $N_{SF}/N_{ASE} = 4.2\ 10^{-7}$; $N_{spont} = 42$. Calculations show that *in the induced super-threshold regime* $N_{SF} << N_A$ at the same parameters of active medium for SF and ASE. Only for a weak near-threshold regime (when $N_{SF} \approx 10$) could be $N_{SF} > N_A$, i.e., so called "weak SF"[88]. The results of present sec.2 are wider than in Refs.[34,35] and are more correct and realistic than ones of initial theories[17,87,88].

3. Some ideology on the induced and superradiant theory.

3.1. The foundation of cross-section's approach. The cross-section approach is very useful in case of so called feeble gain as like as in γ-laser. It is linked with absent of initial coherent «fuse» wave. Ones could to write the probability W(t) of the atomic transition

induced by laser wave in two approaches $W(t) = |\int_0^t dt\ \mathbf{D(t)}\, \mathbf{E}(t)\,|^2 = \int_0^t dt\, \Phi(t)\, \sigma_{ind}(t)$ (19)

here $\mathbf{D(t)}$ and $\mathbf{E}(t)$ are well known vectors of atomic polarization and field, $\Phi(t)$ is the field intensity and $\sigma_{ind}(t)$ is a resonant cross-section. The derivation of (19) and account that $\Phi(t) \sim |\mathbf{E}(t)|^2$ leads to the relation

$$\sigma_{ind}(t) = const\ \mathbf{D(t)}\, (\mathbf{E}(t)/\,|\,\mathbf{E}(t)\,|) \int_0^t dt'\ \mathbf{D^*}(t')\, (\mathbf{E^*}(t')/\,|\,\mathbf{E}(t)\,|) \qquad (20)$$

Approximately ones have $\sigma_{ind}(t) = const\, \langle (\mathbf{D(t)\, e(t)})\, \exp(i\psi(t)) \int_0^t dt'\ (\mathbf{D^*(t)\, e^*(t)})\, \exp(-i\psi'(t'))\rangle_{AV}$ (21)

There are some reasons suppose that $(\mathbf{D(t)\, e(t)})$ is more slow function than $\exp(i\psi(t))$. It leads to

$$\sigma_{ind}(t) \sim const' \int_0^t dt'\ \langle \exp(i\psi(t))\, \exp(-i\psi'(t'))\rangle_{AV} \qquad (22)$$

But $$\langle \exp(i\psi(t))\, \exp(-i\psi'(t'))\rangle_{AV} = \exp(-|t-t'|/\tau_2) \qquad (23)$$

at substitution into (22) gives

$$\sigma_{ind}(t) \sim const' \, (1 - \exp(-t/\tau_2) \qquad (24)$$

where in accordance with equation (8). $$const' = \sigma_{ind}(\infty) \qquad (25)$$

3.2. The foundation of with-path effects (WPE).

This effect exist when a number of photons in a mode is small, i.e., at the condition

$$\Delta t_{em} >> \Delta t_{van} \qquad (26)$$

Here Δt_{em} is a mean time between two successive *emergencies* of the photon in a lasing mode; Δt_{van} is a mean time-life (*vanishing* time) of one photon. It could be, e.g., L/c, see [37], where L is a free path of photon along a mode. It is simple to show that before the generation the ratio (26) is equivalent to the condition

$$L << (4\tau_1 c/\sigma_0 n_+)^{1/2} \qquad (27)$$

Here $c = 3\ 10^{10}$ *cm/s*. At the typical case $\tau_1 \sim 10^{-6}$ s; $\sigma_0 \sim 10^{-21}$ cm^2; $n_+ \sim 10^{21}$ *cm*$^{-3}$; and must be L << 350 *cm*. But at the developed generation the condition (26) turns into a reciprocal ratio $\Delta t_{em} << \Delta t_{van}$ and **with-path effects must be vanished.** The WPE can't to be observed in usual conditions of optics or even the Moessbauer effect because in that conditions the relation (26) can't be fulfilled. But in the beginning of the γ-lasing that effect is very efficient and leads to the growth of the induced threshold in both kinetics, induced and superradiant.

4. Application of the revised theory to the choice of nuclei candidates.

Below this revised theory is applied to the choice of nuclei-candidates. The initial data are placed in the Table 1.

Table 1. Eight candidates produced in photo-nuclear reactions $^Z A_{n+1}(\gamma n)^Z A^*_n$. $^Z A^*_n$ is an excited work isomer, e.g., $^{92}Nb_{42}(\gamma n)\ ^{92}Nb^*_{41}$

Type Work Isotope	+//1D $^{92}Nb_{41}$	+//1D $^{122}Sb_{51}$	+//2D $^{152}Eu_{63}$	+//1D $^{65}Zn_{30}$	+//1D $^{69}Ge_{32}$	+//1D $^{58}Co_{27}$
E_γ (keV)	90.2	61.45	32.6	53.96	85.0	28.1
τ_1 (sec)	6.20(-6)	2.74(-6)	2.38(-7)	2.31(-6)	7.36(-6)	1.51(-5)
α	0.17	0.75	1.2	4.4	1.4	1.5
$p_0 = \sigma_0/\sigma$	340	174	298	351	393	888
λ (Angstrem)	0.137	0.202	0.380	0.230	0.146	0.441
f'	0.30	0.61	0.88	0.60	0.29	0.86
σ_0 (barn)	7.58(4)	2.26(5)	9.24(5)	9.26(4)	4.04(4)	1.07(6)
$\sigma_0 = (\lambda^2/2\pi)(f'w/(1+\alpha))(1/(1+\chi))$; $\chi = \tau_+/\tau_-$; $\sigma_{+-} = \sigma_0/\zeta$; $\sigma_{-+} = g\,\sigma_{+-}$; $\zeta = \tau_1/\tau_2$; $(1/\tau_1) = (1/\tau_+) + (1/\tau_-)$; $(1/\tau_2) = (1/\tau_+) + (1/\tau_-) + \Gamma$						
σ (barn)	223.2	1300	3100	264	103	1200
σ' (b) in Diamond	3.10	3.47	4.75	3.62	3.15	5.63
j_+	2	3	1	1/2	1/2	4
j_-	2	2	0	5/2	5/2	5
$g=(2j_+ +1)/(2j_- +1)$	1	1.4	3	1/3	1/3	9/11

All necessary values are listed below in the specification list.

Specification List. The terms and values adopted for all tentative candidates.

According to above theory, the following terms and values are adopted for all tentative candidates:
branching ratio $w = 1$; times ratio $\tau_1/\tau_2 = 1.1$; initial ELAN's concentration $(n_+/(n_+ + n_-))|_{at\ t=0} \equiv \exp(-x_1) = 0.9$;
a host adopted here is a perfect diamond single crystal of IIa type; hence host atoms' amount density $n' = 1.76\ 10^{23}$ cm^{-3};
adopted optimal relative concentration of working nuclei $n/n' = 0.005$;
adopted optimal working nuclei' amount density $n = (n_+ + n_-) = \text{const} = 0.005\ n' = 8.8\ 10^{20}$ cm^{-3}
$\psi = (n/n')/((n/n')+(\sigma'/\sigma))$ is an interim auxiliary parameter;
$L_0 = (1-\psi)/(n'\sigma')$ is a mean free path of the γ-quantum with account of only the non-resonant loss (photo-effect, Compton-effect, elastic and non-elastic scattering etc.); $L = 2yL_0$ is the length of the Active Medium of DOCLMP-type;
$p = \psi\ p_0\ \tau_2/\tau_1$ is the «reserved amplification» (or alias «reserved yield»);
$p_0 = (\sigma_0/\sigma)$ is the maximal reserved amplification at the most favorable conditions $(\sigma'/\sigma) << 1$, $\tau_2 = \tau_1$;
$a_1 = (m\lambda L)^{1/2} \propto y^{1/2}$ is the cross-size of Active Medium; $V = L^2 m\lambda$ is the volume of Active Medium;
$\Omega = \lambda/L \propto y^{-1}$ is the solid angle of the generation diffraction mode;
$N_0 = 2(m\lambda/n'\sigma'\sigma)\psi\,(1-\psi)y^2 \propto y^2$; m is the amount of diffraction modes in the generated γ-beam;
$m = 1$ is adopted in all present Tables. Also everywhere below for all candidates there are adopted that
$n/n' = 0.005$; $n' = 1.76\ 10^{23}$ cm^{-3}; $\tau_1/\tau_2 = 1.1$, $m = 1$, $n = 8.80\ 10^{20}$ cm^{-3}, $n_+ = 0.9\ n = 7.92\ 10^{20}$ cm^{-3}.

The calculations are much facilitated with use of main interim invariants listed at the table 8 below. These interim values are not depend on the relative length of the dispersed active medium $y = L/2L_0$. The value $n/n' = 0.005$ is optimal. At $n/n' > 0.005$ the clustering increases and leads to a big line broadening. So the main invariants are evaluated at the optimal value $n/n' = 0.005$.

Table 1. The main invariants ψ, p, (N_0/y^2) independent on y evaluated at n/n' = 0.005.
The value $n/n' = 0.005$ is optimal. At $n/n' > 0.005$ the clustering increases and leads to a big line broadening.

Work Isotope	$^{92}Nb_{41}$	$^{122}Sb_{51}$	$^{152}Eu_{63}$	$^{65}Zn_{30}$	$^{69}Ge_{32}$	$^{58}Co_{27}$
ψ at n/n'= 0.005	0.265	0.652	0.765	0.267	0.141	0.515
$p = \psi\ p_0\ \tau_2/\tau_1$	81.9	103	207	85.2	50.4	416
N_0/y^2	4.38(12)	1.15(12)	5.27(11)	5.36(12)	6.19(12)	1.85(12)

Table 2. Parameter y as a function of the total amount N_0 of the work nuclei in the active medium at $n/n' = 0.005$.						
Work Isotope	$^{92}Nb_{41}$	$^{122}Sb_{51}$	$^{152}Eu_{63}$	$^{65}Zn_{30}$	$^{69}Ge_{32}$	$^{58}Co_{27}$
y for $N_0=10^{12}$	0.478	0.933	1.38	0.432	0.402	0.735
y for $N_0=10^{11}$	0.151	0.295	0.436	0.137	0.127	0.232
y for $N_0=10^{10}$	0.0478	0.0933	0.138	0.0432	0.0402	0.0735
y for $N_0=10^{9}$	0.0151	0.0295	0.0436	0.0137	0.0127	0.0232
y for $N_0=10^{8}$	0.00478	0.00933	0.0138	0.00432	0.00402	0.00735

Besides the main invariants of Table 8 there are useful some spatial invariants located in the Table 10 below. In the calculations below according to the Specification List 2 the total amount N_0 of the work nuclei in the active medium at $n/n' = 0.005$ is a given value. Hence the parameter y is a function of the amount N_0. This function $y(N_0)$ is derived from the direct dependence of N_0 from y represented in the Specification List 2 . This function is tabulated in the Table 9.

Table 3. The spatial invariants on y. Spatial invariable coefficients for the calculation of the length L , the transversal size a_1 , the visual volume V, the solid angle for generated radiation W, the number of the working nuclei N_0.						
Invariant	$^{92}Nb_{41}$	$^{122}Sb_{51}$	$^{152}Eu_{63}$	$^{65}Zn_{30}$	$^{69}Ge_{32}$	$^{58}Co_{27}$
L_0 (cm)	1.35	0.570	0.281	1.15	1.55	0.489
$2L_0 = L/y$ (cm)	2.70	1.14	0.562	2.30	3.10	0.979
** Free path L_0 refers to the usual continuous host. So free path in a dispersed half-empty active medium is $2L_0$ and $L/y = 2L_0$						
$a_{10} = a_1 y^{-1/2}$(cm)	6.08(-5)	4.80(-5)	4.62(-5)	7.29(-5)	6.72(-5)	6.57(-5)
$V_0 = V y^{-2}$(cm^3)	9.99(-9)	2.63(-9)	1.20(-9)	1.22(-8)	1.40(-8)	4.22(-9)
$\Omega_0 = \Omega y$(steradian)	5.07(-10)	1.77(-9)	6.77(-9)	9.97(-10)	4.73(-10)	4.50(-9)
$N_{00} = N_0 y^2 = (1/2)nV_0$	4.38(12)	1.15(12)	5.27(11)	5.36(12)	6.19(12)	1.85(12)
The number of work nuclei (on top and lower levels together) in the dispersed active medium is $N_o = y^2 N_{00} = (1/2)\, n\, V_0 y^2$. The optimal $n = 0.005\, n'$. In diamond $n' = 1.76\ 10^{23}$ cm^{-3} and so $n = 8.8\ 10^{20}$ cm^{-3}.						

5. The calculation of the time dependent factor G(t) of the induced gain.

The time dependent factor G(t) of the induced gain function is transferred to the usable form. At the denotations $x = t/\tau_1$; $\mu = \exp(-x)$; $\mu_1 = \exp(-x_1)$; $\zeta = \tau_1/\tau_2$; this gain-factor is transformed to the following form omitted in [35]:

$$G(t) = G(\mu) = (1 - \mu^{\zeta})\,(\mu\,\mu_1 - g) + g\,\mu_1\,(\mu - \mu^{\zeta})/(1 - (1/\zeta)) \tag{28}$$

According to[35] it is necessary to find the numerical approximation

$$G(\mu) \approx G_m - (\mu - \mu_0)^2 K \tag{29}$$

In present work $\mu_1 = 0.9$; $\zeta = 1.1$ and (6.40) has a particular form

$$G(\mu) = (1 - \mu^{1.1})\,(0.9\mu - g) + 9.9g\,(\mu - \mu^{1.1}) \tag{30}$$

A rather good approximation is resulted in a simple procedure: μ_0 coincides with a point of maximum for the right part of (40); and

$$\mathbf{G_m = G(\mu_0)\ ,\ K = G(\mu_0)/(1 - \mu_0)^2} \tag{31}$$

All relations marked by sign # were omitted in Ref.[35] as the trivial ones.

The parameters g, G_m, , μ_0, K of the time dependent gain have much significant role in the calculation of the output generation characteristics. So they are calculated separately for each nucleus candidate and located below in the Table 11.

Table 4. The results of the numerical approximation of the function (42) by the quadratic form (41).						
Work Isotope	$^{92}Nb_{41}$	$^{122}Sb_{51}$	$^{152}Eu_{63}$	$^{65}Zn_{30}$	$^{69}Ge_{32}$	$^{58}Co_{27}$
$g = (2j_+ + 1)/(2j_- + 1)$	1	1.4	3	1/3	1/3	9/11
G_m	0.124	0.0987	0.0425	0.188	0.188	0.138
μ_0	0.723	0.767	0.873	0.608	0.608	0.705
K	1.62	1.82	2.64	1.22	1.22	1.586

6. Calculation of the amount N_{ASE} of photons generated in Amplified Stimulated Emission (ASE) per γ-lasing pulse.

The amount N_{ASE} of the Amplified Stimulated Emission (ASE) [35] is estimated through the above parameters

$$N_{ASE} \approx y^{-1/2}\, N_1 \{[\exp((pG_m - 2)y) - 1]/(pG_m - 2)\}, \tag{32}$$

$$N_1 = (\pi p/K)^{1/2}\,(m/4)\,(\tau_1/\tau_2)\exp(-x_1)\,. \tag{33}$$

this formula is valid at $(pG_m - 2)y \geq 0.5$, i.e., it is more correct than the adequate formulae in the work[18]. Here the formula (33) accounts that the incorrect factor (m/8) in eq. (26) of Ref.[35] needs be changed into the correct factor (m/4). In case $(\tau_1/\tau_2) = 1.1$; $\exp(-x_1) = 0.9$; $m = 1$ the correct working formula is following

$$N_1 = 0.439\,(p/K)^{1/2}\, m\,. \tag{34}$$

Eq.(44) is good valid at a region

$$28 > (pG_m - 2)y > 5 \tag{35}$$

and it gives a new estimate for the ASE threshold condition:

$$p > p_{ind} = 2/G_m\,, \tag{36}$$

which is much more severe than the soft simple balanced Schaulov-Townse condition $p > 1$.

This formula is *good valid* in a region $28 > (pG_m - 2)\,y > 5$ (37)

This formula is *less good* in a region $5 > (pG_m - 2)\,y \geq 0.5$ (38)

but in this last region this formula is more correct than the adequate formulae in the Ref.[18].

In a region $(pG_m - 2)y > 28$ this formula needs be replaced by more correct estimate, see below, formula (39).
In a region $(pG_m - 2)y < 5$ this formula needs be replaced by more correct estimate, see below, formula (6.51).

6.1. The amount N_{ASE} of photons generated in the asymptotic case of $(pG_m - 2)y > 28$.

At $(pG_m - 2)y > 28$ the analytical formula (6.44) gives the non-physical result $N_{ASE} \geq N_0$ and hence needs be replaced by more correct expression. In that case the Zvelto's theory[67] modified in [23,27] could be used. The arbitrary strong non-resonant absorption is accounted in that modified theory of the asymptotic π-pulse[23,27] (see, e.g., formulae (60) - (62) in Ref.[23]). But the original Zvelto's theory[67] is valid only at very feeble non-resonant absorption. Instead of the non-physical result $N_{ASE} \geq N_0$ given by (6.44) ones have according to the theory[23,27] the following strict asymptotic estimation

$$N_{ASE\ asympt} = N_{asympt} = a_1^2\ (p-1)/\sigma_0\ . \tag{39}$$

Such estimates (6.47) in the Tables 17.1 - 17.7 below are marked by the subscription «asympt».

6.2. The induced radiation at a weak and moderate gain $(pG_m - 2)y < 5$.

According to the eq. (6.20) at the approximation

$$G(\mu) \approx (G_m - (\mu - \mu_0)^2 K) \tag{40}$$

and at the account that the γ-lasing can do only in the interval

$$|\mu - \mu_0| \leq \Delta \equiv [(pG_m - 2)/(pK)]^{1/2} \tag{40'}$$

ones get the following formula for the Amplified Spontaneous Emission (ASE)

$$N_{ASE} = 2\ N_s \int_0^{\Delta} d\delta\ (e^{R\,y} - 1)/(Ry); \tag{41}$$

where

$$R = (pG_m - 2 - p\,\delta^2 K)\ ,\ \delta = (\mu - \mu_0). \tag{42}$$

Here $R = 0$ at the point $\delta = \Delta$. But this point is a fictive peculiarity for the integrand which is equal to unity, 1, at this point. Hence at the parameter

$$0 < vy \equiv (pG_m - 2)y < 3 \tag{43}$$

this expression can be estimated as the following cut series

$$N_{ASE} = 2\ N_s\ (v/pK)^{1/2}\ [1 + (5/6)\ (vy) + (19/45)\ (vy)^2 + (87/280)\ (vy)^3] \tag{44}$$

with the relative error less than 20% at $vy<3$. Here the amount of the spontaneous photons in a generating mode is

$$N_S = (1/4)\ y\ p\ m\ (\tau_1/\tau_2)\ \exp(-x_1) \tag{45}$$

and a ratio «signal/noise» = (N_{ASE}/N_s) is proportional to this series (44) too

$$(N_{ASE}/N_s) = 2\ (v/pK)^{1/2}\ [1 + (5/6)\ (vy) + (19/45)\ (vy)^2 + (87/280)\ (vy)^3]\ . \tag{46}$$

Below in the Table 12 *the maximal relative error in results (6.51), (6.53)* is given as a function of $vy \equiv (pG_m - 2)y$.

Table 5. Maximal relative error for the eqs.(51), (53) as a function of the parameter $vy \equiv (pG_m - 2)y$.

vy	0.1	0.5	1.0	2.0	3.0	4	5
Max Relative Error	$6.3\ 10^{-5}$%	0.044%	0.58%	6.1%	19.4%	37.8%	56.3%

Rules: At $vy>5$ the formula (6.44) for N_{ASE} is valid with the accuracy not less than $\pm$ 50%. In case of very big $vy>28$ *when this formula gives a non physical result* $N_{ASE} > N_0$ it needs to use the asymptotic formula (6.48). At small $vy < 5$ the formulae (6.51), (6.53) are valid with enough accuracy pointed in this Table 12.

7. Threshold and initial conditions for the Super-Radiance.

On base of the refs. [34,35] the threshold condition for the Super-Radiance holds the form

$$\mathbf{p > p_{SR}} \tag{47}$$

where

$$\mathbf{p_{SR} = \{F_{TSR}(y)\} \times \{TSRI\}} \tag{48}$$

is the Threshold for the Super-Radiance (TSR) where

$$\mathbf{F_{TSR}(y) = y/[1 - (1 + y)\exp(-y)]} \tag{49}$$

Note that

$$F_{TSR}(y)\,|_{at\ y \to 0} = (2/y)\ \text{Hence}\ \mathbf{p_{SR}} \to \infty\ \text{at}\ y \to 0. \tag{50}$$

i.e., the function $F_{TSR}(y)$-contains the pole in the point $y = 0$.

$$\mathbf{\{TSRI\} = 4\ (\tau_1/\tau_2)\ /\ [(1 + g)\ \exp(-x_1) - g]} \tag{51}$$

the value {TSRI} called as «Threshold Super-Radiance Invariant» is not dependent on the parameter y, see Table 13.
The initial condition for the Super-Radiance which follows from the demand $p_{SR} > 0$ or $\{TSRI\} > 0$ is

$$\mathbf{\exp(-x_1) > g/(1 + g)} \tag{52}$$

The analysis (see [35] sec. 2.2) leads to the next algorithm in order to estimate the amount of γ-quanta in a super-radiant pulse:
I. To evaluate of the parameters p, g , $z=(1+g)\exp(-x_1)$, and to introduce three interim parameters-invariants which are independent on the relative length $y = L/2L_0$ (53)
$\mathbf{A_1 = (p/4)\ z\ ;\ A_2 = (p/4)\ g\ ;\ A_3 = 4\ N_{00}/p}$ where $\mathbf{N_{00} = N_{00}/y^2} = 2(m\lambda/n'\sigma'\sigma)\psi\ (1-\psi)$, see part 1.
II. To estimate the relative length $y = L/2L_0$ and its functions (52)
$(\beta/y) = [1-(1+y)e^{-y}]/y$; $G_1 = (\beta/y)A_1$; $G_2 = (\beta/y)A_2 + (\tau_1/\tau_2)$; $K' \equiv K_{SF} = y\ A_3$. Note that $K' = (4N_0/yp)$ but $N_0 = y^2\ N_{00}$. Note

that K_{SF} for the super-radiance is another value than the parameter K for the induced radiance.

III. To introduce the argument $x = t/\tau_1$ and its functions

$R(x) = K\,[G_1 e^{-x} - G_2]$; $\varphi(x) = G_1\,(1 - e^{-x}) - x\,G_2$; $\xi_1(x) = e^{\varphi(x)}$. (53)

The region of x in which $R(x)>0$ and $\varphi(x)>0$

is determined by the conditions $x< x_c \equiv \ln(G_1/G_2)$ and $(G_1/G_2)(1-e^{-x})> x$

IV. To account the majorant formula

$\varphi'_{maj} = 2\,\ln[(1 + (R/\xi_{in}))/2] - 2[(1 - (\xi_{in}/R))/(1+ (\xi_{in}/R))] > \varphi'$ (54)

which leads to the simple approximate solution (55)

$\xi_2(x_m) < e^{\varphi'(x_m)maj} \cong 23.0$;

$R(x_m)< R(x_m)_{maj} \cong \xi_1(x_m)\,\xi_2(x_m) \cong \xi_1(x_m)\,23.0$;

$\xi_1(x_m) \cong \xi_1(x_c)$;

$x_m = \ln[G_1/(G_2+(R/K_{SF}))]$; (56)

hence $N_{SF}< N_{SF\,maj} \equiv N_{00}\,\xi_1(x_m)\,\xi_2(x_m) \equiv (1 - e^{-y})\,y^{-1}\,(1+g)^{-1}\,\xi_1(x_m)\,\xi_2(x_m)$. (57)

where x_m is a temporal maximum of the SF-pulse, x_c is the point in which $R(x_c) = 0$ and R(x) changes its sign. Here, see above,

$$\xi_2(x_m) < 23.0 \quad (58)$$

and

$$\xi_1(x_m) = (G'/G)^{G'} e^{G-G'}; \quad (59)$$

where $G \equiv G_1$; $G' \equiv G_2$. Hence

$$N_{SF} < (1 - e^{-y})\,y^{-1}\,(1+g)^{-1}\,\xi_1(x_m)\,\xi_2(x_m) < 23.0\,(1 - e^{-y})\,y^{-1}\,(1+g)^{-1}\,(G'/G)^{G'} e^{G-G'} \quad (60)$$

and so

$$\mathbf{N_{SF} < 23.0\,(1 - e^{-y})\,(G'/G)^{G'} e^{G-G'}/(y(1+g))} \quad (61)$$

where $G \equiv G_1$; $G' \equiv G_2$ and hence

$$R(x_m)_{maj} \cong \mathbf{23.0}\,(G/G')^{G'} e^{G-G'} \quad (62)$$

or the compacted final result is so (the number **63** is referred to all complex of results 64 - 72) **(63)**

$\xi_1(x_m) = (G'/G)^{G'} e^{G-G'}$; (64)

$\xi_2(x_m) < 23.0$; (65)

$R(x_m)_{maj}<23.0\,(G/G')^{G'} e^{G-G'}$; $R = 22.97006105\,(G'/G)^{G'}\,e^{G-G'}$ (66)

$N_{SF} < 23.0\,Z_{SF}\,(G/G')^{G'} e^{G-G'}$; (67)

$x_m \cong \ln(G/(G' +(R/K_{SF})) = \ln(G/G') - \ln(1+(R/K_{SF}G')) = x_c - \delta$; (68)

$x_c = \ln(G/G')$; (69)

$\delta = \ln(1+(R/K_{SF}\,G')) = R/(K_{SF}G')$; (70)

because $R/(K_{SF}\,G') << 1$; (71)

where $G \equiv G_1$; $G' \equiv G_2$; $Z_{SF} \equiv (1 - e^{-y})/(y(1+g))$; $K_{SF} = y\,A_3$. (72)

In all calculations the so called invariants are used. Their values are not depend on the regime if a row of parameters are fixed, see the beginning of the Table 6.

Table 6. Parameters-invariants for calculation of the super-fluorescent and induced parts of γ-lasing pulse at common conditions: The time-ratio $\tau_1/\tau_2 = 1.1$, the initial relative inverted population $n_+/(n_+ + n_-) = n_+/n = \exp(-x_1) = 0.9$, the relative concentration of the working nuclei in host $n/n' = 0.005$, the host atoms' amount density in diamond $n' = 1.76\ 10^{23}$ cm^{-3} and so $n = 8.8\ 10^{20}$ cm^{-3}. The initial density of ELAN $n_+ = 0.9\ n = 7.92\ 10^{20}$ cm^{-3} is adopted here for all candidates.

Work Isotope	$^{92}Nb_{41}$	$^{122}Sb_{51}$	$^{152}Eu_{63}$	$^{65}Zn_{30}$	$^{69}Ge_{32}$	$^{58}Co_{27}$
$p = \psi\,p_0\,\tau_2/\tau_1$	81.9	103	207	85.2	50.4	416
$p\,0.99/4 = N_s/y$	20.3	25.5	51.2	21.1	12.5	105
$g = (2j_+ +1)\,/\,(2j_- +1)$	1	1.4	3	1/3	1/3	9/11
Interim invariable parameters for the superfluorescent part in the gamma-lasing pulse, eqs. (47)-(72).						
TSRI	5.50	5.79	7.33	5.08	5.08	5.38
z	1.8	2.16	3.6	1.20	1.20	1.636
g	1	1.4	3	1/3	1/3	9/11
$\mathbf{N_{00}}$	4.38(12)	1.15(12)	5.27(11)	5.36(12)	6.19(12)	1.85(12)
$\mathbf{A_1 = (p/4)\,z}$	36.9	55.6	186	25.6	15.1	170
$\mathbf{A_2 = (p/4)\,g}$	20.5	36.1	155	7.10	4.20	85.1
$\mathbf{A_3 = 4\,N_{00}/p}$	2.14(11)	4.47(10)	1.02(10)	2.52(11)	4.91(11)	1.78(10)
Induced Threshold p_{ind}. Interim invariable parameters for induced part in the gamma-lasing pulse, eqs. (28)-(46).						
$p_{ind} = 2/G_m$	16.1	20.3	47.1	10.6	10.6	14.5
K	1.62	1.82	2.64	1.22	1.22	1.59
N_1	3.12	3.31	3.89	3.67	2.82	7.11

$pG_m - 2$	8.16	8.17	6.80	14.0	7.48	55.4

Tables 7. Gamma-lasing regimes for nuclei-candidates $^{92}Nb_{41}$, $^{122}Sb_{51}$, $^{152}Eu_{63}$, $^{65}Zn_{30}$, $^{69}Ge_{32}$, $^{58}Co_{27}$

Table 7.1. Gamma-lasing regime for $N_0 = 3\ 10^{11}$.

Work Isotope	$^{92}Nb_{41}$	$^{122}Sb_{51}$	$^{152}Eu_{63}$	$^{65}Zn_{30}$	$^{69}Ge_{32}$	$^{58}Co_{27}$
L (cm)	0.71	0.58	0.42	0.55	0.68	0.43
a_1 (cm)	3.1(-5)	3.4(-5)	4.0(-5)	3.5(-5)	3.2(-5)	4.4(-5)
y for $N_0=3\ 10^{11}$	0.262	0.510	0.755	0.237	0.220	0.402
$(pG_m - 2)y$	2.14	4.17	5.13	3.32	1.65	22.3
«Reserved Amplification» **p** . Thresholds $\mathbf{p_{IND}}$ for the Induction and $\mathbf{p_{SR}}$ for the Super-Radiance (Super-Fluorescence)						
$p = \psi\, p_0\, \tau_2/\tau_1$	81.9	103	207	85.2	50.4	416
$p_{IND} = 2/G_m$	32.2	40.6	94.2	21.2	21.2	29.0
$^{**}p_{SR} = F_{TSR}(y) \times TSRI$	50	31.6	31.6	50	**53.2>p**	34.8
** The super-radiance threshold $p_{SR} = F_{TSR}(y) \times TSRI = (y/\beta)\,(\tau_1/\tau_2)\,/((1+g)\exp(-x_1) - g)$, where $\beta = 1 - (1+y)\exp(-y)$.						
$N_{SR} = Z_{SR}\, R_{maj}$	10.8	10.5	6.23	17.4	**NO SR**	296
N_{ASE} at $N_0=3\ 10^{11}$	21	190	110	72	9.4	$9.6\ 10^8$
N_S	5.3	13	39	5.0	2.7	42
N_{ASE}/N_S	3.8 ± 0.3	14 ± 6	2.8	15 ± 4	3.5 ± 0.1	$2.3\ 10^7$
$(N_{SR} + N_{ASE})/N_S$	6.0	15.4	3.0	17.9	3.5	$2.3\ 10^7$
N_{SR}/N_{ASE}	0.51	0.055	0.056	0.24	0	$3.1\ 10^{-7}$
Replications	1	1	1	1	2	1
«Replications» > {6.0/(the least from N_S and $N_{ASE}+ N_{SR}$)} is a minimal number of the γ-lasing pulses in order to have good photons' statistics.						
Temporal induced parameters						
$x_0=\ln[0.9(1+g^{-1})]$	#0.588	#0.434	#0.182	1.281	#1.281	#0.693
x_{+ind}	0.030	0.025	0.016	0.127	0.044	0.005
x_{-ind}	**#0.744**	**#0.583**	**#0.273**	**1.093**	#1.350	**#0.879**
$x_{max\ ind}$	**0.324**	0.265	0.136	**0.498**	0.498	0.350
$\Delta = (x_- - x_+)_{ind}$	0.715	0.558	0.257	0.966	1.305	0.874
THE FINAL PARAMETERS IN THE SUPER-RADIANT (SUPER-FLUORESCENT) ESTIMATIONS FOR $N_0 = 3\ 10^{11}$.						
x_c	**0.191'702'03**	**0.281'167'39**	**0.149'906'03**	**0.352'821'37**	NO SR	**0.616'326'97**
$\mathbf{x_m = x_c - \delta}$	0.191'702'03-d	0.281'167'39-d	0.149'906'03-d	0.352'821'37-d	NO SR	0.616'326'96
$\delta \cong \mathbf{R/(K_{SR}G')}$	1.3(-10)	1.8(-10)	1.2(-10)	2.4(-10)	NO SR	6.4(-9)
ξ_{init}	1.07	1.40	1.55	1.14	NO SR	28.5
$R_{maj} = R_{fin} = \xi_{fin}$	24.6	32.2	35.7	26.1	NO SR	654
$N_{SR} = Z_{SR}\, R_{maj}$	10.8	10.5	6.23	17.4	NO SR	296

Table 7.4. Gamma-lasing regime for $N_0 = 10^{11}$.

Work Isotope	$^{92}Nb_{41}$	$^{122}Sb_{51}$	$^{152}Eu_{63}$	$^{65}Zn_{30}$	$^{69}Ge_{32}$	$^{58}Co_{27}$
Spatial parameters and effective gain $(pG_m - 2)y$ of active medium for $N_0=3\ 10^{11}$.						
L (cm)	0.41	.34	0.25	0.32	0.39	0.23
a_1 (cm)	2.4(-5)	2.6(-5)	3.1(-5)	2.7(-5)	2.4(-5)	3.2(-5)
y for $N_0=10^{11}$	0.151	0.295	0.436	0.137	0.127	0.232
$(pG_m - 2)y$	1.23	2.41	2.96	1.92	0.95	12.9
«Reserved Amplification» **p** and Thresholds $\mathbf{p_{IND}}$ for the Induction and $\mathbf{p_{SR}}$ for the Super-Radiance (Super-Fluorescence)						
$p = \psi\, p_0\, \tau_2/\tau_1$	81.9	103	207	85.2	50.4	416
$p_{IND} = 2/G_m$	32.2	40.6	94.2	21.2	21.2	29.0
$^{**}p_{SR} = F_{TSR}(y) \times TSRI$	80.4	47.6	44.8	81.2	**86.8>p**	54.0
** The super-radiance threshold $p_{SR} = F_{TSR}(y) \times TSRI = (y/\beta)\,(\tau_1/\tau_2)\,/((1+g)\exp(-x_1) - g)$, where $\beta = 1 - (1+y)\exp(-y)$. **86.8>p** in this case the super-radiance is forbidden (NO SR).						
$N_{SR} = Z_{SR}\, R_{maj}$	10.6	9.41	6.14	16.1	**NO SR**	74.4
N_{ASE}	4.9 ± 0.1	31 ± 3	76	13	2.7 ± 0.1	$1\ 10^5$
N_S	3.06	7.5	22	2.9	1.6	24
N_{ASE}/N_S	1.6	4.1	3.5	4.5	1.7	4170
$(N_{SR} + N_{ASE})/N_S$	5.1	5.4	3.7	10.0	1.7	4170
N_{SR}/N_{ASE}	2.2	0.30	0.081	1.2	0	0.00074
Replications	2	1	1	2	4	1

Table 7.3. Gamma-lasing regime for $N_0 = 10^{10}$.

Work Isotope	$^{92}Nb_{41}$	$^{122}Sb_{51}$	$^{152}Eu_{63}$	$^{65}Zn_{30}$	$^{69}Ge_{32}$	$^{58}Co_{27}$
L (cm)	0.13	0.11	0.078	0.99	0.12	0.072

a_1 (cm)	1.3(-5)	1.5(-5)	1.7(-5)	1.5(-5)	1.3(-5)	1.8(-5)
$p = \psi\, p_0\, \tau_2/\tau_1$	**81.9**	**103**	**207**	**85.2**	**50.4**	**416**
$p_{IND} = 2/G_m$	32.2	40.6	94.2	21.2	21.2	29.0
$^{**}p_{SR} = F_{TSR}(y) \times TSRI$	**238>p**	**132>p**	116	**242>p**	**260>p**	154
$N_{SR} = Z_{SR}\, R_{maj}$	**NO SR**	**NO SR**	5.54	**NO SR**	**NO SR**	17.0
N_{ASE}	0.68 ± 0.01	2.00 ± 0.01	3.8 ± 0.1	1.2 ± 0.1	0.45 ± 0.01	140 ± 60
N_S	0.97	2.38	7.1	0.91	0.50	7.6
N_{ASE}/N_S	0.70 ± 0.01	0.84 ± 0.01	0.54 ± 0.01	1.3 ± 0.1	0.90 ± 0.01	19 ± 8
$(N_{SR} + N_{ASE})/N_S$	0.70	0.84	1.3	1.3	0.9	20.7
N_{SR}/N_{ASE}	0	0	1.5	0	0	0.12
Replications	9	3	1	7	14	1

Table 7.4. G amma-lasing regime for $N_0 = 10^9$.

Work Isotope	$^{92}Nb_{41}$	$^{122}Sb_{51}$	$^{152}Eu_{63}$	$^{65}Zn_{30}$	$^{69}Ge_{32}$	$^{58}Co_{27}$
L (cm)	0.041	0.034	0.025	0.032	0.039	0.023
a_1 (cm)	7.5(-6)	8.2(-6)	9.6(-6)	8.5(-6)	7.6(-6)	1.0(-5)
y for $N_0=10^9$	0.0151	0.0295	0.0436	0.0137	0.0127	0.0232
$(pG_m - 2)y$	0.12	0.24	0.30	0.19	0.095	1.29
$p = \psi\, p_0\, \tau_2/\tau_1$	81.9	103	207	85.2	50.4	416
$p_{IND} = 2/G_m$	32.2	40.6	94.2	21.2	21.2	29.0
$^{**}p_{SR} = F_{TSR}(y) \times TSRI$	736>p	400>p	346>p	748>p	808>p	472>p
N_{SR}	**NO SR**	**NO SR**	**NO SR**	**NO SR**	**NO SR**	**NO SR**
N_{ASE} series	0.17 ± 0.01	0.39 ± 0.01	0.64 ± 0.01	0.25 ± 0.01	0.12 ± 0.01	@ 4.7 ± 0.1
N_S	0.31	0.75	2.2	0.29	0.16	@ 2.4
(N_{ASE}/N_S) series	0.55 ± 0.01	0.51 ± 0.01	0.29 ± 0.01	0.86 ± 0.01	0.76 ± 0.01	@ **2.0 ± 0.1**
Replications	35	15	9	24	50	@ **3**

«Replications» > {6.0/(the least from N_S and $N_{ASE} + N_{SR}$)} is a minimal number of the γ-lasing pulses in order to have good photons' statistics. @ This experiment could be referred to the class of the straight experimental demonstration of γ-laser

Table 7.5. Gamma-lasing regime for $N_0 = 10^8$.

Work Isotope	$^{92}Nb_{41}$	$^{122}Sb_{51}$	$^{152}Eu_{63}$	$^{65}Zn_{30}$	$^{69}Ge_{32}$	@ $^{58}Co_{27}$
L (cm)	0.013	0.011	0.0078	0.0099	0.012	@ 0.0072
a_1 (cm)	4.2(-6)	4.6(-6)	5.4(-6)	4.8(-6)	4.3(-6)	@ 5.6(-6)
$p = \psi\, p_0\, \tau_2/\tau_1$	81.9	103	207	85.2	50.4	@ 416
$p_{IND} = 2/G_m$	32.2	40.6	94.2	21.2	21.2	@ 29.0
$^{**}p_{SR} = F_{TSR}(y) \times TSRI$	2300>p	1250>p	1070>p	2360>p	2540>p	1470>p
N_{SR}	**NO SR**	**NO SR**	**NO SR**	**NO SR**	**NO SR**	**NO SR**
N_{ASE} (series)	0.050 ± 0.001	0.11 ± 0.01	0.17 ± 0.01	0.070 ± 0.001	0.036 ± 0.001	@ 0.63 ± 0.01
N_S	0.097	0.24	0.71	0.091	0.05	@ 0.77
(N_{ASE}/N_S) series	0.51 ± 0.01	0.45 ± 0.01	0.24 ± 0.01	0.77 ± 0.01	0.72 ± 0.01	@ 0.83 ± 0.01
Replications	120	55	35	86	167	@@$ 10

@$This experiment could be referred to the class of the straight experimental demonstration of γ-laser.

8. The first stage of choice. The perspectives for the γ-generation theory creation.?

Besides these 6 nuclei the other nuclei (~200) were checked, see the work [E]. The MBE could work on neutron fluxes more effectively than on the gamma-quanta fluxes[1-9,37]. It is apparent that in many cases the value of so called asymptotic pulse (see section before the last table) is rather powerful in order to fuse a more powerful γ-lasers. The generation on the nuclei **«+//1D»**, see work[E] could give a rather intensive, tight, good directed gamma-ray beam. The mean intensities of the asymptotic pulse F_p (W/cm^2) generated on some work-nuclei are given for big N_0 and are varied in the interval 10^9 - 10^{17} W/cm^2. The peak intensities could be more by 1-2 orders than mean ones. In optical diapason the much more big mean intensities are reached. But the frequencies from γ-laser are more by 3-5 orders. On this reason the combination triggering action of γ-beam of the intensity 10^{15} W/cm^2 must be more effective than the combination triggering action of optical beam with 10^{17} - 10^{19} W/cm^2. It leads to the creation of much more powerful **hybridized «residential-nonresidential» many-sectional γ-lasers** «Many-Section» γ-lasers, with other generation theory, see in ref.[A].

PART 2. RADIATION-HEAT THEORY.

A total theory of the radiation-heat regime for the solid active medium of gamma-laser is developed. The phenomena of the microplasma, the collapse of the hyperfine structure (HFS) and the heat blast of the active medium are researched. The question about a compatibility of the different gamma-laser's types with the radiation-heat regimes conditioned by them in the different aggregate states of the active medium is regarded. It is shown that in all cases the heat blast of the active medium is inevitable if the solid phase and the SPTEN-pumping based on the fast separation of the short-lived isomer are not used. The conditions for the generation and cooling are quite different between the «nonresidential» active media and the «residential» ones. Hence they are different also between the first «fuse» γ-lasing section and the subsequent more powerful sections of the compound γ-lasers.

1. Introduction.

The joint theory of the gamma-generation and the radiation heat regime of the active medium (AM) is made on base of a world experience in gamma-laser problem[1-72] analyzing. This analysis is made in a sequence of works [23,27,28-30,32]. The knowledge of that works could to get in right the following «Heat» part of the joint theory.

1.1. High heat release in case of active media based on short-lived isomers. • Naivety of first models for cooling of such short-lived active media. • New type of working body for a feasibility of active medium's cooling in case of its enormous high heat release. • Inapplicability of usual heat conductivity theories. • Simple applicable non-equilibrium model «Free exit of the energy's carriers from the active medium» and its results. The question about a radiation-heat regime of the active medium based on the short-lived isomers has a long history. Very enormous high energy release in active medium was outlined in the first works on the pulse pumping of γ-laser[6,9]. The most part of that energy release in the direct pumpinγ–schemes belongs to the origin fluxes for the pumping (the flows of neutrons, gamma-quanta, electrons, etc.). Later in works [23,27,29] it was outlined that even in the most soft case of the indirect pumping SPTEN the energy release is enormous too ~ 10^{10} - 10^{13} W/cm^3 in case of the work isomer's time-life τ_1~ 10^{-4} - 10^{-6} *s*. In the first works there were made suggestions in order to preserve the active medium from its radiation-heat blast. In accordance with that suggestions the active medium needs to have a needle form and this «needle» needs be dipped in the super-liquid helium-II [1-6,9-12,17]. But indeed such suggestions were reveled as naive after its revision[27,29] because:

• only part of the conversion energy, less than 50%, belongs to the fast origin conversion electrons but another significant part of the conversion energy, about 50%, belongs to the slow Auger and secondary electrons together which stick in any thin needle[27-30].

• the heat transfer from the needle to the liquid helium is impossible if the heat flow exceeds j_{crit} ~ 0.1 W/cm^2 on the outer surface of the needle. E.g., for a commonly accepted[1-17] needle diameter d ~ 10^{-5} - 10^{-4} cm, the heat flow is about qd ~ 10^5 -10^6 W/cm^2 >>>> j_{crit} for the threshold conditions in active medium. For such great heat flow > 0.1 W/cm^2 , the needle is surrounded by a gas bubble and is heated as being a thermally isolated body[27-30]

• it was strictly shown[27] that the electron-conversion energy release stored in the electron subsystem of an initially deep-frozen thermally isolated solid is transferred (with self-acceleration)into the phonon subsystem during a time $t_{transf} << \tau_1$ [27]. This relation is valid at any small time-life of the working isomer, e.g. 10^{-10} -10^{-11}. Because the less is the more is the heat release q and the less is (in accordance with the strict equations[27]). Therefore, for a thermally isolated active medium-system with realistic threshold conditions there is no any hope to obtain the γ-lasing before the heat blasting of the active medium[27].

A feasible mean for the cooling owing to a new type of the work-body was suggested in [27,29]. The main peculiarity of this new work-body's cooling is the embodiment of the active medium and the nearest part of the surrounding cooler into a homogeneous common-master chip. This chip of the dimensions ~ 0.1cm × 0.1 cm × 1cm needs be a high perfect crystal of diamond, or another light perfect crystal which could be constructed from the first light elements from the hydrogen to the carbonic. In turn, this chip needs be carefully mounted in order to provide a good heat contact with a more massive interim solid cooler. It could be, e.g., a big (~ 3 cm × 3 cm × 3 cm) sapphire or a germanium or some else high perfect crystal. In turn, the interim (e.g., sapphire) cooler needs be carefully mounted in order to provide a good heat contact with a big (~ 10 cm × 10 cm × 10 cm) massive outer solid cooler, e.g., a pig from a well refined copper. The last needs be in a good thermal contact with a liquid cooler (or with its vapor). Such work-body construction also needs be moderately pre-stretched or pre-pressed in the care thermostated fixtures in order to avoid the inhomogeneous Doppler shift arising from the temperature expansion of the active medium[27]. An effectiveness of method [27] against a danger of such Doppler shift for a γ-lasing was outlined In Ref.[17].

The detailed properties of the suggested cooling method are available from the Refs.[27-30,32,34,35]. In that series of works some origin theoretical foundations of cooling were developed. The enormous heat release q ~ 10^{11} - 10^{13} W/cm^3 makes the ordinary thermodynamics unusable. Moreover, in this case the weakly non-equilibrium thermodynamics is unusable too. Hence it needs to do new non-equilibrium kinetic theory for the cooling of active medium with the enormous big heat release. The first advanced results in that non-equilibrium theory were reached in works [32,34,35]. But these origin results needs be corrected. Because in that first model the removal of the heat carriers is considered as free. But it is valid only if the free paths of heat carriers (electrons, holes , phonons - all are strong non-equilibrium so-called «injected» quasi-particles) are much more than the transversal size of the active medium.

The concepts of that origin «free removal» theory are contained in Refs.[32,34,35] and are compressed at the Specification List 3 below. The main conclusions of that origin theory are the following:

• • in spite of the enormous heat release q ~ 10^{11} - 10^{13} W/cm^3 the active medium could be kept at low temperature ~ 50 K

during the gamma-lasing process;

• • however a hot (above 30000 K) non-equilibrium microplasma arises in that cold (~50K) solid active medium; the density of that microplasma is about ~ 10^{16} - 10^{18} charged carriers per cm^3;

• • this microplasma breaks the stability of the hyperfine structure (HFS) in the active medium if the last is created from the short-lived ELAN; this circumstance makes useless any attempt to use a hyperfine structure in solid active medium in case of the short-lived ELAN. Hence

• - any attempt to create the inverted nuclear population from the inverse-less nuclear mixture located in the active medium of the short-lived ELAN and de-excited nuclei (see [23,27,28,68]) is useless;

• - the creation of the amplification in the inverse-less mixture of short-lived ELAN and de-excited nuclei (see[23-28] is useless too;

• the optical hyperfine structure cannot be used for the creation of the amplification in the inverse-less mixture because besides the above «microplasma's» hindrances there are the following difficulties

- the optical hyperfine structure in solid is rather strongly broaden by the inhomogeneity of the crystalline local fields about ~ 10^9- 10^{10} s^{-1}, such optical crystalline broadening is by 4-6 orders more than the width of the Moessbauer lines for the short lived nuclei-candidates

- the optical lines in solid are else more strongly broaden into the very wide bars ~ 10^{12} - 10^{13} s^{-1} by the interaction of atomic transitions with the phonons' system. These bars could be narrowed to the inhomogeneous limit ~ 10^9- 10^{10} s^{-1} only at very low temperatures of the host-lattice T_{host} ~ 1 K. Such low temperatures in solid AM on the short-lived ELAN is infeasible [32,34,35].

• • this crisis is overcome in the SPTEN - types of γ-laser because

- the SPTEN - types of γ-laser could use the short-lived nuclei candidates with life-time of the upper working level ~ 10^{-4} - 10^{-6} *s*; the high inversion population ~ 0.9 is achieved in a nuclear beam before its soft transplantation in a host[28-36], hence

• • the SPTEN - types of γ -laser can do without any use of HFS inside of the active medium and particularly;

- the SPTEN - types of γ-laser can do without application of any methods for the narrowing of the work transition lines;

- the SPTEN - types of γ-laser can do without application of any methods for the transformation of non-inverted nuclear mixture into the inverted one in the site of the active medium;

- the SPTEN - types of γ-laser can do without application of any methods for the creation of the amplification without inversion in the site of the active medium.

• • • the main condition of a good cooling contains in the relations between the size of the active medium and the lengths of free paths for the energy-carriers (non-equilibrium «injected» electrons, holes and high frequency phonons) in the site of active medium

$$\Lambda_e(T) >> a_1, \quad (1)$$

$$\Lambda_{ph}(T) >> a_1 \quad (2)$$

these relations depends on the quasi-temperature of the host in the active medium.

• • • In works[32,34,35] the following common remarks were noted:

• at the increasing of the parameter $j = qa_1$ the quasi-temperature T of the active medium needs to be increased

• this increasing of quasi-temperature leads to the contraction of the free paths $\Lambda_{ph}(T)$ and $\Lambda_e(T)$ in the site of active medium

• hence at a certain value $j = qa_1$ the relations (1) and (2) must be broken and hence the active medium must be blasted. The models and the appropriate mathematical methods based on that remarks were completed. The methods and results of their application for the tested candidates are given below after the Specification List . The List contains basic concepts of that methods.

Specification List. **Formulae and Heat-Regime Parameters of Free Exit model in case of Diamond Host.**	
Parameters	Determination and appropriate comments
a_1	«Transversal size» of an active medium. In a demonstration one-mode γ-lasing experiment ones have $a_1 \ll L$ where L is the length of active medium. For a simplicity of calculations the active medium is adopted here as a long bar of a square cross-section. One main side of this bar lies at the boundary between the active medium and the vacuum. The area of this main side is $L \times a_1$. The beam of the ELAN is delivered into active medium through the vacuum. Three other main sides of this bar lie at the conditional boundary between the active medium and the solid cooler. The area of this «cooling» boundary is $3 L \times a_1$. This conditional boundary is not a physical one owing to the embodiment of the active medium and the cooler into a homogeneous common-master chip. Hence there are no ever jump in any physical property (acoustical, optical, chemical, isotopic, magnetic, electrical, etc.). Hence there are no reasons for any temperature jump of Newton or Kapitsa type on that boundary. This circumstance is very important for the cooling of active medium. The outer sizes of that chip needs be by some orders more than the appropriate sizes of the active medium: L_{chip} ~ 10 L , $a_{chip} > 10^3 a_1$. Hence such chip needs have approximately the sizes ~ 0.1cm × 0.1cm × 1cm. The host of that chip is supposed to be diamond II-*a* or some other light perfect materials. That chip needs be carefully mounted with a good heat contact into a massive interim solid cooler (e.g., a big very perfect carefully rectified monocrystal of sapphire, or germanium or silicon , etc.)[27-30]. That interim solid cooler needs be carefully mounted with a good heat contact into a massive outer solid cooler (e.g., a big rather perfect and rectified copper pig) keeping at low temperature (about 1-5 K) in liquid helium or in its vapor.
$q = n_+ E_\gamma \alpha/(1+\alpha)\tau_+ =$	«Energy-release density» arising from the internal conversion averaged over the teeth volume
$j_{AM} = qa_1$	The approximate value of the flux energy density from the active medium AM. At the propagation of the energy flux at the distance $\rho < L$ its value decreases as $j(\rho) \sim j_{AM} a_1/\rho$. But at the distance $\rho > L$ ones have another dependence $j(\rho) \sim j_{AM} (a_1/\rho)^2$. For typical case $a_1 = 10^{-4}$cm, L = 0.5 cm q= 10^{11} W/cm^3 ones have $j_{AM} \sim 10^7$ W/cm^2 .Note, see sec.1, that the gaseous bubble could not to arise only if $j(\rho) \sim j_{AM} (a_1/\rho)^2 < 0.1$W/$cm^2$. Hence it needs be at the outer radius of the working body $\rho_{out} > 10^4 a_1$ = 1cm.
ε_0 = 5.5 eV =	«Minimal energy slit» between the valence zone and conductivity one in diamond [61]

$= 8.81\ 10^{-19}$ J	
ε_p = 13.3 eV/pair = $= 2.1\ 10^{-18}$ J/pair	«Mean energy for the creation of one pair of light charged carriers (electron and hole) in diamond[61]
$\tau_e = 1.48\ a_1/v_e$	«Averaged exit time» for the removing of the non-equilibrium charged carriers from the active medium. The factor 1.48 accounts the averaging of the reciprocal value τ_e^{-1} (the speed of removal) over all possible trajectories of carrier with account of its origin direction of moving. It is accounted that the boundary «active medium/vacuum» reflects the light carrier back in a chance direction.
$v_e \sim 10^8$ *cm/s*	Mean velocity of the «injected» light charged carriers
$\tau_{ph} = 1.48\ a_1/v_{ph}$	«Averaged exit time» non-equilibrium for the removing from the active medium of the non-equilibrium «injected» high frequency phonons. Factor 1.48 accounts the averaging of the reciprocal value τ_{ph}^{-1} (speed of removal) over all possible trajectories of phonon with account of its origin pulse direction. It is accounted that the boundary «active medium/vacuum» reflects the phonons in a chance direction.
$v_{ph} \sim 1.6\ 10^6$ *cm/s*	«Mean velocity» of the non-equilibrium high frequency phonons in case of a diamond host
τ_{ep}	«Time for the transferring» of the non-equilibrium injected «electron-hole system» energy into the «phonons system» energy According to results[35] based on the extrapolating of the experimental data [61] the following temperature dependence is valid $\tau_{ep} \approx \tau_{ep(50K)}\ (50K/T)^{1.5} \approx 3.4\ 10^{-11} (50\ K/T)^{1.5}$ s
Q_e	«Energy-density» of the non-equilibrium charged carriers-system (measured in J/cm^3). In simple quasiballistic approach[32,35] the quasi-stationary energy-density of charged carriers is $\mathbf{Q_e = q\tau_e}$. The other approaches used here are given in the below sections.
$\mathbf{n_e = 2Q_e/\varepsilon_p}$	«Density» (in cm^{-3}) for the amount of non-equilibrium «injected »charged carriers
Q_{ph}	«Energy-density» (measured in J/cm^3) of the non-equilibrium «injected» phonons. In simple quasiballistic approach[32,35] the quasi-stationary energy-density of charged carriers is $\mathbf{Q_{ph} = q\tau_{ph}/(1+\tau_{ep}/\tau_e)}$. The other approaches used here are given in the below sections.
T	«Quasi-temperature» of host which at low temperatures $T<T_D/6$ is linked with the phonons energy-density Q_{ph} owing to the well known *empirical temperature dependence for the heat capacity* $C(T) = C_0\ (T/T_D)^3$. Here in case of diamond single crystal $T_D \approx 1860$ K (Debye temperature) and $C_0 \approx 567.8\ J/cm^3K$. It gives the following dependence $\mathbf{T = (4Q_{ph}T_D^3/C_0)^{1/4}}$ or for a diamond $\mathbf{T = 82.054\ Q_{ph}^{1/4}}$ *K (J/cm3)*$^{-1/4}$ at T<314 *K*.. And vice versa, $\mathbf{Q_{ph} = 2.206\ 10^{-8}\ T^4}$ *J/cm^{3}K^4*
Λ_e	«Free path» for the «hot» (above 30000 *K*) non-equilibrium light charged carriers in a «cold» (below 300 *K*) host. The empirical dependence of free path $\Lambda_e(T)$ for a diamond host is [32,35] $\mathbf{\Lambda_e(T) \approx \Lambda_e(27.3\ K)\ \tau_{ep}(T)/\tau_{ep}(27.3\ K) \approx 0.121\ T^{-1.5}}$ *cm K$^{-1.5}$*
Λ_{ph}	«Free path» for the non-equilibrium injected high frequency phonons in host. This phonons' free path depends on the quasitemperature T of a diamond host according to the semi-empirical data's Table 1 (from Ref.[32]). The approximation $\mathbf{(1/\Lambda_{ph})_{appr} \approx 6.8\ cm^{-1} + 205.0\ Q_{ph}}$ cm^2/J for the reciprocal phonon's free path is represented at the Table 1.
$\Lambda_e(T) >> a_1$, $\Lambda_{ph}(T) >> a_1$	This is the main condition for the success in cooling of the Active Medium (AM). The force of this rule is proved by the satisfactory results in the Table 2. These results are achieved by the methods developed on the base of the origin concepts of works [32,35].

Table 1. Dependence $\Lambda_{ph}(T)$ and $1/\Lambda_{ph}(Q_{ph})$ for diamond II-α derived in work[32] from trial data.

T (*K*)	5	10	20	50	70	110	140	180	250
Q_{ph}(J/cm^3)	1.38(-5)	2.21(-4)	3.53(-3)	0.138	0.530	3.23	8.47	23.2	86.2
Λ_{ph} (cm)	1.5(-1)	1.1(-1)	9.0(-2)	3.0(-2)	1.0(-2)	2.0(-3)	1.0(-3)	3.0(-4)	5.0(-5)
$1/\Lambda_{ph}$	6.8	9.1	11.0	33.0	1.0(2)	5.0(2)	1.0(3)	3.3(3)	2.0(4)
$(1/\Lambda_{ph})_{appr}$	6.8	6.8	7.4	35.0	1.2(2)	6.7(2)	1.7(3)	4.7(3)	1.8(4)

2. Two advanced models for radiation-heat regimes in active medium.

2.1. Non-equilibrium model «Ballistic exit of carriers and their partial returning in active medium». The carrier (electron, hole, high-frequency phonon) emitted in a certain point of the site of the active medium (AM) is moving along a right-line without its scattering unless it removes a site of AM or unless it reaches the boundary between the AM and the vacuum. The carrier could be scattered only on this boundary. The total probability of scattering is unity for each carrier incident on this boundary. Then the scattered carrier moves along a right-line and remove off the AM-site. Inside the AM the energy of electrons and holes is continuously transforming with a rate $1/\tau_{1ep}$ into the phonons' energy. The time τ_{1ep} is a function of the quasitemperature T_1 of a host in the site of AM. But T_1 is, in turn, a function of the phonons' energy density $Q_{1\ tot\ ph}$ in the site of AM. Hence

$$\tau_{1ep} = \tau_{1ep}(Q_{1\ tot\ ph}). \qquad (3)$$

The chip volume outside of the AM is divided into the nearest zone Z_2 and the further cooling zone Z_∞. The radial region of the zone Z_2 is $\Lambda_{2e} > \rho > a_1$. The radial region of the zone Z_∞ is $\Lambda_{2e} < \rho < \infty$. Here the free path Λ_{2e} of the electron (hole) is adopted as a function $\Lambda_{2e}(Q_{2\ tot\ ph})$ of the stationary mean total phonons' energy density $Q_{2\ tot\ ph}$. The latter is a sum of the following parts:

- $Q_{2\ ball\ ph}$ which is a density in the ballistic phonons' flow from the active medium;
- $Q_{2\ diff\ ph}$ which is an averaged energy density of the phonons arisen at the microplasmas' energy dissipation with a rate $Q_{2e}/(\tau_{2ep}(Q_{2\ tot\ ph}))$;
- $Q_{\infty 2\ back\ ph}$ which is an averaged energy density of the phonons which were arisen in the zone Z_∞ and then penetrated into a zone Z_2. Then this density is diffusely reflected by the boundary with vacuum. In a result ones have the following equation

$$Q_{2\ tot\ ph} = Q_{2\ ball\ ph} + Q_{2\ diff\ ph} + 2\ Q_{\infty\ 2\ back\ ph}\ . \qquad (4)$$

The value $Q_{2\ D\ ph\ O^*} = Q_{\infty\ 2\ back\ ph\ O^*} + Q_{2\ diff\ ph\ O^*}$ is the contribution of diffused phonons from the zones Z_∞ and Z_2 in the active medium denoted here as a point O*. This contribution is reflected on the boundary with vacuum. Hence the total phonons' energy density in the active medium is the following sum

$$Q_{1\ tot\ ph} = Q_{1self\ ph} + 2\ Q_{2\ D\ ph\ O^*} \qquad (5)$$

where $Q_{1self\ ph}$ is the «self» part of the phonons energy density which is arising directly in the active medium and $2\ Q_{2\ D\ ph\ O^*}$ is the «returned» part. So there is a pictorial part of the model «Ballistic exit of carriers and their partial returning in active medium».The resultant mathematical development of that model-ideology is given below after the Tables 4 and 4a in which the regimes are evaluated on base of this and further (see sec.2.2) modeling approaches.

2.2. Non-equilibrium model «Exit of carriers with their scattering in active medium». In above model the carriers' scattering inside of the active medium had been neglected. But this scattering leads to the additional accumulation of the energy and plasma in the site of the active medium. Hence it needs to be accounted. Such approach «Exit of carriers with their scattering in active medium» uses the values determined above in 2.1. Some necessary comments are given below in sec.3.

2.3. The tables of radiation-heat regimes. The basic nuclear data are given in the works [C,E,F] reported at the "LO'2000".

Tables 2.1 - 2.5. Radiation-Heat Regimes of the Active Medium at $N_0 = 3\ 10^{11}, 10^{11}, 10^{10}, 10^9, 10^8$

The adopted optimal initial density for all ELAN is $n_+ = 0.9\ n' \ 0.005 = 7.92\ 10^{20}\ cm^{-3}$ is adopted here for all nuclei-candidates in a diamond host $\tau_{1e} = 1.48\ a_1/v_e$; $\tau_{1ph} = 1.48\ a_1/v_{ph}$; $v_e = 10^8\ cm/s$; $v_{ph} = 1.6\ 10^6\ cm/s$; The preblasting heat data (shadowed) are given in the Table 2a.

Work Isotope	$^{92}Nb_{41}$	$^{122}Sb_{51}$	$^{152}Eu_{63}$	$^{65}Zn_{30}$	$^{69}Ge_{32}$	$^{58}Co_{27}$
E_g (*KeV*)	90.2	61.45	32.6	53.96	85.0	28.1
τ_+ (sec)	6.20(-6)	2.74(-6)	2.38(-7)	2.31(-6)	7.36(-6)	1.51(-5)
a	0.17	0.75	1.2	4.4	1.4	1.5
q (W/cm^3)	**$2.68\ 10^{11}$**	**$1.22\ 10^{12}$**	**$9.48\ 10^{12}$**	**$2.42\ 10^{12}$**	**$8.55\ 10^{11}$**	**$1.41\ 10^{11}$**
Table 2.1. $N_0 = 3\ 10^{11}$						
a_1 (cm) at N_0 $3\ 10^{11}$	3.1(-5)	3.4(-5)	4.0(-5)	3.5(-5)	3.2(-5)	4.4(-5)
τ_{1e} (sec)	4.59(-13)	5.03(-13)	5.92(-13)	5.18(-13)	4.74(-13)	6.51(-13)
τ_{1ph} (sec)	2.87(-11)	3.15(-11)	3.70(-11)	3/23(-11)	2.96(-11)	4.07(-11)
Model «Ballistic exit of carriers and their partial returning into active medium».						
τ_{1ep} (sec)	2.52(-11)	1.02(-11)	2.91(-12)	6.94(-12)	1.30(-11)	2.52(-11)
a_1/Λ_{2e}	0.0513	0.166	1.03	0.279	0.114	0.0763
a_1/Λ_{1e}	0.1210	0.325	1.27	0.487	0.240	0.1710
Q_{1e}	0.121	0.585	4.66	1.17	0.391	0.895
$n_{1e\ av}$	2.51(17)	1.21(18)	9.69(18)	2.42(18)	8.12(17)	1.86(17)
$Q_{1self\ ph}$ (J/cm^3)	0.137	1.78	56.1	5.31	0.876	0.143
$Q_{2D ph O^*}$ (J/cm^3)	0.082	0.748	12.5	1.80	0.420	0.0775
$Q_{1tot\ ph}$ (J/cm^3)	0.301	3.28	81.1	8.91	1.72	.298
T_1 (K)	60.8	110.0	246.0	142.0	93.9	60.6
$Q_{2tot\ ph}$ (J/cm^3)	0.0302	0.544	46.3	2.02	0.237	0.0347
T_2 (K)	34.2	70.5	214.0	97.8	57.3	35.4
Model «Exit of carriers with their scattering in active medium».						
$j_{AM} = qa_1$ (W/cm^2)	*8.31(6)*	*4.14(7)*	*3.79(8)*	*8.47(7)*	*2.74(7)*	*5.02(6)*
τ_{1e}	4.59(-13)	5.03(-13)	5.92(-13)	5.18(-13)	4.74(-13)	6.51(-13)
$\tau_{1e}/\tau_{1ep}{}^*$	0.0583	*Blast*	*Blast*	*Blast*	*Blast*	0.0935
$a_1/\Lambda_{1e}{}^*$	0.390	*Blast*	*Blast*	*Blast*	*Blast*	0.626
Q^*_{1e}	0.198	*Blast*	*Blast*	*Blast*	*Blast*	0.188
$n^*_{1e\ av}$	**4.11(17)**	*Blast*	*Blast*	*Blast*	*Blast*	**3.90(17)**
$a_1/\Lambda_{1ph}{}^*$	0.0435	*Blast*	*Blast*	*Blast*	*Blast*	0.0854
T^*_1 (K)	**132.5**	*Blast*	*Blast*	*Blast*	*Blast*	**143.8**
$Q^*_{1tot\ ph}$ (J/cm^3)	6.81	*Blast*	*Blast*	*Blast*	*Blast*	9.44
$Q^*_{1self\ ph}$ (J/cm^3)	6.65	*Blast.*	*Blast.*	*Blast.*	*Blast.*	9.28
Table 2.2. $N_0 = 10^{11}$						
a_1 (cm) at $N_0 = 10^{11}$	2.4(-5)	2.6(-5)	3.1(-5)	2.7(-5)	2.4(-5)	3.2(-5)
τ_{1e} (sec)	3.55(-13)	3.85(-13)	4.59(-13)	4.00(-13)	3.55(-13)	4.74(-13)
τ_{1ph} (sec)	2.22(-11)	2.41(-11)	2.87(-11)	2.50(-11)	2.22(-11)	2.96(-11)
Model «Ballistic exit of carriers and their partial returning into active medium».						
τ_{1ep} (sec)	3.26(-11)	1.32(-11)	3.81(-12)	8.82(-12)	1.73(-11)	3.47(-11)
a_1/Λ_{2e}	0.0287	0.0885	0.524	0.149	0.0588	0.0370
a_1/Λ_{1e}	0.0726	0.1940	0.773	0.299	0.1370	0.0908
Q_{1e}	0.0941	0.456	3.96	0.926	0.297	0.0659
$n_{1e\ av}$	1.95(17)	9.48(17)	8.22(18)	1.92(18)	6.18(17)	1.37(17)
$Q_{1self\ ph}$ (J/cm^3)	0.0637	0.824	28.1	2.58	0.380	0.0558
$Q_{2D ph O^*}$ (J/cm^3)	0.0439	0.428	7.01	1.13	0.221	0.0364
$Q_{1tot\ ph}$ (J/cm^3)	0.152	1.68	42.1	4.84	0.822	0.128
T_1 (K)	51.2	93.4	209.0	122.0	78.1	49.1

$Q_{2tot\,ph}$ (J/cm^3)	0.0128	0.207	14.9	0.762	0.0865	0.0117
T_2 (K)	27.6	55.3	161.0	76.7	44.5	27.0
Model «Exit of carriers with their scattering in active medium».						
$j_{AM} = qa_1$(W/cm^2)	6.43(6)	3.17(7)	2.94(8)	6.53(7)	2.05(7)	3.65(6)
τ_{1e}	3.55(-13)	3.85(-13)	4.59(-13)	4.00(-13)	3.55(-13)	4.74(-13)
τ_{1e}/τ_{1ep}*	0.0304	*Blast*	*Blast*	*Blast*	0.0723	0.0397
a_1/Λ_{1e}*	0.203	*Blast*	*Blast*	*Blast*	0.485	0.266
Q^*_{1e}	0.123	*Blast*	*Blast*	*Blast*	0.542	0.0936
$n^*_{1e\,av}$	2.55(17)	*Blast*	*Blast*	*Blast*	1.13(18)	1.94(17)
a_1/Λ_{1ph}*	0.0118	*Blast*	*Blast*	*Blast*	0.118	0.0150
T^*_1 (K)	**101.8**	*Blast*	*Blast*	*Blast*	**181.6**	**100.5**
$Q^*_{1tot\,ph}$ (J/cm^3)	2.37	*Blast*	*Blast*	*Blast*	24.0	2.25
$Q^*_{1self\,ph}$ (J/cm^3)	2.28	*Blast.*	*Blast.*	*Blast.*	23.6	2.18
Table 2.3. $N_0 = 10^{10}$						
a_1 (cm) at N_0 10^{10}	1.3(-5)	1.5(-5)	1.7(-5)	1.5(-5)	1.3(-5)	1.8(-5)
τ_{1e} (sec)	1.92(-13)	2.22(-13)	2.52(-13)	2.22(-13)	1.92(-13)	2.66(-13)
τ_{1ph} (sec)	1.20(-11)	1.39(-11)	1.57(-11)	1.39(-11)	1.20(-11)	1.67(-11)
Model «Ballistic exit of carriers and their partial returning into active medium».						
τ_{1ep} (sec)	6.19(-11)	2.29(-11)	6.62(-12)	1.57(-11)	3.23(-11)	6.29(-11)
a_1/Λ_{2e}	0.00732	0.0253	0.121	0.0385	0.0148	0.0102
a_1/Λ_{1e}	0.02070	0.0647	0.251	0.0943	0.0397	0.0282
Q_{1e}	0.0513	0.268	2.30	0.530	0.163	0.0373
$n_{1e\,av}$	1.07(17)	5.57(17)	4.78(18)	1.10(18)	3.39(17)	7.76(16)
$Q_{1self\,ph}$ (J/cm^3)	0.00994	0.162	5.39	0.466	0.0605	0.00985
Q_{2PphO}*(J/cm^3)	8.80(-3)	0.115	2.54	0.301	0.0476	8.26(-3)
$Q_{1tot\,ph}$ (J/cm^3)	0.0275	0.392	10.5	1.07	0.156	0.0264
T_1 (K)	33.4	64.9	148.0	83.4	51.5	33.1
$Q_{2tot\,ph}$ (J/cm^3)	1.72(-3)	0.0319	1.48	0.0979	0.0112	1.75(-3)
T_2 (K)	16.7	34.7	90.5	45.9	26.7	16.8
Model «Exit of carriers with their scattering in active medium».						
$j_{AM} = qa_1$(W/cm^2)	3.48(6)	1.83(7)	1.61(8)	3.63(7)	1.11(7)	2.05(6)
τ_{1e}	1.92(-13)	2.22(-13)	2.52(-13)	2.22(-13)	1.92(-13)	2.66(-13)
τ_{1e}/τ_{1ep}*	7.47(-3)	0.0268	*Blast*	0.0435	0.0153	0.0105
a_1/Λ_{1e}*	0.0500	0.179	*Blast*	0.292	0.102	0.0702
Q^*_{1e}	0.0550	0.341	*Blast*	0.776	0.188	0.0411
$n^*_{1e\,av}$	1.14(17)	7.08(17)	*Blast*	1.61(18)	3.90(17)	8.54(16)
a_1/Λ_{1ph}*	8.57(-4)	0.0184	*Blast*	0.0668	5.26(-3)	1.22(-3)
T^*_1 (K)	**60.1**	**128.1**	*Blast*	**177.1**	**96.8**	**60.7**
$Q^*_{1tot\,ph}$ (J/cm^3)	0.289	5.94	*Blast*	21.7	1.94	0.299
$Q^*_{1self\,ph}$ (J/cm^3)	0.271	5.71	*Blast.*	21.1	1.84	0.282
Table 2.4. $N_0 = 10^9$						
a_1 (cm) at N_0 10^9	7.5(-6)	8.2(-6)	9.6(-6)	8.5(-6)	7.6(-6)	1.0(-5)
τ_{1e} (sec)	1.11(-13)	1.21(-13)	1.42(-13)	1.26(-13)	1.12(-13)	1.48(-13)
τ_{1ph} (sec)	6.94(-12)	7.59(-13)	8.88(-12)	7.86(-12)	7.03(-12)	9.25(-12)
Model «Ballistic exit of carriers and their partial returning into active medium».						
τ_{1ep} (sec)	1.12(-10)	4.31(-11)	1.17(-11)	2.82(-11)	5.71(-11)	1.18(-10)
a_1/Λ_{2e}	2.17(-3)	0.00658	0.0326	0.0108	0.0045	2.79(-3)
a_1/Λ_{1e}	6.62(-3)	0.01880	0.0812	0.0297	0.0131	8.38(-3)
Q_{1e}	0.0297	0.147	1.33	0.304	0.0956	0.0208
$n_{1e\,av}$	6.17(16)	3.06(17)	2.76(18)	6.31(17)	1.99(17)	4.33(16)
$Q_{1self\,ph}$ (J/cm^3)	1.836(-3)	0.0259	1.01	0.0840	0.0118	1.63(-3)
Q_{2PphO}*(J/cm^3)	1.93(-3)	0.0233	0.676	0.0698	0.0112	1.66(-3)
$Q_{1tot\,ph}$ (J/cm^3)	5.70(-3)	0.0725	2.36	0.224	0.0342	4.95(-3)
T_1 (K)	22.5	42.6	102.0	56.4	35.3	21.8
$Q_{2tot\,ph}$ (J/cm^3)	2.91(-4)	4.43(-3)	0.206	0.0150	1.96(-3)	2.62(-4)
T_2 (K)	10.7	21.2	55.3	28.7	17.3	10.4
Model «Exit of carriers with their scattering in active medium».						
$j_{AM} = qa_1$(W/cm^2)	2.01(6)	1.00(7)	9.1(7)	2.06(7)	6.50(6)	1.14(6)
τ_{1e}/τ_{1ep}*	2.22(-3)	6.73(-3)	0.0375	0.0111	4.58(-3)	2.84(-3)
a_1/Λ_{1e}*	0.0149	0.0451	0.251	0.0743	0.0307	0.0191
Q^*_{1e}	0.0303	0.157	1.85	0.336	0.0997	0.0214
$n^*_{1e\,av}$	6.29(16)	3.26(17)	3.84(18)	6.98(17)	2.07(17)	4.44(16)
a_1/Λ_{1ph}*	1.26(-4)	1.31(-3)	0.0941	4.53(-3)	5.63(-4)	1.58(-4)
T^*_1 (K)	**38.7**	**76.3**	**215.7**	**103.8**	**62.1**	**37.6**

$Q^*_{1tot\,ph}$ (J/cm^3)	0.0495	0.749	47.8	2.57	0.329	0.0443
$Q^*_{1self\,ph}$ (J/cm^3)	0.0456	0.702	46.5	2.43	0.307	0.0410
Table 2.5. N_0 = 10^8						
a_1 (cm) at N_0 10^8	4.2(-6)	4.6(-6)	5.4(-6)	4.8(-6)	4.3(-6)	5.6(-6)
τ_{1e} (sec)	6.22(-14)	6.81(-14)	7.99(-14)	7.10(-14)	6.36(-14)	8.29(-14)
τ_{1ph} (sec)	3.89(-12)	4.26(-12)	5.00(-12)	4.44(-12)	3.98(-12)	5.18(-12)
Model «Ballistic exit of carriers and their partial returning into active medium».						
τ_{1ep} (sec)	2.11(-10)	8.04(-11)	2.12(-11)	5.20(-11)	1.06(-10)	2.22(-10)
a_1/Λ_{2e}	0.606(-3)	1.84(-3)	0.00901	3.05(-3)	1.28(-3)	0.775(-3)
a_1/Λ_{1e}	1.95(-3)	5.66(-3)	0.0252	9.12(-3)	6.60(-3)	2.49(-3)
Q_{1e}	0.0167	0.0830	0.757	0.172	0.0543	0.0117
$n_{1e\,av}$	3.46(16)	1.72(17)	1.57(18)	3.56(17)	1.13(17)	2.43(16)
$Q_{1self\,ph}$ (J/cm^3)	3.05(-4)	4.38(-3)	0.177	0.0146	0.0203	2.71(-4)
Q_{2DphO^*}(J/cm^3)	3.70(-4)	4.69(-3)	0.152	0.0147	2.28(-3)	3.21(-4)
$Q_{1tot\,ph}$ (J/cm^3)	1.04(-3)	0.0138	0.481	0.044	0.0249	9.13(-4)
T_1 (K)	14.8	28.1	68.3	37.6	32.6	14.3
$Q_{2tot\,ph}$ (J/cm^3)	4.54(-5)	6.88(-4)	0.0311	2.37(-3)	3.14(-4)	4.08(-5)
T_2 (K)	6.74	13.3	34.5	18.1	10.9	6.56
Model «Exit of carriers with their scattering in active medium».						
$j_{AM} = qa_1$(W/cm^2)	1.13(6)	5.61(6)	5.12(7)	1.16(7)	3.68(6)	7.90(5)
τ_{1e}/τ_{1ep}*	6.25(-4)	1.88(-3)	9.26(-3)	3.11(-3)	1.31(-3)	7.99(-4)
a_1/Λ_{1e}*	4.19(-3)	0.0126	0.0620	0.0209	8.81(-3)	5.35(-3)
Q^*_{1e}	0.0168	0.084	0.82	0.177	0.055	0.0118
$n^*_{1e\,av}$	3.49(16)	1.74(17)	1.70(18)	3.68(17)	1.14(17)	2.45(16)
a_1/Λ_{1ph}*	3.48(-5)	1.40(-4)	5.94(-3)	4.25(-4)	7.60(-5)	4.54(-5)
T^*_1 (K)	**24.4**	**47.9**	**124.7**	**65.2**	**39.5**	**23.8**
$Q^*_{1tot\,ph}$ (J/cm^3)	7.87(-3)	0.116	5.33	0.399	0.0537	7.03(-3)
$Q^*_{1self\,ph}$ (J/cm^3)	7.13(-3)	0.107	5.03	0.370	.0491	0.00639
q (W/cm^3)	**2.68 10^{11}**	**1.22 10^{12}**	**9.48 10^{12}**	**2.42 10^{12}**	**8.55 10^{11}**	**1.41 10^{11}**

Table 2a. The pre-blasting radiation-heat regimes.

Model «Exit of carriers with their scattering in active medium».

Work Isotope	$^{92}Nb_{41}$	$^{122}Sb_{51}$	$^{152}Eu_{63}$	$^{63}Zn_{30}$	$^{69}Ge_{32}$	$^{58}Co_{27}$
N_0	3 10^{11}	10^{10}	10^9	10^{10}	10^{11}	3 10^{11}
q (W/cm^3)	2.68 10^{11}	1.22 10^{12}	9.48 10^{12}	2.42 10^{12}	8.55 10^{11}	1.41 10^{11}
a_1 (cm) blast 3.29	4.2(-5)	2.6(-5)	1.7(-5)	2.7(-5)	3.2(-5)	5.6(-5)
a_1 (cm) preblast 4.58	3.1(-5)	1.5(-5)	9.6(-6)	1.5(-5)	2.4(-5)	4.4(-5)
@ $j_{AM\,blast}$ 25.2 #	1.13(7)	3.17(7)	1.61(8)	6.53(7)	2.74(7)	6.38(6)
$j_{AM\,prebl}$ 18.1	8.31(6)	1.83(7)	9.1(7)	3.63(7)	2.05(7)	5.02(6)
$\Theta_{16/11\,blast}$ 4.46	4.84	6.76	18.5	14.7	7.90	4.15
$\Theta_{16/11\,prebl}$ 2.60	2.29	1.75	4.55	3.48	3.89	2.30
*) $(blast/prebl)_{16/11}$ 2.34	2.11	3.86	4.07	4.22	2.03	1.80
τ_{1ph} (sec)	2.9(-11)	1.39(-11)	8.88(-12)	1.39(-11)	2.22(-11)	4.07(-11)
τ_{1e}	4.59(-13)	2.22(-13)	1.42(-13)	2.22(-13)	3.55(-13)	6.51(-13)
τ_{1e}/τ_{1ep}*	0.0583	0.0268	0.0375	0.0435	0.0723	0.0935
a_1/Λ_{1e}*	0.390	0.179	0.251	0.292	0.485	0.626
Q^*_{1e}	0.198	0.341	1.85	0.776	0.542	0.188
$n^*_{1e\,av}$	**2.06(17)**	**3.54(17)**	**1.92(18)**	**8.06(17)**	**5.63(17)**	**1.95(17)**
a_1/Λ_{1ph}*	0.0435	0.0184	0.0941	0.0668	0.118	0.0854
T^*_1 (K)	**132.5**	**128.1**	**215.7**	**177.1**	**181.6**	**143.8**
$Q^*_{1tot\,ph}$ (J/cm^3)	6.81	5.94	47.8	21.7	24.0	9.44
$Q^*_{1self\,ph}$ (J/cm^3)	6.65	5.71	46.5	21.1	23.6	9.28
Q_{2DphO^*}(J/cm^3)	0.082	0.115	0.676	0.301	0.221	0.0775

3. Crucial regime's parameter.

3.1. Notes@: critical curve line $\mathfrak{L}_{crit}\{q, a_1\}$ between the «stationary region» and «region of blast» , «the main parameter» $\Theta_{16/11}$

The host and the work nuclei concentration in it are fixed at calculations overall the Tables 2 and 2a. So in that tables a pair of mutual independent variables q, a_1 (or an equivalent pair q, N) determines a regime of the active medium. It is obvious that a certain critical curve line $\mathfrak{L}_{crit}\{q, a_1\}$ divides the plain $\mathcal{P}\{q, a_1\}$ into two regions , viz., the «stationary region» $\mathcal{P}_{stationary}$ and the «region of blast» $\mathcal{P}_{blast}$.. Let the equation for such critical curve is $\Theta(q, a_1)$ = const. Hence a certain functional $\Theta(q, a_1)$ of two parameters q and a_1 is the same for the different nuclei-candidates in all points of the critical line $\mathfrak{L}_{crit}\{q, a_1\}$ the crossing of which leads to the transition from a stationary regime to the blast. That combination, «the main parameter», is approximately $\Theta_{16/11} = j_{AM}\, a_1^{16/11}$.

Each subindex number in the left column of Table 2a is the ratio of the maximal value to the minimal one in the appropriate line. This ratio gives a rough characteristic for the relative dispersion. E.g., $(\max j_{AM\,blast}/\min j_{AM\,blast}) = 1.61(8)/6.38(6) = 25.2$

*) ***(blast/prebl)***$_{16/11}$ it is the ratio «*blast/preblast*» = $(a_1^{16/11} j_{AM})_{blast}/(a_1^{16/11} j_{AM})_{preblast}$

The meaning of the parameters of the left column in the Table 2a: $j_{AM} = a_1 q$ is the approximative value of the energy density flux; $\Theta_{16/11} = j_{AM}\, a_1^{16/11} = q\, a_1^{27/11}$ is the combined parameter as an approximation to the main parameter.

3.2. The derivation of the combined parameter Θ. It is natural to suppose that the heat regime could be determined mainly by the value $\Theta' = a_1^2 q\,[(a_1/\Lambda_e)+(a_1/\Lambda_{ph})]$ the nature of which is the intensity of the scattered carriers delayed in the active medium. But, see sec.3, Λ_e^{-1}, $\Lambda_{ph}^{-1} \propto Q^{3/8} \propto (qa_1)^{3/8}$. Here $\propto$ is the sign of a proportionality. Hence $\Theta' \propto a_1^3 q\,(qa_1)^{3/8} = q^{11/8} a_1^{27/8}$. So the following functional transformation of the Θ'-parameter as its power 8/11, viz., $\Theta_{16/11} = (q^{11/8} a_1^{27/8})^{8/11} = q\, a_1^{27/11} = j_{AM}\, a_1^{16/11}$ is the equivalent change for the Θ'. The numerical calculation proves that the derived parameter $\Theta_{16/11}$ is the best main parameter among the plurality of the tentative parameters $\Theta_m \equiv a_1^m j_{AM\ prebl}$ with the arbitrary real constant m. Indeed, this parameter $\Theta_{16/11}$ has a minimal ratio $(\max \Theta'_m/\min \Theta'_m)$. Besides the parameter $\Theta_{16/11}$ has the minimal «dispersion» $[\max (\Theta'_{m\ blast}/\Theta'_{m\ preblast})/\min (\Theta'_{m\ blast}/\Theta'_{m\ preblast})]$ along the critical curve $\mathfrak{L}_{crit}\{q, a_1\}$ for the value $(\Theta'_{m\ blast}/\Theta'_{m\ preblast})$. Ergo, the main approximate characteristic, evaluated only through the origin values q and a_1, exists. It is the combined value $\Theta_{16/11} = q\, a_1^{27/11} \approx q\, a_1^{2.4545\ldots} = j_{AM}\, a_1^{16/11}$. At the continuous variation of the active medium's parameters q, a_1 in a certain critical point $(q, a_1)_{crit}$ of that parameters the radiation-heat regime suddenly changes from the stationary state into the strong non-stationary one, i.e., to the blast. It is proved that the «main parameter» $\Theta'_{16/11}$ is approximately one and the same for the different nuclei on the boundary $\mathfrak{L}_{crit}\{q, a_1\}$ between the stationary regime and the blast. The tables 2, 2a support this rule for the main parameter. The more compact crucial form is given below on the base of the above results:

3.3. The compact form of the cruces regime parameter

$$\Theta_{regime} = (q\, a_1^{27/11})/4.84. \tag{6}$$

The radiation-heat regime is stationary and fit for the γ-lasing if $\Theta_{regime} < 1$.

The active medium (AM) is blasted before the γ-lasing at condition

$$\Theta_{regime} > 1 \tag{7}$$

At length $y_m = 1.79$ the AM is blasted. Everywhere at $y < 1.79$ the threshold p_{SR} increases if the length y decreases.

The joint analysis of γ-generation and radiation heat regimes shows that in the stationary heat-regime (no blast) the induced threshold is always less than the super-radiant one

$$p_{ind} < p_{SR} \tag{8}$$

4. Origine basic formulas of the radiation-heat theory.

Evaluation of Q^*_{1e}, $n_{e\ av}$, τ_e, τ_{ph}, τ_{ep}, $T(Q_{ph})$, $\Lambda_e(T)$. Note also that many coefficients are given below with the surplus exactness in order to avoid the big uncertainty in the high power nonlinear transformations and in the nonlinear iteration processes. The sense of the formulas below could be apparent from the Specification List 1 at the inspection of theory given in the sect.5. The total complex of the work formulas must be cumulated here in order to have the success in the inspection of the mathematical section 5.

$$Q^*_{1e} = q / [\tau_{1ep}^{-1} + \tau_{1e}^{-1} \exp(-1.48\, a_1/\Lambda_{1e})] \tag{9}$$

$n_{e\ min} = 2Q_e/\varepsilon_p$, $n_{e\ max} = Q_e/\varepsilon_0$ are the minimum and the maximum for the quasi-stationary non-equilibrium charged carriers density; $\varepsilon_p = 13.25$ eV/pair $= 2.123\ 10^{-18}$ J/pair is the mean energy for one pair creation, $\varepsilon_0 = 5.5$ eV $= 1.602\ 10^{-19}\ 5.5$ J $= 8.811\ 10^{-19}$ J is the minimal energy slit between the valence zone and the conductivity one. These two estimations are approximately equal to a certain «average» $n_{e\ av} = [(1/\varepsilon_p) + (1/2\varepsilon_0)]\, Q_e$ where $[(1/\varepsilon_p) + (1/2\varepsilon_0)] = 1.039\ 10^{18} J^{-1}$; so

$$n_{e\ av} = 1.039\ 10^{18} J^{-1}\, Q_e\,. \tag{10}$$

$q = n_+ E_\gamma \alpha/(1+\alpha)\tau_1 = 1.269\ 10^5\ E_\gamma \alpha/(1+\alpha)\tau_1$ $(J/KeV\ cm^3)$ is the density of energy-release owing to the internal conversion averaged over the teeth volume at $n_+ = 7.92\ 10^{20}$ cm^{-3}; 1 KeV = $1.602\ 10^{-16}$ J .

$\tau_e = 1.48\, a_1/v_e$ is the averaged time for the removing of the non-equilibrium charged carriers from the active medium; here $v_e \sim 10^8$ cm/s is the mean velocity of the light charged carriers.

$\tau_{ph} = 1.48\, a_1/v_{ph}$ is the averaged time for the removing of the non-equilibrium phonons from the AM;; the phonons speed $v_{ph} = 1.6\ 10^6$ cm/s in a diamond is adopted here[69].

$\tau_{ep} = \tau_{ep}(50K)\,(50K/T)^{1.5} = 3.4\ 10^{-11}(50\ K/T)^{1.5}\ s$ (see [35]) is the time for the transferring of the «electron-hole system energy» into the «phonons system energy»;

$T = (4Q_{ph}T_D^3/C_0)^{1/4} = 82.054\,(Q_{ph})^{1/4}\ K\ (J/cm^3)$ is the stationary non-equilibrium quasi-temperature of host; here $T_D = 1860$ K, $C_0 = 567.8$ J/cm^{3}K are the parameters of the empirical temperature dependence for the heat capacity $C(T) = C_0\,(T/T_D)^3$ valid at $T < 314\ K \approx T_D/6$.

$\Lambda_e(T) = \Lambda_e(27.3\ K)\,\tau_{ep}(T)/\tau_{ep}(27.3\ K) = \Lambda_e(27.3\ K)\,(27.3\ K/T)^{1.5} = 8.5\ 10^{-4}\,(27.3\ K/T)^{1.5}\ cm = 0.121\ T^{-1.5}\ cm\ K^{1.5}$ is a free path for the «hot» non-equilibrium light charged carriers at the lattice quasi temperature T (see [35])

5. Non-linear equations' systems for the evaluation of radiation-heat regimes

Here the following dependencies on the phonons energy density approximated on the experimental data for the diamond host at the quasi-temperature $T < 314\ K$ are adopted:

the free path of the «injected» charged carriers could be expressed through the total phonons energy density

$$\Lambda_e = \Lambda_e(Q_{ph}) = B^*\, Q_{ph}^{-3/8}\,; \tag{14}$$

where $B^* = 1.631\ 10^{-4}$ cm $(J/cm^3)^{3/8}$; (14a)

the time of the charged carriers energy degradation into the non-equilibrium high-frequency phonons

$$\tau_{ep}(Q_{ph}) = A^*\ Q_{ph}^{-3/8} \quad (15)$$

where $A^* = 1.617\ 10^{-11}\ s\ (J/cm^3)^{-3/8}$ (15a)

and the reciprocal phonon's free path

$$(1/\Lambda_{ph}) = 6.67\ cm^{-1} + 205.0\ Q_{ph}\ cm^2/J \quad (16)$$

5.1. Non-linear equations' system in model «Ballistic exit of carriers and their partial returning in active medium». In case of the work-isomers with the times relation $\tau_1 >> \max(\tau_{ph}, \tau_e, \tau_{ep})$ the stationary regime is feasible in active medium (AM). This relation is proved at least in all examples of the Table 16 above. On base of the model «Ballistic exit of carriers and their partial returning in active medium» the following equations are built in that stationary case: The phonons' energy density averaged over the zone Z_2

$$Q_{2ph} \equiv Q_{2\ ph\ full\ av} \equiv Q_{2Ball\ ph\ av} + Q_{Dph\ tot\ a} \quad (17)$$

$$Q_{2ph} = \{[C^*\ (a_1/\tau_{1ep}) + D^*]\ (1-a_1/\Lambda_{2e})\ (q\ a_1^2)\}^{8/5} \quad (17')$$

where $\Lambda_{2e} = \Lambda_e(Q_{2ph}) = B^*\ Q_{2ph}^{-3/8}$ (17'')

and hence the right part of eq. (7') is a certain function of the left one. So the eq. (7') leads to a nonlinear task with a consistence. The constants used in the right part of this equation (7') are the following

$C^* \equiv (0.406/B^*)\ (1.48/\ v_{ph}\ v_e) = 2.303\ 10^{-11}\ s^2 cm^{-3}\ (J/cm^3)^{-3/8}$, (17'a)

$D^* \equiv (0.728/A^*)\ (1.48/\ v_{ph}\ v_e) = 4.089\ 10^{-4}\ s\ cm^{-2}\ (J/cm^3)^{-3/8}$, (17'b)

The energy density contains the «ballistic» part (with factor C^*) from the ballistic «self» phonons directly borne in AM and from the mean «diffused» contribution in Z_2 (with parameter D^*) from all zones. The zone Z_2 is determined in the space. The diffused contribution is born at electron-phonon processes in the microplasma. The reflection (on boundary with vacuum) contribution is accounted also in the parameter D^*. The genealogy of the ballistic term $C^*\ (a_1/\tau_{1ep})$ is so:

$Q_{2Ball\ ph\ av}(at\ a_1 < \rho < \Lambda_{2e}) = 0.274 Q_{1self\ ph}\ (a_1/\Lambda_{2e})(1-a_1/\Lambda_{2e}) = 0.274(Q_{1e}\tau_{1ph}/\tau_{1ep})(a_1/\Lambda_{2e})(1-a_1/\Lambda_{2e}) < C^*\ (a_1/\tau_{1ep})(qa_1^2)\}^{8/5}$

at the account that $(1-a_1/\Lambda_{2e})<1$ and that the microplasmas energy density in the AM (zone Z_1) is

$$Q_{1e} = q/(\tau_{1ep}^{-1} + \tau_e^{-1}) \cong q\tau_{1e} \quad (18)$$

and hence is weak dependent on the quasi-temperature in the zone Z_1. This formula allows to evaluate a number of charged carriers in microplasma (see the notation at the end of the table 16)

$$n_{1e\ av} = 1.039\ 10^{18} \mathcal{J}^{-1}\ Q_{1e} \quad (18')$$

Note also the use of the simple relation of the detailed equilibrium in AM at the stationary regime

$$Q_{1self\ ph}/\tau_{1ph} = Q_{1e}/\tau_{1ep}\ . \quad (19)$$

because $Q_{1\ self\ ph} = q\tau_{ph}/(1+\tau_{ep}/\tau_e)$ (19')

and $Q_{1e} = q\tau_{1ep}/(1+\tau_{ep}/\tau_e)$. (19'')

In equation (7') the value τ_{1ep} is a function of a total phonons energy density $Q_{1\ tot\ ph}$ in the zone Z_1, i.e., in the active medium

$$\tau_{1ep} = \tau_{ep}(Q_{1\ tot\ ph}) = A^*\ (Q_{1\ tot\ ph})^{-3/8}, \quad (10)$$

where

$$Q_{1\ tot\ ph} = Q_{1self\ ph} + 2\ Q_{2\ D\ ph\ O^*} \quad (21)$$

and the variables $Q_{1self\ ph}$, $Q_{2\ D\ ph\ O^*}$ are determined below:

$$Q_{1self\ ph} = (Q_{1e}\tau_{1ph}/\tau_{1ep}) \cong (q\tau_{1e}\ \tau_{1\ ph}/\tau_{1ep}) \quad (22)$$

$$Q_{2DphO^*} \cong E^*\ q\ a_1^2 (Q_{2ph})^{3/8}\ [ln(\Lambda_{2e}/a_1) - 0.577 + (a_1/\Lambda_{2e}) - 0.25\ (a_1/\Lambda_{2e})^2] \quad (23)$$

where

$E^* = 4.920\ 10^{-4} cm^{-2}\ s\ (J/cm^3)^{-3/8}$ (23a)

$(\Lambda_{2e}/a_1) = B^*/(a_1 Q_{2ph}^{3/8})$ and $B^* = 1.631\ 10^{-4}$ cm $(J/cm^3)^{3/8}$. (24)

So a complete *system of 8 equations* for the determination of *8 unknown variables* τ_{1ep}; $Q_{1\ tot\ ph}$; $Q_{1\ self\ ph}$, $Q_{2\ D\ ph\ O^*}$, Q_{2ph}; Q_{1e}; $n_{1e\ av}$; (Λ_{2e}/a_1) is formed. The compact notation of that complete system is following:

$\tau_{1ep} = A^*\ (Q_{1\ tot\ ph})^{-3/8}$; (20)

$Q_{1\ tot\ ph} = Q_{1self\ ph} + 2\ Q_{2\ D\ ph\ O^*}$ (21)

$Q_{1self\ ph} = (Q_{1e}\tau_{1ph}/\tau_{1ep})$ (22)

$Q_{1e} = q/(\tau_{1ep}^{-1} + \tau_e^{-1})$ (see(18))

$n_{1e\ av} = 1.039\ 10^{18} \mathcal{J}^{-1}\ Q_{1e}$ (see the notations at the end of Table 2a)

$Q_{2DphO^*} \cong E^*\ q\ a_1^2 (Q_{2ph})^{3/8}\ [ln(\Lambda_{2e}/a_1) - 0.577 + (a_1/\Lambda_{2e}) - 0.25\ (a_1/\Lambda_{2e})^2]$ (23)

$(\Lambda_{2e}/a_1) = B^*/(a_1 Q_{2ph}^{3/8})$ (24)

$Q_{2ph} \cong \{[C^*\ (a_1/\tau_{1ep}) + D^*]\ (q\ a_1^2)\}^{8/5}$ (17')

where $\tau_{ph} = 1.48\ a_1/v_{ph}$, $\tau_e = 1.48\ a_1/v_e$, (see the Specification List 3), $v_{ph} = 1.6\ 10^6$ cm/s; $v_e = 1.6\ 10^8$ cm/s;

$A^* = 1.617\ 10^{-11}\ s\ (J/cm^3)^{-3/8}$ (25a)

$B^* = 1.631\ 10^{-4}$ cm $(J/cm^3)^{3/8}$; (24a)

$C^* \equiv (0.406/B^*)\ (1.48/\ v_{ph}\ v_e) = 2.303\ 10^{-11}\ s^2 cm^{-3}\ (J/cm^3)^{-3/8}$; (27a)

$D^* \equiv (0.728/A^*)\ (1.48/\ v_{ph}\ v_e) = 4.089\ 10^{-4}\ s\ cm^{-2}\ (J/cm^3)^{-3/8}$; (17b)

$E^* = 4.920\ 10^{-4} cm^{-2}\ s\ (J/cm^3)^{-3/8}$ (23a)

The results of the self-consistent solution for such non-linear equations' system is the estimation of a row radiation - heat parameters τ_{1ep}; a_1/Λ_{2e}; a_1/Λ_{1e}; $Q_{1self\ ph}$; Q_{2DphO^*}; $Q_{1tot\ ph}$; $Q_{2\ tot\ ph}$; and the quasi-temperatures T_1, T_2 in the zones Z_1 and Z_2, correspondingly, are given in the Tables 2, 2a. These results are some more sever that the results in «Free exit»-model.

5.2. Non-linear equations' system in model «Carriers' scattering in active medium». The system with account of the scattering in the site of active medium is the following

$$Q^*_{1self\ ph} = q\tau_{1ph}\{[(\tau_{1e}/\tau_{1ep}) + 1 - \exp(-1.48\ a_1/\Lambda_{1e})]/[(\tau_{1e}/\tau_{1ep}) + \exp(-1.48\ a_1/\Lambda_{1e})]\}\ \exp(1.48\ a_1/\Lambda_{1ph}) \quad (25)$$

where all denotations are almost the same as above. Here the star * marks the belonging to the regarding method 3.2. with the account of the scattering directly in the site of the active medium. The expression (15) is the generalization of the expressions for the $Q_{1self\ ph}$, given in more simple models. It holds an apparent structure lightly understandable from the above more simple models. Its structure is clear also from the common positions expanded in Refs.[32,34,35]. Viz.:

- The value $\tau_{1ph}\exp(1.48\ a_1/\Lambda_{1ph})$

is the time for the phonon's removal from active medium at its scattering account [32,34,35].

- The value $[(\tau_{1e}/\tau_{1ep}) + 1 - \exp(-1.48\ a_1/\Lambda_{1e})]/[(\tau_{1e}/\tau_{1ep}) + \exp(-1.48\ a_1/\Lambda_{1e})]$

is a so called «storing factor» which arose as a result of the charged carriers scattering and the transforming of some part of their energy into the non-equilibrium phonons.

- At limit of big free paths when $a_1/\Lambda_{1e} = a_1/\Lambda_{1ph} = 0$ the right part of eq.(15) transforms into the expression

$$Q^*_{1self\ ph}(at\ a_1/\Lambda_{1e} = a_1/\Lambda_{1ph} = 0) = q\tau_{1ph}/[(\tau_{1ep}/\tau_{1e}) + 1] \quad (25')$$

which is well known in the above sections, see eqs. (19), (19'), (19'') and the SPECIFICATION LIST .

- But at the limit of almost zero free paths, $a_1/L_{1e} >> 1$, $a_1/L_{1ph} >> 1$, the right part of eq.(15) transforms into the expression

$$Q^*_{1self\ ph}(at\ a_1/\Lambda_{1e} >> 1,\ a_1/\Lambda_{1ph} >> 1) = q\tau_{1ph}\ [(\tau_{1ep}/\tau_{1e}) + 1]\ \exp(1.48\ a_1/\Lambda_{1ph}) \quad (25'')$$

which is unknown from the above sections and leads to the blasting regimes. The right part of eq. (15') depends on the value

$$Q^*_{1\ tot\ ph} = Q^*_{1self\ ph} + 2\ Q^*_{2\ D\ ph\ O^*} \quad (26)$$

through the interim fragments τ_{1e}/τ_{1ep}, a_1/Λ_{1e} and a_1/Λ_{1ph}, viz.:

- the fragment $$(\tau_{1e}/\tau_{1ep}) = F^*\ a_1(Q^*_{1\ tot\ ph})^{3/8} \quad (27)$$

where $$F^* = 1.48/v_e A^* = 915.3\ cm^{-1}(J/cm^3)^{-3/8} \quad (27')$$

at the adopted above values $v_e = 10^8$cm/s, $A^* = 1.617\ 10^{-11}\ s\ (J/cm^3)^{3/8}$.

- the fragment $$(a_1/\Lambda_{1e}) = Q^{*3/8}_{1tot\ ph}\ a_1/B^* \quad (28)$$

where (see the sections above) $$B^* = 1.631\ 10^{-4}\ cm\ (J/cm^3)^{3/8} \quad (28')$$

- the fragment $$(a_1/\Lambda_{1ph}) = a_1\ (6.67\ cm^{-1} + 205.0\ Q^*_{1\ tot\ ph}\ cm^2/J) \quad (29)$$

The substantiation of this relation is given at the notes to the Table 1 . In tat table the temperature dependence for the phonon free path diamond matrix at temperature T> 50 K has been changed into the approximative dependence of the reciprocal phonon free path from the phonons energy density

$$(1/\Lambda_{ph})_{approximate} \approx 6.67\ cm^{-1} + 205.0\ Q_{ph}\ cm^2/J \quad (30)$$

The constants for diamond were adopted here after the working of the table data for the $\Lambda_{ph}(T)$, see Table 1. In the right part of the equation (16) the contribution $Q_{2\ D\ ph\ O^*}$ is small

$$(Q_{2\ D\ ph\ O^*}\ with\ account\ of\ scattering\ in\ AM) <<< (Q^*_{1self\ ph}\ with\ account\ of\ scattering\ in\ AM) \quad (31)$$

and could be neglected in the approximative evaluations. It is seen from the data of Table 1 because

$$(Q^*_{2\ D\ ph\ O^*}\ with\ account\ of\ scattering\ in\ AM) < (Q_{2\ D\ ph\ O^*}\ without\ account\ of\ scattering\ in\ AM) << (Q^*_{1\ self\ ph}\ with\ account\ of\ scattering\ in\ AM). \quad (22)$$

Hence the use of the majorant value $Q_{2\ D\ ph\ O^*}$ instead of the exact value $Q^*_{2\ D\ ph\ O^*}$ in the approximative estimates is valid. So the following system of 6 equations with 6 unknown interim variables $Q^*_{1self\ ph}$, τ_{1e}/τ_{1ep}, a_1/Λ_{1e}, a_1/Λ_{1ph}, $Q^*_{1\ tot\ ph}$, $Q^*_{2\ D\ ph\ O^*}$ needs be solved in order to evaluate the radiation-heat regime in active medium according to the regarding here model «Carriers' scattering in active medium» :

$Q^*_{1self\ ph} = q\tau_{1ph}\{[(\tau_{1e}/\tau_{1ep}) + 1 - \exp(-1.48\ a_1/\Lambda_{1e})]/[(\tau_{1e}/\tau_{1ep}) + \exp(-1.48\ a_1/\Lambda_{1e})]\}\ \exp(1.48\ a_1/\Lambda_{1ph})$;

$(\tau_{1e}/\tau_{1ep}) = F^*\ a_1(Q^*_{1\ tot\ ph})^{3/8}$;

$(a_1/\Lambda_{1e}) = Q^{*3/8}_{1tot\ ph}\ a_1/B^*$;

$(a_1/\Lambda_{1ph}) = a_1\ (6.67\ cm^{-1} + 205.0\ Q^*_{1\ tot\ ph}\ cm^2/J)$;

$Q^*_{1\ tot\ ph} = Q^*_{1self\ ph} + 2\ Q^*_{2\ D\ ph\ O^*}$;

$Q^*_{2\ D\ ph\ O^*} \approx Q_{2\ D\ ph\ O^*}$. Substantiation of such approach see above. The value $Q_{2\ D\ ph\ O^*}$ was evaluated in a previous section on the model without account of scattering in AM. Here

$F^* = 915.3\ cm^{-1}(J/cm^3)^{-3/8}$;

$B^* = 1.631\ 10^{-4}\ cm\ (J/cm^3)^{3/8}$.

A host's quasi-temperature and a charged carriers density in a site of the active medium could be evaluated almost as in 3.1.:

$T^*_1 = (4\ Q^*_{1\ tot\ ph}\ T_D^3/C_0)^{1/4} = 82.054\ (Q^*_{1\ tot\ ph})^{1/4}\ K\ (J/cm^3)$

$n^*_{1e\ av} = 1.039\ 10^{18} J^{-1}\ Q^*_{1e}$

where $Q^*_{1e} = q/[\tau_{1ep}^{-1} + \tau_{1e}^{-1}\exp(-1.48\ a_1/\Lambda_{1e})]$

4. The general main results of joint «generation - radiation-heat-regime» theory GG&RH.

4.1. There are no long-lived work isomers candidates for g-laser creation. The analysis of all nuclear data-banks shows that all «minute's» isomers have without Borrman effect only very small working ratio $p/p_{ind} < 1$.

4.2. The multi wave Borrman effect is capable only in high perfect crystals and it is impossible at the surface. Hence it is not suit in the SPTEN methods. Hence it is necessary to insert long-lived isomers before the generation in the solid volume. It is infeasible if that work nuclei are excited on the «minute's» levels.
4.3. Hence there are two ways: a) the «two-step» pumping[11] or b) the «two-stage» pumping[22,23]. Both that types of pump have a «transversal» geometry of any pumping radiation. The joint theory show the unfeasibility of both that ways because the transversal humping radiation create the adiabatic isolation around the active medium and it leads to its blast.
4.4. Another type of «longitudinal» pumping is possible only by a tight, powerful, sharp directed g-beam. In that case the crucial regime parameter is less than the unity.
4.5. There are some theories which predict the amplification of g-wave on its path in medium of the «two-step» type.
4.6. There are some theories which predict the frequency transformation of g-wave on its path in presence of powerful laser wave in combination-resonant media ($\omega_\gamma \pm N\ \omega_{las} = \omega_{med}$).
4.7. Long ago the «superdilution» method [23,27] was suggested on base of unusual application of Borrmann effect, when the Borrman wave acts almost only with the work nuclei and almost not do with the host matrix. The super-dilution could reach value $1/10^7$ and even $1/10^8$ at many wave Borrman effect. Hence the energy of the internal electron conversion ~ 10^5 eV could be distributed among 10^7 or 10^8 light atoms. Hence the temperature around work atom will be increased only by 100 -10 K.
4.8. In that superdilution case the cooling is realized owing to the capacity. In contrary to the conductivity method in SPTEN.
4.9. Suppose that the small γ-beam could be transformed (see 4.5, 4.6) into the beam for the fuse the superdiluted active medium.
4.10. The superdiluted medium could have a not restricted cross-section and hence not restricted power of γ-generation, e.g., ~ 10^8 J/pulse, see [49,50].
4.11. In case of superdilution the Borrman effect could in principle to suppress the absorption on mixture and host atoms both together.
4.12. Hence there is a probability to use the nuclei which are discarded now. And to use many other sorts of nuclei.
4.13. But in order to realize that perspectives it needs to create a certain many sectional γ-laser in order to amplify and transform in its frequency the initial small γ-beam of SPTEN γ-laser into the powerful multibeam (many tight parallel microbeams).
4.14. It needs to revise an carefully to check the existing theories in many relevant topics.
4.15. But the first it needs to begin with the development of the SPTEN method and its basis, the Multi Beam Emitters.
4.16. The joint theory shows that the gaseous, plasma's and beam's active media are not realizable even at use of the modern methods of laser cooling[35]. The main reason is the ionization and heat processes linked with the internal electron conversion.
4.17. The joint theory shows that the solid active medium is not usual crystal because it is a mixture of very hot light microplasma and cold solid (below 100 K). Light microplasma has high density ~ , more than 10^{17}-10^{19} cm^{-3}, and high temperature, more than 30000 K.
4.18. At such conditions the hyperfine structure, HFS, is utterly unstable and the collapse of HFS arise.
4.19. Hence all methods based on the HFS will be destroyed in the active medium of γ–laser:
all methods for the work-line narrowing;
all methods to create the inverted population from the inverseless nuclear mixture;
all methods to create the so called «amplification without inversion»
4.20. Of cause all above methods could be applied in the Moessbauer spectroscopy Particularly in order to diminish the resonant absorption in the powerful Moessbauer sources. Appositely the first suggestion of the «amplification without inversion» on base of laser action on the optical HFS was published in 1980 in JETP[23] long before the its «discoveries» in 1995[24,25].
4.21. The active media are divided into two main groups: the residential and non-residential. In the residential case the work nuclei, as like as the residents, are inserted into the active medium long before the γ-lasing. In the non-residential case the e[cited work nuclei are prepared out of the cite of future generation. The joint theory shows that all residential active medium cold be activated or triggered only be other γ–laser beam. Otherwise ones have the adiabatic isolation of active medium and its heat blast.
4.22. The SPTEN which belongs to the non-residential class could overcome all these hindrances 4.17-4.21.
4.23. Hence the SPTEN is the unique method for the creation of γ–beam in order to fuse all other more powerful gamma-lasers.

ACKNOWLEDGMENTS

The Author express his gratitude to V.I.Gol'danskii, Y.M.Kagan, R.V.Khokhlov, Yu.A.Il'inskii, L.A.Rivlin, G.C.Baldwin, V.S.Letokhov, Yu.B.Khariton, A.A.Rukhadze, J.J.Carroll, C.B.Collins, A.N.Starostin for the discussions in divers times.

REFERENCES

All references cited at present work could be found in the paper labeled here as [A]:

[A]. Karyagin S.V. \\ 2000, "Status of gamma-laser problem on current moment'2000: ranging analysis and screening of gamma-laser schemes on their feasibility". Corresponds to the report TuB1-8 at the X Conference "Laser Optics'2000", St.-Petersburg, June 26-30, 2000, Technical Program, p. 16.

Gamma-ray solid laser: variety of work nuclei and host-matrixes in Mendeleev Table screened with use of system of criteria based on joint GG&RH theory.

S.V.Karyagin

Semenov Institute of Chemical Physics, RAS, Prospect Kosygina 4, 117997 (GSP-1), Moscow, GSP-1, Russia
e-mail: chaika@chph.ras.ru ; fax: (095)-137-8318

ABSTRACT

The hosts and nuclei-candidates (mass ~ 46 – 243, transition energy ~ 1 – 200 keV, decay's time 10^{-7} – 10^{+2} s) for gamma-laser (GL) realisation are represented over Mendeleev Table. The choice of active media (nuclei-candidates, hosts) for GL is based on the joint theory of γ-generation and radiation-heat regime (GG&RH) which accounts a big complex of hindrances against GL and thus discards many tentative candidates. Nuclei-candidates are screened at the analyzing of data banks for nuclear transitions. Chosen candidates (~20) could be used due to author's method SPTEN (Soft Prompt Transplantation of Excited Nuclei). The discarded tentative nuclei (~80) with the life-times 10^{-6} - 10^{+2} s are represented too. All analyzed long-lived (~ 0.5 – 10^{+2} s) isomers are turned to be not fit for GL without use of very strong multi-wave Borrman effect even at the supposition of natural line's width. The application of the revealed candidates in two different γ-laser's categories (residential and non-residential) is discussed.

Keywords: quantum nucleonics, isotopes, isomers, Moessbauer effect, Borrman effect, gamma-laser, long-lived and short-lived isomers, residential and non-residential active media, gamma-generation (induced, super-radiant in plasma, in beam, in solid), amplification without inversion, hot microplasma in cold solid, collapse of HFS in active medium by its microplasma

1. Introduction.

From early works up to nowadays a big world experience in γ-laser (GL) problem is stored [1 - 53]. Crisis in GL-problem was reviled just before 1980 [9-11;23]: no real nuclei-candidates, "heat death" of GL, etc. That crisis is conditioned by deep contradiction between the pump and the lasing[9-12,17,23]. It would be prematurely to believe that the GL-problem could be decided finally just nowadays. The start positions for the GL problem decision are just prepared. In works[8,19,27-36] and here a so called «mitigating» or «softening» complex was developed. It is a system of the engineering high technology's means for the GL realization. The last time a special branch of that «softening complex» is quickly developing[28-36]. It is the most feasible model of GL, so called SPTEN (Soft Prompt Transplantation of Excited Nuclei) suggested (1995) and substantiated at large by the Author[28-36]. The precursor of the SPTEN, so called AVLIS (Atomic Vapor Laser Separation), is not fit for the GL creation[7,10,14,38]. The SPTEN is based on a new class of laser separation, so called «Multi Beam Laser Selection» or alias the selection with use of the «Multi Beam Emitter» [28,34,36]]. Each of that work contains the words about much big amount of work-nuclei-candidates. But only the transitions of $^{181}Ta_{73}$ (6.3 keV, 10^{-5}s) and ^{58}Co(28.1 keV, 1.5 10^{-5}s) were used as the examples. Now ones can quite apparently see a plenty of candidates.

2. The choice methods.

The necessary theoretical results, formulae and denotations are given in the previous paper [C-D].
The choice complex consists from the following canons.

1. **Condition on the time-life τ_+ of top work level.** The nuclei-candidates must be in the interval

$$\sim 10^{-7}\ \mathrm{s} < \tau_+ < \sim 10^{+2}\ \mathrm{s} \qquad (1)$$

The right boundary ~10^{+2} s is determined by the enormous difficulties of Moessbauer experiments on nuclei with $\tau_+ > 10^{+2}$ s. The left boundary ~ 10^{-7} s is determined by sharp growth of difficulties with the production, selection and the delivery of the Excited Laser Active Nuclei (ELAN) into the cite for γ-lasing.

2. **Condition on the energy $\mathbf{E}_\gamma$ of work transition.** The nuclei-candidates must be in the interval

$$\sim 1\mathrm{keV} < \mathbf{E}_\gamma < \sim 200\ \mathrm{keV} \qquad (2)$$

The right boundary ~ 200 keV is determined by a very small value of the recoilless probability (Moessbauer's factor) < 0.001.
The left boundary ~ 1keV is determined by the sharp growth of the internal conversion factor α.>> 1000. Hence out of the interval (2) the conditional resonant cross-section σ_0 is much damped because

$$\sigma_0 = (\lambda^2/2\pi)\,(f'w/(1+\alpha))\,(1/(1+\chi));\ \chi = \tau_+/\tau_- \qquad (3)$$

3. **Condition on the time-life τ_- of the lower work level.** This time-life must be in the interval

$$\infty > \tau_- > \sim 10^{-3}\,\tau_+; \qquad (4)$$

The right boundary ∞ corresponds to the stable lower level.
The left boundary ~10^{-3} τ_+ corresponds to the very diffused line with very small damping factor $(1/(1+\chi))$ ~10^{-3}.

4. **Condition on the branching:** $w > 0.001$ (5)

5. **Only the nuclei which answer simultaneously all four conditions (1), (2), (4), (5) together were considered as the tentative nuclei.** Other word, the tentative nuclei for the choice belong to the intersection of four arrays

Laser Optics 2000: Ultrafast Optics and Superstrong Laser Fields, Alexander A. Andreev, Vladimir E. Yashin, Editors, Proceedings of SPIE Vol. 4352 (2001) © 2001 SPIE · 0277-786X/01/$15.00

$$\{\text{array of tentative nuclei}\} = \{\text{array (1)}\} \cap \{\text{array (2)}\} \cap \{\text{array (4)}\} \cap \{\text{array (5)}\} \quad (6)$$

6. The following additional conditions were adopted:

6.1. The optimized restriction on the relative concentration $n/n' \cong 0.005$ (7)

At $n/n' > 0.005$ the sharp growth of the clustering leads to the enormously big time-ratio $\zeta = \tau_1/\tau_2$ (8)

which damps the asymptotic acting resonant cross-sections $\sigma_{+-} = \sigma_0/\zeta$; $\sigma_{-+} = g\,\sigma_0/\zeta$ (9)

where the «longitudinal» time τ_1 and the «crossing» time τ_2 are determined so

$$(1/\tau_1)=(1/\tau_+) + (1/\tau_-);\ (1/\tau_2) = (1/\tau_+)+(1/\tau_-)+\Gamma \quad (10)$$

The decrease of n/n' is undesirable because the important parameter

$$\psi = (n/n')/[(n/n')+(\sigma'/\sigma)] \quad (11)$$

determines the so called «Reserved Amplification» parameter p named as the «Reserved Amplification»

$$p = \psi\, p_0\, \tau_2/\tau_1 \quad (12) \text{ where } p_0 = \sigma_0/\sigma \quad (13)$$

σ is the cross-section of the non-resonant losses (through the photo-effect, Compton effect, scattering) on the atoms with the work nuclei, σ' is the cross-section of the non-resonant losses on the atoms of the light host-matrix. Hence always $(\sigma'/\sigma) << 1$.

6.2. The adopted value for time ratio $\zeta = \tau_1/\tau_2 \cong 1.1$. (14)

To provide this value $\zeta = 1.1$ is difficult but feasible for the most part of candidates. On this reason the comparison and choice of all candidates was executed at one and the same value $\zeta = 1.1$. Of cause, the value $\zeta = 1.1$ is indeed a big allowance for long-lived isomers. But even at such allowance all long-lived isomers were discarded, see the Tables below.

6.3. The adopted value for the ratio $n_+/(n_+ + n_-) \equiv \exp(-x_1) \cong 0.9$ at the initial moment t = 0. The real feasibility of value

$$n_+/(n_+ + n_-) \equiv \exp(-x_1) \cong 0.9 \quad (15)$$

with use of MBE method is substantiated in the talk [B]. In the super-radiant theory a form $\exp(-x_1)$ is adopted instead of the more apparent form $n_+/(n_+ + n_-)$ of the induced theory.

6.4. The degeneracy for both the top and the lower work levels is adopted. In deed, in case of the short-lived isomers the Hyper Fine Structure (HFS) is collapsed 37,40]. Hence in this case the work levels are degenerate. In case of long-lived work-nuclei all HFS-components are strongly overlapped. Hence the γ-lasing effect in this case is like as in case of degeneracy for both levels. In degeneracy case many γ-lasing properties are linked with the degeneracy's' ratio

$$g = (2j_+ + 1)/(2j_- + 1) \quad (16)$$

6.5. The γ-generation into one diffraction mode is regarded. Hence the number $m = 1$ (17)

for the amount of the generation modes is adopted here.

6.6. The Moessbauer factor is evaluated at the Debye approximation with the effective Debye temperature θ_{Mixt} for the mixture heavy atom in a light host $\theta_{Mixt} \cong (A'/A)^{1/2}\, \theta_{Host}$ (18)

here A' is the atomic mass of the host atom; A is the atomic mass of the mixture heavy atom; θ_{Host} is the host's Debye temperature.

7. The threshold parameters evaluated on base of the induced (p_{ind}) and super-radiant (p_{SR}) kinetics revised with account of the most complete complex of hindrances and other adverse obstacles:

For the induced kinetics $p_{ind} = 2/G_m$ (19)

here the value G_m is dependent on a degeneracy ratio **g** only at conditions **6.1-6.3**, see (16) and the Table 10.

For the super-radiant kinetics $p_{SR} = \{TSRI\}\, F_{TSR}(y)$ (20) where $y = L/2L_0$ (21)

is the relative length of the dispersed active medium, $2L_0$ is a free path of γ-quanta with account only non-resonant losses.
The values p_{ind} and {TSRI} are not depend on the length y. The factor $F_{TSR}(y)$ is minimized at

$$y = y_m = 1.79 \quad (22) \quad \text{where} \quad F_{TSR}(y_m) = \min F_{TSR} = 3.35 \quad (23)$$

8. The very perfect natural single crystal of diamond of type IIa is adopted as the best gauge-standard for the host candidates. Such crystal provides the effective cooling of the active medium owing to the low impurities' concentration (less than $10^{17}cm^{-3}$), high sound velocity, high speed of nonequilibrium electrons and holes, not too fast electron-lattice energy exchange, big free path lengths for light carriers at low temperatures, high Debye temperature; it has high Moessbauer factor (~1) for mixture nuclei, low cross-section of nonresonant losses, high stability against radiation damages and a row of other merits.

9. Cruces regime parameter $\Theta_{regime} = (q\, a_1^{27/11})/4.84.$ (24)

The radiation-heat regime is stationary and fit for the γ-lasing if $\Theta_{regime} < 1$.
The active medium (AM) is blasted without γ-lasing at $\Theta_{regime} > 1$ (25)

9a. At length $y_m = 1.79$ the AM is blasted. Everywhere at $y < 1.79$ the threshold p_{SR} increases if the length y decreases.

10. Absence of conditions for the Borrman effect realization. Substantiation is given in works [28-30,32,35].

11. In the stationary regime (no blast) the induced threshold is always less than the super-radiant one

$$p_{ind} < p_{SR} \quad (26)$$

12. The threshold conditions have the forms

for the induced generation regime $p/p_{ind} > 1$ (27) and for the super-radiant regime $p/p_{SR} > 1$ (28)

The threshold ratio p/p_{ind} was calculated for all tentative nuclei. This value is the main characteristic of the candidate owing to the properties 9,11. The tentative nucleus must be discarded if its crucial ratio $p/p_{ind} < 1$.

3. The example of the data-table for the choice.

The Table1 gives the most total representation about the choice method on the examples of two small nuclei groups. Some non-crucial characteristics are given in that tables in order to help any reader to find out the real possibilities SPTEN method in the simplest one-mode case, see, e.g., the values for the asymptotic gamma-π-pulse

$$\Phi_\pi = (p\text{-}1)/\sigma_0\ ;\ \tau_\pi = \tau_1/(p\text{-}1);\ F_\pi = \Phi_\pi/\tau_\pi = 1.6\ 10^8\ (p\text{-}1)^2 E_\gamma/\sigma_0\tau_1 \sim 1.3\ 10^8\ E_\gamma\psi^2\sigma_0/\sigma^2\tau_1 \text{ at } p >> 1.$$

Other values (so called invariants) in the tables are given as like as the introduction in the calculation of the array choice data, they give the systematic overall picture about chosen and discarded nuclei. The other tables are produced by the same method which is used for the Table 1. The Table 7 contains very impotent result: *no one long-lived nucleus* fit for the γ-laser creation was descried even at completely narrowed total line width, i.e., even if $\Gamma\tau_1 = 1$.

Table 1. Six candidates produced in photo-nuclear reactions $^{Z}A_{n+1}(\gamma n)\ ^{Z}A^*_n$, e.g., $^{92}Nb_{42}(\gamma n)\ ^{92}Nb^*_{41}$. $^{Z}A^*_n$ is a work isomer						
Type Work Isotope	±//1 D $^{92}Nb_{41}$	±//1 D $^{122}Sb_{51}$	±//2 D $^{152}Eu_{63}$	±//1 D $^{65}Zn_{30}$	±//1 D $^{69}Ge_{32}$	±//1 D $^{58}Co_{27}$
E_γ (keV)	90.2	61.45	32.6	53.96	85.0	28.1
τ_1 (sec)	6.20(-6)	2.74(-6)	2.38(-7)	2.31(-6)	7.36(-6)	1.51(-5)
α	0.17	0.75	1.2	4.4	1.4	1.5
$p_0 = \sigma_0/\sigma$	340	174	298	351	393	888
λ (Angstrem)	0.137	0.202	0.380	0.230	0.146	0.441
f	0.30	0.61	0.88	0.60	0.29	0.86
σ_0 (barn)	7.58(4)	2.26(5)	9.24(5)	9.26(4)	4.04(4)	1.07(6)
$\sigma_0 = (\lambda^2/2\pi)\ (f'w/(1+\alpha))\ (1/(1+\chi))$; $\chi = \tau_+/\tau_-$; $\sigma_{+-} = \sigma_0/\zeta$; $\sigma_{-+} = g\,\sigma_{+-}$; $\zeta = \tau_1/\tau_2$; $(1/\tau_1) = (1/\tau_+) + (1/\tau_-)$; $(1/\tau_2) = (1/\tau_+) + (1/\tau_-) + \Gamma$						
σ (barn)	223.2	1300	3100	264	103	1200
σ' (b) in Diamond	3.10	3.47	4.75	3.62	3.15	5.63
σ'/σ	0.014	0.0027	0.0015	0.014	0.031	0.0047
j_+	2	3	1	1/2	1/2	4
j_-	2	2	0	5/2	5/2	5
$g=(2j_+1)/(2j_-1)$	1	1.4	3	1/3	1/3	9/11
$p_{SR\,min} = \{TSRI\}\ F_{TSR\,min} = \min$ at $y = y_m = 1.79$, $F_{TSR\,min} = 3.35$; $N_{0\,(max\,SR)} = y_m^2\ N^*$						
Work Isotope	$^{92}Nb_{41}$	$^{122}Sb_{51}$	$^{152}Eu_{63}$	$^{65}Zn_{30}$	$^{69}Ge_{32}$	$^{58}Co_{27}$
ψ at n/n'= 0.005	0.264	0.652	0.765	0.268	0.141	0.516
$p = \psi\ p_0\ \tau_2/\tau_1$	81.8	103	207	85.6	50.2	416
F_π (W/cm²)	2.01(14)	1.65(14)	1.01(15)	2.89(14)	1.11(14)	4.80(13)
For the asymptotic gamma-π-pulse $\Phi_\pi = (p\text{-}1)/\sigma_0$; $\tau_\pi = \tau_1/(p\text{-}1)$; $F_\pi = \Phi_\pi/\tau_1 = 1.6\ 10^8\ (p\text{-}1)^2 E_\gamma/\sigma_0\tau_1 \sim\sim 1.3\ 10^8\ E_\gamma\psi^2\sigma_0/\sigma^2\tau_1$ at $p>>1$.						
$N^* = N_0/y^2$ at m=1	4.38(12)	1.15(12)	5.27(11)	5.40(12)	6.18(12)	1.85(12)
$N_{0\,(max\,SR)} = y_m^2\ N^*$	1.40(13)	3.68(12)	1.69(12)	1.73(13)	1.98(13)	5.93(12)
{TSRI}	5.50	5.79	7.33	5.08	5.08	5.38
$p_{SR\,min}$ = {TSRI} 3.35	18.4	19.4	24.6	17.0	17.0	18.0
$p_{ind} = 2/G_m$	**16.1**	**20.3**	**47.1**	**10.6**	**10.6**	**14.5**
p/p_{ind}	**5.08**	**5.07**	**4.39**	**8.08**	**4.74**	**28.7**
$p/(p_{ind}\,\psi)$	19.2	7.78	5.73	30.1	33.6	55.6
Spatial and heat parameters: In case of diamond host (and at the work nuclei dilution $n/n' \sim 0.005$) the characteristic parameter of a heat regime is the value $\Theta = (q\,a_1^{27/11})/4.84$. At $\Theta < 1$ a heat regime of active medium is stationary. At $\Theta > 1$ a heat regime of active medium is a heat-blast. Hence at a given heat-release q (W/cm³) the following critical parameters are exist: $a_{1cr} = (4.84/q)^{11/27}$; $y_{cr} = (a_{1cr}/a_{10})^2$; $N_{0cr} = y_{cr}^2\ N^* = 13.1\ N^*/(a_{10}\,q^{11/27})^4$ with the main property $a_{1\,preblast} < a_{1cr} < a_{1\,blast}$; $y_{preblast} < y_{cr} < y_{blast}$; $N_{0\,preblast} < N_{0cr} < N_{0\,blast}$						
$q\,W/cm^3$	2.68(11)	1.22(12)	9.48(12)	2.42(12)	8.55(11)	1.41(11)
$a_{10}\,cm$	6.08(-5)	4.80(-5)	4.62(-5)	7.29(-5)	6.72(-5)	6.57(-5)
$a_{1cr}\,cm$	4.20(-5)	2.26(-5)	9.82(-6)	1.71(-6)	2.62(-5)	5.45(-5)
y_{cr}	0.477	0.222	0.045	0.055	0.152	0.688
N_{0cr}	9.97(11)	5.67(10)	1.07(9)	1.62(10)	1.43(11)	8.76(11)
p_{SRcr}	31.5	60.6	335.7	191.6	73.9	24.4
$p_{ind} = 2/G_m$	16.1	20.3	47.1	10.6	10.6	14.5
$p = \psi\ p_0\ \tau_2/\tau_1$ Lasyng type at $N_0 = N_{0cr}$	81.8 IND + SR	103 IND + SR	207 only IND	85.6 only IND	50.2 only IND	416 IND + SR
It is apparent that really always (with the account of radiation-heat regime) $p_{ind} << p_{SRcr}$. It is a reason of a feeble SR-gamma-generation in comparison with an induction generation.						
$N_0 = 10^{12}$						
Work Isotope	$^{92}Nb_{41}$	$^{122}Sb_{51}$	$^{152}Eu_{63}$	$^{65}Zn_{30}$	$^{69}Ge_{32}$	$^{58}Co_{27}$

$y = (N_0/N^*)^{1/2}$	0.478	blast	blast	blast	blast	blast
$p = \psi\, p_0 \tau_2/\tau_1$ Type of generation	81.8 IND + SR	blast No generation	blast No generation	blast No generation	blast No generation	blast No generation
$p_{ind}=2/G_m$	16.1	blast	blast	blast	blast	blast
p_{SR}	31.5	blast	blast	blast	blast	blast
p/p_{SR}	2.60	blast	blast	blast	blast	blast
			$N_0 = 10^{11}$			
Work Isotope	$^{92}Nb_{41}$	$^{122}Sb_{51}$	$^{152}Eu_{63}$	$^{65}Zn_{30}$	$^{69}Ge_{32}$	$^{58}Co_{27}$
y	0.151	blast	blast	blast	0.127	0.232
$p = \psi\, p_0 \tau_2/\tau_1$ Type of generation	81.8 IND + SR	blast No generation	blast No generation	blast No generation	50.2 only IND	416 IND + SR
$p_{ind}=2/G_m$	16.1	blast	blast	blast	10.6	14.5
p_{SR}	80.5	blast	blast	blast	86.8	54.0
p/p_{SR}	1.02	blast	blast	blast	0.578	7.72
			$N_0 = 10^{10}$			
Work Isotope	$^{92}Nb_{41}$	$^{122}Sb_{51}$	$^{152}Eu_{63}$	$^{65}Zn_{30}$	$^{69}Ge_{32}$	$^{58}Co_{27}$
y	0.0478	0.0932	blast	0.0430	0.0402	0.0735
$p = \psi\, p_0 \tau_2/\tau_1$ Type of generation	81.8 only IND	103 only IND	blast No generation	85.6 only IND	50.2 only IND	416 IND + SR
$p_{ind}=2/G_m$	16.1	20.3	blast	10.6	10.6	14.5
p_{SR}	238	132	blast	243	260	154
p/p_{SR}	0.344	0.778	blast	0.352	0.193	2.71
			$N_0 = 10^{9}$			
Work Isotope	$^{92}Nb_{41}$	$^{122}Sb_{51}$	$^{152}Eu_{63}$	$^{65}Zn_{30}$	$^{69}Ge_{32}$	$^{58}Co_{27}$
y	0.0151	0.0294	0.0436	0.0136	0.0127	0.0232
$p = \psi\, p_0 \tau_2/\tau_1$ Type of generation	81.8 only IND	103 only IND	207 only IND	85.6 only IND	50.2 only IND	416 only IND
$p_{ind}=2/G_m$	16.1	20.3	47.1	10.6	10.6	14.5
p_{SR}	736	402	346	754	807	470
p/p_{SR}	0.0111	0.256	0.598	0.114	0.062	0.885
The results of a numerical approximation of function G(t) by quadratic form $G(t) \cong G_m - K_{ind}(\mu - \mu_0)^2$ at $\mu = \exp(-t/\tau_+)$:						
Work Isotope	$^{92}Nb_{41}$	$^{122}Sb_{51}$	$^{152}Eu_{63}$	$^{65}Zn_{30}$	$^{69}Ge_{32}$	$^{58}Co_{27}$
$g = (2j_+ +1)/(2j_- +1)$	1	1.4	3	1/3	1/3	9/11
G_m	0.124	0.0987	0.0425	0.188	0.188	0.138
μ_0	0.723	0.767	0.873	0.608	0.608	0.705
K_{ind}	1.62	1.82	2.64	1.22	1.22	1.586
$p_{ind}=2/G_m$	16.1	20.3	47.1	10.6	10.6	14.5

4. Host matrixes and nuclei-candidates for gamma-lasers in Mendeleev Table.

The main results of choice are represented in a form as like distantly as the Mendeleev Table, see the Table 2. The light atoms which are fit for the host matrixes of the GL's active media are marked by a shadow. Many of that elements were pointed firstly in a work[27]. For the most nuclei the best matrix is a diamond of the IIa-type[27-36]. But in case of small γ-transition energies $E_\gamma < 30$ *keV* ones could to choice some other matrix constructed from more light atoms than carbon, e.g. Be [6] or B [27], or Li [9], or even a solid hydrogen H [27], or hard isotopes deuterium D [27], or tritium T [27]. Besides many composite materials could be prepared from some of the shadowed elements from hydrogen to carbon in combination with the elements N, O, F which are less fit for the GL's active media. Such composites cold be used as host matrixes with high gamma-optical properties and good heat conductivity. The other elements of Mendeleev Table are fit for the surrounding layers of the central matrix. See refs.[14,33-35,39,40]. All denotations are given below:

••••Sc21
$^{46}_{52.012}$ *6.30*

This•••• is a signal about the presence of the chosen work nucleus in the cell of the Mendeleev Table's element marked by row of bold dots. In this case the chosen work-candidate is the nucleus $^{46}Sc_{21}$ with the mass **46**, the energy of the work transition E_γ = 52.012 *keV* and the work ratio p/p_{ind} = *6.30*. The brief notation of all this information is so: $^{46}_{52.012}$ *6.30* . The nuclei which are labeled as ***** were researched (see [G]) on the values of the changing of the optical HFS at the isomeric transitions. The times τ_1, τ_+, τ_- are not pointed in the Table 2. But they could be found in the tables 3 - 8 which contain the more detailed information than the table 2. Particularly the value $p/p_{ind}\psi$ could be found in that tables. The value $p/p_{ind}\psi$ is the work ratio in the unreal (owing to the heat blast !) case of 100% solid substance created only from the ELAN. The important general perspective for the use of the SPTEN as a fuse for the much powerful GL in future is given in [A] and is mentioned in the next Section 5. In deed the specified here nuclei candidates would be used for the creation of the SPTEN γ-laser. But the latter is necessary for the triggering of the more powerful γ-lasers because any powerful γ-laser couldn't do without the triggering by another γ-laser. Such "another" γ-laser could be at near future only the SPTEN γ-laser, see the work [A].

Table 2. Host matrixes and nuclei-candidates for gamma-lasers in Mendeleev table.

H1								**He2**
Li3	**Be4**	**B5**	**C6**	N7	O8	F9		Ne10
Na11	Mg12	Al13	Si14	P15	S16	Cl17		Ar18
K19	Ca20	**• • • • Sc21** $^{46}_{\#44}$ 52.012 *6.30;* ^{43} 78.5 *0.19* ^{45} 151.7 *0.091* ^{46} 12.4 *0.38* 142.5 *0.15*	Ti22	V23	Cr24	Mn25	Fe26 ^{57} 14.4 *4.1*	*** * * * Co27** ^{*58} 28.1 ***28.7*** ^{58} 53.0 ***w3.7*** **• • • • • • • •**	**• • • • • Ni28** ^{63} 86.9 ***1.13***
Cu29	**• • • • • Zn30** ^{65} 53.96 ***8.1*** ^{67} 93.32 ***4.0***	**Ga31• • • •** ^{74} 56.5 ***20.2*** ^{74} 59.7 *0.39*	**Ge32• • • • •** ^{69} 85.0 ***4.7*** ^{73} 13.26 *0.17* ^{75} 139.7 *0.035* ^{77} 159.7 *0.12*	**As33• • • • •** ^{76} 46.04 ***23.5***	Se34 ^{77} 162.0 *0.012* ^{79} 95.7 *0.65*	Br35		Kr36 ^{77} 66.5 *14.4* ^{83}*Kr*9.39 *5.10* ^{79} 130.0 *0.43*
Rb37 ^{83} 5.2 ~~*0.32*~~ ^{83} 42.3 *0.51*	Sr38	Y39	Zr40	**• • • • • Nb41** ^{92} 90.2 ***5.1*** ^{90} 122.4 *0.98*	Mo42 ^{99} 97.8 *0.67*	Tc 43	Ru44 ^{105} 20.55 ~~*7.6*~~	Rh45 ^{100} 74.8 ~~*4.7*~~ ^{105} 129.6 *0.49*	**• • • • • Pd46** ^{107} 115.7 ***1.62***
• • • • • Ag47 ^{110} 1.113 ***1.43*** ^{103} 134.3 *0.27* ^{107} 93.1 *0.041* ^{109} 88.03 *0.042* ^{111} 59.8 *0.017* ^{116} 81.0 *0.25-0.03* ^{118} 127.7 *0.28-0.035* ^{120} 203.0 *0.011*	Cd48 ^{109} 59.9 *0.84*	In49 ^{116} 162.4 *0.058* ^{118} 138.0 *0.13*	Sn50 $^{\#115}$ 100.7 *0.065*	**Sb51• • • • •** ^{122} 61.45 ***5.1*** ^{118} 50.8 *0.17* ^{126} 23.28 ~~*1.1*~~ ^{126} 64.3 ~~*3.0*~~ ^{126} 87.6 ~~*4.7*~~ ^{126} 87.0 ~~*0.20*~~ 22.7 *0.057*	Te52	J53 ^{122} 148.8 *W(0.6-0.1)* ^{120} 72.6 ~~*5.2 - 2.5*~~		Xe54 ^{125} 43.3 ~~*w4.2*~~
Cs55 ^{140} 13.9 ~~*3.7 - 2.5*~~ ^{134} 11.3 *0.25*	Ba56	*La57 ^{137} 72.6 ~~*1.4*~~ ^{138} 72.6 ~~*0.71*~~	Hf72 ^{175} 125.9 *0.72* $^{\#173}$ 90.3 ~~*1.7*~~	*** * * * Ta73** ^{*181} 6.23 *0.25* ^{177} 73.6 ~~*2.0*~~ ^{183} 73.16 ~~*1.9*~~	W74	**• • • • • Re75** ^{177} 84.7 ***1.94*** ^{179} 65.6 ***9.81*** ^{180} 20.2 ~~*13.0*~~	Os76 ^{181} 107.7 ~~*1.2*~~	Ir77	Pt78 ^{187} 117.0 *0.03*
Au79 ^{189} 78.0 ~~*1.1*~~	Hg80	Tl81	Pb82	Bi83 ^{206} 59.9 *0.22*	Po84 ^{207} 68.7 ~~*0.26*~~ $^{\#209}$ 55.2 ~~*0.054*~~ $^{\#210}$ 85.0 ~~*0.099*~~	At85		Rn86
Fr87	Ra88	**Ac89	The mark* * * * * means that the optical HFS was evaluated here in case of the work isomer of «**// 1 D» type.					

Ce58 Pr59	Nd60 ^{140} 42.8 *0.19*	Pm61 Sm62	**• • • • * * * * * Eu63** ^{*154} 68.2 ***3.9;*** ^{152} 32.6 ~~*w 4.4;*~~ ^{152} 89.8 ~~*2.4*~~ ^{152} 19.7 ~~*0.28;*~~ ^{141} 96.4 *0.012*		Gd64 $^{\#153}$ 76.2 *0.83* ^{157} 63.8 ~~*2.4*~~	Tb65 Dy66 Ho67	Er68 $^{\#169}$ 151.7 ~~*0.39*~~ ^{171} 198.0 ~~*0.08;*~~ ^{157} 156.0 *0.03*	**• • • • • Tm69** ^{165} 80.3 ***2.5*** ^{167} 113.3 *0.98*	Yb70	**• • • • • • Lu71** ^{172} 67.5 ***2.4;*** ^{173} 123.7 *W(1.6 - 0.2)* ^{172} 24.0 ~~*3.1;*~~ ^{177} 150.4 ~~*0.42*~~				
Th90	Pa91	U92	Np93	Pu94	Am95	Cm96; ^{243} 87.4 *0.19*		Bk97	Cf98	Es99	Fm100	Md101	No102	Lw103

Table 3. The isomers of type «+//1D» : $p/p_{ind} > 0$ at the absence of Borrman effect, $n/n'=0.005$, $n_+/n=0.9$, $\tau_1/\tau_2=1.1$ and at the time-lives τ_1,τ_+ lying in the first short-lived diapason «//1D» 10^{-4} s > $\tau_1,\tau_+ > 10^{-6}$ s.

Isomers +//1D	46 Sc 21	58 Co 27	58 Co 27	63 Ni 28	65 Zn 30	67 Zn 30	74 Ga 31
E_γ (KeV)	52.012	28.1	53.0	86.9	53.96	93.32	56.5
τ_1 (sec)	1.27(-5)	1.51(-5)	1.51(-5)	2.48(-6)	2.31(-6)	1.33(-5)	7.21(-7)
p/p_{ind}	6.30	28.7	w 3.68	1.13	8.08	4.01	21.5//18.9
$p/(p_{ind}\psi)$	69.2	55.6	w 18.1	12.7	30.1	41.1	79.6//70.0
Isomers +//1D	69 Ge32	76 As 33	92 Nb 41	107 Pd 46	110 Ag 47	122 Sb 51	154 Eu 63
E_γ (KeV)	85.0	46.04	90.2	115.7	1.113	61.45	68.2
τ_1 (sec)	7.36(-6)	2.7(-6)	6.20(-6)	1.30(-6)	9.52(-7)	2.74(-6)	3.46(-6)
p/p_{ind}	4.74	23.5	5.08	1.62	1.43	5.07	3.85
$p/(p_{ind}\psi)$	33.6	53.4	19.2	6.40	8.03	7.78	4.98

Isomers +//1D	165 Tm 69	172 Lu 71	173 Lu 73	177 Re 75	179 Re 75
E_γ (KeV)	80.3	67.5	123.7	84.7	65.6
τ_1 (sec)	1.30(-5)	6.20(-4)	1.06(-4)	7.21(-5)	1.30(-4)
p/p_{ind}	2.46	2.42	w 1.6 // w 0.2	1.94	9.81
$p/(p_{ind}\psi)$	3.33	2.93	w 2.74//w 0.34	2.50	16.6

Isomers of type +//1D are the most preferable for the first direct γ-lasing experiments: 1. Times τ_1,τ_+ are fit for use in the SPTEN-method. 2.The Borrman effect is not necessary.

Table 4. The isomers of type □//1D : $p/p_{ind} < 0$ at the absence of Borrman effect, $n/n'=0.005$, $n_+/n=0.9$, $\tau_1/\tau_2=1.1$ and at the time-lives τ_1,τ_+ lying in the first short-lived diapason «//1D» 10^{-4} s > $\tau_1,\tau_+ > 10^{-6}$ s.

Isomers □//1D	44 Sc 21	73 Ge 32	90 Nb 41	99 Mo 42	109 Cd 48	# 115 Sn 50	118 Sb 51
E_γ (KeV)	78.5	13.26	122.4	97.8	59.9	100.7	50.8
τ_1, τ_+, τ_- (sec)	$\tau_+ = 7.21(-5)$ $\tau_- = 2.21(-7)$	4.26(-6)	8.80(-5)	2.16(-5)	1.73(-5)	$\tau_+ = 2.29(-4)$ $\tau_- = 4.76(-6)$	3.03(-5)
p/p_{ind}	0.185	0.172	0.979	0.673	0.840	0.0651	0.168
$p/p_{ind}\psi$	43.0	0.610	5.76	2.79	1.37	0.402	0.224
Isomers □//1D	122 I 53	140 N d60	#153 Gd 64	167 Tm 69	175 Hf 72	*)181 Ta 73	187 Pt 78
E_γ (KeV)	148.8	42.8	76.2	113.3	125.9	6.23	117.0
τ_1, τ_+, τ_- (sec)	1.01(-4)	9.67(-5)	$\tau_+ = 1.098(-4)$ $\tau_- = 5.05(-6)$	$\tau_+ = 1.30(-6)$ $\tau_- = 1.59(-6)$	7.79(-5)	9.81(-6)	4.47(-4)
p/p_{ind}	w 0.64 - w 0.08	0.185	0.833	0.980	0.719	0.25	0.0297
$p/p_{ind}\psi$	2.86 - 0.358	0.312	1.15	1.64	1.22	0.35	0.0430

Isomers □//1D	206 Bi 83	243 Cm 96
E_γ (KeV)	59.9	87.4
τ_1 (sec)	1.13(-5)	1.56(-6)
p/p_{ind}	0.224	0.192
$p/p_{ind}\psi$	0.311	0.284

The isomers of the type □//1D could be used in the direct gamma-lasing experiments only at the condition of a feasibility of very strong Borrman effect. The value p_{ind}/p shows the minimal ratio for the change in the resonant and non-resonant absorption correspondingly. Other words it needs to get the relation $(\sigma_0/\sigma)_B > (p_{ind}/p)\,(\sigma_0/\sigma)_{usual}$. A ratio $(\sigma_0/\sigma)_{usual}$ corresponds to an usual case without Borrman effect. A ratio $(\sigma_0/\sigma)_B$ corresponds to the use of Borrman effect.

Table 5. The isomers of type «+//2D» : $p/p_{ind} > 0$ at the absence of Borrman effect, $n/n'=0.005$, $n_+/n=0.9$, $\tau_1/\tau_2=1.1$ and at the time-lives τ_1,τ_+ lying in the second short-lived diapason «//2D» 10^{-6} s > $\tau_1,\tau_+ > 10^{-7}$ s.

Isomers +//2D	57 Fe 26	77 Kr 36	83 Kr 36	105 Ru 44	100 Rh 45	126 Sb 51	126 Sb 51
E_γ (KeV)	14.4	66.5	9.39	20.55	74.8	23.28	64.3
τ_1 (sec)	1.38(-7)	2.45(-7)	2.12(-7)	4.91(-7)	3.09(-7)	1.13(-7)	7.93(-7)
p/p_{ind}	4.05	14.4	5.10	7.57	4.66	1.07	3.04
$p/p_{ind}\psi$	6.19	45.0	11.2	12.7	10.4	1.50	4.77
Isomers +//2D	126 Sb 51	120 I 53	125 Xe 54	140 Cs 55	137 La 57	152 Eu 63	152 Eu 63
E_γ (KeV)	87.6	72.6	43.3	13.9	72.6	32.6	89.8
τ_1 (sec)	1.13(-7)	3.32(-7)	2.02(-7)	6.78 (-7)	1.67(-7)	2.38(-7)	5.54(-7)
p/p_{ind}	4.65	5.24//2.53	w 4.17	3.65//2.54	1.35	w 4.39	2.38
$p/p_{ind}\psi$	10.1	8.78//4.24	w 4.96	30.3//43.6	1.71	w 5.73	3.72
Isomers +//2D	157 Gd 64	172 Lu 71	#173 Hf 72	177 Ta 73	183 Ta 73	180 Re 75	181 Os 76
E_γ (KeV)	63.8	24.0	90.3	73.6	73.16	20.2	107.7
τ_1, τ_+, τ_- (sec)	6.64(-7)	4.76(-7)	$\tau_+ 2.31(-7)$ $\tau_- 2.60(-7)$	5.34(-7)	1.59(-7)	1.27(-7)	4.62(-7)
p/p_{ind}	2.36	3.14	1.67	1.96	1.91	13.0	1.16
$p/p_{ind}\psi$	3.69	3.47	2.28	2.42	2.33	23.3	1.69

Isomers +//2D	189 Au 79
E_γ (KeV)	78.0
τ_1 (sec)	2.74(-7)
p/p_{ind}	1.07
$p/p_{ind}\psi$	1.96

The excited nuclei of the type +//2D are more preferable for the γ-lasing than the nuclei of the type □//2D (see Table «Isotopes □//2D» below). The nucleous marked by the sign # is characterized by the complex of the times $\tau_1, \tau_2, \tau_+, \tau_-$ which are determinded in this paper. The values $p/p_{ind}\psi$ correspond to the case of a 100% concentration of the work nuclei.

Table 6. The isomers of type «□//2D» : $p/p_{ind} < 0$ at the absence of Borrman effect, $n/n'=0.005$, $n_+/n=0.9$, $\tau_1/\tau_2=1.1$ and at the time-lives τ_1,τ_+ lying in the second short-lived diapason «//2D» 10^{-6} s > $\tau_1,\tau_+ > 10^{-7}$ s.

Isomers □//2D	83 Rb 37	126 Sb 51	138 La 57	152 Eu 63	#169 Er 68	171 Er 68	177 Lu 71
E_γ (KeV)	5.2	87.0	72.6	19.7	151.7	198.0	150.4
τ_1, τ_+, τ_- (sec)	1.04(-7)	7.93(-7)	1.67(-7)	1.36(-6)	$\tau_+ = 2.89(-7)$ $\tau_- = 4.04(-7)$	3.03(-7)	1.73(-7)
p/p_{ind}	0.318	0.195	0.708	0.282	0.394	0.0836	0.422
$p/p_{ind}\psi$	0.755	0.212	0.895	0.326	0.997	0.306	0.968

Isomers □//2D	207 Po 84	#.209 Po 84	# 210 Po 84
E_γ (KeV)	68.7	55.2	85.0
τ_1, τ_+, τ_- (sec)	2.89(-7)	$\tau_+ = 1.41(-7)$ $\tau_- = 3.61(-8)$	$\tau_+ = 1.38(-7)$ $\tau_- = 6.06(-8)$

The isomers of 0//2D-type could be used as like as the work-nuclei only after the following difficulties will be overcome: 1. Difficulties of the pumping for the times shorter than 10^{-6} s (see this paper). 2. Difficulties of the

p/p_{ind}	0.264	0.0542	0.0987
p/p_{ind} Ψ	0.387	0.213	0.178

strong Borrman effect creation at the conditions of a real γ-lasing experiment (see this paper).

Table 7. The isomers of type □//LL : $p/p_{ind} < 0$ at the absence of Borrman effect, n/n'=0.005, $n_+/n=0.9$, $\tau_1/\tau_2=1.1$ and the time-lives τ_1,τ_+ lying in the available long-lived diapason «//LL» ~ 100 s > $\tau_1,\tau_+ >> 10^{-4}$ s.

Isomers □//LL	43 Sc 21	45 Sc 21	46 Sc 21	74 Ga 31	75 Ge 32	77 Ge 32	77 Se 34
E_γ (KeV)	151.7	12.4	142.5	59.7	139.7	159.7	162.0
τ_1 (sec)	0.912	0.456	27.0	13.7 sec	68.8	76.3	25.2
p/p_{ind}	0.0908	0.377	0.146	0.390	0.0347	0.121	0.0124
p/p_{ind} Ψ	4.18	0.771	6.27	1.63	0.539	2.36	0.212
Isomers □//LL	79 Se 34	79 Kr 36	83 Rb 37	105 Rh 45	103 Ag 47	*)107 Ag 47	*)109 Ag 47
E_γ (KeV)	95.7	130.0	42.3	129.6	134.3	93.1	88.03
τ_1 (sec)	234.6	72.1	0.0113	64.9	8.22	63.9	57.4
p/p_{ind}	0.654	0.428	0.513	0.489	0.271	0.0409	0.0416
p/p_{ind} Ψ	4.77	4.08	0.924	2.46	1.27	0.114	0.108
Isomers □//LL	111 Ag 47	116 Ag 47	118 Ag 47	120 Ag 47	116 In 49	118 In 49	126 Sb 51
E_γ (KeV)	59.8	81.0	127.7	203.0	162.4	138.0	22.7
τ_1 (sec)	93.5	15.1	4.04	0.46	3.12	12.3	15.9
p/p_{ind}	0.0174	0.25//0.031	0.28//0.035	0.0105	0.0584	0.129	0.0571
p/p_{ind} Ψ	0.0291	0.59//0.073	1.19//0.15	0.106	0.0456	0.576	0.0760
Isomers □//LL	134 Cs 55	141 Eu 63	157 Er 68				
E_γ (KeV)	11.3	96.4	156.0				
τ_1 (sec)	65.9	4.76	0.115				
p/p_{ind}	0.254	0.0123	0.0306				
p/p_{ind} Ψ	0.302	0.0209	0.119				

There are apt all long-lived isomers at ~10^{-2} s > τ_1, $\tau_+ >> 10^{-4}$ s. So any isomers of type «+//LL» are not revealed as yet. Long-lived isomers of type «□//LL» could be fit for the γ-lasing only at a very problematic happy use of the rather strong Borrman effect.

Table 8. Denotations in Tables 1 - 8.

116 Ag 47	is the economic «aligned» transformation of the usual standard denotation for the nucleus $^{116}Ag_{47}$
0.28//0.035	the value p/p_{ind} is evaluated with a spread in the interval 0.28> p/p_{ind} >0.035
p/p_{ind}	and the other parameters are evaluated at the following optimal complex of the experimental conditions: No the Borrman effect, n/n' = 0.005, n+/n = 0.9; τ_1/τ_2 = 1.1. The meaning of this values is given in the present paper.
#	In this case, if $\tau_-\sim\tau_+$, the resonant nuclear self-absorption could be sufficiently reduced owing to the decay of the lower work level. Such reduction of the self-absorption is accounted in the estimation of the crucial ratio p/p_{ind}.
***)107 Ag 47; *)109 Ag 47; *)181 Ta 73**	These early candidates for γ-laser are rather well examined. Sorry, but they must be discarded because the types □//1D and □//LL could be used only together with the much strong Borrman effect. The SPTEN method can't use the Borrman effect. In SPTEN case, the active medium is placed in a dispersed (e.g., comb-like or dentate) micro-profile engraved at the surface of the host-crystal. Such irregular microstructure (with an irregular «period» ~ 10^{-6} *cm* cant to make the Borrman effect. There are many other so-called «residential» γ-laser schemes in which the active medium is placed inside the crystal. But in case of short-lived isomers that other methods of pumping give the blast of the active medium before the γ-lasing. In case of long-lived (~ 100 - 10^{-4} s) isomers . At last the gaseous and beams active media are not fit for the γ-lasing even at use of the modern laser-cooling methods (see [40,41]).

5. SUMMARY TABLE

The main results are represented below in the Table 9 and in the notes to it. That notes contain the perspectives for the GL problem.

Table 9. Distribution of nuclei-candidates over three diapasons for the time-life determination

1st short life-time diapason //1D» ~ 10^{-8} s > τ_1 > 10^{-6} s		2nd short life-time diapason //2D» ~ 10^{-6} s > τ_1 > 10^{-7} s		Minute life-time (long-lived) diapason //LL» ~ 10^{+2} s > τ_1 >> 10^{-4} s	
Lasing without Borrman Effect	Amount	Lasing without Borrman Effect	Amount	Lasing without Borrman Effect	Amount
«+//1D», yes: p/p_{ind}>1	#1 ~19	«+//2D», yes: p/p_{ind}>1	~ 22	«+//LL», yes: p/p_{ind}>1	#2 ~ 0
«□//1D», no: p/p_{ind}<1	~ 16	«□//2D», no: p/p_{ind}<1	~ 10	«□//LL», no: p/p_{ind}<1	~ 24

Note #1. The amounts of candidates in this distribution are as yet approximate and could be changed at more care analysis with more reliable and total data-banks.

Note #2. The generation on the nuclei **«+//1D»** could give a rather intensive, tight, good directed gamma-ray beam. The mean intensities of the asymptotic pulse Φ_π (*W/cm²*) generated on some work-nuclei are given in the Tables 1, 2 and are varied in the interval 10^{15} - 10^{9} *W/cm²*. The type **«+//1D»** is achievable in future and could give ~ 10^{16}-10^{17} *W/cm²* for mean intensities. The peak intensities could be more by 1-2 orders than mean ones. In optical diapason the much more big mean intensities are reached. But the frequencies from γ-laser are more by 3-5 orders. On this reason the combination triggering action of γ-beam with 10^{15} *W/cm²* must be more effective than the combination triggering action of optical beam with 10^{17} - 10^{19} *W/cm²*. Such beams from SPTEN-γ-laser could be used In the creation of much more powerful «Many-Section» γ-lasers.

REFERENCES

All references cited at present work could be found in the paper labeled here as [A]:

[A]. Karyagin S.V. \\ 2000, "Status of gamma-laser problem on current moment'2000: ranging analysis and screening of gamma-laser schemes on their feasibility". Corresponds to the report TuB1-8 at the X Conference "Laser Optics'2000", St.-Petersburg, June 26-30, 2000, Technical Program, p. 16.

Author Index